ITALIAN PHYSICAL SOCIETY

CONFERENCE PROCEEDINGS

VOLUME 70

ICCF8

Proceedings of the 8th International Conference on Cold Fusion

edited by F. Scaramuzzi
Lerici (La Spezia), Italy 21-26 May 2000

Centenary 1897-1997

Italian Physical Society
Bologna- Italy

Technical Editing by Carmen Vasini

ISBN 88-7794-256-8

Printed in Italy

Finito di stampare
nel mese di gennaio 2001
Compositori Ind. Grafiche - Bologna

SOCIETÀ ITALIANA DI FISICA

ATTI DI CONFERENZE

VOLUME 70

ICCF8

Atti dell'8ª Conferenza Internazionale sulla Fusione Fredda

a cura di F. Scaramuzzi
Lerici (La Spezia), Italia 21-26 Maggio 2000

Centenario 1897-1997

Società Italiana di Fisica
Bologna- Italia

The International Advisory Committee (IAC)

F. Scaramuzzi, Chairman

J.P. Biberian, France
T. Bressani, Italy
H. Ikegami, Japan
F. Jaeger, USA
J. Kasagi, Japan
X.Z. Li, China
M. McKubre, USA
G. Miley, USA
K. Ota, Japan
G. Preparata, Italy
N. Samsonenko, Russia
C. Sanchez, Spain
M. Srinivasan, India
A. Takahashi, Japan

The Scientific Program Committee (SPC)

F. Scaramuzzi, Chairman

J.P. Biberian, France
F. De Marco, Italy
A. De Ninno, Italy
D. Gozzi, Italy
J. Kasagi, Japan
X.Z. Li, China
M. McKubre, USA
G. Mengoli, Italy
G. Miley, USA
G. Preparata, Italy
C. Sanchez, Spain
V. Violante, Italy

Secretariat

A. De Ninno, Chairwoman
M.L. Ciceroni
S. Ferri
F. Vinciguerra
F. Simoni

ICCF8

CONTENTS

3. TRANSMUTATIONS

4. LOADING OF H(D); MATERIAL SCIENCE

5. Detection of nuclear emissions

6. Experiments with stimulation: energetic particles, E.M.-radiation, ultrasounds

7. THEORIES

FOREWORD

1. HISTORY

Eleven years have passed since Professors Fleischmann and Pons (FP) announced that they had observed the fusion of two deuterium nuclei at room temperature within the lattice of a metal. This announcement produced great excitement, and there were many attempts to reproduce the experiment. It turned out that it was neither easy, nor easily reproducible, and the eventual outcome was the growth of enthusiasm and skepticism at the same time: the enthusiasm of those who succeeded in repeating the experiment and the skepticism of those (the majority) who did not. Within a few months the scientific community took the "semi-official" position that none of it was true and that "Cold Fusion" (CF) did not exist.

This history has created a very strange situation, a divergence increasing in time between official science and a small group of researchers, most of whom have participated in this Conference, who have continued to do research in this field. They had the conviction, better the awareness, that the phenomena under investigation were real and scientifically very interesting. The hope that this research could also have an important practical result, mainly as a new energy source, added charm and passion to this enterprise.

Research in CF has been going on all these years, producing continuous, albeit gradual, progress, mostly in USA, in Japan, in Italy, in Russia, in China, and, to a lesser extent, also in other countries. There have been difficulties in communicating the results obtained within and outside of the CF community: many scientific journals have *a priori* denied access to papers related to CF. In this situation an important role has been played by the International Conferences, of which the present, ICCF8, is the most recent. They have offered an occasion to meet and exchange information among the researchers active in this field, and have provided an important resource with their Proceedings, amounting to a good archive, witnessing the development of CF. I think that it is worthwhile, at this time of the CF history, to review them, thus producing a concise outline of the main events in the field.

The first Conference was sponsored by the "National Cold Fusion Institute" (NCFI), founded by the University of Utah, and was held in Salt Lake City at the end of March 1990. It was called "The first annual Conference on Cold Fusion". There were already major difficulties: the official scientific community had already pronounced its verdict against CF; the NCFI would close shortly afterwards; within the CF community there were two diverging schools, those who believed only the nuclear evidence (mainly neutrons), barely accepted by the scientific community, and those who believed in excess heat, spurned by the scientific community. I must confess that I belonged to the first school, being quite skeptical about heat production, and I participated in the organization of a "dissident" Conference, called "Anomalous nuclear effects in deuterium/solid systems", sponsored by "The Electric Power Research Institute" (EPRI), by the US Department of Energy (DOE) and by the Brigham Young University at Provo (BYU): the Conference was held in Provo, Utah, in October 1990.

At this point two parallel initiatives were proposed: I was asked by the "neutron" people to organize the next Conference in Italy and Giuliano Preparata was asked to perform the same task by the "excess heat" people. There were discussions and correspondence was exchanged between the representatives of the two schools, but eventually wisdom prevailed and it was decided that there would be only one Conference, in Italy, covering all aspects of CF. This was the "Second Annual Conference on Cold Fusion": Tullio Bressani, Emilio Del Giudice, and Giuliano Preparata were the Chairmen, and for the first time an International Advisory Committee (IAC) appeared. The Conference was sponsored by Italian universities, research agencies and industries, and was held in Como at the end of June and beginning of July 1991.

I think that the Como Conference was very important in the development of CF. There were at least two results that have influenced future research: the statement that heat excess in electrolytic cells with heavy water and palladium cathode could be obtained only if the amount of deuterium absorbed in the palladium lattice (the D/Pd ratio) exceeded a threshold value (McKubre), and the correlation between heat excess and the presence of ^{4}He, understood to be a nuclear ash of the fusion process (Miles). Both these features were consistent with the theory presented by Preparata, Bressani and Del Giudice in April 1989. The many confirmations of the production of heat excess also had an important effect on me and on the ENEA Frascati Group: we decided to move from neutron and tritium detection to calorimetry, and eventually we obtained very convincing evidence of the existence of excess heat.

Next Conference was organized in Japan, with the strong encouragement of IMRA, the research enterprise that owed its existence to the determination of Minoru Toyota, an influent member of the Toyota "dynasty". It was sponsored by many Japanese scientific institutions, was held in Nagoya in October 1992, and was chaired by Prof. Hideo Ikegami. This was the first for which the present name and acronym were used: "3rd International Conference on Cold Fusion" (ICCF3). The IAC was also active in this Conference, and a general rule was informally accepted about the frequency and location of the subsequent conferences: there would be a rotation among the three most active continents: Asia, America, and Europe, with roughly one and a half years between successive conferences. Thus we had ICCF4 in December 1993 in Maui, Hawaii, USA, sponsored by EPRI and by the Stanford Research Institute (SRI), chaired by Drs. Tom Passell and Michael McKubre, followed by ICCF5, in April 1995, in Monte Carlo, (almost) France, Europe, organized again by the IMRA laboratories, chaired by Prof. Stanley Pons. Then came ICCF6, in Toya, Japan, in October 1996, organized by the Japanese government enterprise, "The Institute of Applied Energy" of the "New Energy Technology Development Organization" of MITI (the Ministry of International Trade and Industry): it was chaired by Prof. Makoto Okamoto. Finally ICCF7 was held in Vancouver, Canada, in April 1998, and was organized by Eneco, a private company that has always followed attentively the development of CF. Fred Jaeger was its Chairman.

After Asia and America, it was once again the turn of Europe. In Vancouver I was appointed by the IAC to be Chairman of ICCF8, to be held in Italy. The period envisaged was October 1999, but a number of management problems that I had to face in Frascati forced me to propose to the members of the IAC to postpone ICCF8 to the Spring of 2000. They accepted and it seemed advisable, in order to avoid the congestion to be expected in the Rome area during the Holy Year, to have it in a different site. Antonella De Ninno proposed Villa Marigola, a beautiful 18th century

villa upon a hill in a delightful park in Lerici, which is a small town on the Tirrenian sea not far from Genoa. In retrospect it seems to me that this choice was appreciated by the participants in the Conference.

In the course of these years many new features of CF have appeared, only a few of which I will mention here: In FP-type experiments, the "heat after death", i.e., the production of excess heat after the total evaporation of the electrolyte; the possibility of having CF phenomena by coupling hydrogen and nickel (rather than deuterium and palladium); the increasing evidence of "transmutations", i.e., the appearance, after the CF experiment, of nuclei that were absent before; the increasing accuracy in the evidence of nuclear emissions, both in passive and "active" experiments, where by active I mean those in which a stimulation is applied to the system under study (energetic particles, e.m.-radiation, ultrasound). Much theoretical work deserves to be cited: I will limit myself to stating what is, in my opinion, the most important notion, presented first by Preparata as early as in 1989: a collective and coherent interaction among the entities that participate in the CF phenomena is required in order to explain them. The multiplicity of phenomena, together with the limited resources dedicated to this research activity, results in a sparse but fascinating panorama, with many holes still to be filled. Furthermore, all these features have continued to be haunted by the old ghost of the "lack of reproducibility". But in this direction too important progress has been achieved. I will mention here just one episode: at ICCF6 the ENEA Frascati Group presented a measurement in electrolytic cells with heavy water, in which an easily measurable heat excess was obtained with quite good reproducibility; what is most important is that this had been obtained by facing and solving material science problems connected with the absorption of deuterium in palladium, and by carefully designing the samples and the protocol of the experiment.

It is worth remembering that in these years there were three major initiatives:

1. EPRI made an important investment in CF research, initially in a number of areas, eventually mostly in excess heat experiments with D/Pd systems, that were performed at SRI. This project was active for many years and, in spite of good results, was terminated in 1995.
2. I already cited IMRA, an institution tied to the Japanese industry Toyota: three laboratories were created, two of them in Japan (in Sapporo and in Nagoya), and one in Europe, at Sophia Antipolis, near Cannes. This project, too, has been terminated quite recently.
3. Another important Japanese initiative was taken a few years later by the MITI, with an additional contribution from a consortium of industries. A specialized laboratory was built for the purpose, and universities collaborated on more fundamental aspects. This project was terminated in 1998.

One could be tempted to interpret the end of these three important projects as a demonstration that CF research is failing in its objective to become a well defined discipline in science. I am convinced that this interpretation is wrong. Let me explain why. One of the common characteristics of these projects is that they were promoted by agencies (in a general sense) highly interested in the potential energetic applications of CF. Thus, their expectation was to be able to develop practical applications of CF in a few years. This has not happened: in spite of the indubitable scientific realities, progress in CF research has been quite slow, both because of the intrinsic difficulties of the field, and of the very scarce resources that have been dedicated to its study. Thus, it is not surprising that enterprises that were born with the aim of a practical fall-out in short time would give up.

I am convinced that a lot of basic research is still needed in order to better understand the science underlying CF, before practical objectives can be seriously addressed: this can be better pursued by small groups that proceed with this idea clearly in mind. And this is, in my opinion, what is happening. As an example, let me note that at this Conference there were 15 communications by Japanese scientists (more than 20% of the total), mostly from universities, in spite of the disappearance of the two big initiatives quoted above. The research program at ENEA Frascati, funded by the Italian Government, is another meaningful example, which, I hope, will be followed by other initiatives of this kind.

2. ICCF8

2a. Generalities

The Italian research agency for energy and environment, ENEA (*Ente per le Nuove tecnologie, l'Energia e l'Ambiente*), accepted the task of organizing this Conference. There were other important sponsors. One of them was CNR (*Consiglio Nazionale delle Ricerche*), the largest public research agency in Italy. The others were the INFN (*Istituto Nazionale di Fisica Nucleare*), an important research institution, operating in symbiosis with Italian universities in the field of nuclear and sub-nuclear physics, and the Italian physical society, SIF (*Società Italiana di Fisica*). The latter is responsible for publishing these Proceedings. The decision of ENEA to sponsor ICCF8 is part of a more general initiative, taken by the Board of Administration of the Agency in 1998, including the start of a research program, proposed by Giuliano Preparata, with a new laboratory to be built at the ENEA Center of Frascati. This program was started in 1999, and the first results were reported at this Conference.

Unfortunately, on April 24, less than a month before the beginning of ICCF8, Giuliano Preparata died, leaving a sad void in our Group, in the world of CF, and in science. We decided that we would memorialize him in this Conference, dedicating to his memory the very beginning of the meeting. On Monday, May 22, after a brief introduction by me, Martin Fleischmann gave a speech in his memory. The reader will find both texts in the Proceedings.

In organizing ICCF8 I benefited from the expert advice of the IAC, which helped me take the difficult decision to delay the Conference by half a year. When the real work started, I could not have succeeded, without the efficient and intelligent contributions of Dr. Antonella De Ninno. Becoming the head of the Secretariat, she set up and directed a wonderful team, and all together we worked out all the stages of the Conference, from the decision about where to hold it to the editing of the Proceedings. Last, but not least, I wish to recall here the very important contributions of the Scientific Program Committee (SPC): initially a small group of Italian colleagues, it was then enlarged, substantially doubled, by representatives of other countries, in order to help take decisions on the program of the Conference, on its format, and on the publication of the Proceedings.

2b. About criteria

The experience accumulated from the past conferences prompted us to have a single session and to divide the contributions into orals and posters. We decided also to repeat once more the well tested technique of the "poster presentation sessions", preceding the poster discussion sessions: for each poster there would be a three-minute oral presentation, the whole session lasting one hour. We did not have invited talks, and divided the oral presentations into longer ones, the majority (35 minutes, including discussion), and shorter ones (25 minutes, including discussion). We had a total of 26 oral presentations and 51 posters, out of 110 abstracts presented. These criteria were founded on the awareness that, in spite of the eleven years that have passed, this discipline is still young, and it is important to do our best to allow the maximum possible number of participants to communicate the results of their research work.

Knowing that ICCF8 would take place at the end of May at an appealing sea-side site, we decided that we would leave the participant free time to enjoy the place: thus, we concentrated all the oral presentations in the four mornings, Monday to Thursday, from 9 a.m. to 1 p.m.. Then the participants were free for three hours. The afternoon sessions, for three days (we left the Wednesday afternoon free) started at 4 p.m. with the poster presentation session, and continued up to 7 p.m. with the poster discussion. We had three social gatherings: on Sunday afternoon we had a get-together party, on Wednesday evening we had the social dinner, and on Friday 26, after a session on "conclusions", we had a brunch offered to all participants and to their companions.

2c. Attendance

There were 145 participants in the Conference: 41 from Italy, 40 from USA, 24 from Japan, 12 from Russia, and smaller numbers from 14 other countries. We succeeded in helping colleagues who had financial difficulties plus a number of students (a total of more than 20 persons), by waiving the Conference fee, by providing free lodging in Lerici during the Conference, and, in a few cases, we also paid travel expenses.

2d. The scientific outcome

Here, of course, I am expressing my own point of view, for which I take full responsibility. I think that the picture of CF that I described briefly at the beginning of this foreword has been substantially confirmed, but there have also been many important new results, and I would have difficulty in quoting all of them. Let me just mention a few items that, in my opinion, deserve to be emphasized:

- There have been quite convincing confirmations, at least three, of the detection of ^{4}He, understood to be a nuclear ash, in experiments with palladium and deuterium, obtained with different experimental procedures. In some cases the correlation with the heat produced gives support to the figure of 24 MeV per atom as a consequence of a D+D reaction. There was also an interesting evidence of ^{3}He production. The presence of these nuclei is the indubitable signature of a nuclear reaction.

- We had the first presentation of the effect proposed by Giuliano Preparata with the name of Cohen-Aharonov effect, which it has been proposed to rename as the Preparata effect. There was also the first experimental evidence of this effect. This effect could represent a shortcut to most of the material science problems, with the aim of achieving high loading ratios in palladium.
- There were many reports on problems of material science, most of them worked with very advanced techniques and with a sound scientific approach.

But there was such a variety of different experiments and fascinating theories that I would have difficulty in quoting them here. The Conference was quite lively, with interesting discussions.

Given these observations of the state of the art of this discipline, and the indubitable progress that has been achieved in these eleven years, I am still astonished by the lack of communication between the CF world and the "official" scientific community. This is also witnessed by the absence of research on CF in most of the European Countries and by the ostracism to CF publications in most prestigious scientific journals (we are very grateful to "Il Nuovo Cimento" for its open position in all these years, witnessed once more by the decision to publish these Proceedings). In my opinion, there is no doubt that we are facing a subject of enormous scientific interest: it can no longer be denied that there are many different kinds of nuclear reactions that take place at substantially low energies, and that this implies the existence of collective and coherent interactions among the participants in the events under study. Following Preparata's suggestion, one can envisage a totally new way of looking at most of the problems of condensed matter. This should stimulate the "curiosity" of all scientists: physicists, chemists, biologists, and engineers.

Another stimulating aspect is the hope that CF could lead to the solution of the very serious problems that mankind is facing concerning the production of energy. I have no doubts that we are producing particularly "clean" nuclear energy, without nuclear emissions and wastes. On the question of practical energy sources, my opinion diverges from that of many enthusiastic supporters of CF. As I said before, I am convinced that much research has still to be performed in order to better understand the physics at the basis of CF. Considering practical applications will become more and more sensible as we progress in this kind of understanding, and thus it is too early to foresee important practical applications. But, even if there is no certainty that we will succeed in this task, it seems to me that the target is so important that the scientific community should feel the duty of working at it, and this is my invitation to all those who will read this foreword.

4. THESE PROCEEDINGS

On 24th and 25th of February this year at the ENEA Center at Frascati there was a meeting of the (extended) SPC, mostly dedicated to examining the 110 abstracts submitted for presentations at ICCF8. We decided which would be the 77 presentations accepted, and their distribution between oral (long and short) and poster presentations. We discussed the program of the conference and its format. Finally, we discussed the procedure for the publication of the Proceedings. The first decision was to shift the deadline for the presentation of the manuscripts from the date of the Conference to the end of June: it was stressed that in a Conference the authors should be allowed to take inspiration from what they learned during the Conference, if this can

help them to produce more up to date and more critically conceived manuscripts. The other important decision concerned refereeing the manuscripts before accepting them for publication. Here a compromise was necessary, to assure good quality manuscripts but still bring out the Proceedings promptly. It was decided that every manuscript would be submitted to one referee, and that there would be only one interaction between referee and author. Thus, the procedure would consist in sending the manuscript to the referee, obtaining comments, transmitting the comments to the author; and if the referee required a revision of the manuscript, a second version would in turn be sent to the referee, who would give a definitive "yes" or "no" to the publication. In case of controversy, the final decision was left to the editor, i.e., to me. We would use e-mail communication wherever possible. It worked rather well on the average. But I did not succeed in sending the final manuscripts to the publisher before the end of September, as promised in the program. I had to have a one-month delay.

Most of the manuscripts were properly prepared and respected the length limit of 6 pages that we had asked to the authors. However, some were presented with an excessive number of pages. There were also some papers that were presented using a quite poor English, and sometimes the logic of the presentation itself needed to be improved. For each of these cases we asked the authors for a correction: in some cases we succeeded, in some others not. As far as the length is concerned, I decided to accept the papers that exceeded the six pages in the second version (I want to make clear that the paper by Martin Fleischmann was accepted in a version 15 pages long for intrinsical reasons: without all the figures included, he could not have presented his arguments). For the persistent poor presentation of some papers I decided to adopt another "compromise" between pursuing a most thorough and complete diffusion of the information presented at the Conference, and satisfying the quest for a rapid publication of its Proceedings. Thus, in those occasions in which I had not succeeded in obtaining a clear version of the paper in English, and the final decision on its publication was demanded of me, I decided to adopt the following criterion. Let me forget about good English and ability in presenting a scientific paper. I'll just ask the following question: after reading the manuscript, more than once if necessary, do I succeed in understanding what the author is trying to communicate? If the answer is yes, and what the author is communicating is scientifically sound, then I will accept the paper for publication. This happened in a few cases, and I hope that the reader of these Proceedings will forgive me: I thought that the most important issue was to have the information as complete as possible.

In editing the Proceedings I had to decide whether to divide it into categories (chapters), to make it easier to consult. We had not tried to make separate sessions in the Conference on purpose, both because many papers touch different aspects of CF research, and because we thought that a certain variety within a session was recommendable. The former feature occurs also in the editing of manuscripts. In spite of all these considerations, I decided to divide the papers into the seven categories that the reader will find, trying to evaluate in those papers referring to different items which was the most meaningful one. Also here I ask for the clemency of the reader for any mistake that I might have made.

5. ICCF9

On Wednesday May 24 there was a meeting of the IAC. The most important item of the agenda was the decision to be taken for next Conference, ICCF9. It was unanimously decided that next Conference will be held in China, presumably in Bejiing in the Spring of 2002: Prof. Li, Xing Zhong, will be its Chairman. This decision was announced to the participants in the Conference both during the dinner party and at the session on conclusions on Friday 26, where Prof. Li gave a short speech in accepting the nomination.

6. ACKNOWLEDGMENTS

I want here to thank warmly the members of the IAC, of the SPC, the referees and the chairmen, who made this Conference rational and well conducted, and the Proceedings accurate and appealing.

I also thank the sponsors for their much appreciated help. Besides the great Agencies that I quoted above, I want to thank ST Microelectronics, an advanced multinational industry operating (in Italy among other countries) on semiconductors, and Balzers, the well known vacuum industry from Liechtenstein: both gave a financial contribution to the management of the Conference, and both participated with a presentation in the Conference.

A specially warm note of thanks goes to the Secretariat, starting from its head, Antonella De Ninno, to Ms. Maria Luisa Ciceroni, who, together with Ms. Simona Ferri, helped during the Conference preparation, during the Conference itself, and in the editing of the manuscripts; I want here to express my gratitude to Ms. Franca Vinciguerra, who took charge of all administrative procedures, and Mr. Fabio Simoni, who was in charge of the information technology aspects of ICCF8, including the web-page.

A sincere thank goes to the personnel of the ENEA laboratory in Santa Teresa, close to Lerici: their help has been really precious during the development of the Conference. We want to thank in particular Ms. Patrizia Maffei, who gave invaluable help, and the Director of the Center, Dr. Giovanni Scabbia.

Thanks also goes to the personnel of Villa Marigola, starting from the very efficient Mr. Bruno Di Stefani, always ready to solve every problem, and to the personnel of the Symposia Agency, who took care of most of the management problems of ICCF8.

Last but not least, I want to express my gratitude to all participants in the Conference, who made it lively, interesting, and pleasant.

Franco Scaramuzzi
ENEA Consultant

Frascati, October 31, 2000

IN MEMORY OF GIULIANO PREPARATA

Giuliano Preparata died on April 24 in Frascati, and we felt that we had to remember him in this Conference for his important contributions to cold fusion. This is only a brief introduction to the speech in memory of Giuliano that will be presented by Martin Fleischmann, who had been in close touch with him in recent years.

Giuliano became interested in cold fusion immediately after the initial announcement of Fleischmann and Pons in March 1989. I like to remember a paper, written by Giuliano together with Tullio Bressani and Emilio Del Giudice, called "First steps toward an understanding of cold nuclear fusion". The date of appearance on "Il Nuovo Cimento – Note Brevi" is May 1989, and it was received on April 26, 1989. Thus, it was written just a month after the announcement. The important aspect to note is that in this work an original way of looking at the phenomenon was pointed out, consisting in the claim that a coherent and collective interaction among the deuterons, palladiums, and electrons was required to explain the results of the experiments. Shortly afterwards Giuliano Preparata foresaw two features that in these eleven years have been more and more evident. The first feature is the fact that a phenomenon like cold fusion in the palladium lattice could take place only if a threshold in the density of the absorbed deuterium was reached: the value that he evaluated was one deuterium atom per palladium atom. The second was that the outcome of the fusion reaction, differently from what happens in well known high energy D+D fusion reactions, would not be preferably neutrons, or tritium, or other energetic particles, but just ^{4}He, and the excess energy would be transformed into heat.

Giuliano was very active all these years. In particular, the second international Conference on cold fusion was held in Como, at the end of June – beginning of July 1991, and Giuliano, Emilio Del Giudice and Tullio Bressani were the Chairmen. I remember that Conference as the most fruitful in the brief history of Cold Fusion. In fact, in that Conference two important new pieces of evidence were presented: one by Mike McKubre , who found that a threshold was necessary in order to obtain heat excess in his electrolysis experiments (around D/Pd = 0.9), and the evidence by Melvin Miles that ^{4}He could be found and could be correlated with the heat measured. So, the two things that Giuliano had foreseen so early were presented in Como. As you well know, the uncertain reproducibility of these experiments has made it difficult to confirm these results, but in the nine years that have passed since then, in which Giuliano and I have participated in this adventure, we have seen growing evidence of these two facts.

I want to recall what Giuliano did at ENEA. As I said earlier, he died in Frascati; he was in Frascati because he proposed in 1998 the start of a new program, and he was strong enough to convince politicians and research managers to start a serious program and to have it funded by the Italian Government And in fact this program has been started in Frascati mostly because of Giuliano Preparata. He took a sabbatical year from the University of Milan, where he was a Professor, and came to Frascati, and he rented a house, the house in which he died. He spent last year in Frascati being extremely active, encouraging the people in the laboratory. It is easy to perceive the effect of his activism: life in the laboratory has changed since Giuliano came. He also participated in the February two-day meeting of the Science Program Committee: he

was not well, but nevertheless he wanted to participate. He was extremely active, with his intelligent criticism, pointing out faults of the abstracts that he examined: his contribution was very important in making the proper choices for this Conference, and I am very grateful to him for his help.

Let me finish by recalling that Giuliano was not only a dedicated researcher in cold fusion. He was a great scientist. He has shed light in many fields of Physics, and also outside of Physics. It is a pity that he is no longer with us: I think that we must look to his memory for guidance on the future of science in general, and of cold fusion in particular.

Franco Scaramuzzi

GIULIANO PREPARATA: AN APPRECIATION.

M. Fleischmann, E.N.E.A. C.R., Frascati, via E. Fermi, 45,
00044 Frascati (Rome), Italy.

Ladies and Gentlemen and, especially Emilia who is with us today: I really feel quite unequal to this task and, as Franco has said, we are remembering Giuliano especially because of his contributions to the subject which will be the theme of this meeting. However, we should also recall that Giuliano's initial work was in the fields of Nuclear and Particle Physics, Fig 1. One of the problems with which he was especially concerned was the extremely difficult question of why leptons are free whereas quarks are confined (quarks which are the constituents of hadrons). He sought the answer to this problem in the behaviour of the quantum fluctuations which, under certain conditions, form a giant coherent field which confines the quarks. The conundrum of why we cannot obtain free quarks, which has puzzled scientists so intensely, was thereby explained.

I believe that the outcome of Giuliano's early research demonstrated one of his key characteristics namely, that if he thought one line of argument was correct, then he would insist on its validity irrespective of heated arguments to the contrary trying to persuade both him and the Scientific Community at large that he was wrong.

In due course Giuliano's thoughts - and those of Emilio Del Giudice (who is with us today) - turned towards the behaviour of ordinary matter. Of course, there is an analogy between these two research areas because a coherent electromagnetic field establishes the ground state so that we must certainly think about the behaviour of "ordinary matter" in terms of field theory: field theory is not an esoteric subject to be confined to Particle and Nuclear Physics (1). It is equally important in modelling the behaviour of "ordinary matter" and it will probably be found that it is most important of all in Biology.

It is these lines of reasoning which were responsible for the reinforcement and extension of our contacts because I too had been thinking about related problems. I do not want this short presentation to deal with matters with which I had been occupied but it is perhaps somewhat inevitable that I should pay some attention to these topics because they were central to our points of contact. The series of questions which I had started to pose in the 1960's can be summarised by the general question: is it possible to devise electrochemical experiments which demonstrate the need to explain the behaviour of ordinary matter in terms of Quantum Electrodynamics, Fig 2?" I will return to this Figure in due course. Of course, it is the high sensitivity as well as the high time and spatial resolution of electrochemical methodology which makes such a question meaningful

The importance of this aspect lies in the fact that there were only four people known to me who realised that the work which we had started on Cold Fusion had to be part of a wider programme. Giuliano was pre-eminently one of these and the other three are present in

the audience - however, I will not embarrass them by giving their names. One of the topics which came up repeatedly in our discussions which is relevant to part of the work which we want to carry out in Frascati is the well-worn theme of the behaviour of ions in solution . As you will know, the accepted model is that of the Debye-Huckel Theory, where we postulate that a central ion is surrounded by an ionic atmosphere controlled by the electrostatic interaction of the ions. This model was proposed in the 1920's but I would doubt whether Debye would have used this particular model if he had tackled the problem in the 1960,s. We have to bear in mind that we do not have static ions surrounded by static ionic atmospheres because the ions execute Brownian motions, Fig 4. Such random motions must lead to radiation so that the model, Fig 3, can only apply at absolute zero which is an uninteresting limit because we cannot have an ionic solution at this temperature. The model violates the principle of Microscopic Reversibility (i.e. the Second Law of Thermodynamics) at any finite temperature so that we must conclude that it has been formulated within an inapplicable paradigm.

At the time at which I first considered such problems (the 1960,s) I only knew one Theoretical Physicist interested in Quantum Field Theory and his comment was: "well, it is quite obvious, you have to think about this problem in terms of Quantum Electrodynamics" and I replied "Quite so, but how?" I only knew how to tackle a part of the problem so I put the whole matter aside until, in due course, Giuliano, Emilio Del Giudice and I started to discuss this topic once again. They had taken the essential step in 1995 (2) and said: "it is quite obvious that if you have a coherent electromagnetic field, the solvent (in this case water) will divide into coherent and incoherent domains". This is illustrated in Fig 5; models of this kind were very popular in the 19th Century but went out of fashion when Bernal and Fowler showed that you cannot have two sorts of liquids within the context of Quantum Mechanics because the molecules are indistinguishable: there can be only one type of solvent. So here there is one of the big questions namely, while this is true within the framework of Quantum Mechanics, it is not true within the framework of Quantum Electrodynamics which tell us that the model in Fig 5 is entirely feasible. This dichotomy is an interesting illustration of the influence of paradigms on scientific research; we have believed in models of uniform liquids for most of the last century (with the singular and highly significant exception of liquid ^4 He) whereas we know that the properties of liquids are interpreted much better in terms of two-phase models. Such two-phase models were abandoned because they are not consistent with Quantum Mechanics whereas the real point at issue has been the question of the validity of this paradigm in the modelling of liquids.

We realised that if there are coherent and incoherent domains of the solvent, then electrolytes will be confined in the incoherent domains where they will themselves be in a coherent state. This model does actually give a much better interpretation of the properties of electrolyte solutions than does the Debye-Huckel Theory (3). I do not want to labour

this point here: my purpose in raising it is because it has been Giuliano's intention that the programme in Frascati should be much wider than that of "Cold Fusion" alone: one of the topics which we intend to investigate is that of the influence of weak alternating magnetic and electric fields on the conductance of ions in solution , Fig 7. There is now hardly any work on conductance because it is believed that everything in this field is now well-known and well-established. However, the situation is rather similar to that of the Boston Learning Curves: whenever a field becomes unpopular, you can be pretty sure that there is a great deal more waiting to be discovered by changing the methodology (laughter). In fact Fig 7 is based on the approach of Zhadin (e.g. see (4)) and perhaps our Russian colleagues here can tell us more about this subject.

The outline in the preceding paragraph is really somewhat back-to-front because it has been realised for a long time that weak electric and magnetic fields have an enormous influence on biological processes. However, because the Theoretical Physicists cannot think why this should be so, it is believed that the effects must be wrong (laughter). Now, of course, this cannot be true. I see that I am producing some laughter in the audience and I think that Giuliano would have appreciated this and, also, that he would have liked us to take a forward looking view of the subject. What is wrong, of course, is that our model of the world is wrong. If the ions in solution are in a coherent domain, then they behave as though they have a much bigger mass than that of the single ionic species. They can therefore tune into very weak alternating electric and magnetic fields (5). The work of Zhadin et. al will be a starting point for research in Frascati which will also cover several other related projects. I do not believe that this work will make us many friends!

We should note here that there is currently work on the influence of strong magnetic fields on transport processes in which case we observe incoherent scattering (fields in the region of 1 T). The question of the consequences of coherent scattering (fields in the region of 1 nT) leads us into a very wide area in Biology and Physical Chemistry (indeed, Chemistry in general).

I have often wondered why it was that Giuliano's interpretations have raised such intense opposition. It seems to me that this was due to his general approach. He said : let us take an experiment (or a series of observations) and, instead of interpreting it according to the left-hand-side of Fig 9, using the Classical Paradigm to set up a model, let us set up a model within the Quantum Electrodynamic Paradigm and see whether we get a better interpretation (indeed, whether this can explain results otherwise inexplicable). The problem with this approach is that it leads to criticisms both of the model as well as of the way in which the Quantum Electrodynamic Paradigm has been set up in the first place. I believe that Giuliano suffered greatly on both scores because the normal view in Quantum Theory is that the Quantum Electrodynamic Paradigm emerges somehow from Quantum Mechanics, Fig 8. Now Giuliano and Emilio believe that there is really only one paradigm in Nature and that is Quantum Electrodynamics (a view which I share). Classical Mechanics may sometimes be an adequate description while Quantum Mechanics can also

be used in some situations. However Quantum Mechanics is somewhat isolated from the other paradigms, Fig 9.

Giuliano followed the approach you would have expected from a Mathematical Physicist seeking interpretations in terms of a mathematically complete theory, Fig 10, an approach which can (but should not!) lead to the type of opposition I have referred to. It is relevant perhaps that I side stepped issues of this kind by concentrating instead on falsifications of paradigms e.g. by using violations of the Second Law of Thermodynamics, Fig 10 and Fig 4. In any event, we based our work on "Hidden Agendas", Fig 11, in which the need to invoke Quantum Electrodynamics was disguised, the aim being to give a general discussion of such topics at a later date. This approach served us very well up to the premature publicity which surrounded the work on "Cold Fusion".

As I have already said, Giuliano questioned me closely about our work, discussions which were very profitable because we did not have to talk at length about any one project. Giuliano simple said: "hm, yes, next topic" though on occasion he would say "how would you tackle this problem?" These topics were all illustrations of the first six items in Fig 2. However in due course I realised that there was one missing element namely, the direct study of the effects of perturbations of the energy in many-body systems. One can ask: how can it be that biological and chemical systems (I think certain classes of physical systems also) can manipulate small energy quantities so well? The answer of course is that this is incomprehensible except as part of a many-body problem (e.g. see the short description of the effects of weak magnetic and electric fields on the conductance which I have already outlined). In due course Stan Pons and I said: we have the means for one further investigation so let us see whether we can induce nuclear processes in a lattice at low temperatures. So that is why we are here at this Meeting!

Giuliano and Emilio latched on to this project immediately and came to Salt Lake City where Giuliano was going to give a seminar on the underlying theory applicable to "Cold Fusion". Inevitably, Stan Pons and I were very busy and I recall putting the brutal question to Giuliano: (we had had a large number of seminars on the topic all based on the Quantum Mechanical Paradigm which predictably led to the conclusion that "Cold Fusion" was impossible in the absence of special assumption, examples of attempts to save the paradigm) "Professor Preparata (I did not know him that well then) are you going to discuss this problem in terms of Quantum Field Theory?" He replied: "Of course", so I said: "In that case I will come to your lecture". It was illuminating. My wife is here and if you ask her about that day she will tell you that I said: "I have met a man who says exactly what I say. Either we are both crazy or we are both right" (laughter). I also said to Giuliano: "There is this absolutely amazing experiment carried out in 1929 which has since then been totally messed up (expletives deleted) and this is this work of Alfred Coehn on the electrodiffusion of hydrogen in Pd wires", see Fig 12 (6). I have spoken

about this before but I would like to ram this down your throats once again because it does lead on to the work in Frascati which Emilio Del Giudice will outline at this meeting. (7) If you deposit hydrogen electrolytically in the central part of the wire and then apply an electric field along this wire, you find that hydrogen moves more rapidly to the negative end and less rapidly to the positive end than by diffusion alone. Fig. 13 is one of Alfred Coehn's original results. If the polarity is reversed, then one can detect the reversal of the additional motion. This was an absolutely beautiful experiment and the great Walther Nernst congratulated Coehn on the execution of this work. Nernst was not a person to congratulate anybody (laughter). I often describe this experiment as opening the way for some of the ultimate experiments in Physics.

The mobility of the hydrogen followed the Nernst-Einstein relation so that hydrogen had to be present as protons. What is so amazing about these results (and, perhaps, Alfred Coehn did not realize just how amazing they were) is that hydrogen (of deuterium for that matter) is extremely strongly bound in the lattice as can be shown by a Born-Haber cycle. Fig 14 (8). We therefore arrive at a conundrum: how can one have extremely strongly bound hydrogen or deuterium ions in the lattice while at the same time they are free to move? It seems to me that this conundrum can only be resolved within the framework of Quantum Electrodynamics (this is an example of the use of consistencies / inconsistencies to judge the applicability / inapplicability of paradigms, see Fig 10).

What Giuliano realised immediately was that this provided a means of confining deuterium in the lattice (by analogy to the Boehm-Aharonov effect) so that we can create an extended coherent system (the γ-phase) in an high state of charge and thereby induce an high rate of fusion (8). Giuliano and Emilio initially in Milan and then also with Antonella De Ninno in Frascati have achieved in a fairly routine way sustained specific rates of excess enthalpy production in the ~ 10kWcm^ -3 range and, sometimes, rates as high as ~100kWcm^ -3 . This is of course much higher than can be achieved in the systems which Stan Pons and I initially investigated.

I want to close with a personal appreciation of Giuliano. For me it would be wrong to describe him as a man in a million. I think it would be even wrong to describe him as a man in an hundred million. For me he was a man who, with his breadth of vision which latterly extended from cosmology to biology (and which is so necessary in the development of science), who is only found once in a lifetime, perhaps only once in several lifetimes. I am sure that his work will be increasingly appreciated and I am just deeply saddened that he has not lived to witness this himself.

So let us remember Giuliano and let us move forward to this next phase of work in the Natural Sciences. Thinking about Giuliano let us recall that he said that when people maintain that everything is known, then you can be sure that nothing is known. All we can do is to move on to the next phase.

References

1) For a review of a number of topics which have been of key interest to Giuliano Preparata see G. Preparata "Q.E.D. Coherence in Matter", World Scientific Publishing Co. Pte.Ltd., Singapore, 1995; QC 173.454.P74, ISBN 9810222491.
2) R,. Arani, I.Bono, E. Del Giudice and G. Preparata, Int.J. Mod. Phys., B 9 (1995) 1813.
3) E. Del Giudice, G. Preparata and M. Fleischmann, J. Electroanal.Chem., 482 (2000) 110
4) Mikhail N. Zhadin, Vadim V. Novikov, Frank S. Barnes and Nicholas F. Pergola, Bioelectromagnetics 19 (1998) 41.
5) E. Del Giudice, G. Preparata and G . Talpo, "On the "unreasonable" effects of ELF magnetic fields upon a system of ions", submitted for publication.
6) A. Coehn, Z. Elektrochem, 35 (1929) 676..
7) E. Del Giudice, Proceedings of ICCF 8.
8) M. Fleischmann, S. Pons and G. Preparata, Nuovo Cimento 107A (1994) 143.

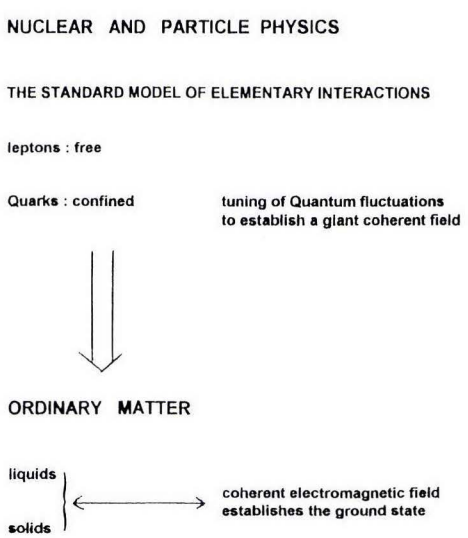

Fig 1 Some of the problems which were central to Giuliano Preparata's research.

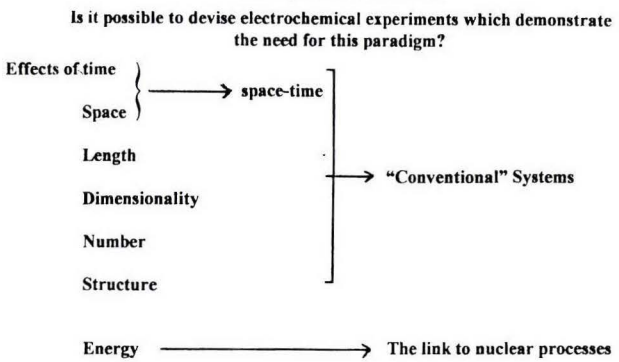

Fig 2 Questions which we posed prior to the development of work on cold fusion ; the special role of research in the latter field.

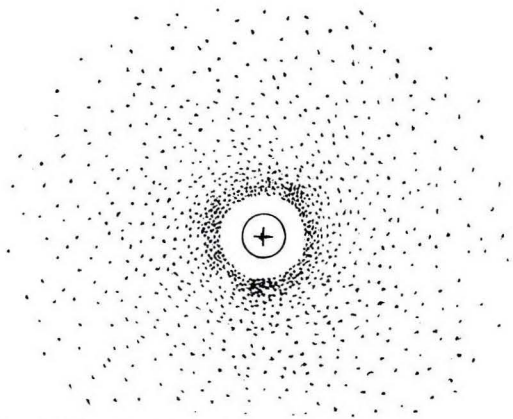

Fig 3 Schematic diagram of the negative space charge around a central positive ion formed by the electrostatic interaction of the ions.

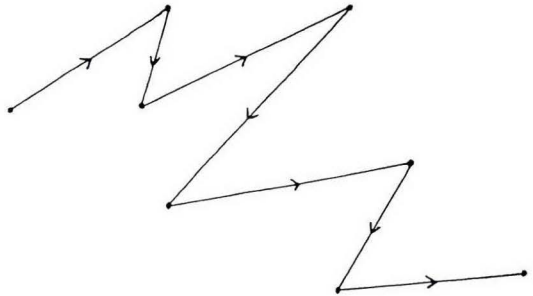

Fig 4 Schematic diagram of the Brownian movements of an ion. The arrows connect the points at which the ions are at rest.

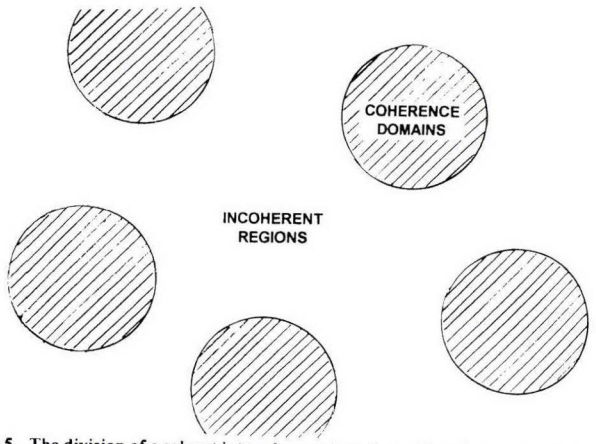

Fig 5 The division of a solvent into coherent domains and incoherent regions.

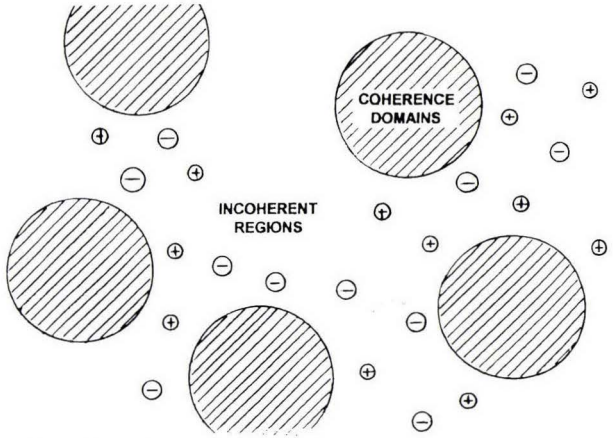

Fig 6 The confinement of ions in the incoherent regions of the solvent.

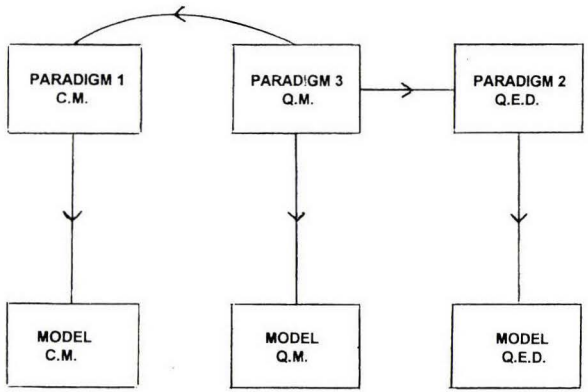

Fig 8 The conventional view of the linkage of the Classical, Quantum Mechanical and Quantum Electrodynamic Paradigms.

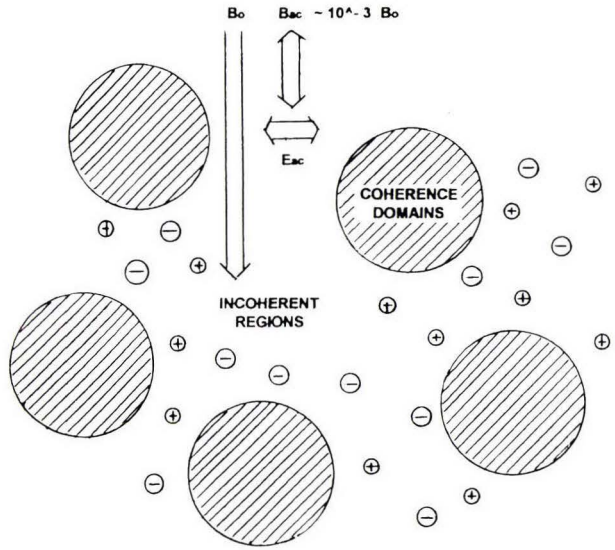

Fig 7 The effects of weak magnetic or electric fields on the motion of ions in solution.

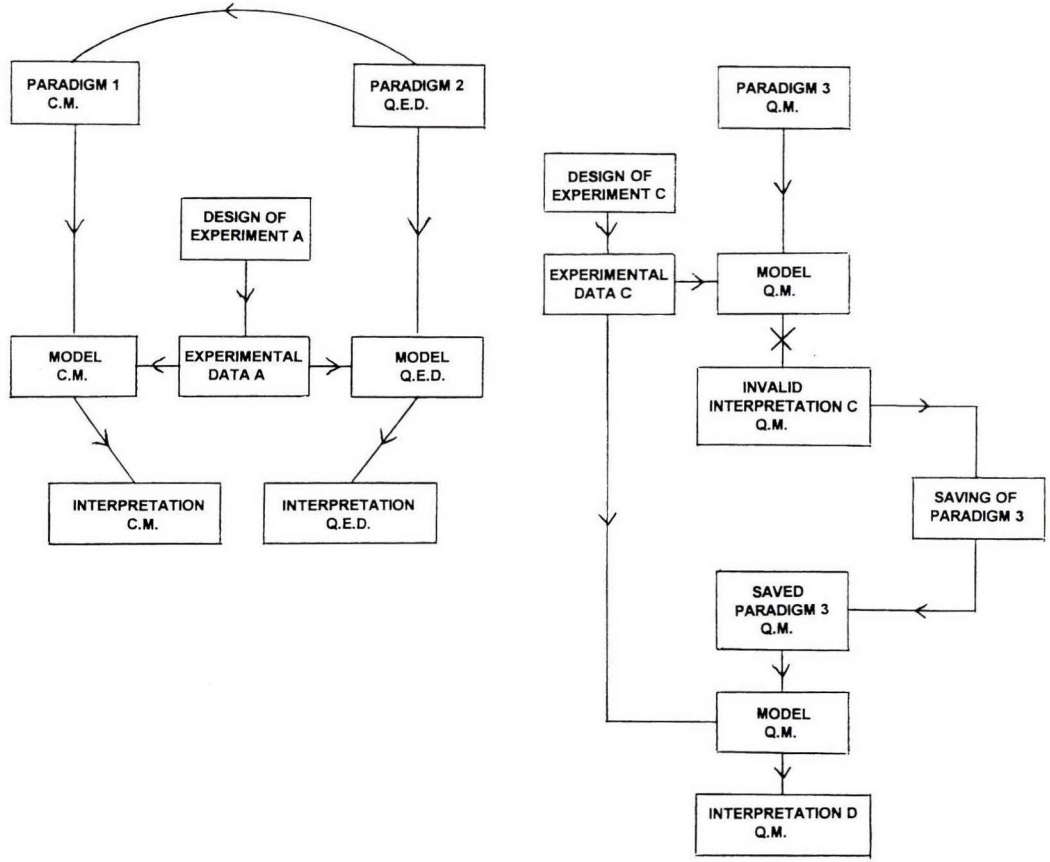

Fig 9 Our view of the status of the Classical, Quantum Electrodynamic and Quantum Mechanical Paradigms.

MATHEMATICAL COMPLETENESS

VIOLATIONS OF THE SECOND LAW OF THERMODYNAMICS

CONSISTENCY OF INTERPRETATIONS

Fig 10 Assessment of the need to invoke the Q.E.D. paradigm.

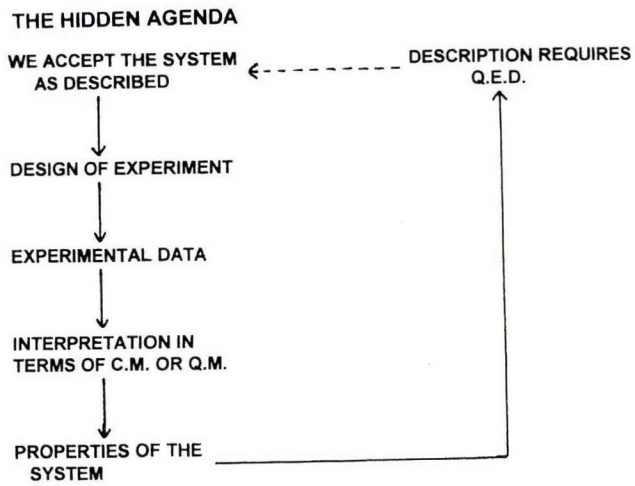

Fig 11 The hidden agenda.

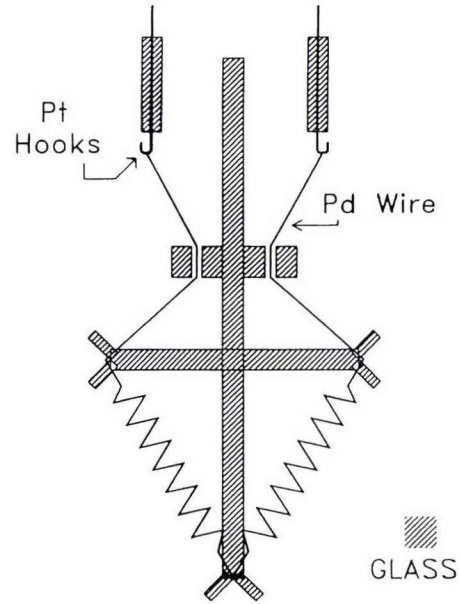

Fig 12 Schematic of Coehn's original experiment for measuring the electrodiffusion of hydrogen along a palladium wire.

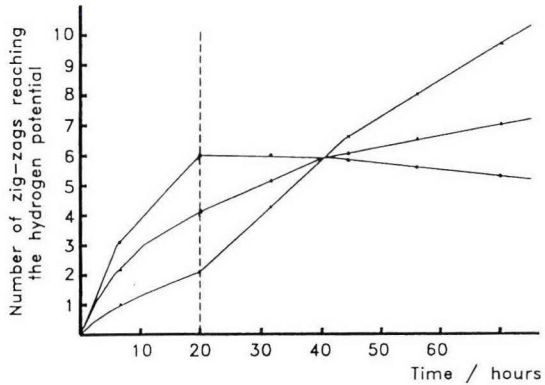

Fig 13 An example of Coehn's measurements (distance between zig-zags = 1.85mm).

CAN A PROPERTY A BE INTERPRETED IN TERMS OF PARADIGM / MODEL X USING ARGUMENT a ?

CAN A PROPERTY B BE INTERPRETED IN TERMS OF THE SAME PARADIGM / MODEL X USING ARGUMENT b?

etc. etc.

ARE a, b .....SELF CONSISTENT? IF NOT, THEN PARADIGM / MODEL X IS INAPPLICABLE.

Fig 15 The question of the consistency of the properties of a system in terms of a given paradigm.

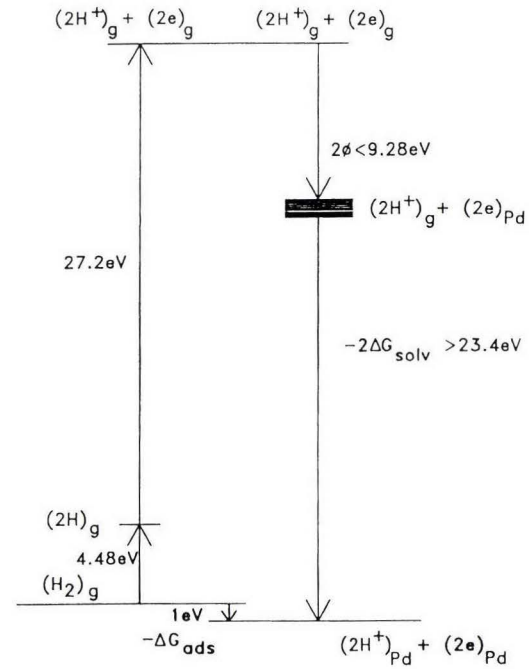

Fig 14 Born-Haber cycle for calculating the solvation energy of H^+ in the Pd host lattice.

CHAPTER 1.

DETECTION OF HELIUM, THOUGHT AS A NUCLEAR ASH

Conference Proceedings Vol. 70
"ICCF8"
F. Scaramuzzi (Ed.)
SIF, Bologna, 2000

The Emergence of a Coherent Explanation for Anomalies Observed in D/Pd and H/Pd Systems: *Evidence for ^{4}He and ^{3}H Production*

Michael McKubre[1], Francis Tanzella[1], Paolo Tripodi[1] and Peter Hagelstein[2]

1 SRI International, 333 Ravenswood Ave. 94025 Menlo Park, CA (USA).
2 MIT, 77 Massachusetts Ave. 02139 Cambridge, MA (USA).

Introduction

Numerous observations have been made of apparent anomalies in carefully performed experimental studies of D/Pd and H/Pd systems. Such anomalies include: prompt emission of electrons and charged particles; unexplained heat in excess of known input sources; the residual presence of light elements (notably ^{3}H, ^{3}He and ^{4}He); the possible occurrence of isotope anomalies in higher mass elements (including the host metal); unusual electrical conductance effects both stable and transient (not discussed in this paper). The features that unify these apparently disparate observations are the common elements of the needed experimental stimuli, and the requirement for extended lattice coherent processes in any obvious explanation.

Presented in this paper are the results of four experiments conducted using palladium structures loaded with hydrogen or deuterium by gas and electrolytic means. The purpose was to evaluate possible evidence for d-d fusion reactions in lattice structures, in the temperature range 25-250°C. Primary evidence sought and evaluated were the appearance of anomalous excess heat accompanied by the production of light isotopes: ^{3}He and ^{4}He.

Description

Experiments were performed in four basic geometries:

1) Open cell electrolysis of D_2O at Pd and Pd-alloy wire cathodes using an accurate integral boundary Seebeck calorimetry.[1] These experiments were designed to replicate earlier observations of Miles et. al.[2] of the correlated appearance of excess heat and helium in glass cells. The experiments at SRI were performed in rigorously metal sealed cells incorporating active exclusion of ^{4}He to increase the measurement sensitivity and accuracy.
2) Loading of D_2 and H_2 into Pd on carbon supported catalyst using modest gas pressures (1-3 Atm.) and temperatures (170°–250°C). These experiments were designed to test the claim by Case[3] to observe excess temperature and increasing ^{4}He levels under similar conditions. Experiments at SRI were performed in sealed Nupro® 50 cc stainless steel vessels connected to a steel manifold. Periodic measurements of ^{4}He were made by direct connection to an Extrel® mass spectrometer capable of resolving the mass-4 peaks of D_2 and ^{4}He. Using information recorded from temperature sensors placed inside and outside active and reference gas cells it was possible to obtain heat-flow calorimetric information at times when the catalyst bed temperature rise was significant.
3) Closed cell electrolytic loading of D into Pd wire cathodes in a rigorously metal-sealed apparatus using highly accurate mass flow calorimetry.[1] These

experiments were intended to replicate earlier results of excess heat measurement at SRI in thermodynamically closed electrolytic loading cells, for which ambient exclusion of ^{4}He was not possible.[4,5]

4) Closed cell electrolytic loading of D (and H) into hollow Pd cathodes sealed to contain small dimension Pd-black powders. These experiments were performed to replicate published results by Arata and Zhang in which excess heat, ^{4}He and ^{3}He, were found to be associated with the electrolysis of such "double structured" cathodes[6] in D_2O, but not in H_2O. In experiments performed at SRI accurate mass flow calorimetry[4] was used to evaluate and compare the heat production of double structured cathodes electrolyzed in D_2O and H_2O in otherwise identical cells. The contents of the cathode void volumes were subjected to retrospective analysis for light isotopes.

Results

Figure 1 presents the results of concurrent excess power and helium measurements performed during open cell electrolysis using two different Pd and Pd-alloy cathodes. In three instances where excess power was measured at statistically significant levels, ^{4}He also was found to be conveyed out of the cell in the electrolysis gases ($D_2 + O_2$). The solid line in Figure 1 plots the regression fit of these data to a line passing through the origin; the dashed line is that expected for ^{4}He generation according to the reaction;

$$d + d \rightarrow {}^4He + 23.82\ MeV\ (\textit{lattice}) \qquad [1]$$

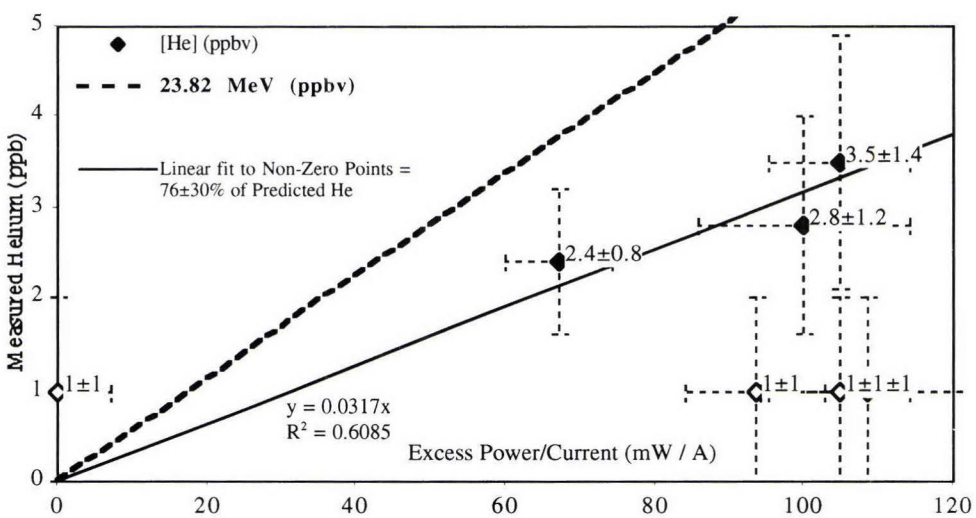

Figure 1 Correlation between rates of Heat and ^{4}He production in Seebeck Calorimeter.

It is clear from the slopes of these two lines that the observed ^{4}He constitutes only 76 ± 30% of the ^{4}He predicted by equation [1]. A more significant problem in Figure 1 is that three further ^{4}He samples, taken at times of non-zero excess power (open diamonds), exhibited helium concentrations only at the level of the analytical uncertainty, as did numerous samples taken in the apparent absence of excess power production. Clearly if ^{4}He is produced in association with excess power, it is not released to the gas phase immediately, or completely.

Experiments in category "2" in which Pd on C catalyst materials were exposed to D_2 and H_2 gases for prolonged periods, exhibited a range of behaviors. Figure 2 summarizes 6 of 16 results obtained in paired cells.

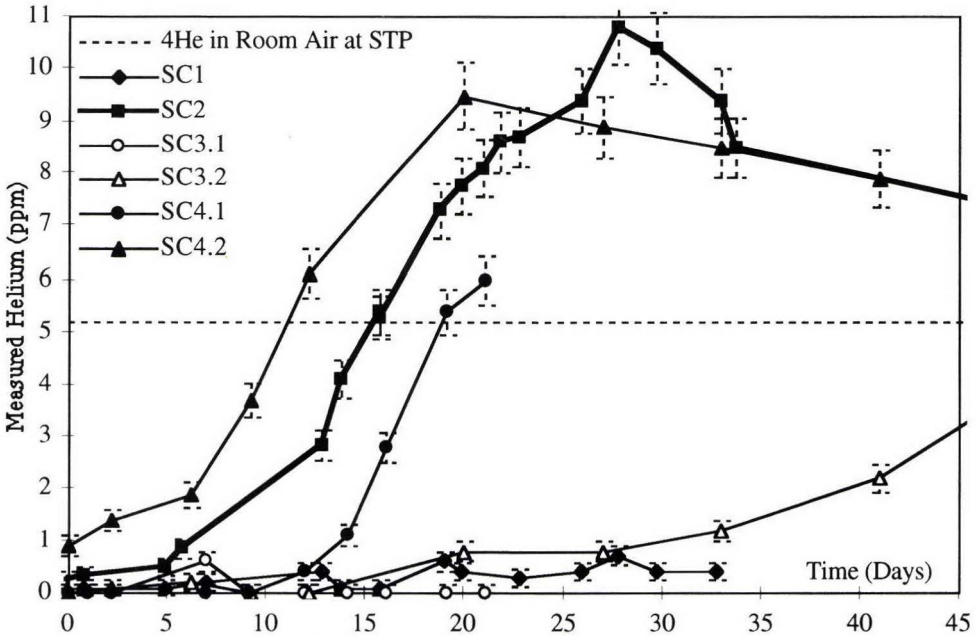

Figure 2 Helium increase in sealed cells containing Pd on C catalyst and D_2 (H_2) gas.

Using direct, on-line, high-resolution mass spectrometric measurement of [^{4}He] we observed the following behaviors:

(i) cells that show no increase of ^{4}He over long periods of time (including all cells operated with H_2 instead of D_2);
(ii) cells that exhibit a slow, approximately exponential increase in [^{4}He] with time;
(iii) cells that display no measurable increase in [^{4}He] for a period of several days, followed by a rapid, approximately linear rise in [^{4}He] to levels sometimes exceeding that of the ambient background.

Using data from temperature sensors placed in the catalyst and gas phases, and situated in the room, we are able to make heat flow estimates in one of two ways:

a) a Gradient method, based on the relationship between the temperature difference between catalyst bed and confined gas, and the heater input power;
b) a Differential method, based on the temperature differences between active and reference catalyst bed sensors, and room temperature, as a function of the relative input heater powers.

The energy estimated in excess of that provided by the heater for these two calorimetric methods is plotted in Figure 3, together with the measured helium concentration during the time of greatest derivative, $\partial[^4He]/\partial t$ in experiment SC2. It is clear that the appearance of excess heat and the apparent increase in $[^4He]$ are temporally correlated.

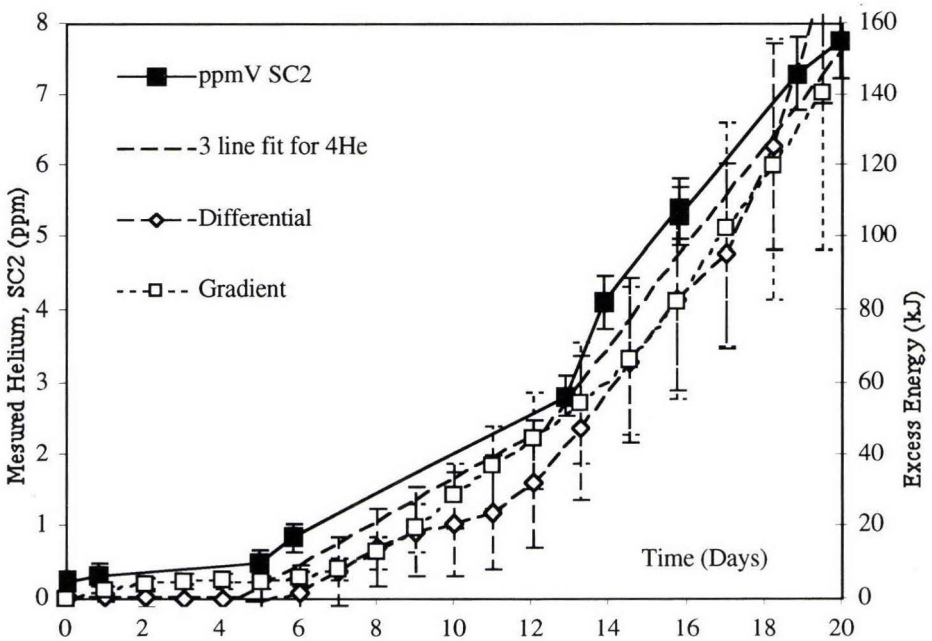

Figure 3 Correlation of Heat and Helium Production in D2 Gas Cell.

In an attempt to establish a quantitative correlation, Figure 4 plots the two calorimetric estimates of excess heat production interpolated from Figure 3, versus the measured increase in $[^4He]$ (the value plotted in Figure 3 minus the ^4He initially present in the D_2 gas). Regression lines through these data incorporating the origin have slopes: $Q=31 \pm 13$ and 32 ± 13 MeV per ^4He atom, respectively, for the gradient and differential calorimetric methods. Although these Q values include that of reaction [1] within their assigned uncertainties, the mean values for the ^4He presented directly to the gas phase for analysis is only ~75% of that predicted by equation [1].

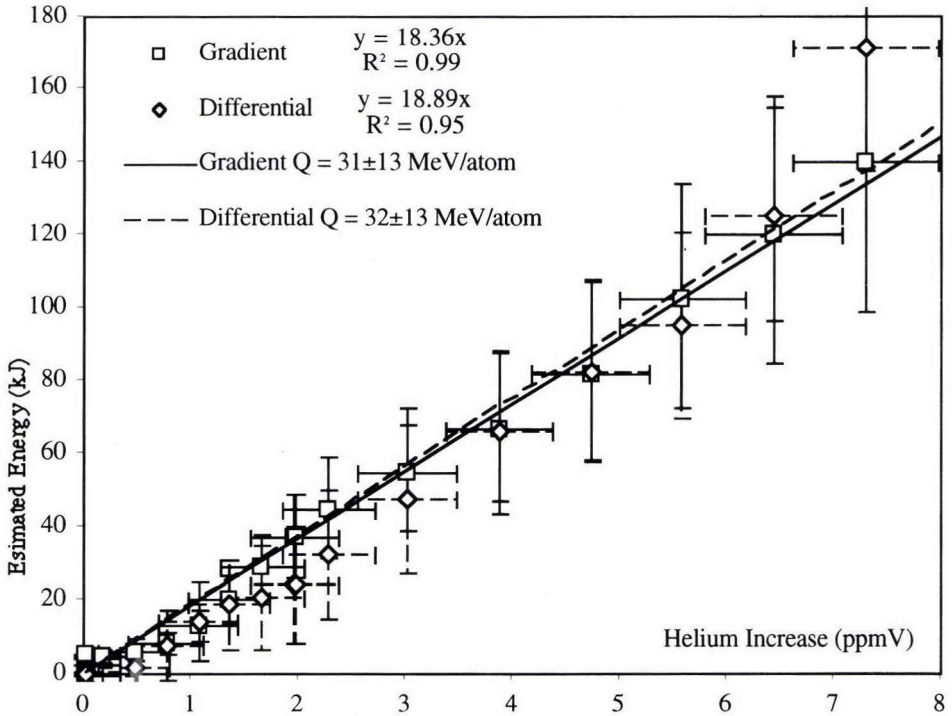

Figure 4 Estimated Energy versus Helium Increase.

Clarification of a possible origin for the apparent ^4He deficit in experiments "1" and "2" can be obtained from the results of experiment "3". Approximately 82 kJ of excess heat was measured in the electrolysis of a 100 mm x 1mm Pd wire cathode in D_2O. This experiment was performed in a rigorously metal sealed and helium leak-tested cell and apparatus provided with the facility to sample the gas in the headspace. When initially analyzed following a period of excess power production, the gas phase contained only 62% of the ^4He expected if reaction [1] were the source of the excess heat. A second sample showed an increase in [^4He] despite the fact that the helium content of the vessel had been diluted with D_2 containing low levels of ^4He, in order to make up the initial gas volume after the first gas sample. Taking these increases as evidence of sequestered ^4He, the cathode was subjected to an extended period (~200 hours) of compositional and temperature cycling by varying the current density in both anodic and cathodic directions.

A mass balance of ^4He was calculated based on two further gas samples: one to determine the helium content of the D_2 gas used initially to fill and refill the sealed metal cell (0.34 ± 0.007 ppmV); the other to measure the final helium concentration in the gas phase after exercising the cathode to release trapped gases (2.08 ± 0.01 ppmV). Taking into account the amounts lost by sampling, and introduced with make-up D_2, a calculated mass balance for ^4He in the gas phase after compositional and thermal cycling of the

cathode results in a number that is 104 ± 10% of the number of atoms quantitatively correlated with the observed heat via reaction [1].

The results of experiment "4" generally confirm those published earlier by Arata and Zhang of the appearance of excess heat in the electrolysis of "double structured" palladium cathodes[6] in D_2O, but not in H_2O. Figure 5 plots the calorimetric results of cathodically exercising two nominally identical cathodes in intentionally similar cells, one in 0.1M LiOD and the other in 0.1 M LiOH. In the same range of input powers, the heavy water cells yields clearly more output heat (plotted as excess power) than does the light water cell.

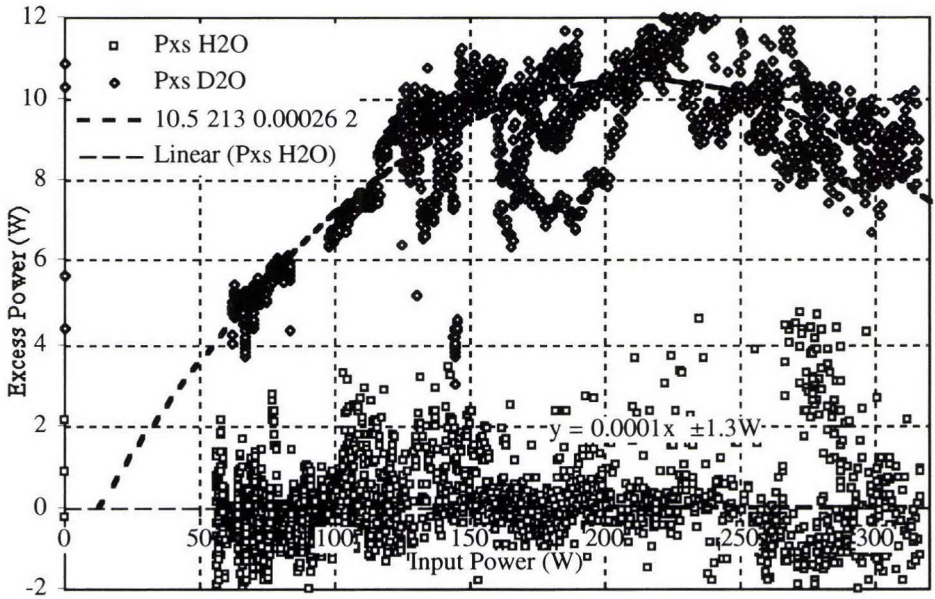

Figure 5 Excess Power versus Input Power measured for Arata-Zhang Double Structured Cathodes using Mass Flow Calorimetry.

The maximum excess power observed in D_2O was 9.9 ± 1.3% of the measured power input, with the average value being approximately half the maximum. The measured power excess exceeded the experimental uncertainty (1-2%) for a period of ~86 days to produce an integrated energy excess of 64 ± 6 MJ for the D_2O cell. For the H_2O cell in the same period of time the measured energy excess was –1 ± 6 MJ.

At the conclusion of the experiment, both cathodes were removed and placed successively in a sealed chamber where they were punctured mechanically, and the gas contents of the cathode void volumes were extracted for analysis[7]. The Pd black powders also were removed and the Pd metal walls of the hollow cathodes were sectioned for analysis.

Significant amounts of tritium and ^{3}He from the decay of tritium were found inside the double structured volume of the cathode electrolyzed in heavy water. Small amounts of ^{4}He were attributed to atmospheric contamination. Detailed results are presented by Clarke et al[8].

Conclusions

There exists a strong time correlation between the rates of heat and helium production measured using on-line high-resolution mass spectrometry. In experiments performed using three different metal sealed cells, three different calorimetric methods, by electrochemical and gas loading means and with ^{4}He analyses made at three different institutional laboratories, there is observed a quantitative or near-quantitative correlation between heat and ^{4}He production consistent with the reaction:

$$d + d \rightarrow {}^4He + 24\ MeV\ \textit{(lattice)}$$

Evidence for near-surface retention of ^{4}He in the lattice can be used to accommodate the discrepancy between measured and expected yields of ^{4}He.

Evidence was obtained for excess heat production in the electrolysis of D_2O using "double structured" cathodes, supporting original claims by Arata and Zhang[6]. Associated with this result, although not quantitatively correlated to it, is the production of a significant amount of tritium and ^{3}He from the decay of tritium within the cathode void volume, suggesting the presence of a second nuclear reaction.

Acknowledgment

Credit for the work summarized in this paper can be attributed largely to the following individuals, without the active support of whom we could not have accomplished this work. Dr. T. O. Passell whose vision made possible the establishment of a research facility, and whose unflagging support and encouragement provided necessary stimulus for our perseverance. Dr. M. Miles and Dr. B. Bush whose pioneering work in correlating the appearance of heat and helium in Pd/D_2O electrolysis provided early incentive for the work described here. Dr Bush also was responsible for the initial confirmation of this correlation, at SRI, and for the implementation of a helium leak-tight mass-flow calorimeter used in subsequent studies. Dr. L. Case provided the impetus to begin our study of temperature, heat and possible nuclear effects in gas phase deuterium/noble metal systems. Without his direct, personal guidance and support, our successful replication of his work would have been far from assured. Finally we wish to acknowledge a huge debt to Professors Y. Arata and Y. Zhang for their dogged support of an innovative concept, and willingness to share their remarkable technology with us. Truly we have advanced on the shoulders of giants.

References

1) M. McKubre et al, "*Energy Production Processes in Deuterated Metals*", EPRI, TR-107843-V1 (1998).
2) M. Miles et al, "*Heat and Helium Production in Cold Fusion Experiments*" "The Science of Cold Fusion", Proc. ICCF2 (June 1991); "*Experimental Evidence for Correlated Heat and Helium Production in Cold Fusion*", Proc. Electrochem. Soc. (1992); "*Correlation of Excess Power and Helium production during D_2O and H_2O Electrolysis Using Palladium Cathodes*", J. Electroanal. Chem., 346 (1993); "*Anomalous Effects Involving Excess Power, Radiation and Helium Production During D_2O Electrolysis....*", Fusion Technology, 25 (1994).
3) L. Case, "*Catalytic Fusion of Deuterium into Helium-4*", Proc. ICCF7, Vancouver, Canada, April 19-24, 1998.
4) McKubre et al, "*Development of Advanced Concepts for Nuclear Processes in Deuterated Metals*", EPRI TR-104195, Final Report on EPRI Contract 3170-01, (1994).
5) McKubre et al, "*Isothermal Flow Calorimetric Investigations of the D/Pd System*" J. Electroanal. Chem., **368** (1994) p. 55.
6) Y. Arata and Y. Zhang, Proc. Japan Acad., **70(B)**, p106, (1994); **71(B)**, p98, (1995); **71(B)**, p304, (1995); **75(B)**, p281, (1999); J. High Temp. Soc., **21**, p130, (1995).
7) B. M. Oliver, "*Helium Analyses of Deuterium Gas and Palladium-Black Samples*", Report of work performed for SRI under Battelle Project Nos. 30776 and 31535, (1999).
8) W. B. Clarke et al, "*Search for ^3He and ^4He in Palladium-Black from Arata-Style Palladium Cathodes, II: Evidence for Tritium Production*", submitted to Fusion Technology, (2000).

Conference Proceedings Vol. 70
"ICCF8"
F. Scaramuzzi (Ed.)
SIF, Bologna, 2000

Definitive Difference among [DS-D_2O], [DS-H_2O] and [Bulk-D_2O] Cells in the Deuterization and Deuterium-reaction

Yoshiaki Arata and Yue Chang Zhang

Cooperation Research Center for Science and Technology, Osaka University
2-1 Yamadaoka, Suita, Osaka, 565-0871, Japan

Abstract: We observed a new phenomena that enormous amount of deuterium/hydrogen can be absorbed quickly as a movable "solute-atom" into fine metal powders embedded inside a double-structure (DS) cathode in the electrolyses of D_2O and H_2O-electrolytes, but such highly deuterated powders can be produced only by using DS-cathode immersed in D_2O-electrolyte; [DS-D_2O], and never generated in H_2O-electrolyte even using the DS-cathode; [DS-H_2O].

On the other hand, [Bulk-D_2O] with bulk-cathode made by bulk Pd metal never produces highly deuterated metal as mentioned above even though using D_2O-electrolyte. In short, the deuterium-concentration generated in [Bulk-D_2O] is found to be much lower than that in [DS-D_2O]. As a result, because of the reason mentioned above, neither excess heat nor ^4He production are observed with both [DS-H_2O] and [Bulk-D_2O] in marked contrast to the case with the [DS-D_2O].

1.Introduction

In order to continuously produce "solid-state nuclear fusion", it is extremely important that the density of deuteriums which must exist as a "solid-solution" in Pd metal, should be higher than that of its "host metal". Such high concentration of deuterium (or hydrogen) has, however, not been realized yet. This is because the deuterium concentration in a normal bulk-solid is essentially based only on "diffusion-effect", so that it merely reaches the thermal equilibrium state with extremely slow speed. Thus, although it is necessary to realize a deuterium concentration much more than 100% (for instance, $D^* \equiv [D/Pd] \gtrsim 250\%$), which is named Ultra High Concentration Condition (UHC-condition), it is impossible apparently to realize each condition by normal diffusion-effect in a host bulk solid as a solid-solution.

It is well-known that all researchers including Fleischmann and Pons[1] have used "Bulk-cathodes" made by bulk-solid. Thus, with such a Bulk-cathode, we cannot expect continuous reaction of the "solid-state nuclear fusion".

In contrast, by utilizing "atom cluster-effect", "spillover-effect" and "Sieverts-Law" stated in Fig. 1, we have made it possible to make the deuterium concentration of UHC-condition (UHC-deuterium) for all over the host-metal.

To realize the UHC-deuterium, the authors developed the Double Structure Cathode (DS-cathode)[2] whose principle is shown in Fig.1. That consists of both an "inner-cathode" (Pd-black) and an "outer-cathode" (Pd-vessel). Pd-black used is extremely fine powder of the nano-scale, which is called "nano-particle" and/or "atom-cluster"[6], and kept in vacuum inside the Pd-vessel.

Compared with the "Bulk-cathode", the DS-cathode provides excellent functions as demonstrated in Fig. 1. These functions are called "DS-function". As a result, the "DS-function" of the DS-cathode provides the capability to generate a tremendous amount of excess energy within highly deuterated solid, while with the "Bulk-cathode" it is impossible at all to realize the "DS-function".

In order to make clear the essential conditions for generating the deuterium nuclear reaction in a

solid, we performed the following three kinds of experiments.

a)-Experiment: Comparison of the "reaction products" between electrolytes of D_2O and H_2O using the same DS-cathode ([DS-D_2O] and [DS-H_2O]).

b) –Experiment: Comparison of the "reaction products" between DS-cathode and Bulk-cathode using the same conditions in size, current and D_2O-electrolyte ([DS-D_2O] and [Bulk-D_2O]).

c) –Experiment: Controlling system to supply a constant output of the excess energy using [DS-D_2O].

2.Experiment

a)-Experiment using [DS-D_2O] and [DS-H_2O] cells [2), 3)]

In order to make clear the difference in the reaction energy generated in both [DS-D_2O] and [DS-H_2O], both cells, each of which is composed with the same DS-cathode, we connected it in series as shown in Fig.2. In this case, electrolytic current and its density passing through both cathodes are the same. Furthermore, because of using the identical DS-cathode in each cell, pure deuterium and pure hydrogen can be filled up essentially by the "DS-Function" to an extremely high pressure over several thousand atmosphere within the DS-cathode in each cell, respectively, during electrolysis over long hours. By this experiment, we have obtained many interesting data as shown in Fig.3, 4 and 5, etc., and more detailed information has been published in Refs.2 and 3.

These experimental results provide the following facts:

1) Tremendous reaction energy generates within the DS-cathode in [DS-D_2O], but no energy is produced in [DS-H_2O] when the chemical reaction energy is subtracted in each cell. "Deuterons-reaction" is created in large quantities within highly deuterated solid, but "hydrogen-reaction" is never created within highly hydrogenated solid.
2) The Pd powders, which generated much of the excess energy in the [DS-D_2O], produced a substantial amount of ^4He as the reaction product. On the contrary, there was no such event in the [DS-H_2O] at all.

b)-Experiment using [DS-D_2O] and [Bulk-D_2O] cells

It is well known that the so-called "cold-fusion" has not been recognized generally in an academic society and also the general public as a new phenomena during ten years after Fleischmann and Pons, and since their experiment, a great number of experiments have been carried out using bulk Pd metal cathodes in electrolysis, but there was no evidence of reproducible yield of any reaction products of both excess heat and helium. These events have been demonstrated by many researchers as shown in Refs.7 and 8 as a typical example. We, thus, thought it would be interesting to compare the conventional "Bulk-cathode" method with the "DS-cathode" method under the same experimental condition.

To clarify the situation, we made a Bulk cathode of bulk Pd metal a cylindrical shape of 14 mm in diameter and 60 mm in length. It was given the same appearance as the DS-cathode, but of course, had no inner structure. We immersed the DS-cathode and the Bulk-cathode in separate but identical electrolysis cells of the same D_2O electrolyte. We stress here that there was no difference in the outlook of the two apparatus. As shown in Fig. 6, we connected the electric circuits in a series so as to allow the application of common electric current, and the procedure for calorimetry was the same as used in the previous **a)**-E experiment.

By this experiment, we have obtained interesting data shown in Fig.7, 8, 9, 10 and 11 etc., and more detailed information has been published in Refs.4 and 5.

As the result, the present experiment has demonstrated for the first time that the non-existence of

excess heat in bulk Pd metal is due to the occurrence of much less deuterization. The reason why dense deuterization is not obtained in [Bulk-D_2O] is that, in bulk metal, only the diffusion effect at normal pressure is utilized. On the other hand, [DS-D_2O] provides extremely dense deuterium (UHC-deuterium) in Pd fine powders, where anomalous deuterium reactions take place.

c)-Experiment of controlling the excess power using [DS-D_2O] cell.

It is very useful for the practice if the nuclear fusion energy of solid-state can be controlled to generate with a certain constant output, which is selected. We established controlling method to supply constant output of the excess energy using [DS-D_2O]. It is considered that this is the first step of the practice for using deuterium nuclear reaction energy within a solid. Following figures demonstrate the typical example of these events, as you see.

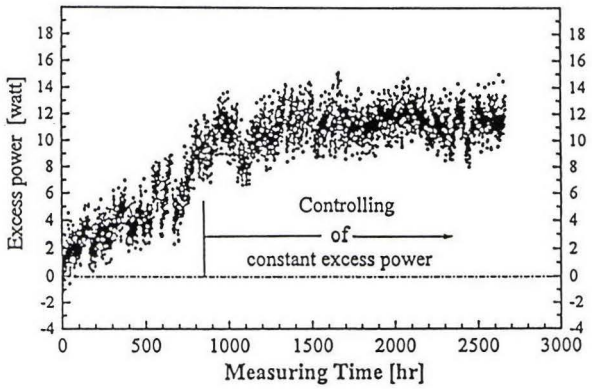

3. Conclusion

The results obtained in the present experiments are summarized as follow:

1) The present experiment has firstly demonstrated that the non-existence of excess heat in bulk Pd metal is due to the occurrence of much less deuterization. The reason why dense deuterization is not obtained in [Bulk-D_2O] is that in bulk metal only thediffusion effect at normal pressure is utilized. On the other and, [DS-D_2O] provides extremely dense deuterium in Pd fine powders, where the anomalous deuterium reaction take place.

2) The combination of "D-atoms" and "Pd-atom clusters" is the best choice at present for "solid-state nuclear fusion" (simply "solid fusion")

3) We developed "controlling system to supply constant-output" is the excess energy using [DS-D_2O] cell, this is the first step of the practical use for the deuterium nuclear reaction energy within a solid.

Acknowledgement

The present study was conducted through a research grant from the Japan Society for the Promotion of Science (JSPS). The authors would like to thank Drs. K. Sugimoto and T. Yamazaki, Professors Emeritus of University of Tokyo, Dr. H. Fujita, Professor Emeritus of Osaka University, and Professor T. Yokobori, M.J.A.

References:

1) Fleischmann, M., and Pons, S.: J. Electronal, Chem. 261 301-308 (1989).
2) Y. Arata and Y. C. Zhang: Jpn. J. Appl. Phys. 37 (1998) L1274.
3) Y. Arata and Y. C. Zhang: Jpn. J. Appl. Phys. 38 (1999) L774.
4) Y. Arata and Y. C. Zhang: Jpn. J. Appl. Phys. 39 (2000) part 1. 7A.
5) Y. Arata and Y. C. Zhang: Proc. Jpn. Acad. B75 (1999) 281.
6) H. Fujita: Mater. Trans. JIM, 35 (1994) 573.
7) N. S. Lewis et al.: Nature 340 (1989) 525.
8) . Nakata, M. Kobayashi, M. Nagahama, H. Akita, N. Hasegawa and K. Kunimatus: ICCF-6 (1996) p.121

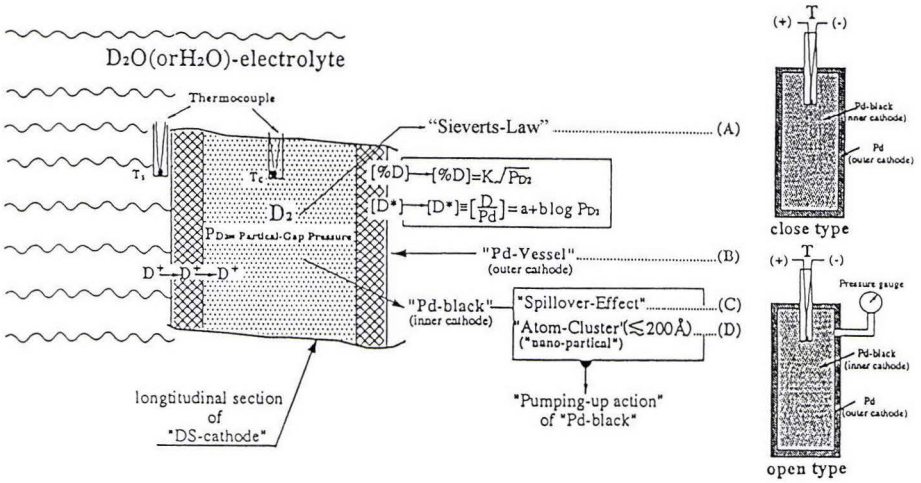

Fig.1. Concept of "DS-cathode" (Double Structure Cathode)

Note (1): Symbols (A), (B), (C) and (D) have special functions ("DS-function") as follows;

(A): Extremely high pressure of D2 gas (or H2) such as over several thousand atmospheres takes place easily inside DS-cathode because of "Sieverts-Law".

(B) Deuterium purity is extremely high inside DS-cathode because Pd-vessel works as a filter.

(C): Deuterium distribution on the surface of all particles of Pd-black instantaneously extends with uniformity and high density because of function of "Spillover-effect"

(D): Pd-black in nano-scale instantaneously absorbs much deuteriums with over 250at% in content because of essential function of "atom-cluster".

Note (2): Close type DS-Cathode (right side) is made airtightly by EB-welding to minimize a redundant inner space, and open type is connected with a pressure gauge to measure inner pressure any time, but existence of reduction inner space can not avoid.

Note (3): DS-cathode in this case was a cylinder with 60 mm in length, 14 mm in diameter and 3 mm in thickness.

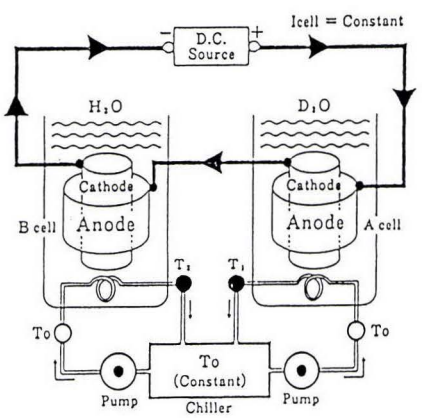

Fig.2. "Double-cell" connected with two unit same cells in series: A-cell (D_2O) and B-cell (H_2O).
Note: Although A and B cells are same construction, electrolyte only is difference

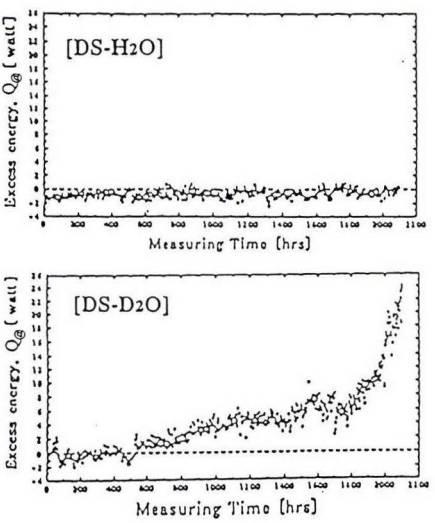

Fig.3. Characteristics of excess energy generated in H_2O-cell (upper) and D_2O-cell (lower). Note: enormous differences of excess energies ($Q_@$) generated in H_2O-cell and D_2O-cell corresponding to the change of measuring time (τ). These experimental data demonstrate that tremendous "reaction excess energy" generates within the D_2O-cell and the "said-energy" does not produce in the H_2O-cell.

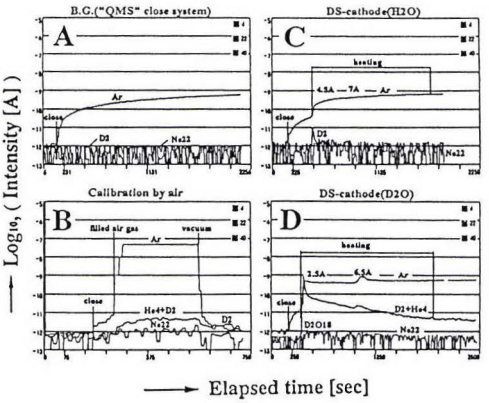

Fig.4. Time charts of the intensities of D_2+^{4}He, ^{22}Ne and ^{40}Ar measured by QMS-A. A) without sample, B) calibration with air (1.1 cm^3 x10^{-2} Torr), C) 20 mg Pd powders from DS-H_2O and D) 20 mg Pd powders from DS-D_2O. The timing of the closure of the chamber and the heating conditions (timing and current) are shown.

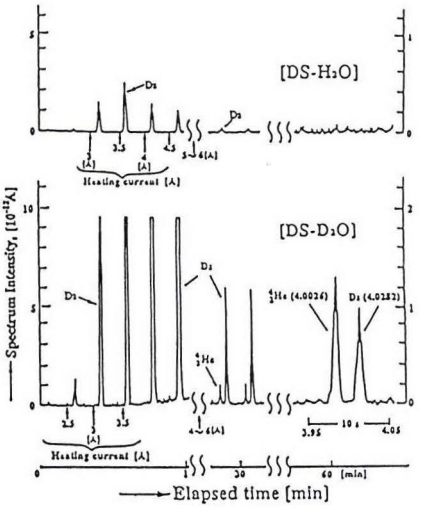

Fig.5. High-resolution M = 4 spectra of 20 mg of the remnant Pd powders after 2000-h electrolysis in the DS-H_2O (upper) and in the DS-D_2O (lower). Examples taken at typical elapsed times (1, 30 and 60 min) during and after heating the sample. The scanning range (M = 3.95-4.05) repeated every 10 s is shown, in which well separated D_2 and ^{4}He peaks are revealed. The vertical unit scale (1x10^{-12} A) corresponds roughly to 10^{-8} cm^3 ^{4}He @STP. The vertical axis for the right-hand spectra is enlarged by five times compared with that for the left-hand spectra.

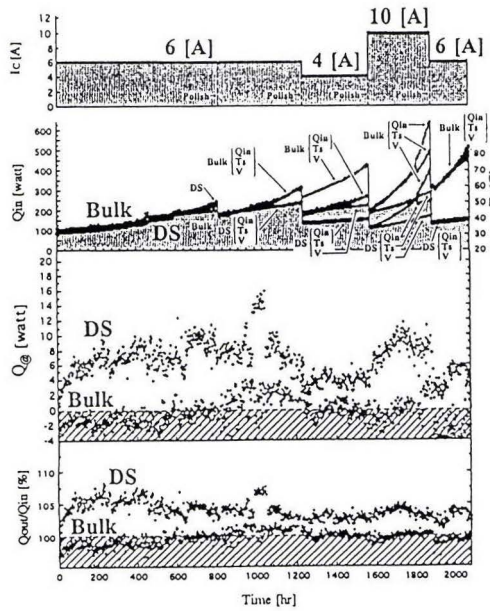

Fig. 7 Chronological records of the experimental conditions and observed quantities in [DS-D2O] and [Bulk-D2O] cells. The electrolytic currents for the two cathodes were commonly regulated to I_c [A] (6→4→10→6) as shown in top side, and $Q_{@}$ (excess power), Q_{out}/Q_{in} (output/input). In this case, over voltage changed about 3 to 5 volts during about 1000 hrs in electrolysis are shown in the lower raw. These parameters are shown chronologically by plotting on top each other. The tremendous excess power $Q_{@}$ is seen clearly in the DS-cathode, while is essentially zero in the Bulk-cathode.

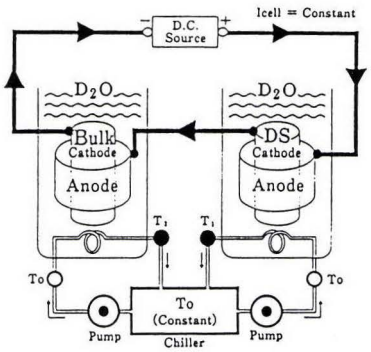

Fig. 6 [Double-cell] system, where [DS-D_2O] cell and [Bulk-D_2O] cell are electrically connected in series. Note: Both cells are constructed identically, except for the cathode.

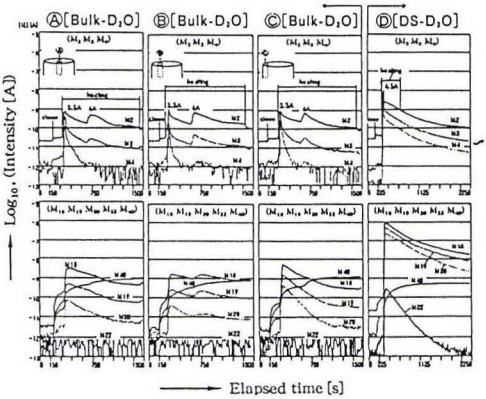

A) Chronological change in intensity of Mass (M2, M3, M4 and M18, M19, M20, M22, M40)

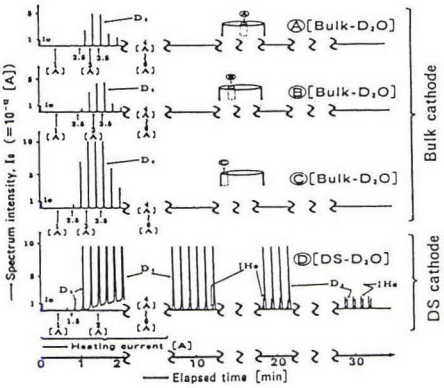

B) Chronological high resolution spectra change of Mass M4.

Fig.8 Definitive difference between the mass analysis results of the elements released from the samples (Pd powder only) taken out of the each cells used as a) Experiments in Fig.7.

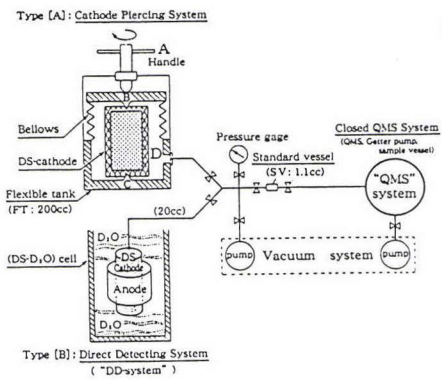

Fig. 9 Layout of the DS-cathode piercing system used in the measuring inner gases generated inside DS-cathode. A flexible tank (FT) with bellow encloses a DS-cathode, which can be pierced with sharp drills by pushing the tip plate B to the bottom plate C without treating the vacuum by using a handle A. The FT is connected to the standard vessel and the QMS system. The valves, pressure gauges and vacuum system also shown.

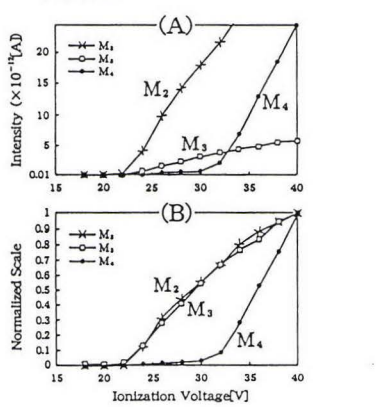

Fig. 11 I-V curves ("Vi-effect"), for M = 2, 3 and 4 groups taken at 5 minutes after t = τ_3 on the sample gas Fig. 11,C. The upper figure (A) is for absolute currents and the lower one (B) normalized. The group M2 contains D and H2. The M3 is found to be mostly HD, while the group M4 is mainly 4He.

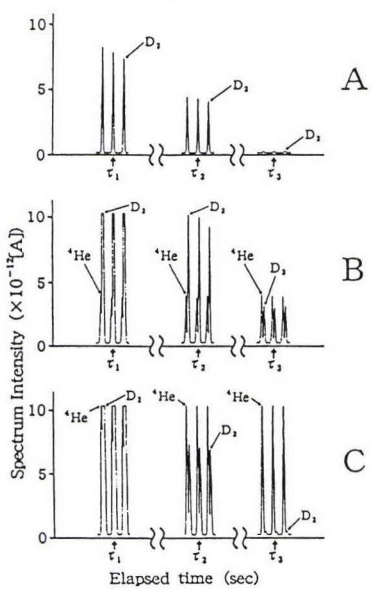

Fig. 10 The M = 4 coupled spectra of QMS taken at different elapsed times (τ_1 = 200s, τ_2 = 400 s and τ_3 = 800s) after introduction of respective sample gases. A: 1.1 cc at 3 Torr before piercing. B: 1.1 cc at 1.1 bar taken at 5 hrs after piecing, and C: 1.1 cc at 1.1 bar taken at 134 hrs after piercing.

Conference Proceedings Vol. 70
"ICCF8"
F. Scaramuzzi (Ed.)
SIF, Bologna, 2000

SEARCH FOR COHERENT DEUTERON FUSION BY BEAM AND ELECTROLYSIS EXPERIMENTS

Yuji Isobe, Shigeo Uneme, Kahou Yabuta, Hiroki Mori, Takayuki Omote, Satoshi Ueda, Kentaro Ochiai, Hiroyuki Miyamaru and Akito Takahashi

Department of Nuclear Engineering, Graduate School of Engineering, Osaka University,
Yamadaoka 2-1, Suita, Osaka, 565-0871, Japan
E-mail: yisobe@newjapan.nucl.eng.osaka-u.ac.jp

[Abstract] Procedures and results of three kinds of experiments i.e., closed type D_2O/Pd electrolysis, electron beam irradiation and ion-beam bombardment on titanium-deuteride (TiDx) have been introduced in this paper. In the electrolysis experiment, upper gas of the electrolysis cell was analyzed using a Quadrupole Mass Analysis System (Q-MAS). Significant amount of helium-4 was detected without neutron emission in several experiments and in one of these experiments, the amount of helium-4 atom in the released gas from the palladium cathode was 8.1×10^{16} atoms. Under electron beam irradiation to highly D-loaded palladium, anomalous spectra were taken in X-ray measurement. In the experiments using deuteron beam and TiDx, responses which suggested 3D multi-body fusion were taken and the reaction rate of which was increased compared to the D(d,p)T reaction rate, below 100 keV. This result may reflect the coherent effect of the solid state in the reactions. From the results of the experiments using proton beam and TiDx, peaks which suggested 3D multi-body reaction were detected with high reproducibility. Moreover, high energetic protons having 17-20 MeV emitted kinetic energy which suggested H-D-D three-body coherent fusion were also detected.

1. Introduction

In lattice dynamic conditions, where plasma oscillation and/or vibrations of deuterium atoms trapped in metal lattice are excited coherently, there is possibility that anomalous nuclear reactions are enhanced drastically compared with random processes, with consideration of the following points:

- Deuterium atoms trapped in metal lattice make well-regulated array symmetrically in metal solid.
- Free electrons which screen the Coulomb potential wall in nuclear fusion process can exist. [1,2]

Some kinds of researches have been performed in our group to induce these reactions and to detect the phenomena. [3-5] In this paper, three kinds of experimental researches, namely closed type D_2O/Pd electrolysis, electron beam irradiations to metal-deuteride and ion-beam bombardment on titanium-deuteride (TiDx) are presented. Detection of ^{4}He atoms accumulated during electrolysis and on-line detection of neutron emission in correlation with heat generation have been tried in the closed type electrolysis experiments. Under electron irradiation on highly D-loaded metals, measurements of charged particles and X-rays associated with coherently induced deuteron fusion have been tried. In ion beam experiments, peaks that might suggest the occurrence of coherently induced multi-body deuteron fusion have been detected with high reproducibility.

Existence of non D-D type nuclear reactions i.e., coherently induced deuteron fusion in lattice dynamics condition, will be recognized by the results of present three kinds of experiments, as explained in the following.

2. Closed Type D_2O/Pd Electrolysis Experiment

On-line measurements of correlation between time-variation of D/Pd ratios, excess power (by mass flow calorimetry) and neutrons (measured by NE213 scintillation counter) and off-line quantitative measurements of ^{4}He atoms accumulated in the cell and the cathodes during electrolysis (by Q-MAS; Quadrupole Mass Analysis System) have been performed using a closed type D_2O/Pd electrolysis system.[4] The upper-cell gas was sent to the Q-MAS after the electrolysis. In addition, the electrolyzed palladium cathode was heated up and released gas from the cathode was also analyzed because it was considerable that ^{4}He generated during electrolysis was trapped in the cathode palladium. By using an improved Q-MAS with a sorption pump for collection of deuterium and hydrogen, quantitative analysis was possible. Results are summarized in Table 1. In three out of seven data, meaningful increase of ^{4}He was recognized. The increased number of ^{4}He atom in the upper-cell gas during electrolysis in exp. 4-7 is summarized in Table 2. In exp. 4, significant increase of ^{4}He was detected (40 times). This result cannot be explained by contamination of air, because much (about 10 Torr of) air-leakage during electrolysis was necessary if the result is assumed to be contamination of air. In this run, ^{4}He atom was detected clearly also in the released gas analysis: 8.1×10^{16} atoms. Considering no ^{4}He atom was detected before the heating up of the cathode and the heating up analysis was completed in few minutes, detected ^{4}He atoms must be released from the cathode. Slight amount of ^{4}He atom (10^{14}-10^{15} atoms) was detected in exp. 2 and exp. 3 in the released gas analysis. No meaningful amount of neutron exceeding the confidence level ($+3\sigma$ ~ 19.5 counts per hour) was detected through this series of experiments. Unfortunately neutron measurement was not performed in exp. 4, but by the results of the other runs, it seems that there is no clear correlation between the ^{4}He generation and the neutron emission. In exp. 3, slight amount of heat generation was detected according with increase of D-loading ratio. The excess power was about 2 W for 60 W input and continued for 130 hours. In the other runs, clear heat generation was not detected.

Table 1: Results of the closed type electrolysis experiments

			^{4}He detection		
Exp. No.	Pd-cathode treatment	Current mode [1]	Upper-cell gas	Released gas [2]	Neutron
1	Annealed	S.U, L.H	No	No	No
2	Anneal + Ti coating	S.U, L.H	Yes (?)	Yes	No
3	Annealed	S.U, L.H	Yes (?)	Yes	No
4	Anneal + Au coating	S.U, L.H, S.T, Co.	Yes	Yes	--
5	Anneal + Au coating	S.U, L.H, Co.	Yes (?)	No	--
6	Anneal + Au coating	S.U, L.H, S.T	No	No	--
7	Anneal + Au coating	S.U, L.H	Yes (?)	No	No

1) S.U: Step up mode
L.H: Low high mode
S.T: Sow teeth mode
Co.: Constant current mode

2) Analysis of released gas by heating up electrolyzed cathode Pd.

Table 2: The number of 4He atoms detected in the upper-cell gas

	Exp. No.			
	4	5	6	7
No. of ^{4}He before electrolysis	1.1×10^{15}	1.1×10^{15}	1.1×10^{15}	1.1×10^{15}
No. of ^{4}He after electrolysis	4.7×10^{16}	4.4×10^{15}	1.7×10^{15}	3.3×10^{15}
Difference	4.6×10^{16}	3.3×10^{15}	6.3×10^{14}	2.2×10^{15}

3. Electron Beam Stimulation Experiments

Figure 1 shows the experimental setup. Two SSBDs for charged particle and two CdTe detectors for X-rays were attached to a vacuum chamber keeping about 10^{-6} Pa. By using two detectors having the same ability and shape, detected signals could be crosschecked. Electron beam was produced by an electron gun, of which energy could be changed continuously from 100 eV to 3 keV, beam current was about 3.5 μA, and beam diameter was about 1mm on target. Pre-D-loaded Ti (TiDx: x~1.5, by gas loading method) or Pd (PdDx: x~0.7, by electrolysis method) was used as a target. Surface of PdDx was coated with cupper layer (~ 0.05 μm) by electroplating method after D-loading by electrolysis method (150 mA/cm^2, 8 hour) for making blocking-layer to prevent loaded deuterium releasing out. Figure 2 shows energy spectra measured with twin CdTe detectors under electron beam irradiation to PdDx. Bumps from 10 keV to 20 keV are recognized in the both of spectra and counts above 20 keV very increased comparing with background (see Table 3). Since electron beam energy was 3 keV, energy of X-rays by slowing down of the electron beam must not exceed 3 keV. These spectra were not detected in other runs, using Ti or TiDx as a target. Considering that resembling spectra were detected by both detectors, these spectra cannot be explained by detectors' malfunction. If these phenomena are due to electromagnetic noise, increase of counts would be detected also in energy spectra by SSBDs, however, no such signals were detected in this run. Therefore, there is every possibility that these spectra are due to a tail of a Compton continuum or a continuous X-rays by slowing down of high energetic charged particles. After this run, a lithium drifted silicon detector Si (Li)

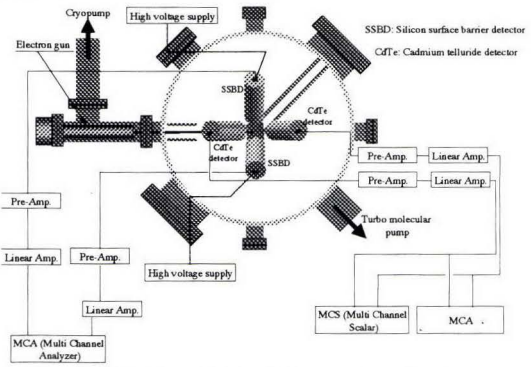

Fig. 1: Schematic view of the experimental setup

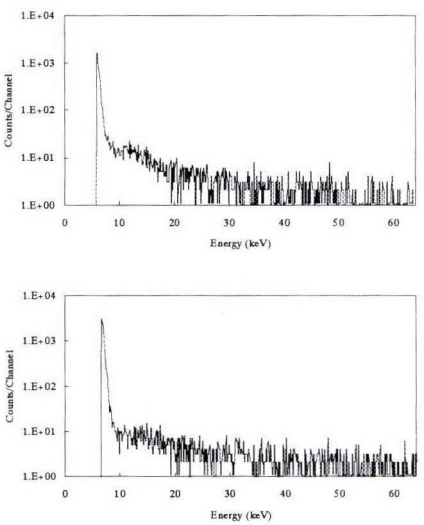

Fig. 2: Energy spectrum measured with CdTe detectors under electron beam irradiation
Beam current, energy: 0.5 μA, 3 keV
Measurement time: 5000 sec.

Table 3: Comparison of foreground count ratio (cps) with background

	CdTe_1		CdTe_2	
	10 keV- 20 keV	20 keV- 60 keV	10 keV- 20 keV	20 keV- 60 keV
Background	6.6E-3 *)	2.5E-2	5.4E-3	2.8E-2
foreground	1.7E-1	1.3E-1	1.2E-1	1.4E-1
Ratio(fore / back)	26	5.2	22	5.0

*) counts par second (cps)

and a HP-Ge detector were set up for low energy X-ray analysis and for γ-rays, respectively. Further experiments are necessary to investigate the origin of these responses.

4. Ion Beam Experiment

4-1. Deuteron Beam Experiment

Charged particles emitted from the TiDx were measured with silicon surface barrier detectors (SSBDs) under deuteron beam bombardment. For identification of the detected charged particles, ΔE&E-counter-telescope which consisted of a thin transmission type detector (ΔE-detector) and a conventional SSBD (E-detector) was used. For the measurement of the total energy of each particle, one more conventional SSBD (Ek-detector) was also set up. Figure 3 shows energy spectra measured with Ek-detector under deuteron beam irradiation to TiDx. Two strange shoulders which obviously differ from the double pile-up responses are recognized between the peak of the D(d,p)T reaction and the double pile-up peak of the D(d,p)T. Looking over the energy spectra measured with ΔE&E-counter-telescope and/or results of experiments with changing the thickness of Al screen foil set in front of the detectors, it was concluded that lower energy shoulder (at 3.4 MeV) is a responses of ^{3}He and the other shoulder is of triton (at 4.3 MeV). These particle conceived to be produced by the 3D multi-body fusion; 3D → t (4.75 MeV) + ^{3}He (4.75 MeV), at deeper place in the target. Considering the energy loss value of each particle (1.4 MeV for ^{3}He and 0.5 MeV for t), the depth where the 3D reaction was induced was estimated to be 3μm-5μm. Scanning range of deuteron beam in Ti is about 2μm, so the reaction was occurred at the end of the beam scanning range or deeper. [6-8] In addition, the yield ratio; [Yield of the ^{3}He]/[Yield of the proton by D(d,p)T reaction], showed a tendency to increase at lower beam energy (see Fig. 4). In general beam/target interaction at low energy, reaction cross-section decreases more than D-D reaction as incident beam energy decreases. Therefore, the detected 3D fusion is not direct interaction with the incident deuteron but may be indirect reactions under coherent effect in the far less energy than the beam. Namely we imagine warm or "cold" fusion.

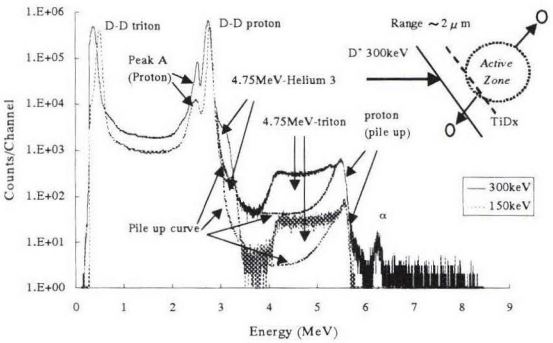

Fig. 3: Charged particle spectra measured with Ek-detector under deuteron beam irradiation to TiDx

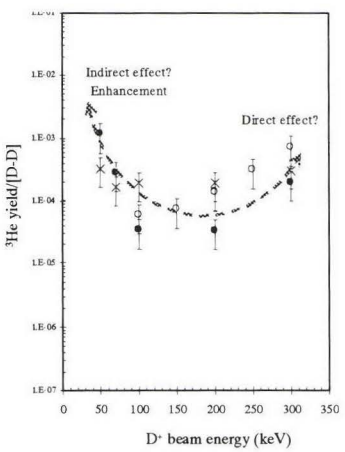

Fig. 4: Variation of the yield ratio, [^{3}He yield]/[D-D], by deuteron beam energy

In Fig. 3, there is a peak, called peak A, at lower energy side of d-d proton peak. This peak was recognized to be a response of proton and the energy of this peak agree with proton of the $^{12}C(d,p)^{13}C$ reaction. However, by the fact of that if the peak is produced by the $^{12}C(d,p)^{13}C$ reaction, peak yield for 150 keV should be less than 1/10 of the observed yield considering the reaction cross-section and peak shape should be of sharp spike. The observed peak-A may include proton responses of anomalously enhanced "cold" D-D reaction process at deeper place in the target.

4-2. Proton Beam Experiment

To investigate whether the indirect coherent deuteron fusion is induced by ion beam stimulation, measurements of charged particles were performed during the proton beam irradiation to TiDx. Figure 5 shows a charged particle spectrum which was taken during proton beam irradiation to TiDx. The peaks at 2.5 MeV and 2.8 MeV were recognized to be α-particles of the $^{15}N(p,\alpha)^{12}C$ reaction and protons of the D-D reaction induced by recoil deuterons by incident proton beam, respectively. Peak around 4.3 MeV was a response of charged particle which was detected with high reproducibility. However, no reactions explaining this peak were found by looking into interactions with impurities. If multi-body deuteron fusion (3 D → t + ^{3}He + 9.5 MeV) was induced in the target at 3 μm-5 μm depth, emitted triton may have about 4.5 MeV kinetic energy at the front of the detector, by the calculation. Since the partner particle, ^{3}He, should have about 3.3 MeV kinetic energy, the response might be covered by the continuum from 2.0 MeV to 3.5 MeV in Fig. 5. This explanation is consistent with the discussion for the results of the deuteron beam experiments. This result suggests that the incident beam played a role only for generating the condition in which the multi-body reactions were induced; multi-body D-reactions are not a direct beam/target interaction. Figure 6 shows a high energetic charged particle spectrum measured in the run using proton beam and TiDx. These signals were supposed to be responses of protons by the HDD reaction, i.e. H + D + D → p (19.1 MeV) + ^{4}He(4.77 MeV), because any other considerable emitted charged particles cannot penetrate through the thick screen foil (Ni: 600 μm thickness) set in front of the detector because of their large stopping power. Although these signals spread from 17.5 MeV to 18.2 MeV, protons having 19.1 MeV kinetic energy should have energetic deviation width of about 1.2 MeV after penetrating through a 600μm thickness Ni sheet as a result of the struggling in materials. In the runs using pure Ti instead of TiDx as a target, these signals were not

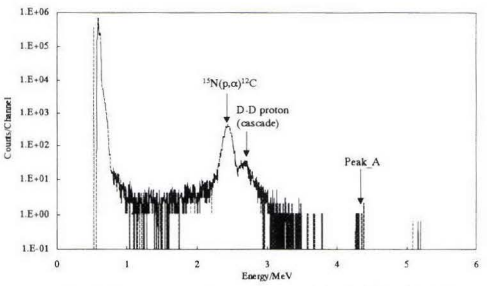

Fig.5: Energy spectrum measured with Ek-detector under proton beam (300 keV) irradiation

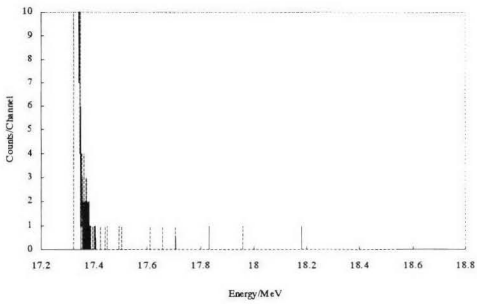

Fig.6: High-energy charged particle spectrum measured under protonbeam irradiation, with 600μm Ni-screen foil

detected. A possible mechanism to explain the production of the HDD reaction is as follows: under the stimulation by ion beam irradiation, two deuterons approach each other closely in transient coherence and D-D pairs are produced transitionally, then, incident proton hits to induce H + D + D reaction.

5. Discussions and Conclusions

It seems that multi-body reactions (3D and 4D) are of key importance to explain the experimental results of the both electrolysis and beam experiments consistently. The outgoing channel of 3D and 4D reaction can be drawn as follows:

$$3D \rightarrow {}^{6}Li^{*}\,(Ei = 25.3\ MeV: 4^{-}) \rightarrow {}^{6}Li^{*}\,(Ei = 2.18\ MeV: 3^{+}) + \text{photon emission (QED-photons)}$$
$$\hookrightarrow d\ (0.47\ MeV) + {}^{4}He\ (0.24\ MeV) \quad (1)$$
$$\rightarrow t\ (4.75\ MeV) + {}^{3}He\ (4.75\ MeV) \quad (2)$$
$$\rightarrow d\ (15.9\ MeV) + {}^{4}He\ (7.9\ MeV) \quad (3)$$
$$\rightarrow n + p + {}^{4}He + 20.1\ MeV, \quad (4)$$

$$4D \rightarrow {}^{8}Be^{*}\,(Ei = 47.7\ MeV: 3^{-}) \rightarrow {}^{8}Be^{*}\,(Ei: I^{\pi}) + \text{photon emission (QED-photons)},$$
where permitted Ei and I^{π} pairs are (25.5 MeV: 4^{+}), (20.0 MeV: 2^{+}),
(16.6 MeV: 2^{+}) and (3.04 MeV: 2^{+}), and ${}^{8}Be^{*} \rightarrow \alpha + \alpha + Ei + 0.0918\ MeV \quad (5)$
$$\hookrightarrow {}^{8}Be^{*}\,(g.s.: 1^{+}) + \text{photon emission (QED-photons)}, \text{ and } {}^{8}Be^{*} \rightarrow \alpha + \alpha + 0.0918\ MeV\,. \quad (6)$$

The detected charged particles in the ion beam experiments may be produced by the reaction (2). But this outgoing channel (2) is supposed to be a minor channel, considering the spin-parity selection rules. The main channels may be (1)(5) and (6). Results of the electrolysis experiments as ^{4}He-generation without neutron emissions can be explained by the reaction (1) and/or (6). There is a possibility that the detected signals under electron beam irradiation were bremsstrahlung X-rays by slowing down of those charged particles by the reaction (1), (5) and/or (6), all of which produce ^{4}He as the effectively same process as $d + d \rightarrow {}^{4}He + 23.8\ MeV$.

These results of the three kinds of experiments can be explained with a common key of multi-body reactions induced with stimulating highly D-loaded metals (TiDx or PdDx). This reaction may be induced under lattice coherent motion in transitional process as suggested in the results of ion beam experiments. It is important task in future to search how these conditions can be realized much more strongly and to work out how 3D or 4D cluster can be made.

References

[1] A. Takahashi et al.: Fusion Technology, 19(1991) pp.380-390
[2] A. Takahashi et al.: Fusion Technology, 27(1995) pp.71-85
[3] A. Takahashi: Proc. of the 7th ICCF, April 1998, pp.378-382
[4] S. Ueda et al.: Proc. of the 7th ICCF, April 1998, pp.398-402
[5] K. Ochiai et al.: Proc. of the 7th ICCF, April 1998, pp.274-278
[6] A. Takahashi et al.: Fusion Technology, 34(1998) pp.256-272
[7] A. Takahashi et al.: Physics Letters A, 255(1999) 89-97
[8] K. Ochiai et al.: Fusion Technology, 36(1999) pp.315-323

Conference Proceedings Vol. 70
"ICCF8"
F. Scaramuzzi (Ed.)
SIF, Bologna, 2000

Finite Element Modeling of the Transient Calorimetric Behavior of the MATRIX Experimental Apparatus: ^{4}He and Excess of Power Production Correlation through Numerical Results

M. McKubre [1], F. Tanzella [1], P. Tripodi [1], D. Di Gioacchino[2], V. Violante [3]

[1] SRI International, 333 Ravenswood Ave, 94025 Menlo Park, CA (USA)
[2] INFN-LNF, Viale Enrico Fermi 40, 00044 Frascati (Italy)
[3] ENEA, Viale Enrico Fermi 45, 00044 Frascati (Italy)

Introduction

The increasing interest in the phenomena concerning the production of excess of power in deuterium loaded palladium led to several different experiments in order to identify the mechanism responsible for this effect that cannot be explained in terms of some chemical reactions to account for the high energy for atom released [1-3]. The "MATRIX" experiment has been conceived for studying the behavior of a catalytic bed of palladium particles on carbon, in equilibrium with deuterium gas (or hydrogen for the calibration). A gas loading strongly reduces poisoning of the host metal during the loading and can be employed successfully in loading thin films and small particles of palladium. The gas loading experiments simplify the measurement of ^{4}He [4-5] that is the expected ashes of the D-D reaction in condensed matter (i.e. palladium lattice). MATRIX experiment is oriented to reveal a correlation between ^{4}He production and excess of power during gas loading of deuterium in palladium. The experiments shown that helium production is strongly correlated with increasing of the system temperature.

Thermal Transient Analysis

An important aspect of the calorimetric study is the evolution of the room temperature: a variation of one degree in the room produces a variation of about 0.4 degrees in the active zone of the experimental device. In order to separate the effect of the excess of power from the effect of the room temperature evolution, a transient calorimetric description of the system is required, including the effect of the room temperature evolution and oscillations in the mathematical description of the experiment. The model studies the system transient by taking into account the non linearity given by the radiative heat transfer, that couples with the convective mechanism on the top of the cell, and the moving boundary conditions given by the room temperature behavior.
The numerical simulation represents a tool able to translate the temperature measurement and map into heat flux evaluation.

Experimental set-up

The experimental system has been realized assembling four 50 cc stainless steel cells (see Fig.1) within a heated stainless steel support that is maintained at a controlled temperature. The environment temperature oscillations are smoothed of about a factor 2.5, therefore typically the temperature oscillations of the catalyst and of the support is in the order of 0.7 degree for a day.

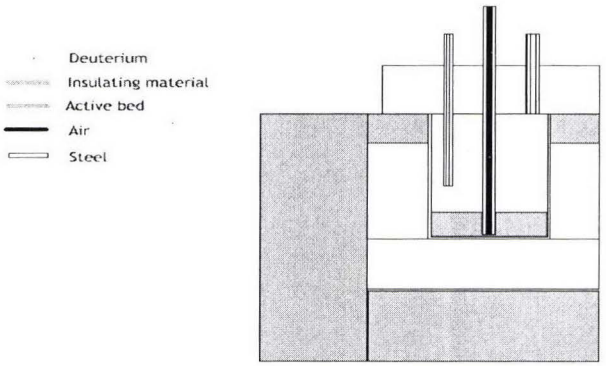

Fig. 1 - Experimental cell

The palladium is contained as supported small particles in the active bed that is placed in the bottom of the cell.
Ten grams of catalyst with 0.4-0.5% wt of palladium, the size of the metal particles is ranging from 10 nm up to 10 μm. A small tube is used to refill the cell with deuterium in order to compensate the adsorption on the catalytic bed.
The pressure of the cell, the catalyst temperature and the gas temperature are continuously monitored during the experiment. The system composed by the four cells and the stainless steel support are thermally insulated from the environment by using $CaSiO_4$ bricks. The loading is carried out by the physical absorption of deuterium gas at a pressure ranging, approximately between 1 and 2 atm; the cell block temperature, during the considered experiment, is maintained at about 516 K, with an oscillation of about 0.7°, while the air temperature oscillates about 1.7° around 303.5 K (see Fig. 2).
The objectives of this static experiment are:

(i) more accurate calorimetry to verify the value of the heat associated with the production of ^4He;
(ii) a parametric study of heat and helium production seeking to maximize these effects;
(iii) analysis of the helium produced in the gas or retained in the bed.

The main features of the experiment are:
Low cost, highly reproducible construction so that a multiplicity of interchangeable cells can be operated in comparative testing.

a) All metal construction and all metal, helium leak tight sealing to retain any helium produced and to exclude ambient sources.
b) Separate admission and sample lines to eliminate the possibility of gaseous cross contamination.
c) Independent, on-line pressure transducers to monitor cell pressure and ensure above atmospheric operation.

d) A constant temperature block having a large thermal conductivity and heat capacity to ensure closely identical cell operation in comparative testing.
e) Well-defined, well-characterized and well-modeled heat transfer so that heat flow calorimetry can be performed absolutely and quantitatively.

Modeling

The solution can be achieved by solving the transient two dimensional heat transfer equation over the domain shown in fig.1. The heat transfer mechanism can be assumed to be convective around the experimental device but coupled with a radiative mechanism on the top due to the high temperature there. The environment temperature is time dependent so that the boundary conditions are moving. Then the first problem to solve is to obtain a proper function approximation for the room temperature.

Equation:

$$\rho c_p \frac{\partial T}{\partial t} = \nabla K \bar{\nabla} T + Q''' \tag{1}$$

B.C.

$$-K \frac{\partial T}{\partial n} = h(T - T_R) + \varepsilon\sigma\left(T^4 - T_R^4\right) \tag{2}$$

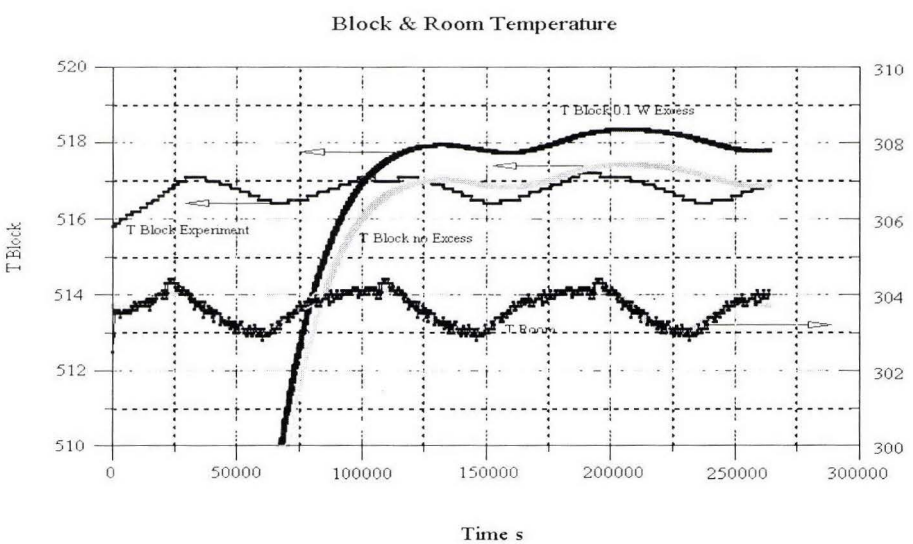

Fig. 2 - Experimental and theoretical values of the block and room temperature evolution

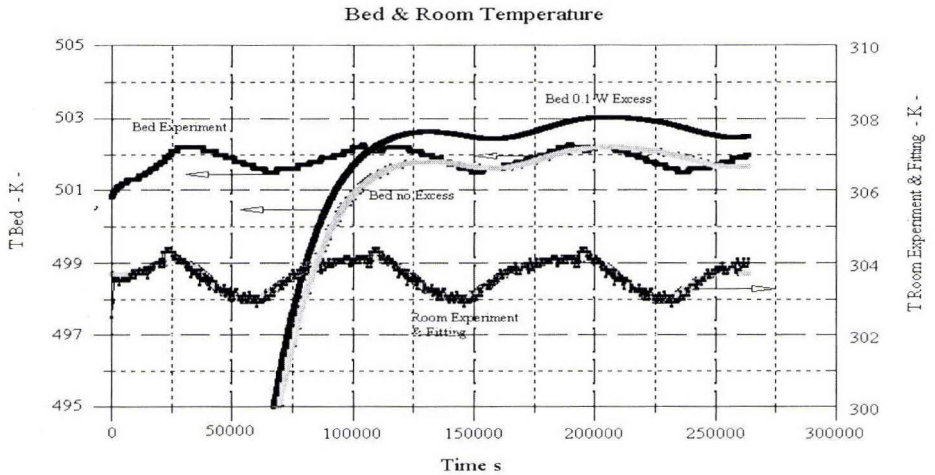

Fig. 3 - Bed and room temperature evolution

ρ is the density (g/cm^3), c_p specific heat (J/g °), T temperature, K conductivity (W/cm^2 °), Q''' thermal load (W/cm^3), *h* convective heat transfer coefficient (W/cm^2 °), T_R the room temperature (time depending), ε the emissivity of the top and σ the Boltzmann coefficient.
The lower curves of Fig. 2, 3 show the room temperature evolution. The upper black curves in Fig. 2 and 3 show the evolution of the block and bed temperature (experimental values) respectively.
The palladium is contained as supported small particles in the active bed that is placed in the bottom of the cell.
We can observe that the noise in the room temperature is smoothed by the device because of its thermal inertia. So we can assume that the real forcing function, that should be applied
as moving boundary condition, is a function obtained by filtering the noise from the room temperature.
This condition can be obtained by means of a Fourier's series development of the experimental data.
In general a function *f(x)* with given values on *2n+1* points can be developed as Fourier's series up to the harmonic *m* as:

$$f(x) \equiv A_0 + \sum_{i=1}^{m}(A_i \cos(ix) + B_i \sin(ix)) \tag{3}$$

$$A_0 = \frac{1}{2n+1}\sum_{j=0}^{2n} f(x_j) \tag{4}$$

$$A_i = \frac{2}{2n+1}\sum_{j=0}^{2n} f(x_j)\cos(\frac{2\pi i}{2n+1}j); \quad B_i = \frac{2}{2n+1}\sum_{j=0}^{2n} f(x_j)\sin(\frac{2\pi i}{2n+1}j) \tag{5}$$

A_i and B_i have been estimated over 250000 s.
The behavior of boundary condition evolution is shown in the figures 2, 3 (see the continuous curve passing through the experimental points of the room temperature).

Results

Figure 3 shows the evolution of the bed temperature (experimental points, theoretical curve without excess of power, and theoretical curve with excess of power).
We can see that the oscillation of the room temperature produces an oscillation of the bed temperature both in the experimental and in the theoretical curves with a delay that is in the range 1×10^4 s. Such a delay introduces an uncertainty of 0.2 degrees, while an excess of power in the order of 0.1 W produces an increasing of the temperature of about 0.7 degrees, as can be easily seen comparing the two theoretical curves in Fig. 2 and 3, so that we can conclude, on the basis of the enhanced modeling, including the transient, that the calorimetric response of the experimental system is accurate enough to detect an excess of power of 0.1W and that a more precise evaluation of the excess of power can be done taking into account the delay effect.
The numerical study reveals that the response of the calorimeter is linear in the investigated temperature experimental range.

References

[1] M.Fleishmann, S.Pons, Electrochemically Induced Nuclear Fusion of Deuterium, J. Electroanal. Chem. **261**, (1989), p. 301.

[2] M. C. H. McKubre, S. Crouch-Baker, A. M. Riley, S. I. Smedly, F. L. Tanzella, Excess Power Observation in Electrochemical Stusies of the D/Pd System; the Influence of Loading, Proc. Third Int. Conf. on Cold Fusion, Nagoya (Japan) October 20-25, 1992, p. 5.

[3] Y. Arata, Y. C. Zhang, Achievement of Solid State Plasma Fusion ("Cold Fusion"), Proc. Intern. Conf. On Cold Fusion, Toya (Japan), Oct. 13-18 1996, p. 129.

[4] D. Gozzi, F. Cellucci, L. Cignini, G. Gigli, M. Tomellini, E. Cisbani, S. Frullani, G.M. Urciuoli, Erratum to "X-Ray, Heat Excess and ^{4}He in the D/Pd System", J. Electroanal. Chem. **435** (1997) 251-271.

[5] M. Miles, B. J. Bush, Search for Anomalous Effect Involving Excess Power and Helium During D_2O Electrolysis Using Palladium Cathodes, Proc. Third Int. Conf. on Cold Fusion, Nagoya (Japan) October 20-25, 1992, p.189.

Conference Proceedings Vol. 70
"ICCF8"
F. Scaramuzzi (Ed.)
SIF, Bologna, 2000

A NEW METHOD AIMED AT DETECTING SMALL AMOUNTS OF HELIUM IN A GASEOUS MIXTURE

A. De Ninno, A. Frattolillo, A. Rizzo, F. Scaramuzzi, C. Alessandrini
ENEA C.R. Frascati, via E. Fermi, 45, 00044 Frascati (Rome), Italy

ABSTRACT

In Cold Fusion experiments it is sometimes important to detect the presence of helium (either ^{3}He or ^{4}He) in the gases evolved in the experiment. In electrolytic experiments there is a mixture mostly composed by H_2 or D_2, O_2, water vapor, and traces of helium; in gas loading experiments there is only H_2 or D_2 besides helium.

The suggested method consists of a static measurement. The mixture to be examined is passed through a catalyzer in order to reduce the amounts of H_2, D_2 and O_2, followed by a cold trap to further remove these gases as well as water vapor and is then stored in a large volume which includes the mass spectrometer head. Then the measuring volume is connected to a getter pump, which removes all residual gases with the exception of noble gases: in particular such a pump is very efficient in pumping out hydrogen and its isotopes. The residue is then measured in a static mode by the mass spectrometer: the use of an high-resolution mass-spectrometer allows a further check of the absence of D_2 (in the case of heavy water).

The apparatus has been calibrated with ^{4}He, and a reproducible dependence of the mass-spectrometer current on the amount of ^{4}He present has been found.

Tests are being conducted aimed at eliminating contamination by ^{4}He from the atmosphere; furthermore, the absence of neon allows us to exclude the possibility of such contaminations.

Current work is concerned with the analysis of gases produced by a Cold Fusion cell generating excess heat.

1. INTRODUCTION

The correlation between excess heat production and the achievement of a high deuterium loading ratio in a host metal M, has been assessed by many experiments [1,2]. This result is consistent with the theory proposed by G. Preparata [3], predicting the formation of coherence domains in the host lattice of a hydrogen-metal system, provided that a sufficiently high ($\geq$1) concentration D/M is reached. Inside such domains, the deuterons behave as a coherent system, resulting in a dramatic change in the cross sections of the D-D fusion reactions, as compared to those measured for the usual "vacuum" conditions. Furthermore, the probability of the reaction:

$$D + D \rightarrow {}^4He + 24MeV$$

increases by many orders of magnitude as compared to those for the other fusion channels. The excess energy, which in vacuo is released as the kinetic energy of the emitted projectiles (nucleons or γ rays), is mostly absorbed by the coherent system as heat, accounting for both the observed excess energy production and the lack of neutrons and other "conventional" nuclear ashes.

If such a theoretical approach is correct, we may expect that ^{4}He is produced during excess heat phenomena. It is therefore important to detect the presence of helium in the gases evolved in *"cold fusion"* experiments, provided that this is to some extent released into the gas phase.

2. TYPICAL COMPOSITION OF THE GAS MIXTURE IN ELECTROLYTIC AND GAS LOADING EXPERIMENTS

The gas mixture in electrolytic experiments consists mainly of hydrogen isotopes (H_2, D_2, HD) and O_2, which are produced at the electrodes, and water vapor (H_2O, D_2O, HDO). In gas loading experiments, hydrogen isotopes are the main components.

Since ^{4}He represents about 5.2 ppm of atmospheric air, it is mandatory to avoid any possible contamination of the gaseous sample from the environment. The maximum care must then be taken

in order to avoid leaks and/or helium permeation phenomena during the experiment, both by using appropriate materials as well as by using adequate high (HV) or ultra-high vacuum (UHV) sealing connections. Moreover, any air initially contained in the experimental volume must be removed before starting the run. The whole circuit must therefore be previously evacuated and/or flushed with some pure gas. It may also be recommendable, in the case of electrolytic experiments, that some purge gas be added to the cell each time a sample is sent to the analyzer. This refilling procedure avoids the need to pump on the liquid electrolyte, and keeps the pressure inside the cell somewhat above the atmospheric pressure, reducing the risk of contamination from the environment. Considerable traces of the purge gas used for this purposes (for instance high purity dry nitrogen) can therefore be found in the gas mixture.

The amount of ^4He eventually produced during excess heat phenomena, is expected to be only a very small fraction of the total gas sample. As an example, let us estimate the composition of the gas mixture in a typical Frascati electrolytic cell. After the initial purging with pure gas, the mixture will be mainly composed of nitrogen and water vapor in equilibrium, at room temperature, with the liquid.

In our present test configuration, the volume available to the gas mixture above the electrolyte level, is about 3 cm^3. The initial nitrogen pressure, after the preliminary purging procedure, is typically set at about 0.11 Mpa. The amount of nitrogen in the experimental volume is therefore around $1.47 \cdot 10^{-4}$ mole.

During electrolysis, D_2O is dissociated at the electrodes according to the reaction:

(1) $$2D_2O \rightarrow 2D_2 + O_2$$

The number of moles of D_2 and O_2 produced per unit time is given by the Faraday low:

(2) $$\frac{dn_{O_2}}{dt} = \frac{1}{2}\frac{dn_{D_2}}{dt} = \frac{1}{2}\frac{dn_{D_2O}}{dt} = \frac{1}{2}\frac{i(t)}{n_e \cdot F}$$

where *i(t)* is the instantaneous electrolysis current (A), $n_e = 2$ is the number of electrons involved in the reaction, and $F = 96484$ C/mole is the Faraday constant. With a typical electrolysis current in the order of 10 mA, we have:

(3) $$\frac{dn_{O_2}}{dt} \cong 2.59 \cdot 10^{-8}\,\text{mole} \cdot \text{s}^{-1}$$

(4) $$\frac{dn_{D_2}}{dt} \cong 5.18 \cdot 10^{-8}\,\text{mole} \cdot \text{s}^{-1}$$

Assuming that all the measured excess power ΔP (watt) gives rise to the formation of ^4He, we can easily estimate the corresponding production rate:

(5) $$\frac{dn_{^4He}}{dt} \cong \frac{\Delta P(W)}{24\text{MeV} \cdot N_A} = 4.32 \cdot 10^{-13} \cdot \Delta P(W)\ \text{mole} \cdot \text{s}^{-1}$$

where N_A is the Avogadro's number. Equation (5) gives an upper bound for the expected helium yield ratio in the gases evolved in an electrolytic experiment, with the further assumption that all the ^4He produced inside the metal is released to the gas phase. For a typical excess heat of a few tens of mW, equation (5) predicts about $10^{-15} \div 10^{-14}$ mole$\cdot s^{-1}$, i.e. about $10^9 \div 10^{10}$ atoms$\cdot s^{-1}$ as an order of magnitude. Comparing this estimation with equations (3) and (4), it is easily seen that the concentration of ^4He in the gas sample is expected to be in the order of a ppm or less, with respect to that of

O_2 and D_2 produced by electrolysis. Also, the concentration of purge gas turns out to be many orders of magnitude larger than that of ^4He.

3. LIMITS OF "CONVENTIONAL" ANALYSIS TECHNIQUES.

Since we need to measure the partial pressure of an extremely rarefied component, the pressure of the gas sample at the ion source must be as high as possible with respect to the ultimate vacuum, in order to maximize the signal to background noise ratio. On the other hand, for a correct estimation of the helium content, the corresponding partial pressure at the ion source must not exceed the linearity range of the analyzer, having a typical upper bound of about $10^{-5} \div 10^{-4}$ mbar. Moreover, the total gas sample pressure cannot rise above some 10^{-3} mbar, in order to prevent the ion source filament from being damaged or switched off by the internal protection circuitry. Conventional analysis methods rely on differential pumping arrangements, or on the diffusion of the gas sample through large impedance circuits, in order to control the amount of gas sent to the analyzer. Both these techniques, however, besides resulting unavoidably in a reduced detection limit, may affect the original composition of the gas mixture in a somewhat uncontrollable way, due to the selective pumping speed and/or selective transmission coefficients for different gases. Moreover, the gas sample is continuously drawn off during the analysis, so that there is no possibility of repeating the measurement or to perform additional checks later on. In a certain sense, these methods can be considered as destructive analysis techniques.

Table 1
Compilation of possible components in the mass range of 1 - 4 m/e

Mass	Ion	Mass (amu)
1	H^+	1.0078252
2	D^+	2.014102
	H_2^+	2.01565
3	$^3He^+$	3.016030
	T^+	3.016050
	HD^+	3.021825
	H_3^+	3.023475
4	$^4He^+$	4.002600
	HT^+	4.023875
	D_2^+	4.028204
	H_2D^+	4.029650

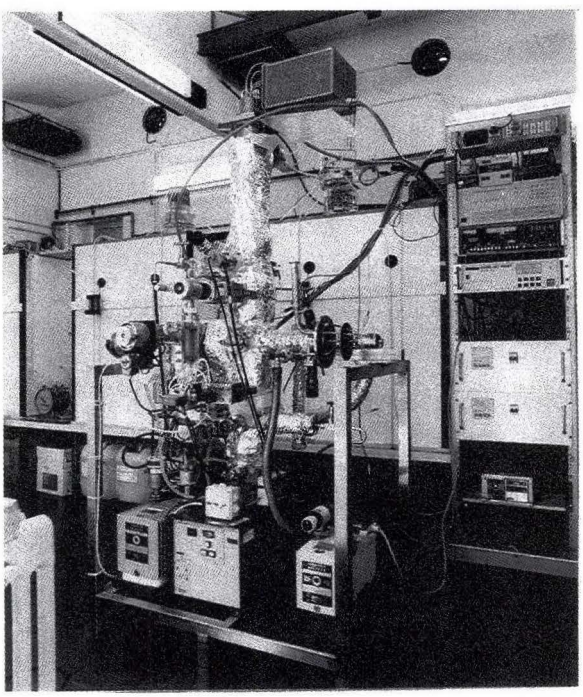

Figure 1. The experimental facility at ENEA Frascati

The presence in the gas mixture of both ^4He and D_2, further complicates the analysis. The masses of the $^4He^+$ and D_2^+ ions are indeed only 0.026 amu apart (see table 1), therefore a high resolution mass spectrometer is required in order to separate the two peaks. Moreover, for a correct measurement of the amount of helium in the gas sample, the contribution of the nearest neighbor D_2 peak to the ^4He signal must be negligible with respect to expected helium ion current intensity. Since in our case the concentration of ^4He is in the order of a ppm compared to that of D_2, an extremely high resolution is required in order to prevent the helium peak from being hidden by the tail of the deuterium peak. This results in a correspondingly large reduction of the mass analyzer

sensitivity and hence of the helium detection limit.. A compromise must thus be chosen between resolution and sensitivity, unless we are able to selectively remove the D_2 from the gas mixture.

4. THE NEW "PSEUDO-STATIC" ANALYSIS METHOD.

The method suggested here relies on the use of a non-evaporable getter (NEG) alloy pump, to remove all the components in the gas mixture (or at least to strongly reduce their concentration), except for noble gases, finally resulting in a gas sample with a high helium concentration, and a total pressure within the linearity range of the QMA (10^{-7} – 10^{-5} mbar), provided that the volume of the UHV analysis chamber has been suitably designed. The mass spectrometer thus operates, during the analysis, in a sort of "pseudo-static" vacuum condition, i.e. with no turbmolecular pumping, but under the selective action of the NEG pump.

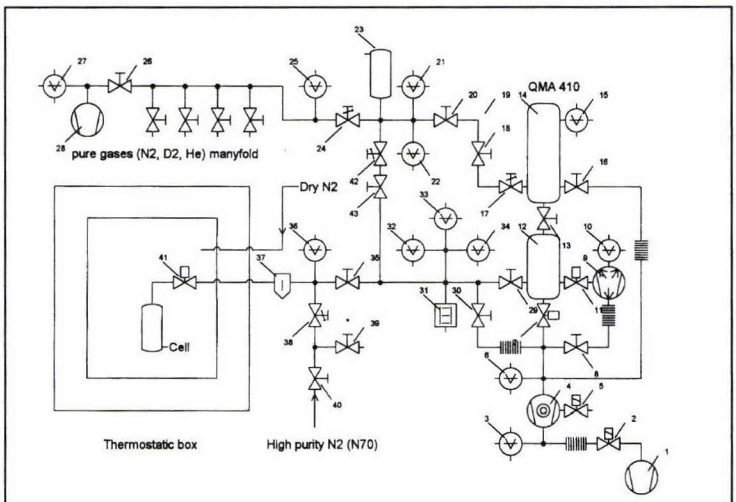

List -Key

1 RP1 Rotary pump
2 AV1 angular valve
3 PG1 Pirani gauge
4 TP1 Pfeiffer TPU 170 turbomolecular pump
5 VV1 Vent valve
6 IG5 hot cathode ion gauge
7 GV1 gate valve DN 100 CF
8 GV8 gate valve DN 40 CF
9 GP1 SAES MK200 SORB AC NEG pump
10 IG3 hot cathode ion gauge
11 GV3 gate valve DN 100 CF
12 Double cross CF100 - CF40
13 GV2 gate valve DN 100 CF
14 UHV analysis chamber with a QMA 410 analyzer
15 IG4 Hot cathode Ion Gauge
16 GV9 gate valve DN 40 CF
17 DV1 Balzers dosing valve
18 BL2 NUPRO diaphfragm valve
19 Known volume 2.64 cc (VCR elbow)
20 BL1 NUPRO diaphragm valve
21 BG1 Absolute Baratron gauge 1 tor FS
22 BG2 Absolute Baratron gauge 0.1 tor FS
23 300 cc SS bottle
24 BMG1 NUPRO metering valve
25 Bourdon gauge
26 AV2 angular valve
27 PG3 pirani gauge
28 PR2 rotary pump
29 GV5 gate valve CF40
30 GV7 gate valve DN 40 CF
31 Liquid nitrogen sorption trap
32 PG2 Pirani gauge
33 IG2 hot cathode ion gauge
34 PT1 piezoresistive gauge
35 BL3 NUPRO valve
36 P2 piezoresistive gauge
37 Pd catalyzer
38 MRG1 regulating valve
39 BL4 NUPRO diaphragm valve
40 BL5 NUPRO diaphragm valve
41 BK1 NUPRO valve
42 BMG2 NUPRO metering valve
43 BL5 NUPRO diaphragm valve

Figure 2. Schematic layout of the analysis system

Two main constraints have to be considered when using NEG pumps: hydrogen isotopes are reversibly sorbed in the bulk getter material (physi-sorption); however, when a sufficiently high concentration of hydrogen is reached, the alloy may become brittle. A second con-straint arises from the progressive degradation of the NEG pump performance with successive exposure to chemically active gases, such as N_2, O_2, CO, CO_2 or water vapor, which are sorbed in a non reversible way at the surface of the alloy (chemi-sorption), resulting in a contamination by oxide or carbide layers. This therefore requires periodic regeneration of the getter material (ST707 alloy) at high temperature (450°C), so as to release all the absorbed hydrogen, while surface contaminants can migrate into the bulk material resulting in a freshly cleaned surface.

Increasing the mass of the NEG alloy will help in reducing the frequency of regeneration cycles, as well as in extending the lifetime of the getter cartridge. Reducing the amount of gas to be sorbed by the NEG pump may also alleviate the problem. This can be accomplished by introducing a cata-

lyzer, which allows the reduction of most of the H_2 (or D_2) and O_2 with formation of water, and a cold trap containing some sorbant material (such as activated charcoal or a molecular sieve) cooled down to liquid nitrogen temperature. Such a cold trap further reduces the O_2 and N_2 content, and eliminates water vapors.

5. PRELIMINARY RESULTS

A facility has been built at ENEA Frascati (figure 1), in order to test the feasibility of such a method. A schematic drawing of the proposed experimental arrangement is shown in figure 2. A turbo-molecular pump ensures an ultimate vacuum of about 10^{-9} mbar inside the UHV chamber, which is periodically baked out at about 250°C in order to reduce the outgassing from the walls. This pump is excluded during the analysis, by closing the gate valve GV1 just before introducing the gas sample. A SAES MK200 non-evaporable getter alloy pump (equipped with a 170 g cartridge of ST707 alloy) keeps the pressure inside the UHV chamber within a $5\cdot10^{-9} - 3\cdot10^{-8}$ mbar range, depending on the cleanness of the getter cartridge surface. Once the gas sample has been introduced into the analyzer, the NEG pump strongly and quickly reduces the concentration of all the components initially present in the mixture, except for noble gases (figure 3). In particular, its pumping speed for H_2 is rated about 500 ℓ/s at room temperature (almost regardless of the amount of hydrogen already sorbed), resulting in a very effective removal of hydrogen isotopes (figure 4). Somewhat higher pumping speeds can be achieved by warming up the getter cartridge, however the corresponding hydrogen equilibrium pressure grows with the temperature. Moreover, the outgassing from the surrounding wall may increase, due to the thermal radiation by the hot cartridge, so we decided to operate the getter pump at room temperature.The ability of the getter pump to effectively reduce the deuterium content below the detection limit in just a few minutes, can easily be observed in the multiple Ion Detection (MID) mode, plotting the ion current signal at mass 4 vs time. When a ^4He-D_2 mixture is introduced into the analyzer, the mass 4 signal rapidly decreases to a

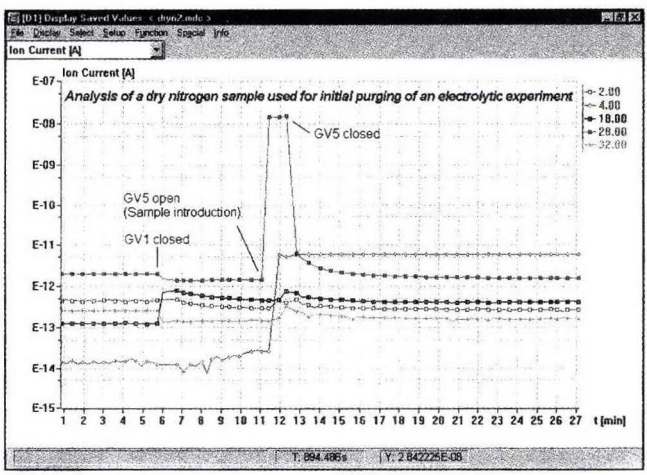

Figure 3. Example of a purge dry N_2 sample analysis. Only a few masses are shown to make the plot more readable. Nevertheless, some interesting observations can be made:

- when excluding the turbomolecular pump (GV1 closed), the observed reduction of the ion current signal at masses 2 (H_2), 28 (N_2) and 32 (O_2) indicates that these gases are effectively pumped by the ST707 NEG alloy. Also mass 18 (H_2O) after a sudden small increase, is reduced by the getter pumping. Mass 4 signal slowly increases as a consequence of the outgassing from the UHV chamber walls, however it remains well below $5\cdot10^{-14}$ A.
- When the gas sample is introduced into the analyzer, a sudden significant increase of mass 28 and mass 4 is observed, while the other masses exhibit just a small increment, quickly recovered by the getter pump. It is interesting to note that, soon after the valve GV5 is closed, stopping the sample admission to the analyzer, the getter pumps out in just a few minutes the considerable amount of nitrogen, while leaving the helium unaltered.
- The dry nitrogen used in these preliminary tests for purging purposes, was taken from the evaporation of a 5 m^3 liquid nitrogen tank. It exhibits a considerable ^4He concentration, which can limit the sensitivity of the analysis system. Ultra high purity N70 nitrogen is going to be used, as soon as a suitable decompression and distribution manifold has been installed.

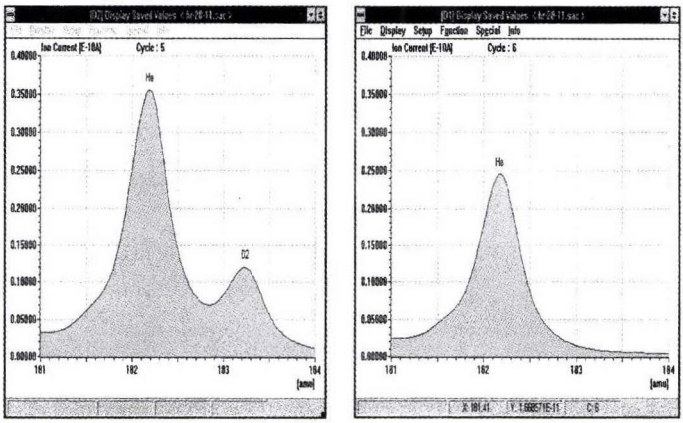

Figure 4. High resolution spectra of a ^{4}He-D_2 mixture.
The first scan above (cycle 5) shows the two resolved peaks. The GV3 was opened at the end of this scan cycle, allowing the getter to pump the deuterium. The following scan (cycle 6), shows that there is no further significant trace of D_2. During these tests, the dwell time was set at 1 s, while the scan width was of 10 amu. This means that the scan time of each cycle was 10s.

constant value, indicating that all deuterium has been sorbed. The asymptotic value of the ion current can thus be safely ascribed to the exclusive contribution of ^{4}He. The high resolution quadrupole mass spectrometer (Balzers QMS421) can however provide a further check of the absence of D_2.

Since inert gases are not sorbed by the getter, the content of argon, neon and ^{3}He can easily be controlled to check against any eventual leakage. Besides Ar^{++} and Ne, heavy water vapor can also contribute to mass 20. D_2O is however sorbed by the getter pump. Moreover, the different contributions to mass 20 can be discriminated in the high resolution mode. This is not true in the case of mass 3 peak, which has contributions by several hydrogen isotopic species (see table 1). The QMS 421 has the potential to resolve the mass 3 peak, but it needs to be upgraded to operate in the second stability region [4]. Nevertheless, hydrogen isotopes are sorbed by the getter pump, so that any significant signal at mass 3 can be considered as representative of the ^{3}He content.

6. CALIBRATION OF THE QMA

The high resolution quadrupole mass spectrometer was calibrated using pure N_2, ^{4}He, D_2, and a ^{4}He-D_2 mixture, as summarized in table 2. Measurements of the ion current vs pressure were carried out in both Scan Analog and MID modes. Pure gas samples were introduced into the analyzer through a dosing valve while pumping by means of the turbomolecular unit, in such a way that a suitable equilibrium pressure was established at each different step. A quite good correspondence was found between calibrations in Scan Analog and MID modes. In the case of ^{4}He, the QMA was also calibrated in the "pseudo-static" vacuum condition, introducing a known amount of gas into the analyzer, while pumping only by the getter unit. The helium pre-load was accomplished by filling a carefully measured known volume (2.64 ±

Table 2

Sensitivities of the QMA 410 for some different gases (70 eV energy of ionization)

Gas sample	Analysis method	QMA resolution	Mass Nr.	Sensitivity (A/mbar)	Sensitivity (A/atom)	Scan mode
N_2	dynamic	Standard	14	7,43E-05		MID
			28	8,53E-04		MID
^{4}He	dynamic	High	182,15	7,12E-06		MID
		Standard	4	1,96E-04		MID
	static	High	182,15	7,01E-06	1,75E-26	ANALOG
			182,15	7,07E-06	1,76E-26	MID
		Standard	4	1,64E-04	4,41E-25	ANALOG
			4	1,88E-04	4,53E-25	MID
D_2	dynamic	High	183,25	1,98E-05		ANALOG
			183,25	1,93E-05		MID
		Standard	2	8,53E-06		MID
			4	6,25E-04		MID

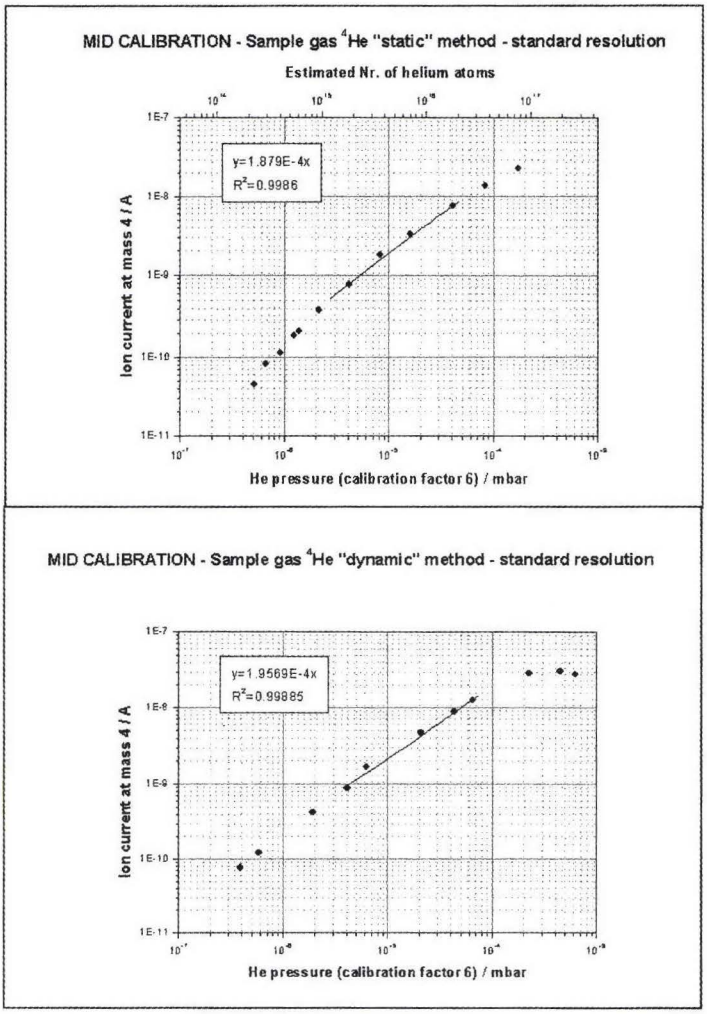

Figure 5. Comparison between "static" and "dynamic" calibrations for ^{4}He in standard resolution mode

0.0031cc) at a known pressure. This latter was monitored by means of two accurate capacitive baratron gauges (BG1 and BG2 in fig. 2). In this way, it was possible to calibrate the system directly in terms of the number of helium atoms introduced into the analyzer. The pressure exerted by the gas sample after being expanded into the analyzer, was monitored by the same ion gauge (IG4) used for the dynamic calibrations, to compare the results. Figure 5 shows the consistency of these two calibrations.

Preliminary tests with a roughly 50% ^{4}He-D_2 mixture were also carried out, to investigate the feasibility of quantitative analysis in the high resolution mode. The mixture was prepared by first replenishing a previously evacuated stainless steel gas bottle (≈ 300 cc) with pure ^{4}He, at a pressure of about 0.4 tor (as measured by the baratron gauge BG1). An almost equal amount of deuterium was then added. The gas mixture was finally introduced into the analyzer through the dosing valve, while pumping by means of the turbomolecular unit. The partial pressures of the two components were estimated, dividing the measured intensities of the two peaks by the corresponding sensitivities previously obtained by calibrating the system with pure gases, and accounting for the relative sensitivities of the hot ion gauge (a conversion factor 6 for ^{4}He and 2.6 for D_2). The measured concentrations turned out to be about 54% of ^{4}He and 46% of D_2.

7. CONCLUSIONS

A new method for the detection of very small amounts of ^{4}He in a complex gas mixture has been proposed, using a NEG pump and a high resolution mass spectrometer.

The preliminary tests carried out with a facility built at ENEA Frascati demonstrate the feasibility of this new concept. Moreover, extensive calibrations performed with different gases in both "dynamic" and "pseudo-static" methods, clearly demonstrate the consistency of the results.

The proposed method preserves the initial helium content of the gas mixture, as well as that of other inert components. This feature has the potential of enhancing the helium detection limit, while ensuring the possibility of performing repeated tests on the same gas sample and to easily check against contamination from the environment.

8. ACKNOWLEDGMENTS

The authors whish to gratefully acknowledge the skilful contribution of Mr. F. Marini, who assembled the facility and constantly assisted us during the experiments.

9. REFERENCES

[1] M. C. H. McKubre et al. Proceedings of ICCF-3, Nagoya, Japan, p. 5 (1993)
[2] K. Kunimatsu et al. Proceedings of ICCF-3, Nagoya, Japan, p. 31 (1993)
[3] G. Preparata. QED coherence in matter, chapter VIII, World Scientific (1995). See also contributions by the same author to the International Conferences on Cold Fusion from 1 to 6
[4] A. Hofmänner et al. Paper presented at the 46th AVS Conference, Seattle, 1999

CHAPTER 2.

EXCESS HEAT AND CALORIMETRY

Conference Proceedings Vol. 70
"ICCF8"
F. Scaramuzzi (Ed.)
SIF, Bologna, 2000

ANOMALOUS EFFECTS INDUCED BY D_2O ELECTROLYSIS AT TITANIUM

M. BERNARDINI[1], C. MANDUCHI[2], G. MENGOLI[1] and G. ZANNONI[2]

[1]CNR IPELP, Corso Stati Uniti 4, 35127 Padova, Italy
[2]Dipartimento di Fisica dell'Università di Padova, via F. Marzolo 8, 35131 Padova

1 Summary

This investigation emphasizes the heat output (≈ 1 W) measured at open circuit after the electrolysis of 0.6 M K_2CO_3 in D_2O at Titanium. This thermal phenomenon then decayed slowly over the course of several days. "Post-mortem" γ-spectroscopy analysis of the Ti samples cathodized in D_2O evidenced transient γ-emissions which cannot be attributed to impurities of the electrolytic system.

2 Introduction

Since Fleischmann and Pons announced they had induced D-D fusion into a Pd lattice by electrolytic deuterium loading [1], it was speculated that the phenomenon might not be restricted to Pd only. Titanium soon appeared a viable alternative to Pd. Thus, the Frascati ENEA group first [2] and others later [3-5], after submitting the Ti – D_2 system to thermal cycles, were able to detect sporadic neutron emissions of energy compatible with D-D fusion. That the Ti lattice could constitute a suitable host for low energy nuclear reactions of hydrogen isotopes is also stressed by recent reports on D^+ implantation onto TiD_2 targets [6-8], whereby unpredicted fusion channels would operate in the solid and thereby greatly enhance the fusion rates.

But what about the induction of nuclear phenomena at Ti by D_2O electrolysis? To address this question, much careful work has been performed by Sanchez and his group [9-10] but without definitive results, due probably to the difficulty of the Ti-water system.

Water discharge at a Ti cathode can lead to Ti hydride formation in acid media [11], where evolving hydrogen directly interacts with the bare metal. Indeed, several reports qualitatively account for Ti hydride formation from acidic electrolytes, whereas hydriding seems hindered at pH ≥ 9 [12]. However, the extent and penetration of the electrolytic reaction are expected to be very low, as indeed confirmed by Escarpizo *et al.* [10].

The efficiency of electrolytic hydriding could therefore be increased by operating at temperatures near boiling, but not in acid electrolytes owing to the possible dissolution of Ti at open circuit. Here we have chosen to perform the electrolytic experiments at temperatures near boiling (95° C) by using a relatively mild alkaline electrolyte (0.6 M K_2CO_3 in D_2O, pD=11.3), wherein the metal is stabilized by surface oxides.

3 Experimental Procedures and Results

3.1 Electrochemical tests

Ti foils (purity $\geq$ 99.5%, 0.02-0.07 cm thick) were supplied by Goodfellow, Johnson Matthey and a local producer. The typical Ti sample working electrode was a square with area of 1.5 cm^2; the counter electrode was a Pt coil; the reference was Ag|AgCl KCl sat. The Ti sample was charged galvanostatically by I = −200 mA for periods $\geq$ 24 h, either at 25° C or at 95° C, while a continous N_2 draft removed the electrolysis gas from the cell.

At electrolysis interruption, we observed the relaxation with time of the open circuit electrode potential and accordingly divided the various Ti samples into three groups: two groups that gave totally different responses and one group that gave intermediate response.

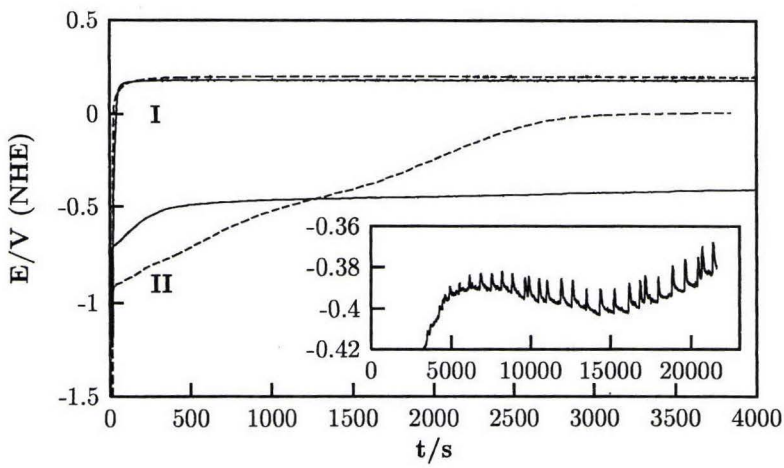

Figure 1: Ti electrode potential transients following the electrolysis interruption

Figure 1 illustrates the two limit behaviours at 25° C (broken curves) and 95° C (plain curves) of two samples I and II. For sample I at both temperatures, electrolysis interruption was followed by a fast potential increase to attain the potential of TiO_2 [11].

For sample II, at 25° C the potential of TiO_2 was eventually achieved after a slowly increasing potential transient, whereas at 95° C the rate of potential increase dropped with fluctuations and oscillations, as the insert of Figure 1 shows. We associate the

behaviour of Sample II with the decomposition (by corrosion) of a bulk hydride phase, the formation of which had occurred much more efficiently at 95° C than at 25° C.

3.2 Calorimetry

The calorimetric runs were carried out at 95° C [13-14]. The core of the calorimetric system was a Dewar electrolytic cell equipped with a refrigerated column to condense the vapour. In addition to the (Ti) cathode and (Ni) anode, the cell was further equipped with a Pt 100 thermometer, a NiCr resistance heater and a glass pipe conveying a controlled N_2 flow ($3.5\,cm^3\ min^{-1}$) into the electrolyte to ensure homogeneous heat distribution.

The cell, filled with 100 ml of 0.6 M K_2CO_3 in D_2O and immersed in a silicon oil bath kept at $95 \pm 0.01°$ C by a Hake F3 thermostat, was made isothermal with the bath by supplying continuously the power required for NiCr resistance. In the experiment detailed below we have chosen to measure the free temperature increments (above 95° C) and convert them into power through repeated calibrations (typical cell constant was $2.0 \pm 0.1°\,C\,W^{-1}$).

Figure 2(a-d) accounts for the evolution with time of the calorimetric response during electrolysis at a Ti cathode from the same batch of sample II (1.2 cm × 2.5 cm × 0.07 cm). The left ordinate gives, with accuracy ±0.1° C, the increment in temperature of the electrolyte (continuous line). The right ordinate gives, with accuracy ±0.1 W, the power correspondingly determined by the cell constant. The accuracy of this datum is lower than that of the thermometric readings since we considered the range 95-97° C, $\Delta T/°$ C linear with P/W. The two broken lines indicate $(E-1.52\,V)\times I$ (*i.e.*, electrolytic joule power - - - -) and $E \times I$ (*i.e.*, total electrolysis power — · —) fed to the cell.

Note therefore that as soon as the electrolysis was initiated (Fig 2a) firstly with I = −75 mA, the electrolyte temperature quickly increased well above the provisions of the Joule effect to then exhibit a smooth decline. This latter trend was reversed by applied -250 mA (Figure 2b) and a temperature jump occurred at electrolysis interruption.

Figure 2a

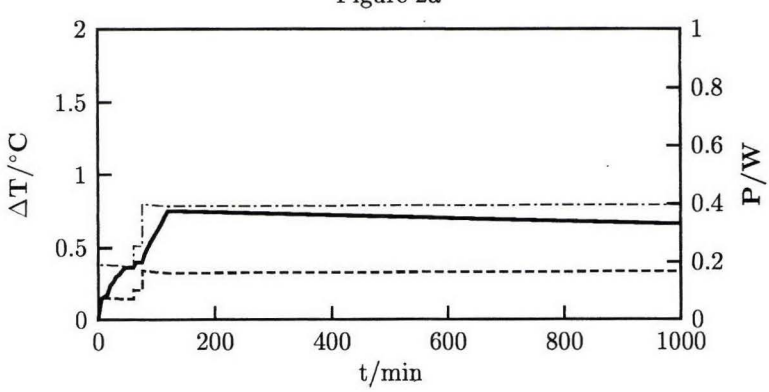

Figure 2b

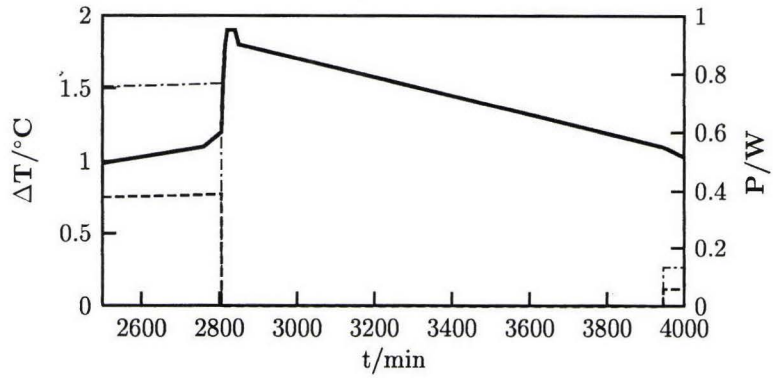

Figure 2c

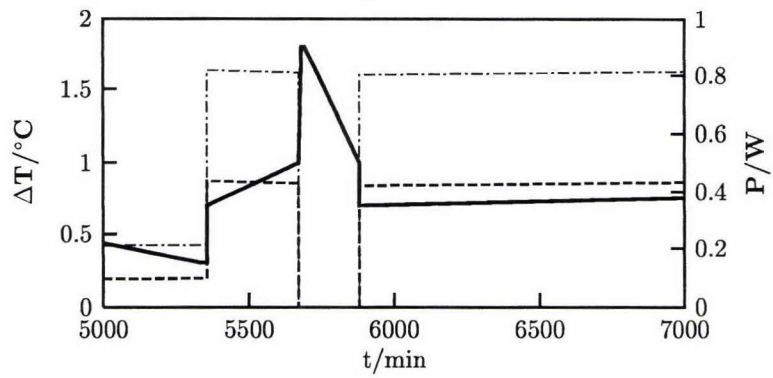

Figure 2d

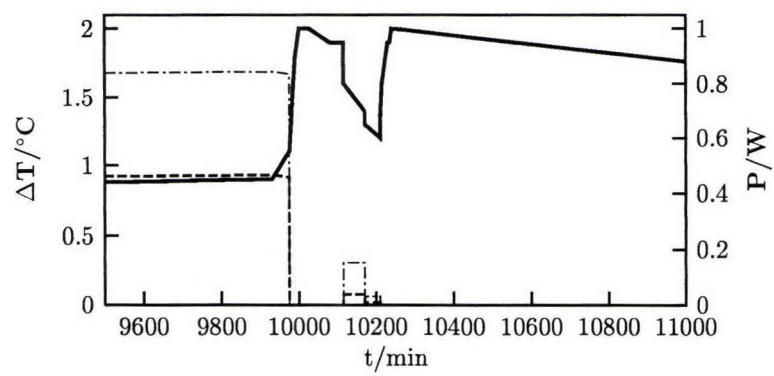

Figure 2: Evolution with time of the calorimetric response.

The relaxation time of the thermal phenomenon (days) clearly had nothing to do with the Dewar cell heat loss characteristics. Upon applying I=-50/-75 mA for $\approx$24 h, the temperature steadily declined as if the thermal phenomenon had been totally quenched (Figure 2c). With I = -250 mA the electrolyte temperature rose, and later, at a new electrolysis interruption, the thermal effect then relaxed much more quickly than before. At this stage, -250 mA were applied for another 3 days (Figure 2d) and when the electrolysis was stopped, the thermal output at open circuit appeared remarkably steady (although it could easily be quenched by applying even - 15 mA as Figure 2d shows). Since then, the spontaneous relaxation of electrolyte temperature required several days, whereby some hundred Kj supply from an unknown source can be inferred.

3.3 γ-Spectroscopy equipment and procedure

To establish whether the anomalous heat release could have involved other anomalous effects such as nuclear transmutations to meta-stable nuclides, some Ti samples (of typical dimensions 4.5 cm $\times$ 1.5 cm $\times$ 0.02 cm) submitted to D_2O (H_2O) electrolytic discharge, were then ("post mortem") examined by γ-spectroscopy, by using two high-resolution Ge γ detectors working in coincidence (Fig 3).

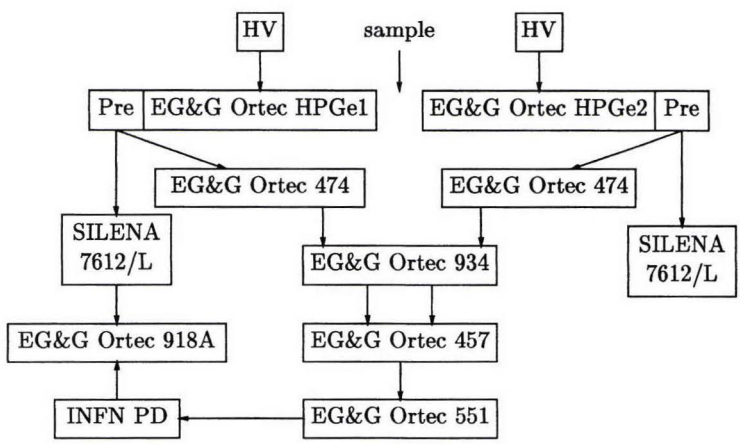

Figure 3: Scheme of the gamma-gamma coincidence system utilizing two Ge detectors.

The linear signals from the amplifiers were first shaped to the best energy resolution (time constant = 6 μs), then amplified and finally sent to the multi-channel analyser for spectral analysis. The analyser accepted the detected signals only when they were above a threshold energy value ($\approx$800 keV) and in coincidence within a pre-fixed resolution time (< 500 ns).

The former condition was controlled by the constant fraction discriminators. The second condition was verified by the time-amplitude converter. The signal from this converter was synchronized with the linear signal entering the analyser in coincidence mode. Energy calibration of Ge detectors was systematically performed both before and after the spectroscopic experiments, by using six lines of the natural background (^{208}Pb,^{228} Th,^{214} Po). In the γ measurements, the maximum deviation was in the range 0.14 – 0.19 keV, whereas the error due to electronics could have reached 0.27 – 0.38 keV.

4 γ-Spectroscopy results

A Ti sample, cathodized some weeks in light water, was examined as preliminary experiment; this constituted the blank for the other experiments.

As γ-cascade source, we have considered the hypothetical occurrence of the nuclear reation

$$^{47}\mathrm{Ti} + \mathrm{H} \rightarrow [\text{intermediate state}] \rightarrow ^{48}\mathrm{V} + 6830\,\mathrm{keV} \quad (1)$$

whereby β^+/EC unstable ^{48}V originates ^{48}Ti*, which then decays to the ground ^{48}Ti state with the two γ photon emissions [15].

After monitoring this sample for over one week, 45 d after the end of the electrolysis, no peak was detected. For the Ti sample cathodized in heavy water, we hypothesized the nuclear reactions producing γ cascades to be:

$$^{48}\mathrm{Ti} + \mathrm{D} \rightarrow [\text{intermediate state}] \rightarrow ^{46}\mathrm{Sc} + ^{4}\mathrm{He} + 3891\,\mathrm{keV} \quad (2)$$

$$^{50}\mathrm{Ti} + \mathrm{D} \rightarrow [\text{intermediate state}] \rightarrow ^{48}\mathrm{Sc} + ^{4}\mathrm{He} + 3686\,\mathrm{keV} \quad (3)$$

The half-life of ^{46}Sc (reaction 2) is 83.81 d and the γ cascade to ^{46}Ti ground state is constituted by two photons of energy equal to 889.277 and 1120.545 keV respectively [15]. The half-life of ^{48}Sc (reaction 3) is 43.7 h and γ cascade to ^{48}Ti consists of γ photons of energy equal to 983.524 keV, 1037.522 keV and 1312.050 keV respectively [15].

In Experiment A, we examined a Ti sample cathodized for 20 d, which eventually showed 0.2 - 0.3 W heat output at open circuit. The sample was placed in the γ spectrometer 8 d after the end of the electrolysis, whereby only the occurrence of reaction (2) was investigated.

Table 1: γ-Spectroscopy Results

Experiment		Length (s)	Energy (keV)		Counts
			Expected	Measured	
A	Run 1	934000	889.277	890.26±0.34	21±7
			1120.545	1122.91±0.35	22±5
	Run 2	647000	889.277	889.55±0.31	4±8
			1120.545	1121.17±0.36	7± 6
B		163000	983.254	982.85±1.24	8±5
			1037.522	1036.44±0.32	17±4
			1312.099	1308 ≈ 1316	4±4

The measure consisted of two spectra acquisition runs lasting 11 d (run 1) and 8 d (run 2), with a 70 d interruption between each run. The data reported in Table I were obtained by a MAESTRO II search program which automatically identified peak energy and area. Compared to the blank, the peak area in run 1 resulted from 3 to 4 standard deviations, whereas in run 2 the said peaks decreased to $\approx$ 1 standard deviation.

In Experiment B, a Ti sample, again cathodized in D_2O for 20 d (excess heat production of ≈ 0.2 W), was introduced into the γ-spectrometer (≈ 2 h later) and monitored for 46 h.

Two of the three expected lines (983 and 1037 keV) were found and metered by the automatic research system (cf. Table I), while the 1312 line was estimated by us, with reference to the backgrounds. The intensity of the automatically detected lines ranged from 4.2 to 1.6σ and was seen to fade by the end of the measurement.

From the data of Table I, corrected for γ-spectrometer efficiency, the radioactivity of either ^{46}Sc or ^{48}Sc was extrapolated to a hypothetical steady state between production and decay to obtain the respective values of $6.5(\pm 1.8)\times 10^{-2}s^{-1}$and $3.2(\pm 0.9)\times 10^{-2}s^{-1}$.

Acknowledgments

The authors wish to thank C. Baiocchi and Profs. F. Gramigna, F. Brandolini, M. Nigro of INFN-Legnaro for making possible our γ-spectroscopy investigation. Thanks are also due to Torresin s.r.l for the Ti supply and to the INFN group of Trieste for the loan of a data acquisition system.

References

[1] Fleischmann M. and Pons S., J. Electroanal. Chem., 261, (1990) 301.

[2] De Ninno A., Frattolillo A., Lollobattista G., Martinis L., Martone M., Mori L., Podda S., and Scarammuzzi F., Nuovo Cim., 101, (1989) 841.

[3] Menlove H.O., Fowler M.M., Garcia E., Miller M.C., Paciotti M.A., Ryan R.R. and Jones S.E., J. of Fusion Energy, 9(4), (1990) 495.

[4] Bressani T., Calvo D., Felicello A., Lamberti C., Iazzi F., Minetti B., Cherubini R., Hague A.M.I., and Ricci R.A., Nuovo Cim. A, 101, (1991) 1413, 1587.

[5] Botta E., Bressani T., Calvo D., Felicello A., Gianotti P., Lamberti C., Agnello M., Iazzi F., Minetti B., and Zecchina A., Nuovo Cim. A, 105, (1992) 1663.

[6] Kasagi J., Ohtsuki T., Ishii K., and Hiraga M., J. Phys. Soc. Japan, 64, (1995) 777.

[7] Takahashi A., Iida T., Miyamaru H., Fukuhara M., Fusion Tech., 27, (1995) 71.

[8] Takahashi A., Iida T., Miyamaru H., Fukuhara M., Fusion Tech., 34, (1998) 256.

[9] Sevilla J., Escarpizo B., Fernandez F.J., Sanchez C., Fusion Tech., 19, (1991) 188.

[10] Escarpizo B., Fernandez F., Sevilla J., Cuevas F. and Sanchez C: in The Science of Cold Fusion, Proceedings of the Second Annual Conference on Cold Fusion, Como June 29-July 4, 1991, edited by T. Bressani, E. Del Guidice and G. Preparata, 33 (Società Italiana di Fisica) 1991, p. 15.

[11] Pourbaix M., Atlas D'Equilibres Electrochim. (Gauthier-Villars, Parigi) p. 213.

[12] Mizuno T. and Enyo M., in Modern Aspects of Electrochemistry, edited by R.E. White et al., Vol. 30 (plenum Press, New York) 1996, p. 415.

[13] Mengoli G., Bernardini M., Manduchi C., Zannoni G., J. Electroanal. Chemistry, 444, (1998) 155.

[14] Mengoli G., Bernardini M., Manduchi C., Zannoni G., Nuovo Cim., 20D, (1998) 331.

[15] in Nuclear Data Sheets, ed. J.K. Tuli, (Academic Press, New York-London) 1977-1986.

Conference Proceedings Vol. 70
"ICCF8"
F. Scaramuzzi (Ed.)
SIF, Bologna, 2000

THE FLEISCHMANN-PONS EFFECT IN A NOVEL ELECTROLYTIC CONFIGURATION

E. Del Giudice, A. De Ninno, A. Frattolillo, G. Preparata[1], F. Scaramuzzi, A. Bulfone, M. Cola, C. Giannetti
ENEA C.R. Frascati, via E. Fermi, 45, 00044 Frascati (Rome), Italy

ABSTRACT

We have designed a new type of cell, containing a thin film Pd cathode deposited on a glass substrate in a "bustrophedic pattern" (width $w = 5\times10^{-3}$ cm, length $l = 100$ cm, and depth $d = 0.5\text{-}2\times10^{-4}$ cm). Such cathodes have a resistance of several kΩ's. In addition to the usual potential difference V_{ac} between anode and cathode, the electric configuration has a further potential difference V_{cc} applied across the cathode. This set up has been designed in order to test a new effect, the Coehn-Aharonov effect. This effect is established in a coherent quantum system, such as that of the D-plasma inside the Pd, due to the turning of the electric into an electrochemical potential, thereby greatly enhancing the loading capability of the electrolytic system.

1. INTRODUCTION

A long sequence of replications (1) of the original Fleischmann-Pons (FP) (2) production of excess heat released by Pd cathodes loaded with deuterium in electrolytic cells has firmly established the existence of a critical loading:

$$x_c = (D/Pd)_c \qquad (1)$$

Thus, excess heat can be revealed only for $x > x_c$ only. These experiments point to the value of $x_c = 1$, as predicted theoretically (3) at an early stage of this research. This high value of x_c has been the cause of a number of the failures in replicating the original FP experiments; loading is thus the decisive factor in producing excess heat.

In 1993 Preparata proposed that a voltage drop applied across the cathode could enhance the loading significantly. This topic is the subject of the presentation (4) at this Conference; here we will give a brief outline. A physical system described by a unique wave function is able to detect an external e.m. potential since the potential is incorporated in the phase of the wave-function; in the case of the magnetic potential this gives rise to the well known Bohm-Aharonov effect (5). The experimental evidence indicates that when $x = 0.65$ the D-Pd system undergoes a phase transition from the usual β-phase to a γ-phase at room temperature, where deuterons migrate from the octahedral to the tetrahedral sites of the Pd lattice and where they can enter into a coherent plasma oscillation. This coherent state of the nuclei fits the above

[1] *Giuliano Preparata died the 24th of April, 2000. We remember him for his passion in the daily experimental work and his generosity in teaching us, day by day, that a physicist is not just an expert of the laws of nature, but is primarily a philosopher fascinated by the laws of nature.*

quantum conditions so that an externally applied electric potential affects the chemical potential of the deuterons. As a consequence we should be able to decrease the chemical potential of deuterons in the γ-phase, host of the D-Pd system, by applying to the cathode a negative potential sufficiently large to transform the cathode into a sink with respect to the electrolyte solution (or, more generally, with respect to the environment). This effect differs from the usual electromigration since it implies a transverse attractions of deuterium into the cathode, with respect to the direction of the field (see Fig.1).

However the application of a voltage across the cathodes of conventional geometry will produce a flow of current, and thereby induce Joule effect which can destroy the coherence. To reduce this adverse effect as much as possible the electrical resistance of the cathode must be made as large as possible. Thus the only viable cathodes are one-dimensional, having a great length and a narrow cross-section. In previous experiments wires having a diameter of 50 μm have been used and energy gains up to 100% have been obtained (6,7,8).

In the present experiment a further reduction of the cross-section has been achieved by using deposited strips of Pd on inert surfaces. These strips have a width of 50 μm and a thickness of 2 μm, the total length being about 1 m. In this way an extra order of magnitude in the resistance has been achieved, decreasing by the same factor the Joule thermal heating.

We present here the first stage of this ongoing experiment.

2. ELECTROLYTICAL LOADING OF A "BUSTROPHEDIC" DEPOSITION

The electrolytic cell is very compact and easy to assemble (see Fig.1b). The maximum external diameter is 8.5 cm. Different types of materials have been used, from Teflon to a thermal hardening resin known as Cybatool. The cell is equipped with a Pt-100 thermoresistor to measure the temperature of the internal volume (a few cm^3) and sits in a thermostat regulated to better than 0.1°C in order to perform a

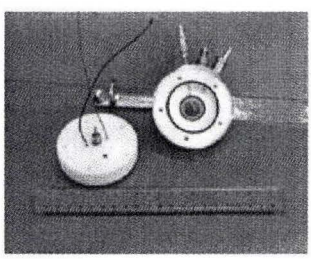

Fig. 1 - The cathode geometry and the cell assembly:

a) The bustrophedic cathode. Six pads have been used to measure independently the resistance of 5 sections of the cathode.

b) The electrolytic cell can hold 1.5 cm^3 of LiOD solution. The Pt anode is welded to one of the two shells, while the Pd cathode is deposited onto a glass contained in the circular housing in the diagram

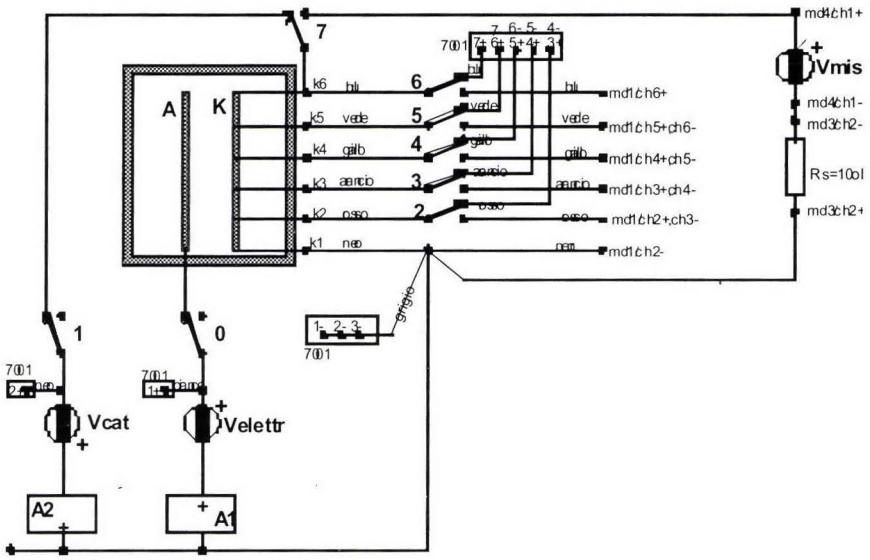

Fig. 2 - Electrical layout of the experiment. The mismatch between the two circuits is based on the opening of relays 1 and 0 when 7 is closed and vice versa; k_1, k_2, ... k_6 are the contacts on the cathode pads (see Fig.1a), the resistance is read as the voltage between two neighboring contacts.

calorimetric measure with a very high accuracy. The cathode is a Pd film sputtered in a UHV chamber onto Vycor glass. In order to prevent detachment of the Pd film from the substrate during loading, a very thin (few hundreds angstroms) Cr "buffer" layer has been deposited below the Pd. The pattern (Fig.1a) has been obtained with photolithographic techniques.

We are interested in studying the loading along the cathode in order to observe the concentration profiles due to the voltage drop across the cathode itself. We have therefore divided the sample into 5 successive segments and have monitored the resistance of each segment. A relay bank allows the separation of the electrolysis circuit during the DC resistance measurement (see Fig.2 for details). The interruption in the electrolysis current is limited to 50 ms. We have observed that such short interruptions do not affect the loading process: in fact, de-loading starts only if the interruption lasts for several hundreds of milliseconds. A computer based program acquires data at chosen time intervals, typically every 10 seconds.

The circuit was equipped with an additional voltage generator to supply an independent extra voltage across the cathode (V_{cc}).

A typical pattern of loading in a 10^{-4}M LiOH solution is shown in Fig. 3. It is clear that there is a delay in loading the less cathodic sections. The rate of loading increases as the sections approach the negative terminal of the voltage supply. In these particular experiments the extra-voltage V_{cc} was switched off. A noticeble feature is that the R/R_0 peak has a value lower than the bulk value reported in literature, which is 2. A change in the electrolyte resistance during the experiment cannot explain such behaviour. In fact, in strong electrolytes the molar conductivity is approximately proportional to the square root of the concentration (Kohlraush's law), while we can

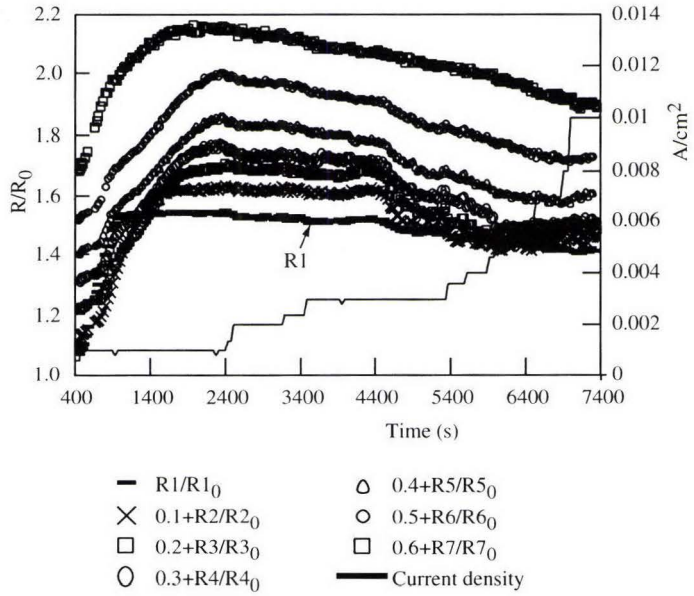

Fig. 3 - Loading curves of different sections of the cathode in LiOH 10^{-4}M solution. The section referred to as "R1" is connected to the negative terminal of the voltage supply. (In this experiment the deposited pattern was divided in 7 rather than 5 sectors, as in Fig. 1)

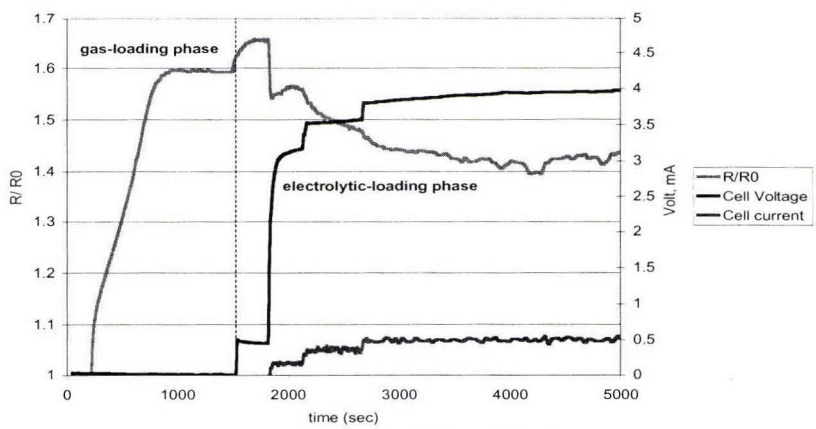

Fig. 4 - Comparison between gas loading and electrolytic loading in the same sample: LiOD solution was added into the cell at the end of the gas loading at 1.2 bar.

assume a linear law for very dilute solutions, as in our case. A shift from $R/R_0 = 2$ (Baranowskji's peak value) to $R/R_0 = 1.65$ (measured value) should be produced by a decrease of the electrolyte resistance of 100%. However, we have measured the conductivity of the solution after a long (4 days) electrolysis at 10 mA, and we found a decrease from 104 ± 1 to 94 ± 1 μS/cm. Gas loading experiments, aimed to check this behaviour, have given the same maximum value ranging from $R/R_0 = 1.65$ to 1.70

(see Fig.4). Thus, we deduce that there must be a physical meaning for this unexpected behaviour.

Our samples have been produced by an ion-assisted sputtering technique. The X-ray diffraction analysis shows a (1,1,1) orientation on the surface with a small tilt of 5° out of plane. The average defect-free crystal volume is about 180 angstrom thick and defects (dislocations) are mainly parallel to the surface. Since the Pd β-phase is characterised by a coherence domain (3) almost spherical in shape, going to one dimension can disturb the coherence of the phase, determining the reduction of the potential wells in the octahedral sites and a decrease in depth of the tetrahedral wells. This in turn leads to an increase of the chemical potential of the electrons. The increase of chemical potential of the β-phase has the effect to shift the crossing point between the curves towards smaller values of x, which means that the γ-phase starts to nucleate at lower concentrations (4). Since the maximum of the Baranowskji's curve can be assumed as the starting point of the γ-phase, we can now understand why the behaviour of thin films is different from that of bulk samples.

In order to evaluate the role of geometry on the sample behaviour, we have compared the loading of a bustrophedic film with that of an electrode of large area deposition obtained with the same sputtering procedure. Using a comparable current density we were not able to "drive" the sample over the maximum of the loading curve in the latter case. In fact, as soon as the current was switched off, the resistance started to decrease.

With the present configuration we were able to reach, in a reproducible way, concentrations as high as $x = 1$ with very low currents (up to a few mA) in very short times (few thousands of seconds). This allowed us to investigate highly loaded samples of Pd-D in a series of experiments aimed to improve the understanding of the physics of this system (9,10).

3. CALORIMETRY

The evaluation of the power dissipated in the cell has been obtained, as usual, through a linear calibration. A measured Joule heating power has been dissipated in the cell and the corresponding increase of the temperature, measured with a Pt-100 sensor dipped into the solution, has been used to calculate the thermal constant of the cell, k. A typical figure is $k = 181 \pm 5$ mW/°C. The thermal stability of the cell, housed in a thermoregulated box is about 0.01°C. Of course, this figure depends very closely on the chosen geometry and on the materials of construction, and can vary from experiment to experiment. We therefore need a very accurate procedure of calibration before each experiment.

We have observed that, whenever $x \cong 1$ is reached, an extra-power is generated inside the cell with an intensity proportional to the concentration (see Fig. 5). In this way we have measured excess specific rates of enthalpy generation of $1 - 2$ kW/cm^3. This figure corresponds to absolute values of the order of tens of milliwatts because of the very small volume of the cathodes ($V_{deposition} = 25 \times 10^{-6}$ cm^3).

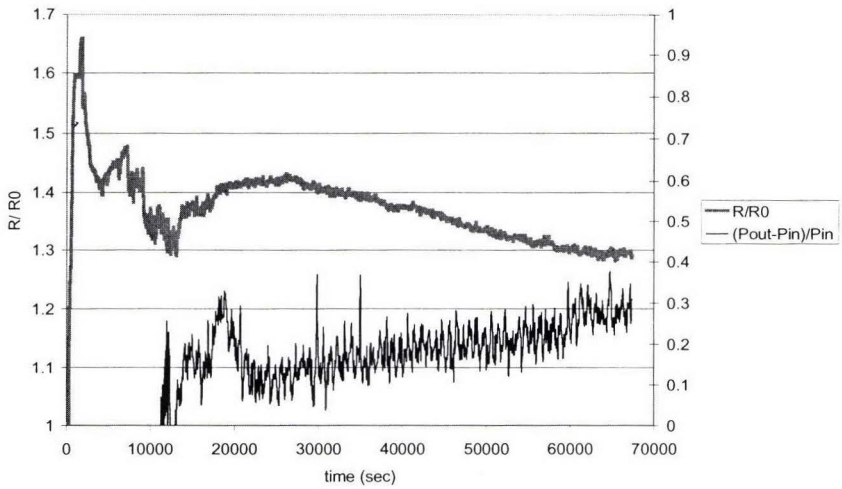

Fig. 5 - Excess power measured during the experiment quoted in fig.4 . The input power was about 60 mW.

One of the key problems for the use of this configuration is the fragility of the cathodes. In fact, the overloading of the sample affects its lifetime, and some of the experiments fail because the cathode breaks. We have tried to solve the problem by using a different experimental set up in which the electrolytic solution flows through the cell in a circuit containing a reservoir at constant temperature. The calorimetry was performed by measuring the difference between the output and the input temperature of the solution. It turned out that the motion of the electrolyte with a velocity comparable to the velocity of the ions in solution can severely affect the loading process. For this kind of small cells the static configuration is therefore most appropriate; the problem of the film overheating has to be solved by increasing the thermal transfer to the substrate.

One further aspect which should be emphasized is that the assumption of a stationary thermal regime inside the cell should not be used. Such an assumption, which allows us to use the linear calorimetry approximation, is probably correct in most of the cases under study when the power dissipated in the cell is small, i.e., the average or the local temperature in the cell does not change appreciably. For the case of large heat generation in the cathode, there will be a strong increase of the temperature near the cathode surface, with the possible formation of a film boiling layer that changes the heat transfer towards the solution. In this condition the thermal constant of the cell will be obviously changed with respect to the stationary conditions. The only reliable method, as stressed both by Martin Fleischmann and Giuliano Preparata, is the isoperibolic calorimetry (6). The method consists in supplying small, well known, amounts of power at definite time intervals, and in monitoring the consequent variations of temperature. This correlation allows us to determine the cell heat transfer coefficient as a function of temperature and time. We have started to analyse our experiment also in the light of these considerations.

4. CONCLUSIONS

The approach used in this experimental campaign was aimed to study the role of the cathode geometry in the deeuterium loading process. We have found that concentrations with x higher than 1 could be obtained easily and in short times in most of the experiments by using thin films. We also have observed an interesting deviation from the Baranowskji's behavior for the R/R_0 versus x graph. We relate this feature to the metallurgic structure of our samples. We have checked this behavior in the case of gas loading also, in order to validate the measurement procedure in electrolysis, obtaining the same R/R_0 versus x behavior.

The peculiar design of the cathode has allowed us to test the so called "Coehn-Aharonov" effect, studying the influence of an electric potential on the chemical potential as in the case of coherent quantum systems. We have observed that the voltage drop across the cathode itself appears to enhance the loading of the Pd film in the most cathodic regions. A very different behavior was observed in an extended sample, without the "bustrophedic" structure, even if made under identical deposition conditions and loaded with the same electrolysis parameters. We have never observed a clear effect of the additional power supply on the loading (V_{cc}), probably because of the competitive Joule heating effect which spoils the coherence inside the metal and favors the de-loading.

Excess rates of enthalpy generation of the order of tens of milliwatts have been measured as soon as the average loading exceeded the threshold $x_c = 1$. Considering the dimensions of the cathodes this figure corresponds about to 1 kW/cm^3.

The experimental set up described in this paper has been limited to demonstrating the effect. We believe that in order to increase the excess power generated by such electrolytic cells a multiple system has to be realized, based on many replicas of the basic cell. The first step of this program is the management of the loading procedure and of the heat measuring system.

In order to achieve the total characterization of the physical phenomena underlying cold fusion, we have started a program on the analysis of ^4He, as a nuclear product of the fusion reaction between two deuterium nuclei. The experimental technique has been presented in this Conference (11). Preliminary results show that the method used has a detection sensitivity which allows the use of the measured number of ^4He atoms to evaluate the rate of nuclear reactions, thereby giving a further confirmation of the calorimetric experiments.

ACKNOWLEDGMENTS

We wish to warmly acknowledge the skill and enthusiastic work of Mr. Fabrizio Marini, who designed and realized the electrolytic cells, and of Mr. Luigi Verdini, who contributed to the elctric set up of the measurement and to the data acquisition process.

BIBLIOGRAPHY

1. Proceedings of the ICCF Conferences
2. M. Fleischmann, S.J. Pons, Journal of Electroanal. Chem., 261, 301 (1989)
3. G. Preparata, 3rd International Conference on Cold Fusion (ICCF3), Nagoya, Japan (1992)
4. M. Cola, E. Del Giudice, A. De Ninno, G. Preparata, this Conference
5. Y. Aharonov, D. Bohm, Phys. Rev. 11, 485 (1959)
6. G. Preparata, M. Scorletti, M. Verpelli, Journal of Electroanal. Chem., 411, 9 (1996)
7. G. Preparata, 6th International Conference on Cold Fusion (ICCF6), Toya, Japan (1996)
8. E. Del Giudice, Workshop on "New Energy from Hydrogen", ENEA Frascati, May 28-29 (1998)
9. R.G. Agostino, R. Filosa, V. Formoso, G. Liberti, A. De Ninno, this Conference
10. E. De Giudice, A. De Ninno, A. Frattolillo, G. Preparata, F. Scaramuzzi, P. Tripodi, this Conference
11. A. De Ninno, A. Frattolillo, A. Rizzo, F. Scaramuzzi, C. Alessandrini, this Conference

Conference Proceedings Vol. 70
"ICCF8"
F. Scaramuzzi (Ed.)
SIF, Bologna, 2000

EXCESS POWER PRODUCTION FROM PLATINUM CATHODES USING THE PONS-FLEISCHMANN EFFECT

Edmund Storms

Energy K. Systems, 2140 Paseo Ponderosa, Santa Fe, NM 87501

ABSTRACT

Excess power was produced using a platinum cathode. Efforts to produce active cathodes by plating palladium onto various metals were largely unsuccessful.

INTRODUCTION

Palladium has been the cathode of choice since Pons and Fleischmann made their original claims. Occasionally, anomalous energy has been claimed to result from other elements such as Pt[1; 2], Au[3], Ti[4]. Thin layers of palladium on various inert substrates have also been claimed to produce anomalous energy [5; 6; 7; 8]. From this collection of experience, one might conclude that any layer of Pd made to stick tightly to the surface of another material would produce energy with greater ease than the bulk metal. This assumption has been found to be false even though such material can achieve a D/Pd ratio greater than 1.5[9]. Layers of electroplated Pd can be just as difficult to reproduce as bulk material. Although several successful samples were made, this paper will describe only one example of uncoated platinum which produced excess energy after being electrolyzed for an extended time in LiOD+D_2O.

EXPERIMENTAL

Calorimeter Design:

The calorimeter, shown in Fig. 1, consists of a Pyrex glass cell surrounded by a water-cooled jacket. This assembly is contained in a vacuum dewar, thereby allowing most of the energy lost through the lid to be picked up by the cooling water. A magnetic stirrer is used to stir the electrolyte, thereby reducing temperature gradients. The entire assembly along with all reference resistors is contained in a constant temperature environment. Table I lists values and uncertainties for the various quantities.

The cell contains three linear thermistors within the electrolyte, one near the top of the solution, one near the bottom, and the third just above the cathode. The anode is equidistant (0.5 cm) from the flat plate cathode (1 cm x 2 cm x 0.01 cm). Temperature of distilled water flowing through the jacket is measured just as it enters the jacket and just as it leaves. Data are recorded every 15 min. using a National Instruments data acquisition system after averaging 15000 values. The flow rate is measured by allowing the water, after it leaves the calorimeter, to fill a container on a balance while the weight and time are recorded every 120 sec. In addition, the cell contains a Pt-coated-carbon recombiner catalyst and an bare Pt wire heater within the solution for calibration. Luggin capillaries allow the voltage between a platinum reference electrode and the cathode to be measured. Because the cell is gas-tight and connected to an oil reservoir, any gas generated within the cell can be detected by weighing oil displaced onto a balance. Samples can be quickly changed or replaced by an inert cathode for calibration. Lengthy studies of inert platinum show a stability of ±75 mW.

Calibration and Error

A typical calibration for the flow-mode is shown in Fig. 2, using a clean piece of platinum for the cathode. Values are taken both going up and going down in applied power in

the same manner as the sweeps described later. The standard deviation of the electrolytic values from the least-squares line is ±30 mW which is the same as the standard deviation from a constant value when stable excess energy is being observed at low applied power.

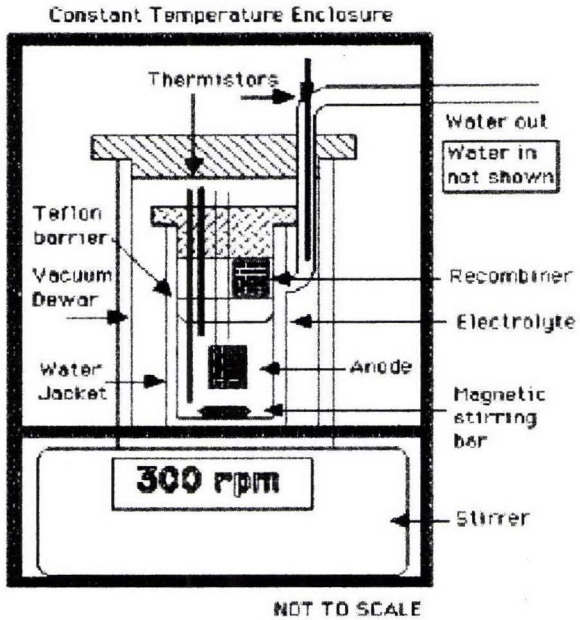

Figure 1. Drawing of the calorimeter. The electrolyte is 65 ml of 0.3 N LiOD and the anode is Pt mesh. The cell lid is Lucite and the Dewar lid is expanded foam insulation. All thermistors are glass covered. Time to reach a steady temperature is 50 min.

TABLE I
Summary of uncertainties in measured quantities

Water temperature entering the jacket = 20±0.02°
Environment temperature = 20±0.03°
Flow rate = 31.00±0.05 g/min (long term variation)
Precision of current measurement = ±<0.001 A
Precision of voltage measurement = ±<0.001 V
Precision of temperature measurement = ±<0.005°
Absolute accuracy of temperature measurement = 0.1°
Stirring rate = 300 rpm ± 1 rpm
Average heat capture efficiency = 98±0.5%

This scatter increases to ±0.1 W at the upper limit of applied power (27 W). A zero drift as much as -0.05 W has been observed over an extended time. Consequently, changes in excess energy production are more accurate than absolute values. Good agreement between the electrolytic- and Joule-based calibrations shows that the location of heat production does not affect the accuracy of the device. Doubling the fluid flow from 22.3 g/min to 45.3 g/min caused a change in the calibration constant from 0.0732 W/degree-g/min to

0.0738 W/degree-g/min, indicating that good thermal mixing is achieved in the exiting cooling water. Because samples can be easily changed, the cathode is frequently replaced by clean platinum when the need arises, to recalibrate. Good stability is shown by a scatter of only ±1.6% in the calibration constant when measured many times over three months.

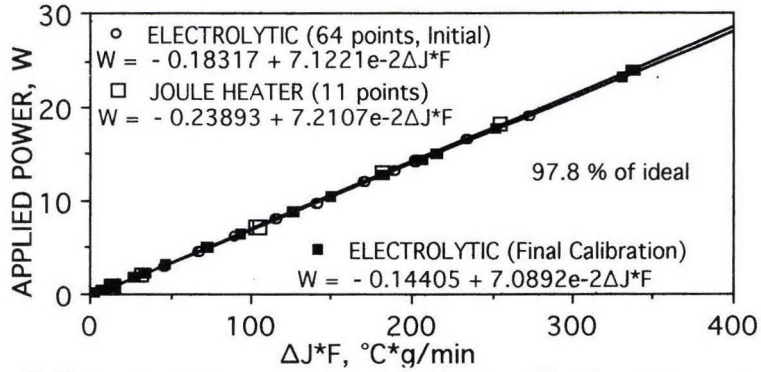

Figure 2. Comparison between electrolytic and heater calibrations before and after the study using the flow method. The heater and electrolysis agree within 1.2%.

The cell can also be used as a rough isoperibolic calorimeter by measuring the average temperature between the electrolyte and the cooling jacket. However, this method is not stable, in spite of active stirring, because of changes in convection within the electrolyte and within the jacket. Figure 3 shows how the average temperature across the cell wall changed between the first and final calibration using the electrolytic method and clean Pt.

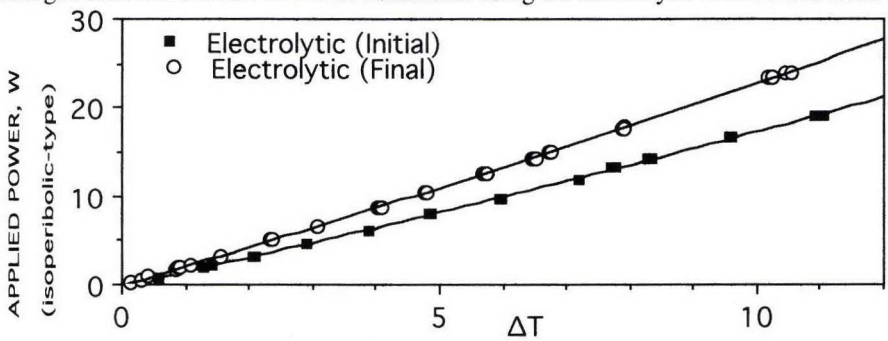

Figure 3. Comparison between applied electrolytic watts and the average temperature across the jacket for two calibration runs.

Excess Energy Measurement

Figures 4, 5, and 6 show the time history for excess power (EP) production using a platinum cathode which had been subjected to electrolysis for many hours without subsequent cleaning. Current sweeps consist of stepping the current up in value, waiting for the calorimeter to achieve steady-state (50 min), taking five values, and repeating the process. After reaching 3 A, the current is reduced in steps. Notice in Fig. 4 that the expected EP was achieved at 0.5 A and 1.0 A, but decayed away when 1.5 A was applied. A sweep taken after the decay showed very little EP. After the current was turned off for a brief time, the study was resumed in Fig. 5. Notice that the EP again gradually increased after 0.5A was applied. Sweep #3 again showed EP and this continued while 0.75A and

1.0A were applied. However, application of 1.5A again caused the EP to decay away. Once again the current was turned off. Application of 0.5 A, shown in Fig. 6, again produced EP. The calorimeter was calibrated at 430 h using the internal heater and later using an inert Pt cathode. This experience shows a consistent pattern of behavior which was repeated once again, but is not shown here.

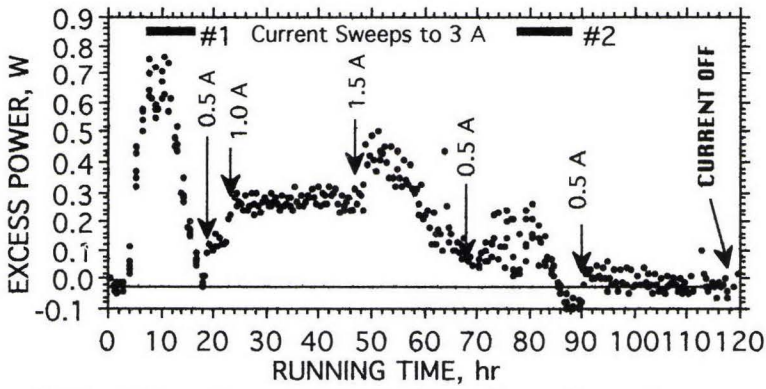

Figure 4. Time history of excess power production from a Pt sample.

The first sweep is shown as applied current vs EP in Fig. 7. Notice that excess power is indicated by the isoperibolic method during this initial sweep. Later sweeps do not show an effect because the calibration constant changed, as indicated in Fig. 3. Also notice that the excess power falls on a higher line upon reduction in applied current. Subsequent cycles, as shown in Fig. 8, produce excess power that falls consistently on this higher line which extrapolates to zero EP at zero applied current, in contrast to the behavior of palladium. Palladium requires a critical applied current before EP is produced because the leakage rate into the metal has to be overcome before the required critical composition can be achieved on the surface. Figure 9 shows the sweeps taken using different numbers of values to produce the plotted average and these are compared to values obtained using the heater as a calibration. Apparently, the measured EP is not affected by the number of points averaged.

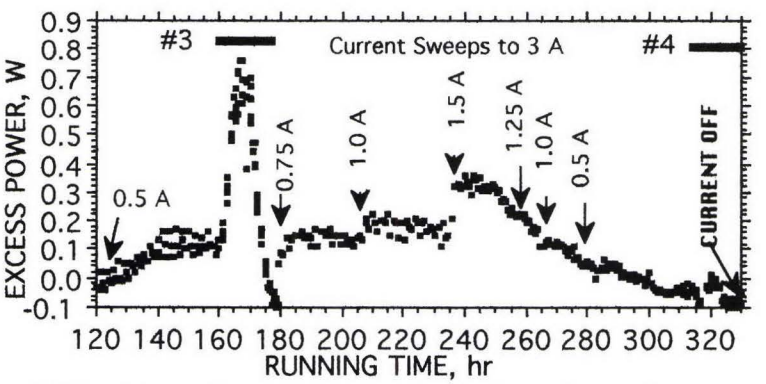

Figure 5. Time history of excess power production from a Pt sample.

DISCUSSION

A large average composition within the cathode is thought required to produce excess energy. Yet many researchers have failed to produce excess power after achieving large compositions, for example Nakata et al.[10]. Now, metals that do not even dissolve hydrogen are found to make excess energy. Clearly, additional variables are operating.

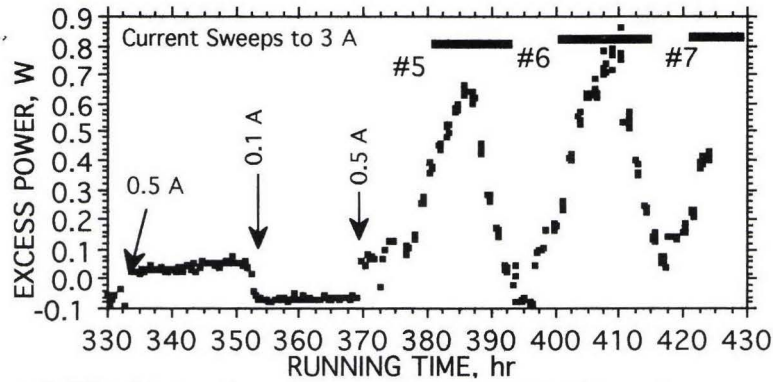

Figure 6. Time history of excess power production from a Pt sample.

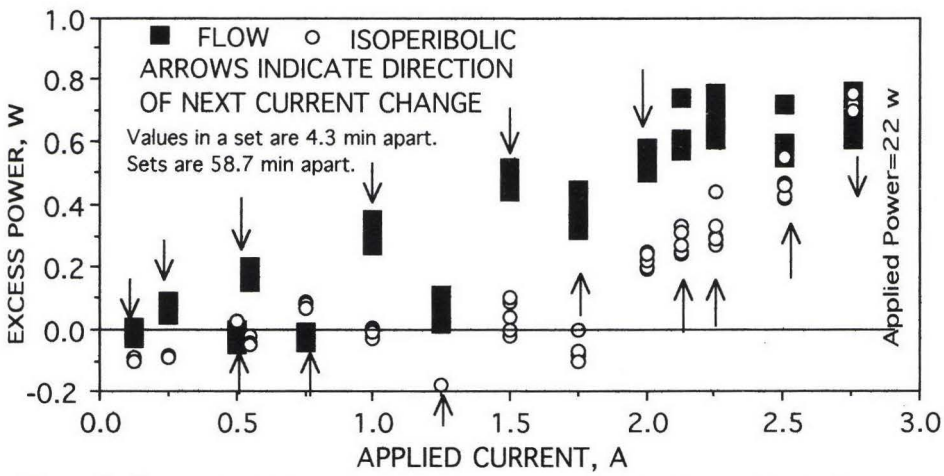

Figure 7. Comparison between excess energy measured using flow method and isoperibolic method during the initial current sweep.

In the case of platinum, this study suggests that an energy-active layer of unknown composition can deposit on a Pt surface. This observation might also be related to the frequent detection of Pt on the Pd cathode after excess energy is observed. Such a layer is slow to form, which is consistent with the observed long delay in producing excess energy, and, for this sample, it is unstable. Is it possible that such a layer might be the active material in all studies, even when palladium is used?. McKubre et al. [11] also suggest that a critical layer is required to maintain the required high composition in Pd. Perhaps this is the actual active material. If this is the case, the bulk properties of palladium are only impor-

tant in that they must support a critical concentration within this layer. Since palladium can easily permit loss into the metal, such material might be the worst substrate to use. Platinum, gold, and other inert materials would appear to be better choices. Use of such materials would only require forming the active layer without a need to use special batches of the substrate. If this suggestion is true, significant changes in various theories will be required.

More detail and the raw data can be accessed at http://jedrothwell.home.mindspring.com.

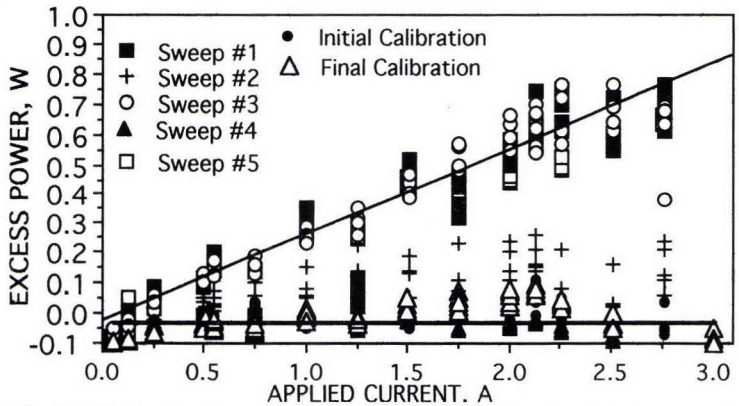

Figure 8. Applied current vs excess power for the various sweeps, compared to Pt calibrations taken before and after the study.

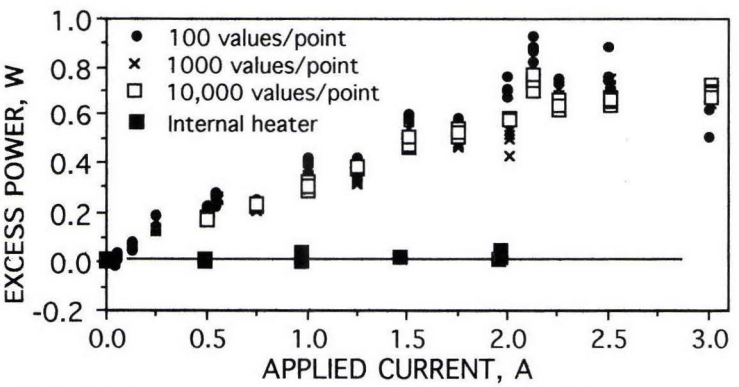

Figure 9. Applied current vs excess power for sweeps using different number of values to average are compared to the heater calibration.

References

[1] Lonchampt, G., Biberian, J.-P., Bonnetain, L., and Delepine, J. 1998. "Excess Heat Measurement with Pons and Fleischmann Type Cells" *Proc. of the Seventh International Conference on Cold Fusion*, April 19-24, Vancouver, Page 202.

[2] Dash, J. "Chemical Changes and Excess Heat Caused by Electrolysis with H2SO4-D2O Electrolyte", *Proc. Sixth International Conference on Cold Fusion,Progress in New Hydrogen Energy*, Oct. 13-18, 1996 (M. Okamoto, ed.) New Energy and Industrial Technology Development

Organization, Tokyo Institute of Technology, Tokyo, Japan (1997), Vol. 2, page 477.

[3] Ohmori, T., Mizuno, T., and Enyo, M. 1996. "Isotopic Distributions of Heavy Metal Elements Produced During the Light Water Electrlysis on Gold Electrodes", J. New Energy **1**, #3, 90. See also: Notoya, R. and Enyo, M.1992. "Excess Heat Production during Electrolysis of H_2O on Ni, Au, Ag and Sn Electrodes in Alkaline Media," *Proc. Third International Conference on Cold Fusion*, October 21-25, Nagoya Japan, *Frontiers of Cold Fusion*, (H. Ikegami, ed), published by Universal Academy Press, Inc., Tokyo, Japan, p. 421; Ohmori, T. and Enyo, M. 1993. "Excess Heat Evolution During Electrolysis of H_2O with Nickel, Gold, Silver, and Tin Cathodes," Fusion Technol. **24,** 293.

[4] Klopfenstein, M. F., and J. Dash, "Thermal Imaging during Electrolysis of Heavy Water with a Ti Cathode", Proceedings of *The Seventh International Conference on Cold Fusion*, Vancouver, Canada, April 19-24, 1998, ENECO, Inc., Salt Lake City, UT. (1998), page 98.

[5] Bush, R. T. and R. D. Eagleton. "A Calorimetric Study of the Excess Heat Effect in Thin Films of Palladium", Presented at Second Annual Conference on Cold Fusion, June 29-July 4, 1991, Como, Italy. (not in Proc., but on vidio tape).

[6] Szpak, S., P. A. Mosier-Boss and J. J. Smith, " On the Behavior of Pd Deposited in the Presence of Evolving Deuterium", J. Electroanal. Chem. 302 (1991) 255. See also: M. H. Miles, "Report on Calorimetric Studies at the NHE Laboratory in Sapporo, Japan", Infinite Energy, 5, #30 (2000) 22.

[7] Miley, G. H., and J. A. Patterson, "Nuclear Transmutations in Thin-Film Nickel Coatings Undergoing Electrolysis", J. New Energy **1**, #3 (1996).

[8] Patterson, J., "Method for Electrolysis of Water to Form Metal Hydride", US Patent 5,318,675, June 7, 1994.

[9] E. K. Storms, "My life with cold fusion as a reluctant mistress", Infinite Energy **4**, issue 24 (1999) 42.

[10] T. Nakata, M. Kobayashi, M. Nagahama, H. Akita, N. Hasegawa, and K. Kunimatsu, "Excess Heat Measurement at High Cathode Loading by Deuterium During Electrolysis of Heavy Water using Pd Cathode", *Proc. Sixth International Conference on Cold Fusion,Progress in New Hydrogen Energy*, Oct. 13-18, 1996 (M. Okamoto, ed.) New Energy and Industrial Technology Development Organization, Tokyo Institute of Technology, Tokyo, Japan (1997), Vol. 1, page 121.

[11] McKubre, M. C. H., S. Crouch-Baker, F. L. Tanzella, M. Williams and S. Wing, "New Hydrogen Energy Research at SRI", *Proc. Sixth International Conference on Cold Fusion,Progress in New Hydrogen Energy*, Oct. 13-18, 1996 (M. Okamoto, ed.) New Energy and Industrial Technology Development Organization, Tokyo Institute of Technology, Tokyo, Japan (1997), Vol. 1, page 75.

Conference Proceedings Vol. 70
"ICCF8"
F. Scaramuzzi (Ed.)
SIF, Bologna, 2000

SOME EXPERIMENTAL RESULTS ON HEAT MEASUREMENT DURING WATER ELECTROLYSIS

K.Ota, T.Okabe, H.Kudo, M.Fujii, N.Motohira and N.Kamiya

Department of Energy and Safety Engineering, Yokohama National University
79-5, Tokiwadai, Hodogaya-ku, Yokohama240-8501, JAPAN

Abstract

It is important to establish a precise heat measurement system to confirm the excess heat owing to cold fusion phenomenon. We have been developing two types of flow calorimetry systems. Among them we obtained 99% heat recovery using the improved NHE type calorimeter and have almost established the absolute measurement of the heat during electrolysis.

During the electrolysis using small metal rods (Ni,Pd and Ti) as the cathode in Li_2SO_4-H_2O solution, the excess heat that was over 5% of the input power was not observed. During the electrolysis using porous Ni or Pd wire cathode in K_2CO_3-H_2O solution, the large excess heat was not also obtained. However, we observed the unusual increase of the electrolyte temperature at the very beginning of electrolysis. This excess energy was small (about 1kJ) but we could not find any chemical reactions that correspond to this excess heat.

1. Introduction

More than 10 years has past since the first announcement of the cold fusion by Fleischmann and Pons[1] Since then, many people have worked on this field and many reports have been published. However, there remains some uncertainty especially for the excess heat. Many reports claimed the excess heat. However, most of them were low reproducible and the amounts of excess heat were very small.

In order to confirm the small excess heat, the precise calorimetry is inevitable. We are developing two kinds of flow calorimetry systems. One is the Yokohama type calorimeter that has triple walls to keep constant temperature in the vessel. The other was the NHE type calorimeter that originally designed by the NHE project (Japanese cold fusion project) which uses the vacuum insulation around the electrolysis cell.[2]

Excess heats were reported not only with D_2O system but also with H_2O system using K_2CO_3 or Li_2SO_4 electrolyte. In this study we will report firth the development of our flow calorimetry systems and in the second, show the results of heat measurements in K_2CO_3-H_2O and Li_2SO_4-H_2O systems.

2. Improvement of flow calorimetry system

2.1 Yokohama type flow calorimetry system

The electrolysis cell for this type was a closed cell with recombiners at the upper part. The cooling water goes through the copper tubing and the temperature difference between the inlet and the outlet was measured. The electrolysis cell was placed in the vessel that has triple walls. The triple walls were thermally controlled separately and precisely. The temperature in the vessel was controlled ± 0.01℃ at the room temperature range of 23 ± 3℃. The heat recovery of this calorimeter was rather small (89-97%). However we can use this system at 70℃ or higher temperatures. Figure 1 shows an example of the heat recovery. In this case the heat recovery was $91.5 \pm 0.08\%$ and the systematic error was estimated to be $\pm 1.5\%$ at the input power of 5W.

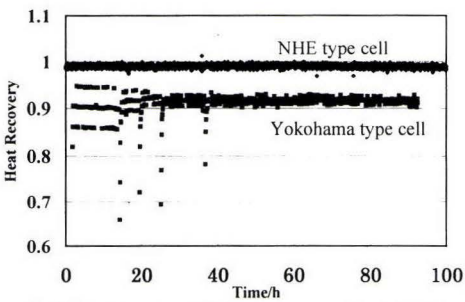

Fig.1 Heat recovery of Yokohama type cell and NHE type cell

2.2 NHE type flow calorimeter

The NHE type cell was also a closed cell with recombiner. The cell has a double structure. The inner cell is hanged to the outer cell. Both cells are thermally insulated by vacuum. The cooling water flows from top to bottom along the wall of the inner cell. The heat recovery was measured by the temperature difference of cooling water. The electrolysis was carried out at a constant current and the total input power was fixed using a joule heater in the inner cell. These controls and the data acquisition were curried out automatically using a personal computer. In order to obtain an accurate data and an absolute value, the heat recovery of the system is important. In this study the heat recovery (H.R.) was obtained by the following equation.

H.R = $4.181 \times 0.9975 \times$ (the amount of the cooling water) $\times \Delta$ T/Total Power

4.181 $JK^{-1}g^{-1}$ and 0.9975 gcm^{-3} were the specific heat capacity at the ambient pressure and the density of the cooling water at 23℃. Δ T is the temperature difference between the

outlet temperature and the inlet temperature of the cooling water. Fig.1 also shows the H.R. of the NHE type flow calorimeter where the total input power was increased from 5W to 5.3 W. In this case the average H.R. is 99.0±0.04%. Fig. 2 shows the dependence of the temperature difference on the input power. The linear relationships is clearly observed. Considering the slope of the line and the sensitivity of the thermometer (0.01℃), we can measure a small heat of 30 mW.

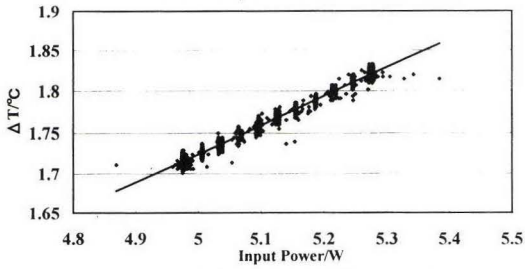

Fig.2 Dependence of the temperature difference on input power using NHE type cell

3. Heat measurement in electrolysis with light water

3.1 Packed-bed cell system [3-5)]

Patterson et al claimed huge amount of excess heat using Packed-bed cell.[3)] We simulated the Patterson cell by using small metal rods (Ni, Pd and Ti). The electrolysis was performed in a cell that was made of acrylic resin. We used a galvanostat for electrolysis. We set up degasser in front of the cell inlet to remove bubbles from electrolyte. Electrolyte used in experiment was 1 M Li_2SO_4-H_2O solution. The electrolyte is circulated in this system. The flow rate of electrolyte was 10 ml/min or 45 ml/min and the temperature of the electrolyte was kept at 20℃ at the inlet of the cell. In order to estimate the amount of the recombination of H_2 and O_2, the current efficiency was measured using a gas flow meter of soap membrane. For these experiments we did not use the precise calorimeter, since we expected a large excess heat as that of Patterson.[3)]

Table1. Heat balance of electrolysis in Li_2SO_4–H_2O solution

Run Number	Cathode Electrode	Cell Current(A)	Cell Voltage(V)	Heat Balance Average
R5	Ni	0.5～ 1.0	10.6～27.2	1.02
R6	Ni	0.5～ 1.0	7.1～20.7	1.01
R7	Ni	0.5～ 1.0	8.1～16.9	1.00
R8	Ni	0.5～ 1.0	11.3～20.8	1.02
R10	Pd	0.5～ 1.0	9.6～ 18.8	1.03
R11	Pd	0.5～ 1.0	9.6～ 25.9	0.99
R12	Pd	0.5～ 3.0	9.2～ 38.0	1.01
R13	Pd	0.5～ 3.0	6.5～ 36.2	1.01
R14	Ti	0.5～ 1.0	18.3～ 35.2	1.02
R15	Pd	0.5～ 1.0	18.7～ 33.8	1.03

Table 1 shows the some results using small Ni rods (2 mmϕ ×2 mm, 12g), Pd rods (1 mmϕ ×2 mm, 520 pieces)and Ti rods(1 mmϕ × 2 mm, 520 pieces)for cathode. Anode was Pt mesh anode (3 cmϕ, 55 mesh), and electrolyte was 1 M Li_2SO_4-H_2O solution. The temperature of the water bath where the electrolyte solution went out and in, was controlled at 20℃ and the flow rate of the electrolyte was 45 ml/min. The electrolysis was conducted at a constant current. The current was increased by 0.1 A every other day from 0.5 to 1.0 A. The same electrode was used repeatedly for these experiments. Figures 3 and 4 show the cell current, the cell voltage and the heat balance for the electrolysis using Ni rods. The decrease of the cell voltage is observed in the figure 3. The decrease would be due to the increase of the surface area of the electrodes. Figure. 4 shows the heat balance of the some experiment (R8). The heat balance does not depend on the cell current. The average heat balance was 1.02 at this case and 2% excess heat might be possible. However, we could not confirm the excess heat, considering the distribution of the data. Table 1 shows the results of the several packed-bed experiments. The heat balance is also more than 1.0 in most cases. However, the excess is 1～3% and very small. We could not observe the large excess heat in our system as reported by Patterson et al.[3)]

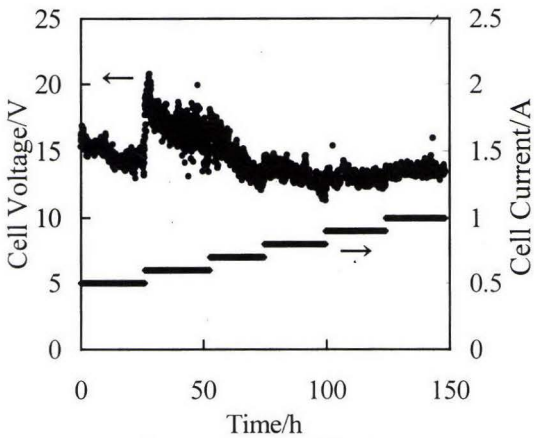

Fig.3 Cell current and cell voltage at R8

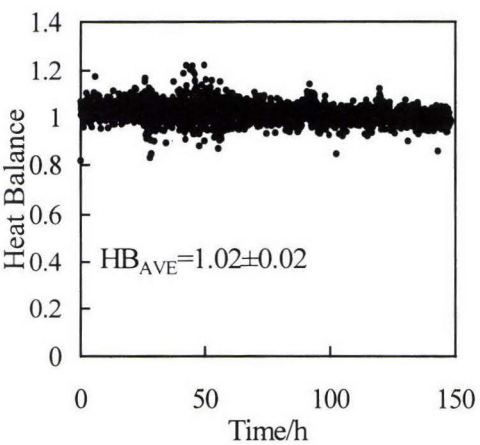

Fig.4 Heat balance at R8

3.2 Heat measurement in electrolysis with K_2CO_3-H_2O solution.

Excess heat productions were reported by Notoya[6-8] and Ohmori[9] in K_2CO_3-H_2O system. We used porous Ni seat (10×15×1 mm) or Pt rod (1 mmϕ×25 mm). The anode was Pt rod (1 mmϕ×25 mm). The electrolyte was 0.5 M K_2CO_3-H_2O solution (50 ml). The electrolysis was conducted at a constant power or a constant current. For the heat measurements we used the Yokohama-type flow calorimeter.

We have performed the electrolysis about 100 times. Table 2 shows the some typical results. In these cases the heat recovery is ranged from 0.88 to 0.95. These data shows that we could not get excess heat. However, in several cases, the temperature of the electrolyte increased more than we expected at the beginning of electrolysis. Normally, the temperature of the electrolyte should follow the following equation before getting the steady state at the beginning of electrolysis.

$$T(t) = R_q W_{in} + T_{cool} - \tau \exp(t/R_q C) \qquad (1)$$

$$\tau = R_q W_{in} + T_{cool} - T(t=0)$$

R_q is the heat resistance (WK^{-1}). W_{in} is the input power (W). T_{cool} is the temperature of cooling water. T(t) is the temperature at time t. C is the heat capacity of cell (WK^{-1}).

Table.2 Heat recovery of electrolysis in K_2CO_3-H_2O solution using Yokohama type flow calorimeter.

Run Number	Cathode	Input Power	Heat Recovery
2h0601	Pt	5W	0.95
2h0603	Ni	5W	0.88
2h0704	Ni	5W	0.88
2h1402	Pt	1A	0.90
2h1406	Pt	1A	0.91
2h1504	Pt	1A	0.89

Figure 5 shows the temperature duration of the electrolyte at the beginning of Run 2h0704. The temperature trend is different from that of eq.(1). We observed the temperature peak around 2 h that could not be expected theoretically. The maximum difference is 0.7℃. From the difference of these temperatures, we calculated the excess heat was 1700 J in this case. This phenomena could not be observed always. We clearly observed this phenomenon 14 times out of 100 runs and the excess is 340～1700 J.

These are very small heat and some chemical reaction might be responsible. Possible reactions owing to the excess heat are the oxidation of metal (anode), and the hydride formation (cathode). Masses of Ni and Pt electrodes used in experiment was 60 mg and

850 mg, respectively. If all these electrodes become NiH_2, $Ni(OH)_3$ or $Pt(OH)_2$ completely. The heats of reactions were 26 J, 69.3 J and 1530 J, respectively. The heat of the hydride formation of Ni or the oxidation of Ni is very small and could not explain the excess heat of this study. The oxidation of Pt might be a possible explanation thermochemically. However, Pt anode is usually very stable and only the surface of the Pt anode would be oxidized. The heat of oxidation of Pt anode might be less than 100 J. No other chemical reactions that produce heat are thermochemically possible. We could not explain the small excess heat by any chemical reaction.

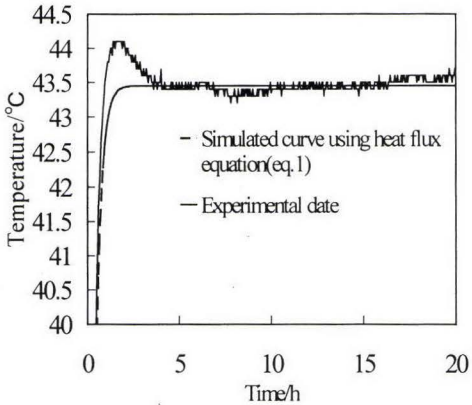

Fig.5 Temperature duration of the electrolyte and the theoretical curve at Run 2h0704.

4.Conclusion

During the electrolysis in 1 M K_2CO_3+H_2O using Ni and Pt cathode, we could not obtain excess heat from the increase of the temperature of the cooling water. However, the unexpected temperature increase of electrolyte was observed at the beginning of electrolysis. The amount of the excess heat was very small but we couldn't find any chemical reaction for this excess heat. During the electrolysis in 1 M Li_2SO_4+H_2O using Ni, Pd and Ti rods the large excess heat could not be obtained, although the average heat balance was a little over 1.0. We are under developing of two kinds of flow calorimeter systems. However, the small excess heat of less than 30 mW is very difficult to confirm. Further development is necessary to measure the small excess heat.

References

1) A.Kubota, et al; Proc.ICCF6,52(1996)
2) M.Fleischmann, S.Pons, et al; J.Electroanal. Chem., **289**, 293(1989)
3) James A.Patterson, U.S.Patent, 5318675
4) G.H.Miley et al,Proc.ICCF6,629(1996)
5) D.Cravens, Proc.ICCF4,79(1995)
6) R.Notoya, Fusion Technol.,**24**,202(1993)
7) R.Notoya, Fusion Technol.,**26**,205(1994)
8) R.Notoya,Y.Noya and T.Ohnishi, Fusion Technol.,**26**,179(1994)
9) T.Ohmori and M.Enyo,"Frontiers of Cold Fusion",Univ.Acad.Press, Tokyo,427(1993)

Conference Proceedings Vol. 70
"ICCF8"
F. Scaramuzzi (Ed.)
SIF, Bologna, 2000

Ni-H Systems

E.G. CAMPARI(1), S. FOCARDI (1), V. GABBANI (2),
V. MONTALBANO (2), F. PIANTELLI (2), E. PORCU (3),
E. TOSTI (3) and S. VERONESI (2)

(1) *Dipartimento di Fisica, Universitá di Bologna, Bologna - Italy*
(2) *Dipartimento di Fisica e centro IMO, Universitá di Siena. Siena - Italy*
(3) *Fiat Avio, Colleferro - Italy*

Abstract

We report the results obtained in three different laboratories on the Ni-H system during several years of experiments. Heat production was observed in different cells for long periods, with a maximum power of 70 W. In several occasions we detected gamma ray emission and in one case also a neutron emission. The analysis of Nickel samples which loaded Hydrogen gas showed the existence of other elements not present in the original specimens. Finally, we present tracks detected in a diffusion chamber of ionising particles from a specimen which produced heat.

1 Introduction

The observation by one of the authors (F. Piantelli) of an anomalous behaviour of the system Ni-H was the starting point of a systematic research on these effects [1]. Different cells and specimens were built and put into operation in order to study the characteristics of the phenomenon. For a detailed description of the cells, the reader is referred to [2] [3]. Nickel specimens or specimens of other nickel plated materials, were put into our cells and treated at various temperatures and hydrogen pressures in order to obtain a high level of H-loading. In some cases a relevant absorption was obtained, while other specimens, even if treated in a similar manner, absorbed much less. Typical values of pressure and temperature employed in the loading operations were in the 200÷1000 mbar and 700÷800 K range. The use of subatmospheric pressures guarantees that the observed pressure decreases were due to Hydrogen absorption and not to cell leakage. During the treatments for loading Hydrogen or as a consequence of Hydrogen absorption, a series of different phenomena, which will described in the following, were observed.

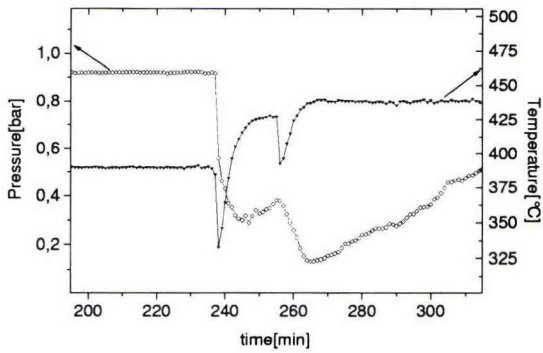

Figure 1: Two pressure shocks causing the sample temperature increase (Termocouple Tc1, figure 1b of reference [2]).

2 Heat production

Apart from the first experiment, whose results are reported in [1], where a heat production effect was deduced by measuring the specimen temperature, in all subsequent experiments heat production was measured with reference to the temperature of the external walls of the cells. In practice, in an initial phase the cell was calibrated: a curve describing the temperature difference between external cell walls and room vs. input power was obtained in equilibrium conditions at a low Hydrogen pressure (200 mbar).

This curve can be approximated as linear in a range of the order of a hundred degrees kelvin and used to calculate the heat exchanged on the basis of the Newton law of convection. The total thermal power emitted from the cell can thus be deduced from a measurement of two temperatures: the wall and the room temperature. Whenever the difference of the two, for a given input power, is above the calibration curve, there must be a power excess coming from inside the cell. In practice the horizontal distance of a point from the curve gives the value of the produced power, as can be seen for example in figure 6 of reference [2]. The apparatus sensitivity to heat production is of the order of a few watts. For this reason we could not observe an eventual excess power production below that a threshold. Usually, the heat production is triggered by a thermal or pressure shock, consisting of a sudden change of input power or of the inside pressure, as shown for example in figure 1. The initial temperature decrease observed in correspondence of pressure jumps is caused by drawing into the sample region of low temperature hydrogen. The successive increase of equilibrium temperature puts in evidence a power production.

For the best case, we obtained an excess peak power up to 70 W, with an average over a period of 10 months of 40 W. During that period of time it was also possible to

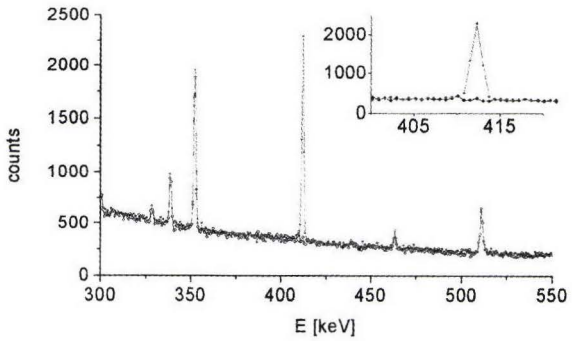

Figure 2: HpGe spectra of activated and not activated Gold. Details of the region around 412 keV are shown in the insert.

stop (typically with an inverse shock) and resume heat production many times. The overall energy production, corresponding in the two best cases [2] to an amount of 600 MJ and 900 MJ, respectively, cannot be explained by chemical reactions because of the low quantity of materials inside the cells. In other shorter experiments, lasting not more than one month, a power production of the order of tents watts was obtained.

3 Neutron emission

Thanks to the long period of heat production of some of the cells it was possible to search for radiation coming from the system, which would be a proof of nuclear reactions occurring inside the cells. In one case alone, we detected neutron emission. This was associated with a spontaneous increase of about 10 W of the power emission, which was kept constant by decreasing the input power. As reported in detail in [4] two methods were used to detect neutrons: one based on the activation of a Gold sheet, the other consisting of counting the neutrons by means of ^{3}He detectors. The activation method is based on the high thermal neutron capture cross section by ^{197}Au, which turns into ^{198}Au. This last isotope decays into an excited state of ^{198}Hg with a 2.7 day halflife. A 411.8 keV gamma ray is emitted in the decay to the ground state of ^{198}Hg. A 5.1x2.4x0.06 cm^3 Gold sheet placed inside a paraffin box was left for 12 days near the cell emitting neutrons. Successively, the sheet was placed above a HpGe detector and the 411.8 keV gamma rays were recorded. The spectrum obtained is shown in figure 2. In the same figure we report in order to exclude effects from cosmic neutrons, the spectrum recorded after the sheet container was kept 12 days 10 m far from the cell. For comparison with the effect produced by an Am-Be neutron source of known strength, it was possible to deduce the intensity of the neutron flux coming from the cell, which resulted in about 6000 neutrons/second. During the same period

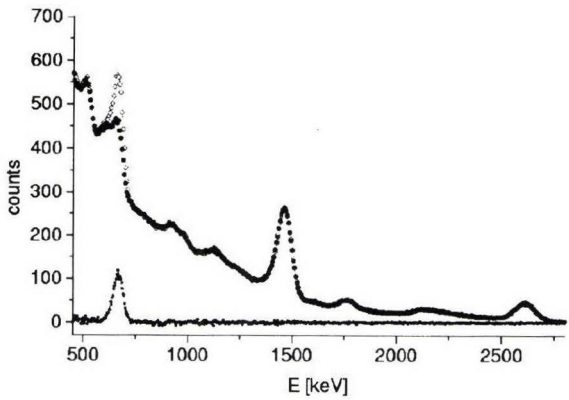

Figure 3: Two consecutive weekly averages of 12000 s NaI spectra, and (lower curve) their difference.

two ^{3}He counters with paraffin and cadmium shielding were placed one near the cell, the other 10 m far away from the cell. Thank to a calibration with the Am-Be source, the counting difference between them permitted us to determine a flux of about 110 neutrons/second from the cell. The apparent disagreement between the two figures can be explained by the time distribution of the neutrons impinging on the near counter, which shows a characteristic arrival in short bursts [4]. Later on, the neutron flux died away. For a period of three months it was monitored by three ^{3}He counters placed near the cell. Data referring to this period, on subtracting the background, give a flux of 2-5 neutrons/seconds. Successively, the heat production was stopped and so did neutron emission. Considering the overall power emitted from the cell and an energy of the order of 1 MeV for each neutron emitted, the ratio between the number of neutron observed and the number of neutron expected is of the order of 10^{-11}.

4 Gamma emission

Another important proof of the existence of nuclear reactions is the emission of gamma rays from the samples. They were measured mainly by means of NaI detectors and also with the use of a HpGe detector. They occurred during periods of cell operation in various experiments. Figure 3 shows two NaI spectra. Each represents the average of 50 runs each lasting 12000 s acquired consecutively. In addition to peaks due to natural background, an extra peak whose energy of 665±1 keV was measured with a HpGe detector is visible. The 665 keV peak intensity increased with time, as evidenced by the reported difference between the two spectra.

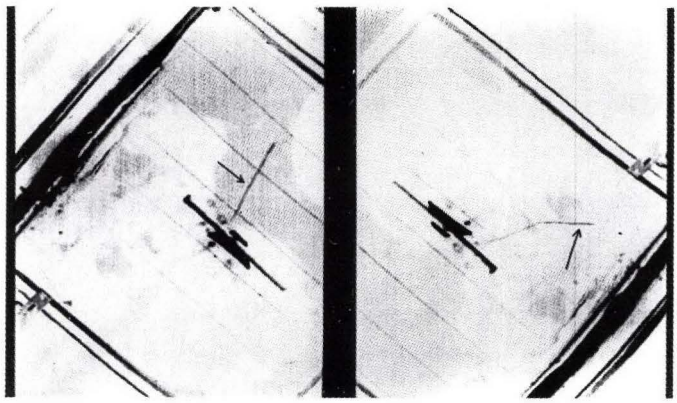

Figure 4: Two tracks from a sample which produced energy.

5 Charged particle emission

The specimen which produced up to 70 watts, at the end of the experiment was extracted from the cell. Two months later it was placed in a diffusion chamber, borrowed from a student laboratory. As shown in figure 4, tracks coming from the sample appeared. The strong ionisation and the absence of straggling allows us to exclude electrons as responsible for the tracks. Unfortunately, this simple kind of chamber cannot be used to make a quantitative and precise measurement. Nevertheless, on having observed tracks of length up to 9 cm, α particles can also be ruled out. In fact α particles of this range would have an energy of about 20 MeV, which is too high for α emission from known radioactive elements.

6 Surface analysis

A surface analysis of the specimens after conclusion of their treatments in the cells was done on some of the first samples [5] and later systematically. These studies were performed by means of a SEM microscope with EDX probe. This analysis was suggested by the observation that those samples which produced energy had a different surface appearance with respect to that at the beginning of the experiment. The surface appeared corroded and sometimes little spots were present. The results of these analysis can be summarised as follows. Whenever there was heat production or a sensible Hydrogen loading, elements not previously detectable by SEM were detected on the surface. These elements are usually found in little spots or in the corroded regions. We found F, Na, Mg, Al, Si, P, S, Cl, K, Ca, Cr, Mn, Fe, Cu, Zn. Apart light elements, not detectable by SEM, we found in practice, with the exception of Sc, Ti, V and Co, all the elements lighter than Ni, plus Cu and Zn. In each spot only some of these were detected, but their EDX signal was in some cases even stronger than that of Nickel. The proportion of the elements changes from place to place. Other

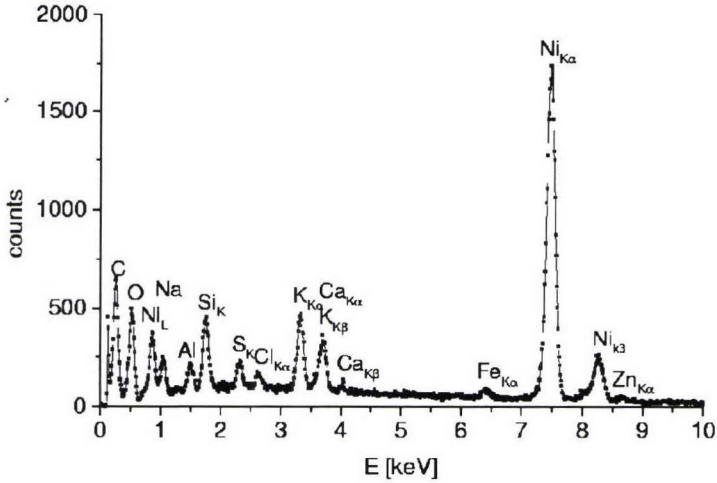

Figure 5: EDX spectrum showing the appearance of elements absent before the run.

authors, working with electrolytic systems, reported the presence of elements different from those initially present in the specimens (see for instance [6] [7]). Figures 5 reports the EDX spectrum relative to a spot with other elements not present before the treatment.

References

[1] S. Focardi, R. Habel and F. Piantelli, Nuovo Cim. A, 107 (1994) 163.

[2] S. Focardi, V. Gabbani, V. Montalbano, F. Piantelli and S. Veronesi, Nuovo Cim. 111A, 1233 (1998).

[3] S. Focardi, V. Gabbani, V. Montalbano, F. Piantelli and S. Veronesi, Asti Workshop on Anomalies in Hydrogen/Deuterium loaded Metals, Italian Physical Society, Conference Proceedings, vol 64, W.J.M.F. Collis editor, Asti 27-30 November 1997.

[4] A. Battaglia, L. Daddi, S. Focardi, V. Gabbani, V. Montalbano, F. Piantelli, P.G. Sona and S. Veronesi, Nuovo Cim. 112A, 921, (1999).

[5] S. Focardi, V. Gabbani, V. Montalbano, F. Piantelli and S.Veronesi, Atti Accad. Fisiocritici, Serie XV, Tomo XV, (1996) pgs. 109-115.

[6] G. H. Miley and J. A. Patterson, Infinite Energy, 19, July-August 1996.

[7] T. Ohmori and M. Enyo, Jour. New Energy 1, 1(1996), 15.

Conference Proceedings Vol. 70
"ICCF8"
F. Scaramuzzi (Ed.)
SIF, Bologna, 2000

Confirmation of heat generation and anomalous element caused by plasma electrolysis in the liquid

Tadahiko MIZUNO, Tadayoshi OHMORI[1], Kazuhisa AZUMI, Tadashi AKIMOTO and Akito TAKAHASHI[2]

Hokkaido University, Kita 13 Nishi 8, Kita-ku, Sapporo 060-8628, Japan
1: Catalysis Research Center, Hokkaido University, Kita 11 Nishi 10, Kita-ku, Sapporo 060, Japan
2: Department of Nuclear Engineering, Osaka University, Yamadaoka 2-1, Suita, Osaka 565-0871, Japan

Abstract

Plasma was formed on the electrode surface in a liquid electrolyte when a metal cathode was polarized high voltage electrolysis in the solution. During the plasma electrolysis a large amounts of heat are sometimes generated. The heat can exceed input substantially, and in some cases by up to 200 percent of input power. At the same time, anomalous elements were detected in the electrolyte and on the electrode surface. Based on the heat and the product, we hypothesize a nuclear reaction that can be induced by photon activation on the cathode element.

1. Introduction

We previously reported that anomalous isotopes are created on metal surfaces and surface regions, which cannot be explained by ordinary electrolysis.[1] In other words, this extruded material consists of elements, which cannot conceivably be contamination, because the isotopic distribution of most of the elements is unnatural. It is thought that this indicates what type of reaction affecting the nucleus has occurred. We expect to clarify the reaction mechanism by analyzing these reaction products. The plasma phenomenon has been in the literature [2-9] for quite a long time. The reaction mechanism of plasma discharge is not understood in as much detail as ordinary electrochemical reactions.

2. Experimental Method

2.1 Electrolysis system

Heat was measured by a method that combined open cell isoperibolic calorimetry and flow calorimetry. The cell is a cylindrical glass vessel, 100 mm in diameter and 150 mm tall. A magnetic stirrer to ensure uniform temperature distribution mixes the electrolyte. It has two layers, or chambers. The anode, cathode and electrolyte are placed in the inner chamber. The outer chamber is filled with primary cooling water and heat exchanger coils (Teflon tubing). During electrolysis, secondary-cooling water flows through the coils and removes heat from the primary cooling water. Thermocouples are installed in the heat exchanger coils inlet and outlet, in Tee fittings, to perform flow calorimetry. Cooling water is circulated through the Teflon tubing from a constant temperature bath with an FMI precision metering pump with 1% precision; for example, 4.26±0.05 g/s. This pump circulates water at any rate from 1 to 20g/s. The flow rate is verified by collecting the water in a flask for a fixed period of time and weighing it on a precision scale.

2.2 Heat calibration

The heat balance is obtained with the following formulas:
Input (Joules) = I (current)×V (volts)×t (Time)
Output (Joules) = Hw (heat of solution and cell)+Hc (heat of coolant)+Hr (heat release)+Hv (heat of vapor) + Hg (heat of water decomposition)

All data, including voltage, current, temperature, and mass of secondary cooling water, are collected with a data logger for each 10s. Current is determined by measuring voltage through a shunt. Cell voltage is measured by attaching sensor wires directly to the electrode leads in the top of the cell. Data from the logger is captured by the computer, and finely recorded on diskette. All electric lead junctions from the thermocouples to the logger are compensated.

The heat balance was calibrated by changing the input power of the Joule heater immersing in the electrolyte. The out/input ratio stayed at 0.89 during the calibration run except when the cell was boiling, and during glow discharge boiling seldom occurred. The results show that a large change in input has no effect on the heat recovery calibration. In other words, changes in input power can be precisely monitored by the flow calorimetry method and by the open cell isoperibolic method. The only difficulties arose when the input power is very low, because the temperature precision was only 0.1C, and below 70W measurement accuracy suffered.

2.3 Electrolyte and Cathode Material Preparation

The electrolyte solution was prepared with Milli-Q pure distilled water that is filtered. It was used after being redistill in quartz glass. Ultra high pure reagents were used for the K_2CO_3 electrolyte. High purity of tungsten plate (99.98%) was used for the cathode. Platinum wires or mesh were used as the counter electrode and electrode lead wires.

2.4 Analysis of generated element

Materials in the solution and deposition bottom of the cell were calibrated by ICP analysis. The element on the electrode surface was analyzed by the EDX. The elements were then melted by an acid and calibrated by ICP method.

3. Results

When we increased the input voltage, excess heat was clearly generated. A typical result is shown in fig. 1, with a tungsten electrode of 0.5mm thickness; the graph on the left shows changes of input current, voltage and the electrolyte temperature during electrolysis. The figure on the right shows the input and output in watts and the ratio between them. The output heat showed slight excess comparing with the input power after 2,000s of plasma electrolysis start. After the 3,000s, the excess was considerably larger than the heat measurement error of 20W and reached 30-40W of average during the plasma electrolysis.

Tungsten samples of 0.3-mm thickness also produced significant excess heat generation. A typical result is shown in fig.2. Excess heat was observed after only 100s of plasma electrolysis. At the time, the excess was considerably larger than the heat measurement error of 20W, reaching 40W average for the first 1,500s of plasma electrolysis. The output and input ratio changed over time. For the first 1,000s, excess was 20%, but after 1,600s it increased to around 60%, with fluctuations. The ratio again increased up to 300% after 3,000s then fell back to one after the voltage decreased to 100V. The total output heat power during plasma electrolysis was

estimated as 388.7kJ while the total input electric power of 334.3kJ. Excess heat is 54kJ or 16% of input power.

After the voltage fell to 100V, the output and input ratio seems to fall gradually below unity. The ratió slowly increased after the voltage decreased into 60V. A possible reason is that the electrolysis temperature rose close to boiling point during glow discharge, and heat was lost to the water vapor released from the cell. Although we did not measure heat lost to vapor, the overall balance during glow discharge remained well in excess of unity because so much excess heat was generated. After the voltage was lowered, excess heat stopped although large losses to vapor continued, so ratio fell under unity. At 60 volts, glow discharge stopped, the boiling ceased, and the heat losses to vapor declined, so the balance returned close to unity.

It has been established that at the extraordinary excess heat generation is sensitive to many parameters, such as electrolysis and electrode material. Especially, it can depend on the electrolysis temperature, input voltage and the duration of plasma discharge. We had no excess heat at the beginning of the plasma electrolysis even the temperature and the input voltage were quite high, at 100V and 85C. However, after several hundred seconds of plasma electrolysis, we always observed large excess heat generation. We conclude that if we attain sufficiently high temperature and voltage, and hold them, we observe excess heat with 100% of reproducibility.

It is apparent that excess energy production depends on electrolysis voltage and the temperature of the electrolyte solution. The discharge voltage at which excess heat production begins is quite different as these conditions vary. Even when these conditions are satisfied, other parameters, such as the shape of the cathode, cause dissimilar discharge conditions. The spectrum of light from the reaction shows that two kinds of reactions can occur[10]. A reaction in which hydrogen dominates in the spectrum, or a reaction in which the alkaline in the electrolyte and the cathode metal, which have no direct role in the reaction, are more pronounced in the spectrum. In the latter case the electrochemical potential near the electrode is large. We assume this affects the excess heat generation.

After excess heat was produced, many elements were found in the electrolyte, the eroded and precipitated cathode material, and on electrode surface. On the other hand, there were fewer elements when no excess heat was measured. Several elements were detected on the cathode surface after excess heat evolution, including Cl, Ca, Ti, Fe and Zn. The distribution of the elements was different in different parts of the electrode surface. Most were found around the center of sample. Meanwhile, other elements were detected in the solution, which were not the same as those found on electrode surface and the deposition at the bottom of the cell. Typical element distributions are shown in the Table1. A clear difference can be seen between the case when excess heat was generated, and when it was not.

4. Discussion

In evaluating heat production, is necessary to consider whether the heat might have been produced by chemical changes. After discharge electrolysis it is clear that the cathode material was worn down and precipitated to the bottom of the cell in the form of fine particles. Because this material was entirely made up of pure metal, the destruction must have been caused by hydrogen corrosion as well as heat damage. Therefore chemical changes cannot explain the heat. Ignoring the fact that this is impossible, let us consider some hypothetical chemical reactions:

$2W+3O_2=2WO_3 + 200.84kJ$

$WO_3+H_2O=H_2WO_4 + 179kJ$

In other words if 183.85g of tungsten reacted the maximum heat generation from this reaction would be 380kJ. The actual volume of excess heat measured using flow calorimetry was 54.4kJ for the case of plasma electrolysis with 200V of input for 3.1ks. The mass of tungsten removed in the reactions described above was 0.1g, and if we assume hypothetically that all of this material reacted, the heat would have been only 0.207kJ or 0.38% of the actual excess heat observed. The heat production in this experiment cannot begin to be explained as a chemical reaction.

This discussion has been predicated on the supposition that the tungsten underwent a chemical reaction, but in reality the tungsten found at the bottom of the cell was recovered as pure metallic fine powder, so no chemical reaction occurred. Furthermore, the decomposition of carbonates in a water solution is an endothermic reaction, so in this case 274kJ/M of heat would be absorbed, therefore even assuming that a reaction occurred no excess heat would be produced. Ordinarily, when metal is transformed into a hydride, it produces on the order of 200kJ/M, the exact amount depending on the metal. If a hydride was formed, based on the amount of tungsten lost from the cathode, the excess heat from the reaction should have been 0.1kJ approximately, which is simply too small to make a difference. In short, the actual heat that might have been produced from potential chemical reactions is essentially nonexistent.

5. Conclusions

According to the many reported experiments, almost of papers reported that there were no radioisotopes and no or very weak radiation such as neutron and other gamma or x-ray detected during and after the cold fusion experiment. So then, We have to explain the fact by a proper mechanism that produce the no radioactive materials by the treatment of the electrochemical reactions. Here, Takahashi[11] make progress the mechanism of photo-fission for the case of palladium that had been used properly for the cold fusion experiment. We can understand that the same discussion would be taken for the case of Tungsten electrode.

The discussion was not only the case of Palladium electrode but also essentially consist for Tungsten electrode. There are two peaks for the element distribution of the product of Tungsten electrode as shown in table 1. One peak is the major element of iron and zinc and other is the In. The total generated amount of element for the case of excess heat evolved was calibrated as the order of mg. Meanwhile, the total excess heat was calculated as the order of 10^6J from the products. The mechanism is well explained the excess heat evolution. We can say the photo-fission mechanism explain the amount of excess heat and the distribution of the element generation during the electrochemical treatment.

References

1. T. Mizuno et al., Electrochemistry, 64, No.11, (1996) 1160.

2. E. M. Drobyshevskii, Y.A. Dunaev and S. I. Rozov, Sov. Phys. Tech. Phys., 18 (1973) 772.
3. V. M. Sokolov, Sov. Phys. Tech. Phys., 29 (1984) 1112.
4. E. P. Koval'chuk, O. M. Yanchuk and O. V. Reshetnyak, Phys. Lett. A, 189 (1994) 15.
5. E. M. Drobyshevskii, B. G. Zhukov, B. I. Reznikov and S. I. Rozov, Sov. Phys. Tech. Phys., 22 (1977) 148.
6. A. Hickling and M. D. Ingram, Trans. Faraday Soc., 60 (1964) 783.
7. A. Hickling, Modern Aspects of Electrochemistry No. 6, Ed. by J. O'M Bockris and B. E. Conway, Plenum Press, New York (1971) 329-373.
8. S. K. Sengupta and O. P. Singh, J. Electroanal. Chem., 301 (1991) 189.
9. S. K. Sengupta and O. P. Singh and A. K. Srivastava, J. Electrochem. Soc., 145 (1998) 2209.
10. K. Azumi, T. Mizuno, T. Akimoto and T. Ohmori, J Electrochem. Soc., 146 (1999) 3347.
11. A. Takahashi, M. Ohta and T. Mizuno, Proc. 8-th Int. Conf. Cold Fusion, (2000).

Table1 Analytical results of the total element in the electrolysis system

Element	Before (mg)	After electrolysis Large excess heat	After electrolysis Small excess heat
Al	0 .006	1.2	0.5
Si	1.4	2.0	1.5
P	0.5	0.5	0.5
S	0.4	0. 6	0.6
Cl	0.8	1.0	0.85
Ca	0.06	0.45	0.12
Ti	0.001	0.8	0.15
Cr	0.001	1.4	0.005
Fe	0.024	2.5	0.055
Ni	0.001	0.02	0.004
Cu	0.14	0.03	0.16
Zn	0.001	0.75	0.001
Ge	0.01	1.2	0.01
Pd	0.01	0. 5	0.01
Ag	0.01	0. 12	0.01
In	0.01	1.1	0.01

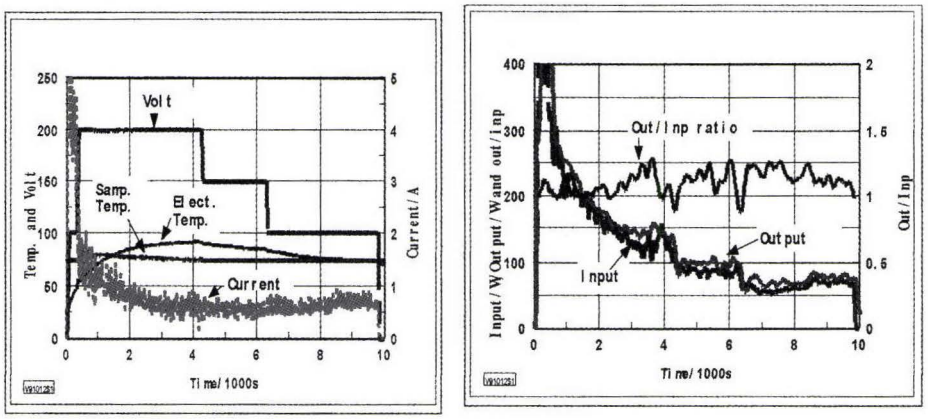

Fig. 1 Result of small excess heat of 0.5-mm thickness Tungsten plate in 0.2 M K2CO3.
Left; Changes of input volt, current, electrolyte temperature and electrode temperature (vertical scale, 1/10).
Right; Changes of input, output and their ratio during plasma electrolysis.

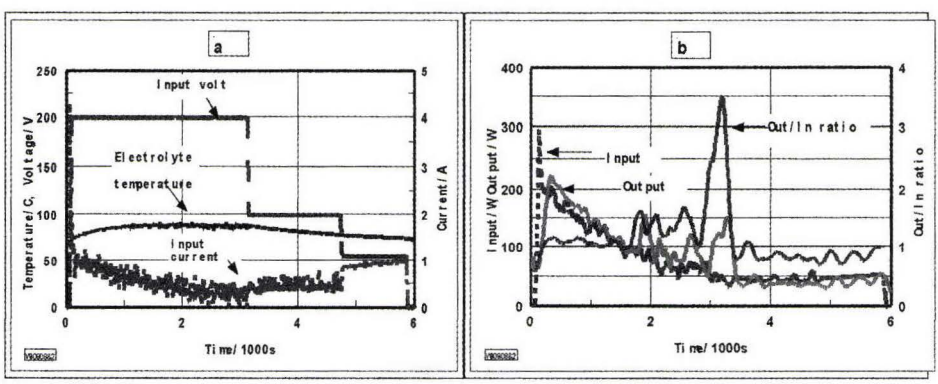

Fig.2 Result of large excess heat generation during plasma electrolysis of Tungsten electrode.
Left; Changes of input volt, current, electrolyte temperature.
Right; Changes of input, output and their ratio during plasma electrolysis.

Conference Proceedings Vol. 70
"ICCF8"
F. Scaramuzzi (Ed.)
SIF, Bologna, 2000

An Energy Amplifier Device

U. Mastromatteo – Sensors & Actuators development Manager

STMicroelectronics
Via Tolomeo, 1 – 20010 Cornaredo (MI), Italy
Phone: +39 0293519416, Fax: +39 0293519354,
E-Mail: ubaldo.mastromatteo@st.com

Abstract.
After more than ten years from the beginning of the experiments, in laboratories of many countries, aimed to confirm the phenomenology claimed by Fleischmann and Pons in March 1989, in which the lattice of hydrogen-loaded metals nuclear reactions can take place at temperatures not above a few hundreds degrees centigrade; the scientific certainty of this possibility has been achieved.
Actually, the work of cold fusion experimenters is now mainly devoted to finding the best technological approach to activate these phenomena in a reproducible, efficient, clean way.
A more attractive approach uses a simple nickel layer at high temperature in a hydrogen environment.
Many experiments using this kind of approach demonstrated a very interesting correlation between excess heat coming from hydrogen-loaded nickel and electrical, thermodynamic conditions of the system.
Using a peculiar system configuration devoted to the qualitative study of these phenomena, in recent experiments it was possible to evaluate approximately the average micro-system amplification. Moreover, in the spots where excess energy melted the material, the amplification was estimated to be larger than 10.
Under way is an effort to change the system to control, with a suitable feedback block, the local amplification values, in order to extend them in a stable way to the main part of the active material.
A general partitioning of the Energy Amplifier System is showed in figure 1.

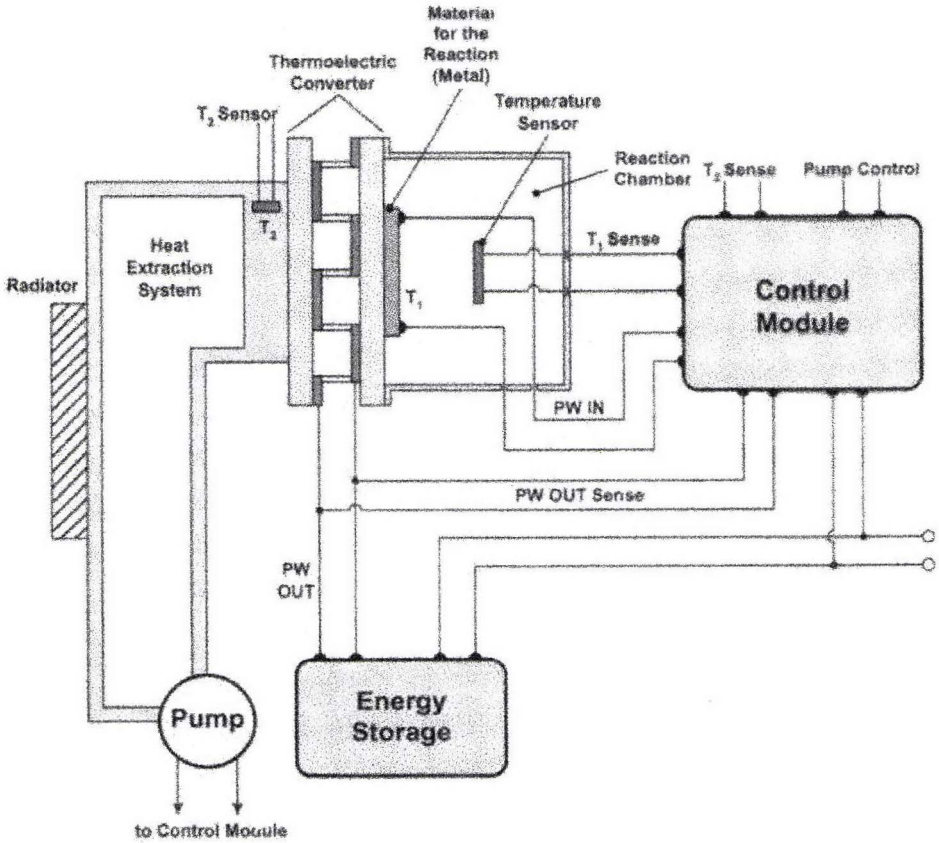

Figure 1 - The energy amplifier & other control modules

Introduction

In a previous paper[1,2] we described the preliminary results obtained in experiments devoted to study the behavior of very thin nickel layers at high temperature (350 – 450 °C) in presence of hydrogen.

The reason for this research is in the possibility, claimed by numerous researchers in Italy and abroad, that in peculiar thermodynamic conditions in the nickel hydrogen system, exoenergetic nuclear phenomena may occur.

The used samples were small silicon chips, in which separated by a dielectric layer, two nickel resistors were constructed. The dimension of such resistors being 3.3 mm in length, 10 microns in width and 0.1 micron in thickness.

One of these two resistors is placed on a SiO_2 layer (inert even at very high temperature), while the other is on a special dielectric layer with high content of hydrogen bonds (10% of Si-H, N-H are present in a PECVD (Plasma Enhanced Chemical Vapor Deposition) silicon nitride, which means a concentration higher than $1x10^{22}$ cm^{-3}).

To induce hydrogen absorption, a suitable hermetic stainless steel chamber has been set up in which it is possible to put the sample and reduce the pressure below 10^{-3} torr. Heating the sample at a temperature higher than 350 °C, a slow release of H^+ from broken hydrogen bonds in the PECVD silicon nitride is produced (the solid source underneath the nickel resistors). In a few experiments a hydrogen atmosphere is created, filling the chamber with Forming gas (5% H_2 in N_2) and heating the samples.
To heat the cell it is possible to use the polysilicon heater underneath the solid source or the nickel resistors as showed in the schematic cross section of the cell (Figure 2).
During the initial phase of this work, mainly devoted to the comprehension of the material behavior, the short duration of the experiments and the flexibility of the system, allowed us to evaluate several boundary conditions.
On the basis of the experimental conditions, it is possible to separate the tests in different groups: a first one with the samples under vacuum and with the hydrogen released by the solid source, a second one with the gas H_2/ N_2 in the chamber, a third one in the N_2 environment using the solid source, and a fourth, covering the resistors with a solid source layer on top to avoid the nickel oxidation, making the experiments in air under an optical microscope to observe in real time the nickel layer changes. A fifth recent group of experiments has been performed, putting the samples in a SEM chamber and biasing the nickel resistor with high-density current pulses. The use of the SEM chamber allowed us to follow in real time the changes in the nickel layer structure (in two cases a low quality video tape recording was possible).
The main difference between the experiments is in the power needed to heat the samples, because the thermal resistance with vacuum and with the gas differs more than one order of magnitude.
So in the case of vacuum the current in the nickel (when used as heater) was 3-4 times lower than in the case of gaseous atmosphere.
When the polysilicon heater was used, the changes in the nickel layer, produced in a longer time, were more uniform in terms of area involved, but in this case it was not possible to evaluate any energy amplification.
However the hypothesis that is possible to formulate about the observed phenomenology can include these tests as well.
It may be useful at this point to remember that all the tests performed can offer us only a qualitative evaluation of the material behavior. This is due to the very small thermal capacitance and very high thermal resistance of the system.
These two conditions are both implying a strong and fast temperature rise, even if the energy generation spots are random and short.
As mentioned above, the main purpose of the initial phase of this research was a qualitative evaluation of the nickel-hydrogen behavior. So to start a quantitative evaluation phase, some changes are necessary in the system to correct its limitations.
The main action is the reduction of the thermal resistance of the system. This may be obtained using larger size nickel samples, directly in contact with a silicon substrate and performing the test in an H_2 gas atmosphere.
This change in the system heat sinking also increases the thermal capacitance of the samples, avoiding fast temperature rising in case of excess power production in the nickel layer.
Hence, the samples should work long enough to allow a clear quantitative measurement of the amplification and probably of nuclear transmutation in the material.

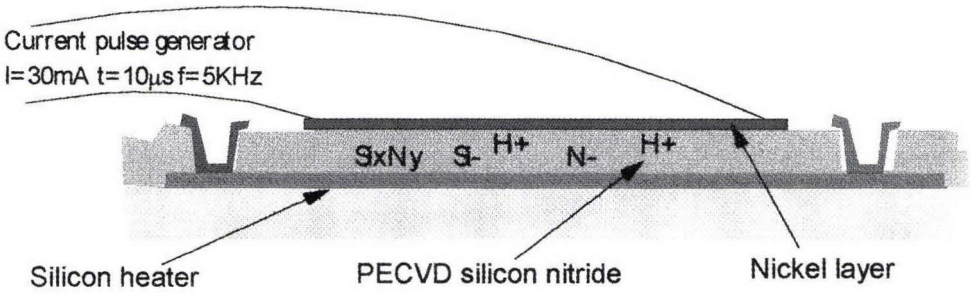

Figure 2 - Schematic cross section of the cell

The don Borghi's work.

The interpretation of the old and new results is based on don Borghi's experimental work. To whoever is not aware of it and its theoretical foundations, due to the difficulties of providing here even a short review, I recommend examining the papers mentioned in the references[3]. To be sure, theoretical quantum mechanics can provide objections to the theoretical foundations of don Borghi's work, also consider that it was done around the 1940. Nevertheless, it is the opinion of experts in the nuclear field that the experimental results remain qualitatively incontrovertible[4,5,6].

Let's now take a look at the analogies between don Borghi's reactor and the structure of the samples we designed to verify the nickel behavior in the presence of hydrogen at high temperature:

1. When, usually at temperatures above 250-300 °C, the nickel layer absorbs hydrogen, this is ionized and in the metallic lattice behaves like a plasma. If we imagine $1cm^3$ of nickel with 10^{-3} as <H/Ni> ratio, the plasma pressure is $(10^{-3}/6.59)x22.4x10^3$ atmospheres (3.4 atm).
2. Using current pulses it is possible to increase the probability of creating neutral particle trough electron-proton interaction, at such low energies to have immediate absorption into nickel nuclei.

In practice, what in don Borghi's reactor was obtained by the RF electric field in the H_2 gas, is automatically produced by the simple absorption in the nickel lattice. Also, the opposed movement of electrons and protons induced by the anodic current is induced simply by biasing the metallic layer endings. Moreover, in the metallic lattice there is a perfect current confinement with the possibility of reaching very high current densities.

Results from six different system configurations (4 and 5 are equivalent);

1. Tests with indirect heating, samples in vacuum and hydrogen solid source (Figure 3);

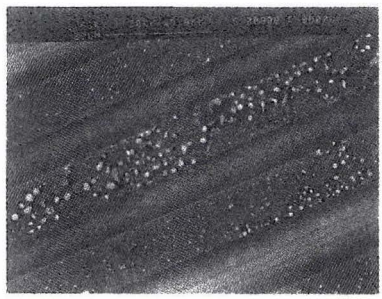

Figure 3 - Nickel resistor showing melted areas

2. Tests with DC direct heating, samples in vacuum and hydrogen solid source;
3. Tests with H_2/ N_2 3% gas and DC direct heating (Figure 4);

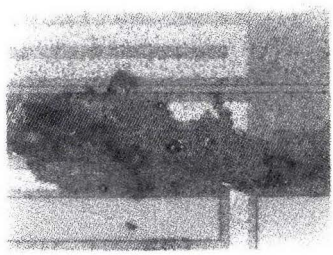

Figure 4 - Nickel resistor showing large melted areas

4. Tests in N_2 gas, solid source for the hydrogen and DC direct heating;
5. Tests done in air with DC/AC direct heating and the nickel resistor interposed between two hydrogen solid source layers (Figure 5);

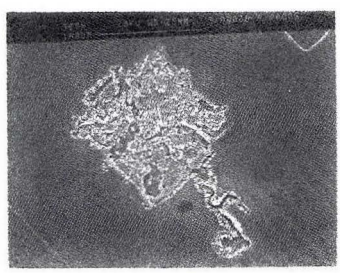

Figure 5 - Nickel resistor showing melted area

6. Tests under vacuum, direct heating by high density current pulses ($3x10^6$ A/cm2) and hydrogen solid source (Figure 6);

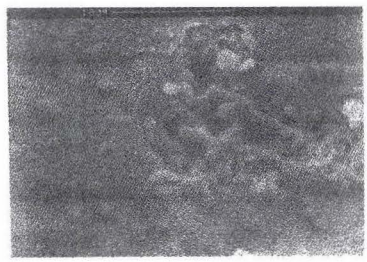

Figure 6 - Nickel resistor and underneath material melted

Heating method	*Sample Environment*	*Current density A/cm²*	*Hydrogen source*	*Power supply*	*Amplification*
Indirect	Vacuum	0	Solid	DC	~1
Direct	Vacuum	$.5\ 10^6$	Solid	DC	~1
Direct	Gas H_2+ N_2	$2\ 10^6$	Gas	DC	>1
Direct	Air/ N_2	$2\ 10^6$	Solid	DC/AC	>1
Direct	Vacuum	$3\ 10^6$	Solid	Pulse	>10

The above table summarizes the test conditions and results.

In conclusion, we succeeded in obtaining under vacuum, with low power-in and energy pulses, what we obtained in DC power with a power twenty times higher. The common parameter in the tests giving excess energy is the current density.

The energy amplifier device.

What we have described above allowed us to make an approximate evaluation of the amplification factor. It is valuable only in the case of pulsed input power, when the energy is lower than the energy necessary to induce the nickel and also the underneath polysilicon heater melting. In the case of DC power-in, the amplification is not easily valuable because the short duration of the excess energy production (needed to destroy the sample), hasn't got a corresponding time interval on which to integrate the input power energy calculation.

Excess energy generator model.

The thermal behavior of the system can be evaluated using the electrical equivalent circuit showed in the figure 7

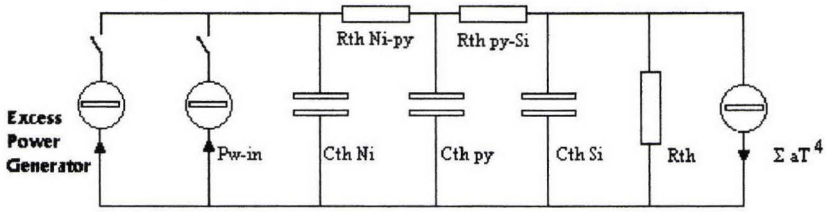

Figure 7 – Electrical equivalent circuit

Symbols legend:
Cth Ni = nickel layer thermal capacitance;
Cth py = polysilicon heater thermal capacitance;
Cth Si = silicon substrate thermal capacitance;
Rth Ni-py = PECVD silicon nitride layer thermal resistance;
Rth py-Si = silicon oxide layer thermal resistance;
Rth = silicon substrate thermal resistance;
ΣaT^4 = energy lost by irradiation;

The excess power generator represents the energy per second generated in the nickel layer through the nuclear reaction chains induced by electron-proton interactions.
So let's try to arrange on the basis of a very simple classical calculation a qualitative model of the excess energy power generator.

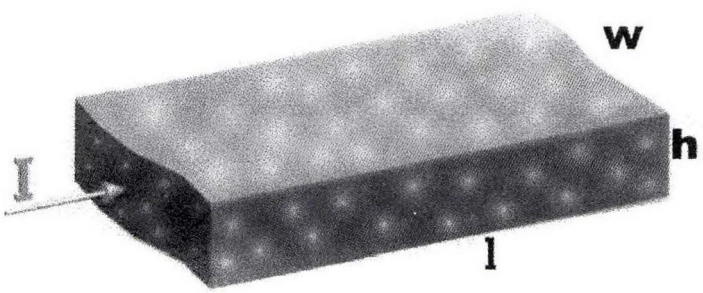

Figure 8 - a small fragment of the nickel resistor can be schematized like a box.

The complete sample is 1cm long, 10 μm wide, and .1 μm thick; so in what follows we will refer to these dimensions for modeling the microsystem thermal parameters (Figure 8).
Inside the nickel the electrons movement gives the current. The interaction we think is based on nuclear chain reactions occurring when the electron-proton distance is less than the "r_o" (2.5×10^{-13} cm) value (don Borghi theory). To calculate the number of interactions, we proceed classically.

The charge **"e"** which moves with a speed **"v"** explores a volume $\pi r_o^2 v$ per second (σv).

The number of electrons pushed by the electric field in the unitary volume is:

$$n = \frac{I}{e} * \frac{\ell}{vV}$$

where

$$\frac{I}{e} \qquad (e = 1.6 \cdot 10^{-19} C)$$

is the number of particles crossing each second the section "***wh***" of the nickel resistor, "***l/v***" is the time necessary to cross the length "***l***" of the sample and "***V***" is the sample volume ("***lhw***").
Hence:

$$n = \frac{I}{e} \bullet \frac{\ell}{v \cdot w \cdot h \cdot \ell} \Rightarrow \frac{J \cdot w \cdot h}{e} \bullet \frac{\ell}{v \cdot w \cdot h \cdot \ell} \Rightarrow \frac{J}{e \cdot v}$$

(where J is the current density).
Multiplying the single particle explored volume by the number of particles per unitary volume, we obtain how many times the unitary volume is explored each second (cm^3/sec).

It is:

$$\frac{J}{e \cdot v} \sigma \, v \Rightarrow \frac{J \sigma}{e}$$

To know the number of interactions per second we have to multiply the value above by the number of proton targets in the unitary volume; this number is given by the molar concentration ratio <H/Ni> divided by the molar volume (of the nickel if we suppose it is not changing too much after hydrogen absorption), multiplied by Avogadro's number N_a (6.023×10^{23}). (The molar volume is the atomic weight divided by the specific weight 58/8.9).

So the number of interaction per second and per unitary volume is:

$$\frac{J \sigma}{e} \langle H/Ni \rangle \frac{8.9}{58} N_a$$

If each event is associated an energy "***Ei***" and the total volume of the sample is "V_{ol}", we obtain a generator with power given by:

$$NEi \Rightarrow \frac{J \sigma}{e} \langle H/Ni \rangle \frac{8.9}{58} N_a V_{ol} Ei$$

Ei can easily be closed to 1 Mev.

Before going to set the parameters in the equivalent thermal circuit, it is necessary to make a hypothesis about how the cross section "σ" may change with the temperature change. If we consider that the temperature changes almost linearly, the electric resistance due to the

increased collisions of the electrons with the lattice, in the same way we can consider the "σ" variation versus temperature[7].

Hence: $\sigma(T)=\sigma_o(1+\alpha\Delta T)$

If, for a given sample, we set:

$$\beta = \frac{Ei\sigma_o}{e}\frac{8.9}{58}N_a V_{ol}$$

The generator power becomes:

$$P_{Wexc}(J,T,\langle H/Ni\rangle) \Rightarrow J\beta(1+\alpha\Delta T)\langle H/Ni\rangle$$

For the sample used in most of our experiments $\beta = 1.8\text{x } 10^{-4}$ (Wcm^2A^{-1})
In the case of ***Ei*** = 1Mev, being ***J*** in the range of $2 - 4\text{x}10^6$ A/cm^2, even for <H/Ni> around 1/2000 the extra power is more than 1 Watt. This means that, without a suitable duty cycle for the input power switching "***J***", the sample can quickly reach a temperature of more than 1000 °C.

Results and Conclusions

The equivalent thermal circuit has been used to simulate the behavior observed during the test in two different conditions and the fitting is very good. In one test an increase of 200 °C has been observed driving the input power at 40 mW (average value) using 10 μs pulses and 1 KHz as frequency. The temperature rise is equivalent in our model to an extra power of 244 mW and a <H/Ni> ratio of $9.7\text{x}10^{-3}$; the power amplification considering only the power input in the nickel (270 mW were supplied to the polysilicon heater) is about 6.
In another test, the input power was all supplied to the nickel using 10 μs pulses at a frequency of 6 KHz with a current density of about $3\text{x}10^6$ A/cm^2 corresponding to an average total power of about 500 mW. This second test produced the melting of nickel and of the polysilicon underneath in large spots. A very conservative calculation of the excess power in the melted spots gives a value of $.77\text{x}10^{-3}$ for <H/Ni> and a minimum of 3 as energy amplification.

A new energy amplifier has been set up changing the thermal elements that in the previous gave up the sample destruction at very low amplification levels. The new one is able to dissipate several watts without exceeding 600°C. This condition will allow us to have longer working time amplifying 20 times an input power of few hundreds mW. The proper hydrogen concentration in the nickel will be achieved using a gaseous hydrogen source (pure or diluted).

The thermal equivalent circuit of the new samples to test the energy amplifier is shown in the figure 9. The symbols meaning n this case is: Cth = total thermal capacitance; Rth = total thermal resistance, because only a very thin dielectric layer separates the nickel from the substrate.

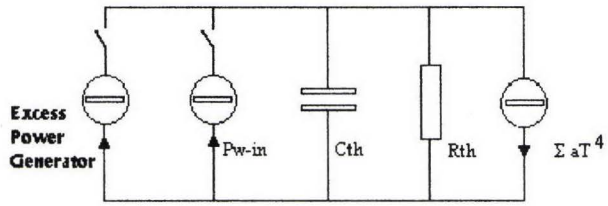

Figure 9 – New samples electrical equivalent circuit

Acknowledgments

The author is indebted to Dario Galletti for technical assistance in failure analysis of samples and SEM observations of experiments; to Franco Coccetta for technical assistance during recent experiments and for computer simulation of electrical equivalent circuits.

References

1. U. Mastromatteo – "Hydrogen loaded thin nickel layers show high temperature hot spots" - Proc. 3rd Asti Workshop-Conf. Proc. SIF – Vol 64 (1999)
2. U. Mastromatteo – " Very thin nickel layers heated over Curie temperature show high temperature spots in hydrogen loading experiments" – Proc. ICCF-7 Vancouver (1998)
3. C. Borghi et al. – "Experimental evidence on the emission of Neutron from Cold Hydrogen Plasma" – Comunicaones do CENUFPE- n. 8 Recife (Brazil) (1969); Phys.At.Nucl. 56,993(1993)
4. L. Daddi – "Dai miniatomi ai maxineutroni: intrappolamento e cattura di elettroni come precursori di reazioni nucleari a bassa energia" – Pubblicaz. Scient. Accademia Navale di Livorno – Livorno 1998
5. E. Conte – " On a Theoretical Explanation of Cold Fusion of Protons and Electrons into Neutrons" – Infinite Energy 24, 49 (1999)
6. L. Daddi – "On the Detection of Cold Fusion Neutrons by Radioactivation" – Proc. 3rd Asti Workshop-Conf. Proc. SIF – Vol 64 (1999)
7. C. Kittel – "Elementary Solid State Physics" – Wiley & Sons NY (1962)

Conference Proceedings Vol. 70
"ICCF8"
F. Scaramuzzi (Ed.)
SIF, Bologna, 2000

Measurements of Excess Heat in the Open Pd|D_2O Electrolytic System by the Calvet Calorimetry

Z.-L. Zhang, W.-S. Zhang, M.-H. Zhong and F. Tan

Institute of Chemistry & Center for Molecular Science, Chinese Academy of Sciences
P.O. Box 2709, Beijing 100080, P.R. China; E-mail: wszhang@a-1.net.cn

Abstract

Excess heat was observed in the Pd|D_2O electrolytic system using a Calvet type microcalorimeter. It was found that the average excess power was 0.025 W over 79 hours period. This result corresponds to a volume excess power of 8.75 W /cm^3 Pd or a surface excess power of 0.044 W /cm^2 Pd, and a specific excess heat of 2.48 MJ/cm^3 Pd or 228 eV/atom Pd. The current density and D/Pd ratio for excess power production were lower than the recognized 'threshold' values 100–150 mA/cm^2 and 0.83–0.92 D/Pd, this indicates that the critical requirement for reproduction of the anomalous heat can be 'cut down' using high sensitivity calorimetry. By comparison with that of the Pd|D_2O system, no anomalous excess heat was measured in the Pd|H_2O electrolytic system within the experimental uncertainty.

1. Introduction

Since the discovery of the anomalous excess heat in the Pd|D_2O electrolytic system [1], there have been continuing controversies on this result in the scientific community; one of the problems is the calorimetric method. As predicted by Storms in an extensive review [2], the isoperibolic calorimetry used by Fleischmann and other researchers introduces some uncertainty and complexity, *e.g.* the problems of inhomogeneous distribution of temperature in the electrolyte, recombination of D_2 and O_2 gas in the cell and effect of the stagnant water layer at the cell wall on the thermal conductivity of the wall etc. Strictly speaking, the isoperibolic calorimeter usually measures overall heat but not power at any time in a process. Another widely using method in cold fusion experiments, the mass-flow calorimetry, is adapted but not preferred means in power measurement at present. On the other hand, the Calvet calorimetry has been used in thermokinetics for more than a half century. It not only provides a high sensitivity but also depends weakly on the thermal homogeneity (the isoperibolic assumption) in the measuring vessel. The great differences between these three methods can be demonstrated by the magnitudes of the minimum value of current density for excess heat production in the Pd|D_2O electrolytic system. Based on the results measured by the isoperibolic and mass-flow calorimetry, Fleischmann *et al* [1], McKubre *et al* [3] and other researchers all mentioned that the minimum current density (known as the 'threshold value') is 100–150 mA/cm^2. Nevertheless, Bush and Lagowski [4], and our results showed that 10–50 mA/cm^2 is enough to produce excess heat using the Calvet calorimetry. This fact indicates that the anomalous excess heat can be easily detected, in other words the critical requirement for reproducibility of the anomalous excess heat can be 'cut down', by using high sensitivity calorimetry.

Starting in 1989, our group has been continually involved in studying the anomalous excess heat in the Pd|D_2O (H_2O) electrolytic system by the Calvet calorimetry [5] as well

as some material and electrochemical characteristics of Pd|D (H) electrode [6]. In the present paper, we report some of the result obtained in the last experiment.

2. Experimental

The electrolytic cell consisted of a glass vessel (inner ϕ 12 × 40 mm) and electrodes in the $LiNO_3 + D_2O$ solution as shown in Fig. 1. The cathode was made of a palladium wire (ϕ 0.2 × 50–90 mm, 99.9% purity) wound round a PTFE rod, each cathode end was spot welded to two platinum leads (ϕ 0.2 × 50 mm) for measuring atomic ratio of D/Pd by the resistance method. The anode was made of a platinum wire (ϕ 0.02 × 100 mm) wound round another PTFE rod. All platinum wire leads were covered with thin-walled PTFE tubes to minimize their contact with electrolyte and catalysis of $D_2 + O_2$ combination. Both the cathode and anode were partially inserted in an appropriately machined PTFE piece, which ensured good permanent positioning of the electrodes and fixed distance (ca. 2 mm) between them. A diaphragm made of a PTFE plate with thin holes in it was used in the cell to separate the cathode and anode compartments and to prevent from D_2 and O_2 gas bubbles mixing. The 5 M $LiNO_3$ heavy water solution was prepared by dissolving $LiNO_3$ (No. 3 reagent plant of Shanghai, AR) in D_2O (Beijing chemical plant, 99.8% isotopic purity). The cell was filled with about 2 ml of the electrolyte solution.

The electrolytic cell was coiled with an isolated resistance wire as a calibration heater and placed in a stainless steel container (inner ϕ 16.9 × 60 mm). An appropriate amount of silicon oil was filled in the space between the glass vessel and stainless steel wall for good heat conductivity.

Figure 2 shows the experimental apparatus. A microcalorimeter, LKB 2107 made in Sweden, was employed in our work, it is a kind of instrument used to determine the heat flow evolved or absorbed in a process undergoing in a system and it is used widely in thermokinetic studies. The overall thermal flux produced in the system converts to electromotive force, and has a simple linear relationship to the output signal in voltage. This sort of calorimetry avoids the problem of inhomogeneous distribution of temperature in the isoperibolic calorimetry, and has much more sensitivity than the mass-flow calorimetry. The effect of slight temperature fluctuation around the calorimeter is eliminated by the twin cell design. The temperature in the air bath in which the calorimeter is mounted was maintained at 40.00 ± 0.02 °C.

With multiplexed computer data acquisition, the data associated with the input power, output power and D/Pd ratio were displayed in real time on the computer monitor and also stored on disc using a software package.

Finally, all electrolysis was carried out under the galvanostatic condition, the applied current was typically between 25 and 30 mA, which was measured as a voltage drop across a standard resistor. The light water solution was used in blank experiments for comparison.

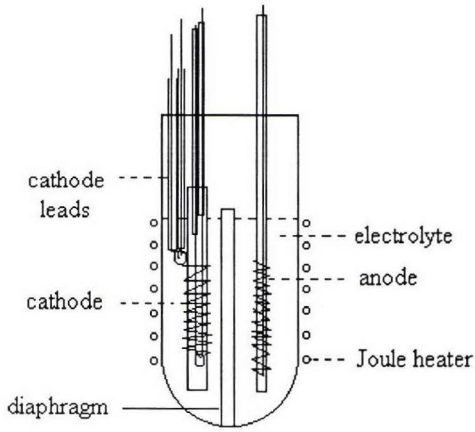

Fig. 1. Schematic diagram of the electrolytic cell.

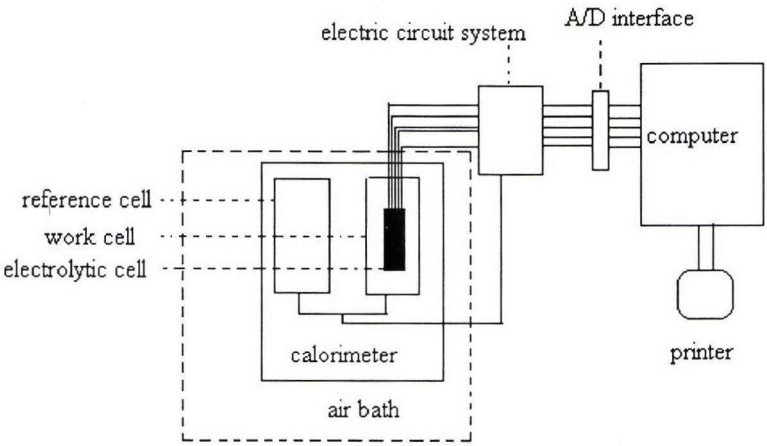

Fig. 2. Schematic diagram of the experimental apparatus.

3. Results and discussion

In order to verify the accuracy and reliability of the calorimeter, a number of calibration experiments were performed with Joule heating after the temperature in the air bath and calorimetric experimental zero were stable. It was found that the precision was better than ± 2% with the applied power being just about that of the electrolysis and the device constant did not change within the error 1% before and after the electrolysis.

A run of calorimetric experiment on the Pd|D_2O (H_2O) electrolytic system was always carried out over several days. In general, the calorimetry on the electrolytic system lasted about 20 hours. Between two calorimetric experiments, the calorimeter was calibrated and heavy water (light water) was added into the electrolytic cell to compensate the D_2O (H_2O) consumption in electrolysis and the evaporation in the gas stream escaping from the cell

although the latter was very small.

The excess power is calculated from the input, output and water electrolysis powers:

$$P_{ex} = P_{out} + IV_{th} - IV \qquad (1)$$

where P_{out} is the output power measured by the calorimeter; I is the applied current; V is the measured potential drop across the electrolytic cell; V_{th} is the thermoneutral potential in the water electrolysis, V_{th} = 1.524 and 1.478 V at 40 °C for D_2O and H_2O, respectively.

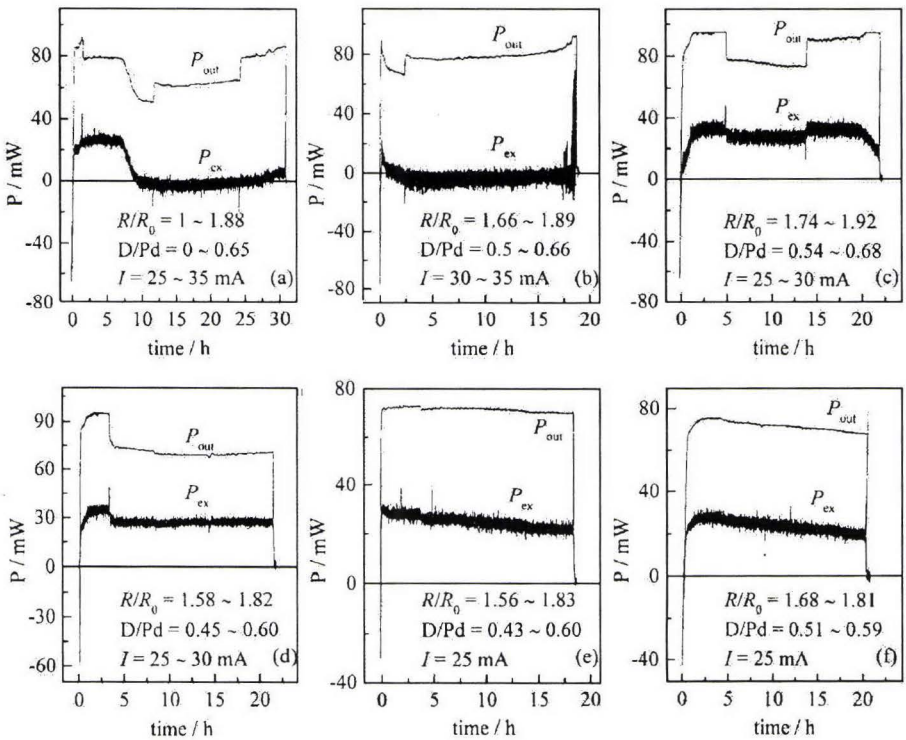

Fig. 3. Calorimetric results of Pd|(5M $LiNO_3$ + D_2O) system, T = 40 °C, sizes of Pd cathode: ϕ 0.2 × 91 mm.

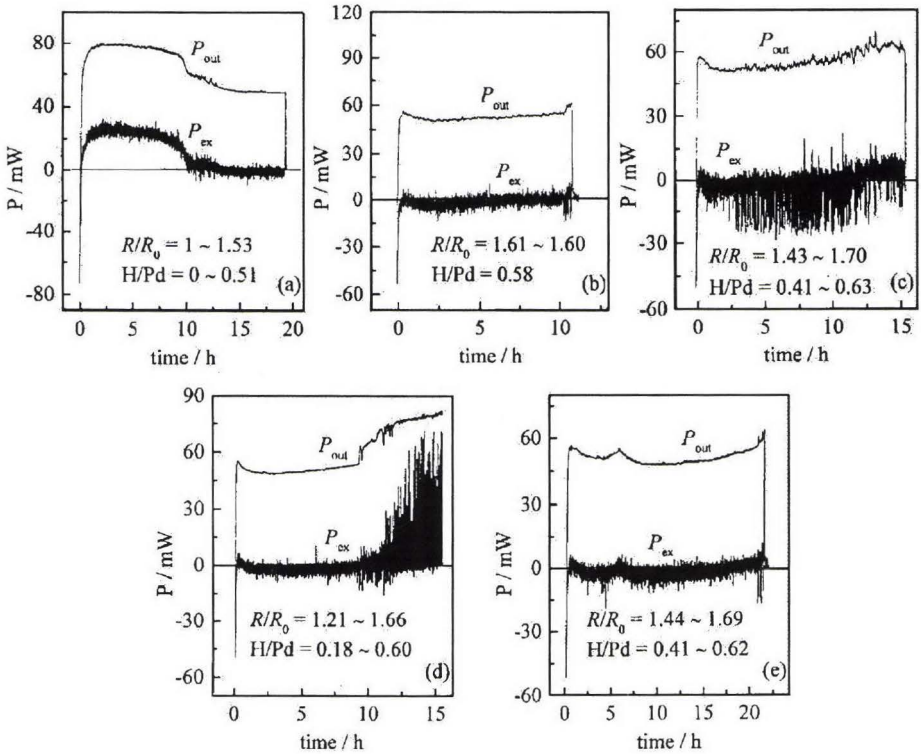

Fig. 4. Calorimetric results of Pd|(5M $LiNO_3$ + H_2O) system, T = 40 °C, I = 25 mA, sizes of Pd cathode: ϕ 0.2 × 55 mm.

There have been seven runs of calorimetric experiment on Pd|D_2O (H_2O) electrolytic systems being performed in two months period. Most of Pd|D_2O systems exhibited excess heat in different magnitudes of excess power and sustaining time. Two runs of calorimetric results throughout the experiments for Pd + D_2O and Pd + H_2O systems are shown in Figs. 3 and 4, respectively. Each figure shows the output power and excess power calculated according to Eq. (1) in less than one-day period. The applied current, resistance ratio of PdH_x to Pd (R/R_0) and loading ratio of D/Pd are noted in each figure.

By Figs. 3 and 4, we find that both the D_2O and H_2O systems exhibit excess heat (ca. 500–800 J) at the beginning of electrolysis. Because it is greater than the enthalpy of palladium deuteride (hydride) formation (≤ 5 J) and any chemical process associated with $LiNO_3$ is endothermic, so we only attribute it to unknown chemical process, which needs further research in future. Subsequently, both these two systems experience the trivial time of no excess heat. The distinction between them appears at the latter time, we find the excess heat is produced in the Pd|D_2O system on the third day and it lasts for 4 days; otherwise, the Pd|H_2O system exhibits no any excess heat during the rest time and it also provides a calibration for the calorimeter in some sense. These results clearly indicate that the Pd|D_2O electrolytic system produces anomalous excess power.

For result in Fig. 3, the average excess power over 79 hours is 0.025 W which corresponds to a volume excess power of 8.75 W /cm^3 Pd or a surface power of 0.044 W /cm^2 Pd. The maximum excess power shown in Fig. 3 is 0.035 W, the ratio of excess power

to input power ranged from 48% to 83%. The overall excess heat corresponds to 2.48 MJ/cm^3 Pd or 228 eV/atom Pd which appears to be well beyond any chemical process can be expected to release.

Our calorimetric results showed an excess power that was quite in line with other positive results reported up to now. In particular, if we consider the excess power per unit electrode surface area as a function of the current density, our result is beyond the general behavior pointed out by Storms [2] by considering many calorimetric measurements on the $Pd|D_2O$ system in various laboratories. The applied current density for production of the excess heat in Fig. 3, 44–53 mA/cm^2, is lower than the 'threshold' value 100–150 mA/cm^2 mentioned by Fleischmann, McKubre and other researchers [1,3,7]. However, it is consistent with the result of Bush and Lagowski [4] who found 10–30 mA/ cm^2 is enough to produce excess heat using the Calvet calorimetry. At the same time, the loading ratios accompanying the excess heat production in Fig. 3 are between 0.51–0.68 D/Pd which are lower than the 'threshold' value, 0.83–0.92 D/Pd, first mentioned by McKubre *et al* [3] and Kunimatsu *et al* [7]. Both results indicate the 'threshold' current density and D/Pd ratio for anomalous heat production may be 'cut down' using a high sensitivity calorimeter. Of course, our experiment was performed at a higher temperature (40 °C) than before used (20–30 °C), this difference may cause the triggering condition of the excess heat being modified. On the other hand, these results are qualitative and the quantitative relation of excess power *vs.* current density and loading ratio needs further research in future works.

Acknowledgements

This work was supported by the Natural Science Foundation of China under Grant No. 19455001 and the President's Innovation Foundation in Chinese Academy of Sciences.

References

[1]FLEISCHMANN M., PONS S. AND HAWKINS M.: J. Electroanal. Chem., 261, (1989) 301; errata, J. Electroanal. Chem., 263, (1989) 187.

[2]STORMS E.: Fusion Tech., 29, (1996) 261; Infinite Energy, vol. 5, #21, (1998) 15.

[3]MCKUBRE M.C.H., CROUCH-BAKER S., RILEY A.M., SMEDLEY S.I. AND TANZELLA F.L.: in Frontiers of Cold Fusion, Proc. 3rd Int. Conf. on Cold Fusion, edited by H. IKEGAMI, Nagaya, Japan, October 21-25, 1992, (Universal Academy Press, Tokyo) 1993, pp. 5.

[4]BUSH B.F. AND LAGOWSKI J.J.: in Proc. 7th Int. Conf. on Cold Fusion, Vancouver, British Columbia, Canada, April 19-24, 1998, pp.38.

[5]ZHANG Z.L. *et al*: AIP Conf. Proc. 228, Provo, UT, 1990, pp. 572; Fusion Facts, 1994, #2, pp. 27; J. Thermal Analysis, 45, (1995) 99.

[6]ZHANG W.S. *et al*: J. Electroanal. Chem., 434, (1997) 31; 445, (1998) 55; 458, (1998) 107; 474, (1999) 123 & 130; 481, (2000) 13; J. Alloys Comp., 302, (2000) 258.

[7] KUNIMATSU K. *et al*: in Ref [3], pp. 31.

Conference Proceedings Vol. 70
"ICCF8"
F. Scaramuzzi (Ed.)
SIF, Bologna, 2000

Calorimetric Studies of Palladium Alloy Cathodes Using Fleischmann-Pons Dewar Type Cells

Melvin H. Miles*
New Hydrogen Energy Laboratory
3-5 Techno-Park 2-Chome Shimonopporo
Atsubetsu-Ku, Sapporo-004, Japan

ABSTRACT

My first three experiments conducted at NHE using the Fleischmann-Pons (F-P) Dewar type cells investigated the Pd-Ce-B, Pd-B, and Pd-Ce alloy cathodes. Significant excess power was produced from the cells using the Pd-B and Pd-Ce alloy cathodes. The Pd-Ce-B alloy, in contrast, showed no measureable excess power effects. Previous experiments at China Lake using similar Pd-B alloy cathodes prepared by the Naval Research Laboratory (NRL) produced excess heat in seven out of eight experiments. The same Pd-Ce cathode that was used at NHE also produced significant excess power in previous experiments at China Lake. Due to the controversy over methods of data analysis for the F-P cells (see ICCF-5 Proceedings, 1995, pp. 105-115), I developed my own methods while at NHE. As I refined my methods for evaluating the calorimetric measurements, they approached more closely the methods outlined by Fleischmann and Pons in their Icarus Systems handbooks available at NHE. The method previously developed by NHE for the analysis of the F-P cells showed no excess heat for any of these same three experiments. The major problem with the NHE method is that a single calibration was used in determining the effective radiative heat transfer coefficient for the cell. An incorrect heat transfer coefficient can readily confuse the excess heat effect with the calorimetric error for the system. Calorimetric results for the same experiment using the NHE method, my method, and the F-P method for data analysis are compared. The fact that the alternative NHE method showed no excess heat for F-P cells illustrates the problem in transferring calorimetric methods from one laboratory to another. The second laboratory often fails to follow directions and makes changes that compromise the calorimetry. Similar problems were encountered in the attempt to transfer the China Lake calorimetry to NRL, hence excess heat was not observed.

INTRODUCTION

The New Energy Development Organization (NEDO) of Japan made it possible for me to return to cold fusion and to perform calorimetric experiments for a five-month period as a Guest Researcher at the New Hydrogen Energy (NHE) laboratory in Sapporo, Japan. Two types of isoperibolic calorimeters were used in these studies (1) China Lake type calorimetric cells where the heat transfer is mainly by conduction, and (2) Fleischmann-Pons Dewar type cells where the heat transfer occurs mainly by radiation. The excess power measured at NHE in the China Lake calorimetric cells has been reported elsewhere [1-5]. The focus here will be on three experiments using Pd-Ce-B, Pd-B, and Pd-Ce alloy cathodes in Fleischmann-Pons Dewar type cells. Previous experiments at China Lake using similar Pd-B alloy cathodes prepared by the Naval Research Laboratory produced excess heat in seven out of eight experiments [6,7]. The same Pd-Ce cathode that was used at NHE also produced significant excess power in previous experiments at China Lake [6,7]. The Pd-Ce-B alloy cathode prepared by NRL had never been previously investigated.

* Present address: NAWC Weapons Division, Code 4T4220D, China Lake, CA 93555 USA.Fax: (760) 939-1617. E-mail: milesmh@navair.navy.mil; melmiles@ridgecrest.ca.us

EXPERIMENTAL

The Pd-Ce-B and Pd-B (0.5 weight % boron) alloy cathodes were prepared at the Naval Research Laboratory [8], and the Pd-Ce alloy was obtained from Martin Fleischmann. In order to test possible effects of different polishing procedures, the Pd-Ce-B sample was polished using only silicon-carbide paper while the Pd-B sample was polished using normal NHE procedures involving diamond paste. The third sample, Pd-Ce, gave excess heat in a previous study at China Lake [6,7], but now contained a deep, long crack that was difficult to remove. This sample was polished by NHE procedures to remove the crack, while the final polish used silicon-carbide paper. The final dimensions of these three rods were 4.40x20.05 mm for the Pd-Ce-B sample (V=0.305 cm^3, A=2.92 cm^2), 4.71x20.1 mm for Pd-B (V=0.350 cm^3, A=3.15 cm^2), and 3.16x19.54 mm for Pd-Ce (V=0.153 cm^3, A=2.02 cm^2). These cathode rods were each spot welded on the side to platinum lead wires. Quick-setting Epoxy was used to cover the spot weld area, the top of the cathode, as well as the end of the glass tubing containing the platinum lead wire.

These electrodes along with the platinum anode cage structures were assembled in three similar Fleischmann-Pons cells. The platinum wire spiral anode was supported by a thin Kel-F disk containing glass rods at the base of the cell. Each cell also contained a resistive heater and two thermistors (short and long). The long thermistor was positioned in the bottom part of the cell above the electrodes while the short thermistor was located near the mid-point of the cell. The top of each cell contained a special Kel-F plug cap which seals in all of the components which protrude through it. This is to restrict all vapor to exit the cell strictly through the distillation tube also mounted in the cap. For experiments involving boiling of the electrolyte, the vapor is condensed and collected in a flask resting on an electronic balance. The Kel-F caps were sealed to the Dewar cells using clear silicon rubber and cured overnight.

The three Fleischmann-Pons cells were placed in a large water bath containing a glass window that allowed direct observations of the electrolysis. Each cell was filled with 90 cm^3 of 0.1 M LiOD+D_2O. The D_2O used throughout these experiments was from Isotec, Inc. (99.9 atom % D). The Dewar glass dimensions were 25.0 cm in height with the top 8.0 cm silvered. The outside circumference of the Dewar cell was 13.3 cm with an inner diameter of about 2.5 cm. It was determined that 82 cm^3 of the LiOD solution filled each cell to the bottom edge of the silvered portion. This mark was frequently used to determine the amount of D_2O required in refilling the cell. A special port in the cell top sealed with a solid glass rod was used to add D_2O with the aid of a graduated glass hypodermic syringe (5.0 cm^3) fitted with a stainless steel needle. An exact record was kept for all D_2O additions for each cell.

Each Dewar cell was connected to the Icarus 2.00 data acquisition system via eight connections: anode, cathode, short thermistor (2), long thermistor (2), and resistive heater (2). The power to each cell was controlled by its own potentiostat/galvanostat (Hi-Tek DT 2101) while a fourth instrument supplied power to the resistive heaters in each cell. A reading for the cell voltage, two cell temperatures, bath temperature, cell current, and time was recorded every 300 seconds for each of the three cells. These readings were also shown in real-time on the console display. This Icarus 2.00 system was similar to those used in earlier work in the IMRA-Europe laboratory in France.

CALORIMETRIC EQUATIONS AND MODELING

The Dewar-type Fleischmann-Pons electrochemical calorimetric cells are silvered in their top portions, thus heat transfer is confined almost exclusively to radiation across the lower, un-silvered region. The calorimetric equations, therefore, are given by

$$P_{calor} = P_{EL} + P_X + P_H - P_{out} - P_{gas} \quad (1)$$

where

$$P_{EL} = [E(t)-\gamma E_H]I \quad (2)$$

$$P_{out} = k_R (T^4_{cell} - T^4_{bath}) \quad (3)$$

$$P_{gas} = (\gamma I/F)\{[0.5\, C_{P,D2}+O.25\, C_{P,\,O2}+0.75\, (P/(P^*-P))C_{P,D2O\,(v)}]\Delta T + 0.75\, (P/(P^*-P))\, L\} \quad (4)$$

$$P_{calor} = C_{P,D2O\,(l)}\,[M^o(1+\beta)\,(\gamma It/2F)]\,(d\Delta T/dt) - (1+\beta)\,(\gamma I/2F)C_{P,\,D2O\,(l)}\cdot\Delta T \quad (5)$$

Excess power is represented by P_X and the power added to the cell via the calibration heater is given by P_H. The silvering of the top portion of the cell results in a radiative heat transfer coefficient (k_R) that is nearly independent of time. The thermoneutral potential (E_H), the heat of evaporation of D_2O (L), each heat capacity value (C_P), and the vapor pressure of D_2O (P) were always calculated based on the measured cell temperature (T_{cell}). The equations for these temperature-dependent calorimetric parameters are presented elsewhere [6]. The faradaic efficiency for the water electrolysis (γ) was always unity based on the D_2O consumption. Equations 1-5 are consistent with those reported previously by Fleischmann and Pons (9).

The use of Equations 1-5 to determine any excess power (P_X) requires the accurate determinations of two critical cell parameters: (1) the radiative heat transfer coefficient (k_R) and (2) the water equivalent of the cell ($M^oC_{p,D2O(l)}$) where M^o is the moles of D_2O initially present in the cell as well as at the refilled level. The values for M^o is 4.97 moles of D_2O for these experiments. The actual value to be used for the water equivalent is increased somewhat by the glass and other components of the cell. The accurate methods for determining these key cell parameters are presented in detail elsewhere [10-12].

Due to the rather long time constants of these Dewar-type cells (90 minutes), the actual temperature of the cell represents a large averaging effect for any variations in the power added to the cell. Therefore, the data analysis for these cells must involve extensive averaging over rather long time periods to accurately determine any excess power. For example, an experimental variation of only ±0.01°C in a single measurement of either the cell temperature or the bath temperature produces a variation in P_{calor} (Eq. 5) of ±15 mW. This is due to the large value of $M^oC_{p,D2O(l)}$ (450 J/K) multiplied by $d\Delta T/dt$ (±0.01K/300 seconds). Another variation results from experimental fluctuations in the cell voltage due to gas bubbles. For example, a change of ±0.02 V in the measurement of $E(t)$ in Eq. 2 at a cell current of 0.5 A will give an experimental variation of ±10 mW for the electrochemical power added to the cell. These variations in the cell temperature, bath temperature, and cell voltage measurements can give compound fluctuations of ±40 mW in any measurement of excess power based on a single point. Data averaging of all these measurements is an absolute necessity for accurate results using the Fleischmann-Pons calorimetry. Generally, an 11 point running average of the cell temperatures and voltages covering 55 minutes is used by Fleischmann [10-12].

RESULTS AND DISCUSSION

Due to the controversy involving NHE over methods of data analysis for the Fleischmann-Pons Dewar type cells [13], I developed my own methods for evaluating the calorimetric measurements. This report is based on my extensive notebook recordings of the cell

temperatures, voltages, and currents from the console display during the workday at the NHE laboratory. This data was further selected for periods of nearly steady state conditions ($d\Delta T/dt \approx 0$) where the P_{calor} term (Eq. 5) is small. This minimizes errors due to the $M\mathcal{C}_{p,D2O(l)}$ term. The NHE methods assumes a value of 490 J/K for $M\mathcal{C}_{p,D2O(l)}$ [13]. However, both theoretical and experimental determinations yield a significantly lower value of 450 J/K for the water equivalent of these cells [10-12]. Averaged values of $d\Delta T/dt$ (Eq. 5) were used in all calculations.

The main controversy involving NHE and Martin Fleischmann is the method of determining the radiative heat transfer coefficient (k_R) for these Dewar type cells [10-13]. The NHE method relies on a single determination of k_R based on the very first application of the resistive heater (Day 3 for these experiments). Possible problems for this single determination of k_R is that the cell currents were much lower than normal (0.15 A) during this early stage of the experiments. Cell temperatures, therefore, were also rather low during this period. Another problem is that the time period of six hours for the application of the resistive heater was too short to establish a good baseline due to the long time constant for these cells (90 minutes). Furthermore, any early development of excess power and "positive feedback" would seriously compromise this single determination of k_R. This is indeed the case for the Pd-B study where both excess power and positive feedback are present for the calibration period selected [10-12]. Any error in k_R would produce a shift in the baseline for zero excess power, thus real excess power would be readily confused with errors in the calorimetry.

My method of data analysis for the Fleischmann-Pons calorimetry differs significantly from that reported by either Martin Fleischmann [9-12] or by NHE [13] and is much simpler to understand. It consists of the following steps:

1. Equations 1-5 are used exactly with all parameters calculated for the measured cell temperature. Modern computers make this quite feasible.
2. Experimental values at nearly steady state conditions ($d\Delta T/dt \approx 0$) are selected to minimize errors due to the $M\mathcal{C}_{p,D2O(l)}$ term (Eq. 5). An estimated value of $M\mathcal{C}_{p,D2O(l)}$ is calculated.
3. The pseudo radiative heat transfer co-efficient (k'_R) is calculated from Eq. 1 by assuming that there is no excess power ($P_X=0$).
4. The actual radiative heat transfer co-efficient (k_R) for the cell is determined by averaging over a selected time period where k'_R was high.
5. The value obtained for k_R in Step 4 is used in Eq. 1 to determine the excess power for each measurement. Averaging techniques for the cell temperature and cell voltage improve the accuracy.

This method is based on the fact that any excess power in the cell will cause k'_R to decrease. Time periods where k'_R remain high can then be assumed to represent actual periods of small or zero excess power. This method can only underestimate the amount of excess power since the value of k_R determined will be too small if any excess power were actually present. This value of k_R represents an average of many measurements under typical cell operating conditions and is related to the lower-bound value used by M. Fleischmann [10-12].

The use of this method for the Pd-Ce-B cathode suggests that the excess power, if any, is quite small for this experiment. The average experimental error in k'_R for the entire data set assuming no excess power is only ±0.93%. Using the time period between 1033800 to 2159400 seconds (13 days) yields a radiative heat transfer coefficient of $k_R = 8.46 \pm 0.06 \times 10^{-10}$ W/K^4 for the Pd-Ce-B cell. This time period covers typical operating conditions for the cell (0.3-0.6 A). The value

for k_R was then used in Equation 1 to calculate the excess power for the Pd-Ce-B cell. The results are shown in Figure 1.

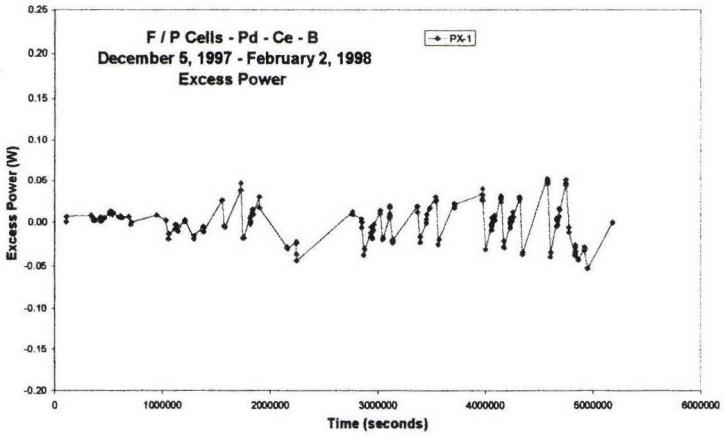

Figure 1. Excess power measurements for the Pd-Ce-B cathode.

The excess power is near zero during the entire 60 days of this experiment. The ratio of the power out ($P_{out}+P_X$) to the power in (P_{EL}) for this experiment is X=1.002±0.008, this there is no average excess power effect within an error range of ±0.8%. Improvements in this data analysis would require the exact determination of $M\,C_{p,D2O(l)}$ for this cell as well as further averaging of the cell voltages and the cell and bath temperatures. Extensive use of the daily application of the resistive heater could lead to improved k_R values for this cell, however, the six-hour heater time period used by NHE is simply too short for establishing accurate baselines.

This same method of data analysis was applied to the Pd-B cell. The resulting radiative heat transfer coefficient for the Pd-B cell was k_R =8.11±0.10x10^{-10} W/K^4 using the time period of 2847900 to 3973800 seconds (13 days). The excess power that is calculated from Equation 1 using this k_R value is shown in Figure 2.

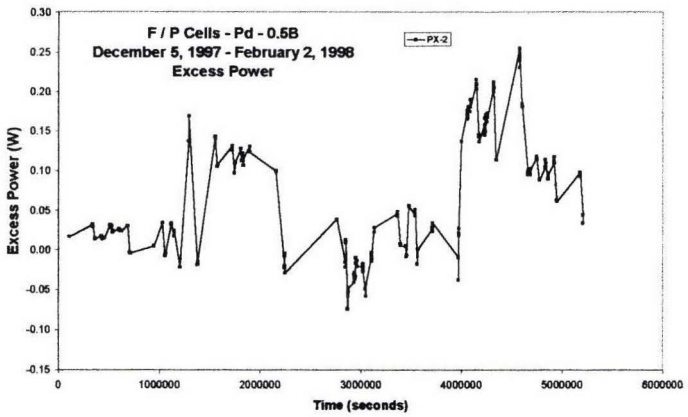

Figure 2. Excess power measurements for the Pd-B cathode.

Figure 2 shows two different episodes of significant excess power production for the Pd-B cell. The excess power reaches levels exceeding 200 mW or 0.6 W/cm^3. For the first significant episode of excess power near 1500000 seconds, the applied cell current was typically near 0.5 A with an input power of 2.6 W and a cell temperature of 50°C. For the second large episode of excess power at 4500000 seconds, the applied cell current was again near 0.5 A, but the input power was now 3.7 W with a cell temperature of 60°C due to the passivation of the electrodes. The cell currents were generally in the range of 0.4 – 0.6 A during these experiments. This study indicates that the NHE polishing procedures do not hinder the production of excess heat.

The Pd-B results in Figure 2 show periods where the excess power becomes more negative than 50 mW. The presence of excess power during the period selected for the evaluation of the radiative heat transfer coefficient would result in a k_R value that is too small, thus negative P_X values would be expected. A detailed evaluation of the experiment by Martin Fleischmann using the entire data set yields a value of k_R =8.5065x10^{-10} W/K^4 with $M\mathcal{C}_{p,D20(l)}$ = 450 J/K [10-12]. The use of these cell parameters eliminates negative results for the excess power. Furthermore, the actual excess power shows the same general trends as in Figure 2, but the excess power is significantly higher [10-12]. The boil-off phase for this experiment yields large excess power effects in the range of 3 to 27 W/cm^3 [10-12].

The flawed NHE method [13] applied to the Pd-B data yields a value of k_R =7.93504x10^{-10} W/K^4 that is much too small. This produces large oscillations in the excess power centered around zero that are confused with errors in the Fleischmann-Pons calorimetry. This single determination of k_R based on the first application of the resistive heater is obviously incorrect. Numerous serious errors in the NHE method for this experiment are documented elsewhere [10-12].

The same method of data analysis applied to the Pd-Ce cell also shows the presence of excess power. The radiative heat transfer coefficient obtained for this cell was k_R =8.00±0.08x10^{-10} W/K^4 using the time period of 1033800 to 1381800 seconds (4 days) involving cell currents of 0.3 to 0.6 A. The excess power that is calculated from Equation 1 using this k_R value is shown in Figure 3.

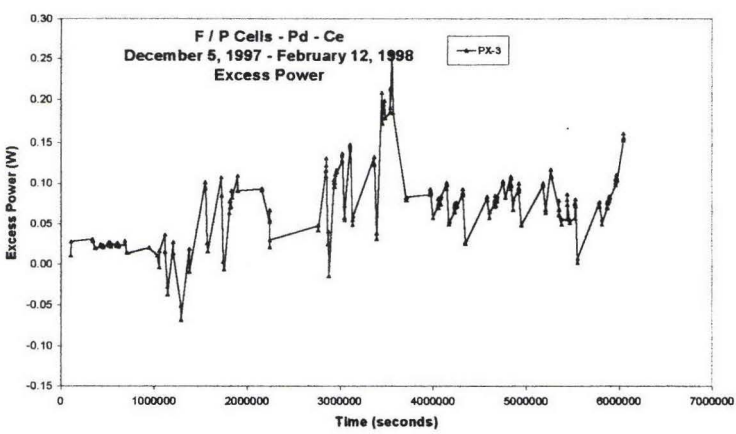

Figure 3. Excess power measurements for the Pd-Ce cathode.

The Pd-Ce alloy began producing significant excess power after fifteen days of electrolysis and

gave a fairly steady level of about 100 mW with a peak of 250 mW (1.6 W/cm^3). A negative episode of excess power exceeding 50 mW suggests that the value for k_R and hence the excess power is actually larger. The flawed NHE method [13] applied to this same data again shows no excess power and large calorimetric errors. An incorrect determination of k_R has once again confused the excess heat effect with calorimetric errors. The precise analysis of this data by Martin Fleischmann is in progress [14].

The fact that the alternative NHE method [13] shows no excess heat for the F-P cells used in these experiments illustrates the problem in transferring calorimetric methods from one laboratory to another. The second laboratory generally does not understand the system, fails to follow directions and makes changes that compromise the calorimetry. Similar problems were encountered in the attempt to transfer the China Lake calorimetry to the Naval Research Laboratory. The NRL laboratory scaled up the size of the system, added extra lead wires for loading studies, failed to average the data, and had poor room temperature control, thus their calorimetric error soared ten-fold to ±200 mW [8]. The excess power for the Pd-B (Fig. 2) and the Pd-Ce (Fig. 3) cathodes would not be detectable using a calorimeter with an error of ±200 mW. A general rule for excess heat measurements is that the calorimeter must be capable of detecting 1 W/cm^3 based on the volume of the cathode. Typically, the calorimetric error must be less than ±20 mW for these studies.

SUMMARY

The Fleischmann-Pons calorimetry requires the accurate determination of the radiative heat transfer coefficient, k_R, and the water equivalent of the cell, $M^{\circ}C_{p,D20(l)}$. The alternative NHE method [13] is a complete failure in the accurate determination of k_R, thus excess heat is confused with the calorimetric error for the system. These new experiments using palladium alloys in F-P Dewar type cells show significant excess power for Pd-B and Pd-Ce alloys. Previous China Lake experiments [5] also showed excess heat for these materials. My simplified method of data analysis for the Pd-B experiment shows the same general pattern for excess power as found in the more detailed and more accurate methods used by Martin Fleischmann [10-12].

ACKNOWLEDGEMENT

The author is grateful to the New Energy Development Organization (NEDO) of Japan and the New Hydrogen Energy Laboratory for the opportunity for this research. The author especially thanks Dr. N. Asami for making this an enjoyable experience. The author also thanks Masao Sumi and Mari Hosoda for their help in these experiments along with Linda S. Miles for figures and manuscript preparations.

REFERENCES

1. M.H. Miles, *J. Electroanal. Chem.*, **482** (2000) 56.
2. M.H. Miles, 1999 Pacific Conference, ACS Western Regional Meeting, Ontario, California, October 6-8, 1999, Abstract No. 255.
3. M.H. Miles, 4th Asti Workshop on Anomalies in Hydrogen/Deuterium Loaded Metals, Asti, Italy, October 22-24, 1999, Societá Italiana Di Fisica (in press). See also *Infinite Energy*, Vol. 5, Issue 30 (2000) 22.
4. M.H. Miles, Bulletin of the American Physical Society, Vol. 45, No. 1, Minneapolis, MN, March 20-24, 2000. Abstract C 324, p. 234.
5. M.H. Miles, "Electrochemical Calorimetric Studies of Palladium and Palladium Alloys in Heavy Water", NEDO Final Report, March 31, 1998.

6. M.H. Miles, B.F. Bush and K.B. Johnson, "Anomalous Effects in Deuterated Systems" NAWCWPNS TP 8302, Sept. 1996.
7. M.H. Miles and K.B. Johnson, "Progress in New Hydrogen Energy", M. Okamoto, Editor, ICCF-6 Proceedings, Japan, Vol. 1, pp. 20-28, October 13-18, 1996.
8. D.D. Dominguez, P.L. Hagans, and M.A. Imam, A Summary of NRL Research on Anomalous Effects in Deuterated Palladium Electrochemical Systems", NRL/MR/6170-96-7803, January 9, 1996.
9. M. Fleischmann, S. Pons, M.W. Anderson, L.J. Li, and M. Hawkins, *J. Electroanal. Chem.*, **287** (1990) 293.
10. M. Fleischmann, M.H. Miles, and M.A. Imam, ICCF-8 Proceedings, Lerici (La Spezia), Italy, May 21-26, 2000 (in press).
11. M. Fleischmann, M.H. Miles, and M.A. Imam, "Calorimetric Analysis of a Heavy Water Electrolysis Experiment Using A Pd-B Alloy Cathode", NRL Report (in press).
12. S. Szpak, M. Fleischmann, M.H. Miles, S.R. Chubb, and T.A. Chubb, "The Behavior of the Pd/D System: A Decade of Research at Navy Laboratories", NRaD Report (in press).
13. T. Saito, M. Sumi, N. Asami, and H. Ikegami, "Proceedings of the 5th International Conference on Cold Fusion", ICCF-5, Monte Carlo, Monaco, April 9-13, 1995, pp. 105-115.
14. M. Fleischmann and M.H. Miles (in progress).

Conference Proceedings Vol. 70
"ICCF8"
F. Scaramuzzi (Ed.)
SIF, Bologna, 2000

"CASE STUDIES" OF TWO EXPERIMENTS CARRIED OUT WITH THE ICARUS SYSTEMS.

M. H. Miles,* M. A. Imam,** and M. Fleischmann***

*Naval Air Warfare Weapons Division, China Lake, CA 93555-6100, U.S.A.

**Naval Research Laboratory, Washington,D.C. 20375, U.S.A.

*** ENEA, Frascati Research Centre, 00044 Frascati, (Rome), Italy.

I. ABSTRACT.

The publication of the Final Report of the New Hydrogen Energy (N.H.E.) Group on their investigations of the Pd/D systems (1) prompts us to analyse a number of experiments carried out with the ICARUS Systems (2), (3). As the reproducibility of such experiments remains low, our analyses rely on a series of "Case Studies" which use appropriate parts of the methodologies developed for these systems (2), (3) (see) also (4), (5),(6),(7),(8).

In this paper we present selected parts of such "Case Studies for two experiments carried out in the N.H.E. Laboratories; full details will be given elsewhere (9). The first experiment, designated as FP2 - 9506203 - 556l used a 2mm diameter x l2.5mm length Pd cathode supplied by the IMRA-Materials Laboratory; the second FP2-97120402 - M7C2, was carried out by one of us (M.H.M.) also in the N.H.E. Laboratories. This experiment used a 4.75mm diameter x 20.1mm length Pd - 0.5%B cathode (prepared by M.A.I. in the Naval Research Laboratory, Washington, D.C.). Contrary to the conclusions reached in the N.H.E. report (1) we find that these experiments show "Heat-after-Death" and excess enthalpy generation at temperatures close to the boiling points of the electrolytes. The experiment using the Pd-B cathode also shows excess enthalpy generation in other temperature regions as well as the very early development of "positive feedback" (compare (10),(11),(l2)). Such "positive feedback" complicates the analyses of the experiments. The "Case Studies" of these experiments also lead to the identification of errors in the execution and analyses of the experiments carried out by the N.H.E. Group.

2. EXPERIMENT DESIGN AND RESULTS.

In common with other experiments carried out in the N.H.E. Laboratories, measurements were made using an ICARUS-1 type Calorimeter illustrated schematically in Fig. 1 Figs 2 and 3 show respectively the "raw data" for an early stage and part of the final day of the measurement sequences for the experiment with the Pd-cathode; Fig 4 gives these data for the key day of operation of the experiment with the Pd-B cathode. We note that experiment FP 2-9506203-566l has been carried out in accord with the instructions for the ICARUS Systems (2), (3) in that the measurement cycles lasted 2 days. This allowed the use of calibration pulses of 12-hour duration (see Fig 2) leading to the complete relaxation of the temperature perturbations. However, the majority of the experiments carried out in the N.H.E. Laboratories used measurement cycles lasting just l day such as those illustrated in Fig 5.

Data acquisition was carried out with an ICARUS-2 type system (3). However, as far as experiment FP2-9506203-5661 is concerned, it appears that the software controlling the data acquisition computer has been rewritten because the times for measurements with the "short thermistor", Fig 1, do not coincide with those for the "long thermistor" (which themselves coincide closely with those for the measurements of the cell current, cell voltage and bath temperature). This change is not crucially important for the preliminary data analyses described in this paper (except for the loss of redundancy in the measurements and, especially, for the evaluation of the evaporation to dryness on Day 29 of the experiment) because the synchronised data are sufficient to allow such analyses. A more serious matter is the loss of synchronisation of the calibration pulses, Fig 5. In consequence, the data evaluation must be restricted to the differential heat transfer coefficients determined locally e.g. $[k_R']_{11}$ and $[k_R']_{12}$. The more precise integral heat transfer coefficients (e.g. $[k_R']_{21}$ and $[k_R']_{31}$ and accurate integral heat transfer coefficients (e.g. $[k_R']_{22}$ and $[k_R']_{32}$) will have serious errors unless this loss of synchronisation is taken into account 9); this applies especially to the true heat transfer coefficient, $[k_R']_{32}$, which we believe has been used extensively in the interpretations carried out by the N.H.E. Group.

3 DATA EVALUATION FOR EXPERIMENT FP2-9506203-5661

3A. THE DIFFERENTIAL LOWER BOUND HEAT TRANSFER COEFFICIENTS FOR DAYS 5-26.

The first stage in the ICARUS data evaluation scheme is the examination of these coefficients, designated as $[k_R']_{11}$, and of the relevant 11-point means, $[k_R']_{11}$ of $[k_R']_{11}$ see e.g. (4), (5), (10), (11),(12). Here we assume initially that there is a zero rate of excess enthalpy generation, hence $[k_R']_{11}$ is a lower bound. The development of excess enthalpy generation is then shown by falls in $[k_R']_{11}$; conversely decreases in excess enthalpy generation are shown by increases in $[k_R']_{11}$; see e.g. (8). It will be evident that if there is no excess enthalpy generation (e.g. in suitable "blank" experiments), then $[k_R']_{11}$ will be identical to the true heat transfer coefficient, $[k_R']_{12}$, obtained by applying appropriate calibration pulses. We believe that this condition applies to the major part of experiment FP2-9506203-5661 viz. to Days 5 - 26 (9).

The coefficients $[k_R']_{11}$ discussed in this paper have been obtained in a second cycle of calculations where the first cycle leads to the water equivalent to be used in this second cycle. The need to use such a second cycle will be discussed elsewhere, (9); we note that this procedure does not appear to have been followed in the evaluations carried out by the N.H.E. Group.

We also note that the expected value of the water equivalent is in the range 450-460 JK^- 1 whereas the measured values are in the range 490- 525 JK^-1. We take this increase to be due to the "overfilling" of the cells with electrolyte and/or D_20 which must have contained ~6 Moles of D_20 rather than the ~5 Moles as given in the instructions for the ICARUS Systems (2), (3). This "overfilling", which is also indicated by the rise of $[k_R']_{11}$ for the initial stages of the measurement cycles, Fig 6 (see also (9)), must be taken into account in the analysis of the "evaporation to dryness" on Day 29 (see Section 3C below).

The lack of control in the replenishment of the D_20 content of the electrolyte is also shown by the variability of $[k_R']_{11}$ under nominally identical conditions. Thus the extrema of the

behaviour for the polarisation carried out at a cell current ~ 0.5A shows a 0.36% change in $[k_R']_{11}$. This is outside the error limits specified for the ICARUS Systems.

Fig 6 shows that the derived values of $[k_R']_{11}$ vary with the cell current; we see also that these values are much larger than those calculated using the Stefan - Boltzmann coefficient and the radiant surface area (this is especially true of the values determined at the higher cell current). Furthermore, close inspection of the data on expanded scales, e.g. Fig 7, shows that there are changes in $[k_R']_{11}$ during the application of the calibration pulse, for $t_1 < t < t_2$, as compared to the behaviour for $t < t_1$ and $t > t_2$. All these facts show that either or both of the input enthalpies to the cell and heater are in error : the test for the absence of such effects has always been used for assessing the satisfactory execution of the experiments, (13). We believe that all these observations can be explained by power dissipation in the leads external to the cell due to the use of the wiring supplied for the ICARUS-1 Systems (2) to connect the cells to the ICARUS-2 VERSION (3).Fig 8 A shows the effects of including an 1 Ohm lead resistance in the current leads external to the cell (this resistance is the median value of the lead resistances supplied with the ICARUS-1 Systems). It is evident that the values of $[k_R']_{11}$ determined at the two cell currents are now in reasonable accord and, moreover, that these values are close to those predicted from the Stefan-Boltzmann coefficient and the radiant surface area. However, we also note that the errors introduced by the mismatch of the enthalpies delivered to the cell and heater now have the opposite sign to those in Fig 7. It is evidently necessary to correct also for power losses in the leads to the calibrating heater and Fig 8B shows the effects of including an 1 Ohm resistance in these leads. The offset seen in Fig 8A can be seen to be reduced; however, a complete cancellation of this offset requires us to assume a resistance of 2.5 Ohms in these leads, Fig 8C, and this particular value also removes the offsets throughout the measurement sequence. However, such an high value of the lead resistances is unlikely and it may well be therefore that the enthalpies delivered to the calibration heater were lower than those given in the "raw data" for this experiment. A further discussion of these particular aspects will be given elsewhere (9).

We note finally that the inclusion of the power dissipation in the external wiring in the enthalpy input to the cells leads to an overestimate of $[k_R']_{11}$ by ~ 5% (and the raising of the errors in the precision of $[k_R']_{11}$ from 0.1 to 5%). It is possible that these errors are the principal cause of the observation that $[k_R']_{11}$ can exceed the true value $[k_R']_{12}$ (1) although there are further factors which can lead to the underestimate of $[k_R']_{12}$ (9), (14).

The further discussion of this particular experiment given in this paper will be based on the uncorrected values of $[k_R']_{11}$ as the corrections of the "raw data" for unknown external resistances can hardly be justified (however, see Sections 3C and 3D).

3B. THE DIFFERENTIAL LOWER BOUND HEAT TRANSFER COEFFICIENTS FOR DAYS 27-28.

The operation of the cell on Days 27-28 has been excluded from Section 3A principally because $[k_R']_{11}$ shows a significant fall with time during this penultimate measurement cycle (9). Such decreases are due to the development of excess enthalpy generation as the cell temperature increases. However, Fig 9 shows that the derived values of $[k_R]_{11}$ now become sensitive to the atmospheric pressure (due to the sensitivity of the enthalpy of evaporation to this variable as the temperature increases). Unfortunately, it appears that the on-line

pressure sensor supplied with ICARUS-2 was disconnected so that it is not possible to evaluate this measurement cycle with complete certainty. However, increases of $[k_R]_{11}$ with time can be excluded as the surface area available for heat transfer decreases with time (compare Fig 8). It follows that value of the atmospheric pressure $P^* > 1$ must be excluded. The atmospheric pressure which must have applied to the operation of the cell towards the end of Day 28 can be specified more closely by considering the evaporation to dryness on Day 29 (see Section 3C). The cell is driven to dryness at 23,000s after the start of the measurement cycle and we can therefore determine the value of P* required to achieve this condition at this time (9). This pressure lies between 0.975 and 0.980 Ats which thereby also determines the variation of $[k_R]_{11}$ with time, Fig 9.

3C ENTHALPY BALANCES AND RATES OF EXCESS ENTHALPY GENERATION FOR t < 23,000S OF DAY 29

The most direct way of estimating these quantities is illustrated in the Tabulation, Fig 10, which gives directly the excess enthalpy required to achieve complete evaporation of the D_20 content of the electrolyte. If we assume that this is generated at a constant rate, we then arrive at a mean rate of excess enthalpy generation. It is important to realise the this calculation is quite independent of all the information required for the calculation of the time dependence of the rates of excess enthalpy generation, see the Tabulation in Fig 11, except for the need to specify the volume of electrolyte in the system (a minor correction required is that for the variation of the enthalpy of evaporation with concentration). The calculation has therefore been given for the nominal cell contents of 5 Moles as well as for 6 Moles of D_20. We believe that the actual volumes are closer to the latter rather than the former figure in view of the evident "overfilling" of the cell.

It will be seen that the Table given in Fig 10 also contains a second estimate in which the enthalpy input to the cell has been corrected to allow for power dissipation in the external leads (see Section 3A) together with a correction to the heat transfer coefficients. The excess enthalpy terms are not markedly affected by these corrections i.e. the estimates are "robust".

The simplicity of this calculation must be contrasted with the complexities of calculations of the variation of the rate of excess enthalpy generation with time, Fig 11. Such calculations have been carried out so far within the framework of "ideal solution theory" which may not be adequate for the concentrated electrolyte developed in the cell. Detailed calculations will be presented elsewhere (9); however, we note here that it is impossible to achieve a satisfactory interpretation of the evaporation to dryness for any plausible values of the reflux ratio while in the absence of reflux, the rates of evaporation require negative rates of excess enthalpy generation at long times, a behaviour which is forbidden by the Second Law of Thermodynamics. We believe that these contradictions are due to errors in the concentration and volume of electrolyte. Furthermore, the "long thermistor" and Pd cathode may not have been in the positions shown in Fig 1 which are required to allow the evaluation of the data during evaporation to dryness.

In view of the uncertainties in the interpretation of the data at long times for Day 29, we have evaluated the rates of excess enthalpy generation shown in Fig 13 at times t < 10,000s.

3D HEAT-AFTER-DEATH ON DAY 29 FOR t >23,700s.

The cooling of cells following evaporation to dryness is possibly the simplest calorimetric experiment which can be devised for "Cold Fusion" Systems (4), (5),(15). There is now no thermal input to the cell and no evaporative cooling so that the interpretation of such experiments is especially straightforward.

Inspection of the cooling curve for t > 23,700s, Fig 3, shows that this cannot possibly be explained by the cooling of an empty cell with the heat transfer coefficient which applies to such cells (l5): the rate of cooling is too slow which can only be explained by enthalpy generation in the system. Fig 12 compares the behaviour derived from the cooling curve shown in Fig 1 with that predicted in the absence of excess enthalpy generation.

The rates of excess enthalpy generation can evidently be derived from the difference between the radiative output from the cell and the change in enthalpy content of the calorimeter. Fig 13 shows the relevant data and it appears that at t = 0 for the cooling curve (i.e. at 23,700s) the rates lie between those calculated for the cell filled with electrolyte for P* = 0.985 and P* = 0.980 Ats. (see Section 3C).

4.DATA EVALUATION FOR EXPERIMENT FP2 - 47120902-M7C2.

Pd-B alloy electrodes of the type used in this experiment had been shown to give excess enthalpy generation in previous experiments (16), (17). An evaluation of the experiment discussed here but using a different methodology has also been presented at ICCF-8 (18) while full reports of the ICARUS - type analysis will be given elsewhere (9), (19), (20).

Comparison of the "raw data" for the experiment with the Pd-B cathode, Fig 4, with those for the Pd cathode, Fig 2, shows that the approach to the steady state is delayed for the former electrode following the application of the heater calibration pulse. This is an immediate indication of the onset of "positive feedback": an increase in the rate of excess enthalpy generation induced by the increase in the cell temperature, here due to the imposition of the calibration pulse (compare e.g. (12)).It is of special interest that such "positive feedback" develops at such an early stage of the experiment. However, it is not possible to determine at the present time whether this effect is a general feature of the use of Pd-B alloys.

The presence of "positive feedback" greatly complicates the evaluation of the data because it is not possible in general to calibrate "closed loop" systems in the presence of such feedback.

4A. THE N.H.E. EVALUATION

The Group at N.H.E. have quoted a single value of the "true heat transfer coefficient" $[k_R']_{12}$ = 0.793504 x 10^- 9 WK^- 4 , on Day 3 of this experiment (i.e. for the data in Fig 4) and have used this value for all further evaluations. The magnitude of the calibration pulse, ΔQ ~ 0.2500W during $t_1 < t < t_2$ has also been excluded in the calculations; furthermore, the water equivalent 490 JK^-1 contained in the original parameter listing for the ICARUS-Systems (2),(3) has been used throughout rather than to revise the value to that applicable to this experiment.

We arrive at the data shown in Fig 14 and can identify an immediate shortcoming of the procedure used by N.H.E.: it is not possible to determine whether $[k_R']_{11}$ during $t_1 < t < t_2$

falls on the same straight line as the values for $t < t_1$ and $t > t_2$ (compare Fig 7). Proceeding further with the N.H.E. style analysis we derive the rates of excess enthalpy generation shown in Fig 15. We can see that this evaluation must be subject to one or several errors. In the first place, it is not possible for the cell to be endothermic during $t_1 < t$ and $t > t_2$ as the endotherminity of the cell reaction has already been fully taken into account by using the thermoneutral potential. Secondly, we note that it has been maintained (21) that the N.H.E. methodology recovers the magnitude of the heater calibration pulse, ΔQ, during $t_1 < t < t_2$ together with any rate of excess enthalpy generation. Fig 15 shows that this is incorrect. The values of the rates of excess enthalpy generation are smaller than ΔQ if we fix the base-line at $Q_{excess} = 0$. If we fix the base-line at the level of the negative rate of excess enthalpy generation for $t < t_1$, then $Q_{excess} > \Delta Q$ during $t_1 < t < t_2$. The methodology used by N.H.E. can, in fact, only be used under an highly restricted range of conditions which do not apply to this particular measurement cycle (14).

4B THE ICARUS-TYPE EVALUATION.

In view of the very early development of "positive feedback" we can only evaluate the "true heat transfer coefficient, $[k_R']_{12}$" at times close to t_1. Such an evaluation shows that $[k_R']_{12}$ must be at least 0.83808 x 10^-9 WK^-4 while the water equivalent, 454 JK^-1, is close to the expected value. Use of this value and inclusion of ΔQ in the enthalpy input to the cell gives the variation of $[k_R']_{11}$ with time shown in Fig 16. The fact that the application of the calibration pulse leads to a build up of excess enthalpy generation (and hence to a fall of $[k_R']_{11}$) can now be clearly seen : (more complete discussions will be given in (9), (19) and (20).

In view of the intervention of "positive feedback", we are unable to apply the methodology for the evaluation of the "integral lower bound heat transfer coefficients, $[k_R']_{21}$ and $[k_R']_{31}$" as well as of the "integral true heat transfer coefficients, $[k_R']_{22}$ and $[k_R']_{32}$" in the manner set out in the Handbooks (2), (3). However, as the effects of "positive feedback" are relatively small and confined in the time-domain, Fig 16, we can include the additional rates of enthalpy input in the integral of the total enthalpy and evaluate the target "true integral heat transfer coefficient, $[k_R']_{352}$ as well as the water equivalent, Fig 17. We obtain the values $[k_R']_{352}$ = 0.85065 x 10^-9 WK^-4, water equivalent = 450 JK^-1 .However, we note here that in general the coefficient $[k_R']_{252}$, based on the backward integration of the data sets, is to be preferred to $[k_R']_{352}$ which is based on forward integration (9), (14), (19), (20). In view of the fact that this evaluation of the "true heat transfer coefficient" requires a special approach, it is necessary (and advisable) to investigate whether the value can be confirmed using other parts of the experiment. One such confirmation can be obtained from the initial parts of the experiment where the rate of any excess enthalpy generation must be small. In this region we can show that the maximum value of $[k_R']_{11}$ is closely similar to $[k_R']_{352}$ (9), (19), (20) (compare (4), (5)). A second confirmation can be obtained on Day 61 where we must again have a low rate of excess enthalpy generation (see Section 3C). In this case we find that $[k_R']_{11}$ agrees with the value of $[k_R']_{352}$ determined above together with the time-dependence of $[k_R']_{11}$ as given by appropriate "blank" experiments (8), (14).

4C. ADDITIONAL COMMENTS ON THE RATES OF EXCESS ENTHALPY GENERATION.

Fig 18 gives the rate of excess enthalpy generation determined with the correct value of the "true heat transfer coefficient". The near zero value for $t < t_1$, the build-up due to "positive feedback" during $t_1 < t < t_2$ and the relaxation of this effect for $t > t_2$ can now be clearly seen.

Fig 19 gives the corresponding plot evaluated by analogy to the procedure used by the Group at N.H.E. The near zero rate for $t < t_1$, steps of $Q = 0.25W$ at $t = t_1$ and $t = t_2$, the build-up of excess enthalpy generation during $t_1 < t < t_2$ and the decay for $t > t_2$ are now evident.

Fig 20 gives the integrals of the rates of excess enthalpy production for the whole of the experiment when using the heat transfer coefficient determined by N.H.E. The large negative excess enthalpies are clearly not acceptable as they violate the Second Law of Thermodynamics.

Fig 21 gives a plot corresponding to Fig 20 but based on the true heat transfer coefficient evaluated in the present report. We can see that the negative excess enthalpies are now eliminated.

4D THE BEHAVIOUR ON DAY 68: EVAPORATION TO DRYNESS AND HEAT-AFTER-DEATH.

The analysis for the period $0 < t < 21,300$s during which the cell is driven to dryness is similar to that presented in Section 3C and will be presented elsewhere (9), (14), (20).
The analysis of the cooling curve for the period $21,300s < t < 86,400s$ is similar to that which has been given in Fig 12 except that it is necessary to allow for a low level of enthalpy input from the Galvanostat during the initial part of this period. Fig 22 shows the specific rates of excess enthalpy generation as the cell is being driven to dryness as well as during the observation of Heat-after-Death. As for the case of experiment FP-9506203-5661, Fig 13, it appears that the rates converge to a common value in the region where dryness is achieved

The full discussion of this experiment (9), (19), (20), will also comment on other periods during which it is possible to observe Heat-after-Death. This includes the period $2,400s < t < 32,400s$ during which the cell was disconnected from the Galvanostat and the period Day 25 + 76,300s < t < Day 26 + 22,300s during which there was a marked reduction in the cell current (the conditions follow Scenario 1 for the observation of Heat-after-Death (6), (7)). This period of operation is of special interest because the rate of excess enthalpy production exceeded the rate of enthalpy input to the cell.

5. CONCLUSION.

The two experiments used to illustrate this paper show all the features to which we have previously drawn attention: excess enthalpy production in Pd-based cathodes charged with deuterium, "positive feedback", evaporation to dryness, Heat-after-Death. The results obtained contradict those reported by the group at N.H.E. and it is therefore important that this group should present a detailed evaluation of these (and other!) experiments.

The results obtained also demonstrate the need for adopting a flexible approach to the evaluation of data.

We believe that the observations of Heat-after-Death are of special significance because they point the way towards the construction of energy efficient systems based on electrochemical charging. One of the shortcomings of research hitherto has been the failure to integrate this phenomenon into the methodology. We note also that any future work on this aspect should take due account of the long term maintenance of enthalpy production at zero enthalpy input provided the systems are maintained at elevated temperatures (22).

References

1) Information about this Report is available in Infinite Energy 30(2000)
2) Hand book "ICARUS" Isoperibolic Calorimetry ;Acquisition, Research and Utilities System "Version 1, Low Power Measuring System for Three Cells, December (1993), Technova Inc., 13th Floor, Fukoku Seimei Building , 2-2-2 Uchisaiwai-cho, Chiyoda-ku, Tokyo 100,Japan.
3) Handbook: "ICARUS 2": Isoperibolic Calorimetry: Acquisition, Research and Utilities System" Version 2.00 February (1995), Technova Inc., 13th Floor, Fukoku Seimei Building, 2-2-2 Uchisaiwai-cho Chiyoda-ku, Tokyo 100, Japan.
4) Martin Fleischmann and Stanley Pons, Proceedings of the Third International Conference on Cold Fusion, Editor ; H. Ikegami, Universal Academy Press, Frontiers of Science Series no 4 (FSS-4), ISSN 0915-8502, ISBN 4-946443 -12-6 (1993) 118.
5) Martin Fleischmann and Stanley Pons, Phys. Lett. A 176 (1993) 118
6) S. Pons and M. Fleischmann, Proceedings of the Fourth International Conference on Cold Fusion, EPRI TR-104188-V2 (1994) page 8-1
7) S. Pons and M. Fleischmann, Trans. Fusion Technology, 26 (1994) 87
8) Martin Fleischmann, Proceedings of the Seventh International Conference on Cold Fusion, ENECO Inc., Salt Lake City, U.S.A. (1998) 119
9) M.H. Miles, M.A. Imam and M. Fleischmann, to be published
10) M. Fleischmann, S. Pons, Monique Le Roux and Jeanne Roulette, Proceedings of the Fourth International Conference on Cold Fusion, EPRI TR-104188-VI (1994) page 1-1
11) M. Fleischmann, S. Pons, Monique Le Roux and Jeanne Roulette, Trans. Fusion Technology, 26 (1994) 323.
12) M. Fleischmann, Proceedings of the Fifth International Conference on Cold Fusion, IMRA Europe SA, Valbonne, France (1995) 140
13) Report on the First Set of Experiments carried out under the NEDO / NHE Project at the Sapporo Laboratories, June 1994
14) Second Report on the Experiments carried out under the NEDO / NHE Project at the Sapporo Laboratories, December (1994)
15) S. Pons and M. Fleischmann, Trans. Fusion Technology 26 (1994) 87
16) M.H. Miles, B.F. Bush and K.B.Johnson, "Anomalous Effects in Deuterated Systems", NAWCW PNS TP 8302, September (1996)
17) M.H. Miles and K.B. Johnson, in "Progress in New Hydrogen Energy", Editor : M. Okamoto, Proceedings of ICCF-6, Vol. 1 (1996) 20
18) M.H. Miles, Proceedings of ICCF-8, (2000)
19) M.H. Miles, M. Fleischmann and M.A. Imam, "Calorimetric Analysis of a Heavy Water Electrolysis Experiment Using a Pd-B Alloy Cathode", NRL Report (in press)

20) S. Szpak, M. Fleischmann, M.H. Miles, S.R. Chubb and T.A. Chubb, "The behaviour of the Pd / D System : A Decade of Research at Navy Laboratories" NRaD Report (in press)
21) Toshiya Saito, Masao Sumi, Naoto Asami and Hideo Ikegami, Proceedings of the Fifth International Conference on Cold Fusion, IMRA Europe S.A., Valbonne, France (1995) 105
22) G. Mengoli, M. Bernardini and G. Zannoni, J. Electroanal. Chem., 444 (1998) 155

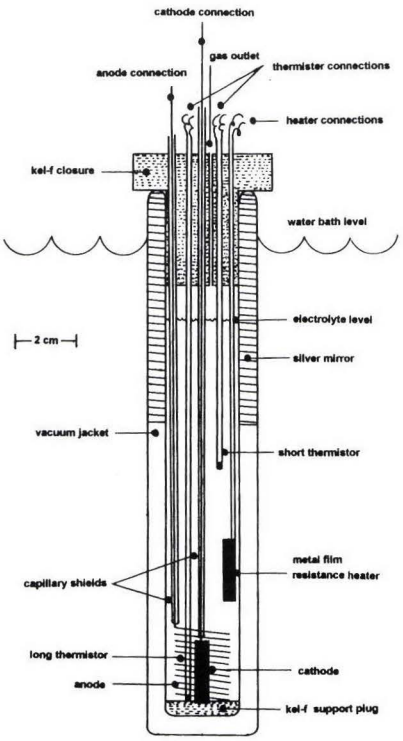

Fig 1 ICARUS-1 type cell; diagram approximately to scale

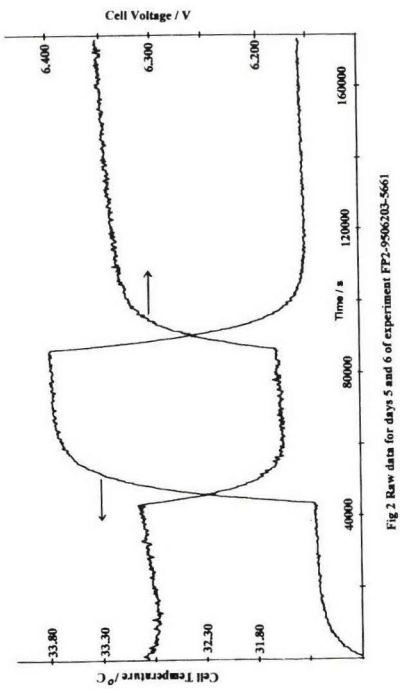

Fig 2 Raw data for days 5 and 6 of experiment FP2-9506203-5661

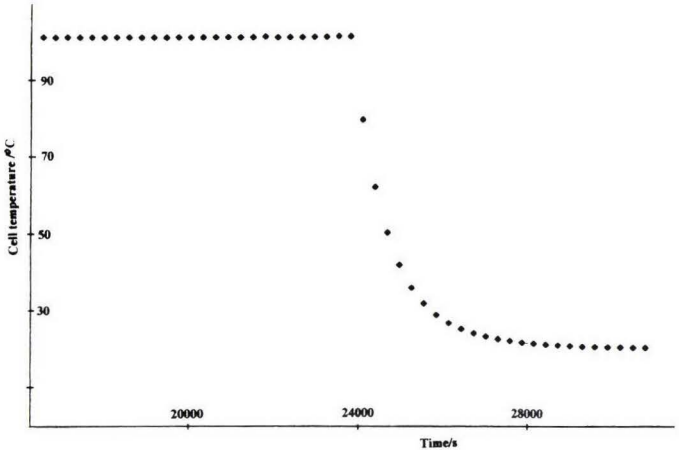

Fig 3 Cell temperature ("long thermistor") for FP2-9506203-5661; dryness at 23,700s

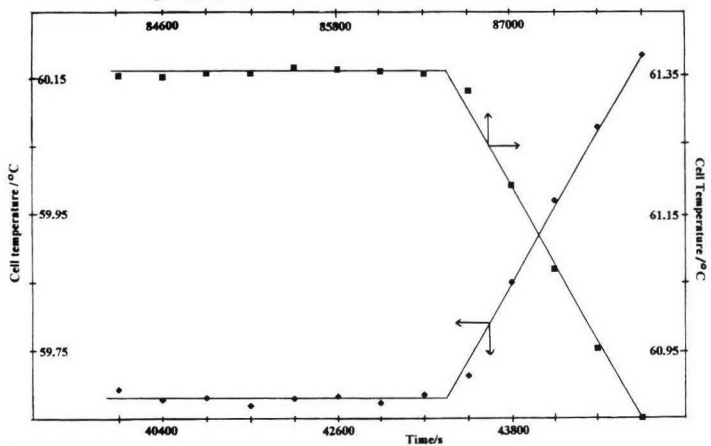

Fig 5 The mean cell temperatures for days 13 to 28 in the region of application and cessation of the calibration pulses

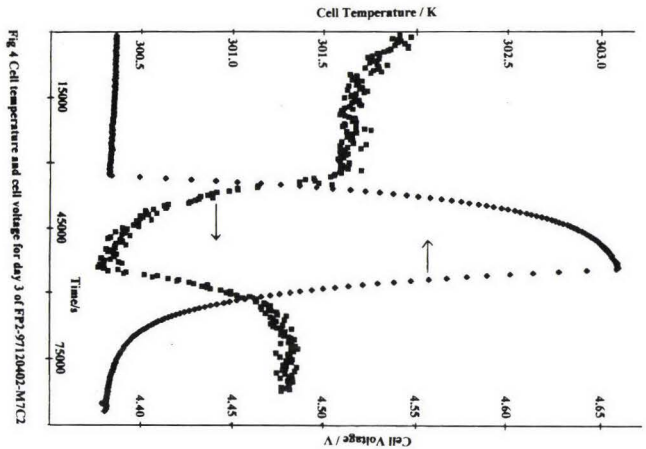

Fig 4 Cell temperature and cell voltage for day 3 of FP2-97120402-M7C2

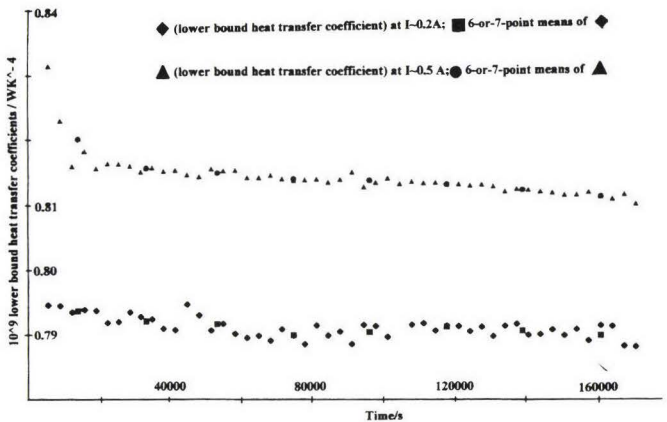

Fig 6 The mean lower bound heat transfer coefficients for Days 9 to 10 and 11 to 12; water equivalent = 490JK^ -1

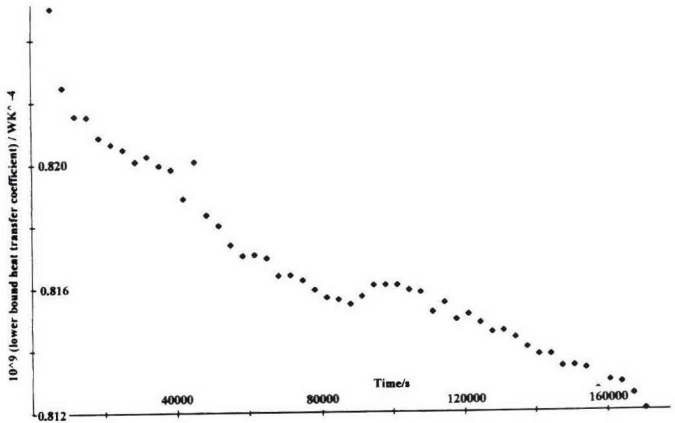

Fig 7 The central region for days 13 to 26

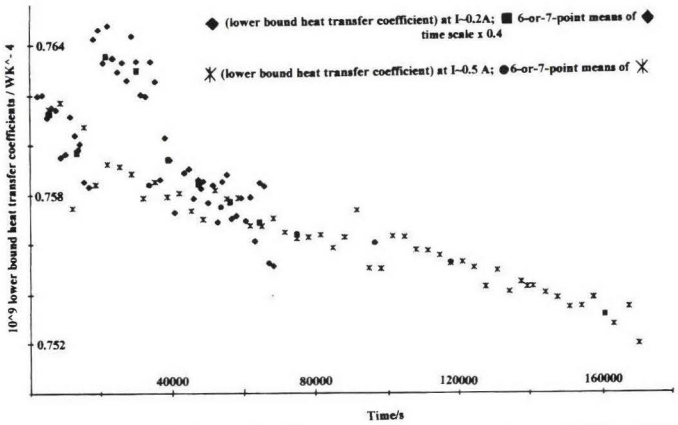

Fig 8A The mean lower bound heat transfer coefficients for days 9 to 10 and 11 to 12; 1 Ohm resistance in current leads.

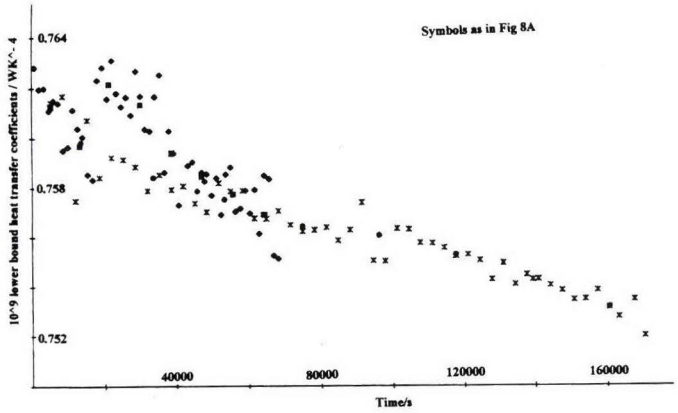

Fig 8B The mean lower bound heat transfer coefficients for days 9 to 10 and 11 to 12; 1Ohm resistance in current and heater leads.

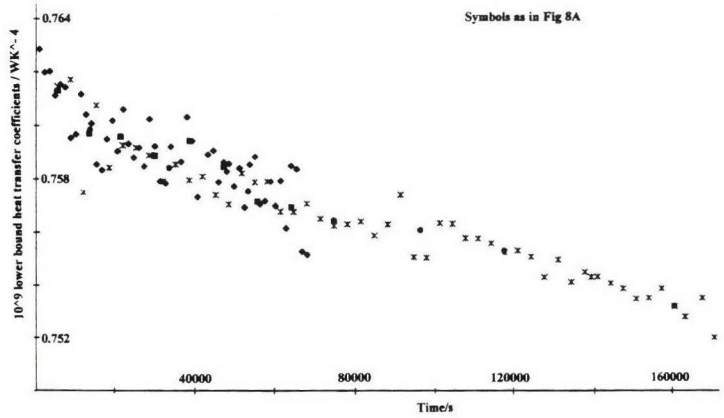

Fig 8C The mean lower bound heat transfer coefficients for days 9 to 10 and 11 to 12; 1Ohm resistance in current and 2.5 Ohm resistance in heater leads.

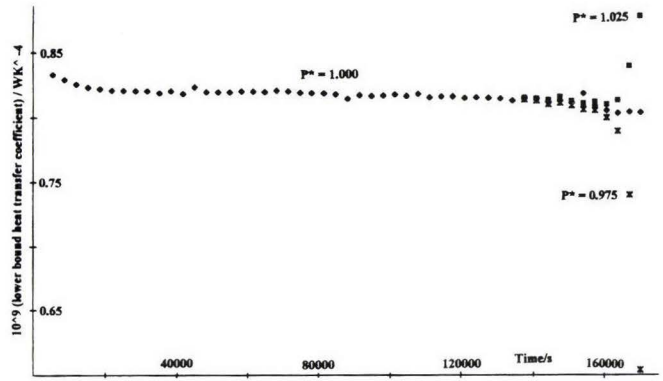

Fig 9 The lower bound heat transfer coefficient for Days 27 to 28 at P* shown

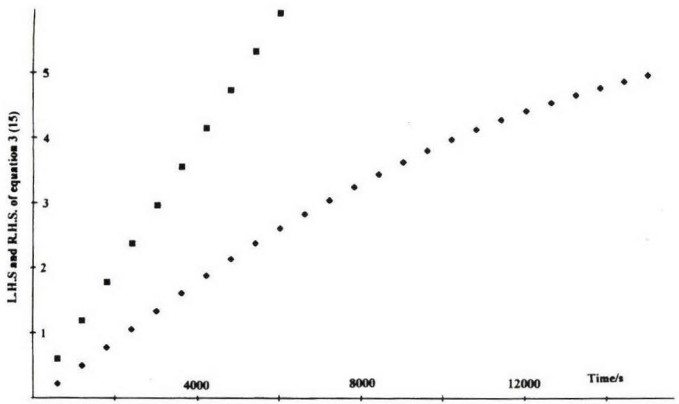

Fig 12 Cooling curves on day 29; ■ prediction for Q=0; ◆ behaviour derived from Fig 4

	DATA AS GIVEN		DATA ALLOWING FOR DISSIPATION OF POWER IN CELL LEADS	
ENTHALPY INPUT	403,921 J		392,071 J	
ENTHALPY OUTPUT	235,567 J		225,476 J	
ENTHALPY FOR HEATING CELL	522 J		522 J	
ENTHALPY AVAILABLE FOR EVAPORATION	168,354 J		166,073 J	
	5 MOLES D_2O	6 MOLES D_2O	5 MOLES D_2O	6 MOLES D_2O
ENTHALPY REQUIRED FOR EVAPORATION OF	208,363 J	250,036 J	208,363 J	250,036 J
EXCESS ENTHALPY REQUIRED	40,531 J	82,204 J	42,290 J	83,963 J
MEAN RATES OF EXCESS ENTHALPY GENERATION	1.71 W	3.46 W	1.78 W	3.54 W
MEAN SPECIFIC RATES OF EXCESS ENTHALPY GENERATION	43.05 W	88.1 W	45.3 W	90.1 W

Fig 10 The enthalpy balances for t < 23,700 of day 29

COLLIGATIVE PROPERTIES OF SOLUTIONS

INFORMATION REQUIRED	COMMENTS
SOLUBILITY	KNOWN
BOILING POINT	KNOWN
ATMOSPHERIC PRESSURE	NOT KNOWN PRESSURE SENSOR DISCONNECTED?
REFLUX RATIO	NOT KNOWN
POSITION OF TEMPERATURE SENSOR	NOT KNOWN
CONCENTRATION	NOT KNOWN
VOLUME OF ELECTROLYTE	NOT KNOWN
DEVIATIONS FROM IDEALITY	NOT KNOWN

Fig 11 Information required for the calculation of the rates of excess enthalpy generation on Day 29

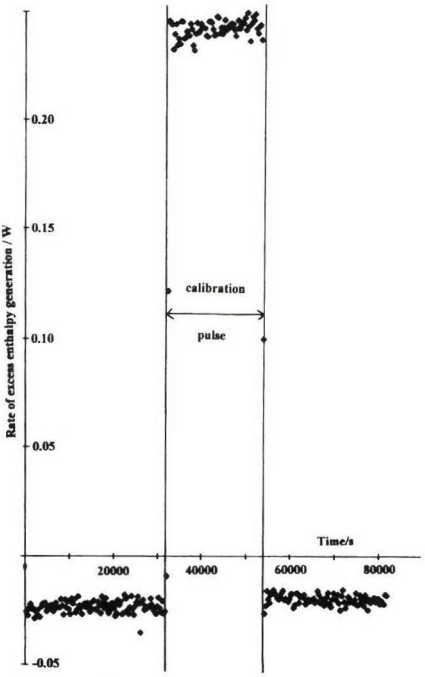

Fig 15 The rate of excess enthalpy generation; NHE Analysis

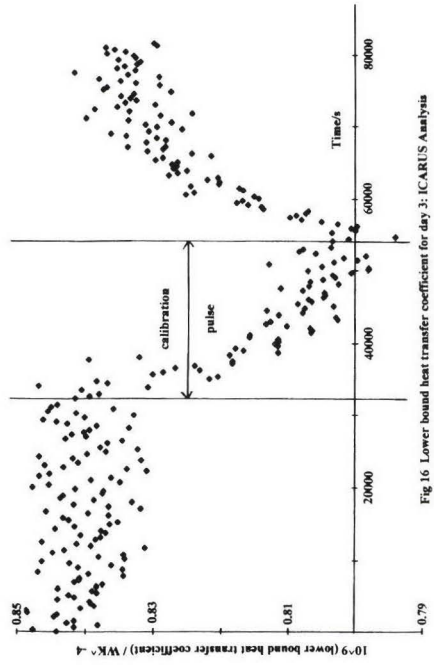

Fig 16 Lower bound heat transfer coefficient for day 3: ICARUS Analysis

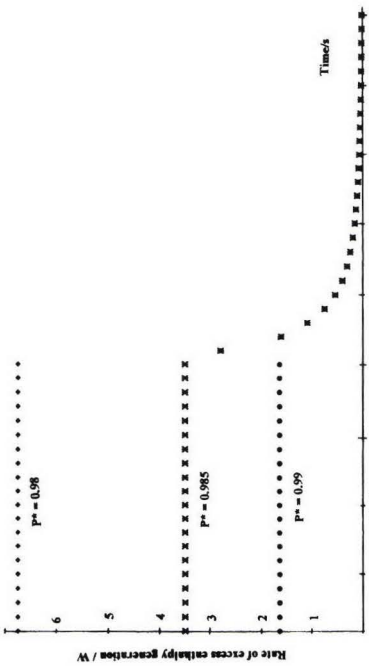

Fig 13 The rate of excess enthalpy generation on day 29

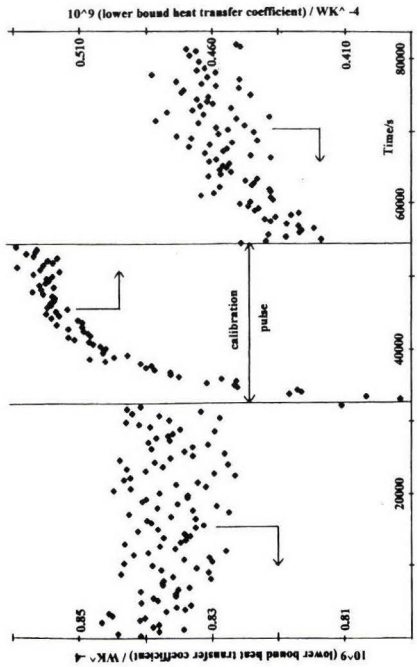

Fig 14 Lower bound heat transfer coefficient for day 3: NHE Analysis

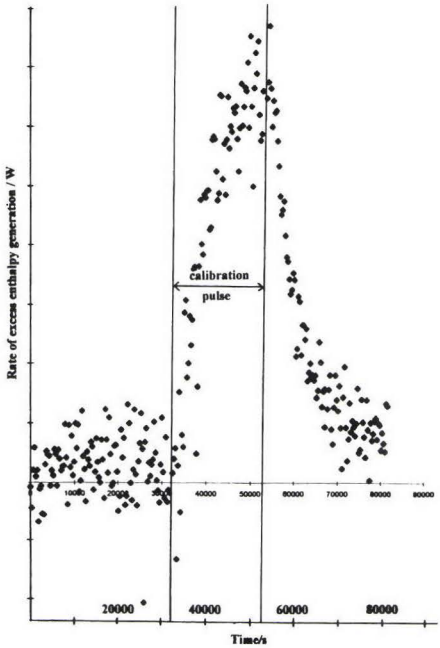

Fig 18 The rate of excess enthalpy generation on Day 3: ICARUS Analysis

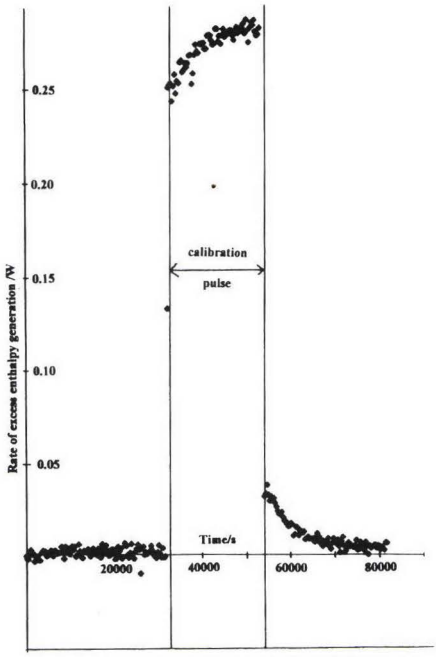

Fig 19 Rate of excess enthalpy generation on Day 3 ICARUS Analysis by analogy to the N.H.E. procedure.

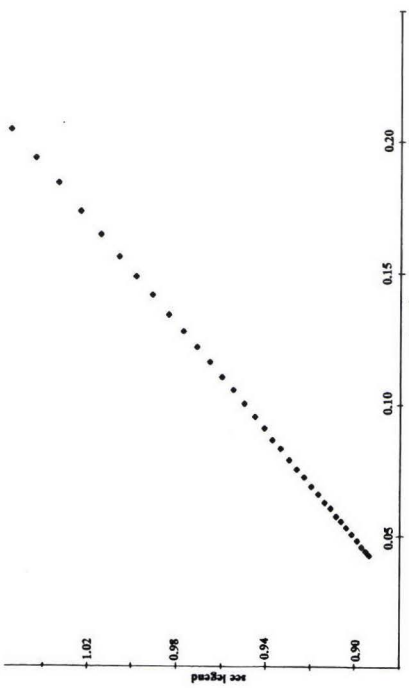

Fig 17 Evaluation of $[k_e]_{263}$ and of the water equivalent for the third measurement cycle and with correction for the effects of "positive feedback".

$$\text{Ordinate} = [k_e]_{263} + \frac{\int_{t_1}^{t} \text{net enthalpy input d}\tau - [\text{net enthalpy input } (t_1)][t - t_1]}{\int_{t_1}^{t} f_2(\theta)\, d\tau} \qquad \text{abscissa} = \text{water equivalent} \times [\Delta\theta(t) - \Delta\theta(t_1)] \frac{}{\int_{t_1}^{t} f_2(\theta)\, d\tau}$$

$$\text{where } f_2(\theta) = [\theta_{am} + \Delta\theta(t)]^4 - [\theta_{am} + \Delta\theta(t_1)]^4$$

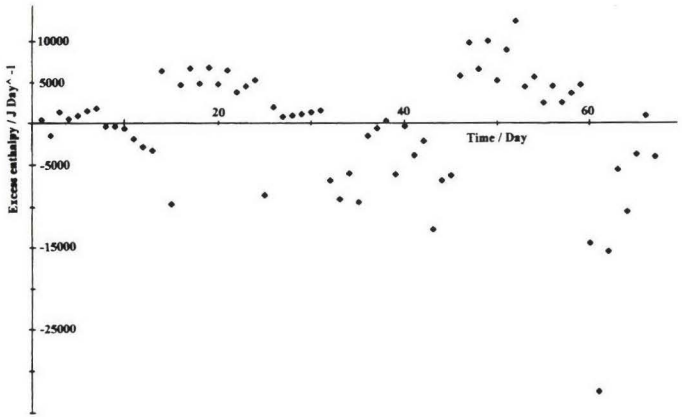

Fig 20 Excess enthalpies using N.H.E. procedure

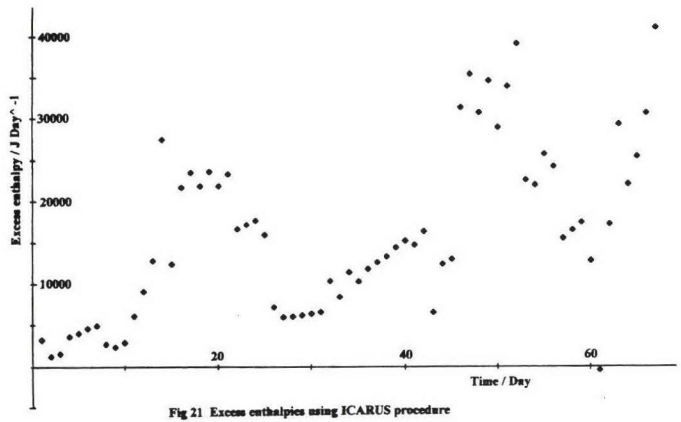

Fig 21 Excess enthalpies using ICARUS procedure

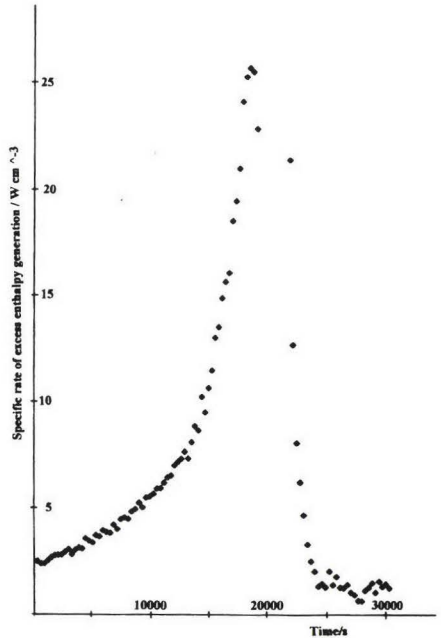

Fig 22 Specific rate of excess enthalpy production on Day 29 for $0 < t < 21{,}000$s and $21{,}000 < t < 30{,}000$s

CHAPTER 3.

TRANSMUTATIONS

Conference Proceedings Vol. 70
"ICCF8"
F. Scaramuzzi (Ed.)
SIF, Bologna, 2000

Nuclear Transmutation in Pd Deuteride

Xing Z. Li, Yun J. Yan[1], Jian Tian, Ming Y. Mei,
Yan Deng, Wei Z. Yu, Guo Y. Tang[1], and Dong X. Cao[2]
Antonnella De Ninno[3]

Department of Physics, Tsinghua University, Beijing 100084, CHINA
[1]Institute of Material Science, Department of Material Science, Tsinghua University
[2]Deparment of Engineering Physics, Tsinghua University
[3]Frascati Laboratory, ENEA Research Center, 00044 Frascati, Rome, ITALY

Abstract

Using Preparata (Cohn-Ahranov) effect, Pd hydrides and deuterides are loaded with high loading ratio (R/Ro<1.3) in a specially designed electrolytic cell. Ni is found as a new element in the Pd deuteride. No source of contamination has been identified for this Ni, of which concentration reaches 10% on some local surface regions. The morphology of this Ni component is studied using secondary electron emission and back scattering electrons. Pd film underlined with a Cr layer is a new configuration among this kind of nuclear transmutatiom experiments

1. Introduction

High loading ratio(R/Ro<1.3) has been reached in palladium hydrides and deuterides in the Frascati Laboratory (ENEA). A unique technology, which is described in paper [1],

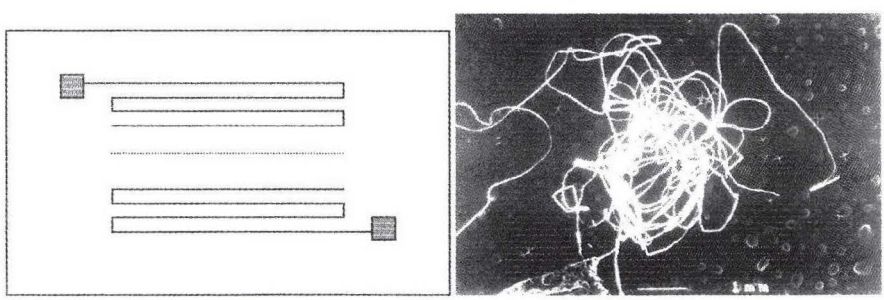

Fig.1 The schematics of the palladium wire before loading(left), and the image of palladium wire after loading(right)

is applied to make a long thin Pd wire on the surface of the glass substrate. The size of Pd wire is 2μ×50μ×1000mm. Then, it is possible to applied a voltage along the wire in order to create the Cohn-Ahranov effect to facilitate the loading process. Since it was first proposed by late Professor G. Preparata, it is renamed by Professor E. Giudice as "Preparata effect" in memory of this pioneer in "cold fusion" research. With this technique, high loading has been reached with high reproducibility. "Excess heat" has been found in this Pd deuteride, and the helium correlation has been investigated. It is natural to study the possible "nuclear transmutation" phenomena in these samples. Two samples of Pd deuteride and one sample of Pd hydride were sent to Tsinghua University to analyze the new elements in these samples using scanning electron microscopy at Institute of Material

Science of Tsinghua University. New elements are identified by characteristic X ray using EDX mode. Careful studies are followed to eliminate any possible contamination. Ni was the most evident new element, Zn, Fe etc. are found as well. It provides the new evidence of the "nuclear transmutation" phenomena in the metal deuterides.

2. Sample Preparation

In order to have a large voltage drop along the palladium wire, we need a long and thin wire. It is realized by Frascati Laboratory (ENEA). The palladium is sputtered on the surface of a piece of glass substrate. Then the lithographic technique is used to cut the thin film into a shape of zigzag ("bustrophedic") wire as shown by Fig.1. The width of the wire is 50 microns, and the thickness of the thin film is about 2 microns. The total length of the Pd wire is 100 cm on the glass substrate which has a size of $2.5 \times 3.5 \cdot cm^2$. There are six squares which are connected to the Pd wire at six points including both ends and four intermediate points equally distributed along the wire. When this sample is emerged into the electrolyte to start the electrolytic loading process as a cathode, the square parts are covered by a small rubber O-ring to keep away the electrolyte. A small indium bead is put inside the O-ring. This elastic indium bead plays a roll of bridge to connect the palladium wire to the power supply. During the sputtering process a thin layer of chromium is sputtered first to improve the adhesion of the palladium to the surface of glass substrate. However, due to the deformation after the loading, the Pd wire detached from glass substrate as shown by the right part of Fig.1.

3. Scanning Electron Microscopy

Two months after the high loading, a field emission scanning electron microscopy (JOEL, JSM-6301 F) was used to detect the new elements on the surface of the palladium wire. Although we know from the manufactory(Balzers) that the palladium is as pure as 99.99%, we may still check the impurity in the sputtered sample in the following two ways:

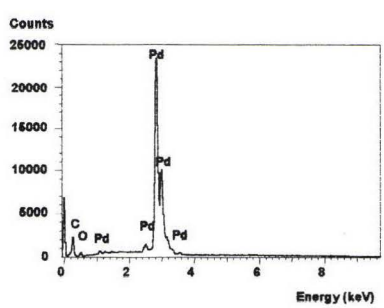

Fig.2 Pure Pd in Square Region

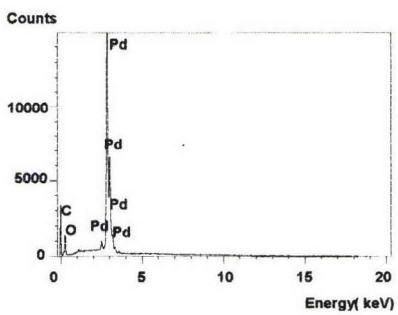

Fig.3 Pure Pd in Crystal Region

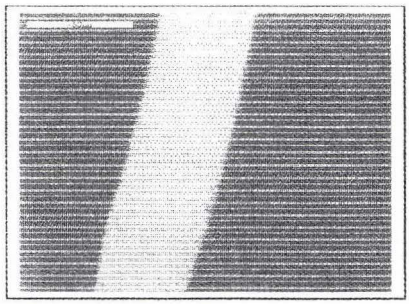

Fig.4 ×700 Back Scattering Electron image of Pd wire with no black spots

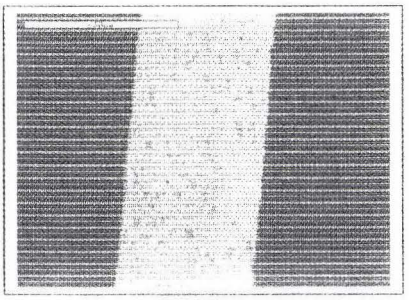

Fig.5 ×1000 Back Scattering Electron image of a section with a crystal region and black spots

(1)Detect the elements first on the square part, because it is supposed to be separated from the electrolyte there. The deuterium is loaded into this part through the diffusion process inside the palladium wire. We do not expect a high loading in these six squares. Figure 2 shows the EDX spectrum of the square part. The palladium peaks are well identified, and the only impurities we are able to detect are the carbon and oxygen. This carbon may be from the rubber O-ring, or from the vacuum pump oil during the sputtering process.

(2)We found a section of wire with a clear crystal shape (straight boundary in a trapezoid shape in Fig.5). We could not find any new elements on this trapezoid region (Fig.3), although it contacts the electrolyte directly, and it is supposed to have similar loading as the vicinity. It is a good evidence to show that the electrolyte is pure as well without any heavy metal contamination.

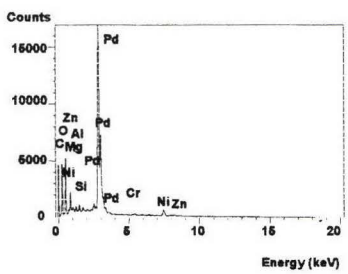

Fig.6 EDX spectrum at the black spot showing Ni peaks etc.

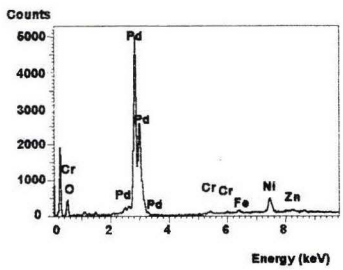

Fig.7 The highest nickel peaks ever observed in this D/Pd sample. (10% of Ni is estimated in the surface layer)

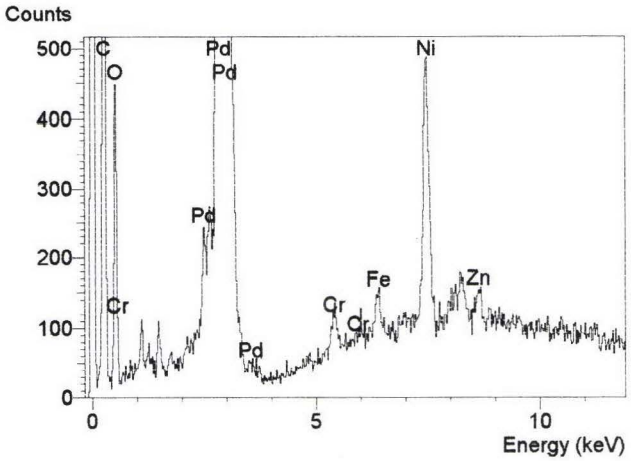

Fig.8 The EDX spectrum details near the highest Ni peak

With these detection, we are sure that even if after sputtering process, after the contact with electrolyte for several days, the sample is still a pure Pd sample except carbon and oxygen which will not interfere the later nuclear transmutation results.

After careful scrutiny, we found that some sections were different from the other parts in back scattering electron (BSE) image (see Fig.4 and Fig.5). In the black spots, the EDX spectrum showed clear peaks for Ni, Zn, Fe and Cr, etc.(Fig. 6 ,7, .8).

Various black spots in the back scattering electron image mean the lower average Z number in the local area (Z number for Zn, Ni, Fe, and Cr is 30, 28, 26, and 24, respectively. They are all less than Z number for Pd, which is 46). Having searched a lot of black spots we found some spots with the highest nickel peaks. The preliminary quantitative analysis showed that the local nickel component may be as high 10% as shown by Fig.7. The Fig.8 is an enlarged spectrum to show the local details. In the past, most of previous work for nuclear transmutation are done for the nickel in hydrogen [2], or with nickel layer under the Pd layer, there was no chance to observe this nickel component enhancement.

The highest Ni peaks were found in certain regions which looks like a crater in the back scattering electron image (Fig.9). In deed they were small beads if we look at them in the secondary electron image (Fig,10). Secondary electron emission coefficient is strongly dependent on local curvature. Usually, the higher curvature region would have a greater

emission coefficient.

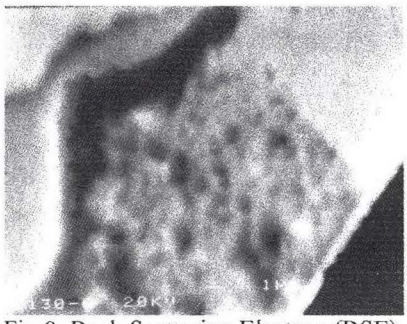

Fig.9 Back Scattering Electron (BSE) image of the highest Ni region

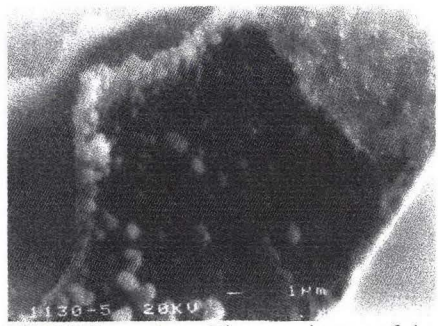

Fig.10 Secondary Electron image of the same highest Ni region as that of BSE

4. Contamination

Contamination has been a big concern in the studies of "nuclear transmutation". Haviing inspected the impurities in electrolyte, in the original Pd, and in the sputtering processes, we suspected the substrate. Is there any nickel in glass substrate or in the chromium layer? We found a section of Pd wire which clearly showed the interfaces among the Pd wire, Cr layer and substrate glass (Fig. 11). A piece of glass shell was peeled off from the back side of Pd wire; then, we may detect the Cr layer between glass substrate and Pd wire (the medium gray portion of the Pd wire in Fig.11). It clearly show that even in this Cr layer, there is no trace of Ni (Fig.12). Then we directly analyze the components in the glass region. It is shown in Fig.13. Although there is a lot of barium and calcium, there is no Ni either.

5. Concluding Remarks

As a part of the anomalous nuclear phenomena [2-6] in metal deuteride, we found the high Ni component in the highly loaded Frascati sample. We could not identify any possible contamination sources of this high Ni component yet.

Acknowledgements

This research is a collaboration between different laboratories in different countries. The Chinese part is supported by State Commission of Science and Technology (#1997567), Natural Science Foundation of China (#19645005), and Fundamental Research Fund of Tsinghua University. This proceedings' paper is finalized at University of Bologna with a grant from ICTP TRIL program with Professor S. Focardi.

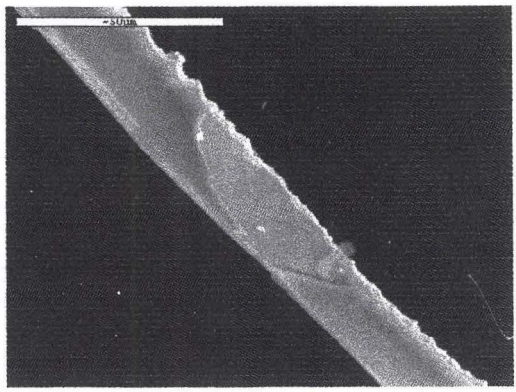

Fig.11 The interfaces between Pd thin wire, Cr layer and glass substrate. The dark parts at two ends of Pd wire are the glass shell on the backside of Pd wire. The central gray part is the layer between glass shell and the Pd wire.

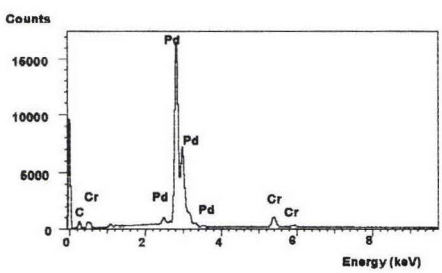

Fig.12 Chromium peaks on the layer between Pd thin wire and glass.

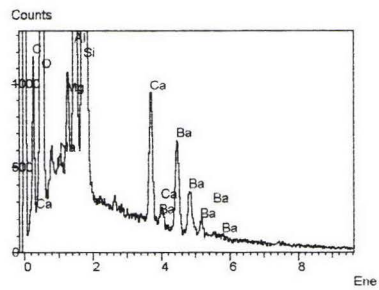

Fig.13 EDX spectrum on the glass substrate surface

References

[1] Antonella De Ninno, et al., *Proceedings of ICCF-8*, May 21-26,2000, Lerici, Italy, Italian Physical Society.

[2] T. Mizuno, et al., *Denki Kagaku*, vol.64 (1996) no.11, p.1160.

[3] G. Miley, et al., *Journal of New Energy*, vol.1 (1996) no.3, p.5.

[4] T. Ohmori, et al., *Fusion Technology*, 33 (1998) 367.

[5] G. S. Qiao, X. Z. Li, et al. *Journal of New Energy*, vol.2 (1997) no.2, p.48.

[6] L.C. Kong, X.Z.Li, et al. *Journal of New Energy*, vol.3 (1998) no.1, p.20.

Conference Proceedings Vol. 70
"ICCF8"
F. Scaramuzzi (Ed.)
SIF, Bologna, 2000

TRACE ELEMENTS ADDED TO PALLADIUM BY EXPOSURE TO GASEOUS DEUTERIUM

Thomas O. Passell* and Russell George**

***TOP Consulting **Saturna Corporation**

Abstract

This is an experimental program to investigate possible trace element changes brought about in palladium (Pd) after extensive electrolysis in heavy water electrolytes as well as long time contact of particulate Pd with gaseous deuterium. Of particular interest are cathodes and particulate Pd which had experienced episodes of excess heat production beyond all electrical and other inputs. This paper details the careful analysis by neutron activation analysis (NAA) of a set of three samples of finely powdered Pd exposed to high deuterium pressures (hundreds of atmospheres) near room temperature at the core of hollow cylindrical Pd cathodes. A fourth sample of unused Pd powder from the same batch used in the cathodes was analyzed as a control. The most prominent change observed in the three active samples versus the virgin Pd was the Zn-64 content. The active samples showed an increase in the Zn-64 isotope of 6 to 14 times that in the virgin Pd. Speculation regarding the source of this increased zinc varies from contamination during electron beam welding (used to seal off the hollow core) to nuclear reactions generated by high pressure deuterium gas on the large surface area Pd particles in the core.

Introduction

Palladium (Pd) cathodes electrochemically charged with deuterium (D) have exhibited episodes of excess heat beyond all inputs.(1-5) To confirm or refute the suspicion of a possible nuclear reaction producing the excess heat, trace element changes were measured in particulate Pd exposed to very high deuterium pressures generated in the hollow core of cylindrical Pd cathodes in a series of experiments by Arata and Zhang.(1) Independently in a completely different type of experiment, Mo, Cai, Wang, Wang, and Li reported observations of increased zinc for Pd exposed to hydrogen and deuterium gas.(6) In addition they reported observing an altered ratio of Zn-64 to Zn-68 relative to that of naturally occurring zinc. They speculated that the extra zinc observed may have been produced by some nuclear process induced by the hydrogen or deuterium on the Pd metal surface, since it was unlikely that contamination by handling or experimental processes

would have given zinc with an altered relative abundance of Zn-64 and Zn-68.

The present study attempted to check the hypothesis put forward by Mo et al (6) on other Pd exposed only to gaseous deuterium (with some mixture of light hydrogen inevitably present in deuterium).

Experimental

The samples of particulate Pd weighing from 5 to 16 milligrams each were sent to the University of Texas for NAA.(7). All elements susceptible to NAA at a flux of 1E12 n/cm2-sec under an irradiation of 3 hours were detected by means of their emitted gamma rays as detected in an intrinsic germanium crystal operated at 77°K. Since NAA is isotope specific, certain changes in the isotopic ratios within palladium were also accessible by this method, for example the Pd-102/Pd-110 ratio. Analyses were mostly dependent upon the ratios of gamma ray integrated photopeaks within a given sample and hence were less subject to errors in sample weighing or comparisons between separate samples. Since not all the samples could be simultaneously gamma counted, small corrections had to be made for different times of decay after irradiation, as these different decay times affected the ratios of gammas from isotopes of different half lives.

Results

Table I shows the increases in the elements iridium (Ir) and gold (Au) in addition to the increase in zinc (Zn) relative to the virgin material (Sample D). In one instance, Sample B showed a DECREASE in Ir from the virgin material. The conventional explanation for such increases is the cathodic deposition of electrolyte impurities on the cathode surface. However, all these samples were protected from the electrolyte inside the gas-pressure-tight hollow core of the cylindrical cathode. The only remaining possibility of contamination would be in the process of cathode preparation. Once the Pd powder is placed inside the core of the cathode, it had to be electron-beam welded because the deuterium pressure could reach extremely high values during electrolysis. In fact, some cathodes failed in a burst mode during electrolysis due to this pressure if not properly welded. It is possible that the high temperatures experienced by the welded region could have vaporized various impurities in the Pd and the vapors carried down for deposition on the Pd powder. While this scenario is plausible for the relatively volatile zinc, it is less likely for gold and iridium. For example, zinc has a boiling point of 907°C, whereas iridium and gold have boiling points of >4800°C and 2600°C respectively.

The zinc concentrations observed in the powder are by far the highest of any observed impurity, ranging between 102 PPM to 248 PPM by weight assuming the zinc is natural zinc. Since we only measure the Zn-64 isotope via its neutron capture product isotope, Zn-65, the Zn-64 concentrations are about half the above numbers (Zn-64 is 48.6% of natural zinc).

The conditions of irradiation apparently obscured the appearance of the prominent gamma ray of the Zn-69m isotope from Zn-68 neutron capture, so the attempt to check whether the zinc observed had an unnatural ratio of Zn-64 to Zn-68 failed. The Zn-69m half-life is nearly the same as that of Pd-109 (both about 13.8 hours) and the gamma rays of the latter were so dominant that we failed to resolve the 438.5 keV gamma of Zn-69m. The above

assumes that the Zn-68 isotope is actually present, even at some different ratio than that of natural zinc.

Discussion

The samples analyzed along with its virgin material were volunteered by Dr. Arata and Dr. Zhang of Osaka University. However, the precise amounts of excess heat produced by the cathodes in which the powdered Pd was contained has not yet been made available. Arata and Zhang's published work shows data from similar cathodes which produced about 30 to 40 megajoules of excess heat over the most active 2 month period of their electrolysis.(1) If one assumes that some nuclear process produced each excess Zn-64 atom at about 10 Mev per atom, and further that some 12 grams of powdered Pd was contained in each cathode hollow core, and further that our sample of 5 to 15 milligrams was a representative sample of the full 12 grams present, then one obtains an expected amount of excess heat of 20 Megajoules.

The only heat producing nuclear reaction capable of producing Zn-64 is the fission of palladium isotopes or proton capture in impurity copper. While some copper impurity is undoubtedly present, it is not readily measured by NAA under these circumstances and even if present, it is not likely to be so large as several hundred PPM. However, new short irradiations (to observe Cu-66 with its 5.1 minute half life) are planned to check for this possible copper impurity.

We are thus left with the possibility of Pd fission, a process giving about 20 to 30 Mev per fission (10-15 Mev per fission product atom). To check this possibility we attempted to measure any change in the ratio of Pd-102 and Pd-110 from that of the virgin material. Table I shows a roughly 20% increase in the Pd-110/Pd-102 ratio in the A and C samples but only about 5% in sample B, the latter not outside the limits of error. If the apparent depletion in Pd-102 relative to Pd-110 is confirmed, this may indicate that the lighter isotopes of Pd are more susceptible to fission than the heavier ones. Clearly these three experiments are only suggestive at present.

The proof of a nuclear source for the increased zinc (and possibly other multi-isotope elements), will be resolved by NAA or other methods that show the isotopic abundance ratios to be significantly different from those found naturally. Otherwise, a contamination source is indicated.

The small increases in iridium and gold in the active samples relative to the virgin sample find no ready explanation. Both elements are considerably less volatile than zinc and hence are less likely to be carried from the site of electron beam welding to the powder. It may be we are seeing the natural variation of these impurity elements - that is - they are not uniformly distributed in the powdered Pd. In one case, (sample B in Table I) iridium shows a factor of 2 decrease rather than the factors of three and four increases observed for samples C and A respectively. Gold shows the smallest increase (10%) in sample B with increase factors of 1.7 and 5.3 for samples C and A respectively. No nuclear processes that have a positive Q value can be readily identified to suggest a nuclear reaction origin for these elemental impurity increases. However, a commonly observed impurity in palladium is platinum, from which both iridium and gold could be produced by positive Q nuclear reactions with protons or deuterons. However we observe at most

Table I. Neutron Activation Analysis Results for Impurities in Palladium Exposed to Gaseous Deuterium

SAMPLE	Zn-64 Content PPM by Weight	Zn-64 Ratio Relative To Unused (Virgin) Palladium Sample D (One Sigma)	Iridium Content PPM by Weight	Gold Content PPM by Weight	Pd-110/Pd-102 Relative to the Ratio Observed in Unused Pd i.e., Sample D (One Sigma)
ARATA A	50	6.6 (1.6)	4.1	55	1.24(0.11)
ARATA B	121	14.4 (3.2)	0.2	11	1.06(0.06)
ARATA C	58	8.3 (2.1)	3.1	17	1.21(0.11)
ARATA D (VIRGIN)	8	1.0 (DNA)	0.5	10	1.00 (DNA)

only a few PPM of platinum in these powdered Pd samples.

Conclusions

These measurements are so far only suggestive of possible nuclear reactions occurring in deuterated palladium. Some suggestive early results from gas loaded palladium was given by Mo, Cai, Wang, Wang, and Li (6). They found alterations in the Zn-64/Zn-68 ratios from gas-exposed samples relative to the same ratios in natural zinc. The most severe alteration showed an enhancement of the Zn-68 to Zn-64 ratio by 20% relative to the ratio for natural zinc. Their unexposed palladium showed no zinc present. Gas-exposed palladium is likely to be reacting at its surface and hence the products of such reactions should be concentrated at the surface. Experiments should be performed which separately measured surface material and material well below the surface. The study by Mo et al used thin wire samples rather than powder, in which such differentiation between surface and bulk would be more practical.

It is possible that conventional explanations will be found for these results, namely that of contamination during electron beam welding for gas tight closure of the hollow core. Experiments are currently under way for NAA of Pd powder that was exposed in the hollow core of a cathode producing NO excess heat under electrolysis with normal light water electrolysis may be persuasive in answering this question.

Acknowledgments

We are indebted to the University of Texas staff at their research reactor for neutron irradiations and subsequent counting of the samples by germanium gamma ray detectors, in particular Dr. Felib Iskander. Thanks are also due to Dr. Y. Arata and Dr. Y. Zhang for allowing us to analyze their Pd samples.

References

1. Arata, Y., and Zhang, Y., "Achievement of Solid-State Plasma Fusion ("Cold Fusion"), Proceedings of the Sixth International Conference on Cold Fusion, Volume 1, pp 129-135, October 13-18, 1996, Toya, Japan
2. Fleischmann, M., Pons, S., and Hawkins, "Electrochemically Induced Nuclear Fusion of Deuterium", Journal of Electroanalytical Chemistry, Volume 261, (1989), 301-308
3. Fleischmann, M., Pons, S., Anderson, M., Li, L., and Hawkins, M., "Calorimetry of the Palladium-Deuterium-Heavy Water System", J. Electroanalytical Chemistry, Vol 287 (1990) pp 293-348
4. McKubre, M., Crouch-Baker, S., Rocha-Filho, R., Smedley, S., Tanzella, F., Passell, T., and Santucci, J., ""Isothermal Flow Calorimetric Investigations of the D/Pd System", J. Electoanalytical Chemistry, Vol.368 (1994), pp. 55-66
5. Miles, M., Johnson, K., and Imam, M., "Heat and Helium Measurements Using Palladium and Palladium Alloys in Heavy Water", Proceedings of the Sixth International Conference on Cold Fusion, Vol. 1, pp 20-28.
6. Mo, D.W., Cai, Q.S., Wang, L.M., Wang, S.Z., and Li, X.Z., "The Evidence of Nuclear Transmutation Phenomena in Pd-H System Using NAA", Proceedings of the Seventh International Conference on Cold Fusion, page 259-263, April 19-24, 1998, Vancouver, B.C., Canada, Published by ENECO, University of Utah Research Park, 391-B Chipeta Way, Salt Lake City Utah 84108
7. Iskander, F., Private Communication (1999)

Conference Proceedings Vol. 70
"ICCF8"
F. Scaramuzzi (Ed.)
SIF, Bologna, 2000

EXPERIMENTAL OBSERVATION AND STUDY OF CONTROLLED TRANSMUTATION OF INTERMEDIATE MASS ISOTOPES IN GROWING BIOLOGICAL CULTURES

Vladimir I.Vysotskii[1], Alla A. Kornilova[2], Igor I. Samoylenko[3], German A. Zykov[1]

[1]Kiev Shevchenko University, Radiophysical Faculty, Kiev, Ukraine
[2]Moscow State University, Physical Faculty, Moscow, Russia
[3]Gamaleya Institute of Epidemiology and Microbiology, Moscow, Russia

Abstract

For the first time the experimental study of cold nuclear transmutation of intermediate mass isotopes was carried out in growing microbiological culture with controlled conditions of growth. With the help of time-of-flight mass-spectroscopy the formation of rare Fe^{54} isotope from Na^{23} and P^{31} isotopes in sugar-salt nutrient medium was observed. Combined and independent Mossbauer and mass-spectroscopy investigations of nuclear transmutation of Mossbauer isotope Fe^{57} in growing biological cultures were also carried out.

1. Introduction

The problem of nuclear transmutation of elements and isotopes at low interaction energy (at room temperature) in biological objects is discussed. Several years ago [1,2] we have made Mossbauer studies of light (D^2) and intermediate (Mn^{55}) cold isotopes transmutation in several microbiological cultures. We have conducted a series of experiments based upon new technology employing the precise methods of Mossbauer spectroscopy. The experiments were based on the $Mn^{55}+d^2=Fe^{57}$ reactions in growing microbiological culture in heavy-hydrous (D_2O) sugar-salt nutrient medium deficient in Fe but additionally containing Mn. The reaction result is generation of stable rare Fe^{57} isotope, concentration of which in the natural iron is very low. In these experiments the formation of Fe^{57} isotope from Mn^{55} and the light isotope D_2 in nutrient medium based on heavy water was observed by Mossbauer effect.

Our new report considers the results of both time-of-flight mass-spectroscopy study of nuclear transmutation of intermediate mass isotopes in growing microbiological cultures and combined (Mossbauer and mass-spectroscopy) investigations of nuclear transmutation of isotope Fe^{57} in the same cultures.

We have carried out investigations aimed at discovery and investigation of such nuclear transmutations. We believe that this aim can be achieved only if an isotope obtained in the process of transmutation does not have any analogues in the nutrient medium where the culture is growing (along with inevitably present admixtures of this isotope). As far as we know, none of the previously conducted researches contains reliable data confirming the possibility of cold transmutations for intermediate mass isotopes.

2. Experimental method and procedures

Our experiments on nuclear transmutation of intermediate mass isotopes are based on the expected $Na^{23}+P^{31}=Fe^{54}$ reaction in growing culture in sugar-salt nutrient medium deficient in Fe but containing controlled quantity of Na^{23} and P^{31} isotopes. The reaction results in generation of the rare Fe^{54} isotope, concentration η=5,8% of which in the natural iron (mainly Fe^{56} with natural concentration η=91,7%) is very low. Iron (any isotopes) in small amounts is necessary for the culture growth. If the conditions of nonbarrier cold fusion are satisfied [1-3], the formation of Fe^{54} takes place. The formed Fe^{54} nuclei during the time $\Delta t \approx 10^{-10}$—$10^{-11}$ s are converted to atoms (or ions) and will be utillized by the growing culture for making its

structure. The research was carried out on the basis of bacterial culture ***Bacillus subtilis.*** The Fe^{54} isotope obtained in small quantities can be easily discovered by the means of time-of-flight mass-spectroscopy. This method allows to monitor the isotope contents of all components of the nutrient medium, the initial culture and all samples of the culture after its growth has finished.

The course of the experiments was as follows. The previously obtained culture after centrifuging, washing and post-growth was placed in flasks with sugar-salt nutrient medium containing salts of Mg, Ca, K, Na, sucrose and 100 ml of pure H_2O water.

The composition of the nutrient medium is shown in the table.

Components	Concentration in the medium (%)	Admixture of Fe (no more) relative (%)	Admixture of Fe (no more) absolute (g)
Sucrose	2	10^{-4}	2.10^{-4}
$MgSO_4$	0,05	2.10^{-4}	10^{-5}
$CaCO_3$	0,2	$1,5.10^{-4}$	3.10^{-5}
KCl	0,05	3.10^{-4}	$1,5.10^{-5}$
$NaNO_3$	0,5	2.10^{-4}	10^{-4}
K_2HPO_4 (in transmutation experiments)	0,2	5.10^{-4}	10^{-4}
Pure distilled water H_2O	100 (100 ml)	10^{-7}	10^{-5}

In accordance with the degree of purification of all nutrient medium ingredients (chemically pure category), the possible content of Fe as an admixture does not exceed $m(Fe^{54}) \approx 5.10^{-4}$ g or $N(Fe^{56}) \approx 4.10^{17}$ Fe^{56} atoms. In accordance with the natural content of Fe^{54} isotope (5,8% of the total Fe), its possible quantity as an admixture does not exceed $m(Fe^{54}) \approx 3.10^{-5}$ g. The total mass and total number of atoms of Na^{23} isotope in $NaNO_3$ salt are $m(Na^{23}) \approx 0.13$ g and $N(Na^{23}) \approx 2,8.10^{21}$. In transmutation experiments, the K_2HPO_4 salt containing less than $\Delta m_{Fe} \approx 10^{-4}$ g of Fe admixture and $m(P^{31}) \approx 0.1$g and $N(P^{31}) \approx 1,1.10^{21}$ atoms of basis P^{31} isotope was added to the nutrient medium. All initial dry ingredients of the sugar-salt nutrient medium were investigated on the time-of-flight mass-spectrometer. The same investigation was held with a part of the bacterial culture inoculum.

A typical experiment concerning the nuclear transmutation of elements consisted of growing the microbiological culture in 2 disks simultaneously (see Fig.1).

The first disk contained the fully-compounded hydrous nutrient medium (including $NaNO_3$) but without K_2HPO_4, the second one — the same hydrous nutrient medium with K_2HPO_4 present. Several series of such control and transmutation experiments were held for different cultures, different times of growth Δt (24, 48 and 72 hours) and different growth modes (in still disks and media and in suspension stirring mode using magnet stirring device). The cultures were grown in the thermostat at the optimal temperature 32^0 C. After completing each series, the obtained biological substance was separated using a centrifuge, cleaned in the distilled water and dried. The total masses of the dried cultures were about 0.3-0.7 g.

A typical series of mass-spectrum measurements consisted of three main procedures:

a) mass-spectrum investigation of pure natural iron (the basic experiment for obtaining the reference mass-spectrum of all isotopes of iron);

b) investigation of the cultures which have been grown in the medium with presence of Na^{23} ($NaNO_3$ compound) and without P^{31};

c) investigation of the cultures which have been grown in full-compounded hydrous nutrient medium with presence of both P^{31} (K_2HPO_4 compound) and Na^{23} ($NaNO_3$).

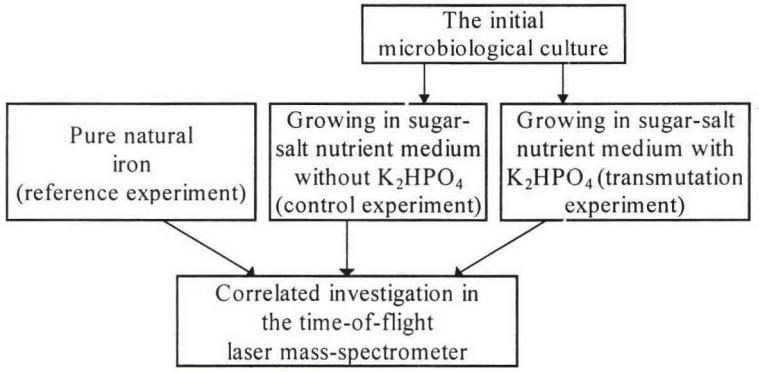

Fig.1. The scheme of experiment on transmutation and mass-spectroscopy investigation of isotopes in growing microbiological cultures

The investigated objects were put together in the same vacuum chamber of the laser mass-spectrometer. The cultures were placed on the Pb holder surface in separate microtroughs.

The ruby laser pulses (duration τ=40 ns, wave-length λ=0.63 μm, energy W=0.2 J, size of laser pulse focus D≈100 μm, laser plasma temperature KT≈100 eV) were aimed at each microtrough in turn. The resulting single-charged ions of different isotopes A_i with masses $M_i=A_iM_0$ after energy selection had equal energies $W_0 \approx 40$ eV but different velocities $v_i=(2W/M_i)^{1/2}$ and times of flight $t_i=L/v_i$ to the detector. Here L≈100 cm is the distance of the ions flight from the laser focus to the detector. Each mass-spectrum was measured during the single laser pulse. The spectra were recorded on the multitrace oscilloscope with memory and later processed on the computer.

3. Results and discussion

The mass-spectrum of the isotopes of natural iron (fig. 2a — reference experiment) allows to carry out exact identification and quantitative interpretation of the summarized spectrum of the impurity (Fe^{56} and Fe^{54}) and synthesized (Fe^{54}) iron isotopes in the researched cultures for the cases b and c (fig. 2b — experiment on transmutation at Δt=72 hours, fig. 2c — control experiment). In these experiments the changes of relation of isotope concentrations from natural value $\eta(Fe^{54})/\eta(Fe^{56}) \approx 0{,}06$ (for the case of pure natural Fe and for impurity Fe in the control experiment) to $\eta(Fe^{54})/\eta(Fe^{56}) \approx 0.2 - 0.25$ (for the experiment on transmutation) were observed. For the several more optimal regimes of culture growth we have obtained $\eta(Fe^{54})/\eta(Fe^{56}) \approx 0.5 - 0.8$. The recurrence of outcomes was close to 100%.

The averaged experimental coefficients of $Na^{23}+P^{31}=Fe^{54}$ transmutation equal

$\lambda_P = N(Fe^{54})/N(P^{31})\Delta t = [\eta(Fe^{54})/\eta(Fe^{56})]\, N(Fe^{56})/N(P^{31})\Delta t \approx$ $(3\text{-}6).10^{-10}$ (synthesized Fe^{54} nuclei per s and per single P^{31} nucleus);

$\lambda_{Na} = N(Fe^{54})/N(Na^{23})\Delta t = [\eta(Fe^{54})/\eta(Fe^{56})]\, N(Fe^{56})/N(Na^{23})\Delta t \approx$ $(1\text{-}2).10^{-10}$ (synthesized Fe^{54} nuclei per s and per single Na^{23} nucleus).

The research of mass-spectra of the dry sugar-salt nutrient medium (before and after the action of the same laser pulse) was also carried out. The measurements have shown that the relation of concentrations $\eta(Fe^{54})/\eta(Fe^{56})$ both in the separate components of the nutrient medium and in their mixture (especially in the mixture of the main salts $NaNO_3$ and K_2HPO_4) remains natural and equals about 0.06. This confirms the conclusion that the formation of Fe^{54} isotope and changes of the isotopes relation $\eta(Fe^{54})/\eta(Fe^{56})$ observed at the growth of culture in an optimal medium with the presence of Na and P salts is the result of cold nuclear

transmutation $P^{31}+Na^{23}=Fe^{54}$ and is not connected to the thermal action of laser inpulse on the target in the mass-spectrometer (i.e. the reaction of nuclear transmutation it is not a result of the possible "wàrm fusion" at KT=100 eV in the laser pulse focus).

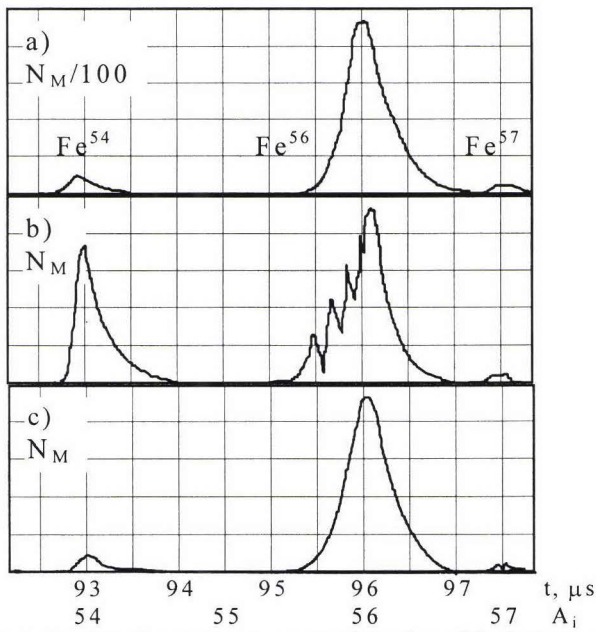

Fig.2. A typical series of mass-spectrometer detection of Fe isotopes: a - reference experiment on pure natural Fe, b - experiment on transmutation (the culture grown in the medium with the presence of P^{31} and Na^{23} isotopes) , c - control experiment (the culture grown in the medium without P^{31} isotope); t is the measured time of flight of the isotope ion from the target to the detector, A_i is the atomic number of the isotope.

As a result of the analysis of the main experiment 2b on transmutation and both the reference 2a and the control experiment 2c one can say:

1) in the grown microbiogical cultures, the sugar-salt components of the nutrient medium and in the natural iron the relations of Fe^{54} and Fe^{56} isotopes concentrations are natural $\eta(Fe^{54})/\eta(Fe^{56}) \approx 0{,}06$;

2) in the sugar-salt components of nutrient medium and in the microbiogical cultures grown in the control experiment we have observed the same natural relation $\eta(Fe^{54})/\eta(Fe^{56}) \approx 0{,}06$ of Fe^{54} and Fe^{56} isotopes concentrations;

3) during the culture growth the Fe^{54} isotope isn't extracted from the glass of the disk;

4) the formation of the Fe^{54} isotope and the changes of the isotopes relation $\eta(Fe^{54})/\eta(Fe^{56})$ observed during the culture growth in the optimum medium with the presence of Na and P salts is not a result of the possible "wàrm fusion" $P^{31}+Na^{23}$ in the laser focus plasma of the mass-spectrometer.

Summarizing the mentioned results and discussion of the experiments we can state that the creation of the Fe^{54} isotope as a result of nuclear transmutation in growing biological medium was observed and verified using the time-of-flight mass-spectroscopy method.

4. Combined investigations of nuclear transmutation of isotopes in growing cultures

The problem of reliability of the experimental results of the low-temperature isotope transmutation process is one of the most important. This aim can be achieved only by using several independent methods of investigation with the same object.

We have carried out investigations aimed at combined but independent Mossbauer and mass-spectroscopy investigation of nuclear transmutation of isotopes in microbiological cultures. These experiments were based on the expected $Mn^{55}+d^2=Fe^{57}$ reactions in growing microbiological culture in the heavy-hydrous (D_2O) sugar-salt nutrient medium deficient in Fe but additionally containing Mn. The reaction results in generation of the rare stable Fe^{57} isotope, concentration of which in the natural iron (mainly Fe^{56}) is very low (≈2.2%).

The course of the transmutation experiments was discussed in our previous investigation [1,2]. The research was carried out on the basis of the yeast culture ***Saccharomyces cerevisiae***, selected according to the possibility of its growth in light and heavy water media. The previously obtained cultures after centrifuging, washing and post-growth were placed in a flask with sugar-salt nutrient medium containing the salts of Mg, Ca, K, ammonium tartrate, sucrose and pure water (D_2O with Mn in transmutation experiments, H_2O with Mn or D_2O without Mn in control experiments). In accordance with the degree of purification of all nutrient medium ingredients (chemically pure category), the possible content of Fe^{56} as an admixture did not exceed $m(Fe^{56})\approx 1{,}1.10^{-6}$g and $N(Fe^{56}) \approx 0{,}9.10^{16}$ atoms. In transmutation experiments, $MnSO_4$ containing $m(Mn^{55}) \approx 2.10^{-4}$g and $N(Mn^{55})\approx 1{,}8.10^{18}$ of Mn^{55} atoms of basis stable Mn^{55} isotope was added to the sugar-salt nutrient medium. The total mass of the culture grown during 72 hours in the optimal medium (D_2O and $MnSO_4$) was near 0.2 - 0.5 g.

The figure 3 presents the results of Mossbauer investigation of this culture. The figure 3a presents the Mossbauer spectrum of ***Saccharomyces cerevisiae*** culture grown during $\Delta t = 72$ hours in the nutrient medium of optimal composition, containing D_2O and $MnSO_4$. The full number of Fe^{57} atoms (calculated by analysis of this Mossbauer spectrum) and their mass are the following: $N(Fe^{57}) \approx 0{,}87.10^{16}$, $m(Fe^{57}) \approx 10^{-6}$g.

The spectrum 3b corresponds to the same culture grown in the medium containing H_2O and $MnSO_4$, and the spectrum 3c — to the medium with D_2O, but without $MnSO_4$. The coefficient of transmutation (obtained by Mossbauer spectroscopy) equals

$$\lambda_a^{(Mossb)} \approx N(Fe^{57})/N(Mn^{55})\Delta t \approx$$

$1{,}7.10^{-8}$ (synthesized Fe^{57} nuclei per s and per single Mn^{55} nucleus).

The figure 4 presents the result of mass-spectrum investigation of this culture. The figure 4a (reference experiment) presents the results of mass-spectoscopic investigation of isotopes of the natural iron, the figure 4b (additional basic experiment) presents the mass-spectrum of the natural single-isotope Mn chemical element, the figure 4c (control experiment) presents the mass-spectrum of the same ***Saccharomyces cerevisiae*** culture grown in the heavy water nutrient medium with D_2O, but without Mn^{55} isotope (without $MnSO_4$ salt), the figure 4d presents the summarized spectrum of the impurity (Fe^{56} and Fe^{54}) and synthesized (Fe^{57}) iron isotopes in the researched culture grown in the heavy water nutrient medium with D_2O and with the Mn^{55} isotope presence.

On the one hand the relation of isotope concentrations in the control experiments (and in the pure natural Fe) equals the natural value $\eta(Fe^{57})/\eta(Fe^{56}) \approx 0{,}02$.

On the other hand the relation of isotope concentrations in the same culture that was grown during the transmutation experiments and investigated by mass-spectoscopy is much larger:

$$\eta(Fe^{57})/\eta(Fe^{56}) \approx 0.7\text{-}0.9.$$

It follows from these investigations that the total mass and total number of synthesized Fe^{57} isotope nucleus (atoms) equal $m(Fe^{57}) \approx [\eta(Fe^{57})/\eta(Fe^{56})]\, m(Fe^{56}) \approx (0{,}8\text{-}1).10^{-6}$ g and

$N(Fe^{57}) \approx (0.6\text{-}0,8).10^{16}$. The coefficient of transmutation (obtained by the method of time-of-flight mass-spectroscopy) equals

$$\lambda^{(Mass\text{-}spectr)} \approx N(Fe^{57})/N(Mn^{55})\Delta t \approx [\eta(Fe^{57})/\eta(Fe^{56})]\, N(Fe^{56})/N(Mn^{55})\Delta t \approx (1\text{-}1,3).10^{-8}$$ (synthesized Fe^{57} nuclei per s and per single Mn^{55} nucleus).

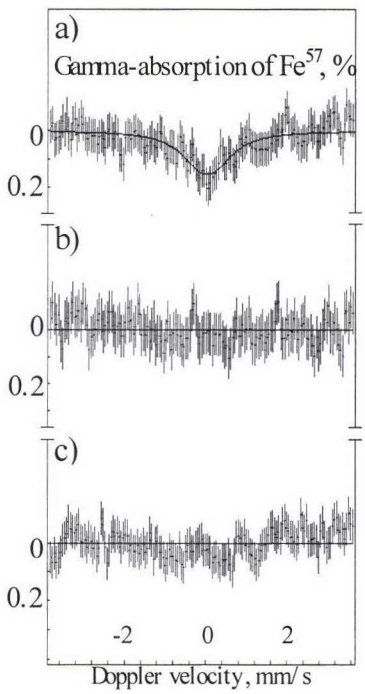

Fig 3

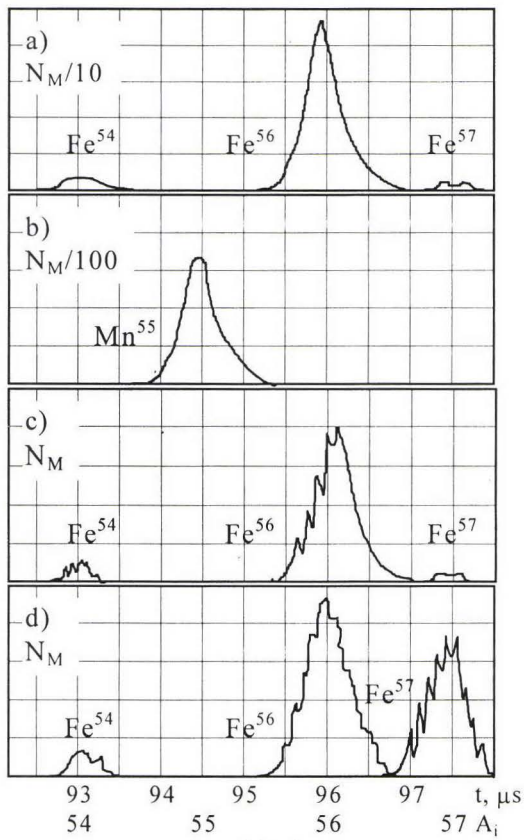

Fig. 4

It follows from our calculations that the coefficients of light (D^2) and intermediate (Mn^{55}) isotopes cold transmutation investigated by both the Mossbauer spectroscopy and the time-of-flight mass-spectroscopy are approximately equal and exceed by two orders of magnitude the same transmutation coefficient for the case of intermediate (Na^{23} and P^{31}) isotopes transmutation. We assume that in these cases a short-term elimination of the Coulomb barrier of the pair nuclear reactions in micro-potential holes with the structure that is close to parabolic [1-3] takes place. This condition is realized in the volume of growing microbiological culture.

1. Vysotskii V.I., Kornilova A.A., Samoylenko I.I. //Progress in New Hydrogen Energy. The Sixth Conf. on Cold Fusion, Proc., v.2, 1996, 687-693.

2. Vysotskii V.I., Kornilova A.A., Samoylenko I.I. //Cold Fusion and New Energy Technology, v.2, n. 10, 1996, p. 63

3. Vysotskii V.I. Proc. Fourth International Conference on Cold Fusion (Lahaina, Hawaii, December 1993), Ed. T.O.Passell (EPRI, 1994), v. 4, p. 20-1.

Conference Proceedings Vol. 70
"ICCF8"
F. Scaramuzzi (Ed.)
SIF, Bologna, 2000

NUCLEAR PRODUCTS AND THEIR TIME DEPENDENCE INDUCED BY CONTINUOUS DIFFUSION OF DEUTERIUM THROUGH MULTI-LAYER PALLADIUM CONTAINING LOW WORK FUNCTION MATERIAL

Yasuhiro IWAMURA, Takehiko ITOH and Mitsuru SAKANO

Advanced Technology Research Center, Mitsubishi Heavy Industries, Ltd.
1-8-1, Sachiura, Kanazawa-ku, Yokohama, 236-8515, Japan
E-mail: iwamura@atrc.mhi.co.jp

[ABSTRACT]
Two kinds of experimental methods have been designed to induce nuclear reactions in Pd-D system. One is the D_2 gas diffusion method, and the other is the electrolysis diffusion method. Common feature of the methods is to cause continuous diffusion of deuterium through a multi-layer Pd that contains low work function material(CaO, TiC, Y_2O_3, etc..). Time dependence of nuclear products(Mg, Si, S, F, Al) were observed by the D_2 gas diffusion method, in which the products were analyzed WITHOUT taking the multi-layer Pd out of the apparatus. The time dependence of the products were reproduced qualitatively. $^{33}S/^{32}S$ of the products was one order larger than that of natural abundance. Fe isotope ratio anomaly of the multi-layer Pd obtained by the electrolysis diffusion method were confirmed by SIMS and TOF-SIMS. Si powder products detected after electrolysis amounted to 0.057g, and its isotopic composition was anomalous.

1. INTRODUCTION

Nuclear reactions observed in the low energy deuteron and metal system have been investigated intensively. However, the nature of the phenomena is still unclear. Our experimental results so far let us to assume that necessary conditions to induce nuclear reactions in solids are as follows; (i) existence of a low work function material near the Pd surface, (ii)enough diffusion flux of deuterium, (iii) high D/Pd on the Pd surface.

To meet with the assumptions, we have contrived two kinds of experimental methods characterized by "multi-layer Pd" and "continuous diffusion of D" as shown in Fig.1. The multi-layer Pd consists of Pd thin film, low work function material and Pd bulk. It corresponds to the assumption(i). Enough diffusion flux of deuterium, assumption(ii), is satisfied with the composition shown in the lower figure. Deuterium atoms are provided with D electrolyte or D_2 gas and released from the vacuum side. They are controllable by the applied electric current or D_2 gas pressure. As for the assumption(iii), enough D/Pd ratio on the Pd thin film is considered to be attained by our methods.

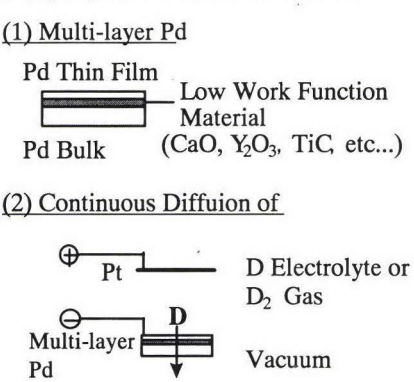

Fig.1 Features of the Present Method

2. EXPERIMENTAL

Figure 2 show the cross sectional view of the D_2 gas diffusion apparatus. The feature of this method is that it can analyze the surface of a Pd sample by XPS (X-ray Photoelectron Spectroscopy) WITHOUT taking it out of the apparatus. Therefore it is possible to avoid contamination onto the Pd sample from outer environment. This newly developed apparatus can provide the data of time dependence of detected nuclear products.

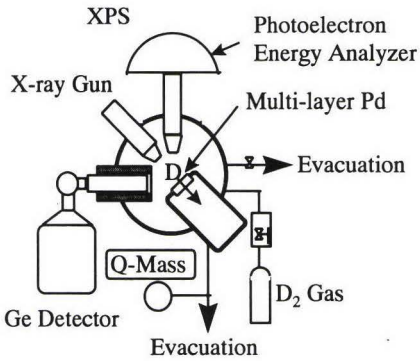

Fig.2 D_2 Gas Diffusion Method

The apparatus consists of two vacuum chambers, a X-ray gun and an electrostatic analyzer for XPS , a mass spectrometer and a Ge semiconductor detector. One chamber is fulfilled with D_2 gas, and the other chamber is evacuated by a turbo molecular pump. These two chambers are divided by a multi-layer Pd composed of Pd thin film(400 angstrom), low work function layer(typically CaO; 1000 angstrom) and Pd sheet(25mmX25mmX0.1mm).

Procedure of an experiment is as follows. At first, the surface of a multi-layer Pd in the vacuum chamber is analyzed by XPS to confirm that the surface of the Pd sample is clean. Next, D_2 gas is fulfilled into a chamber and deuterium atoms diffuse from the D_2 side chamber to the vacuum side chamber. At this moment nuclear reaction occur on the multi-layer Pd containing low work function material. After certain period(from 2days to 1 week) of deuterium diffusion through the Pd sample, the D_2 side chamber is evacuated and the surface of the Pd sample is analyzed by XPS in the chamber. The new elements which did not exit on the Pd sample at the beginning of the experiment can be detected. In case of obtaining time dependence of the products, the process mentioned above should be repeated.

Experimental results using the electrolysis type of apparatus were presented at ICCF-7[1]. Schematic view of the electrolysis diffusion method is shown in Fig.3. Details of the apparatus are given in the reference[1],[2]. The feature of this apparatus is that much larger reaction rate is possible because D/Pd on the Pd surface is larger than that of D_2 gas diffusion method. We can estimate excess heat and radiation with this type of apparatus, although element and mass analysis of the Pd sample become possible after the end of an experiment.

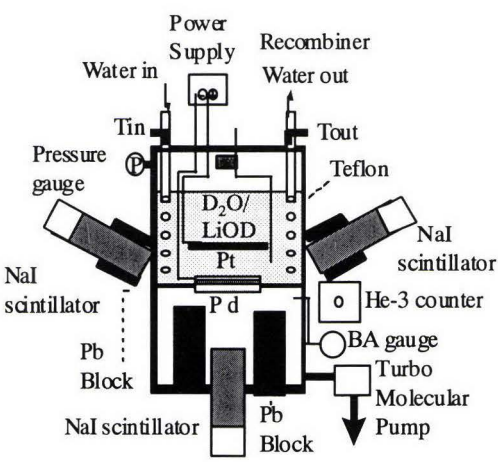

Fig.3 Electrolysis Diffusion Method

3.RESULTS AND DISCUSSION

Experimental results by the D_2 diffusion method are shown in Fig.4-6. We tried three kinds of materials; normal Pd, multi-layer Pd(Pd/CaO/Pd) and Li doped multi-layer Pd(Pd,Li/CaO/Pd).

Figure 4 shows the time dependence of C on the normal Pd(Pd only) sample which existed as an impurity at the beginning of the experiment. C usually exist on the surface of a Pd sample unless we remove it. Therefore, C and Pd are detected by XPS on the normal Pd sample. The numbers of C atoms detected by XPS did not change for two cases(No.1, 2), although the initial C and experiment time were different each other. No time dependence of C were observed if the Pd only samples were used.

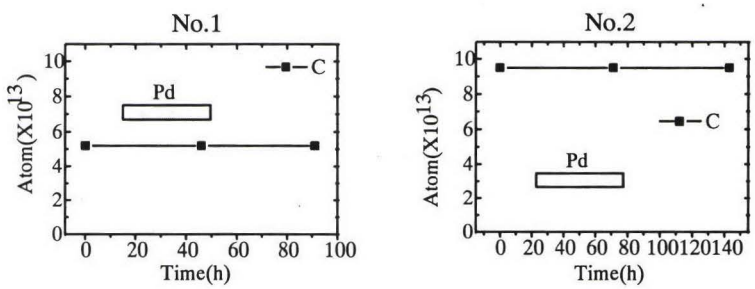

Fig.4 Time Dependence of C(impurity) detected on the Pd only samples

Multi-layer Pd gave us the entirely different results. Time dependence of C, Mg, S, Si on the multi-layer Pd(Pd/CaO/Pd) are shown in Fig.5 At first, we will explain the result of experiment No.3. There were no elements except C and Pd at the beginning of the experiment. No Mg, Si and S existed on the sample. Mg, Si and S peaks emerged and the C peak decreased after 42 hours of deuterium diffusion through the multi-later Pd. At 116 hours, S and Si increased and Mg decreased. As for No.4 experiment, amount of C was slightly larger than that of No.4. Mg, Si and S were detected again after 24 hours. After that, Mg decreased, Si and S increased, and C decreased monotonously as shown in the right figure. These results indicated that the behavior of C, Mg, S, Si were reproduced qualitatively.

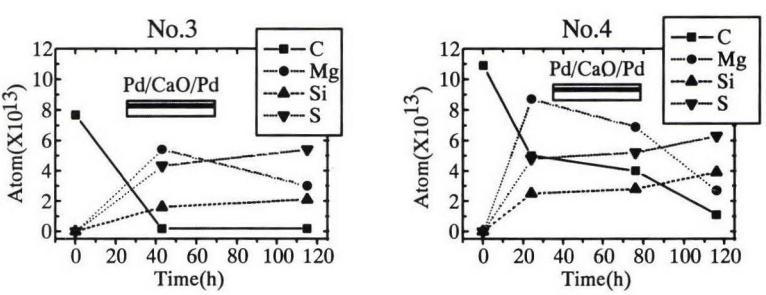

Fig.5 Time Dependence of C, Mg, Si, S detected on the Pd/CaO/Pd samples

Examination on isotope ratio of the detected elements was carried out. Table1 shows comparison between multi-layer Pd and normal Pd on isotopic abundance of S. The sample No.1 and No.4 after experiments were analyzed by SIMS(Secondary Ion Mass Spectroscopy). S on the No.1 sample was detected by SIMS, although No S was detected by XPS. Since the sensitivity for S of SIMS is higher than that of XPS. S on the No.4 sample were observed by both XPS and SIMS. As for ^{36}S, no effective counts were obtained because abundance of ^{36}S is very small.

Although secondary ion intensity of the No.4 was larger than that of the No.3, $^{34}S/^{32}S$ was almost equal to each other. $^{34}S/^{32}S$ is nearly equal to the natural abundance. On the other hand, $^{33}S/^{32}S$ of the Pd/CaO/Pd(No.4) was one order larger than that of Pd only(No.1). $^{33}S/^{32}S$ of the No.1 was nearly equal to the natural abundance. These results shown in the table1 indicates that isotopic abundance of S on the multi-layer Pd(No.4) was anomalous and S on the normal Pd seemed natural.

Table1 Comparison between Multi-layer Pd and Normal Pd on Isotopic Abundance of S

Type of Sample	Secondary Ion Intensity (cps)			Isotope Ratio	
	^{32}S	^{33}S	^{34}S	$^{33}S/^{32}S$	$^{34}S/^{32}S$
Pd/CaO/Pd(No.4)	$1.93X10^4$	$4.89X10^3$	$1.05X10^3$	0.25	0.054
Pd Only(No.1)	$9.70X10^2$	1.0X10	5.0X10	0.010	0.052
Natural Abundance	-	-	-	0.0079	0.044

Let us discuss on the above experimental results on the multi-layer Pd. The first point is the time dependence of C, Mg, Si, S. These elements were detected by XPS without taking the multi-layer Pd out of the vacuum chamber. The surface of the sample was just only exposed with D_2 gas. Therefore it was difficult to add these elements on the surface of the multi-layer Pd, or remove them from it. Especially Mg once increased and decreased. It is very difficult to explain their behaviors by certain contamination processes. The second point is that product S had anomalous isotopic abundance. As shown in Table1, $^{33}S/^{32}S$ is one order larger than natural isotope ratio. If the S were contaminant, such efficient isotope separation was possible? According to the points, we can conclude that it is strongly suggested that Mg, Si, S are formed by certain nuclear reactions.

If these elements are nuclear products, they are basically explained by the EINR(Electron-Induced Nuclear Reaction) model[2]. Experimental results enable us to make an interpretation that C was transmuted to Mg, Si, S. The EINR model gives the following explanation. At first deuterium nuclei capture electrons and form di-neutron clusters. Simultaneously, the di-neutron clusters react with C, and produce Mg. After that, Mg reacts with di-neutron clusters again and is transmuted into Si or S.

$$ {}^{2}_{1}d + {}^{0}_{-1}e \rightarrow {}^{2}_{0}n + \nu \qquad (1) $$

$$ {}^{12}_{6}C \xrightarrow{6^2_0 n} {}^{24}_{12}Mg \xrightarrow{2^2_0 n} {}^{28}_{14}Si \qquad (2) $$

$$ {}^{12}_{6}C \xrightarrow{6^2_0 n} {}^{24}_{12}Mg \xrightarrow{4^2_0 n} {}^{32}_{16}S \qquad (3) $$

In the Pd/CaO/Pd experiments, impurity C was transmuted into Mg, Si, S. Next experiments were performed aiming that Li will be transmuted into the other elements.

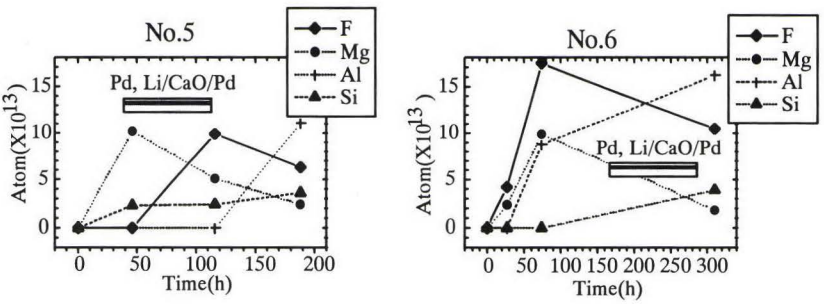

Fig.6 Time Dependence of F, Mg, Al, Si detected on the Pd,Li/CaO/Pd samples

Experimental results on Li doped multi-layer Pd are shown in Fig.6. Lithium atoms were doped by the electrolysis of LiOD solution onto the surface of the multi-layer Pd(Pd/CaO/Pd). The new elements F, Al emerged in the both cases; No.5 and No.6. F once increased and decreased. Al increased monotonously. Behaviors of F and Al were similar to Mg and Si, respectively, though emergence time of F and Al in the case of No.5 is difference. Mg and Si are considered to be originated from impurity C. We observed F and Al by adding Li on the surface of multi-layer Pd, therefore we assume that F and Al were transmuted from the added Li as shown in the following equations.

$$ {}^{7}_{3}Li \xrightarrow{6^{2}_{0}n} {}^{19}_{9}F \xrightarrow{4^{2}_{0}n} {}^{27}_{13}Al \qquad (4) $$

At present, the model is theoretically incomplete. However, it is noticeable that the similar explanation is possible between the transmutations of C and Li.

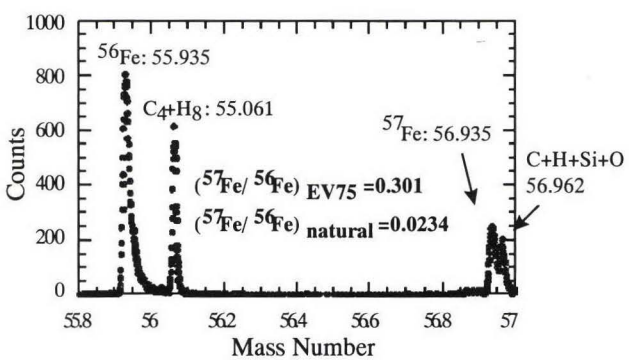

Fig.7 Fe Isotope Anomaly observed by TOF-SIMS

Next, experimental results obtained by the electrolysis diffusion method are described. Excess heat and nuclear products were observed for almost all the cases we tried using the multi-layer Pd. Isotopic composition of the obtained product were often different

from natural abundance. The authors usually estimate the isotopic composition of a product by SIMS. Figure 7 presents an example that Fe isotope ratio anomaly was confirmed by both SIMS and TOF-SIMS(Time of flight SIMS). Better mass resolution can be obtained by TOF-SIMS. According to the SIMS analysis for sample(EV75) in Fig.7, $^{57}Fe/^{56}Fe$ was estimated at 1.8; very high value compared with natural abundance 0.0234. TOF-SIMS analysis gave 0.301 for $^{57}Fe/^{56}Fe$ as shown in Fig.7. Anomalous large $^{57}Fe/^{56}Fe$ was obtained on a multi-layer sample(EV75) by both SIMS and TOF-SIMS, though $^{57}Fe/^{56}Fe$ did not agree with each other. The reason is considered that $^{57}Fe/^{56}Fe$ depend on the analyzed position on the sample. Variation of isotope ratio depending on the location of analysis are often observed[1].

As excess heat increased, the amount of nuclear products increased. Figure 8 shows an example of Si powder product. In this case, large excess heat more than input power was obtained. The powder is SiO_2, because Si was oxidized by O_2 in the air after being taken out of the experimental apparatus. Amounts of the Si reaches to 0.057g.

In order to evaluate Si contamination, we made a list of candidates of contamination source; solution, multi-layer Pd, Pt anode, Ni cooling pipe, Polypropylene and Teflon in the experimental apparatus. Maximum quantity of Si contaminants was estimated at 0.023g, which is smaller than that of obtained Si powder.

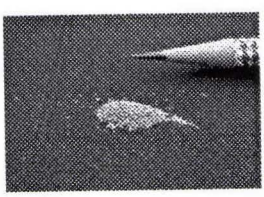

Fig.8 Detected Si Powder

Table 2 Isotope Ratio of Detected Si Powder

Isotope	Detected Si Powder		Si Standard Solution		Natural Abundance(%)
	Intensity (cps)	Isotope Ratio(%)	Intensity (cps)	Isotope Ratio(%)	
^{28}Si	4,300	96.1	3,256	92.5	92.23
^{29}Si	70	1.6	149	4.3	4.67
^{30}Si	105	2.3	110	3.2	3.10

The isotope ratios of detected Si powder are shown in Table 2. ICP-MS(Inductively Coupled Plasma Mass Spectrometry) was applied to the analysis, the tabulated values were averaged by 5 times measurements. ^{29}Si of detected Si powder is smaller than Si standard solution as shown in the table. The isotopic composition of Si powder detected in the apparatus after an experiment was different from natural Si abundance.

Judging from the above results, the authors consider that the detected Si powder is composed of nuclear products and Si impurities in the solution. We should confirm this result by performing the experiments with the improved solution that contains small amount of Si.

[REFFERENCE]

[1]Y.Iwamura, T.Itoh, N.Gotoh, M.Sakano, I.Toyoda and H.Sakata, "Detection of Anomalous Elements, X-ray and Excess Heat Induced by Continuos Diffusion of Deuterium Through Multi-Layer Cathode(Pd/CaO/Pd)", Proc. of ICCF-7, Vancouver, Canada, April 19-24, 1997, p167

[2]Y.Iwamura, N.Gotoh, T.Itoh and I.Toyoda, "Detection of Anomalous Elements, X-ray and Excess Heat in a D2-Pd System and its Interpretation by the Electron-Induced Nuclear Reaction Model", *Fusion Technology*, vol.33, No.4, p.476, 1998

Conference Proceedings Vol. 70
"ICCF8"
F. Scaramuzzi (Ed.)
SIF, Bologna, 2000

X-ray Spectrometric Analysis of Carbon Arc products in Water

Teruo Hanawa
Osaka University
Suita Osaka 565-0871, Japan

Abstract

Energy dispersive X-Ray spectrometry, methods of X-ray fluorescence (XRF) and Particle Induced X-ray Emission (PIXE) were applied to analyze the product of carbon arc in light water. The result revealed increase or appearance of many kind of elements; Si, S, Cl, K, Ca, Ti, Cr, Mn, Fe, Co, Ni, Cu, Zn, and possibly heavier elements, however, the relative abundance including null varied case by case. Among them, a dominant product Fe was found only in the larger debris.

Among XRF inspections applied to the arc traces of used electrodes, an anode showed metallic elements, which suggests that transmutation reactions take place on the anode surface.

1. INTRODUCTION

The generation of iron from carbon arc was discovered by Osawa [1] in 1964, since then no scientific study had been done on this interesting subject until early nineties: Ogura et al.[2,3] reported their analysis of carbon arc product in water applying ICP-MS in 1990 and 1992, however, a problem had been involved in their sampling method ; they analyzed only the filtrate. In 1994, Sandaresan and Bockris [4] verified the appearance of iron in the carbon detritus produced from carbon arc in water under the existence of dissolved oxygen, Singh et al. [5] found out that iron from carbon arc had the same isotope composition as the natural iron, and that elements such as Si, Ni, Al, Cr, Mn were also accompanied with Fe.

Considering the importance of carbon arc in the field of cold fusion, more studies are required. In the present study adopting X-ray spectrometry as the analytical means, much more elements than reported are easily identified and the site of nuclear reaction can be located as the discharge part of anode.

2. EXPERIMENTAL

2-1 Materials: Two kind of highest purity carbon rods (6 mm in diameter) for emission spectroscopy were used, the one being soft type made in Hitachi Chemical Co., and the other hard type from Toyo Tanso Co.. The highest purity water (R>18.2 MΩ·cm) used for XRF analysis was the product of Osaka University. The arcing was done in a Teflon beaker (1 litter), and only plastic devices were used in the sampling stage (Quality of water used in the case of PIXE analysis was not so high; R >10 MΩ·cm and Pyrex glass beaker was used).

2-2 Power Source: A DC welder (single phase, full wave rectifier with a choke coil, max. capacity 50 A). The current was measured by a digital clamp meter.

2-3 Analysis: At the beginning, PIXE (Particle Induced X-ray Emission) was applied for the elemental analysis because of its high performance in speed and accuracy; however, its use was very limited due to the time-sharing usage imposed on this apparatus connected to an accelerator. Thus, an energy dispersive fluorescent X-ray spectrometer, SEIKO-SEA2001 was adopted, in which a sample is illuminated by a collimated beam of the characteristic X-rays of Rh, the diameter and the dominant energy of the beam being 10 or 3 mm and 20.2 keV, respectively. The fluorescent X-rays are detected by a SSD cooled by liquid nitrogen, and processed to a spectrum as shown below. The time necessary for data acquisition was around 30 min.

2-4 Sampling : The position of carbon electrodes was manually controlled to ignite arc. The arc current and the inter electrodes potential varied irregularly, and the arc itself disappeared occasionally, the typical input power being about 600 W (around 30 A, 20 V). Under this condition, enough amount of carbon debris for the analysis was obtained within 1 hour including intermissions for cooling to avoid excessive vaporization of the water.

The arc treated water was kept still for one day after the carbon rods had been removed. After decanting excessive water, much reduced volume of water containing carbon debris was transferred to a small beaker, then the debris was pipetted to a sample holder made of ash less filter paper for XRF analysis, weight of the dried sample being around 5 mg. In the case of PIXE analysis, arc-treated water containing carbon debris was filtered though a membrane filter. The filtrate was heat concentrated about 100 times, 50 micro litter of which was pipetted on a thin Mylar film of the sample holder. Thin filter (bore size = 0.4 micro meter) carrying debris was used as the sample.

After weighing each electrode, an end part having the trace of arc was cut off from the rod for the analysis, and one of the opposite end was scraped off with a diamond file or a piece of alumina ceramic to produce carbon powder to be used as the control sample.

3. RESULTS AND DISCUSSION

Comparison between PIXE spectra A and C in Fig.1 reveals considerable increase of Fe, slight increase of Ca, Mn, Ti, and newly appeared Cu, Zn which have not been reported. In addition, the most interesting finding derived from comparison between A and B is that almost all Fe exists in debris larger than about 0.4 micro meter. Further discussion on the spectrum B cannot be made at present due to lack of the corresponding control.

After picking off the first debris, the arced water segregated enough amount of deposits for XRF analysis successively accompanied with decreasing Fe content; an example is shown in Fig.2, where larger Fe signal in the control is due to considerable contribution from filter paper used as the substrate. Since the successive deposition is thought as the result of coagulation of colloidal particles having successively decreased size, the XRF observation accords with the conclusion derived from PIXE stated above.

In the later experiment, analysis was extended to the arced point of the carbon rods, but all measurement failed to detect metallic elements except one case in which sodium carbonate solution was used instead of pure water. In this experiment, arc current suddenly increased over 60 A after net arcing time of 10 min. at the current around 35 A, which caused break down of the power source. In this case, weight loss of the anode was 271 mg. XRF analysis applied to both electrodes revealed that metallic elements appeared only on the trace of arc in the anode as shown in Fig.3. From these observations, an idea that negative oxygen ions transported to the anode may react with carbon to produce Fe under the intense electron bombardment from the arc. In addition, the fact that Fe is always found in larger debris seems to suggest that the transmutation reactions may have some coherence. Anyways, more extended studied are necessary to understand the behavior of this interesting and important system.

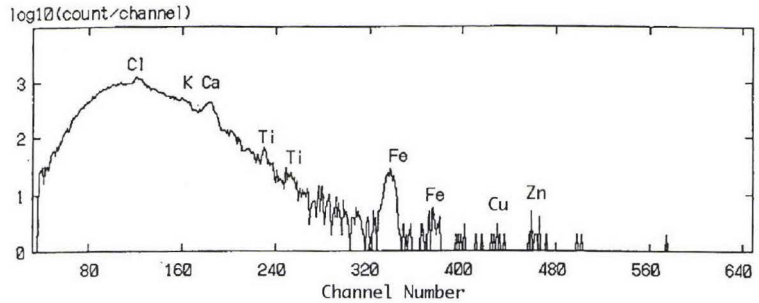

A. PIXE SPECTRUM OBTAINED FROM CARBON ARC DEBRIS ON A MENBRAIN FILTER

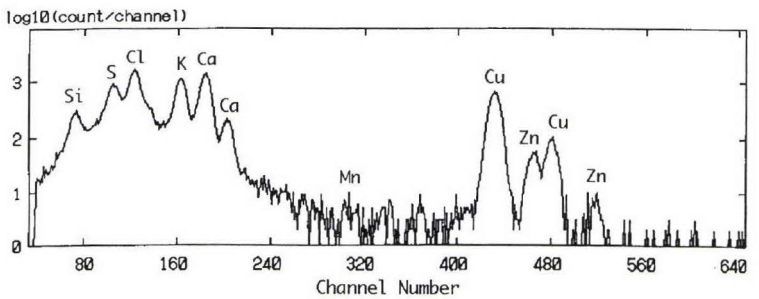

B. PIXE SPECTRUM OBTAINED FROM CONCENTRATED LIQUID

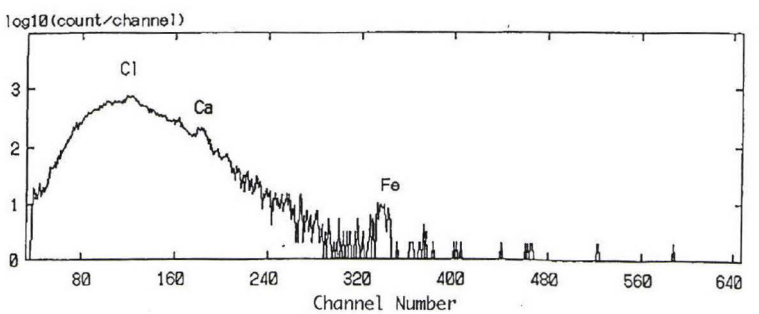

C. PIXE SPECTRUM OBTAINED FROM THE CONTROLE SAMPLE

Fig.1 PIXE SPECTRA OBTAINED FROM 2 PHASES OF ACRBON ARC PRODUCT IN WATER SEPARATED BY A FILTER

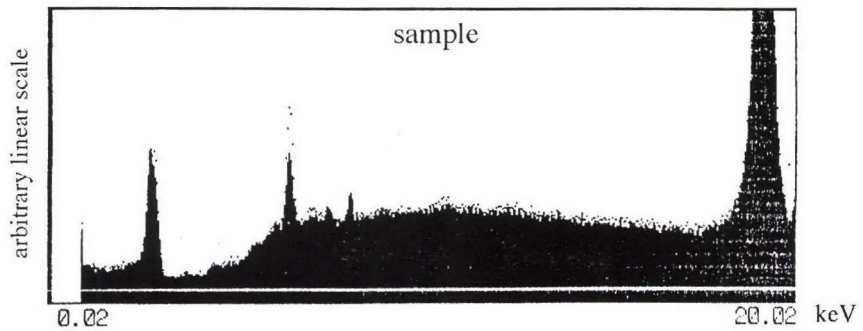

A. XRF spectrum obtained from in-water carbon arc debris

Dotted line: 1st deposit

Filled pattern: 2nd deposit

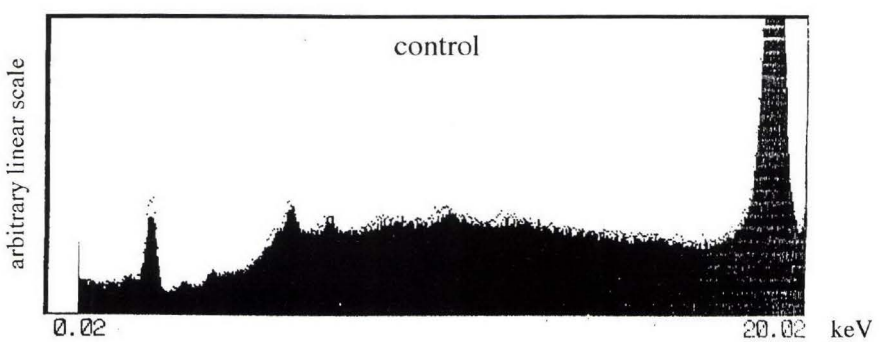

B. XRF spectrum obtained from carbon powder

Fig.2 XRF spectra obtained from Carbon debris and its control supported on ash less filter papers.

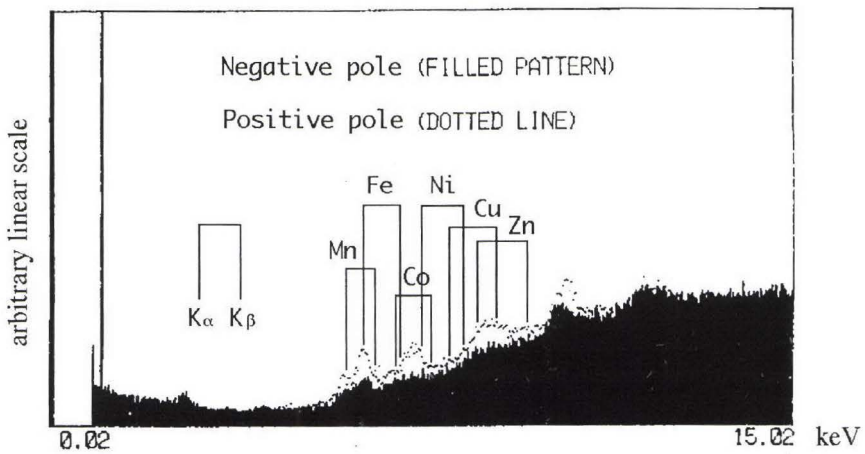

Fig.3 XRF SPECTRA OBTAINED FROM THE ARC TRACES IN THE ANODE AND CATHODE

Acknowledgement:

The author wish to express his sincere thanks to Prof. Akito Takahashi of Osaka University for his encouledgement and valuable discussions. Also thanks are due to president Dr. Ryoda Sato of Manyo Industries Co. Ltd. For his kind permission for free use of his factory. Further the author wish to express his thanks to Prof. Hiroshi Miyake of Kobe Marchantile Marine University for his kind guidance in performing PIXE analysis.

Reference:

1. G.Oshawa, East-West Inst. Magazine (Mar.1965)
2. I. Ogra, I. Awata, T. Takigawa and K. Nakamura, Annual Rept. Atomic Energy Res.Inst., Kinki Univ. 27, 1 (1990)
3. I. Ogura, I. Awata, T. Takigawa, K. Nawamura, O.Horibe and T. Koga, Chem. Express, Vol.7, No.4, 257 (1992)
4. R. Sundaresan and J. O'M. Bockris, Fusion Technol. 26, 261 (1994)
5. M. Singh, M.D.Saksena, V.S.Dixit, and V. B. Kartha, Fusion Technol. 26 (1994)

Conference Proceedings Vol. 70
"ICCF8"
F. Scaramuzzi (Ed.)
SIF, Bologna, 2000

HYDREX CATALYZED TRANSMUTATION OF URANIUM AND PALLADIUM

EXPERIMENTAL PART

J. Dufour, D. Murat, X. Dufour and J. Foos

CNAM. Laboratoire des Sciences Nucléaires 2 rue CONTE 75 003 Paris France

Introduction :

By submitting various metals (U, Pd) containing hydrogen (from 2,000 to 700,000 atoms of hydrogen for 1,000,000 atoms of the host metal) to the combined action of electrical currents and magnetic fields, we have observed a sizeable exothermal effect (from 0.1 to 10 watts). This effect is beyond experimental errors, the energy output being typically 110 to 250 % of the energy input and not of chemical origin (exothermal effect in the range of tens of MJ/mole of the metal under study). The calorimetric measurements have been made using calorimeters exchanging heat with a heat sink maintained at a regulated temperature : either by using a differential calorimeter or by measuring the temperature difference between the processed sample and the heat sink. Together with this exothermal effect, we have seen the apparition, in the treated samples of significant amounts of chemical species : Zn , Mg and Cu in the case of Palladium [1], Pb, Yb, Lu and Hf in the case of uranium (by ICP-MS analysis of the total treated sample after dissolution compared to the corresponding virgin samples of the same batch). Such apparition of new compounds have been observed by many experimenters (see for instance [3],[4] and [5]). Compared to the amount the new species formed the energy produced is typically in the range of 150 to 400 MeV per new atom found in the treated samples.

Experimental :

Case of palladium :

The calorimetric experiments have already been described [1] and will thus be only summarized here. The most interesting results were obtained when an ozonizer discharge

was struck through (light) hydrogen isotopes, contacting a palladium electrode (experiment 3H06) [1].
The palladium was in the form of a thin wire (diameter 250 µm, 60 cm long), placed in the center of a pyrex tube (outside diameter 3 cm, 70 cm long) and parallel to the axis of this tube. The wire was held in position by two small steel springs, connected by small brass hooks to the two fittings closing the ends of the pyrex tube. The palladium wire served as the inner electrode of the ozoniser. The outer electrode was a copper tube (inside diameter 3 cm, 40 cm long), placed round the pyrex tube, at equal distance from both ends of the pyrex tube. The pyrex tube was filled with hydrogen. The outer electrode was then connected to the ground and the inner electrode to the high (2 to 3 kV) AC voltage generated by a coil. An ozoniser discharge was thus struck through the hydrogen, between the palladium wire (and more precisely, the 40 cm of this wire facing the copper tube) and the pyrex tube serving as the ozonizer dielectric. With this design, there is no contact between the discharge and the outer copper electrode. Note that in this experiment, the loading of hydrogen in the palladium and the excitation of the hydrogen in the loaded palladium (by a combination of current pulses and magnetic fields they create) is carried out simultaneously during the experiment.

The chemical composition modifications were assessed in the following way : after the experiment, the palladium wire was removed from the reactor and a 20 cm piece (in the center of the 40 cm facing the outer copper electrode and weighting 120 mg) were dissolved and analyzed by ICP-MS (CEA at Bruyères-le-Chatel) for all elements, except Fe, Ru, Rh and Ag that were assessed by ICP-AES. A virgin sample of palladium wire of the same batch and same length was also analyzed according to the same procedure.

Case of uranium :

Uranium of nuclear purity, in the form of lathe turnings and coming from the same batch (150 g) was used for both blanks and active experiment. Contrary to the case of palladium, the hydrogen loading was done before the experiment and the activation was thus done during the experiment on the preloaded sample. Uranium is easy to hydrogenate, up to UH_3 (2 hours at 250°C, under 20 bars of Hydrogen). Three hydrogen/uranium systems were used :

- solid metallic uranium, containing 700 to 2400 atomic ppm of hydrogen. (Uranium obtained by reduction of the oxide always contains that amount of hydrogen).
- uranium hydride of various H contents (from UH to UH_3) obtained from the Uranium batch and from ALPHAGAZ Hydrogen (quality U).

The following excitation means were applied simultaneously on the preloaded Uranium :

-electrical current, in the form of either dc pulsed current (with frequency 5 KHZ) or high frequency ac current (with frequency 5 to 20 MHZ)
-magnetic field of intensity up to 1 T generated by permanent magnets (Fe, B, Nd or Co, Sm). the magnetic field is applied in a direction parallel to the current direction.
-temperature from 40°c to 250°c

The calorimetric experiments were carried out in 2 different set-up :

-for experiments using 5 kHz pulsed DC current, a differential excess power measurement was used. It has been described in details elsewhere [2].

-for experiments using high frequency (10 MHz) AC current, the excess power measurement was done by measuring the temperature of the sample, enclosed in a reactor exchanging heat with a temperature regulated water bath. Precautions have been taken for measuring the high frequency electrical power input (use of HF probes, with range 0.5 to 1,000 kHz to measure the voltages, use of a thermal ammeter to measure the intensity).

The chemical composition modifications were assessed by mass spectrometry :

-low or medium resolution ICP-MS for all species (from Be to U) and for lead isotopic ratios

-thermal ionisation mass spectrometer for uranium isotopic ratios.

The ICP-MS measurements were performed by two different laboratories (Cogema at Pierrelate and CNRS central lab at Solaize) and the thermal ionisation MS only by the first laboratory. The results by ICP-MS from both laboratories are very comparable.

The dissolution procedure (by HCl or HNO_3) of the samples have been described in [2].

Experimental results :

Case of palladium :

Excess energy :

Table 2 below summarizes the thermal results obtained in experiment 3H06 (light hydrogen / palladium). It can be seen that very significant excess energy production have been observed, on long periods.

Table 2 Period	Duration (second)	H consumed (mMole H)	Excess energy on period (J)	Mean excess power (W)	Exc.Ene. eV per atom H	Power Input (W)
CAL	230 000	0	0			Calib.
INC	695 000	9.88	1 737 500	2.5	1 800	Increasing
I	1 390 000	9.63	5 838 000	4.2	6 300	115
II	342 000	1.41	1 846 000	5.4	13 600	150
III	767 000	5.44	6 596 000	8.6	12 600	150
Total	3 424 000	26.36	16 018 300	4.7	9 000	

Note that the combustion of all the hydrogen used in the experiment (26.36 mMole H) would have yielded 6,400 J, to be compared with 16,018,300 J actually obtained.

New species in the treated sample :

Table 3 summarizes the variations in chemical species between the virgin and the treated sample. Note that the figures are for the 20 cm of wire that were analysed. When required (calculation of energy per atom, these figures are multiplied by 2).

Table 3 :

Elements	3H06	Blank	3H06 – Blank
Li	5.2×10^{14}	1.0×10^{14}	0.04×10^{16}
Mg	2.5×10^{17}	2.2×10^{16}	23.0×10^{16}
Al	7.2×10^{16}	2.7×10^{15}	7.0×10^{16}
Cr	1.1×10^{16}	1.3×10^{15}	0.97×10^{16}
Mn	3.9×10^{14}	2.6×10^{14}	0.01×10^{16}
Fe	2.8×10^{16}	1.3×10^{16}	1.6×10^{16}
Ni	3.3×10^{15}	2.5×10^{15}	0.09×10^{16}
Cu	4.7×10^{15}	1.8×10^{15}	0.3×10^{16}
Zn	4.8×10^{16}	4.8×10^{15}	4.3×10^{16}
Ir	2.3×10^{14}	1.9×10^{14}	3.8×10^{13}
Pt	3.0×10^{14}	5.2×10^{14}	-2.2×10^{14}
Au	2.9×10^{14}	4.0×10^{14}	-1.1×10^{14}

The total amount of new atoms that appear in the sample (40 cm) is roughly 74.6×10^{16}, corresponding to an average excess energy per new atom formed of some 130 MeV. This is the order of magnitude of fission reactions .

When these results were obtained, we attributed the apparition of new species to pollution due to the action of the discharge. We have revisited our experimental set-up and now draw the following conclusions :

-Zn, Cu, Ni, Fe, Mn and Cr are indeed present in the reactor (steel spring and brass hook holding it), but they are at some 10 to 15 cm from the discharge and a transport mechanism to the palladium wire is not at all obvious.

-Al is certainly present as a constituent (2 to 3%) in the pyrex glass struck by the discharge, and we see a 30 times increase of its content in the treated sample. But B, which is also a constituent of the pyrex (up to some 15%) shows no variation in the treated sample. On the contrary, Mg which is a trace component of the pyrex glass used, shows a 10 times increase. Moreover, if we attribute the apparition of Al and Mg to the effect of the discharge, this transport would involve 3 times more Mg atoms than Al.

The only new species appearing in the treated sample which might reasonably be accounted for by pollution by the discharge, is thus Al. The three major new species (Mg, Zn and Fe), amounting to some 58×10^{16} atoms have thus likely been generated in the palladium (40 cm), yielding a mean energy per atom of some 170 MeV, which is an upper limit of the energy released per atom by the treatment to which the palladium has been submitted. Note that Zn have been observed by other experimenters [3],[4] and [5].

Case of Uranium :

Excess energy :

Table 3 below gives the measured excess energy, and the main operating conditions. The energy of reaction per mole of uranium excludes a chemical origin of the phenomenon.

Table 3

Sample Reference	Frequency kHz	Temperature Range °C	Duration s	Total excess Energy (J)	Energy of Reaction MJ/mole U
U2-JD8 (C)	5	170	153700	184400	19,5
U4-JD7 (B)	5	200	162000	129600	57,1
U7-JD6 (A)	5	160-210	15000	56200	24,5
990801	5	190		< 17000	< 4,5
990901	5	190		141500	42,7
MHz1 1+2	9600	40-50	353940	49700	104,7
.					
MHz3	9600	40-50	172250	88340	100,1
MHz4 1+2	8700	40-50	1871400	94600	61
MHz4-5	5100	40-50	30000	2700	18

Table 4 below shows the influence of the operating parameters : the excess power increases when the current increases and for the same current intensity, the excess power is higher in the MHz range than in the kHz one. On the contrary, the activation energy of the reaction is higher for the kHz range than for the MHz one.

Table 4

Sample Reference	Fréquence kHz	Maximum Excess power (mW)	Intensity (A)	P max/I (mW/A)	Activation Energy Ev/atom
U2-JD8 (C)	5	1500	13,000	115	5,5-8
U4-JD7 (B)	5	1000	15,000	67	5,5-8
U7-JD6 (A)	5	4000	16 to 0	250	5,5-8
990801	5	50	1,200	42	5,5-8
990901	5	800	14,000	57	5,5-8
MHz1 1+2	9600	380	0,500	760	1,5-3
MHz3	9600	150	0,300	500	1,5-3
MHz4 1+2	8700	250	0,225	1111	1,5-3
MHz4-5	5100	90	0,180	500	1,5-3

New species in the treated sample

2 new chemical species appear in the treated samples, both well above the detection limits of the ICP-MS (5 µg per liter) :

-lead (a very common specie) in quantities up to 5000 ppm
-lutetium (a very rare specie) in ppm quantities

Table 5 below gives the main results obtained. It can be seen that the energy of reaction per mole U is in the range of tens of MJ/mole, excluding a chemical origin of the exothermal reaction observed. The energy per atom of Lu is in the fission range.The energy per atom of lead is puzzling, varying from α emission range (samples (A), (B), (C) and MHz1 1+2) to a very low value (sample 990901). For this, we propose the following explanation :

Table 5

	Sample weight (mg)	Energy of Reaction MJ/mole U	Lead ppm	Lu ppm	Energy of Reaction KeV per Pb	Energy of Reaction KeV per Lu
U2-JD8 (C)	553	19,5	440,00		1879	
U4-JD7 (B)	540	57,1	209,00		2780	
U7-JD6 (A)	545	24,5	156,00		1615	
990801	888	< 4,5	23,70	0,30	< 3215	< 210180
990901	788	42,7	4844,00	0,47	131	1341200
MHz1 1+2	180,3	104,7	16,90	2,13	13180	104443
MHz3	210	100,1	2,00			
MHz4 1+2	368	61	2,90	0,96		441068

The activated samples have high to very high lead contents. The isotopic composition of this lead is within the range of terrestrial leads, but different from that of the blanks. (20 blank uranium samples have been analysed, yielding a mean lead content of 1.8 ppm). Two possible sources of pollution by lead have been identified. Their isotopic composition does not match neither the one of the blanks nor the one of the activated samples. (taking into account the uncertainty on measurement of the isotopic ratios).It is thus quite certain that the samples have been polluted by lead, but we cannot exclude that we have a mixture of external lead and of lead coming from the reaction (in smaller quantities but with different isotopic composition). Taking into account a smaller lead content in the treated samples would result in a higher energy per atom Pb.

As regards Lu, we have found an anomaly at mass 176, which can be attributed to the presence of Hf and Yb, together whith Lu in the samples.

Finally we can conclude from these results that one class of reaction product resulting from the activation of uranium, might be nuclei ranging from Pb to Lu,Hf and Yb and that the reaction energy might be in the range of fission reactions.

Conclusion :

The experimental results reported above, point to nuclear reactions occurring in Pd and U when these metals, containing hydrogen, are submitted to the action of electrical and magnetic fields. The energies of reaction seem to be in range of fission reactions. A tentative explanation is given in the article "The Hydrex concept. Effect on heavy nuclei"

[1]J.Dufour, J.Foos, J.P. Milot and X.Dufour : From cold fusion to "Hydrex" and "Deutex" states of hydrogen *"Proceedings ICCF6"* (1996) p482-495
[2] J.Dufour, D.Murat, X.Dufour and J.Foos : Hydrogen triggered exothermal reaction in uranium metal *"Phys Lett A"* In press
[3] T.O Passel *"Proceedings ICCF8"* (2000) to be published.
[4] X.Z Li *"Proceedings ICCF 8"* (2000) to be published.
[5] G.H Miley *"Proceedings ICCF8"* (2000) to be published

CHAPTER 4.

LOADING OF H(D); MATERIAL SCIENCE

Conference Proceedings Vol. 70
"ICCF8"
F. Scaramuzzi (Ed.)
SIF, Bologna, 2000

HEAT PRODUCED DURING THE ELECTROLYSIS OF D_2O WITH TITANIUM CATHODES

J. Warner and J. Dash
Physics Dept., Portland State University, P.O. Box 751, Portland, OR 97207

Abstract. Cold rolling 20% appears to increase both the amounts of excess heat and reproducibility obtained by electrolysis of acidified D_2O with titanium cathodes. Unexpected elements such as chromium and iron were detected on the surfaces of cathodes after electrolysis. The presence of chromium was confirmed by neutron activation analysis.

Experimental Methods and Results. Experiments have been performed using titanium cathodes with various amounts of deformation by cold rolling, which increases the amount of lattice disorder and stress in the cathodes.

The first calorimetric system employed is referred to as the "8-cell" system. Each cell is comprised of a small double-walled beaker with a temperature-transducer in the dead airspace between the cell walls. The inner chamber holds the catalyst, electrolyte and electrodes. Each cell is sealed to minimize gas losses. Seven of the eight cells were wired in series so the same, constant current passed through each cell. One of the seven cells is a control cell with platinum anode and cathode and electrolyte containing sulfuric acid and light water in the ratio one mole H_2SO_4 to 99 moles H_2O. The eighth cell, which was empty, was used to monitor ambient temperature. The remaining six experimental cells consisted of three pairs of cells, with the cells in each pair as identical as possible. The three pairs differed from each other in one parameter such as cathode size (from 0.12 to 0.34 cm^2) or degree of deformation. The experimental cells all contained Pt anodes, Ti cathodes (foils, triangular in shape) and an electrolyte composed of the ratio one mole H_2SO_4 to 99 moles D_2O. All of the data is stored in a computer for later analysis. To analyze the experiment, the following equation is used [1]:

$$\frac{dH_e}{dt}(Excess) = \frac{\Delta T_e}{\Delta T_c}(V_c I - \frac{dH_c}{dt}(esc)) + \frac{dH_e}{dt}(esc) - V_e I - \frac{dH_{TiO_2}}{dt} - [\frac{dH_{TiD_2}}{dt} - \frac{dH}{dt}(esc)] \quad (1),$$

where subscript c refers to the control cell, subscript e refers to the experimental cell, dH_e/dt (Excess) is the enthalpy released by cold fusion (or other unknown processes), ΔT is the temperature difference between the cell and its surroundings, VI is the power input into the cell, dH/dt (esc) is the recombination enthalpy lost by each cell due to escape of gases from the cell, dH_{TiO2}/dt is the enthalpy due to the formation of titanium dioxide which results from erosion of the cathode during electrolysis, and [dH_{TiD2}/dt - dH/dt (esc)] is the enthalpy loss due to the large difference between the enthalpy of formation of TiD_2 and the enthalpy of recombination of D_2O. Lost recombination enthalpy is determined from the weight lost by each cell during each experiment.

The other calorimeter employed is a Seebeck envelope calorimeter (SEC) from Thermonetics Corp., which allows for scaled up experiments (cathode areas from 2.81-4.29 cm^2). The cathode foils are shaped to maximize the uniformity of the electrical current density to make the erosion more uniform, thus giving the cathode a longer life. The SEC used here measures 18 cm by 18 cm by 18 cm in the inner cavity. Heat flows from the cell through air in the calorimeter and through the Seebeck envelope to an aluminum jacket incorporating constant temperature water-cooling coils.

The millivolt output signal, which is related to the heat release via an accurate calibration process, is fed to a computer for storage[2]. If no temperature difference between the cavity and the water jacket exists, no heat flux is measured and no signal is generated. If the cavity temperature is greater than the water jacket temperature, a positive signal is generated. The SEC was calibrated using two different methods: (1) a control cell with Pt anode and cathode in a light water/ sulfuric acid electrolyte (three data points) and a cell with a resistor immersed in water (16 data points). The SEC gives a linear input vs. output relationship over the range of interest:

$$\text{Power Output (Watts)} = 0.216 \text{ W/mV} \times \text{SEC output (mV)} + 0.029 \text{ W} \qquad (2),$$

with a coefficient of determination R^2 of 0.9996. The 0.029 W intercept at zero SEC output compensates for thermal leakage along wires fed through a 0.6 cm inner diameter tube inserted into the inner cavity of the SEC. These wires include the power leads to the cell, the leads to measure cell voltage, and the thermocouples used to monitor temperature on the outside of the cell.

According to the suppliers, the titanium used in this study (99.99 % Ti, metals basis) was hot worked from the ingot stage to about 5 mm thickness. It was then cold rolled to 0.5 mm thickness (about 90% reduction in thickness). It is sold in the cold rolled condition. The Ti was obtained from two vendors: Alfa Aesar which reported impurities of 3 ppm Fe, 2 ppm K, 2 ppm Mn, 1 ppm Cr and 20 other elements $\leq$ 1 ppm. This was the Ti used in the 8-Cell "as received" condition. The remainder of the data in fig. 1 was obtained using Ti supplied by Aldrich, which reported that the only impurities detected were 30 ppm Ca and 8 ppm Al. The experimental results are shown in fig. 1, in which the excess power output (W) is a function of percentage reduction in thickness by cold rolling of the titanium cathodes prior to electrolysis. The error values shown in fig. 1 vary from one experiment to another but the largest error values encountered are those reported. As a conservative estimate, only those data points above 100 mW will be reported as excess heat.

With the titanium cathodes in the as received condition, 3 of 8 experimental cells (38%) showed excess heat. The current densities at the cathode for the 8-cell experiments were 0.6 to 3.3 A/cm^2 with voltages from 1.8 to 6.0 V. The SEC cathode current densities ranged from 0.3 to 0.7 A/cm^2 with voltages between 4.3 to 6.0 V. There was no correlation between current density and excess heat. When the as received Ti was cold rolled to 20% reduction in thickness, 6 of 8 cells (75%) produced excess heat. Increasing the amount of cold rolling to 40% gave excess heat for 2 of 2 experimental cells, but the magnitude of the excess heat was not as great as that observed for three of the cells in which the Ti had been cold rolled 20%. At 50% reduction in thickness, 2 of 6 cells gave excess heat, and the magnitude was less than that observed at lower amounts of deformation. There were 7 experimental cells in which the titanium was cold rolled to 65% or greater reduction in thickness. None of these cells produced excess heat.

A possible reason for the results in fig.1 is that cold rolling increases the degree of disorder of the material, which increases the absorption of deuterium and hydrogen, and this enhances the excess heat effect. De Ninno et al [3] concluded that a grain size of about 50 μm gives the maximum concentration of hydrogen in Pd. Both smaller and larger grain sizes reduced the concentration of hydrogen. Further support comes from Kamiya et al[4].

Their studies found that the H/Pd absorption ratio was maximum (0.924) at 30% cold working and decreased to 0.842 at 90% cold work. Shock loading, another process which increases crystalline disorder, has been found to increase the photocatalytic activity of TiO_2 powder by a factor of two to three[5]. The optimum shock pressure was found to be 16 GPa. Photocatalytic activity decreased at higher shock pressures, but it was still much higher than observed for the unshocked powder.

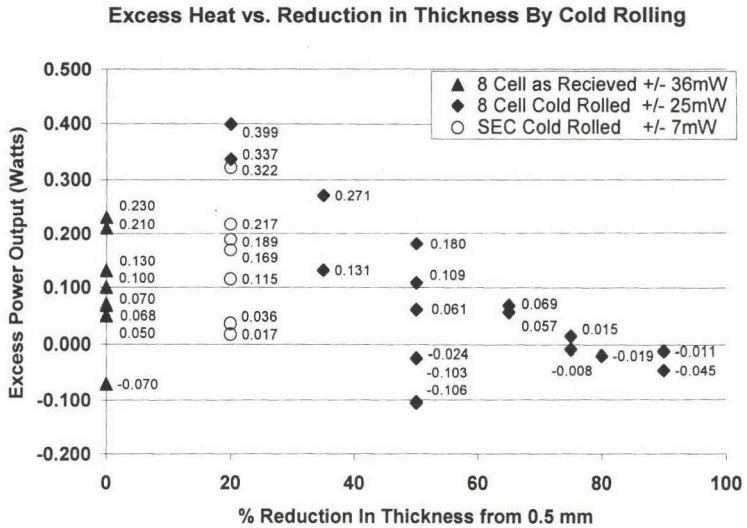

Figure 1. Excess heat as a function of reduction in thickness by cold rolling of the as received titanium.

A further example of excess heat can be found in fig. 2. Here, cell 2 of experiment 2 during the Summer of 1999, in which the titanium cathode was cold rolled to a reduction of 20% in thickness (from 0.5 mm to 0.4 mm), had almost the same power input as the control cell (fig. 2, left). There is however, a 6°C higher temperature in the experimental cell than in the control cell, for a period of 400 minutes (fig. 2, right). One would not expect this kind of behavior from two cells that are identical except for the substitution of a Pt cathode and light water in the control cell.

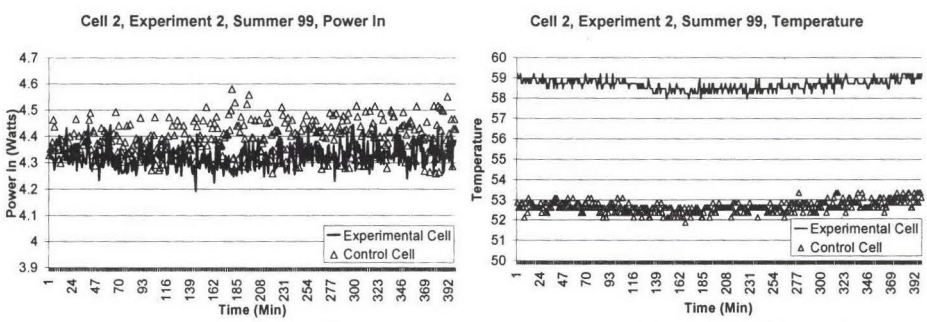

Figure 2. Comparison of power input and temperature of experimental cell 2 and the control cell for experiment 2, summer 1999.

A comparison of enthalpy output of a cell and the enthalpy released due to the formation of titanium deuteride can also be made. SEC cathode 3 (0.3194 g) was electrolyzed for 186 hours, and using the enthalpy of formation of TiD_2 (94KJ/mol) one calculates an enthalpy change of 627 joules. In addition, the cathodes were found to erode during electrolysis at the rate of about 0.3 nm per second. The precipitate was analyzed by x-ray diffraction and found to be to TiO_2. The enthalpy of formation of TiO_2 (913KJ/mol) can be used to calculate an enthalpy change of 2,302 joules. The total enthalpy change due to these chemical reactions is 2,929 joules, far less than the actual excess enthalpy output of 179,000 joules, which was calculated using equation 1.

Scanning electron microscopy (SEM), energy dispersive spectrometry (EDS), and neutron activation analysis (NAA) have been employed in the analysis of cathodes. It should be noted that EDS analyzes the surface to a depth of about 1μm, whereas NAA is a bulk analysis technique. Figure 3 shows one of the localized regions analyzed during a post experiment analysis of SEC cathode 1 using SEM and EDS. Pre-characterization of this cathode shows a flat, featureless topography with 100% titanium, whereas the post-characterization showed localized regions of changes in topography and composition. Figures 4, 5, 6, and 7 show the EDS data that corresponds to this region. Figure 4 shows that the area S14 is composed of 100% titanium while fig. 5 (S15) has a trace amount of Fe, 99% Ti and 1% Cr. Figure 6 shows < 1% S, < 1% Fe, 89% Ti and 10% Cr and fig. 7 shows about 9% Al, <1% S, 2% Fe, 79% Ti and 9% Cr.

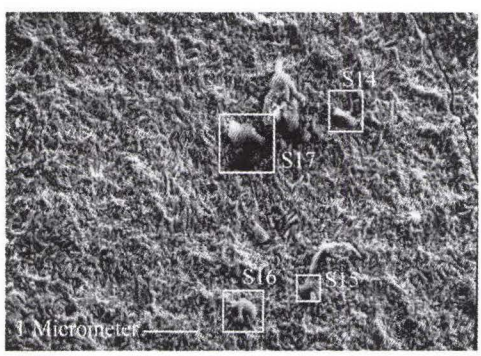

Figure 3. Region of SEC 1 titanium cathode after electrolysis. The squares locate regions where EDS spectra were obtained.

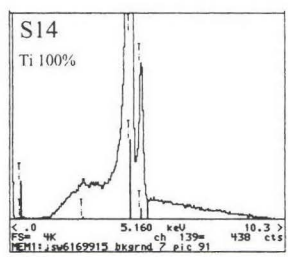

Figure 4. EDS spectrum from region S14 in fig. 3. Ti is the only element detected.

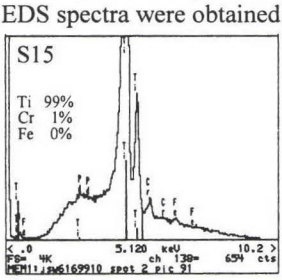

Figure 5. EDS of area S15.

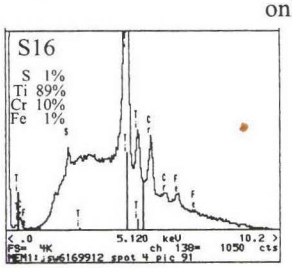

Figure 6. EDS of area S16.

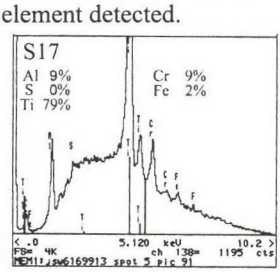

Figure 7. EDS of area S17.

These results are typical and have been found on about half of the experimental cathodes that have yielded excess heat. It should be pointed out that thorough SEM and EDS analysis of these electrodes is very tedious and time consuming. It is likely that further efforts would result in the discovery of unexpected elements on all of the electrodes that produced excess heat. The presence of Cr in an excess heat-producing titanium cathode has been confirmed by NAA analysis performed at the Reed College Nuclear Reactor facility in Portland, OR. Chromium (28 +/- 12 ppm) was found in an excess heat-producing cathode, which weighed about 5 mg, and in about 800 mg of the electrolyte from the same cell after electrolysis (0.5 +/- 0.1 ppm). This shows that most of the chromium is in the electrolyte, suggesting that it was formed by a surface reaction and was transported to the electrolyte by erosion of the titanium cathode. Using NAA analysis, no chromium was found in either the titanium cathode (cut from same batch) or in the electrolyte (drawn from same mixture) of an identical cell electrolyzed in series, which did not produce excess heat.

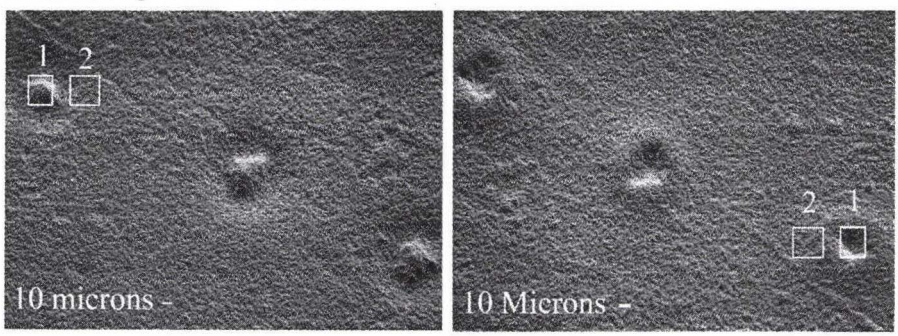

Figure 8. Changes in topography on a Ti cathode. The three mound-like features in the left photo appear to be valleys when the photo is inverted (right photo).

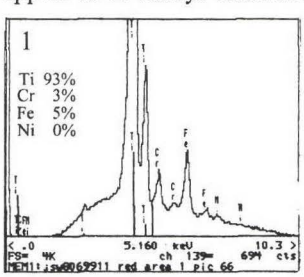

Figure 9. EDS of area 1 in fig.8.

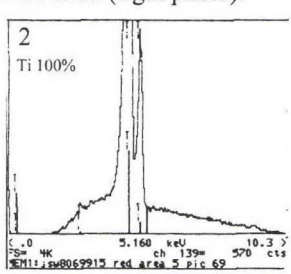

Figure 10. EDS of area 2 in fig. 9.

Figure 8 shows three similar formations, which were found on a cathode that did not yield a reasonable steady state period. Due to this it is unknown if this cell produced excess heat or not. It was determined from a SEM photo that these were not present before the experiment. One can see from the EDS spectra in figs. 9 and 10 that area 2 shows 100% Ti while area 1 shows 93% Ti, 3% Cr, 5% Fe and a trace of Ni. Depending on the orientation of this picture, the features may look like hills or valleys.
With the aid of a light microscope it was determined that these features are valleys (about 4 μm deep) with rims. It may be possible for transmutation to occur without producing

significant levels of excess heat. Previous studies showed that unexpected elements were associated with certain topographical features which were found on Pd cathodes after electrolysis [6-8].

One possible explanation for the appearance of these new elements after an experiment is that these elements are impurities, which are being deposited during electrolysis. If this were the situation, then one would expect that Pt from the anode, which is the most abundant impurity and which can be deposited at a lower potential than either H or D, would appear on the Ti cathode. This is seldom observed. Secondly, it is found that the cathodes erode at a rate of about 0.3 nm per second. Over a 166-hour period, SEC cathode 6 lost 43% of its original thickness. It would be difficult to deposit material onto a cathode that erodes at the rate of about one atomic layer per second. Another possible explanation for the appearance of new elements is that impurities diffuse from the bulk of the material to the surface during electrolysis. Using the Boltzmann equation, a conservative calculation for room temperature diffusion showed that the average length of travel over a 166 hour period to be of the order of 10^{-12} mm. A travel length of 10^{-1} mm would be needed to diffuse from the bulk to the surface. Electromigration could enhance diffusion, but this should produce much more uniform distributions of diffusing elements, not the localized concentration levels ~10^4 times the bulk concentration adjacent to regions where no Cr or Fe is detected. Another factor which makes electromigration an unlikely explanation for the observations is that Ca, the most abundant impurity (30 ppm) in the Ti cathodes used to obtain figs. 4,5,6,7,9 and 10 is not present in any of those spectra. It should be noted that the melting point of Ca is about ½ the melting temperature of Cr and Fe, so Ca should diffuse much more rapidly than Cr or Fe.

Discussion of Results. A 20% reduction in thickness, which is in addition to cold rolling performed by the manufacturer, gave the best heat and reproducibility results, with 6 of 8 cells showing excess heat. The mechanical treatment of the cathode by cold rolling appears to be an important variable in the excess heat effect. The SEC experiments used much larger Ti cathodes than the 8- cell experiments, but the rate of excess heat production was about the same for both. The reason for this result is not known. Unexpected elements such as chromium have been found in about half of the excess heat producing cells. The NAA data cited above suggests that a nuclear reaction occurred, which converted Ti to Cr. The Cr content obtained could account for about 10^{15} events, which could release a few thousand joules of excess heat, far less than that observed. Therefore, other nuclear reactions may also have occurred in order to account for the observed excess heat (~ 10^5 joules).

We realize that absolute proof of transmutation requires extraordinary evidence. We have been gathering evidence for about a decade, and it all seems to fit the conclusion that transmutation occurs, both on Pd [6-8] and on Ti cathodes. Reference 8 includes documentation of time-dependent changes in morphology and microcomposition of a Pd cathode which occurred long after electrolysis was completed. In addition, analyses obtained by secondary ion mass spectroscopy have shown that changes in isotopic abundance occur on the surfaces of Pd cathodes after electrolysis [7, 9].

Also, analyses performed after electrolysis by inductively coupled plasma mass spectroscopy showed that changes in isotopic abundance occurred in both a Ti cathode and in the electrolyte[10].

We will continue our efforts to obtain irrefutable evidence. In the meantime, we can only conclude that our results suggest that transmutation is highly probable.

References

[1] WARNER J.: M.S. Thesis, Portland State University, 1998.

[2] BUSH B. AND LAGOWSKI J.: Proc. ICCF-7 (ENECO, Salt Lake City) 1998, pp. 38-42.

[3] DE NINNO A., ANTISARI M., GIANGIORDANO C.: ibid, pp. 103-107.

[4] KAMIYA N., SAKAI Y., WATANABE Y., YAMAZAKI O., MOTOHIRA N., OTA K., AND MORI K.: Proc. ICCF-6 (New Energy and Industrial Technology Development Organization and the Institute of Applied Energy, Japan) 1996, pp. 203-207.

[5] LIU J., YU Y., LI Y., HE H., TAN H., AND XU K.: Chem. Abs., 131, (1999) 1303.

[6] DASH J., NOBLE G., AND DIMAN D.: Trans. Fusion Tech., 26, (1994) 299 - 306.

[7] DASH J., Progress in New Hydrogen Energy, M. Okamoto, ed., (New Energy and Industrial Technology, Tokyo, 1997) pp. 477- 481.

[8] DASH J., KOPECEK R., AND MIGUET S., Proc. 32nd Intersociety Energy Conversion Engineering Conf., vol. 2, (1997) pp. 1350 -1355.

[9] SILVER D., Ph.D Dissertation, Portland State University, 1998.

[10] KLOPFENSTEIN M., AND DASH J., Proc.ICCF - 7 (ENECO, Salt Lake City) 1998, pp. 98 - 102.

Acknowledgments. We are indebted to the referee for valuable suggestions. Neutron activation analysis was performed by S. Frantz and C. Melhus, Reed Reactor Facility, Portland, OR. This research was supported by a gift from the New York Community Trust and by the U.S. Army Research Office under grant number DAAG 55-97-1-0357.

Conference Proceedings Vol. 70
"ICCF8"
F. Scaramuzzi (Ed.)
SIF, Bologna, 2000

ADVANCES IN THIN-FILM ELECTRODE EXPERIMENTS

George H. Miley, Giovanna Selvaggi, Andy Tate, Maria Okuniewski, Mike J. Williams, D. Chicea[1], Heinrich Hora[2], Jak Kelly[3]

LENR Laboratory, 100 NEL, University of Illinois, 103 S. Goodwin Avenue, Urbana, IL, 61801, Tel.: (217) 333-3772, Fax: (217) 333-2906
Email: g-miley@uiuc.edu

[1]Physics Department, University Lucian Blaga of Sibiu,
Str. Dr. Ion Ratiu nr. 7-9, Sibiu, 2400, Romania

[2]Dept. of Theoretical Physics, University of New South Wales,
Sydney NSW, 2052, Australia

[3]Physics, University of Sydney, Sydney, NSW, 2006, Australia

ABSTRACT

Prior thin-film electrode (layers of order of 1000's of Angstroms) studies have revealed important advantages. Reasonable reproducibility has been demonstrated, an extremely high power density is obtained in the film, and reaction rates can be optimized through selection of materials and interfaces.

New work reported here involved studies of hydrogen isotope loading dynamics using thin Pd wires along with excess heat studies using unique thin-film electrodes coated on a glass plate. The wire results demonstrate a distinctive time correlation between the onset of excess heat production and loading. The plate electrodes confirm the earlier observation of very high excess power densities from thin-film designs.

INTRODUCTION

Research has focused on enhancing reaction rates using electrodes with thin metallic films highly loaded with hydrogen isotopes (>0.95 protons or deuterons per host metal atom). We have successfully used nickel, palladium, and titanium films, the most concentrated reactions occurring with multiple films of alternate metals such as nickel/palladium which produced evidence that this energy release has a nuclear origin. The total energy produced over three four-week runs far exceeds any chemical source and isotopic reaction products have been observed. Here recent flat-plate thin-film electrode experiments are described that achieved 100-200 W/cm^3 power production in the films. This result provides a start towards a practical power unit could be using a design with a film "packing fraction" (volume of film per cell volume) of about 20%, giving an overall cell power output $\geq$ 10 W/cm^3.

BACKGROUND

The present thin-film cell concept is related to, but is a radical departure from the original Pons-Fleischmann "cold fusion" experiment (Fleischmann 1989). Their goal was to create D-D reactions by loading deuterium (D) into a palladium lattice by electrolytic technique. In contrast the present Low Energy Nuclear Reaction (LENR) studies have the goal of proton reactions with the electrode material itself. Such reactions were initially postulated after Hora, Miley, et al. introduced the concept of enhancing reactions via the Swimming Electron Layer (SEL) effect (i.e. creating a high electron density) at interfaces between multi-layer thin films composed of metals with differing Fermi levels (Hora, et al., 1993). After initial experiments to demonstrate the SEL effect failed when the films "flaked" off of the substrate (Miley, et al., 1994), Miley and collaborators (Miley and Patterson, 1996, Miley, et al., 1996, Miley, 1997, Miley, 1998) used improved thin-film

electrode technology and precision analysis techniques to obtain quantitative transmutation data on the proton-metal reaction. These experiments documented absolute isotope production rates and provided insight into reaction "signatures" such as the "four peak" yield curve in mass number and also documented emission of soft x-rays and betas (vs. high, energy radiation). Concurrently, various transmutation observations have been reported by others, further supporting hypothesis of a p (or D) reaction with electrode materials (e.g. in the prior ICCF-7 proceedings, see Iwamura et al., 1998; Mo et al., 1998; Notoya, et al. 1998; and Ohmori and Mizuno, 1998; also related papers in the present ICCF-8 proceedings).

Advantages of Thin-Film Electrodes

The key feature of the University of Illinois approach involves use of multiple layer thin films laid down on the substrate via a unique sputtering process (Miley and Williams 1997). Other researchers have generally employed "thick" electrodes which are notoriously non-reproducible, probably due microcracking of the electrode, combined with subtle differences in crystalline structure induced in the manufacturing process. Sputtering the thin films offers better control and consistency in the crystalline structure of the electrode. Further, the flexibility of the film facilitates stress release, helping prevent microcracking. Films can be loaded with protons quickly (within 30-60 min.) in an electrolytic cell (vs. weeks for solid electrodes). This in turn makes a phased loading program feasible time-wise, starting with low loading rates and gradually increasing the rate.

Basic Spiral-Wire Electrode Loading/Reaction Experiments

In support of the thin-film electrode studies, a basic hydrogen isotope loading experiment was performed using a 50-μm diameter Pd wire, 1-m long, as the cathode. This wire was spiraled around a 30-cm long Teflon support to form the cathode. The selection of a very long wire length is intended to enhance electromigration effects, hence maximize the loading (Celani et al., 1998, 1999). A thicker platinum wire, also spiraled around the support, served as the anode. This unusual configuration provides electrode-loading properties similar to a thin-film, but also allows for easy measurement of loading dynamics using a resistance technique. The wire was carefully pre-conditioned by pre-stressing and annealing to provide reconstruction of the crystalline structure. An identical second cell with a non-reacting platinum wire cathode was constructed to provide reference ("Blank") calorimetric data. Both cells used the same power supply with an applied voltage of ~5 V and current of 5-50 mA. The electrolyte was a 10^{-5} M/l $CaSO_4$ in D_2O, cf. Celani et al., 1998. Integrated circuit temperature transducers were used for the calorimetric measurements. The various data channels were connected through a multiplexer switch unit, allowing real-time on-line data acquisition. This circuitry included super-position of AC current on top of the steady-state DC current to provide continuous monitoring of the wire's electrical resistivity during the run. The resistivity is in turn directly correlated with the deuterium loading (e.g. see McKubre 1992).

The loading process started with a low build-up rate and stepped up over several weeks; allowing time for natural annealing so as to prevent microcracking. The measured resistivity ratio, R/Ro (Ro = initial resistivity), increased up to 1.87, then reversed in slope drastically dropping down to 1.54. This behavior indicates the loading passed through 0.75 atoms D/Pd at the maximum resistivity and then continued to 0.97-0.98 atom D/Pd. At that point, cf. Fig. 1, the resistance ratio suddenly underwent a violent oscillation and then dropped back to a lower steady-state value.

Earlier Celani et al. (1999) observed a related loading oscillation. They speculated that it was caused by the rapid onset of anomalous heating in the wire, but they did not observe such heating directly. Alternately, Celani et al. also suggested that the effect could be caused by formation of the 'so-called', D-Pd "γ phase". In related work, Tripodi et al. (2000) proposed a fluctuation process due to a superconducting state which occurs in the "γ phase", associated with a simultaneous H (D) diffusion from octagonal to tetrahedral sites with relative filling of the latter, cf. Oriani (1994). A prime objective of the present work was to observe the time correlation excess heat release during this process, and the result is shown in Figs. 1 and 2. Here the time scale is expanded in seconds since initiation of the run.

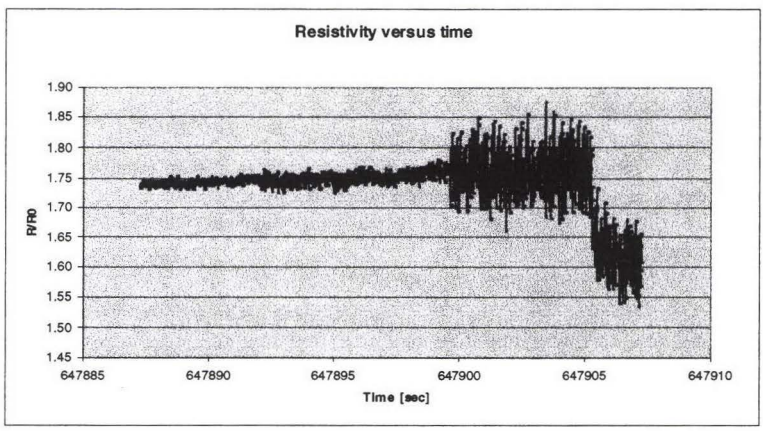

Figure 1. Plot of the ratio of the wire resistance to its initial value. A resistivity oscillation occurred simultaneously with the burst of excess heat. After the end of this recording, the oscillation damped out but R/Ro remained in the 1.65-1.70 range for the remainder of the run.

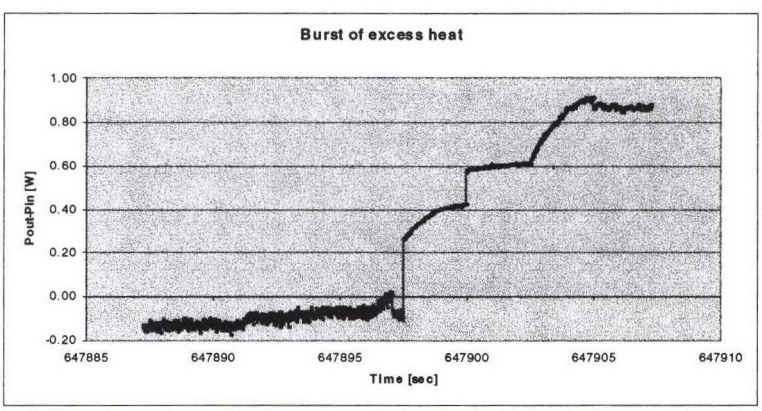

Figure 2. A burst of excess heat occurred seconds before the resistivity oscillation.

As seen from Figs. 1 and 2, the resistivity oscillations were accompanied by a sudden burst of high excess power ("excess" power, or heat, is defined as the difference

between the power output and the power input). The initiation of this oscillation occurred naturally during the loading process without application of any external stimulus. Following this initial burst, an "excess" power of ~1 W (input power of ~ 150 mW) was obtained for several hours before damage to the cell wiring forced shutdown of the run. The continual production of excess power suggests that an exothermic phase transition can be ruled out as the heat source since the total energy release is too large. Likewise, the dynamics of the excess heat burst rule out possible chemical energy sources. Thus, this result provides strong evidence for a nuclear source of energy. A next step planned to verify this involves analysis of the wire cathode for reaction products.

The "excess" heat results (Fig. 2) and are well out of the uncertainty limits associated with the resistivity and power measurements. An uncertainty of ± 0.1 is associated with each R/Ro point based on a random resistivity measurement error of 2 Ohms. An uncertainty of ± 45 mW is inferred from an error propagation analysis of temperature measurements, assuming a slow change in any power transient. The power five-second burst in Fig. 2 is not correctly recorded by the calorimeter which was calibrated for quasi-static operation. If adiabatic conditions are assumed over the short burst (a reasonable assumption) the instantaneous power exceeded 1 kW. Subsequently, when the power returned to equilibrium at ~ 1 W, the calorimetric scale in Fig. 2 should be reasonably accurate.

In summary, this wire experiment clearly demonstrates the connection between a high deuterium (or proton) loading and the "excess power" phenomena. In addition to the unique electrode configuration the pre-conditioning and controlled set-up program are equally important factors that enabled this dynamic measurement.

RECENT EXCESS POWER AND LOADING EXPERIMENTS

Recently, the LENR group initiated work to develop a small, inexpensive demonstration cell (Miley et al., 1999). Initial results are summarized briefly here.

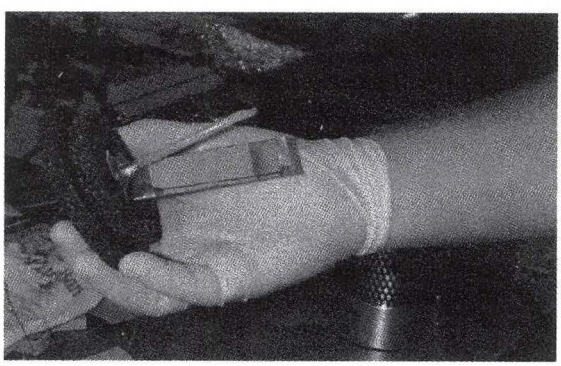

Figure 3. Photograph of a multi-layer thin-film electrode on glass substrate being inserted into a cell.

For compactness, these new experiments employed a unique electrode configuration where the thin-film cathode is sputtered onto a small glass plate the size of a microscope slide (Fig. 3). The anode can be sputtered onto a separate region of the slide (or may be a separate wire). This electrode assembly is then inserted in a small, insulated Dewar along with appropriate temperature sensors to perform calorimetry. As stressed

earlier, a major issue is survival of the thin-film during the harsh conditions encountered in a run. Methods were developed to enhance bonding by pre-sputtering surface preparation, by use of substrate bonding materials, and by annealing.

These cells were purposefully designed to operate at relatively low powers and temperatures (few 100 mW and <30° C) to simplify the experiment. Basically the cells employed carefully calibrated isoparabolic-type calorimetry in an open system. To date, 14 runs have been carried out with a variety of thin-film and foil coatings for the cathodes. Further details about the operating conditions, calibration, error analysis and data reduction are presented in Miley (1999a). Some typical results are summarized in Table I along with a typical excess power histograph in Fig. 4 for layered Pd-Ni films (5 alternating ~ 1000 Å layers ending with Pd on the outer surface). These exploratory runs involved some variations in the electrode coating, the electrolyte and the run conditions; thus, some differences in excess power were expected. Typical coatings included Ni, Pd and Ti and electrolytes ranged from 1-molar Li_2SO_4 in H_2O or D_2O. While the H_2O based runs with Pd-Ni films produced somewhat higher excess heat than D_2O, more experiments are needed to quantify the differences.

Table I: Typical Thin-Film Electrode Results

Run #	Thermal Input Power (W)	Output Power (W)	Excess Power (W)	Total Excess Energy (kJ)
1_1	0.138	0.408	0.266 ± 0.036	113
1_2	0.074	0.195	0.121 ± 0.016	61

All of the thin-film electrodes consistently produced excess power, six producing >80% excess, a goal for these experiments. The estimated uncertainty in the excess power levels is about ± 20 mW, so the results reported are thought to be quite definitive despite the relatively low absolute power levels. Factors included this estimate involve random errors in thermocouple readings/calibrations plus possible temperature gradients in the electrolyte, gas recombination, and effects from room temperature variations. A reference experiment was also performed with a non-loading, electrode that indicated an excess power ~1mW, well within the uncertainty limits.

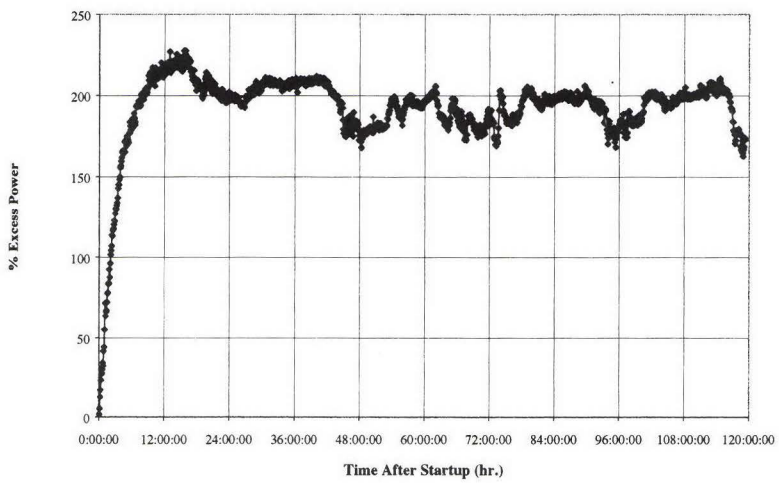

FIGURE 4. PERCENT OF EXCESS POWER VS. TIME FOR RUN 1_1

While the absolute excess powers were low, when computed on the basis of power-per-unit-volume (or weight) of metal film very high excess power densities of ~10-20 W/gram of metal (Pd, Ni, etc) are obtained. For comparison, note power densities of 0.1-0.4 W/g reported by Miles, 1995, using solid Pd electrodes or ~0.006 W/g reported from "Case Catalyst" type experiments (McKubre, 1999). The high power densities achieved in the present experiments is encourages the possibility of developing a practical power source. A suitable cell configuration may have electrode metal films filling 20% or more of the total cell volume, potentially giving overall cell power densities of order of 20 W/cm^3.

PRIOR STUDIES OF REACTION PRODUCTS

The nuclear origin of the excess power observed in these recent experiments can be inferred from earlier thin film studies where reaction products were measured using a variety of analytic methods (Miley and Patterson, 1996, Miley, et al.; 1996, Miley, 1997; Miley, 1998). A key finding was that a large array of "new" elements (i.e., different from the electrode material) appear after the run, many with significant deviations from natural isotopic composition. Based on these observations, especially the "four peak" mass distributions, a semi-empirical theory that assumes proton-metal reactions, termed RIFEX, (Miley, 1997, 1998, 1999) has been proposed to explain these reaction characteristics while the overall energetics of the process are examined in a companion paper (Miley 2000). The nuclear basis was further elaborated via a magic number correlation (Hora et al., 1998) and the connection to astrophysical processes elucidated (Hora et al., 2000). An alternate theory to explain the "four peak" distribution has been proposed by Stoppini, 1998 while Fisher, 1998 suggests polyneutrons play a role.

CONCLUSIONS

The research described here demonstrates the potential for excess heat production via LENRs. As seen from the citations, related phenomena have also been observed worldwide. However, the present approach employing multi-layer thin-films offers several very important practical advantages: fast loading with minimal microcracking, a very high excess power density in the electrode metal, and negligible high-energy radiation emission.

While the excess power obtained in these preliminary experiments is encouraging, higher total powers are desirable for a practical power unit. Such a scale-up would require further optimization of the electrode design and incorporation of multiple electrodes to increase the "packing fraction" of film material. The first step requires advances in research, while the second represents a reasonably straightforward "mechanical-type" modification. Other technology studies would be needed to address lifetime issues, energy extraction, and power control techniques.

ACKNOWLEDGEMENTS

Partial support of this work by Cold Fusion Technology, Inc. and by the NY Community Trust is gratefully acknowledged. Comments and critiques by Ed Storms, J. Rothwell and G. Malove are also appreciated.

REFERENCES

Celani, F. et al., 1998, "The Effect of γ-β Phase on H (D)/Pd Overloading", *Proc., 7th Intern. Conf. on Cold Fusion*, ICCF-7, April 19-24, Vancouver, BC, Canada, (ENECO, Salt Lake City, UT), pp.62-67.

Celani, F. et al., 1999, "A Preliminary D/Pd Loading Study: Anomalous Resistivity Transition Effect", *Proc., Asti Workshop on Anomalies in H/D Loaded Metals*, ASTI '97, Societa Italiana di Fisica, Bologna, Italy, pp 7-16.

Fisher J., 1998, "Liquid Drop Model for Extremely Neutron-Rich Nuclei" *Fusion Technology*, vol. 34 (1), p. 66-75.
Fleischmann, M. and Pons, S., 1989, "Electrochemically Induced Nuclear Fusion of Deuterium," *J. Electroanal Chem.*, pp.261-301.

Hora, H., Kelly, J. C., Patel, J. U., Prelas, M. A., Miley, G. H., and Tompkins, J. W., 1993, "Screening in Cold Fusion Derived from D-D Reactions," *Physics Letters A*, vol. 175, pp. 138-143.

Hora, H., Miley G. H., Kelly, J. C., and Narne, G., 1998, "Nuclear Shell Magic Numbers Agree with Measured Transmutation by Low-Energy Reactions," *Proc., 7th Intern. Conf. on Cold Fusion*, ICCF-7, April 19-24, Vancouver, BC, Canada, (ENECO, Salt Lake City, UT), pp. 147-151.

H. Hora, G. H. Miley, 2000, "Heavy Nuclide Synthesis by Neutrons in Astrophysics and by Screened Protons in Host Metals", *Czechoslovak J. of Physics,* vol. 50 no. 3, pp.433-439.

Iwamura, Y., Itoh, T., Gotoh, N., Sakano, M., and Toyoda, I., and H. Sakata, 1998, "Detection of Anomalous Elements, X-Ray and Excess Heat Induced by Continuous Diffusion of D Through Multi-Layer Cathode (Pd/CaO/Pd)," *Proc., 7th International Conf. on Cold Fusion*, ICCF-7, April 19-24, Vancouver, BC, Canada, (ENECO, Salt Lake City, UT), pp. 167-171.

McKubre, M. 1999, "Recent Loading and Excess Heat Experiments at SRI", *Proc., ASTI Workshop on Anomalies in H/ Loaded Metals,* Nov. 27-30, Asti, Italy, Societa Italiana di Fisica, Bologna, Italy.

McKubre, M., 1992, "*In Proc., On Hydrogen Storage Materials, Batteries and Electrochemistry*," Eds, D.A. Corrigan and S. Srinivasan, Electrochem Soc. Inc, NYC, NY, p. 269.

Miles, M., 1995, "The Extraction of Information From an Integrating Open Calorimeter in Fleischmann-Pons Effect Experiments", *Proc., 5th Intern. Conf. on Cold Fusion*, ICCF-5, Monte-Carlo, Monaco, (ICCF-5, Valbonne, France) pp. 97-104.

Miley, G. H., Hora, H., Batyrbekov, E. G., and Zich, R. L., 1994, "Electrolytic Cell with Multilayer Thin-Film Electrodes", *Transactions, Fusion Technology*, vol. 26, no. 4T, Part 2, pp. 313-320.

Miley, G. H., and Patterson, J. A., 1996, "Nuclear Transmutations in Thin-Film Nickel Coatings Undergoing Electrolysis," *J. of New Energy*, vol. 1, No. 3, pp. 5-30.

Miley, G. H., Narne, G., Williams, M. J., Patterson, J. A., Nix, J., Cravens, D., and Hora, H., 1996, "Quantitative Observation of Transmutation Products Occurring in Thin-Film

Coated Microspheres During Electrolysis," *Proc., 6th Intern. Conf. on Cold Fusion*, ICCF-6, October 13-18, The Inst. of Applied Energy, Hokkaido, Japan, Vol. 2, pp. 629-644.

Miley, G. H., 1997, "Characteristics of Reaction Product Patterns in Thin Metallic Films Experiments," *Proc., ASTI Workshop on Anomalies in H/D Loaded Metals,* Nov. 27-30, Asti, Italy, Societa Italiana di Fisica, Bologna, Italy, pp. 77-87

Miley, G. H. and Williams, M., 1998, "Method for Sputtering Thin Metallic Films on Millimeter Diameter Polyester Spheres," ANS 1998 Winter Meeting, Washington DC, November 15-19.

Miley, G. H., 1998, "Possible Evidence of Anomalous Energy Effects in H/D-Loaded Solids Low Energy Nuclear Reactions (LENRs)", *J. of New Energy*, Vol. 2 (3-4), pp. 6-13.

Miley, G. H., 1999, "Emerging Physics for a Breakthrough Thin-Film Electrolytic Cell Power Unit", *AIP Conf. Proc. 458,* STAIF 99, American Institute of Physics, Melville, NY, pp. 1227-1231.

Miley, G. H., Chicea, D., Williams, M. J., Okuniewski, M. A., Selvaggi, G., Tate, A. N., 1999a, "Infinite Energy" Kit Project Report", FSL no.746, Fusion Studies Lab, University of Illinois, Urbana, IL.

Miley, G.H., 2000, "On the Reaction Product and Heat Correlation for LENRs", these proceedings.

Mo, D. W., Cai, Q.S., Wang, L.M., Wang, S. Z. and Li, X.Z., 1998, "The Evidence of Nuclear Transmutation Phenomenon in Pd-H System Using NAA (Neutron Activation Analysis)," *Proc., 7th Intern. Conf. on Cold Fusion*, ICCF-7, April 19-24, Vancouver, BC, Canada, (ENECO, Salt Lake City, UT), pp 259-263.

Notoya, R., Ohnishi, T., and Noya, Y., 1998 "Products of Nuclear Processes Caused by Electrolysis on Nickel and Platinum Electrodes in Solutions of Alkali-metallic Ions," *Ibid*, pp. 269-273

Ohmori, T. and Mizuno, T., 1998, "Strong Excess Energy Evolution, New Element Production, and Electromagnetic Wave and/or Neutron Emission in the Light Water Electrolysis with a Tungsten Cathode," *Ibid*, pp. 279-284.

Oriani, R. A., 1994, "The Physical and Metallurgical Aspects of Hydrogen In Metals", *Trans. Fusion Technology*, vol 26, No. 4T part 2, pp. 235-266.

Stoppini, G., 1998, "Nuclear Processes in Hydrogen Loaded Metals", *Fusion Technology*, vol. 34 (1), p. 81.

Tripodi, P., Di Gioacchino, D. and McKubre, M. C. H., 2000, INFN-LNF and SRI International, private communication, September.

Conference Proceedings Vol. 70
"ICCF8"
F. Scaramuzzi (Ed.)
SIF, Bologna, 2000

Electronic fingerprint of D site occupation in Pd deuterate

R.G. Agostino, R. Filosa, V. Formoso, G. Liberti
Laboratorio 'Metal Hydrides for Energy Storage' - INFM - Unità della Calabria c/o Dipartimento di Fisica, Università della Calabria, 87036 Arcavacata di Rende (Cs),
A. De Ninno
ENEA/ERG/FUS, C.R.E., C.P. 65, 00044 Frascati, Rome, Italy
F. D'Acapito, S. Colonna
Gilda beamline, ESFR, Grenoble, France

Abstract

The PdD_x system is probably the most widely studied of the simple deuterates. The evolution of its structural and electronic features associated to the deuterium content are matter for several publication and only few regions remain to be investigated [1]. An extremely interesting topic concerns the interstitial site occupation at very high D concentration. Here we present our *work-in-progress* results in the field.

We investigate this topic looking to the structural and electronic changes induced by D absorption on Pd thin wire. The tool we use is 'X-ray absorption spectroscopy' performed in-situ on a Pd wire charged by electrochemical methods.

1. Introduction

The X-ray Absorption Spectroscopy (XAS) technique has the ability to probe both electronic parameters (from the x-ray absorption near edge structures, XANES). In fact, the fluorescence yield induced by the absorption of a x-ray photon (h□ > 24340 eV) is proportional to the Pd empty electronic states above the Fermi level. Increasing the photon energy we can probe the local geometry (from the extended x-ray absorption fine structures, EXAFS). This feature is strictly related to the photoelectron diffraction path into the solid. Both these characteristics are element specific. Thus, with the combination of XANES and EXAFS one can study the geometric and electronic structure at the same time [2]. Furthermore it is even possible to measure in the original environment with the electrochemical cell with different deuterium concentrations [3].

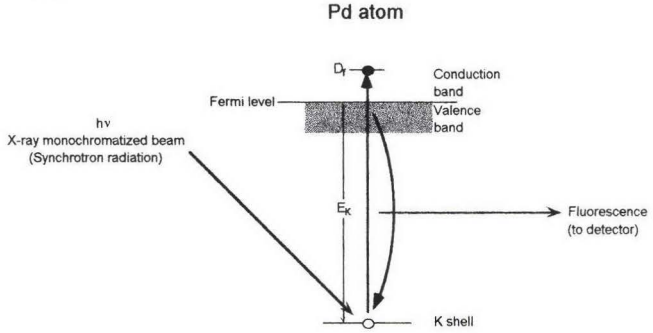

Fluorescence induced by X-ray absorption by Pd K-shell electron

$$F_K(h\nu) = P_{Kf}\, R_f = 2\pi/\hbar\, |\langle f|\, \underline{V}\, |K\rangle|^2\, D_f(h\nu - E_K)$$

P_{Kf}	X-ray absorption cross section
R_K - 1	Radiative de-excitation probability
$D_f(h\nu - E_K)$	Local density of electronic empty states

2. The experiment

The use of XANES and EXAFS techniques in the *in situ* measurements can be performed at high photon fluxes. The 3rd generation synchrotron radiation sources combine high-energy photons to high fluxes allowing this kind of analysis. Recent measurements performed on similar systems pointed out the feasibility of this kind of measurements on samples immersed in an electrochemical cell [3]. The X-ray absorption experiment reported here was performed at GILDA beam-line of ERSF light source facility in Grenoble (France).

The Pd electrode is deposited on a glass window that seals one side the electrochemical cell. The electrode dimensions are: thickness 5000Å, width 50μ and length 1m. More details on the experimental set up are given in another paper in these Proceedings (4). The D concentration is monitored by R/R_0 simultaneous 4-point measurement (where R_0 is the initial wire resistance). D absorption is induced by biasing the Pd deposit up to 8 V relative to the Pt counter-electrode and a maximum power of 200 mW. Due the limited Pd surface area, the D_2 out-gassing is relatively limited. The electrolyte temperature was monitored during the experimental run.

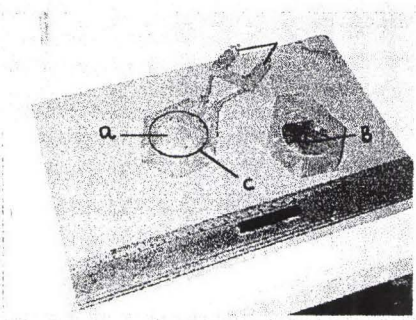

Specially designed electrochemical cell (open):
A: supported Pd wire sample
B: Pt counter-electrode
C: Viton o-ring

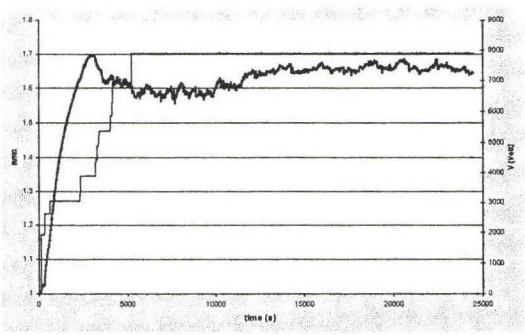

Loading curve versus time during X-ray absorbtion.

3. The calculation

The study of the deuterium induced features is performed during the D loading in Pd deposited film (each loading cycle take place in several minutes). The changes in the chemical bonding of the Pd deuteride is studied on the XANES spectra. The fig. 4a) shows how the main features of the absorption spectrum modify their energy position and shape with the D content. A separate monitoring of the D concentration is given by the R/R_0 ratio whose values are reported aside.

In order to extract the main structural characteristics (atomic position, lattice parameter, atomic vibration, ...) from the measured spectra, they have to be compared with the FEFF calculation results. FEFF is an automated program for ab initio multiple scattering calculations of x-ray absorption fine structure. The preliminary results of this analysis are reported on fig. 4b). We simulated the spectra relative to a series of PdD clusters (radius r_c =

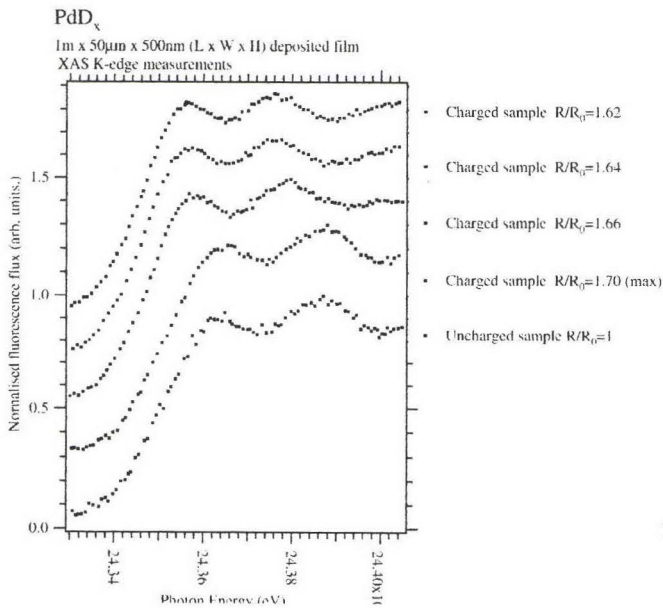

Fig. 4a) Measurements

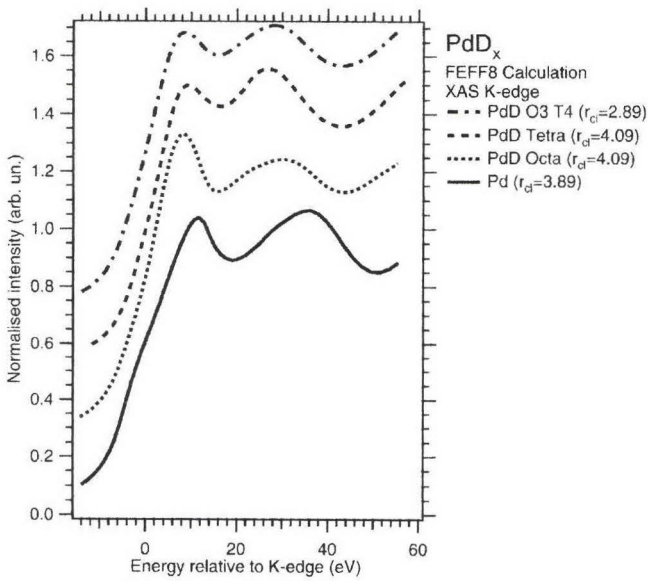

Fig. 4b) Calculations

n.n. distance) in which D nuclei occupy only octahedral sites or only tetrahedral sites or both. As it is clear from the reported calculation, the XAS spectra are a site occupation signature.

Next steps in the analysis are:
- perform an evaluation of the n.n. distance from the EXAFS signal (not shown);
- evaluate the D concentration through an appropriate analysis of the R/R_0 data;
- simulate all the different site occupation configuration.

References

1. see Wipf, Helmut, Hydrogen in metals III : properties and applications - Berlin : Springer, 1997 and references therein.
2. D.A. Tryk et al. J. Electrochem. Soc. 142, 824 (1995); Mukerjee et al., J. Electrochem. Soc. 142, 1409 (1995); Mukerjee et al., J. Electrochem. Soc. 142, 2278 (1995).
3. R. G. Agostino, G. Liberti, V. Formoso, E. Colavita, A. Zuettel, C. Nuetzenadel, L. Schlapbach, A. Santaniello, and C. Gauthier, Phys. Rev. B in press; see also SRN 11, (1998) - A monographic issue on in-situ synchrotron based electrochemical experiments.
4. G. Preparata et al. "The Fleishmann-Pons effect in a novel electrolytic configuration", These Proceedings.

Conference Proceedings Vol. 70
"ICCF8"
F. Scaramuzzi (Ed.)
SIF, Bologna, 2000

HIGH HYDROGEN LOADING INTO THIN PALLADIUM WIRES THROUGH PRECIPITATE OF ALKALINE-EARTH CARBONATE ON THE SURFACE OF CATHODE: EVIDENCE OF NEW PHASES IN THE Pd-H SYSTEM AND UNEXPECTED PROBLEMS DUE TO BACTERIA CONTAMINATION IN THE HEAVY WATER.

F. Celani[1], *A. Spallone*[1], *P. Marini*[2], *V. di Stefano*[2], *M. Nakamura*[2], *A .Mancini*[3], *S. Pace*[1], *P. Tripodi*[1], *D. Di Gioacchino*[1], *C. Catena*[4], *G. D'Agostaro*[4], *R. Petraroli*[5], *P. Quercia*[6], *E. Righi*[1], *G. Trenta*[1].

(1) INFN-LNF, Via Enrico Fermi, 00044 Frascati (Roma), Italy
(2) EURESYS, Via Lero 30, 00129 Roma, Italy
(3) ORIM SrL, Via Concordia 65, 62100 Piediripa (MC), Italy
(4) ENEA-CR Casaccia, Via Anguillarese 301, 00060 Roma, Italy
(5) Perkin Elmer Italia, Via A. Ciamarra 209, 00173 Roma, Italy
(6) ASL-RM H, Via E. Fermi, 00044 Frascati (Roma), Italy

Abstract

A new procedure has been developed at INFN Frascati Laboratory in order to achieve a very high Hydrogen or Deuterium electrolytic loading into a long and thin Palladium wire. This technique consists in the addition of a very small amount of alkaline-earth elements into a very diluted acidic solution.

Because of enhancing pH values around the cathode, during the electrolysis, carbonates are able to precipitate onto the cathode's surface forming a thin layer which strongly increases the Pd loading; a computer simulation has been developed to find out the proper working conditions for the carbonates precipitation.

Loading results of Hydrogen were excellent (H/Pd≅ 1). The evidence of a new phase in the Pd-H system was inferred from the basis of the variation of the thermal resistivity coefficient of the Pd wire as a function of the H/Pd ratio.

Less satisfactory results were obtained for Deuterium (D/Pd≈ 0.85, no excess heat) because of inorganic and organic contamination normally present in ordinary heavy water. A novel procedure to purify heavy water, developed at INFN-LNF, has permitted to achieve interesting loading, up to D/Pd≅ 0.97, for several days and evidence of overheating of Pd wire i.e. "excess heat".

We have discovered that the obtained poor results with the heavy water are mainly due to the presence of two kinds of new bacteria living in the commercial reactor-grade heavy water we have used for the loading tests. We named such bacteria (Ralstonia and Stenotrophomonas genera) "Detusculanense" specie.

Introduction

After ten years of experiences the appearance of excess heat, in the so called "Cold Fusion Phenomena", according to our opinion it seems to be related to the contemporary occurrence of two different and well defined processes:

a) *Overloading* of Deuterium in the Palladium lattice and, simultaneously,
b) *Movement* of Deuterium into the Palladium, without losing of overloading.

The main problem in these kinds of experiments, since 1989, has been the *poor reproducibility* of results.
According to our experience, the typical excess power (during the rare "lucky" conditions we have dealt with) was about 5 ÷ 10% of the total input power; such an excess power rose, in our "best experiment", up to a maximum value of 200% for many hours [Ref. 1], corresponding to a remarkably large absolute power value (over 100 Watts). During this "best experiment", obtained with a long (180cm) and thin (0.1mm) Pd wire, the very large excess power lasted over 12 hours (Fig.1) and we were able to make several different controls (about the realty and the absolute value of excess power). During this phenomenon we switched off electrolysis current for some minutes and the plot clearly shows the wire de-loading; after switched on again, wire re-loaded and gain recovered but the effect extinguished in a few hours.

In order to reduce the irreproducible results we decided to develop and test a new electrolytic procedures starting, as a reference, from the simpler Hydrogen/Palladium system.
The main targets, " a really suitable" for new loading technique were the following:

- H/Pd: > 0.95 → R/Ro: <1.5;
- Time to get H/Pd >0.95: <50 hours;
- Stability of overloading: > 4 hours;
- Success rate: >60%.

The maximum loading ratio H/Pd or D/Pd, ever achieved by gas pressure at room temperature, according to the literature, is 0.97 at 50000 atmosphere of pressure (Baranowski data, presented at the Conference of Kawasuci, Japan, Oct.'94). The aim of our new procedure is to approach and even overcome such a value.
It is, in fact, a common experience in Cold Fusion studies that, in order to achieve "anomalous excess heat" it is necessary (but not sufficient) to overcome a certain threshold in the high level region of the D/Pd ratio: M. H. McKubre, at SRI International, performed some systematic studies about this aspect [Ref. 2].

– *Typical experimental problems*

During the loading, the Pd volume increases up to 13%, usually in a not homogeneous way. This kind of behaviour is the origin of several drawbacks, capable to seriously affect the loading process:

a) superficial cracks (paths for H or D de-loading);
b) dislocations, internal vacancies (production of, high pressure, micro-bubbles of H_2/D_2 inside the defects).

Both the problems are known to be related to the purity and "history" of Pd.

In order to reduce the influence of these hardly controllable parameters, various procedures have been generally adopted. The most common of them can be summarised as following:

a) large (>500mA/cm2) current density, in order to increase, according to the Tafel law, the cathodic over-voltage;

b) time pattern of current (like, e.g., the "low-high Takahashi procedure", developed at Osaka University since 1991 or the "high peak- power pulse method", developed at INFN-LNF since 1994).

Such procedures in any case do not solve completely the problem of reproducibility.

INFN-LNF procedure

The loading measurements, expressed as H/Pd or D/Pd, were performed on-line and in-situ, by measuring the variations of Pd resistance [Refs. 3,4], which are known to change, depending on the ratio of H/Pd and D/Pd (fig. 2) [Refs. 5].
The main characteristic of our method is to induce the precipitation of carbonates, directly on the wire surface, during the electrochemical loading of the Pd wire, as far as to form a semi-permeable, thin and homogeneous barrier, which allows the entrance of Hydrogen or Deuterium into Pd lattice as atomic H or D [Ref. 6]. Such a barrier acts as a poison for the recombination processes: $H+H=H_2$ or $D+D=D_2$.
Such a layer was expected to increase the cathodic over-voltage, through the inhibition of the H-H recombination process.

A peculiar electric circuit has been developed in order to achieve a complete decoupling between electrolysis dc-current (power supply) and Pd wire ac-current (resistance measuring) (Fig.s 3, 4). Furthermore, the cathodic electrolytical current is periodically inverted in such a way that, alternatively, (using a 100 seconds period square wave) the most-cathodic part of the wire is converted into the less-cathodic one and vice-versa: such a procedure (using the "twin relay control" block reported in the plot) is useful for a more homogenous loading.

A further important characteristic is the wire's diameter, which is as thin as 50 micrometers in our recent experiments. This allows for the following advantages:

- High current densities can be achieved with low electrolytic currents (and consequently low input power).
- Because of the high value of the wire's resistance the relative error of the loading of the Pd wire is strongly reduced.
- The loading kinetics are increased.
- The dimension of the H/D bubbles released during the electrolysis, for geometrical reasons, cannot exceed the diameter of the wire. Taking into account that the internal pressure of a bubble of gas increases by decreasing its diameter, it is convenient, in order to prevent eventual de-loading, to maintain as low as possible such a diameter.
- Possibility of changing, in large amount, the pH range (9-13) of the solution just around the cathode surface, by changing the electrolysis current density: specific computer simulations were developed for this purpose (Fig.s 5; 6), [Ref. 6].

Other important characteristics of our method regarding both the electrolyte composition and the procedure for the acquirement of the proper coating on the cathodic surface, can be shortly summarized:

- It is possible to obtain an electrolytic environment (around the cathode) where, depending on the electrolyte composition and the current density, it is possible to control the solubility of alkaline earth carbonates. It is well known in fact that, depending on the electrolytic current, the pH around the cathode rises up, allowing carbonates precipitation: their solubility is actually pH controlled.

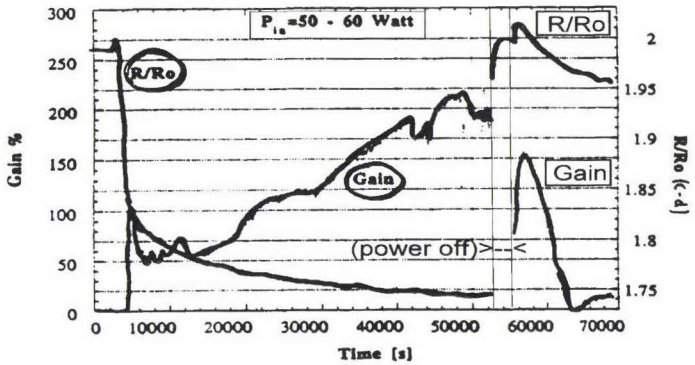

Fig. 1 – Excess heat evidence: Once, a test provided a very large amount of excess power (up to 100 W) correlated to the R/Ro resistivity drop (high D/Pd loading) with a thin long Pd wire; this effect lasted for many hours.

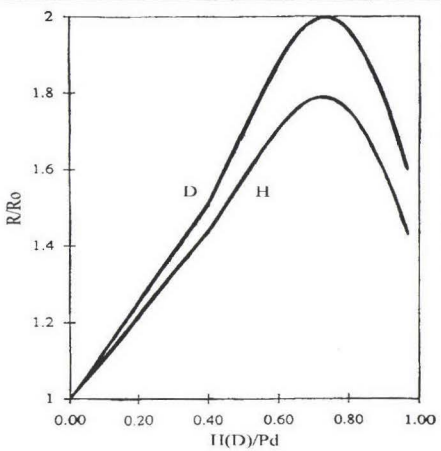

Fig. 2 –
Normalised Palladium resistance versus Hydrogen (Deuterium) molar fraction of Pd. Peak value is: H/Pd= 0.75, R/Ro= 1.78 (Hydrogen) and D/Pd= 0.75, R/Ro= 2.0 (Deuterium).
Maximum known loading is H(D)/Pd= 0.95 at R/Ro= 1.4

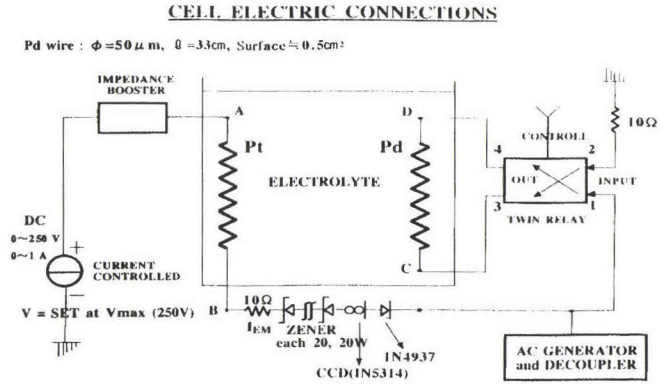

Fig. 3 – Apparatus set-up: electrolytic cell, D.C. power supply block and a.c. resistance measurement block; all electric and thermodynamic parameters are acquired by several Digital Voltmeters (DVM) controlled by a computer.

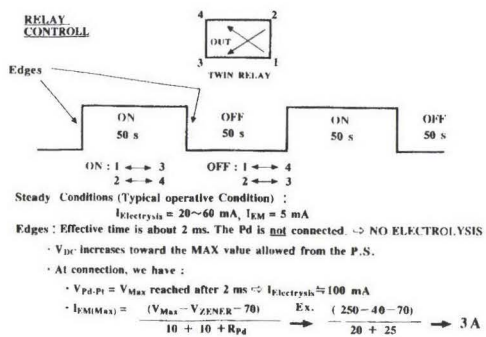

Fig. 4 – Detail of the electrolysis control logic: The "twin relay control" block and diodes chain have been used to improve the loading.

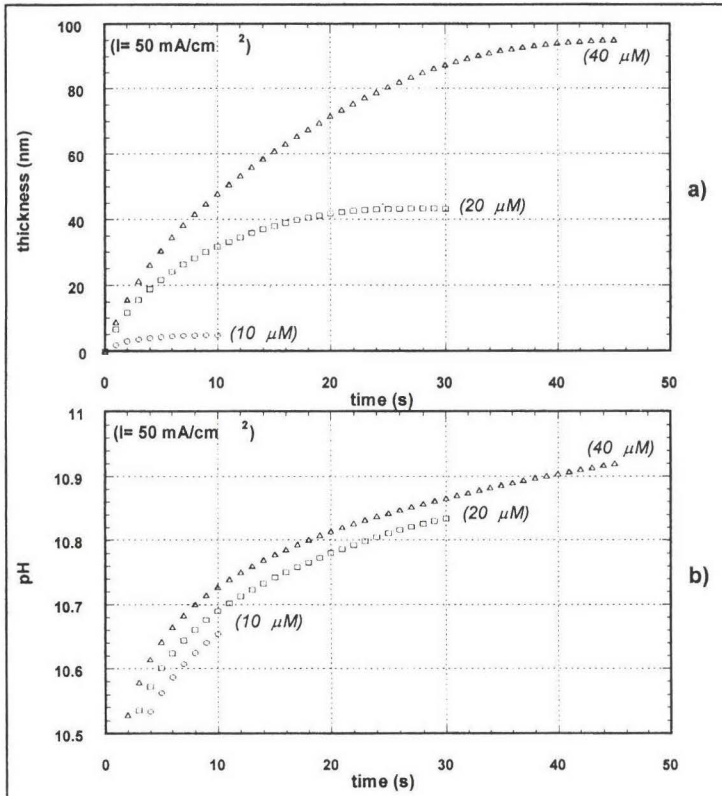

Fig. 5. – *Computer simulation at constant current density of 50 mA/cm^2, wire diameter 50 μm.*

a) $SrCO_3$ deposition thickness, versus time, at 10, 20, 40 μM of Sr^{2+} ions concentrations;

b) pH variation versus time at 10, 20, 40 μM of Sr^{2+} ions concentrations.

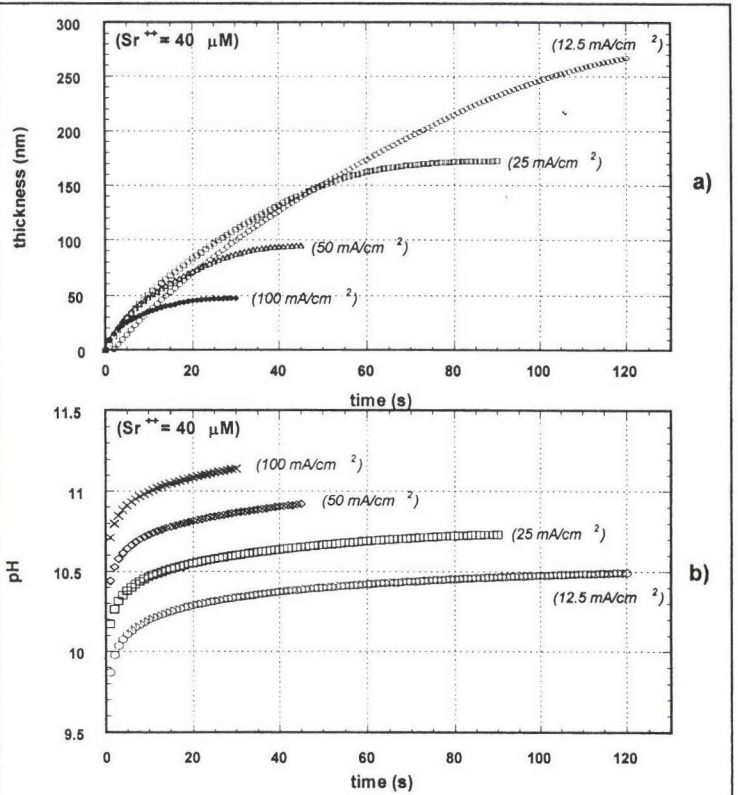

Fig. 6. – *Computer simulation at constant concentration of 40μM Sr^{++} ion concentration, Pd wire diameter 50 μm.*

a) $SrCO_3$ deposition thickness versus time at 12.5, 25, 50, 100 mA/cm^2 ;
b) pH variation versus time at 12.5, 25, 50, 100 mA/cm^2 current density. A comparison with other fits indicates that the slope of the curve becomes more flat when the loading (at low current) is very high.

- It is possible to control the thickness of the deposit, in a feed-back way, changing the amount of acid and therefore the pH of the solution or by properly changing the values of the current density.

Finally, it has been shown that H and D are present in the Pd lattice as protons and deuterons; it is therefore possible to promote their movement by applying an electric field along the wire. It is known that the electro-migration effect is controlled by the drop of voltage along the wire and such a drop is easy to be obtained with a thin wire.
As far as the cracks problem is concerned, since 1998 we have found out that the addition of very small amount of mercury ions ($HgCl_2 \approx 10^{-6}$M) to the electrolyte is very effective. Mercury, galvanically deposits on the cathode surface, because of the formation of amalgams with Pd, is capable to strongly reduce the harmful effects of cracks [Ref. 7].

The differences between the old procedure, based on the use of LiOD as electrolyte, and the new one fully developed since April 1998 (explorative, wide-range, experiments started from 1994), is summarised in Tab. 1.

	Old procedure (conventional)	**INFN protocol**
Cathode	Rods, plates	Thin wires 50 – 100 microns
pH	Strongly alkaline (13 – 14)	Slightly acid (4.5 – 5.5)
Electrolyte	LiOH, LiOD	$CaCl_2$-$SrCl_2$
Concentration	0.1 – 1 M	10^{-5} – 10^{-4} M
Voltage	< 30V	50 – 250V

Tab.1. Comparison between the old procedure and the new INFN – LNF protocol.

-- Critical points

The *purity* of the *water* is one of the most important and *critical* points of our procedure.
We want to stress that the composition of our electrolytic solution is close to a pure water (only extremely low amount of electrolytes are added); a typical composition in our experiments (Pd wire, 30cm of length and 50μm of diameter) is the following:

- H_2O = 1200cc (66.6 mole);
- HCl = $2*10^{-5}$ moles;
- $SrCl_2 = 2*10^{-5}$ moles (1mol of Sr=88g, then *only 1.8 mg of Sr*);
- $HgCl_2$ (Anti Cracking Agent) = 10^{-6} moles

The impurities normally dissolve in the light or the heavy water, can be divided in three groups:
a) Inorganic substances (solid, liquid, gaseous, light water contamination into heavy water);
b) Organic substances (generally expressed as total carbon);
c) Bacteria.

The typical amount of impurities in both waters are the following:

H_2O:

1) Inorganic substances
   a) Deionised, ≈ 10mg/l => not good;
   b) Bidistilled , ≈ 0.3mg/l => good;
2) Organic substance ≈ 0.2 mg/l;
3) Livings = 0 (if properly saved, after high temperature distillation with acidified $KMnO_4$, in sterilized vessels).

D_2O:

1) 10-20 mg/l inorganic substance (distillation is strongly required);
2) about 10 mg/l organic substance [Ref. 8];
3) Livings: 60-700 bacteria/ml, depending on production batches, was measured at ENEA-Casaccia Laboratories (Rome, Italy).

According to our investigations, we found that some of the bacteria, normally present in the heavy water, could be quite deleterious to our loading protocol:

a) they are able to change the solution pH because of the acidic properties of some products of their metabolism;
b) they tend to organize colonies on the surface of the cathode, in that competing with the appropriate carbonates coating;
c) they prevent the proper galvanic deposition of the anti-cracking agent on the cathode.

Procedures for D_2O purification

Several operations have to be performed in order to purify (#1) and to maintain purity (#2, #3) the working heavy water (1 litre):

1) Bacteria "depletion" by the following multi- steps procedure:
   a) addition 1 g of $KMnO_4$ + 1 cc of H_2SO_4 (96%) (=> pH= 1.3); keep at 80 °C for 1 hour;
   b) several vacuum distillations (by Rotavapor) at 30 °C, until pH 5.5 ÷ 6 has been reached;
   c) addition of LiOD up to obtain pH=13; keep at 80 °C for 30 minutes;
   d) several vacuum distillation at 30 °C until a.c. resistivity> 400 Kohm·cm and pH =7 ÷ 8;
2) Addition of colloidal silica (particles diameter 12 nm) + glutaraldehyde as bactericide (from KEMPRO Italiana), to reduce the growing speed of bacteria after purification;
3) Addition of $HgCl_2$ (10^{-6} M) only when D/Pd>0.90.

Identification and characterization of bacteria

The bacteria existing in the heavy water have been characterized by means of the following techniques:

- phenotypic characterization;
- cellular lipid and fatty acid analyses;
- phylogenetic analysis of 16S rDNA nucleotide sequences, adopting the most advanced procedures and reagents recently developed by Perkin Elmer Biosystems.

Two genera of bacteria, both Gram-negative, have been identified and both have been registered as ***new species*** at the GenBank of the "National Center for Biotechnology Information – National Institutes of Health" (Bethesda, MD, USA) and DNA Data Bank of Japan "Center for Information Biology, National Institute of Genetics" (Mishima, Shizuoka, Japan).
The bacteria belong to genera: Ralstonia and Stenotrophomonas. The name given to both new species is: ***Detusculanense.***

The biological analyses have shown why such bacteria were so deleterious to our protocol:

a) they are able to "metabolise" alkaline earth ions (in particular Sr^{++} up to a concentration as large as $2 \cdot 10^{-2}$ M), preventing in this way the precipitation on the cathode surface of the carbonate coating;
b) they are able, furthermore, to "metabolise" even the very poisonous $HgCl_2$ up to a concentration of 10^{-4} M, so inhibiting its anti - cracking action.

Results

As reported in detail in our another paper (see, A. Spallone et al.) at the same Conference, we can claim that the prefixed target has been completely achieved for H loading (H/Pd>0.98). The loading stability lasts for days [Ref. 9].

In these experiments some measurements of the thermal resistivity coefficient (α_T) of the hydrogen loaded Pd wire have been carried out at H/Pd ratios higher than 0.8. It is known that such a coefficient monotonically decreases, by increasing the H/Pd value (from $\alpha_T = 4.1 \cdot 10^{-3}$ K^{-1} when H/Pd = 0, to $\alpha_T = 2.0 \cdot 10^{-3}$ K^{-1} when H/Pd = 0.7) [Ref. 10].

We have found that at higher H/Pd values, the thermal coefficient shows an abrupt increase. When the loading ratio is as high as R/Ro $\cong$ 1.15 at room temperature, we measured for the thermal resistivity coefficient the value: $\alpha_T = 5.5 \cdot 10^{-3} \pm 1.5 \cdot 10^{-3}$ K^{-1}.

This value is remarkably higher than that of the pure (H de-loaded) Pd wire. The evidence of such an abrupt change in slope of the thermal coefficient resistivity, at very high values of the H/Pd ratio, strongly suggests that a new phase in the Pd-H system has been able to nucleate.

About D loading, we found strong differences when the heavy water was used "as received" and when it was been previously purified according to the above mentioned procedure.
In the first case loadings exceeding D/Pd = 0.92 (Fig. 7) can be hardly achieved. No thermal anomalies were ever observed.
In the second one (Fig. 8) loading values in the range D/Pd 0.97 ÷ 0.98 have been obtained for several days. When we reduced the electrolysis current from 40 to 25 mA (high->low current) an anomalous effect occurred: instead of obtaining a de-loading of the wire (as expected by Tafel effect) we recorded an apparent increase of loading for some minutes, followed by the usual, slow de-loading. A possible explanation could be that the wire was actually and continuously emitting excess heat; when the current was reduced, the excess heat progressively had been vanishing, reducing at the same time the actual wire's temperature. So, what could appear a further loading is simply a drop down of the wire resistance due to a drop down of the wire temperature. In absence of a flow calorimeter, we were able to evaluate a rough and conservative estimation of excess heat: 0.5 W respect to 2.0W of input.

CONCLUSIONS

In conclusion the following statements can be proposed:

1) The problem to get H/Pd > 0.97 in a *reproducible* way has been solved by the use of $SrCl_2$-HCl-CO_2 and small amounts of $HgCl_2$ as electrolytes (*the Pd wire surface is coated with thin layers of $SrCO_3$ and amalgam of Hg*). Our results have been successfully reproduced by Pirelli (Milan, Italy) and SRII (Stanford, USA);
2) The same procedure, using D_2O, was less efficient because of bacteria contamination;
3) Properly purified D_2O and a new circuitry allowed us to get large loading (D/Pd> 0.97); strong indications of anomalous "excess heat" (about 0.5 W over 2 W of input power) in a reproducible way (3 times) were observed;
4) Further work on D_2O "purification" is needed; "sterile" electrolysis seems to be necessary.

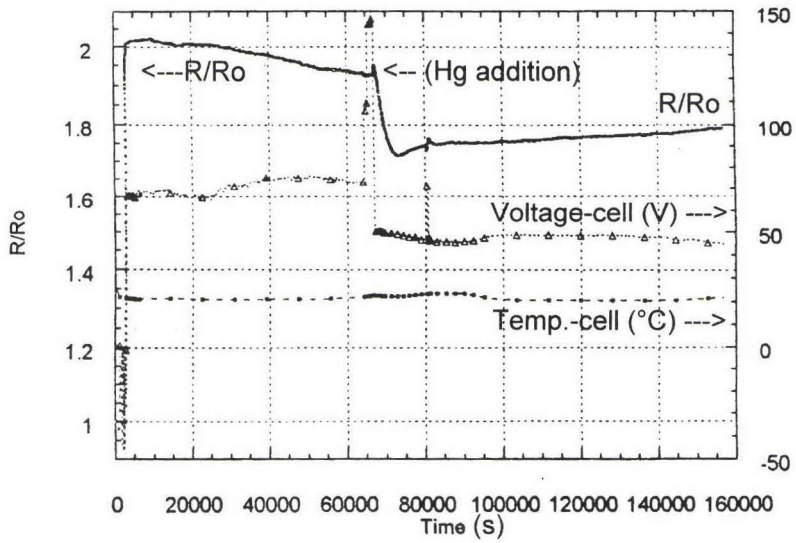

Fig. 7 – Commercial reactor-grade D_2O test: D/Pd= 0.92 is achieved after Hg addition. The loading goes to decrease in the time; no thermal anomalies have been observed.

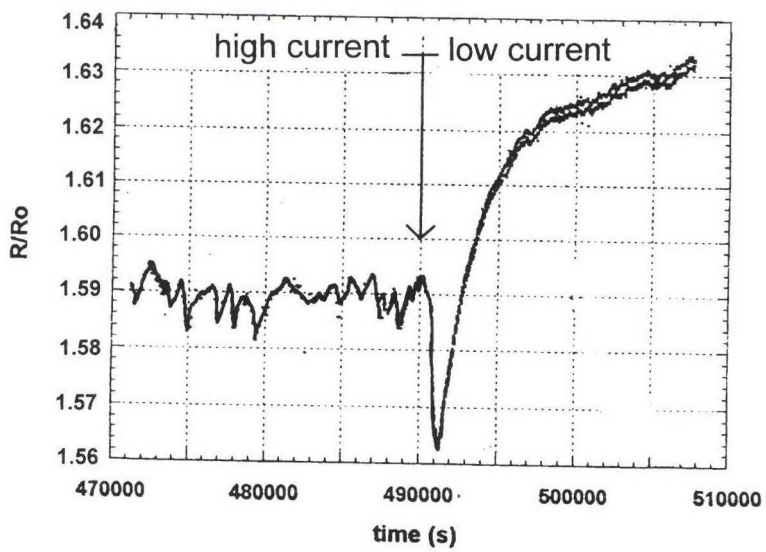

Fig. 8 – LNF-purified D_2O test: After LNF-purification procedure, a high loading (D/Pd= 0.97) have been achieved, lasting several days; an anomalous loading effect occurs after decreasing electrolysis current: it can be explained with a higher temperature of wire occurred during the loading.

The identified bacteria seem to be able to metabolise dangerous heavy metals (Cd, Cr, Pb, Hg). Studies are in progress and they will be published in a future paper.

Acknowledgements

We would like to thank (we will be always in debt with him) Prof. **Giuliano Preparata** (Milan University, Italy), who was the first person (since 1994), to introduce us to some specific properties of thin Pd wires from the point of view of H/D overloading.

We are very sad: He passed away on April 24, 2000 (just one month before the beginning of this Conference). For most of the authors of the present paper Giuliano was not only a Scientist involved in the same field of Research but, overall, a personal, old, friend.

We thank Prof. Jean Paul Vigier (Paris University, France), both for some useful criticism and several suggestions about the comparison of numerical simulation with experimental data.

Dr. Naoto Asami, Dr. Kazuaki Matsui and their colleagues at NHE (presently at IAE Tokyo, Japan) gives us several suggestions and experimental data (obtained in their Laboratories) about purity of H_2O and D_2O: they clarified to us something problematic on their purification.

Prof. Piergiorgio Sona (ENEL Ricerca, Milan, Italy) spent a lot of time on discussions with us about catalytic proprieties of surfaces and methods to modify them.

Prof. Edmund Storms (ENECO, USA) gave us some useful suggestions regarding the more useful acid (between HCl and H_2SO_4) capable to insure the constant of pH during the electrolysis.

Mr Francesco Todarello (KEMPRO Italiana, Ariccia, Italy) provided us information about methods used in the distillation of light water (industrial grade) to reduce the problem of bacteria growing. He developed new types of colloidal silica for our specific purposes.

We are deeply indebted with Prof. Lino Daddi (Accademia Militare Navale, Livorno, Italy) who gave us several information about the proper procedures for the purification of the light water in comparison with the heavy water.

References

[1] F.Celani et al., *Progress in New Hydrogen Energy - Vol. 1* (Proc. ICCF6, Oct. 13-18, 1996, Sapporo, Japan), 93-104 (1996)

[2] M.C.H. McKubre et al. *Frontiers of Cold Fusion* (Proc. ICCF3, 1992, Nagoya, Japan), 5(1993)

[3] B. Baranowsky and R. Wisniewsky (1969), *Phys. Stat. Sol.* **35**, 539

[4] J.C. Barton, F.A. Lewis and I. Woodward (1963), *Trans. Faraday Soc.* **59**, 1201

[5] M. McKubre et al. *Conf. Proc. ICCF1* (Salt Lake City, Utah) March 28-31 1990, p.20-31

[6] F. Celani et al. "High Hydrogen loading of thin Palladium wires through alkaline-earth carbonates precipitation on the cathodic surface. Evidence of a new phase in the Pd-H system." *Published by INFN-LNF-00/006 (P), 6 Marzo 2000* – (To be published by *Physics Letter A*)

[7] F. Celani et al. "A study on the electrochemistry parameters to achieve reproducible high H/Pd values in relation to 'anomalous' excess heat; proteobacteria contamination problematics." Presented at the "*IV Workshop on Anomalies in Hydrogen/Deuterium Loaded Metals*", 22-24 Oct. 1999, Asti, Italy. Publishing by SIF, ed. Compositori, Bologna (Italy) as Conference Proceedings.

[8] Naoto Asami, Institute of Applied Energy, Tokyo (Japan), May 1999; *(private communication).*

[9] A. Spallone et al. "A reproducible method to achieve very high (over 1:1) H/Pd loading ratio using thin wires in acidic solution with addition of very low concentration impurities." Presented at the "*IV Workshop on Anomalies in Hydrogen/Deuterium Loaded Metals*", 22-24 Oct. 1999, Asti, Italy. INFN- *LNF- Report 00/018 (P), 27 Giugno 2000.* Publishing by SIF, ed. Compositori, Bologna (Italy) as Conference Proceedings.

[10] B. Baranowski, Filipek et al. (1990), *J. Less Common Metals* , **158**, 347

Conference Proceedings Vol. 70
"ICCF8"
F. Scaramuzzi (Ed.)
SIF, Bologna, 2000

NEW ELECTROLYTIC PROCEDURE FOR THE OBTAINMENT OF VERY HIGH H/Pd LOADING RATIOS. PRELIMINARY ATTEMPTS FOR ITS APPLICATION TO THE D-Pd SYSTEM

A. Spallone[1], *F. Celani*[1], *P. Marini*[2], *V. Di Stefano*[2]

(1) INFN-LNF, Via Enrico Fermi, 00044 Frascati (Roma), Italy
(2) EURESYS, Via Lero 30, 00129 Roma, Italy

Abstract

A new electrolytic protocol is proposed, capable of insuring a very high Hydrogen loading of thin Palladium wires. The main characteristic of the procedure consists in the use of a particular electrolyte containing very small amounts of alkaline-earth metals dissolved in a diluted acid solution (H_2O+HCl).

The addition of alkaline-earth metals to the electrolyte appears to be decisive for the achievement of H/Pd loading ratios close to 1. Two independent Research Groups have tested the protocol with similar results.

Probably because of the presence of contaminants in the heavy water, less satisfactory results have been obtained for the D/Pd loading ratios (best result: R/Ro = 1.52; D/Pd ≅ 0.97)

Introduction

It is generally known that in cold fusion experiments, in order to obtain stable and reproducible excess heat it is necessary to achieve and maintain very high D/Pd (>> 0.85) loading ratios [Ref. 1].

The poor results, especially from the point of view of their reproducibility, generally achieved by the conventional electrolytic techniques, based on the use of LiOH solutions, induced us to develop a completely different approach.

In order to increase the cathodic overvoltage, which is known to be the main controlling parameter of the H(D) Pd loading, we tried to modify the nature of the cathode, by inducing the formation of a very thin layer of an alkaline-earth carbonate on its surface [Ref. 2].

After the first encouraging results, we decided to carry out a systematic work, starting with light water, in order to define the best composition of the electrolyte and the most effective loading procedure.

With reference to the paper presented by Celani et al. [Ref. 3], which is substantially a comprehensive panorama over all the activities carried out by our group in the last two years, the present one shows in detail the most significant results of the experimental work.

Experimental Apparatus

A schematic diagram of the experimental set-up is shown in Figure 1. The electrolytic cell consists of a Pd cathode (a thin wire - diameter 50 μm – length 19 cm), a Pt anode of the same length (diameter 200 μm) set at a distance of 1.5 - 2 cm form the cathode, both plunged in a glass

beaker filled with about 400 ml of H_2O+HCl solution. The cell is placed into a two litre water bath in order to reduce the temperature fluctuations around the room temperature (usually kept at 22 °C). Cell, bath and room temperatures are continuously monitored and recorded.

The power supply can operate as a constant D.C. current generator or, optionally, as a constant D.C. voltage generator. The cathode is grounded. The voltage is applied to the anode electrode through a home-made impedance adapter circuit (impedance booster), in order to avoid a current feed-back from the A.C. measuring circuit. The latter is essentially composed by a pulse generator (having sinusoidal, square and triangular wave selection) and a ground home-made coupling circuit (ground return, both for the D.C. and A.C. generators).

The D.C. generator can be applied to the edge points A or B of the anode whereas the A.C. generator can be applied to the edge points C or G of the cathode. The Pd wire voltage pick-ups C,D,E,F,G allow for the measurements of the resistances of the correspondent wire segments (CD= bottom, DE=down, EF=up, FG=top). In the present work the length of the CD and FG segments has been set to 0, so that in the following, reference will be made to only two segments, i.e. DE= "down" and EF= "up", both of length 9.5 cm.

The loading ratio is inferred by means of the well known relationship [Ref.s 4,5,6] between resistance and H(D) content in the Pd matrix (Fig. 2) and continuously monitored.

The Pd cathode, because of its favourable surface/volume ratio, allows for a faster Hydrogen absorption and its high resistivity improves both the accuracy and the precision of the measurements. Furthermore, the 1/r dependence of the electric field around the wire allows for a sharp increase of the pH value just in its proximity, thus promoting the carbonate precipitation in that region only (see after).

Composition of the electrolyte

The set of experiments which led us to the final choice of the electrolyte composition is extensively described in Reference 2. Here only the essentials will be treated.

It is known that Hydrogen can enter a metal only if it is present on its surface in the form of H atoms. In the case of the electrolytic Hydrogen loading of a Pd cathode, after the first rapid absorption (absorption isotherm - $\alpha+\beta$ phase), the Hydrogen loading progressively slows down until it comes to an end, no matter how much is the applied current density. This is mainly due to the catalytic properties of the Pd surface. In fact, even though Hydrogen atoms are continuously formed at the Pd cathode during the electrolysis, they rapidly recombine to form the Hydrogen molecule, thus hindering the absorption process, (a fact consistent with the very low overvoltage measured with Pd cathodes). It is also known that catalytic surfaces can be poisoned by films of adsorbed or deposited substances. On the basis of this assumption we tried to alter the Pd surface through the local precipitation of inorganic substances. The final choice has fallen upon alkaline earth carbonates and among them Strontium carbonate.

The choice of the alkaline earth metals was dictated by the fact that they do not discharge to form a metallic layer, which can eventually hinder the Hydrogen absorption due to the low Hydrogen permeability typical of most metals. Mercury, for example, even though it effectively poisons the Pd surface, is able to stop any Hydrogen exchange. We found it useful only as an extremely thin layer, very hardly controllable through the concentration of Hg ions in the electrolyte. Instead, because of its solubility product, the local precipitation of $SrCO_3$ is easily controlled through Sr^{++} concentration, pH, and current density. Because of their higher solubility product both $CaCO_3$ and $BaCO_3$ are less effective [Ref. 2ùç]. The proper Sr^{++} concentration range is within 30 to 70 μM/l. Sr^{++} is added as $SrCl_2$. By setting the pH at 4.5 with HCl additions, the proper CO_2 concentration is that one insured by maintaining the electrolyte exposed to open air.

Experimental

Effect of Sr^{++} additions

After a start-up procedure, common to all experiments, consisting in:

1) The Pd wire is Joule heated (500 mA) in air (up to roughly 600 °C) in order to completely eliminate occasional residual Hydrogen and to relax mechanical stresses due to the wire cold-working.
2) The cell is filled with pure distilled water (400 cm^3).
3) A small quantity of HCl is added till the pH of the solution is around 4.5 (the required amount is about 20 μM)

the electrolysis starts with the application of 5 mA current. This current value is maintained until the cathode reaches a first asymptotic loading value (Fig. 3). At this point the electrolysis current is varied according to the following sequence:

Turned off (partial deloading) - turned on (high current loading till next asymptotic value) - turned off (partial deloading)- Turned on (low current loading till next asymptotic value).

It will be referred to this sequence as to the *off-high-off-low* (OHOL) current sequence.

By repeating the sequence, the loading ratios H/Pd tend to become higher until a final asymptotic value is reached, subjected to no further improvement.

In order to point out the effectiveness of the Sr addition to the electrolyte a blank test has been carried out by operating with an electrolyte containing only HCl.

In Figure 4, it is shown that the final maximum loading ratio R/R_0 obtained by the above described procedure is ≈ 1.50.

At this point the current was turned off in order to allow for a complete deloading of the Pd cathode (Fig. 4).

$SrCl_2$ is then added (50 μM) to the electrolyte and the electrolysis is started again with the same set of conditions (5 mA). The OHOL sequence has then been applied and repeated until a final asymptotic value of R/R_0 of 1.15 has been reached (Fig.s 5, 6 and 7). Therefore it is proved that the Sr addition is decisive for the achievement of extremely low R/R_0 values.

Substantially the same results have been obtained by substituting the Cl^- ions with SO_4^- ones.

Effect of Hg^{++} additions

Tests using $HgCl_2$ at a concentration of $\approx 10^{-6}$ M (pH=4.5) have shown that a Hg coating forms quickly, thus covering the Pd cathode and blocking the loading at around the peak (R/Ro=1.75). The block could not be removed even by strongly increasing the current or by repeatedly applying the OHOL sequence.

Further tests [Ref. 7] carried out with remarkably lower $HgCl_2$ concentrations ($\approx 10^{-8}$ M) have shown a very slow loading (two days) up to a final asymptotic value of R/Ro=1.35. It was observed that even by turning off the current, the deloading rate was extremely low, suggesting that even at such a low concentration an impermeable Hg layer finally forms on the Pd surface.

In another experiment (Fig. 8), to the Sr^{++} containing electrolyte, $HgCl_2$ was added up to a concentration of 10^{-5} M. A strong loading occurred (R/Ro= 1.10 and 1.15 respectively for "up" and "down" sectors). This suggests that Mercury could not form a continuous coating because of the presence on the cathode surface of a previously precipitated $SrCO_3$ layer.

Thermal resistivity coefficient of the Pd-H cathode.

As described in an our previous works [Ref. 8], for the first time we measured the thermal resistivity coefficient of the Pd cathode (α_T), when R/R_0= 1.2. Such a coefficient is known to decrease as the H concentration in Pd increases between H/Pd=0.1 (α_T= $4.1 \cdot 10^{-3}$ K^{-1}) up to

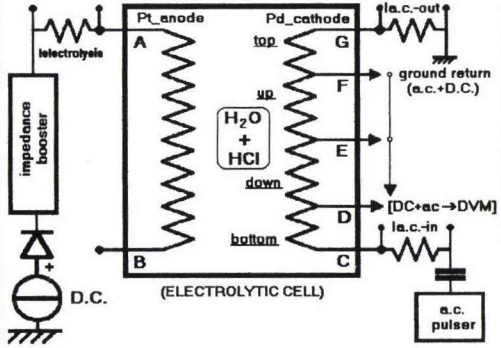

Fig. 1 – Apparatus set-up: electrolytic cell, D.C. power supply block and a.c. resistance measurement block; electric and physical parameters are acquired by Digital Voltmeters (DVM) controlled by a computer.

Fig. 2 – Normalised Palladium resistance versus Hydrogen (Deuterium) molar fraction in Pd. Peak value is: H/Pd= 0.75, R/Ro= 1.78 (Hydrogen) and D/Pd= 0.75, R/Ro= 2.0 (Deuterium).
Maximum gas loading achieved: H(D)/Pd= 0.95 at R/Ro= 1.4 (1.6).

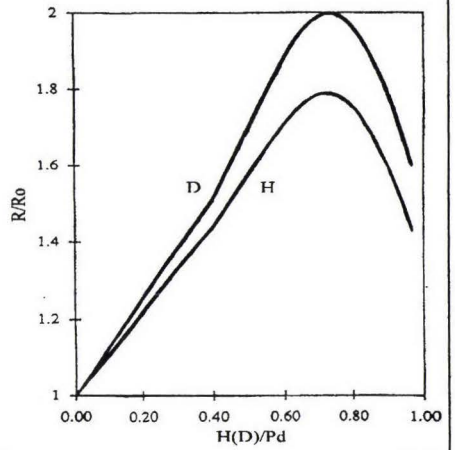

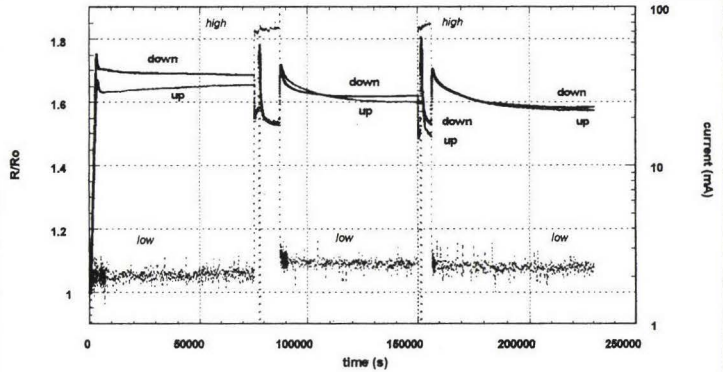

Fig. 3 – HCl blank test: beginning of loading + OHOL sequences.

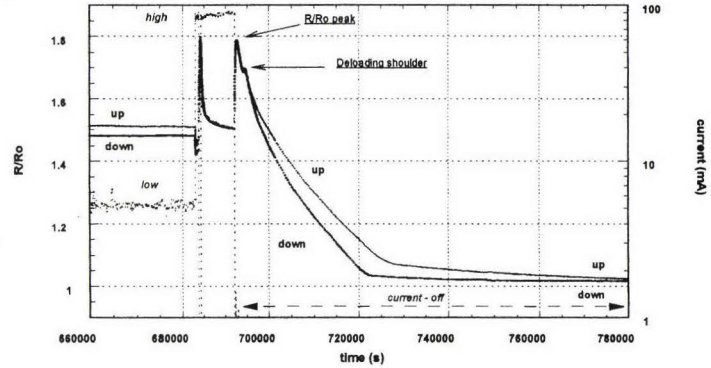

Fig. 4 – HCl blank test: final maximum loading; the complete deloading of the cathode is shown.

H/Pd=0.7 ($2.0 \cdot 10^{-3}$ K^{-1}), which is the maximum H concentration for which there were available data [Ref. 9]. The result of our measurements at R/R_0=1.2 (H/Pd close to 1) is $\alpha_T = 3.5 \cdot 10^{-3}$ K^{-1}.

A further value of $\alpha_T \cong 6.0 \cdot 10^{-3}$ K^{-1} has been found at H/Pd a bit closer to 1 (R/Ro = 1.15). These results show that between H/Pd=0.7 and H/Pd $\approx$ 1, there must be a minimum value of α_T, probably rising rapidly in the H/Pd region close to 1. This strongly suggests that a new phase is starting to nucleate inside the Pd-H β phase.

Finally, the existence of a change of phase seems to be indicated by the presence of a characteristic shoulder (Fig. 4), which appears in the R/Ro versus time deloading curve, just after the peak has been overcome. The occurrence of the shoulder (roughly around H/Pd=0.65) after the peak, might be connected with the end of β phase and the beginning of $\alpha+\beta$ phase, sequentially occurring during the deloading.

Preliminary Pd-D loading experiments

When our batch of commercial heavy water was used for preparing the electrolytic solution, according to the above described protocol, the best loading obtained was D/Pd=0.75. Taking into account that our procedure requires the absence of any foreign substance in the electrolyte apart from Sr^{++} ions and CO_2, it will be clear that even the small amounts of impurities (inorganic, organic and biologic materials) normally present into that commercial heavy water, could have seriously impaired the proper formation of the thin layer of $SrCO_3$ on the Pd surface.

Another batch of guaranteed higher purity heavy water was employed and the composition of the electrolyte was the same one used for H loading.

High purity heavy water is remarkably hygroscopic. Consequently, the electrolytic cell was excluded from the contact with ambient air. The necessary supply of CO_2 was assured by a flow of air, dried by bubbling it into concentrated sulphuric acid, and subsequently into heavy water.

It is to be noted that with the experimental set-up used for D loading, both ends of the up and down sectors of the Pd wires were protected with a drop of silicone sealant for a total length of roughly 4 mm (about 4% of their length). These portions of the cathode are not in contact with the electrolyte and cannot be directly loaded. In this conditions it was found that the maximum numerical value of R/Ro read by the instruments was 1.96 instead of 2.0. Therefore the values of R/Ro, reported in the Figures from 9 to 12 are about 2% lower than the correct ones.

In Figure 9 the effect of the OHOL sequence is shown with some detail. These results are rather inferior if compared with the ones obtained with H loading.

After several attempts it was found effective to increase the deloading time during the off portion of the OHOL sequence, allowing for an almost complete deloading. Some of the results are shown in Figure 10. After several new OHOL sequence applications a final asymptotic value of R/Ro=1.62 (at 25 °C) was achieved. The current was then increased up to 30 mA. It can be seen that an R/Ro value of 1.55 was rapidly achieved. By lowering the applied current the R/Ro value rose to 1.65. By again increasing the current up to 90 mA a R/Ro value of 1.52 was obtained (Fig. 11). In the same figure it is shown that by turning the current off, the deloading process proceeds regularly with a peak of R/Ro at 1.95. It should be noted that the deloading rate of the D loaded wire is significantly lower than that observed with the deloading of the H-loaded wire (Fig. 4). Such a difference could be due to the difference between the length of the deloading time within the OHOL sequence.

The previously reported "loading ramps" effect [Ref. 10] has been observed to occur sometimes when loading is quite high (R/Ro< 1.75). We observed this effect to occur several times especially in the "up" wire sector (Fig. 12), when R/Ro decreases under 1.65 (cycles oscillating between 1.643 and 1.647, with a period roughly of 1 hour, even lasting for about 1 day and disappearing when R/Ro rises up over 1.66).

In a previous paper [Ref. 11], we conjectured that this effect could be located within just a few small fractions of the wire achieving very high loading (R/Ro< 1.5), thus giving rise to "bursts" of

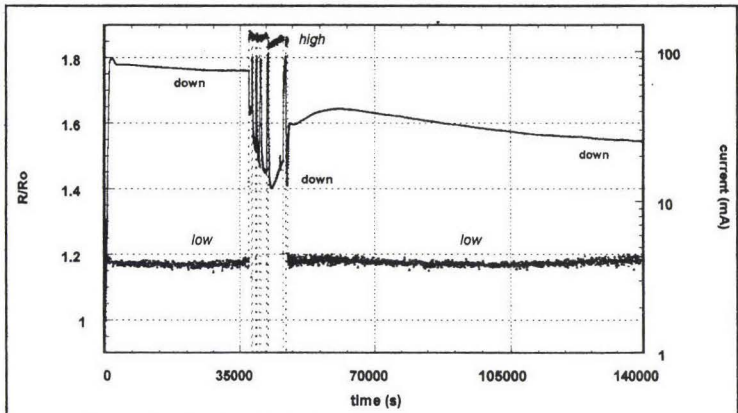

Fig. 5 – Sr test: beginning of the loading + OHOL sequence; R/Ro is reduced from 1.75 to 1.55 (back to low current).

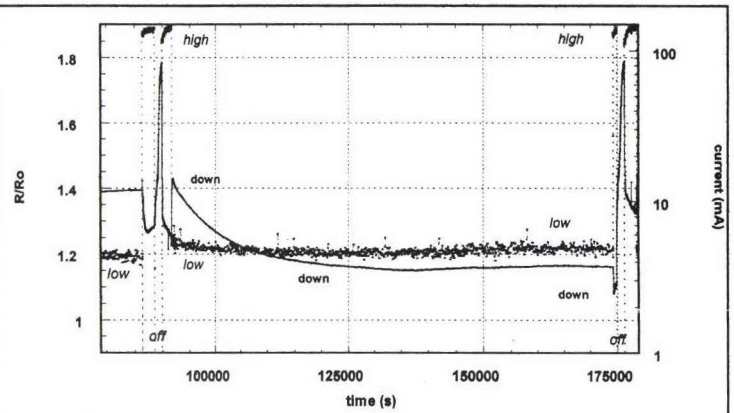

Fig. 7 – Sr test: maximum final loadings: R/Ro= 1.15 at low current (5 mA, 7 V) and 1.05 at high current (120 mA).

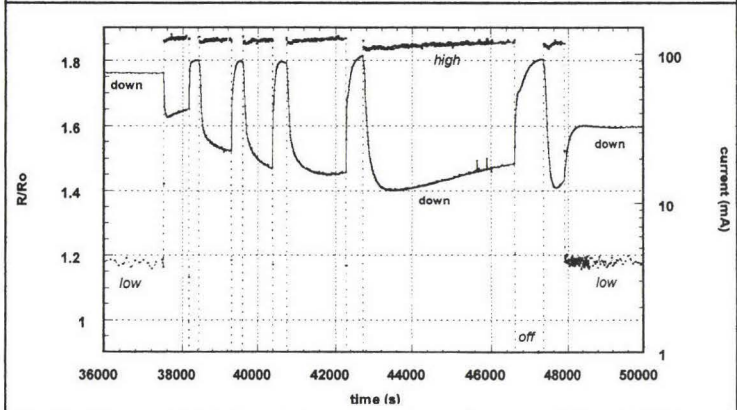

Fig. 6 – Sr test: detail of OHOL sequence ("down" sector); R/Ro= 1.40 is achieved at high current.

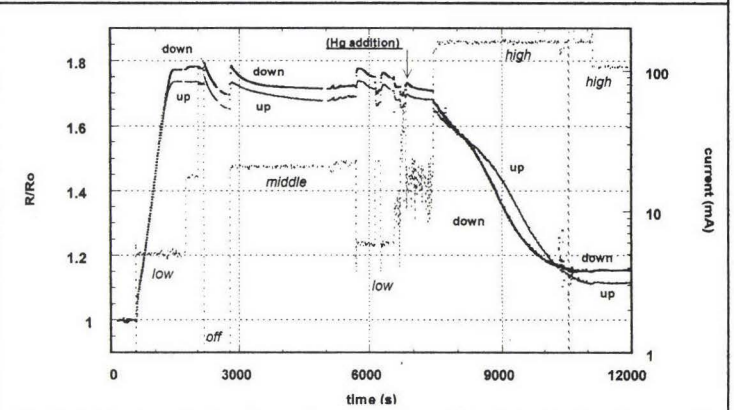

Fig. 8 – Hg test: an addition of Hg to the solution (containing Sr) and a sharp increase of electrolytic current, allow for a fast and strong loading .

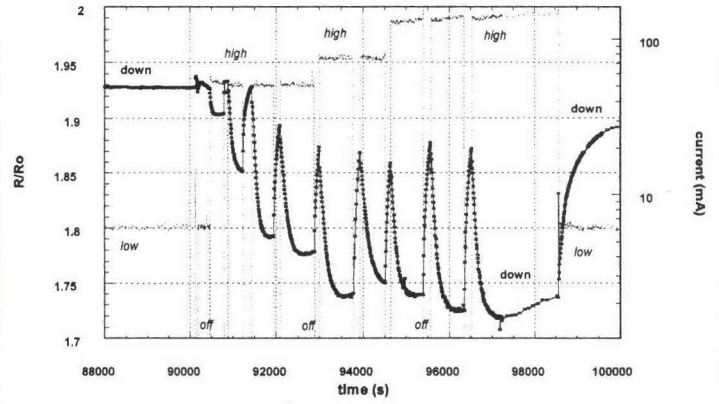

Fig. 9 – D_2O test: detail of OHOL sequence; maximum loading: R/Ro → 1.72

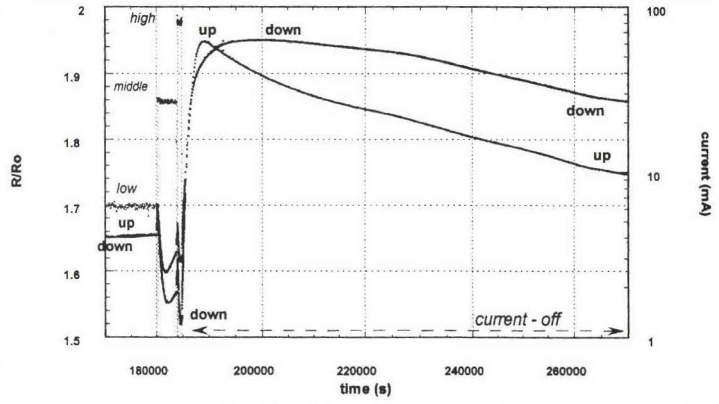

Fig. 11 – D_2O test: starting from R/Ro= 1.65, by increasing the current up to 90 mA, R/Ro= 1.52 was obtained. In OFF, a very slow deloading occurs.

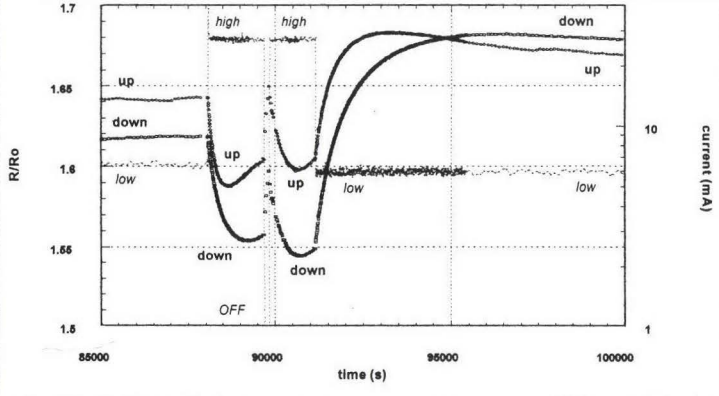

Fig. 10 – D_2O test: final value after the new OHOL sequence (R/Ro ≅ 1.62); the current was switched up to 30 mA and R/Ro = 1.55 was achieved.

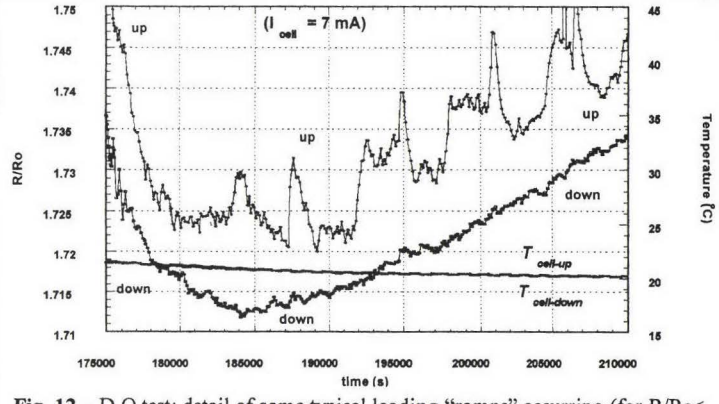

Fig. 12 – D_2O test: detail of some typical loading "ramps" occurring (for R/Ro< 1.75) at low current for the "up" sector only.

heat production which locally rise the wire resistance, but that are on the average too small to be detected by the sensors as cell temperature rise.

Conclusions

In conclusion a protocol for the obtainment of high H/Pd and D/Pd values has been developed, in agreement with the hypothesis of a modification of the catalytic properties of the Pd-cathode surface, through the formation of thin layers of $SrCO_3$, by local precipitation due to pH increase at the cathode surface.

The Pd-H loading protocol has been tested by Pirelli-Cavi SpA Research Laboratory (Milan), by Dr D. Garbelli Group (under the supervision of Ing. F. Fontana) and the Stanford Research Institute (CA), by Dr P. Tripodi Group (under the direction of Dr M. McKubre) and was found to be effective. In particular by the Pirelli Group has shown detailed evidence of the deposited layer on the Pd surface through the use of a SEM apparatus (as it is reported by Dr Garbelli at this same Congress).

Acknowledgements

We are indebted to Eng. Alfredo Mancini for his precious support. We are grateful to Dr. Daniele Garbelli and Eng. Flavio Fontana for their important help and we want to thank Dr Paolo Tripodi and Dr Mike McKubre for their useful suggestions. Finally, we wish to thank Prof. Sandro Pace appreciating so much his useful criticism.

References

[1] M.C.H. McKubre et al. *Frontiers of Cold Fusion* (Proc. ICCF3, 1992, Nagoya, Japan), 5(1993)

[2] F. Celani, A. Spallone et al. "High Hydrogen loading of thin Palladium wires through alkaline-earth carbonates' precipitation on the cathodic surface. Evidence of a new phase in the Pd-H system." Published by *LNF-00/006 (P), 6 Marzo 2000* --- To be published by *Physics Letter A*

[3] F. Celani, A. Spallone et al. "A study on the electrochemistry parameters to achieve reproducible high H/Pd values in relation to 'anomalous' excess heat; proteobacteria contamination problematic." Submitted to the *IV Workshop on Anomalies in Hydrogen/Deuterium Loaded Metals*, Conf. Proc. 22-24 Oct. 1999, Asti, Italy

[4] B. Baranowski and R. Wisniewski (1969), *Phys. Stat. Sol.* **35**, 539

[5] J.C. Barton, F.A. Lewis and I. Woodward (1963), *Trans. Faraday Soc.* **59**, 1201

[6] M. McKubre et al. *Conf. Proc. ICCF1* (Salt Lake City, Utah) March 28-31 1990, p.20-31

[7] A. Spallone, F. Celani et al. "A reproducible method to achieve very high (over 1:1) H/Pd loading ratio using thin wires in acidic solution with addition of very low concentration impurities." Submitted to the *IV Workshop on Anomalies in Hydrogen/Deuterium Loaded Metals*, Conf. Proc. 22-24 Oct. 1999, Asti, Italy --- Published by INFN: *LNF-00/017 (P), 27 Giugno 2000*

[8] P. Marini et al. *XXI Secolo Scienza e Tecnologia* , Anno **X** - Num. **1**, pg. 34-41 (1999)

[9] B. Baranowski, Filipek et al. (1990), *J. Less Common Metals* , **158**, 347

[10] F. Celani, A. Spallone, P. Tripodi et al. "Deuterium overloading of palladium wires by means of high power μs pulsed electrolysis and electromigration: suggestions of a 'phase transition' and related excess heat." *Physics Letters A*, 214 (1996) 1-13

[11] A. Spallone, F. Celani et al. "A preliminary D/Pd study: anomalous resistivity transition effect." "*Asti Workshop on Anomalies in Hydrogen/Deuterium Loaded Metals*" (SIF-Conf. Proc. Vol. 64 pg 7-16, Asti 27-30 Nov. 1997) Edit by W.J.M.F. Collis, Compositori–Bologna, Italy (1999).

Conference Proceedings Vol. 70
"ICCF8"
F. Scaramuzzi (Ed.)
SIF, Bologna, 2000

HYDROGEN/DEUTERIUM LOADING IN THIN PALLADIUM WIRES

D. AZZARONE, F. FONTANA, D. GARBELLI

Pirelli Cavi e Sistemi Advanced Research, viale Sarca, 222, 20126 Milan, Italy

ABSTRACT

The main goal of this work was to describe our investigation in the loading processes of Hydrogen/Deuterium in thin Palladium wires. The Palladium wires (50μm diameter) are electrolitically loaded. The loading ratio (x=H/Pd) was estimated through the measurement of the wire resistance.

The protocol used permits to load Hydrogen into Palladium with very good reproducibility to very high loading ratio. For Deuterium the reproducibility and the loading ratio are not so good. The possibility to keep thin Pd wires loaded with low power during the electrolysis and even with zero power after the electrolysis, was tested and confirmed for Hydrogen.

It is possible very high loaded wires are used in the future to perform calorimetric measurement.

1 INTRODUCTION

The capability of Palladium of absorbing Hydrogen (H) and its isotopes like Deuterium (D), is known since 1866. It is easy to load Hydrogen (and Deuterium) at room temperature inserting Pd in H_2/D_2 gas up to a loading ratio x=[H]/[Pd]~0.7. Higher loading ratios (x>0.97) can be achieved with gaseous techniques with very high pressure (~10^9 Pascal) or with electrochemical loading with high current density and long time.

A new successful method for electrolytic loading of H in Pd was developed by INFN Celani group [1,2] and confirmed by other labs [3,5,6,7,8]. The scope of this article is to describe the tests performed with this method for the loading of Hydrogen and Deuterium in thin Palladium wires. The on-line evaluation of the loading ratio was performed using the calibration curve shown in fig. 1; it gives the loading ratio x=H(D)/Pd as a function of the resistance ratio R/R_0. The main goal of these experiments was the achieving of good (x>0.85) D-loading ratio. This is a necessary

condition in order to obtain cold fusion evidence [4] and is a necessary preliminary step before the starting of calorimetric experiments.

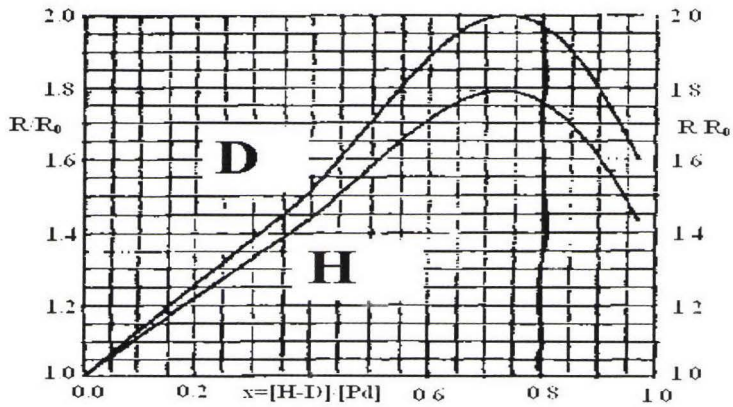

Figure 1 - Baranowsky curves. This curves give the relations between the normalised resistance (R/R_0) of hydride and the loading ratio x=[H(D)]/[Pd].The bottom curve is of Hydrogen while the top one of Deuterium. Data are available up to x=0.97 (R/R_0 =1.43 for H, R/R_0 =1.60 for D).

2 EXPERIMENTAL SET-UP

The loading of Palladium wires was done by electrolysis with the apparatus here described.

2.1 The electrolytic cell

The cell geometry structure is shown in figure 2. It is made using a glass cylinder (diameter ~ 7.5 cm, height ~ 11 cm) with an external sheath where a fluid can flow. In the cell there is a central vertical cathode and 4 vertical parallel wires in symmetrical positions to form the anode. The internal volume was about 400ml. The internal temperature of the cell is measured with 4 thermoresistances (2 Pt100 and 2 Pt1000) placed inside the cell. The cathode is a Pd wire 50 μm in diameter, 9-11cm long, the anode is a Pt wire 400-500 μm in diameter.

2.2 The solution

The solution was obtained adding different chemicals to bidistilled light water for H loading or heavy water (by Ontario Hydro) for D loading. The quantities of chemicals were not rigidly defined, and different kind of tests were performed with some of the following substances and quantities:

HCl (10^{-4}-10^{-5} Mol/l). It was always added to water before the experiment started.

$SrCl_2$ (10^{-4}-10^{-5} Mol/l). It was almost always used, added usually before the experiment started.

$HgCl_2$ (10^{-5}-10^{-7} Mol/l). Sometimes it was added to the solution during the electrolysis when the wire was already loaded (x>0.7), sometimes it was added to the sol0ution at start. Little quantities of Hg (~10^{-7} Mol/l) have the objective of increasing the wire loading while great quantities (~10^{-5} Mol/l) can create a superficial layer that blocks the Hydrogen into the Pd lattice so that the unloading is reduced or even stopped.

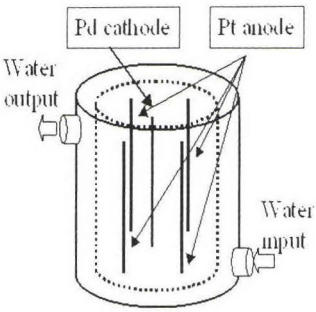

Figure 2 - Approximate scheme of the cell. The cathode and anode positions are shown.

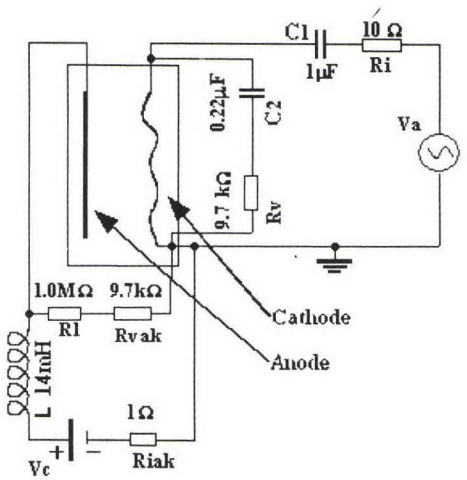

Figure 3 – The supply and measurement circuit. The right part is used to measure the wire resistance while the bottom part is used to supply the electrolytic current. See section 2.3 for details.

2.3 Power supply and measurement

Figure 3 shows the electrical circuit used in the experiments. The electrolytic current is generated by *Vc* and detected through the *Riak*. Anode-cathode voltage is measured through a voltage divider (*R1*, *Rvak*) in order to avoid excessive voltage input on the measurement multimeter. In order to measure the cathode resistance a sinusoidal current (frequency=50kHz) is supplied by generator *Va* and voltages are detected on the *Ri* and *Rv* resistors (*Rv* and *C2* are not strictly necessary, the voltage can be measured directly on the cathode). The inductance *L* and the capacitor *C1* avoid interactions between the two parts of the circuit.

2.4 Limits of the resistance measurement and temperature correction.

The greatest uncertainty on the R/R_0 measurement is caused by the temperature variation: $R=R_0 \cdot (1+\alpha T)$ where R is the resistance at temperature T, R_0 The resistance at 0°C and α the temperature-resistance coefficient that is a function of the loading ratio. During the loading the temperature could vary (usually less than 5°C) because of the electric power dissipated into the cell. So, in order to have a precise estimation of R/R_0 it was necessary to correct the raw data. This correction was precise, and usually negligible, when $0 \leq x \leq 0.7$ because α is well known in this range of loading ($\alpha \sim 2\text{-}4 \cdot 10^{-3}$ $°C^{-1}$) [1,6,7,8]. When $x>0.7$ the coefficient α is poorly known, so only a rough estimation of R/R_0 is possible. In this case a mean value around $4 \cdot 10^{-3}$ $°C^{-1}$ was used and an uncertainty of about 0.02 on R/R_0 is introduced for the typical temperature variation.

3 HYDROGEN LOADING RESULTS

The first set of experiments was performed with Hydrogen – i.e. light water. Most of the results of a previous set of measurement (see [3,8]), evidentiated the possibility of reaching very high loading ratio. These results were obtained using solutions with HCl, $SrCl_2$ and a "low" (10^{-7}-10^{-6} Mol) quantity of $HgCl_2$. The addition of more and more $HgCl_2$ (up to 1.5 10^{-5} Mol) could even block the Hydrogen inside the Palladium also after the end of the electrolysis. To sum up the results described in Ref. 3, it is possible:

- to reach very high loading with Hg-doped solution ($R/R_0<1.2$; $x>0.97$) but without complete reproducibility,
- to obtain high reproducibility of good loading, i.e. it is always possible to obtain $R/R_0<1.4$ and often we obtained $R/R_0<1.3$,
- to keep the wire loaded without electrolysis current by formation of a thin Hg superficial layer (few μm) using "high" Hg-doped (~10^{-5} Mol) solution,
- to measure physical characteristics of high H-loaded Pd. In particular the resistance-temperature coefficient was measured. It has a sharp increase when $x>\sim0.7$.

New trials have demonstrated the possibility to achieve $R/R_0\sim1.25$ without the use of $HgCl_2$. This shows uncertainty about optimal electrolytic composition.

The graph in figure 4 shows the loading result of an experiment performed with the following solution: 0.40l H_2O + $1.0\cdot10^{-4}$Mol HCl + $1.0\cdot10^{-4}$Mol $SrCl_2$; current density $J_{ak}=125$ mA/cm^2 , cathode-anode voltage $V_{ak}=30\rightarrow34$ V.

Relative resistance ratio R/R_0 and electrolytic current density (J_{ak}) are plotted as function of time in the same figure. In few minutes resistance ratio achieves maximum at 1.78 and then it quickly goes down to 1.65, then it slowly decreases down to $R/R_0\sim1.26$, in about 30 hours. This values are far below Baranowsky curve limit ($R/R_0=1.43$): we had certainly reached loading ratio $x=[H]/[Pd]>0.97$

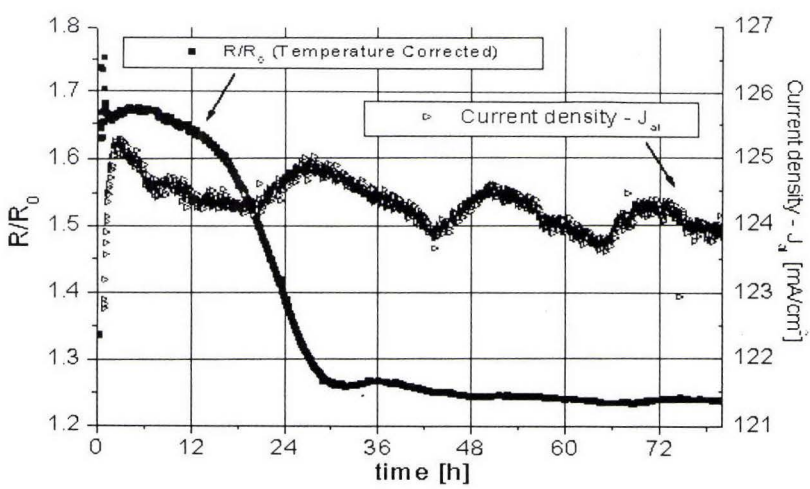

Figure 4 - Example of Hydrogen loading. The electrolysis current density (J_{ak}) and the loading ratio (R/R_0) are shown. See text and table 1 for more details.

4 DEUTERIUM LOADING RESULTS

The use of D instead of H, i.e. the substitution of light water with heavy water, isn't straightforward. In particular, the use of heavy water produces as a consequence: 1) less reproducibility of the results, 2) less loading ratio, 3) different behaviour with Hg-doped solution (it wasn't possible to keep Deuterium inside Palladium after electrolysis).

A possible cause of these results (worse than Hydrogen ones) is the lower purity of commercial heavy water in respect of bidistilled light water. Light water impurities are very low (chloride, phosphate, nitrate and sulphate <0.1 ppm; any metal<0.01ppm). In D_2O, instead, there is at least $KMnO_4$<10ppm and probably similar concentration of other impurities. A more precise quantitative analysis is not available yet.

A good example of loading is depicted in figure 5. It was obtained with a protocol almost equal to the one used for Hydrogen experiment shown in figure 4: solution 0.40l D_2O + $1.0 \cdot 10^{-4}$Mol HCl + $1.0 \cdot 10^{-4}$Mol $SrCl_2$; current density J_{ak}=130→140 mA/cm^2, cathode-anode voltage V_{ak}=27→34 V. Nevertheless, some differences can be noticed with respect to the light water experiment previously described. In particular, the loading ratio (for the minimum R/R_0~1.61) is only x~0.92. Moreover the resistance signal is much more noisy when R/R_0<~1.65. This effect couldn't be ascribed to the couple of deloading cycles performed. In fact this is a common procedure often performed and that sometimes grants an increased loading ratio. It is also important to point out the long-term stability of the loading (after 3 days the experiment was terminated). Other experiments with similar protocol gave similar results, in particular it was possible to reach R/R_0<1.70 with this kind of protocol in most of the cases.

The use of $HgCl_2$ with heavy water did not give easily reproducible results and it had a large dispersion of the loading ratio values.

An optimal loading protocol has not been found yet, because of the limited statistic

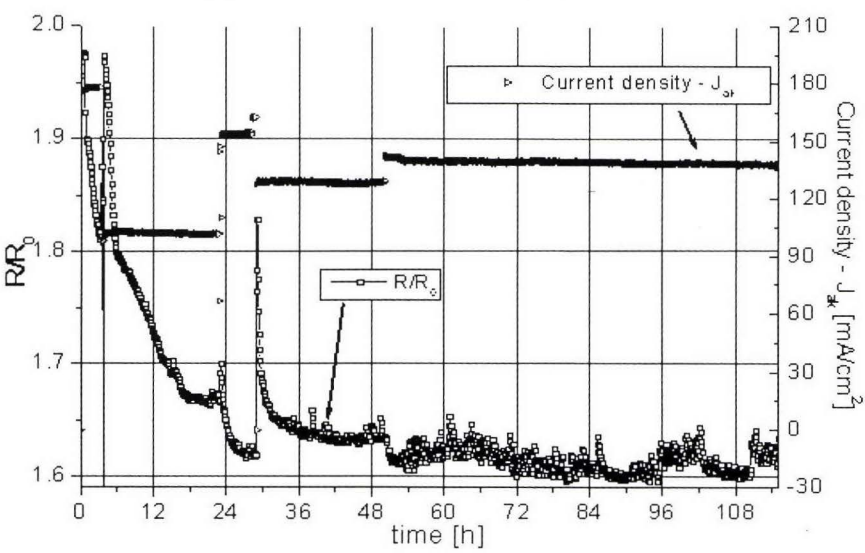

Figure 5 - Deuterium loading example. See text for other details about this experiment.

and the variability of the results. Anyway, this non-uniformity of the results could be due also to the non-uniform behaviour of the wire. Previous experiments performed with 2m long wires showed a different behaviour of adjacent pieces of wire during the loading even if the experimental condition were obviously the same for whole wire [3].

5 CONCLUSION

The goal of achieving high loading ratio [H]/[Pd]>0.97 (R/R0 =1.4) in thin wires of Palladium has been obtained through the loading method previously described. Nevertheless the reproducibility for achieving the highest loading ratios (R/R0 <1.3 i.e. [H]/[Pd]~1) is still not optimal.

The Deuterium loading system shows differences from Pd/H system and with this loading method it was possible to achieve and to keep a loading of x=[Pd/D]~0.95-0.96 (R/R_0~1.65-1.60) for a long time. According to widely accepted ideas, this result is a necessary condition for the onset of cold fusion mechanism.

Future development will analyse the calorimetric behaviour of high loaded Pd wires looking for excess heat production.

ACKNOLEDGEMENTS

We are grateful to Francesco Celani, Antonio Spallone and their entire group for the helpful discussions and suggestions.

REFERENCES

[1] P. Marini, V. Di Stefano, F. Celani, A. Spallone, *21° Secolo*, February 1999, p. 34 (in Italian).

[2] F. Celani et al., http://wwwsis.lnf.infn.it/pub/LNF-00-006(P).pdf, 2000.

[3] D. Azzarone, *"Il sistema palladio/idrogeno: procedure atte al raggiungimento di alti caricamenti"*, university thesis (in italian), 1999.

[4] M. Mc Kubre et al., *proc. ICCF4*, p. 5, 1994.

[5] A. Spallone, F. Celani, P.Marini, V. Di Stefano, A. Mancini, *proc. 4th Asti Workshop on Anomalies in Hydrogen/Deuterium loaded Metals, 1999.*

[6] F.Celani et al, *proc. of 4th Asti Workshop on Anomalies in Hydrogen/Deuterium loaded Metals*, 1999.

[7] P. Tripodi, M. McKubre, F. Tanzella, P. Honnor, 10, *proc. of 4th Asti Workshop on Anomalies in Hydrogen/Deuterium loaded Metals*, 1999.

[8] D. Azzarone, F. Fontana, D. Garbelli, *proc. of 4th Asti Workshop on Anomalies in Hydrogen/Deuterium loaded Metals*, 1999.

Conference Proceedings Vol. 70
"ICCF8"
F. Scaramuzzi (Ed.)
SIF, Bologna, 2000

Effects of Temperature on Loading Ratios of Hydrogen (Deuterium) in Palladium Cathodes under the Galvanostatic Condition

W.-S. Zhang [a,b], Z.-L. Zhang [a] and X.-W. Zhang [b]

[a] Institute of Chemistry, Chinese Academy of Sciences, P.O. Box 2709, Beijing 100080 P.R. China; E-mail: wszhang@a-1.net.cn; Fax: +86-10-62559373.
[b] Institute of Applied Physics and Computational Mathematics, P.O. Box 8009 Beijing 100088, P.R. China

Abstract

On the basis of the thermokinetics of the hydrogen (deuterium) evolution reaction and the thermodynamics of Pd+H(D) system, we analytically and numerically discuss effects of temperature on the loading ratio of hydrogen (deuterium) absorption into electrodes of β-phase PdH_x (PdD_x) under the galvanostatic charging condition. It is found that the change of the loading ratio with temperature depends on the absorption enthalpy, adsorption enthalpy and apparent activation energy of the exchange current density of the Tafel reaction. Our theoretical predictions fit the available experimental results well.

1. Introduction

It is verified experimentally that the anomalous excess heat production in the $Pd|D_2O$ electrolytic system depends on the D/Pd ratio, the space gradient of deuterium concentration and cell temperature etc. [1-3]. However, because not all of these variables are orthogonal, it is necessary to establish their dependent relation in further research. One of these relations is the loading ratio as a function of temperature [4-8]. Mengoli *et al* have found that the loading ratio of D in Pd, x_D decreases with temperature by a slope of $\partial x_D/\partial T \sim -1.1 \times 10^{-3}$ K^{-1} under the potentiostatic charging condition in the temperature range from 25 °C to 90 °C [4]. The same group have also found that $\partial x_H/\partial T \sim -1.6 \times 10^{-3}$ K^{-1} under the galvanostatic charging condition and $\partial x_H/\partial T \sim -8.7 \times 10^{-4}$ K^{-1} under the potentiostatic charging condition with the H_3PO_4 electrolyte from 25 °C to 175 °C [6]. In addition, Asami *et al* found that $\partial x_D/\partial T \sim -2.0 \times 10^{-3}$ K^{-1} from 25 °C to 80 °C [8]. Although these temperature effects can be explained qualitatively by the thermodynamics of Pd+H(D) system [9] and the kinetics of the hydrogen evolution reaction (HER) [10–13], the quantitative analysis is absent up to now. In this paper, we will deal with this subject in detail.

2. Model

Consider hydrogen absorption into a PdH_x electrode in the HER (taken to include D, the same below). At the outer surface, there are three steps, i.e. the Volmer, Tafel and penetration reactions taking place at the same time [10,11]. The rate of the Volmer step is the applied current density (CD) and the rate of the Tafel step is:

$$j_T = 2r^2 \Gamma_s^2 F\left\{A_{+T} f(1-\theta)^2 \exp\left(-\frac{E_{+T}}{RT} - \frac{U_s\theta}{RT}\right) - A_{-T}\theta^2 \exp\left(-\frac{E_{-T}}{RT} + \frac{U_s\theta}{RT}\right)\right\} \quad (1)$$

Because the penetration reaction is very rapidly, it is in pseudo-equilibrium [11] and we have the isotherm:

$$\frac{\theta}{1-\theta}\exp\left(\frac{U_s\theta}{RT}\right) = \exp\left(-\frac{\Delta S_{sb}}{R} + \frac{\Delta H_{sb}}{RT}\right)\frac{x}{1-x}\exp\left(\frac{U_b x}{RT}\right) \quad (2)$$

In Eqs. (1) and (2), A_{+T} and A_{-T} are the Arrhenius frequency factors of the rate constant for H_2 dissociation and H combination reactions; E_{+T} and E_{-T} are the corresponding activation energies; U_b is the non-ideal interaction energy of H in the bulk of the β-PdH_x, U_b = 44.9 kJ mol^{-1} for both H and D [9]; U_s is the heterogeneity energy of the Frumkin adsorption, its value depends on the additives in the electrolyte and pH value; f is the fugacity of H_2 gas; x is the H/Pd atomic ratio; r is the surface roughness factor; $\Gamma_s = 2.2 \times 10^{-9}$ mol H cm^{-2}, is the maximum H molar number of available sites per real unit area; θ is the fractional surface coverage of H on Pd. The other symbols have their usual meanings.

3. Results

3.1. Equilibrium state

Prior to detailed discussing the situation of HER, we focused on the equilibrium state. To be specific, the electrode reaction is confined to the normal condition of f = 1 atm and 0 °C ≤ T ≤ 100 °C. The first assumption means that the partial pressure of hydrogen is equal to that of circumstance, this can be realized through carrying out experiment under H_2 gas atmosphere or blowing hydrogen gas from the bottom of cell. Although many experiments are employed without the blowing H_2 gas and the initial state differs from this equilibrium state, the hydrogen bubbles produced in the HER makes the H partial pressure is approximately equal to 1 atm, hence the corresponding equilibrium state is the same as that in the hydrogen atmosphere. These choices of pressure and temperature ensure the Pd+H system is in the β-phase in equilibrium or in the HER.

We can obtain the exchange CD (per real unit area) of the Tafel reaction as a function of T. Contrary to one's expectation, it is the weak adsorption rather than the strong adsorption dominates the H absorption into the β-PdH_x electrode as verified experimentally and theoretically [10–12]. Therefore, the Frumkin adsorption reduces to the Langmuir type with $U_s\theta \to 0$ and $1 - \theta \to 1$. The exchange CD of the Tafel step is:

$$j_{0T} = 2\Gamma_S^2 F A_{+T} f_{H_2} \exp\left(-\frac{E_{0T}}{RT}\right) \quad (3)$$

with $E_{0T} = 2\Delta H_{gs} + E_{-T}$, is the apparent activation energy of j_{0T}, and it was observed that E_{0T} = 27 kJ mol^{-1} in 0.5 M H_2SO_4 [10]; ΔH_{gs} is the adsorption enthalpy of H on Pd.

It is easy to obtain the relationship between the hydrogen pressure and the loading ratio using Eq. (2) and the equilibrium result of Eq. (1):

$$f^{1/2} = \exp\left(-\frac{\Delta S_{gb}}{R} + \frac{\Delta H_{gb}}{RT}\right)\frac{x}{1-x}\exp\left(\frac{U_b x}{RT}\right) \quad (4)$$

with $\Delta S_{gb} = \Delta S_{sb} + R/2 \ln(A_{+T}/A_{-T})$ and $\Delta H_{gb} = \Delta H_{sb} + (E_{+T} - E_{-T})/2$. This equation is exactly the isotherm of H absorption into the β-PdH_x, it is found that $\Delta S_{gb} = -53.5$ and -53.1 J mol^{-1} K^{-1}, and $\Delta H_{gb} = -50.1$ and -47.7 kJ mol^{-1} for H and D, respectively. Although changes of entropy and enthalpy in each step may be influenced by the Pd surface property or solution composition, their sums must be constant values as are indicated by Eq. (4). The loading ratio changing with temperature under a fixed pressure is:

$$\frac{\partial x}{\partial T} = \frac{\Delta H_{gb} + U_b x}{RT^2\left(\frac{1}{x(1-x)} + \frac{U_b}{RT}\right)} \tag{5}$$

which is -1.0×10^{-3} K^{-1} for both H and D in Fig. 1, the curve $j = 0$. These curves are the isobar of H(D) absorption into the β-PdH_x (PdD_x) under 1 atm pressure.

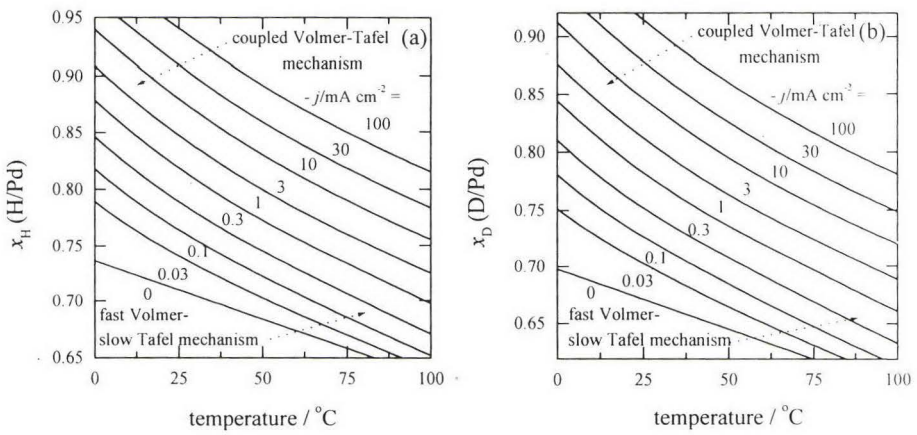

Figure 1. Effects of temperature on the loading ratio for (a) H, and (b) D absorption into a β-phase Pd|H(D) electrode under the galvanostatic charging condition. Current densities are shown besides each curve. The parameters: $A_{+T} = 6.24 \times 10^{11}$ cm^2 atm^{-1} mol^{-1} s^{-1}, $A_{-T} = 3.51 \times 10^{25}$ cm^2 mol^{-1} s^{-1}; $E_{+T} = 27$, $E_{-T} = 83$, $U_s = 15$ kJ mol^{-1}; $\Delta H_{sb} = -22$ and -19.8 kJ mol^{-1} for H and D respectively; $\Delta S_{sb} = 78.53$ J mol^{-1} K^{-1}; $r = 1$, $f = 1$ atm.

3.2. Fast Volmer–slow Tafel mechanism

Because there are two mechanisms of the HER, i.e. the fast Volmer–slow Tafel type at low CD in acidic solution and coupled Volmer–Tafel type in basic solution or at high CD in acidic solution, taking place on the Pd electrode, we will discuss the steady-state absorption in these two situations successively. For the first mechanism, the Tafel step is irreversible and the Volmer reaction is in pseudo-equilibrium, the value of θ is small and the adsorption can be simplified to the Langmuir type as in discussion about j_{0T}. Substituting Eq. (2) into Eq. (1) gives:

$$j = -j_{-T} = -2r^2 I_s^2 F A_{-T} \exp\left(-\frac{2\Delta S_{sb}}{R}\right)\left(\frac{x}{1-x}\right)^2 \exp\left(\frac{2\Delta H_{sb} + 2U_b x - E_{-T}}{RT}\right) \quad (6)$$

which describes x as a function of j. Hence we obtain the loading ratio changing with temperature:

$$\frac{\partial x}{\partial T} = \frac{\Delta H_{gb} + U_b x - E_{0T}/2}{RT^2\left(\frac{1}{x(1-x)} + \frac{U_b}{RT}\right)} \quad (7)$$

which is -1.2×10^{-3} K^{-1} for H and -1.5×10^{-3} K^{-1} for D in Fig. 1.

3.3. Coupled Volmer–Tafel mechanism

Consider the HER is far from equilibrium, both the Volmer and Tafel steps are completely irreversible. The adsorption is the Frumkin type at intermediate surface coverage, this means the exponent term is prominent in the hydrogen adsorption isotherm. Eliminating the factor $\exp(U_s\theta/RT)$ between Eqs. (1) and (2) gives:

$$j = -j_{-T} = -2r^2 I_s^2 F\theta(1-\theta)A_{-T} \exp\left(-\frac{\Delta S_{sb}}{R}\right)\frac{x}{1-x}\exp\left(\frac{\Delta H_{sb} + U_b x - E_{-T}}{RT}\right) \quad (8)$$

this equation describes the relation between j and x. We can obtain the loading ratio changing with T:

$$\frac{\partial x}{\partial T} = \frac{\Delta H_{gs} + \Delta H_{gb} + U_b x - E_{0T}}{RT^2\left(\frac{1}{x(1-x)} + \frac{U_b}{RT}\right)} \quad (9)$$

which is -2.4×10^{-3} K^{-1} for H and -2.7×10^{-3} K^{-1} for D in Fig. 1. In the deduction, the contribution originated from the term $\theta(1-\theta)$ is omitted as it is a slowly varying quantity.

Fig. 1 shows x changing with T based on Eqs. (1) and (2) under the galvanostatic charging condition. The related parameters, noted in the caption of Fig.1, result in $\theta_0 = 0.01$ and $j_{0T} = 0.01$ mA cm^{-2} at 298.15 K. These choices ensure the adsorption in equilibrium is weak; the HER is along the fast Volmer–slow Tafel mechanism while $-j \leq 1$ mA cm^{-2} or the coupled Volmer–Tafel mechanism while $-j >> 1$ mA cm^{-2} around the ambient temperature. The activation energies are chosen to ensure that $E_{0T} = 27$ kJ mol^{-1}, $\Delta H_{gb} = -50$ kJ mol^{-1} for H and -47.8 kJ mol^{-1} for D as were observed experimentally [9,10]. All of these parameters are adjusted to simulate the HER in the aqueous acidic solution under the circumstance pressure although our method and conclusion are beyond this confinement.

We find the amplitude of $\partial x/\partial T$ increases with increasing CD and/or decreasing temperature. The dependence of $\partial x/\partial T$ on T is easy to understand by Eqs. (5), (7) and (9) in which the amplitude of $\partial x/\partial T$ is inversely proportional to T. As far as the effect of CD is concerned, we find the HER changes from the equilibrium state to the fast Volmer–slow Tafel mechanism and up to the coupled Volmer–Tafel mechanism with increasing CD, and corresponding $\partial x/\partial T$ is expressed by Eqs. (5), (7) and (9), respectively. Because the terms $\Delta H_{gb} + U_b x$, ΔH_{gs} and E_{0T} in the numerators have the same sign (< 0), so the increase of $|\partial x/\partial T|$ with CD is obvious.

The change of x with T has two origins: one is the thermodynamic contribution as the isobar shown in Fig. 1 or indicated by Eq. (5) and the same term appeared in Eqs. (5), (7) and (9); another is caused by the kinetic process. A crude but intuitive explanation can understand the reasons of x changing with T. Because x is determined by the relative CD, j/j_{0T} [12], so changes of j/j_{0T} reflect the change of x in some way. For the galvanostatic charging, j_{0T} increases with T; this makes j/j_{0T} decreases with T, hence x decreases some more rapidly than in the equilibrium case.

By comparison our theory with experimental results in Ref. [6,18], we find that $\partial x_H/\partial T \sim -1.6 \times 10^{-3}\ K^{-1}$ and $\partial x_D/\partial T \sim -2.0 \times 10^{-3}\ K^{-1}$ under the galvanostatic charging condition lie in the corresponding ranges of our results shown in Fig. 1, although the relevant experimental parameters are not available. This indicates our theory is appropriate.

4. Discussions

In this paper, we specifically discuss the situation of HER in the acidic solution; there is a change of HER mechanism from the fast Volmer–slow Tafel type to the coupled Volmer–Tafel type with increasing CD. But for the basic solution, the valid CD range for the fast Volmer–slow Tafel mechanism is very narrow even disappears; otherwise, the coupled Volmer–Tafel mechanism dominates the HER in a wide CD range due to a small value of j_{0V}/j_{0T} and a large heterogeneity energy U_s [10]. Of course, our method and results can be applied to this situation with some parameters modified. On the other hand, additives and Pd alloy electrodes are always used to improve the electrode performance for H absorption in experiments. Their effects can be manifested by the same formulae with some parameters adjusted as well.

In the paper, we mainly discuss the loading ratio changing with j under the galvanostatic charging condition. However, our theory can be applied to the problem for the maintenance the loading ratio by increasing the amplitude of j at high temperature. The solution is directly given by Eqs. (6) and (8).

It must be pointed out that our theory is more phenomenological than fundamental. A general treatment should be based on the absolute rate theory and consider subtle effects of temperature on all aspects of the Pd|H electrode process, *e.g.* the temperature dependence of solute activity, the activation free energy of each step and other related issues. Of course, it needs more experiment details as well. However, our results give the most primary effects and there are some experiment evidences supporting our conclusions. Although the systematic experimental study on this subject is absent up to now, we hope our work can stimulate further researches on this issue.

Acknowledgements

The work is supported by the Natural Science Foundation of China under Grant No. 19455001, President Innovation Foundation in Chinese Academy of Sciences, Pan-Deng Project of Department of Science and Technology of China under Grant No. 95–YU–41 and Foundation of China Academy of Engineering Physics.

References

[1] MCKUBRE M.C.H., CROUCH-BAKER S., RILEY A.M., SMEDLEY S.I. AND TANZELLA F.L.: in Frontiers of Cold Fusion, Proc. 3rd Int. Conf. on Cold Fusion.

edited by H. IKEGAMI. Nagaya, Japan, October 21-25, 1992, (Universal Academy Press, Tokyo) 1993, pp. 5.
[2] KUNIMATSU K., HASEGAWA N., KUBOTA K., IMAI N., ISHIKAWA M., AKITA H. AND TSUCHIDA Y.: *ibid*, pp. 31.
[3] MCKUBRE M.C.H., CROUCH-BAKER S., HAUSER A.K., SMEDLEY S.I., TANZELLA F.L., WILLIAMS M.S. AND WANG S.S.: in Proc. 5th Int. Conf. on Cold Fusion, Monte-Carlo, Monaco, April 9-13,1995, pp.17.
[4] MENGOLI G., FABRIZIO M., MANDUCHI C., MILLI E. AND ZANNONI G.: J. Electroanal. Chem., 390, (1995) 135.
[5] WARK A., CROUCH-BAKER S., MCKUBRE M.C.H. AND TANZELLA F.L.: J. Electroanal. Chem., 418, (1996) 199.
[6] BERNARDINI M., COMISSO N., FABRIZIO M., MENGOLI G. AND RANDI A.: J. Electroanal. Chem., 453, (1998) 221.
[7] AKITA H., TSUCHIDA Y., NAKATA T., KUBOTA A., KOBAYASHI M., YAMAMOTO Y., HASEGAWA N., HAYAKAWA N. AND KUNIMATSU K.: in Proc. 5th Int. Conf. on Cold Fusion, edited by T.O. PASELL AND M.C.H. MCKUBRE, Vol. 1, December 6-9, 1993, Lahaina, Maui, HI, (Electric Power Research Institute, Palo alto, CA) 1994, pp. 21-1.
[8] ASAMI N., SENJUH T., UEHARA T., SUMI M., KAMIMURA H., MIYASHITA S. AND MATSUI K.: in Proc. 7th Int. Conf. on Cold Fusion, Vancouver, British Columbia, Canada, April 19-24, 1998, pp. 15.
[9] WICKE E. AND BRODOWSKY H.: in Hydrogen in Metals II, Application Oriented Properties, edited by G. ALEFELD AND J. VÖLKL, Topics in Applied Physics, vol. 29, (Springer, Berlin) 1978, pp. 73.
[10] ENYO M.: in Kinetics and Mechanism of Electrode Processes, edited by B.E. CONWAY, J.O'M BOCKRIS, E. YEAGER, S.U.M. KHAN AND R.E. WHITE, vol. 7, (Plenum Press, NY) 1983, pp. 241.
[11] ZHANG W.S., ZHANG X.W. AND LI H.Q.: J. Electroanal. Chem., 434, (1997) 31.
[12] ZHANG W.S., ZHANG Z.L., ZHANG X.W. AND WU F.: J. Electroanal. Chem., 474, (1999) 123.
[13] ZHANG W.S., ZHANG Z.L. AND ZHANG X.W.: J. Electroanal. Chem., 474, (1999) 130.

Conference Proceedings Vol. 70
"ICCF8"
F. Scaramuzzi (Ed.)
SIF, Bologna, 2000

Loading Palladium with Deuterium gas while lowering temperature

E. Del Giudice, A De Ninno, A. Frattolillo,
G. Preparata, F. Scaramuzzi, P. Tripodi
ENEA – Centro Ricerche, C.P. 65 – 00044 Frascati

1. Introduction

It is well known that the equilibrium value of the D/Pd ratio in Palladium deuteride is an inverse function of temperature and a direct function of pressure: the graph in Fig. 1a, taken from ref.1, together with the derived Fig.1b, illustrates this issue. It is also well known that the diffusion coefficient (in this case, for D in Pd) decreases as temperature decreases.

The experiment that we have designed consists of increasing the charging ratio of D in a Pd sample immersed in a D_2 gas atmosphere, by lowering the temperature of the sample at a substantially constant pressure. In order to reduce the negative effect of the decreasing diffusion coefficient, a thin film of deposited Pd has been selected as the sample. Its geometry – a long (1 m), flat (2 x 50 μm^2) strip – allows also for the application of an electric difference of potential at its terminals, in order to explore the Coehn-Aharonov (Preparata) effect (see Cola et al. in these Proceedings).

The amount of D_2 absorbed can be measured by the change of pressure in a closed circuit of known volume and temperature distribution, part of which consisting of the experimental cell. The measurement of the electric resistance of the Pd strip gives complementary information about its loading.

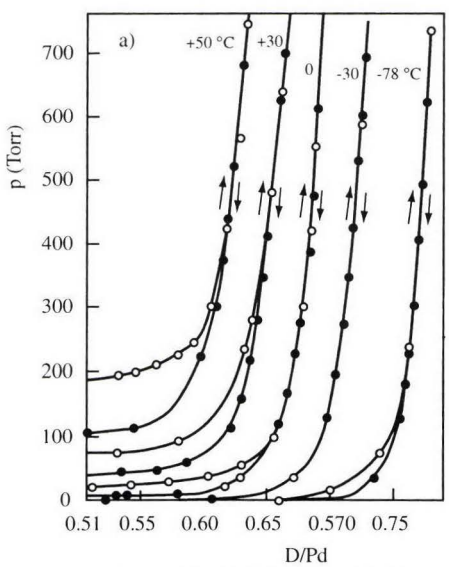

Fig.1a. Isotherms for Pd-D in the β phase (1)

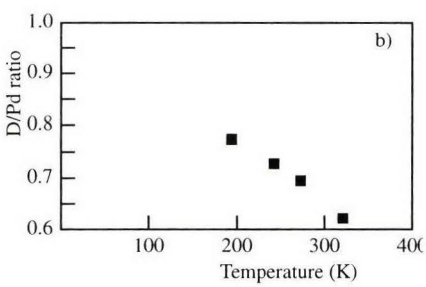

Fig.1b. Data obtained from Fig.1a by cutting the graphs at p = 500 torr

The first test here reported was mainly intended to check the cryogenic system, and to evaluate the possibility of a sensitive calorimetry. Eventually, preliminary assessments of the system behavior were made using measurements of the resistivity of Palladium as a function of temperature.

The temperature can be lowered from room temperature to about 10 K by isothermal steps. A cryostat based on a closed cycle refrigerator (Cryodyne) is used.

2. The cryostat

The Cryodyne closed cycle refrigerator (2) is structured in two stages: the first has a minimum temperature of about 50 K, and the second a minimum temperature of about 10 K. For both, the application of a thermal load shifts upwards the minimum temperature: typically, a heat load of 10 W on the second stage will shift its minimum temperature to about 20 K.

The cryostat has been designed keeping in mind the typical run for this type of measurement. Starting from room temperature, the Pd sample immersed in a D_2 gas atmosphere can be cooled down to the minimum possible temperature, in successive steps, in each of which thermodynamic equilibrium will be reached. This requires long duration (up to hours) for each step. Once at regime, for each step the temperature will be uniform in the experimental cell to better than 0.1 K. Thus, the cryostat has to be able to operate continuously for days, so as to reach constant and uniform temperatures throughout the whole experimental range quoted above.

Figure 2 shows a schematic drawing of the cryostat. A high thermal conductivity shield, S_1, is attached to the first stage and encloses the rest of the apparatus: it has the task of shielding the apparatus from radiation coming from the room temperature walls of the vacuum can, when working at low temperatures. Another high thermal conductivity shield, S_2, is weakly attached to the second stage: it is mechanically attached with low thermal conductivity materials, but there is also a tailored heat resistance, R_1, consisting of a copper wire of appropriate size. The same kind of thermal link is established between this shield and the cell: also here there is a tailored heat resistance, R_2, besides the low conductivity mechanical connection. This second shield represents a uniform temperature environment for the cell, which facilitates its thermoregulation. Thermometers and heaters are located both on the second shield, S_2, and on the cell. These constitute the basic elements for thermoregulating independently the two elements: commercial Lake-Shore instruments (3) have been used. The operation is illustrated as follows: take, for example, the maximum temperature required for the cell, say 300 K. With the Cryodyne operating, and thus with the first stage at 50 K and the second at 10 K, the S_2 shield is brought and thermoregulated at a temperature slightly lower than the cell, say 280 K: it has been calculated and checked experimentally that this requires dissipation of a power of about 5 W on the S_2 heater, which is a quite acceptable thermal load for the Cryodyne second stage. The cell is then thermoregulated at 300 K: in order to achieve this, a power of about 0.5 W has to be dissipated in the cell heater. We will show below how this mode of operation allows accurate calorimetric measurements to be made. Once the measurement at this temperature has been performed, the set points of the two thermoregulators are

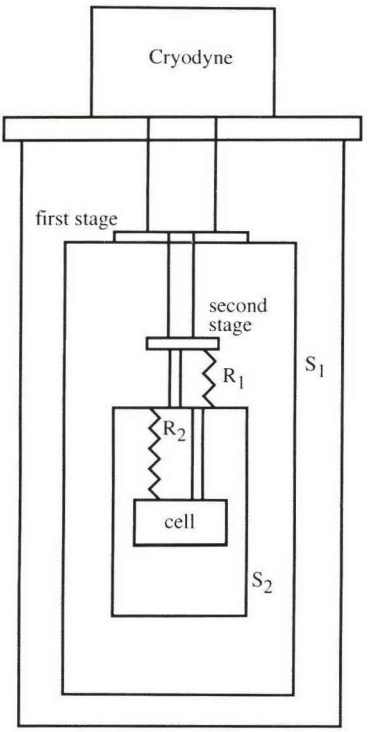

Fig. 2. Schematic drawing of the cryostat

displaced to the following (lower) temperature step: it takes a few hours to reach thermal equilibrium at a new temperature.

The tests performed up to now have shown a satisfactory performance of the cryostat, permitting work at all temperatures from 300 to 35 K (in order to reach still lower temperatures, a second thermal shield will have to be added). In the whole range the cell temperature has been found to be constant with an error of $\pm$ 0.02 K, even for periods as long as many days.

3. Calorimetry

It has been noted that the temperature of the cell is intentionally kept higher than that of the S_2 shield (by 5 to 20 K, depending on the temperature range). This implies that a certain amount of power be dissipated on the cell in order to maintain this temperature difference, typically of the order of hundreds of mW's. If some unknown source of heat appears, the power required for the thermoregulator to keep that temperature constant will decrease: the measurement of such a change in power is then the measurement of the unknown power. In the example shown in Fig. 3 the temperature of the cell and the power on its thermoregulator are reported as a function of time. The temperature of the cell was

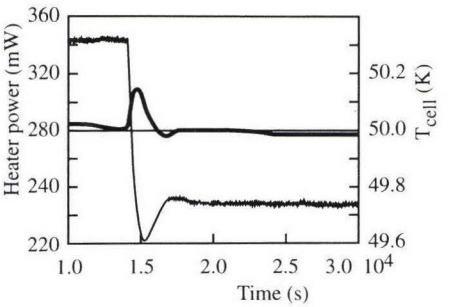

Fig.3. The calorimetric features of the system: a supplementary power is applied at t = $1.4x10^4$ s, and the power of the thermoregulator heater is decreased by the same amount. The temperature has a small transient increase.

50 K (the temperature of S_2 was 35 K), and the power on the cell was initially 342 mW. At a defined time ($1.4x10^4$ s) a supplementary heat power was added, by applying a voltage of 15 V to the Pd strip, whose resistance was roughly 2000 Ω. The temperature had a transient change (5 minutes) of about 0.1 K due to the different location of the thermometer and the source of heat, eventually returning to its original value; the power on the thermoregulator showed a decrease of 114 mW, as expected. Note that the sensitivity of the method is of a few mW's. This technique should therefore allow the detection of small heat excesses where cold fusion effects are present.

4. Measurement of charging ratio

The aim of the experiment is to measure the charging ratio D/Pd of the sample as a function of temperature. The objective is to have D_2 gas in a closed system, consisting of the cell together with a second volume at room temperature. This second volume (including the dead space of the pressure meter) is larger than that of the cell and a capillary tube connects the two parts. With a decrease of temperature, the pressure will change, both because of the change in temperature of the gas in the cell, and because of the absorption of D_2 in Pd. Calculation of the first effect, and subtraction from the total change in pressure, allows the measurement of the amount of D_2 absorbed by the Pd sample, thereby providing an absolute measurement of the D/Pd ratio. In order to be able to make this correction, the cell and the room temperature volumes must be accurately thermoregulated (the capillary tube, in which a temperature gradient will be established, will impose a small correction, presumably within the acceptable error). In the application of the system, "blank experiments" (runs without the Pd film) will provide the base line behavior with all necessary corrections, including change in the adsorption of D_2 on the walls of the system.

The small amount of Pd used in the present geometry (in the order of 1 mg) requires a very high accuracy in the measurement of the pressure: with the volumes presently chosen, the change of D/Pd ratio from 0.6 to 1.0 (the starting value will be reached at room temperature) will correspond to a change in pressure of 5 mbars, which requires in turn work at rather low D_2 pressures. One can foresee that this deficiency can be overcome

using a differential system, with two identical cells (and cell volumes) initially at the same pressure, one of which is a "blank cell" (no Pd); in this case the difference in pressure between the two cells would be measured as a function of temperature. Such a system should allow the use of relatively high pressures, but requires high precision in its construction. A further option is to increase the amount of Pd used in the experiments. Both of these modifications are currently being investigated.

The pressure meters available at the time of the measurements reported here did not have sufficient accuracy to allow the determination of absolute D/Pd ratios. We have therefore worked instead at a constant pressure of 1 bar and have confined the measurements to those of the electrical resistance which are reported in the next section.

5. Measurement of resistance

The Pd film was deposited on a glass square plate, in what is termed a bustrophedic configuration: the total length was about 1 m, the section of the film being 2 x 50 μm^2. The film was divided in 5 sections, so that the resistance of each section could be measured, together with the total resistance. Fig. 4 shows the design of the system. A constant voltage was applied across the film, the current flowing in it being measured, as well as the potential drops on each section. Typical values are 1 V for the potential, and hundreds of ohms for the resistance of each section. Here we will report data of one of the sections, which is similar to the behavior of all the others.

In the preliminary test reported here the system was first cooled from room temperature to the minimum temperature of 30 K with the cell under vacuum. The resistance of the Pd film was measured, in order to define the temperature coefficient for this particular sample. The graph in Fig. 5 shows the change in resistance of one of the sections: the average value of the temperature coefficient of the resistivity is 0.0031, which is not far from the values found in the literature (0.0033 - 0.0037).

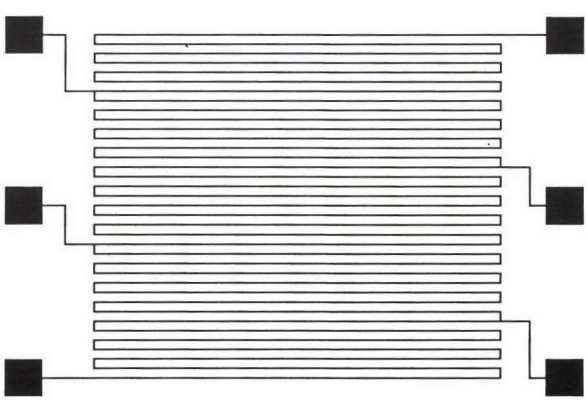

Fig. 4. The "bustrophedic" pattern of the Pd film

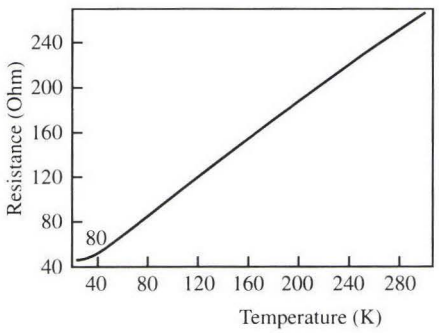

Fig. 5. The change of the resistance of one of the sections of the Pd film, under vacuum, as a function of the temperature T.

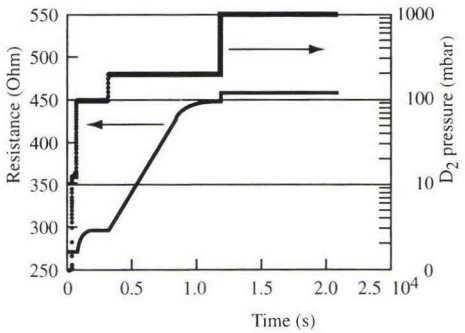

Fig. 6. The change of the resistance of the same section as in Fig. 5 as a function of time, during the procedure of gas loading, at different pressures; the values of the pressure are also reported. The temperature of the system was 300 K.

The sample was then heated again to 300 K, and at this temperature D_2 gas was admitted to the cell circuit. This was done step by step, referring to 4 different values of the gas pressure: 10, 100, 200, 1000 mbar.

The graph shown in Fig. 6 shows the change in resistance of the same section as in Fig. 5 as a function of time; the values of the pressure are also reported. It can be seen that there was no detectable change at 10 mbar while the maximum change was obtained between 100 and 200 mbar.

The measurement of the D/Pd ratios, as outlined in section 4, is currently being investigated.

Acknowledgments: the authors want to express their appreciation and warm gratitude to Mr. Luciano Mori for his skilled contribution to the construction and test of the apparatus.

Bibliography

1. S.E. Segre, P. Batistoni, L. Bertalot, L. Bettinali, M. Martone, S. Podda, A search for neutron emission from deuterated palladium, "Understanding Cold Fusion Phenomena", Conference Proceedings, Vol 24, The Italian Physical Society, 155 (1990).
2. CTI-Cryogenics, USA, Cryodyne Cryocooler, model 1020C.
3. Lake Shore Cryotronics, Inc., USA, Temperature Controller, model DRC

CHAPTER 5.

DETECTION OF NUCLEAR EMISSIONS

Conference Proceedings Vol. 70
"ICCF8"
F. Scaramuzzi (Ed.)
SIF, Bologna, 2000

Study of the Neutron and γ-Emission From the Palladium-Deuterium System in the Process of the Transformation of the Crystalline Structure.

V. D. Dougar-Jabon*, V. I. Kariaka**, N. V. Samsonenko**

*Escuela de Fisica Universidad Industrial de Santander, Bucaramanga, A. 678, Colombia
** Peoples `Friendship University of Russia, Moscow 117198, Russia

Abstract.

Gamma radiation and neutron emission under the different conditions stimulating the transformation in the palladium – deuterium crystalline system were examined. In the experiments the process of the multiple recycles of $\alpha \leftrightarrow \beta$ transition, the primary recrystallization at t^0=(300-500) ^{0}C and the accumulative recrystallization at t^0=(500-800) ^{0}C were studied. The neutron emission from the Pd sample was detected during the accumulative recrystallization. No γ - radiation from Pd –D system was discovered in all the experiments.

I. Introduction .

The deuteron acceleration in the crystalline structure can occur during the crystalline transformation of different types. The crack and break formations in the crystal can stimulate the parametric divergent oscillations and the increase of particles energy in the layers of atoms near the crack boundary [1]. The charged particles in the region of a break can gain the energy sufficient to start the reaction of D+D nuclear fusion if the ions of deuterium are present in the region of material break. The analysis of the model of ions acceleration in the crystals allowed to clear up that the similar phenomena can appear during the transformation of the crystalline lattice in the processes of phase transition or polarization reversal, i. e. without crystal destruction [2]. The theoretical investigations permitted to create a rather general model of formation of energetic particles during the transformation of the crystalline lattice. From the general point of view it is clear, that the process of the particles acceleration in the crystalline structure is determined by a) the system geometry, b) the characteristics of the energy supply to the particles, c) the accelerated particles density. Several experimental investigations were carried out for verification of the theoretical conclusions. The experiments with the deuterated ferroelectric crystals of DTGS (the system geometry and the

deuterium density were not changed considerably, the energy supply to the particles was determined by the polarization reversal) and $LiTaO_3$ (the deuterium density was changed) have shown a small additional (over background) neutron emission from the samples that possibly was due to the deuteron acceleration in these crystals [3]. In the further experiments with the ferromagnetic materials [4] (the energy supply was determined by the magnetization reversal of the samples) the neutron emission from the samples was not discovered possibly because of the poor density of deuterium in the samples. Based on the analysis of these experimental results the palladium – deuterium system was chosen for the further investigation. The properties of Pd are rather promising for the acceleration of deuterium particles. First of all the Pd is able to absorb up to 70 at % of hydrogen under the normal conditions. Furthermore during the hydrogen absorption Pd changes considerably its crystalline structure. In this way in Pd – D system it is possible to change the deuterium density in the wide range. The generation of the defects and lattice distortion during the cycles of deuterium absorption – desorption leads to the variation of the system geometry, the lattice transformations can supply the energy to the deuterium particles.

II. Transformation of the crystalline structure in Pd – H system.

The properties of palladium – hydrogen system are well-known. The β-phase, created during the hydrogen absorption, possesses a grater specific volume. Because of this fact the internal pressure in the crystal augments and that leads to the essential growth of the dislocation density and lattice distortion in α - and β - phases as well. The properties of Pd-H system depend substantially of the temperature. Up to 100 ^{0}C at atmospheric pressure there are no considerable changes of the material structure. At 100-150 ^{0}C no substantial desorption of hydrogen occur but $\beta \rightarrow \alpha$ transition begins and the amount of the α-phase augments. It is important to notice that during the $\beta \rightarrow \alpha$ transition the material inherits the β- phase defects and its additional production continues. At 150 ^{0}C the hydrogen desorption starts, the $\beta \rightarrow \alpha$ transition accelerates. This process is finished at 300 ^{0}C on the whole. The multiple $\alpha \leftrightarrow \beta$ transition in the temperature range mentioned above leads to the considerable accumulation of the crystal distortion. If later on the sample is exposed to annealing at 300 ^{0}C the process favors the development of the small crystallites arising all over the volume of the large crystallites initially created in palladium [5]. Annealing at 400 ^{0}C leads to the further development of the primary recrystallization. Above 500 ^{0}C the accumulative recrystallization takes place, in consequence the dimension of the crystallites augments 7-10 times. To obtain the large crystallites in the sample the annealing at (800-900) ^{0}C during several hours is necessary.

III. Experiments with palladium – deuterium system.

In the experiments the possibility of deuteron acceleration was studied under the different conditions stimulating the transformations in the palladium – deuterium system:

1. The process of the multiple recycles of deuterium absorption up to 70 at.% in the gaseous phase at P=760 Torr , t^0= 100 ^{0}C and the gas desorption at P=10^{-3} Torr and t^0= 200 ^{0}C.

2. The primary recrystallization of the sample at t^0= (300-500) ^{0}C after several $\alpha \leftrightarrow \beta$ transitions.
3. The accumulative recrystallization at t^0= (500-800) ^{0}C.

The palladium samples were of the size of few millimeters and its total mass was equal to 3,7 g. The samples preparation consisted in its degassing and annealing at t^0= 800 ^{0}C during 5 hours. Then the samples were saturated with deuterium in a quartz chamber furnished with the next components:

- Turbomolecular pump to create a vacuum of $1 \cdot 10^{-5}$ Torr.
- Injection system to fill the chamber with deuterium at pressure (0,01-1,0) at.
- Heater to rise the samples temperature.

A quantitative characteristic of deuterium absorption was a reduction of a gas pressure in the quartz chamber. Two blocks consisting of 10 proportional He^3 counters were used for neutron registration. A 1024 channel pulse – in – height discriminator served for detection of the amplitude distribution signals. The total efficiency of neutron registration was estimated as 3% in accordance with measurements made with a 600n/s Cf^{252}- source. 3 NaI(Tl) detectors of γ - radiation were used as diagnostic devices of the possible electromagnetic radiation from the samples. The efficiency of the registration system was equal to 45% for the energy 60 Kev, 4% for 662 Kev and 1,2% for 1800 Kev. The installation permitted to detect neutron – neutron and gamma – gamma coincidence during the time of 500 μs. In the experiments it was possible (taking into account the devices geometry and the background level) to defect with 90% confidence level the γ - radiation from the Pd samples not less than 730 signal/s and neutron emission – 1 neutron/s. A principal scheme of the experimental devices is shown in Fig. 1.

The neutron emission and γ-radiation were detected during the successive intervals of 10 minutes. The control experiments consisted in the background level registrations in different cases (without samples in the camera, or with the samples, saturated by hydrogen). The typical results of neutron registration taken during the experiments on $\alpha \rightarrow \beta$ transition, $\beta \rightarrow \alpha$ transition, primary and collective recrystallization is shown in Fig.2. The analysis of the neutron measurements made it clear that during $\alpha \leftrightarrow \beta$ transitions and primary recrystallization there were no substantial deviations from the background level, and only at collective recrystallization it was possible to notice the growth of the neutron emission from the Pd samples. For the verification of the discovered effect the series of experiments following in the interval of few days were carried out. The palladium saturation by deuterium was within (8÷30) at. %. The experiments demonstrated a good reproducibility of the effect (Fig. 3). As a rule the neutron emission increased in (20-60) min after the heater was switch on and sample temperature reached 800 ^{0}C. The effect continued (10-20)min.

In all the experiments the γ - radiation from the Pd – D system was not discovered (Fig. 4). Nor γ - radiation neither neutron emission were discovered in the palladium – hydrogen control experiments.

Conclusions

In the experiments with deuterium the neutron and γ - emission from the palladium samples was not detected in the processes of $\alpha \leftrightarrow \beta$ transition and primary recrystallization. An excess of neutron emission above the background level (~80%) with a good

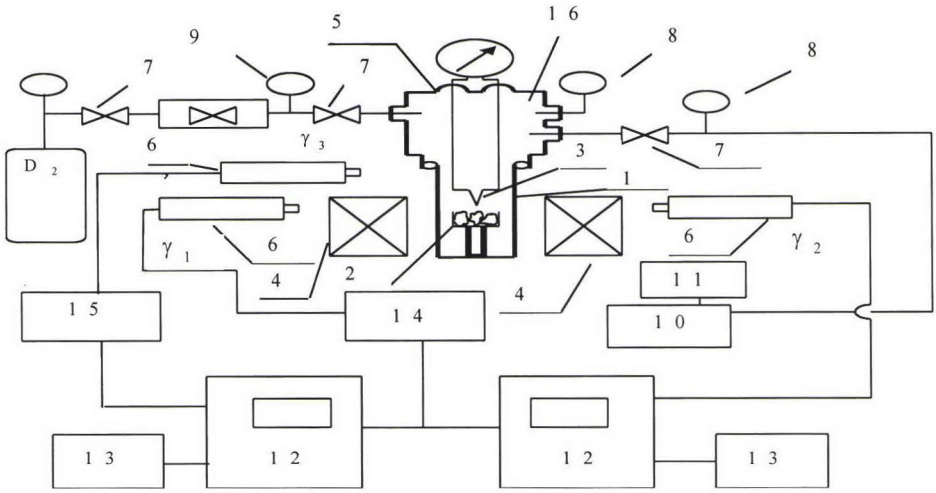

Fig. 1. A principal scheme of the experimental devices. 1-quartz reaction chamber; 2 - Pd samples; 3 - thermocouple; 4 - He^3-detectors with paraffin moderator; 5 - lead – in of thermocouple; 6 – NaI detectors of γ-radiation; 7 – pressure regulators; 8 – manometers; 9 – vacuummetre; 10 – turbomolecular pump; 11 – rough pump; 12 – pulse-in-height analyses; 13 – digital typer; 14 – coincidence scheme; 15 – pulses generator; 16 – upper part of the reaction chamber.

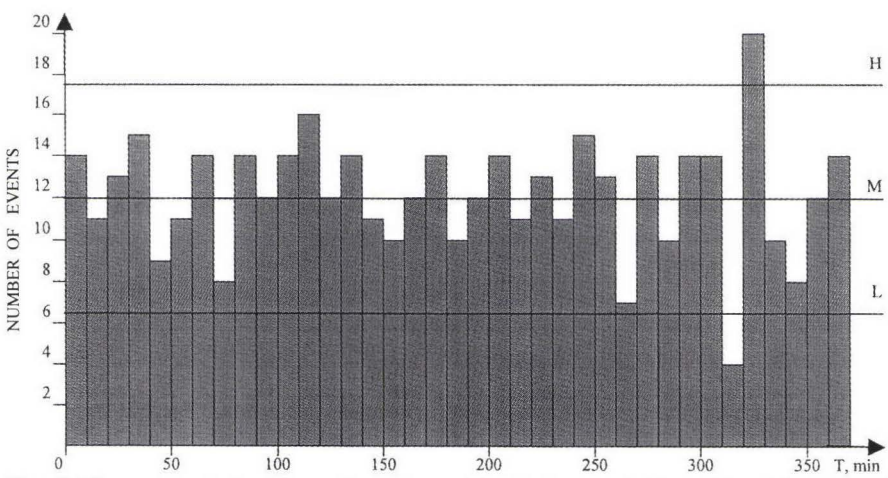

Fig. 2 Neutron emission from the Pd samples during α→β transition (30-100) min, β→α transition (100-210) min, primary recrystallization (210-320) min, collective recrystallization (320-350) min. M is the average background level, H and L are the limits of the background variation at 90% confidence levels.

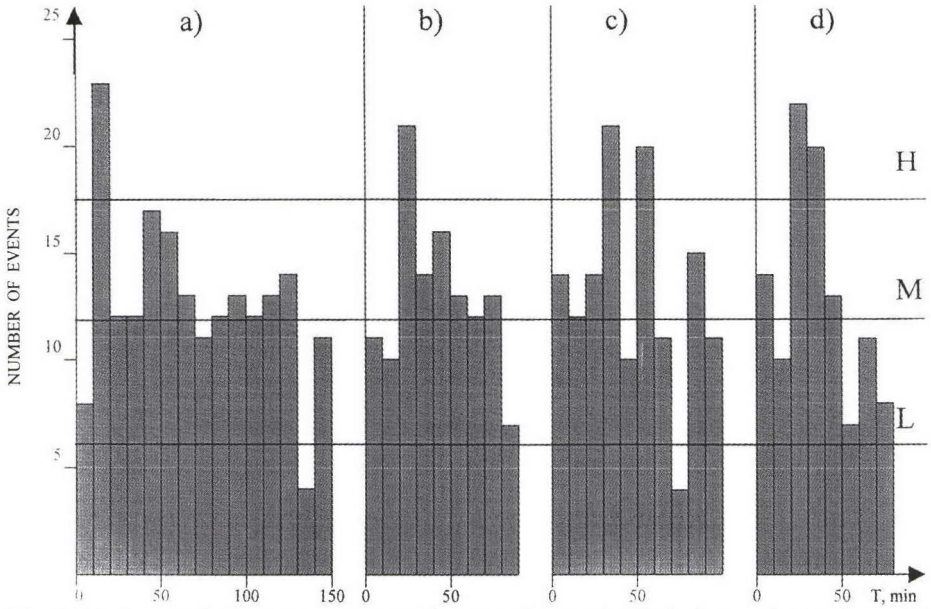

Fig. 3. Neutron emission measurements in 4 experiments (with the intervals 2-4 days). Points "0" in the pictures correspond to the beginning of samples heating. Pictures a), b), c), d) correspond respectively to different values of initial saturation (26 at % D; 8,6 at % D; 8,4 at % D; 9,6 at % D).

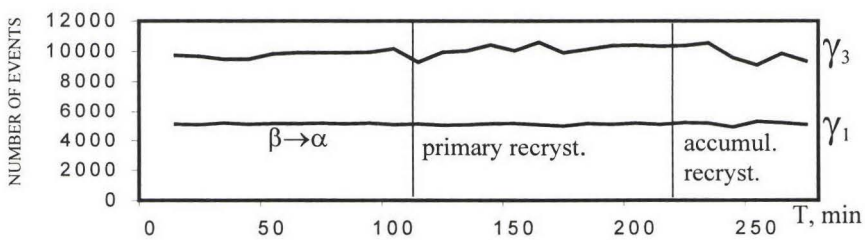

Fig. 4. Results of the γ - measurements during $\beta \rightarrow \alpha$ transition (0-110)min, primary recrystallization (110-220)min, accumulative recrystallization (220-250)min. γ_1 – signals from the reactor chamber protected by the Pb shield. γ_3 – the background level.

reproducibility was discovered during the Pd – D experiments in the temperature range corresponding to the collective recrystallization (500-800) ^{0}C. The effect was observed after the single cycle of $\alpha \leftrightarrow \beta$ transition. The deuterium concentration in Pd samples before heating was equal to (8-30) at.%. The duration of the effect did not exceed (10-20) min. The change of the experimental conditions (grater initial deuterium concentration in Pd, recrystallization in the vacuum etc.) reduced the effect or led to its disappearance.

References

[1] G. V. Fedorovich. Sov. Phys. JTP. V 63, N10. p. 64 (1993)
[2] G. V. Fedorovich Transaction of Fusion Technology, V. 26 N4T, part 2, p. 474-479 (1994)
[3] G. V. Fedorovich, V. D. Dougar-Jabon, V. I. Kariaka, N. V. Samsonenko
Proc. of the 2-nd Russian Conf. on Cold Fusion, Moscow, p. 123-131, (1995)
[4] V. D. Dougar-Jabon, V. I. Kariaka, N. V. Samsonenko
Proc. of the 5-nd Russian Conf. on Cold Fusion, Moscow, p. 87-92, (1998)
[5]V. A. Goltsov. Mater. Sci. and Eng., V. 49, N2, p. 109-125, (1981)

Conference Proceedings Vol. 70
"ICCF8"
F. Scaramuzzi (Ed.)
SIF, Bologna, 2000

DIRECT OBSERVATION AND EXPERIMENTAL INVESTIGATION OF THE PROCESS OF GAMMA-DECAY CONTROLLING IN QUANTUM NUCLEONICS

V. I.Vysotskii[1], A. A.Kornilova, A. A. Sorokin, V. A. Komisarova, S. I. Reiman, G.K. Riasnii
[1]Kiev Shevchenko University, Kiev, Ukraine; [2]Moscow State University, Moscow, Russia

Abstract
The aims of the present experiments were direct observation and investigation of the controlled gamma-decay of radioactive nuclei by delayed gamma-gamma coincidence method. In the experiments with gamma-source Co^{57} (Fe^{57*}) and with gamma-absorber made of stable Fe^{57} isotope we have discovered the change (increase) of radiative life-time of excited nucleus (in relation to resonant Mossbauer gamma-channel of decay) by 10-40% and total life-time (including non-controlled non-Mossbauer gamma-radiation and non-controlled electron conversion channels of excited nucleus decay) by 1%.

1. Introduction

The problem of controlled spontaneous gamma-decay (controlled gamma-radioactivity) is one of the most interesting in nuclear physics. In the case of free space without any material bodies the spontaneous gamma-decay is non-controlled process. Corresponding probability

$$A_{eg} \equiv 1/\tau = (4\pi^2\omega_{eg}|\mathbf{d}_{eg}|^2/3\hbar)\,\rho(\omega_{eg}) = 4\omega_{eg0}{}^3|\mathbf{d}_{eg}|^2/3\hbar c^3 \quad (1)$$

of this decay are fully determined by the matrix element $\mathbf{d}_{eg}$ of nucleus dipole moment and spectral-volume density $\rho(\omega)=\omega^2/\pi^2c^3$ of the modes of free quantized electromagnetic field.

Here τ is the radiative life-time in free space (without adjacent material bodies).

The total life-time of this excited nucleus in free space $\tau_{tot}=\tau/(1+\alpha) \equiv 1/\lambda$ is also the constant. Here α is the coefficient of internal electron conversion for the nuclear transition $E_e \rightarrow E_g=0$; $\lambda = 1/\tau_{tot}$ is a constant of nuclear decay. For the case of radiation transitions of higher multipolarity the expressions for radiative and total life-times also are constants.

The problem becomes very complicated in the important case when material bodies are present in the surrounding space. It is usually stated that in all cases with presence of any material bodies at macroscopic distance $L>>\lambda_{eg}$ from the excited nucleus the expression for the life-times τ and τ_{tot} remains the same or changes by unmeasurably small value. Such supposition is erroneous.

It was shown [1] that spontaneous gamma-decay is a process of an excited nucleus relaxation, the phase premises of which are caused by interaction with fluctuating state of the thermostat controlled by the resonant screen situated at the distance $L>>\Lambda_{eg}$ from the nucleus. The phenomenon of controlled nucleus gamma-decay is a result of interaction of the nucleus with zero-energy modes, interaction these modes with the atoms of controlled (and controlling) screen, and interaction of the nucleus with the system of atom electrons.

We have carried out investigation aimed at direct experimental discovery (based on the theory [1] of controlled gamma-decay) of the phenomenon of radioactive nuclei gamma-decay controlling. The experiment was done using decay of excited state of Fe-57 isotope, under conditions where the linewidth is small on account of the Mossbauer effect. External observations of the decay rate indicate a small, but nonetheless statistically significant modification of the decay rate.

2. The model and theory of controlled nuclear gamma-decay

It was shown [1] that spontaneous gamma-decay is a process of an excited nucleus

relaxation, the phase premises of which are caused by interaction with fluctuating state of the thermostat. We have considered [1] the general system which included the excited nucleus, the system of this nucleus electrons, the system of zero-energy (in vacuum state) electromagnetic modes with frequencies ω_β and the screen — the system of N atoms with resonant frequencies ω_{ns} situated at the large distance $L>>\Lambda_{eg} \equiv 2\pi c/\omega_{eg}$ from the nucleus. We have obtained [1] the solutions of the problem of gamma-decay for this system

$$|A(t)|^2 = \exp(-t/\tau^*_{tot}) \equiv \exp(-\lambda^* t) \qquad (2)$$

for the cases of resonant and non-resonant screen.

It was shown for the first time [1] that if the screen made from resonant ($\omega_{n0} \approx \omega_{eg}$) atoms acts on the excited nucleus inside the solid angle $\Delta\Theta \leq 4\pi$, the result is the change of both the radiative life-time

$$\tau^* = \tau/\{Re[(1-2i\tau\Delta\omega_0)[1-f(\Delta\Theta/4\pi)(1-(1+iG/2-\Delta\Omega)^{-4})]]\} \equiv \tau/\{(1-f\Delta\Theta/4\pi)+(f\Delta\Theta/4\pi)\tau/\tau^*_{ef}\} \qquad (3)$$

and the total life-time of the nucleus

$$\tau^*_{tot} = \tau/\{\alpha+Re[(1-2i\tau\Delta\omega_0)[1-f(\Delta\Theta/4\pi)(1-(1+iG/2-\Delta\Omega)^{-4})]]\} \equiv \tau/\{\alpha+1-(f\Delta\Theta/4\pi)(1-\tau/\tau^*_{ef})\} \qquad (4)$$

Here $\Delta\omega_0 = \int 2\omega_\beta^3 |\mathbf{d}_{eg}|^2 d\omega_\beta/3\pi\hbar c^3(\omega_\beta - \omega_{eg})$ is the radiative shift of excited energy level of the nucleus (radiation correction or nuclear analog of the Lamb shift for atom electrons);

$G = 2N\pi^2|\mathbf{D}_{eg}(\omega_n)|^2/3\tau^*\hbar v_0[(\omega_{n0}-\omega_{eg})^2+(1/2\tau^*)^2]$; $\Delta\Omega_{res} = [(\omega_{n0}-\omega_{eg})\tau^*/\pi]\,G$;

v_0 is the quantizing volume of the electromagnetic mode; N is the total number of resonant atoms of the screen in the volume v_0; $\mathbf{D}_{eg}$ is the matrix element of screen atom dipole momentum; f is the parameter of recoil-free resonant radiation (parameter of Mossbauer for Mossbauer nucleus);

$$\tau^*_{ef} \equiv \tau/Re\{(1-2i\tau\Delta\omega_0)(1+iG/2-\Delta\Omega)^{-4}\} = \tau/\{1-(4\pi/f\Delta\Theta)(1-\tau/\tau^*)\}$$

is the effective radiative life-time for Mossbauer component of controlled radiative gamma-decay for gamma-radiation inside the solid angle $\Delta\Theta$ blocked by the resonant screen.

In the case of the ideal resonant screen (at $f = 1$ and $\Delta\Theta = 4\pi$) we have $\tau^*_{ef} = \tau^*$. Without screen (e.g at $\Delta\Theta \to 0$) we have $\tau^* = \tau$ and $\tau^*_{ef} = \tau$. It follows from this consideration that τ^*_{ef} is the changed life-time of radiation decay in the case of presence of an ideal screen.

The expressions (3) and (4) were obtained under the condition that all electromagnetic modes are quantized at approximately same values of relation N/v_0. If the resonant atoms of the screen are identical to the researched atom with the excited nucleus, we have $\mathbf{D}_{eg} \equiv \mathbf{d}_{eg}$ and $|\mathbf{D}_{eg}|^2 = 3\hbar c^3/4\tau\omega_{eg}^3$.

For the case when the excited nucleus is a Mossbauer one, the screen is made from Mossbauer resonant atoms and the usual condition of small modification of a electromagnetic modes spectrum $G<<1$ holds, at exactly the resonant state $\omega_{n0} = \omega_\beta$ we have

$$\tau^*_{tot} \approx \tau/\{\alpha+1-f\tau\Delta\omega_0 G\,\Delta\Theta/\pi)\} \approx \tau_{tot}\{1+2f\Delta\Theta\,\tau\,\Delta\omega_0\,\pi c^3 N/v_0\,(\alpha+1)^2\,\omega_{n0}^3\}, \qquad (5)$$

$$\tau^* \approx \tau/\{1-f\tau\Delta\omega_0 G\,\Delta\Theta/\pi)\} \approx \tau\{1+2f\Delta\Theta\,\tau\,\Delta\omega_0\,\pi c^3 N/v_0\,(\alpha+1)\,\omega_{n0}^3\}. \qquad (6)$$

It follows from the expressions for τ^*_{tot} and τ^* that the decay parameters for the case when resonant screen is present greatly depend on the sign and magnitude of the radiation shift $\Delta\omega_0$ of the resonance energy level position. E.g., when the radiation shift is absent (at $\Delta\omega_0 = 0$), we have $\tau^*_{tot} = \tau_{tot}$, $\tau^* = \tau$. At positive sign of this shift (at $\Delta\omega_0 > 0$) we have decelerated (partially suppressed) nuclear decay and $\tau^*_{tot} > \tau_{tot}$, $\tau^* > \tau$. For the opposite case of negative sign (at $\Delta\omega_0 < 0$) we have accelerated decay and $\tau^*_{tot} < \tau_{tot}$, $\tau^* < \tau$. Unfortunately the values of $\Delta\omega_0$ for nuclei are unknown.

For the case of non-resonant screen (at $\omega_{ns} \neq \omega_{eg}$, $|\omega_{ns}-\omega_a| >> 1/\tau^*$) we have other results:

$$\tau^*_{tot} = \tau/\{\alpha+1-(\Delta\Theta/4\pi)[1-(1-\Delta\Omega_{nres})^{-4}]\} \approx \tau_{tot}\{1-\Delta\Omega_{nres}\,\Delta\Theta/\pi(\alpha+1)\}, \qquad (7)$$

$$\tau^* = \tau/\{1-(\Delta\Theta/4\pi)[1-(1-\Delta\Omega_{nres})^{-4}]\} \approx \tau\{1-\Delta\Omega_{nres}\,\Delta\Theta/\pi\} \qquad (8)$$

Here

$$\Delta\Omega_{nres} = 2(N/v_0)\pi\Sigma_s|\mathbf{D}_{eg}(\omega_{ns})|^2(\omega_{ns}-\omega_{eg})/3\hbar[(\omega_{ns}-\omega_{eg})^2+(1/2\tau^*)^2] \approx$$

$2(N/v_0)\pi \int f(\omega_{ns}) \{|\mathbf{D}_{eg}(\omega_{ns})|^2 (\omega_{ns}-\omega_{eg})/3\hbar[(\omega_{ns}-\omega_{eg})^2 + (1/2\tau^*)^2]\} d\omega_{ns}$; (9)

$f(\omega_{ns})$ is the function of distribution of frequencies of screen absorption.

It was shown [1] that resonant screen effect in all cases appears to be more significant than the nonresonant one. This result also follows from (7-9): in the case of ideal nonresonant screen we have $f(\omega_{ns}) = \text{const}$ and $\Delta\Omega_{nres} \to 0$ because of a peculiarity of the intergrand function in (9) (this function is odd). As a result from (7) and (8) we have $\tau^*_{tot} \to \tau/(\alpha+1)$, $\tau^* \to \tau$.

3. **Direct experimental observation and study of the process of controlled radioactive and excited nuclei radiative gamma-decay**

In our previous work the phenomenon of controlled decay was studied indirectly by investigating two related phenomena: increase of the spontaneous gamma-radiation intensity in the solid angle that wasn't blocked by the resonant screen [2], and the change of spectral width of the emitted gamma-radiation at presence of the resonant screen [3]. The aim of the present experiments was to observe directly and examine the law of the controlled gamma-decay of the second quantum of gamma-cascade (Fig.1) of radioactive $Co^{57}(Fe^{57*})$ nucleus at resonant screen presence by the delayed gamma-gamma coincidence method.

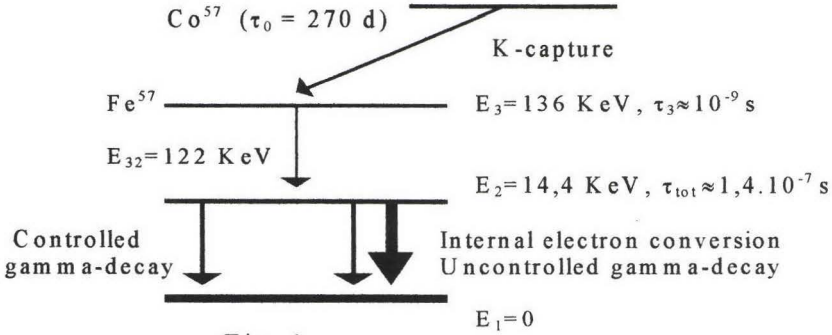

Fig. 1

The $Co^{57}(Fe^{57*})$ radioactive isotope with energy $E_{21} \approx 14.4$ keV of controlled nuclear gamma-transition 2→1, internal electron conversion coefficient $\alpha \approx 8.2$, total life-time $\tau_{tot} = ln2\ T_{1/2} \approx 1{,}4.10^{-7}$ s and decay period $T_{1/2} \approx 0{,}98.10^{-7}$ s for this nuclear transition and with very small activity Q=10 μKu was used as a source of controlled Mossbauer radiation 1. This source had the spectrum in the form of a single line of natural width. The source had thickness about 5 μm, was fixed on the surface of Plexiglas disc with thickness 2 mm and put in the center of the resonant absorber 2, having a form of cylinder with diameter $2R \approx 0.8$ cm and length $L \approx 2.5$ cm, made of stable Fe^{57} isotope in stainless steel. The thickness (surface density) of this Fe^{57} absorber was $\sigma_m \approx 7$ mg/cm^2. For the case of pure resonant Mossbauer radiation, the transparency coefficient of this absorber was $K \approx 10^{-4}$. For the case of non-resonant radiation, we had almost full transparency with $K \geq 0.8$. The total number of Fe^{57} nuclei on the length of resonant absorbtion of gamma-quanta with energy 14.4 keV on the internal surface $S_0 \approx 2\pi RL$ of the quantization volume $v_0 \approx \pi R^2 L$ equals about $N \approx 10^{19}$. For this absorber we had $N/v_0 \approx 10^{19}$ cm^{-3} and $\Delta\Theta \approx 3\pi$.

Behind the diaphragm 3 there was an amplitude detector 4 (thick NaJ(Tl) crystal with thickness about 4 cm) for detection of the first quantum of decay gamma-cascade with high energy $E_{32} \approx 122$ keV. Behind the diaphragm 5 there was another amplitude detector 6 (thin NaJ(Tl) crystal with thickness about 0.1 mm) for detection of the second quantum of decay

cascade with energy $E_{21} \approx 14.4$ keV. The signal processing system picked out the part of amplitude spectrum close to the gamma-line with $E_\gamma \approx E_{21}$.

The law of gamma-decay $|A(t)|^2 = \exp(-t/\tau^*_{tot}) \equiv \exp(-\lambda^* t)$ of the second transition of the cascade from the excited state with energy $E_2 \approx 14.4$ keV to the final ground state $E_2 = 0$ of Fe^{57} nucleus was the object of our investigation. Two signals from the detectors 4 and 6 were used in the processing system 7 to obtain the law of gamma-decay. The measurements of the delay of the second quantum of gamma-cascade were performed in two regimes.

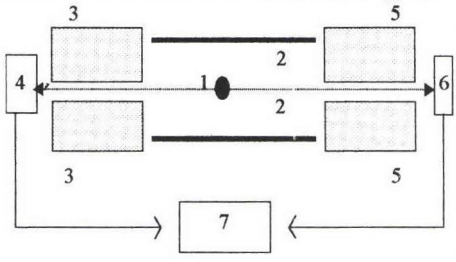

Fig.2

In the first regime (see Fig. 2) the measurements corresponded to presence of the resonant absorber cylinder 2 (resonant screen) only. For this regime the total and radiative life-time were equal (see (5) and (6))

$\tau^*_{tot(res)} \equiv \tau^*_{tot} \approx \tau_{tot}\{1+ 2\, f\, \Delta\Theta\, \tau\, \Delta\omega_0\, N\pi c^3 / (\alpha+1)^2\, v_0\, \omega_{n0}{}^3\}$;

$\tau^*_{(res)} \equiv \tau^* \approx \tau\{1+ 2\, f\, \Delta\Theta\, \tau\, \Delta\omega_0\, N\pi c^3 / (\alpha+1)\, v_0\, \omega_{n0}{}^3\}$.

In the second regime (see Fig. 3) another cylinder 8 made of lead with diameter $D_1 \approx 1.4$ cm, length $L_1 \approx 5$ cm and thickness of the wall $\Delta D_1 \approx 0{,}5$ cm was put around the resonant absorber cylinder. It totally absorbed both the resonant and the non-resonant radiation in the range of energies close to $E_\gamma \approx E_{21} \approx 14{,}4$ keV.

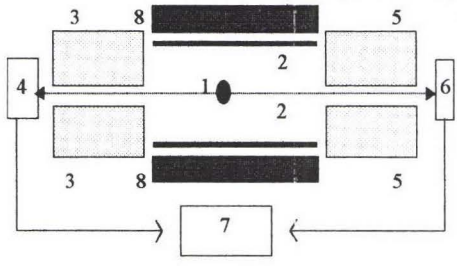

Fig.3

This corresponded to completely non-selective (non-resonant) absorber ("black" screen). For this regime

$\tau^*_{tot(nres)} \approx \tau/(\alpha+1) \equiv \tau_{tot}$; $\tau^* \approx \tau$.

The same results $\tau_{tot} = \tau/\alpha$ and $\tau^* = \tau$ were obtained in the case of free space without a screen.

Such method of investigation excludes the uncontrolled influence of reverse scattering of the resonant gamma-quanta after change from the pure resonant absorption (case 1) to the non-resonant one (case 2) (such influence would occur if the resonant absorber cylinder were simply taken off the source).

Each series of experiments in both regimes lasted $\Delta t = 10$ hours. The measured law of gamma-decay of the second transition $2 \to 1$ of the cascade $3 \to 2 \to 1$ in the final ground state of Fe^{57} nucleus (after three series of experiments) is presented on Fig. 3. In the experimental arrangement shown on Fig. 4 (time calibration is about $\delta t \approx 4.7$ ns per channel) the contribution of the Mossbauer scattering was the same in both types of measurements – with and without the "black" lead screen surrounding the Mossbauer screen. It is known that the resonantly scattered radiation is delayed with respect to the primary beam. In the case of a strict resonance between the source and the (thick) scatterer, which takes place here, this delay is equal to τ_{tot}, and the time distribution of the scattered radiation is characterized by the decay constant $\lambda_s = 1/2\tau_{tot}$. Formulas for total intensities of registered both direct and scattered resonant gamma-quanta of nuclear decay with energy $E_{21} \approx 14.4$ keV in both regimes are the following

$J_1(t) = J(0)\,[(1-g)\exp(-\lambda^* t) + g\exp(-\lambda^*_s t)]$, $J_2(t) = J(0)\,[(1-g)\exp(-\lambda t) + g\exp(-\lambda_s t)]$

The exact contribution of the resonance scattering was difficult to estimate *a priori*. However, considering the geometry, the recoilless fraction, and the internal conversion of the 14.4 keV transition, it could not be large enough to be resolved directly in the measured time spectra. Thus, we compared the effective decay constants of the time spectra measured with and without the Pb screen. Visually both spectra were practically identical. The fit of the experimental points by the single-exponential decay, taking into account the time resolution of the coincidence spectrometer (≈5 ns) and the accidental background, is shown on Fig. 4. The experimental points were fitted in the time range of the order of 900 ns, i.e. about 6.5 total life-times τ_{tot} of the 14.4 keV level.

It is seen that the experimental points in the apex of the curve lie lower than the fitting curve, which evidences a contribution of the delayed scattered radiation.

The computer simulation showed that the observed discrepancy could be attributed to $g \approx 0.1$ contribution of the components with $\lambda_s = 1/2\tau_{tot} \equiv \lambda/2$ and $\lambda^*_s = 1/2\tau^*_{tot} \equiv \lambda^*/2$.
So any difference in the decay constants for the spectra measured with and without the Pb screen should be attributed to the influence of the latter.
with presence of Fe^{57} screen

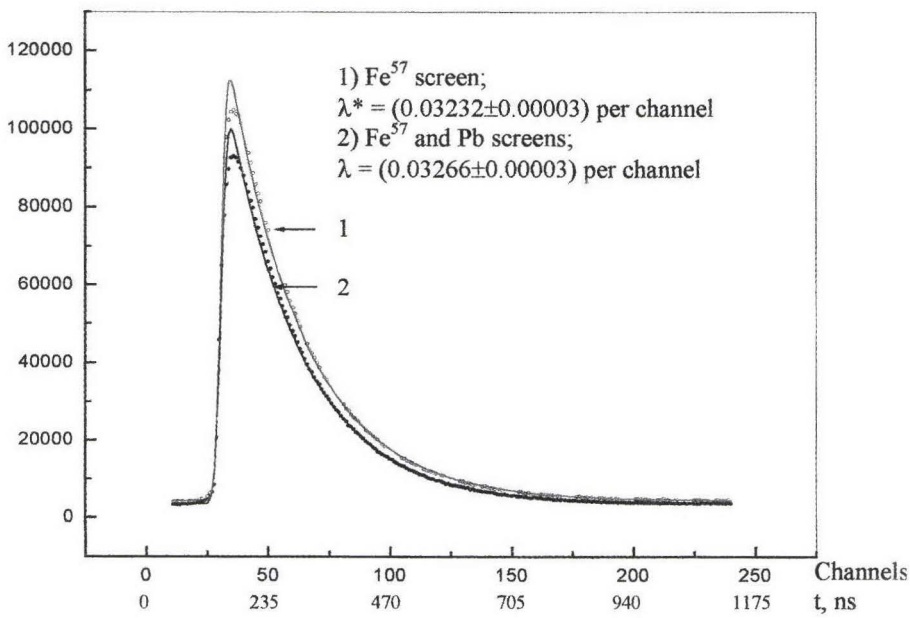

Fig. 4

The decay constants, obtained from the fits are the following:
λ^*=(0.03232±0.00003) per channel ≈ (0.6877±0.0006).10^7 s^{-1} with presence of Fe^{57} screen;
λ=(0.03266±0.00003) per channel ≈ (0.6950±0.0006).10^7 s^{-1} with presence of Fe^{57} and Pb screens.

It is seen that in the second case the decay is slower, and the difference is well beyond the statistical uncertainty. The relative difference $\Delta\lambda/\lambda = (\lambda - \lambda^*)/\lambda = (0.0106\pm0.0018)$, may be ascribed to the retarding effect of the "black" lead screen. The averaged results (for three series of experiments) for changed total life-time τ_{tot}, radiative life-time τ and effective radiative life-time τ_{ef} equal

$\Delta\tau_{tot}/\tau_{tot} \equiv [\tau^*_{tot(res)} - \tau^*_{tot(nres)}]/\ \tau^*_{tot(nres)} \approx [\tau^*_{tot(res)} - \tau_{tot}]/\tau_{tot} \approx (0.92\pm0.17).10^{-2}$;

$\Delta\tau/\tau \equiv [\tau^*_{(res)} - \tau^*_{(nres)}]/\tau^*_{(nres)} \approx 0.092\pm0.017$;

$\tau^*_{ef}/\tau = 1/\{1-[4\pi/f(\Delta\Theta)](1-\tau/\tau^*)\} \approx 1.32\pm0.05$ (10)

It follows from these results and equation (6) that the magnitude of the radiative shift of excited nucleus level Fe^{57} equals $\Delta\omega_0 \approx 10^{13}\ s^{-1}$ and the sign of the shift is positive.

4. **Conclusion**

The results of the presented experiments prove the main conclusion of the theoretical analysis about the possibility of controlled influence of a thin resonant screen on the temporal, amplitude and space characteristics of spontaneous decay and excited nuclei radiation. By optimization of decay controlling system parameters (using the nuclei without the electron conversion decay channel $\alpha\rightarrow0$, the resonance absorbers with a maximum solid angle screening $\Delta\Theta\rightarrow4\pi$, with maximum weight part of the gamma-radiative resonance channel $f\rightarrow1$) it is possible to achieve significantly higher influence upon the spontaneous decay characteristics and, respectively, sharp increase of total life-time $\tau^*_{tot} >> \tau_{tot}$.

Among other conclusions, the obtained results in fact prove the existence of a peculiar macroscopic "distance effect" predicted above, namely the dependence of the effectiveness of quantum spontaneous decay process of the excited nuclei on macroscopically remote position $L>>\lambda_{eg}$ (e.g. about several cm) from the excited nucleus of a resonant absorbing screen (unlike, for example, Kazimir's effect manifesting itself only at microscopic distances).

In conclusion we would like to note that the effect of influence upon the spontaneous radiation characteristics of excited (radioactive) nuclei may manifest itself not only for Mossbauer nuclei and transitions but also for other excited states and nucleus types provided the existence for them of an obviously expressed resonance absorbtion.

1. Vysotskii V.I. // Physical Review C, v.58 (1998) 337.

2. Vysotskii V.I., Bugrov V.P., Kuzmin R.N., Kornilova A.A. and Reiman S.I. // Hyperfine Interactions, v.107 (1997) 277.

3. Vysotskii V.I., Bugrov V.P., Kornilova A.A. and Reiman S.I. International Conf. on the Physics of Nuclear Science and Technology, 1998, New York, Proceedings, v.2, p.1739-1743.

Conference Proceedings Vol. 70
"ICCF8"
F. Scaramuzzi (Ed.)
SIF, Bologna, 2000

Evidence for DD – reaction and a long – range alpha emission in Au/Pd/PdO:D heterostructure as a result of exothermic deuterium desorption

A.G.Lipson[1,3], B.F.Lyakhov[1], A.S.Rousstesky[2], N.Asami[3]

[1] Institute of Physical Chemistry, Russian Academy of Sciences, 31 Leninsky prospect, 117915 Moscow, Russia

[2] Lebedev Physics Institute, Russian Academy of Sciences, 117924 Moscow ,Russia

[3] Institute of Applied Energy, New Hydrogen Energy Laboratory, Sapporo 004, Japan

Abstract

Low intensity nuclear emissions (neutrons and charged particles) due to exothermic deuterium desorption from Au/Pd/PdO heterostructure loaded with deuterium by electrolysis have been studied with NE - 213 neutron detection facility as well as SSB and CR - 39 charged particle detectors in low background conditions with large statistics . The levels of neutron and proton emissions are found to be close one another and after background subtracting (Au/Pd/PdO:H count rate) consist of: I_n == (19 ± 2)□10^{-3} n/s and I_p = (4.0 ± 1.0)□ 10^{-3} p/s in 4□ solid angle, respectively. These yields of DD- reaction products in Au/Pd/PdO heterostructure comply with the mean DD reaction rate of $\lambda_{dd} \sim 10^{-23}$ s^{-1} per DD pair or $Y_{dd} \sim 10^{-18}$ per DD – pair of mobile deuterium in crystalline lattice. The long – range alpha emission ($E_\alpha \sim 8.0 – 14.0$ MeV) that is absent in a natural background charged particle spectra has been also observed in our experiments with both D and H - loaded heterostructure samples.

1. Introduction

The problem of Lattice Induced Nuclear Reactions (LINR) or the existence of so called " Cold Fusion " at present time is still opened. Despite 10 years of essential efforts of many research groups in various countries, to this date there are no convincing nuclear data that would confirm generation of DD - reactions in solids at room temperature. In dozens of such experiments on neutron and charged particle detection, the problem of very low intensity of the observed emissions has been complicated by total irreproducibility of nuclear results [1-3].

All known features of LINR allow to formulate this phenomenon as follows: Under the term of LINR (with respect to DD - reaction) could be appreciated anomalous (in terms of conventional nuclear processes in vacuum) , random and rare nuclear effects in crystalline lattice of essentially non - equilibrium deuterated solids, which are induced by sharp changes in their structure, i. e. phase transitions, deuterium loading, mechanical strains and so on. In accordance with consideration proposed, to generate DD - type nuclear reaction in Pd lattice, a principal condition could be creation of large fluctuations of elastic energy in the sample or/and high screening potential for deuteron Coulomb barrier [4].

In 1992, a Au/Pd/PdO heterostructure was developed and studied in Institute of Physical Chemistry of RAS (Moscow) [5,6]. It possesses a high deuterium capacity at electrochemical loading and simultaneously deuterium transport in such a kind of heterostructure is more intensive compared to pure Pd foils, due to very high mobility of deuterons at the Pd – PdO interface [7]. Recently, at a low energy deuteron

implantation ($2.5 < E_d < 10$ keV) in Au/Pd/PdO heterostructure the highest screening potential U_S = 600 eV has been observed [8], which also indicates the excellent conditions for deuteron screening in such kind of samples, despite of small loading ratio (x = D/Pd = 0.11).

In a present paper we show the results of DD - neutron and charged particle measurements carried out during spontaneous and induced deformations upon exothermic deuterium desorption in a thin Au/Pd/PdO:D heterostructure loaded with deuterium. We demonstrate that in experiments with the Au/Pd/PdO:D system, the 2.45 MeV neutrons, 3.0 MeV protons and long – range alphas are detected.

2. Experimental Technique and Methods

2.1 Sample Preparation and Charachterization

1. Cold - rolled Pd - foils (99.99 %) 8 - 300 μm thick with the area S = 4.0 * 2.0 cm^2 annealed in vacuum 10^{-5} Pa at T = 1000 C have been affected to oxidation by butane - oxygen torch at T = 1000 C during 10 - 20 s. As a result, the gray color layer about 30 nm thick has been formed at the both Pd sides, having the $PdO_{0.57}C_{0.08}$ composition, in accordance the SIMS data.The PdO/Pd/PdO samples obtainedwere covered from one side by teflon mask and electrochemical gold coating of 0.2 μm thick has been deposited at its free side. After this procedure the teflon mask was removed and final annealing at T = 300 C has been carried out.

2. Deuterium (hydrogen) loading of heterostructure samples has been carried out by electrolysis in 1M solution of $NaOD/D_2O$ (1M - $NaOH/H_2O$) at current density J = 20 mA/cm2 during t = 5 - 100 min, depending on sample thickness. The mean volume loading ratio after electrolysis estimated by anodic polarization was x = D/Pd = 0.7. During electrolysis process and after its finishing a strong cross bending of the sample was observed [5,6,12].

3. After the electrolysis finishing, the samples were washed in pure $D_2O(H_2O)$, short dried and fixed in a special sample - holder. In order to provide more uniform and intensive exothermic D - desorption the samples were tightly compressed in a normal direction to their surface with a stress value P = 20 MPa. To detect charged particle emission with SSB - detectors the sample was fixed only from its both ends and placed in vacuum 10^{-1} Pa.

4.Typical detection time in each run of measurement was varied from 5000 to 40000 s. This time is corresponded to a total deuterium (hydrogen) escape from Au/Pd/PdO heterostructure for a used sample thickness range.

5. The plastic deformation of the sample compressed with the stress P = 20 MPa which is higher than plastic limit (E = 9.0 MPa) was about 2 – 3 % and slightly changed during deuterium desorption from the sample [6].

2.2. Neutron and charged particle measurement systems

In order to detect neutrons from the cell with compressed Au/Pd/PdO:D(H) samples two independent 5 - inch NE - 213 liquid - scintillator detectors were used

being installed at a distance of 24 cm one against another. The sample fixed in the sample – holder was placed exactly between the two detectors at a distance of 12 cm from the each. To decrease a natural neutron background the detectors were surrounded by boron containing polyethylene and all set up was placed in the underground laboratory of Hokkaido University under 10 m of the heavy - weight concrete. Owing to such an underground shielding, the 1 order of magnitude decrease in neutron background has been achieved compared to ground - based conditions.To increase the accuracy and reliability of neutron spectra measurements the High gain (System 1) and Low gain (System 2) methods have been used simultaneously for neutron detection. The High gain system is operated in 0.8 - 3.5 MeV range of proton recoil edge, while Low gain system within the 1.0 - 7.1 MeV, respectively. To exclude detection of gammas during neutron detection, the pulse shape analyzer was used that allowed at a high confidential level to separate gamma and neutron pulses. In the energy interval corresponding to a 2.45 MeV neutron peak location (2.0 - 3.0 MeV) the efficiencies values for Systems 1 and 2 were: ε_1 = 4.0 % and ε_2 = 4.7 % respectively. We have to emphasize that the detector efficiency and neutron background condition used allow to increase sensitivity with respect to 2.5 MeV neutrons in our experiment, at least, by 1 order of magnitude compared to previous well - known spectral neutron measurements [2,3] in metal - deuterium systems.

Vacuum measurement of total spectra of charged particle emission were carried out for samples with thickness of 40 - 60 μm in the Department of Nuclear Engineering of Osaka University [12]. Typical background spectra for about 1 - week continuous observation almost do not contain events with energies higher than 7.7 MeV. The background count rate in the energy interval of interest (1 - 4 MeV) in which DD - protons have been expected is very low and has not exceeded 0.15 count/h. In order to establish the thickness dependence of 3 MeV proton yield a special series of measurement with samples of the thickness within 8 - 300 μm has been carried out in the proton spectral range of 2.5 - 3.5 MeV.

In the special measurement of a long – range α - particle emission from heterostructure samples in the air - atmosphere (in Laboratory of Nuclear Science, Tohoku University) the SSB ΔE – E counter telescope has been applied consisting of calibrated thin ΔE – detector (h = 20 μm) and thick E – detector (E = 100 μm). The detector pair have TDC - time gate of coincidence about 20 ns. The requirement of coincidence between ΔE and E detectors completely eliminates the electromagnetic noise and enables unambiguous identification of charged particle type.

In order to confirm the results of SSB measurement, and check the yield of D(d,p)T reaction, an independent CR - 39 track detector technique has been also applied to detect charged particles. To improve the accuracy of CR - 39 detection we searched simultaneously for tracks of 3.0 MeV protons and 1.0 MeV tritons that are both the products of D(d,p)T reactions [13].

3. Experimental Results and Discussion

3.1. Neutron measurement results

1. For mechanically strained Au/Pd/PdO:D (foreground runs) and Au/Pd/PdO:H (background runs) samples the 50 independent measurements have been carried out with $t = 1*10^6$ s total detection time. It was established that count rate of neutrons having energy En > 2.0 MeV in deuterated heterostructure exceeds the

similar value detected in the backround runs at significant level. After subtracting of Au/Pd/PdO:H control experiment data from the foreground the clear peak in the range of 2.5 ± 0.1 MeV for both independent NE - 213 detectors is appeared (**Fig.1,2**).

2. Taking into account a total measurement statistic with statistic weight of each run the average neutron emission count rate in 2.45 MeV peak for both NE - 213 detectors after background subtracting (**Fig.2**) is: $<\Delta N> = (1.67 \pm 0.17) * 10^{-3}$ cps. Or taking into account the total efficiency of detecting system in the 2.0 - 3.0 MeV spectral interval in reference to fast neutron (ε = 9.4 %) the DD - neutron emission intensity is equal to:

$$\mathbf{I_n = (18.5 \pm 1.9) * 10^{-3}\ n/s}$$ in 4 π solid angle.

3. Neutron emission observed during exothermic deuterium desorption in the strained Au/Pd/PdO:D heterostructure has non - uniform stochastic character and is coincided in its duration to characteristic time of a total deuterium escape from the sample.

4. Precense of peak located at 2.45 MeV is accompanied to a broad continuum in the range of higher energies by the 6.0 MeV, as it usually takes place for the typical DD - neutron spectra (**Fig. 1b**). The absence of such a continuum from the low enrgy side at $E_n < 2.0$ MeV (**Fig.1a,b**) could be explained on one hand, by very low intensity of emission observed and high enough background level at low enrgy, due to peculiarities of NE - 213 response function; on another hand, it may be concerned to inelastic scattering of emitted neutrons by the sample and sample - holder material.

3.2. DD - proton measurement results

1. Measurement of charged particle emission with SSB – detector upon the exothermic deuterium desorption from Au/Pd/PdO:D heterostructure of 40 – 60 μm thick in vacuum showed that in the 1.0 - 4.0 MeV energy range that is corresponed to DD - reaction proton peak position the statistically significant excess of count rate above the background level (Au/Pd/PdO:H) is observed .After background subtraction the "proton" peak position is $E_p = 2.5 \pm 0.5$ MeV (**Fig.3**) and average proton emission intensity, taking into account SSB - detector geometric efficiency (ε = 3.4 %) is:

$$\mathbf{<I_p> = (4.0 \pm 1.0) * 10^{-3}\ p/s}$$ in 4 π solid angle.

2. Measurement of D(d,p)T reaction yield in similar Au/Pd/PdO:D(H) samples of 30 μm thick in air atmosphere with calibrated CR - 39 track detectors has been carried out by determintaion of pt - track density (p - track diameter is in the range of 5.0 μm, t - track : 6.5 - 7.5 μm). The precense of pt - double tracks indicate the sample sites where the probability of DD - reaction is higher than in other points of heterostructure surface.The pt track density for Au/Pd/PdO:D samples is 6 time above the similar one for both intial Au/Pd/PdO heterostructure and control samples Au/Pd/PdO:H. After background subtracting the yield of 3.0 MeV proton from DD - reaction, measured by CR - 39 track detectors I_{pt} is close to the average $<I_p>$ value estimated with SSB - detector:

$$\mathbf{I_{pt} = (5.9 \pm 1.1) * 10^{-3}\ s^{-1}}$$ in 4 π solid angle.

3. The obtained 3.0 MeV proton yields are 3- 4 times less than measured level of 2.5 MeV neutron emission. Some diminishing of proton yield compared to neutron could be explained by 3.0 MeV proton energy losses (~1.0 MeV/6 μm Pd) in the sample. It also indicates that DD – reaction in heterostructure used is initiated in the process of deuterium diffusion across the sample.Those conclusion is confirmed by experiments on 3.0 MeV proton detection in the samples with different thickness (8 -

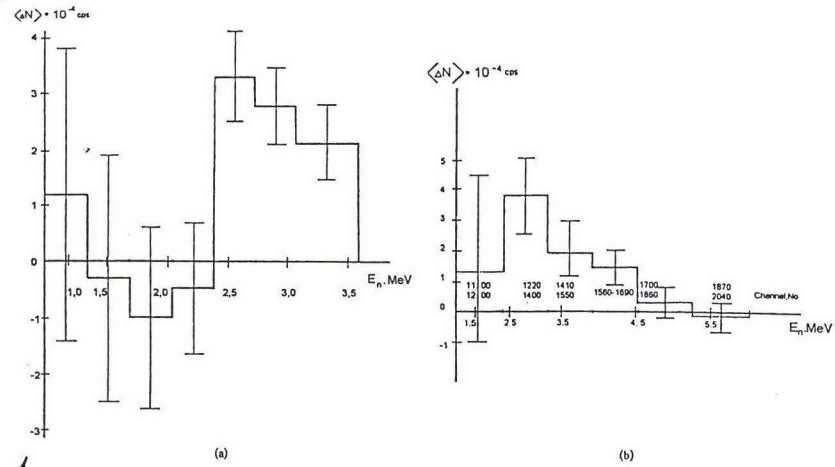
⟨ΔN⟩ · 10⁻⁴ cps
E_n, MeV
1,0
1,5
2,0
2,5
3,0
3,5
(a)
⟨ΔN⟩ · 10⁻⁴ cps
11 00
12 00
1220
1400
1410
1550
1560-1690
1700
1850
1870
2040
Channel No
E_n MeV
(b)

Fig. 1

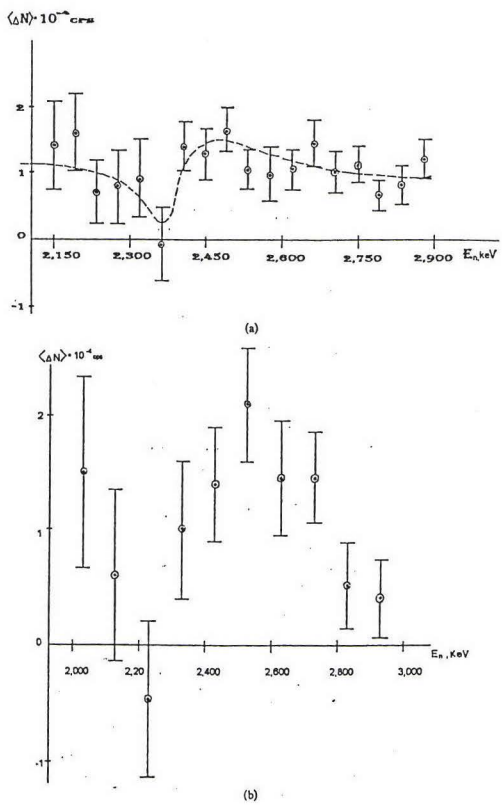
⟨ΔN⟩ · 10⁻⁴ cps
2,150
2,300
2,450
2,600
2,750
2,900
E_n keV
(a)
⟨ΔN⟩ · 10⁻⁴ cps
2,000
2,20
2,400
2,600
2,800
3,000
E_n, KeV
(b)

Fig. 2

300 μm). From this experiment it is possible to conclude that 3.0 MeV proton emission is not detected for the samples with thickness h > 60 μm.

3.3. Long – range alpha – particle emission

The emission of DD – fusion protons during the exothermic deuterium desorption in Au/Pd/PdO:D heterostructure is accompanied by charged particle which spectra extended beyond the 8 MeV. Later, it has been shown in the joint studies with Japanese research groups from Osaka and Tohoku Universities using SSB - detectors that few monoenergetic bands of alpha – particles in the range of 8.0 – 11.7 MeV are emitted in the process of hydrogen (deuterium) desorption from hetetrostructure samples. In order to determine the energy and type of emitted particles the ΔE – E SSB detector pair has been applied in the air atmosphere. It was shown that alpha particle emission in the range of 8.0 – 14.0 MeV is accompanied by the deuterium or hydrogen desorption from Au/Pd/PdO:D(H) samples and has a good reproducibility (**Fig 4 a,b**). At the same time alpha – band within the 8.0 – 10.0 MeV interval is observed only for deuterated samples and not appeared in the case of Au/Pd/PdO:H one. The total α - emission intensities in the range of 8.0 – 14.0 MeV, taking into account ΔE – E detector efficiency (ε = 5.0 %) were:

$<I_\alpha>_D = (4.1 \pm 0.6) * 10^{-4}$ s^{-1} in 4π solid angle for Au/Pd/PdO:D,

$<I_\alpha>_H = (3.1 \pm 1.2) * 10^{-4}$ s^{-1} in 4π solid angle for Au/Pd/PdO:H samples.

It should be emphasized that alpha – particles emitted in these experiments have energies much higher compared to natural background isotopes. The nature of alpha emission observed is not clear at present time. However, it is established that high energy alpha emission in deuterited solid structures always detected under a high internal strain in crystalline lattice caused by presence of hydrogen (deuterium) atoms in it. We can speculate that mechanism of a long – range alpha emissions is concerned to multi – body fusion (3D and 4D – type), producing alphas with energies of 5.75, 7.9, 9.95 and 12.8 MeV [14]. The bands of such an alpha energy one may find in the spectra obtained (**Fig 4 a,b**). Another alternative model of a long range alpha – emission may be concerned to coherent energy transfer from He^{4*} compund nuclei to Pd nucleus caused the emission of alphas with energies up to 20.0 MeV [15]. However both models suggested [14,15] can not explain the high – energy α - emission in Au/Pd/PdO:H – samples. In order to establish a mechanism of a long – range alpha emission in Au/Pd/PdO:D(H) systems the additional experimental data is highly desirable.

4. Conclusions

Data obtained allow to estimate an average DD - reaction rate per DD - pair in the Au/Pd/PdO:D heterostructure due to exothermic deuterium desorption. Taking into consideration the average deuteron concentration in the sample for Foreground runs (N_d = 1.0 * 10^{20} D/ cm^2 of heterostructure) and mean DD reaction yield in accordance to our experimental data, we obtain the mean rate of DD - reaction in Au/Pd/PdO:D sample : $\lambda_{dd} \sim 10^{-23}$ s^{-1} per DD pair. This DD- reaction rate is much lower than it was claimed for the excess heat production and comparable with so called "Jones level"[2].

The mean rate of DD – reaction being obtained in the present study is at least 2

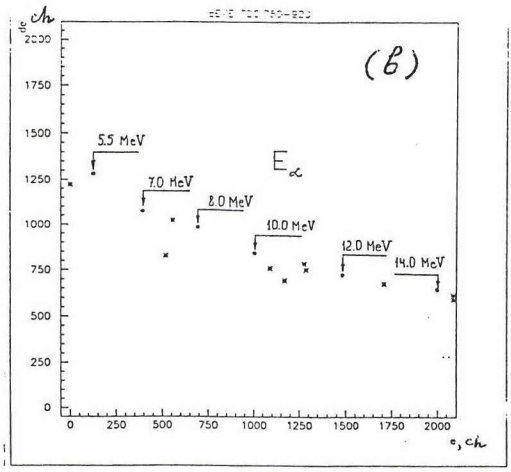
(B)
5.5 MeV
7.0 MeV
8.0 MeV
10.0 MeV
12.0 MeV
14.0 MeV
E_α
0 250 500 750 1000 1250 1500 1750 2000
e, ch

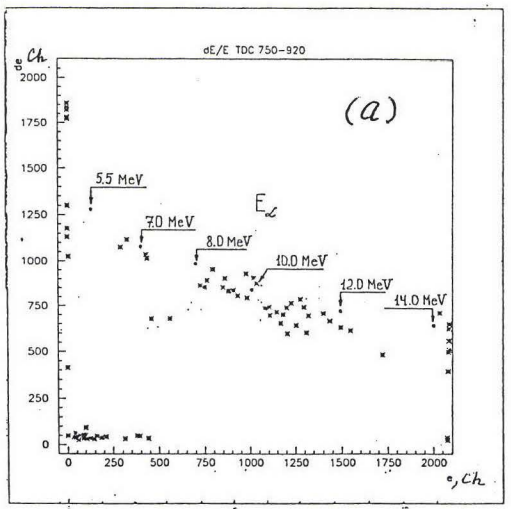
dE/E TDC 750-920
(a)
5.5 MeV
7.0 MeV
8.0 MeV
10.0 MeV
12.0 MeV
14.0 MeV
E_α
0 250 500 750 1000 1250 1500 1750 2000
e, ch

Fig. 4

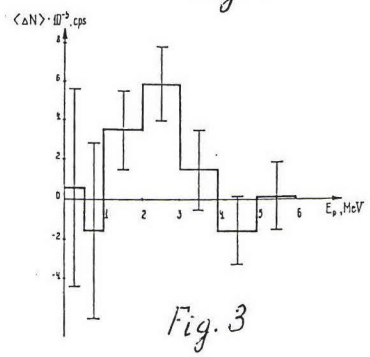
$\langle \Delta N \rangle \cdot 10^{-3}$, cps
E_p, MeV

Fig. 3

orders of magnitude lower than it was estimated in previous works [5,6], where proportional BF-3 thermal neutron detector has been applied. The mean rate of DD – reaction (λ_{dd}) is usually derived quite similar to ref. [2], where λ has been determined as a ratio between neutron count rate and total deuterium concentration in crystalline lattice of the sample used. However, in accordance with recent data [8] a large enhancement of DD – reaction in metals has been observed only for systems with high deuterium mobility. In this connection, we can suggest to estimate DD – reaction yield in Au/Pd/PdO:D experiments using only change in "mobile" deuterium concentration. As a mobile ones it is possible to consider such deuterons that are desorbed from the sample during experiment. Let us consider DD – reaction yield in terms of mobile deuterium for 2 cases: a) present experiment and b) experiment [5,6] with similar, electrochemically loaded Au/Pd/PdO:D samples which were tested in the regime of fast spontaneous thermal deuterium desorption, similar to [6].

a. The change in "mobile" deuterium concentration $N_m(D)$ can be estimated, in average, using measurement of deuterium concentration in the sample N(D) before and after compression in Foreground run (Fig.6). Before neutron detection (after electrochemical loading) $N^1(D) = 1.1 * 10^{20}$ D/cm^2 ; after the finishing of Foreground run with compression $N^2(D) = 7.0 * 10^{18}$ D/cm^2. The sample's area is S = 9.0 cm^2. So, the mean rate of deuterium desorption, taking into account Foreground time $\tau = 3.6 * 10^4$ s [12] is : $N_m(D) \approx N^1(D)S/\tau = 2.5 *10^{16}$ D/s. And DD – reaction yield with respect to 2.5 MeV neutrons, having intensity $I_n = 0.02$ n/s in 4π solid angle is: $\mathbf{Y_{DD}}$ = **$1.6 * 10^{-18}$ reaction per DD - pair.**

b. For this case , neutron detection has been carried out with BF-3 proportional detector (without neutron energy analysis) during fast thermal desorption of deuterium that accompanied by spontaneous plastic deformation of the sample [5]. In accordance with work [6] parameters of experiment were the next: $N^1(D) = 1.1 * 10^{20}$ D/cm^2 , $N^2(D) \leq 10^{17}$ D/cm^2 ; S = 4.0 cm^2 and time of thermal desorption of deuterium is τ = 300 s. The neutron emission intensity was $I_n = 0.92$ n/s. Then we have $N_m(D) = 1.3 * 10^{18}$ D/s per sample and $\mathbf{Y_{DD}}$**= 1.4 * 10^{-18} reaction per DD – pair**. At the same time, estimation of DD – reaction rate λ_{dd} for total (initial) deuterium concentration in the sample during experiment [5] gives : $\lambda_{dd} \sim 2*10^{-21}$ s^{-1} per DD pair.

As one can see, the yields of DD – reaction with respect to "mobile" deuterium are close one to another for both cases a) and b). So we can conclude that in both experiments, despite of different experimental condition there were observed DD – neutrons as a product of mobile deuteron fusion.

Aknowledgements

This work was performed as a part of the New Hydrogen Energy Project of New Energy Development Organization (NEDO), Japan. The authors are grateful to Prof. J. Kasagi and Prof A. Takahashi for their help in SSB measurements and CR - 39 calibration as well as to the late Prof. M. Okamoto, K. Matsui , Dr. A.V. Strelkov , Dr. P. Tripodi, Dr. M. Miles and Prof. G.I. Merzon for friutful discussions. Authors also thanks to R. Shimada, S. Miyashita, H. Kamimura, T. Senju, E. Kennel and Y. Isobe for their help in experiments preparation.

REFERENCES

1. B.V. Derjaguin, A.G. Lipson, V.A. Klyuev et. al. , Nature, **341**, 492 (1989).
2. S.E. Jones, E.P. Palmer, J.B. Czirr et. al., Nature , **338**, 737 (1989).
3. E. Botta, T. Bressani, D. Calvo et. al. , Nuovo Cimento **105A**, 1662 (1992).
4. P. L. Hagelstein, Hyperfine Interact. , **92** , 1059 (1994).
5. A. G. Lipson , B. F. Lykhov, D. M. Sakov and B. V. Derjaguin, Rus. J. Tech. Phys. Lett., **18**, 58 (1992).
6. A.G. Lipson, B.F. Lyakhov and D.M. Sakov, Rus. J. Tech. Phys., **66**, 174 (1995).
7. E. Yamaguchi and T. Nishioka, Jpn. J. Appl. Phys. **29**, L666 (1992).
8. H. Yuki, J. Kasagi, A.G. Lipson et. al., JETP Lett. **68**, 785 (1998).
9. H. Yuki, T. Sato, J. Kasagi et al. , J. Phys. G: Nucl. Part. Phys., **23**, 23 (1997) .
10. U. Greife, F. Gorris, M. Junker et al. , Z. Phys **A351**, 107 (1995) .
11. A.A. Naqvi, Nucl. Inst. Meth. **A 325**, 574 (1993).
12. A.G. Lipson, B.F. Lyakhov, A.S. Roussetsky et al., Fusion Technology, **38** (9), 2000 (in press).
13. A.S. Roussetsky, in Proceedings of ICCF – 8, 2000.
14. A. Takahashi, Fusion Technology, **26** (4T), part 2, 451 (1994).
15. P.L. Hagelstein, Abstracts of ICCF – 8 , 064, Villa Marigola, Lerici, Italy, May 21-26, 2000.

FIGURE CAPTIONS

FIG. 1 Total difference between the sums of all Foreground and Background neutron spectra (with full statistic treatment), taken for 120 channels: for System 1 (a); for System 2 (b).

FIG. 2 Difference between the sums of all Foreground and Background neutron spectra within the 2.0 - 3.0 MeV energy range, taken for 20 channels : for System 1 (a) ; for System 2 (b).

FIG. 3 Total difference between all Foreground and Background runs (with full statistic treatment) for charged particle emission.

FIG. 4 Spectra of long - range alpha – particles detected by $\Delta E - E$ detector pair in air – atmosphere: (a) - for Au/Pd/PdO:D samples, ($\tau = 2*10^6$ s); (b) - for Au/Pd/PdO:H samples ($\tau = 4.5 *10^5$ s).

Conference Proceedings Vol. 70
"ICCF8"
F. Scaramuzzi (Ed.)
SIF, Bologna, 2000

TRITIUM PRODUCTION IN PALLADIUM DEUTERIDE/HYDRIDE IN EVACUATED CHAMBER

H. Yamada, S. Narita, I. Inamura, M. Nakai, K. Iwasaki and M. Baba

Department of Electrical and Electronic Engineering, Iwate University, Morioka 020-8551 Japan

ABSTRACT

The controlled out-diffusion method was employed to induce a nuclear reaction in a palladium(Pd) plate with a MnOx film. The time-resolved mass spectra for Pd deuteride revealed tritium(T) production during the out-diffusion experiment. Similar time behaviors of mass number 1-4 and 6 in the spectra was also observed for Pd hydride. Film blackening was observed for most Pd deuteride as well as Pd hydrides using a normal monochromatic negative photographic film. The radiation from the Pd plate consists of two kinds of components for a Pd hydride. Secondary ion mass spectroscopy has shown considerable increase in counts of Li for Pd hydride after the out-diffusion experiment.

1 INTRODUCTION

Among several experimental methods for nuclear reaction in solid, the controlled out-diffusion one invented by Yamaguchi et al. [1] has the advantage of involving smaller contamination in the reaction vessel with respect to other methods. In addition, the method is expected to yield higher reproducibility in the analysis of the electrode surface, near which is thought to be the center of the reaction.

As most of the systems for investigating the reaction include a pre-amplifier which would be affected by electromagnetic interference. It is better to employ another supporting detection method free from such interference. One available for the supporting method is autoradiography with use of X-ray film as a photon detection passive device. This method has shown the production of tritium [2], β emission [2] from Pd deuteride after discharge and β-emission [3] from Pd deuteride/hydride during discharge. Some anomalous emission from Pd deuteride/hydride has been detected without discharge by this method [4]. Autoradiography has also been applied to detect radiation from protons impinged Pd hydride [5]. In this study, the authors have used an high sensitive monochromatic negative film instead of X-ray film.

2 EXPERIMENTAL

2.1 MATERIALS

The rectangular Pd(99.99% pure) plate sample of $0.3 \times 12.5 \times 25$mm was prepared according to the following procedure. After washing with acetone and aqua resia, it was vacuum annealed at 800℃ for 3h under $\sim 10^{-3}$Torr then cooled down to room temperature in a furnace for 8-10h. Next, one side of the Pd plate was coated with a MnOx film of 20-40nm thickness by sputtering in an argon working gas at 80mTorr, followed by loading of deuterium or hydrogen gas (99.6 % pure) under 6atm pressure for ~24h. The D or H to Pd loading ratio was measured to be 0.3~0.7. The impurities in the Pd were typically Pt(0.1ppm), Rh(1.8ppm), Ag(1.5ppm), Si(2.1ppm), Mg(1.1ppm), and

numerous other metals with lesser concentrations. The deuterium gas with no detectable tritium ($<0.25nCi/cm^3$) was used for the study. The hydrogen used was research grade.

2.2 APPARATUS

A stainless-steel vacuum chamber of cylindrical shape with volume capacity of $880cm^3$ was used. The Pd plate set in the center of the chamber was connected to a constant current DC power supply through a 0.78 Ω current limiting series resistor to flow a current through the Pd. Temperature of the surface of Pd sample was measured by a thermocouple (±0.5℃ precision) and a computerized recorder with digital multimeter to take date once every 9sec. A quadrupole mass spectrometer(QMAS) (AQA-100R, ANELVA) was employed for mass spectrometry of the gas in the chamber.

2.3 PROCEDURE

A current 0.5~4A was flowed through the Pd for 3h in DC mode under pressure of about 10^{-4}Pa. Temperature measurement of the Pd started ~1h before the current flowing. Monitoring gas of mass numbers less than 22 started several min before the current flowing. These measurements continued simultaneously for the 3h and lasted up to 1h after stopping the current flowing. The total number of runs for Pd deuteride and Pd hydride were 59 and 42, respectively. After the measurements, the Pd plate was autoradiographated to detect γ and X-ray photons and charged particles using monochromatic negative film(FUJI PHOTO FILM CO. LTD, NEOPAN 400 PRESTO). For autoradiography, the Pd plate was directly sandwiched using two sheets of negative film. The film with Pd plate had been kept in a dark box carefully to avoid unexpected photons from the outside during exposure time. The film exposure time was 3-8days. The film development was enhanced to ~8 times than usual by increasing development time to 8min and development temperature to 27℃ (using FUJI PHOTO FILM CO. LTD, SUPER PRODOL). Secondary ion mass spectroscopy (SIMS) for randomly selected areas of particular interest Pd hydride was sometimes performed after the experiments. The primary ion in SIMS was ^{69}Ga, the counting time was 5min and the measured area was 80×80 μ m size for all the spectroscopy.

3 RESULT AND DISCUSSION

3.1 MASS SPECTROSCOPY BY QMAS

Fig. 1 shows time behaviors of ion currents for mass number 1-6, 12 and 16 in the test chamber without Pd sample after several forward runs. The bar chart shown on the right side of the figure gives values of each ion current at 1h 59min after the beginning of measurement. Considerable ion current corresponding mass number 1 was detected, which indicates H^+existed as dissolved ion from H_2. Though an high current was seen for mass number 4 as residual D_2 gas, almost no current for mass number 6 was observed. It means almost no D_3 gas existed in the test chamber.

Fig. 2 shows time behaviors of ion currents with Pd deuteride for DC flow, where the dashed line indicate the time when current flow was started. The sudden increase in ion current for mass number 2, 3,4,5 and 6 is due to gas release from the Pd sample induced by current flow. To the contrary, the currents for mass number 1,12 and 18 are seen to decrease gradually, which means that these gases with mass number 1, 12 and 18 had been existed in the test chamber before the forward run. Since H^+ was decreasing, Pd did not

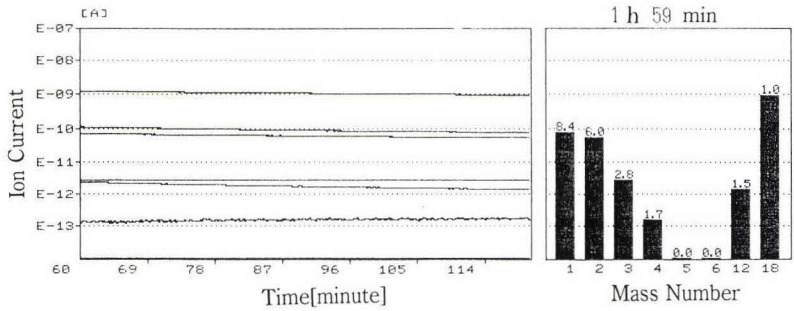

Fig.1 Time behavior of ion currents for mass number 1-6, 12 and 18 without Pd sample

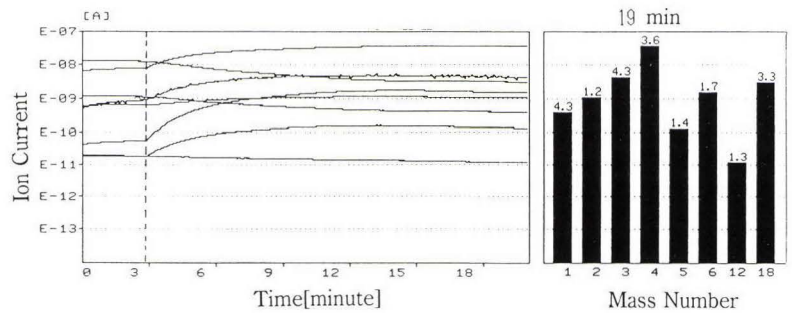

Fig.2 Time behavior of ion currents for mass number 1-6, 12 and 18 with Pd deuteride

release H_2, HD and HT which are thought to be the origin molecules of H^+. Thus, mass number 2 ,3 ,4 , 5 and 6 should correspond D, T and/or ^3He, D_2 and/or ^4He, DT and T_2, respectively. The existence possibility of ^6Li as gas is thought to be little at the experimental temperature. Consequently, T is thought to be released from Pd sample, because almost no mass number 6 was seen in background as seen in Fig. 1.

Fig 3 and 4 show similar time behaviors for Pd deuteride. The ion current for mass number 22 is seen to increase while that of 19 decrease gradually in Fig. 3. Thus, the ions corresponding to mass number 19 and 22 could be HDO and T_2O, respectively, though small amount of ^{19}F and ^{22}Ne might be released from the Pd. The T_2O could consist of T released from the Pd and residual O in the chamber.

A difference in time behaviors of ion currents is seen between mass number 4 and 6 in Fig. 4. The current for mass number 4 keeps almost constant after reaching an highest value while that for mass number 6 decreases gradually after 10min from the beginning of measurement. This difference also indicates that gas components of mass number 6 is different from those of mass number 4. Consequently, the molecule with mass number 6 could not be D_3 but be T_2. Since the diffusion constant of $D(7.3 \times 10^{-7} m^2/s)$ is slightly larger than that of $T(6.1 \times 10^{-7} m^2/s)$ in Pd, the gradually decrease in ion current for mass number 6 would indicate that most of the T existed in near surface of the Pd. Furthermore, considerable current level for mass

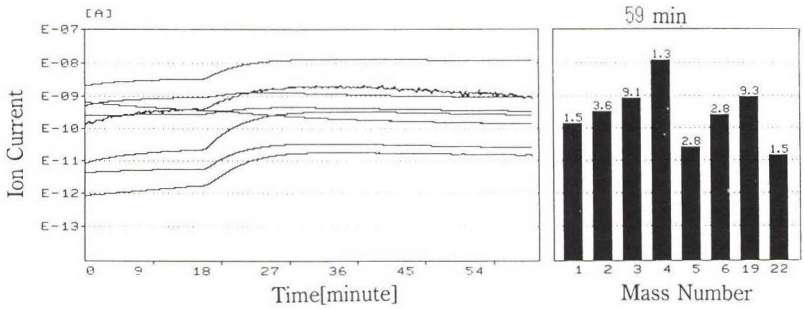

Fig.3 Time behavior of ion currents for mass number 1-6, 19 and 22 with Pd deuteride

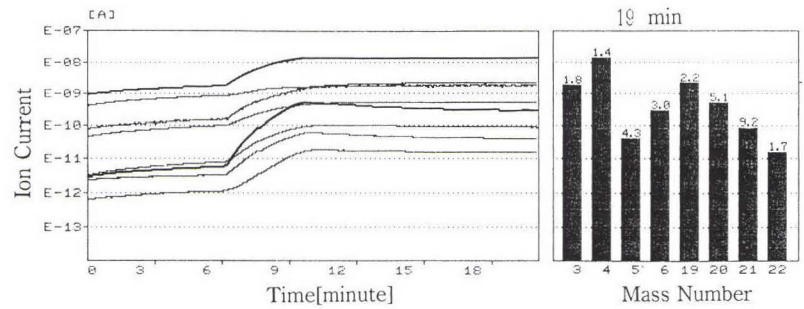

Fig.4 Time behavior of ion currents for mass number 3-6 and 19-22 with Pd deuteride

number 6 is seen in Fig. 4 before the start of current flow. It means that a small amount of T_2 gas had been released from the Pd before the current flow. Several kind of elements [6,7] and ^4He [7] were reported to be observed in Pd deuteride/hydride without discharge.

Time behaviors of currents for Pd hydride are shown in Fig. 5, indicating that gases with mass number 1-4 and 6 were released from the Pd sample. In this case, mass number 3 might be correspond to HD or T, and mass number 4 to D_2 or HT. Thus, D and/or T are considered to be produced in the Pd.

The tritium density reported by the supplier is less than 8.3×10^{-14} and that measured for residual stocked gas in the cylinder is less than 0.25nCi/cm^3. Supposing that higher limit of 0.25nCi/cm^3 was taken as the tritium density, the D_2 gas in loading cell contained 1.03×10^{-11}gram of tritium. On the other hand, the current level for mass number 6 was usually more than 10^{-2} of those of mass number 4 with Pd deuteride. Thus, the released T can be estimated to more than 3×10^{-5}gram from these values and the weight difference between before and after experiment. Therefore, even though supposing that whole the tritium in the loading cell with volume of 80cm^3 under 5atm was absorbed in the Pd sample and was released during experiment, the amount of tritium monitored with the QMAS is at least 3×10^6 times larger than that contained in D_2 gas in the cell before loading. It should be concluded that T was produced in Pd deuteride. Similarly, the amount of T and D in H_2 gas before experiment are too low to explain the

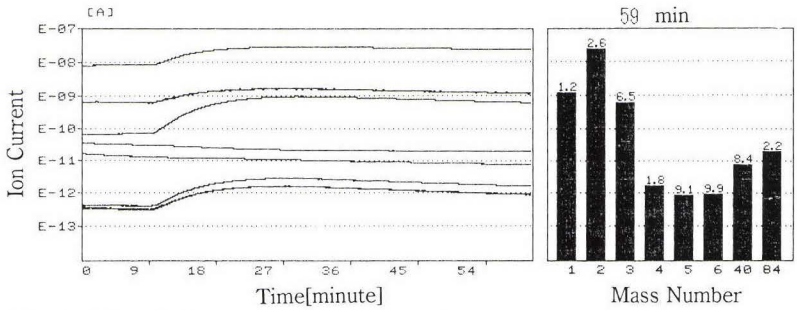

Fig.5 Time behavior of ion currents for mass number 1-6, 40 and 84 with Pd hydride

large amount gas monitored for mass number 2 and 3 in the experiment, which supports that D and/or T was produced in Pd hydride.

3.2 AUTORADIOGRAPHY

Typical autoradiographies for Pd hydride after experiment are shown in Fig. 6. The Lower photographic film was directly contacted with the Pd surface with MnOx film. As the part of photographic film contacted with MnOx film has not been exposed, T would not be produced in this area or a radiation from nuclear products could not penetrate the MnOx film. Of particular interest is the fact that the stronger exposed part in the upper photographic film correspond to the boundary area between the exposed area and non exposed one of the lower photographic film. This means that a nuclear product with stronger radiation was produced in a boundary area between bore and MnOx covering area and that the radiation penetrated the 0.3 mm thickness Pd plate. The radiation would be X-ray due to Bremsstrahlung caused by the deceleration of electron from β-ray decay of tritium in the Pd plate near its surface. The active nuclear reaction is considered to occur when D is released from the Pd and then the D density becomes high in the boundary area. This is supported the fact that the Pd with large decrease in loading ratio after experiment has a tendency to give more film blackening. Pd plates with marked decrease in loading ratio during the exposure time also has a tendency to give higher blackening to negative film. Moreover, the Pd which showed more deformation during loading or during experiment has a tendency to give more film blackening. McKubre et al. [8] have reported that excess heat production need the presence of some flux of D passing through the interface.

3.3 SECONDARY ION MASS SPECTROSCOPY

SIMS was performed for several Pd hydrides before and after experiment; three randomly selected areas of each Pd sample were analyzed. A marked increase in counts of Li after experiment was sometimes observed; a Pd hydride showed increase in the content of the Li two hundreds of times. Contamination due to atmospheric exposure seems to be little.

The whole set of results gives the suggestion that possible nuclear reactions perhaps occurred in the narrow near surface layer, producing new impurity elements such as T and Li. The radioactivity of the sample after experiment may be a result of a nuclear reaction different from that occurred

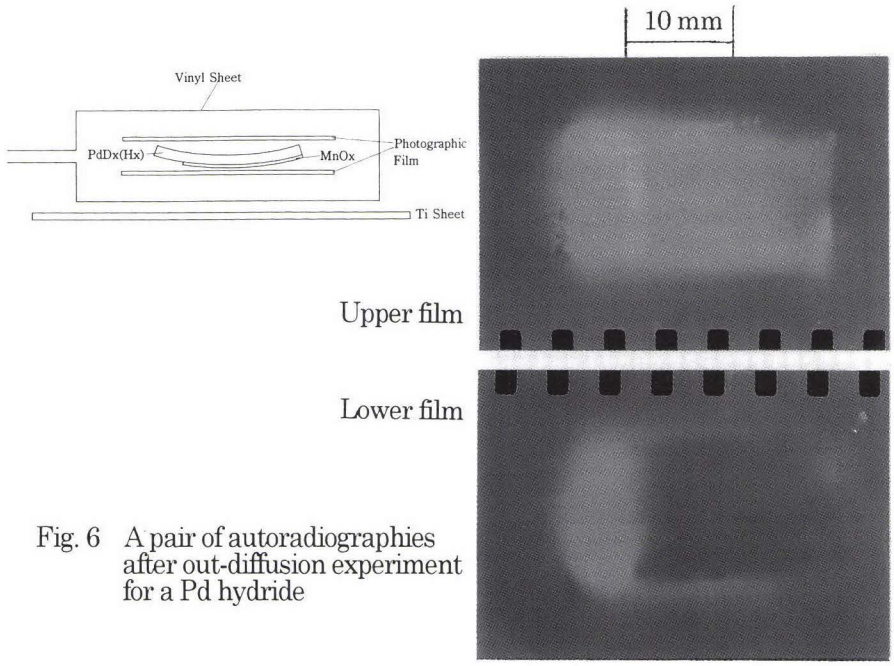

Fig. 6 A pair of autoradiographies after out-diffusion experiment for a Pd hydride

in plasma at high energy region. From the point of view that Pd hydride also yield similar result as Pd deuteride, proton and deuteron should have similar role in the reaction.

4 CONCLUSION

Sudden increase of partial pressure for gases with mass 3, 4, 5 and 6 were observed from Pd deuteride with a MnOx film just after the beginning of DC flow in a evacuated chamber. Time-resolved mass spectra revealed that the gas corresponding to mass number 6 is T_2. That is, tritium was produced in the Pd after loading of deuterium. Similar time behaviors of mass number 1-4 and 6 were also observed for Pd hydride, suggested that similar reaction with tritium production occur in Pd hydride as well. The autoradiograph for almost all Pd samples gave blackening part on the normal monochromatic negative film, indicating beta and/or X-ray was radiated from the Pd. Such a film blackening was obtained without setting in the reaction chamber Pd deuteride as well as Pd hydride. It shows that the reaction would also take place by only loading of deuterium or hydrogen.

REFERENCES

1 E. Yamaguchi et al., Japanese J. Appl. Phys., Vol. 29, L. 666 (1990)
2 I. B. SAVVATIMOVA et al., Fusion Technol., 26, 389 (1994)
3 J. DUFOUR, Fusion Technol., 24, 205 (1993)
4 R. K. ROUT et al., SHRIKHANDE, Fusion Technol., 30, 273 (1996)
5 A. R. CHINDARKAR et al., Fusion Technol., 26, 197 (1994)
6 G. S. QIAO et al., J. New Energy, 2, 48 (1997)
7 L. C. KONG et al., J. New Energy, 3, 20 (1998)
8 M. C. H. McKubre et al., Proceeding of 5th ICCF, p75 (1996)

Conference Proceedings Vol. 70
"ICCF8"
F. Scaramuzzi (Ed.)
SIF, Bologna, 2000

EXPERIMENTAL EVIDENCE OF NUCLEAR REACTIONS IN DEUTERATED TITANIUM SAMPLES UNDER NON-EQUILIBRIUM CONDITIONS INDUCED BY TEMPERATURE VARIATION

Dan Chicea, Dorin Stoicescu

Physics Dept., University Lucian Blaga of Sibiu

ABSTRACT

Several experiments of loading Titanium samples with Deuterium from the gas phase, of changing the temperature of the samples over a wide range and of monitoring the neutron emission were done. Neutron emissions in very low intensity bursts, still significantly above the background were recorded, revealing that low energy nuclear reactions in condensed matter can be produced with a very low rate, which occasionally can be high enough to become detectable.

I. INTRODUCTION

Since the first announcement [1], which stated that nuclear fusion of Deuterium nuclei occurred at low temperature without any external acceleration, experimental work to verify the statement and to investigate the processes has been done all over the world [2] - [5] in sophisticated and in poorly equipped laboratories as well.

In order to verify that nuclear reactions occurred in condensed matter, nuclear radiation should be present; i.e. γ rays, charged particles or neutrons should be detected to a significantly high level during the experiment. In the experiments described hereafter, the neutrons, which are assumed to be produced in the nuclear reaction:

$$d + d = {}^3He + n + 3.27\ MeV \quad (1)$$

were searched for. In Eq. (1) the energy of 3.27 MeV resulting from the nuclear reaction is divided between the neutron and the ^{3}He nucleus; the neutron will have 2.45 MeV [6]. The experiment was focused on searching for neutrons and not the γ radiation or charged particles because the neutrons are less attenuated by the 2 cm thick stainless steel wall of the reactor used for loading the samples.

II. EXPERIMENTAL SETUP

A non-spectrometric system, consisting of a BF_3 proportional counter (Nuclear Enterprise), an electronic counter and a printer was used for the fast neutron detection. In order to reduce the background produced by the natural 1.46 MeV γ line of the ^{40}K contained in concrete, a 5-cm thick Lead slab served as a ground shield for the experiments

performed in the Nuclear Facility of I.T.I.M. Cluj - Napoca. The BF_3 detector, with a cathode of 2 cm diameter, has a pressure of 400 Torr and an active zone 20 cm in length is placed (by producer) in a 30 cm diameter polyethylene moderator. The sensitivity is 4 (imp/sec)/(n/cm^2 sec) for thermal neutrons, provided by producer and consistent with the results of the check performed on a regular basis.

III. THE NEUTRON BACKGROUND

At first the neutron background was monitored to determine the occurrence of the counting rates above the background with more than 3 standard deviations (3σ). It is a standard practice to define a neutron emission from a sample, or event, to be a counting rate higher than the background with more than 3σ [7]. Several simple experiments were performed to assess the natural occurrence of such high-count rates.

The counter worked with counting cycles of 10 minutes, printing each result. The counting time was not changed during the experiments, therefore all the results refer to 10 minutes. Three background monitoring runs, each lasting more than the experiments that were performed. We define the e/t value as the ratio of the high count rates to the total number of records for the time span of the experiment. The highest e/t ratio was 0.7%, therefore it might be considered that a rate higher then 1 % in an experiment can be associated with a neutron emission.

Another method employed to test if a sample emitted neutrons was to analyze the distribution of the recorded values. A Poisson or a Gaussian distribution indicates that the neutrons are produced by one source. Distortion of a normal distribution indicates a perturbation produced by additional source [7]. For a Gaussian distribution, the theoretical standard deviation can be computed as:

$$\sigma_t = \sqrt{< N >} \quad (2)$$

where <N> is the average of the recorded values. The standard deviation can be computed using the experimental recorded values as:

$$\sigma_e = \sqrt{\frac{\sum_{i=1}^{n} (N_i - < N >)^2}{n-1}} \quad (3)$$

where n is the total number of recordings. If the relative difference, $(\sigma_e - \sigma_t)/\sigma_t$ is large then the distribution has a distortion. The highest relative difference for the neutron background is 8%. Next section presents the procedure employed for preparing the samples and for loading them with Deuterium.

IV. SAMPLE PREPARATION AND LOADING

A Titanium surface requires a special activation treatment for the Deuterium to be absorbed in the bulk. Special caution must be taken that the sample surface does not come in contact with organic substances for that location would not absorb Deuterium.

After surface activation samples are placed in a stainless steel reactor that can withstand a 9 MPa pressure from Hydrogen isotopes and temperatures ranging from –250 °C to 900 °C. The gas is removed from the reactor using a vacuum pump and the samples are maintained at 10^{-1} Torr and 500 °C for three hours to ensure a complete sample degazing. All four samples were activated in this manner, but the loading process was conducted differently for each of them as will be discussed. The samples consisted of Titanium small slabs, 1.5 mm x 8 mm x 9 mm.

The absorbed Deuterium mass was calculated using data from pressure and temperature monitoring in a known volume for the first three samples and by weighing the sample precisely for the fourth of them.

After the first sample was activated, the Deuterium gas at a pressure of 7.15 MPa filled the reactor containing the sample at a temperature of 500 °C and then the temperature decreased slowly as the electric heater was disconnected. Subsequently the reactor valve was closed. The pressure decreased rapidly as Deuterium was absorbed into the sample.

The same procedure was used to load the fourth sample while the second sample after activation was maintained at a temperature of 820 °C for 10 minutes with the Deuterium at an initial pressure of 8.25 MPa and then cooled at 13 °C during 3 minutes. These samples presented loading ratios between 0.573 and 1.93. The third sample was activated and then maintained at 680 °C with the initial Deuterium gas pressure of 6 MPa; the reactor with the sample was maintained at this temperature for 5 minutes and then cooled at 13 °C during 3 minutes. The reactor was closed as soon as the Deuterium reached the pressure of 6 MPa. This different treatment was applied to establish a lower value for the loading ratio and a higher pressure of the Deuterium gas in the cold reactor. After that more temperature variation cycles were done with the sample inside, allowing it to absorb Deuterium several more times.

Loading pressure and temperature, sample mass and loading ratio X defined as the number of D over the number of Titanium host lattice ions, for the four samples are presented in Table I.

Sample	Initial Pressure, MPa	Initial Temperature, °C	M_{Ti}, g	M_D, g	$X=N_D/N_{Ti}$
1	7.15	500	9.70	0.2322	0.573
2	8.25	820	6.90	0.556	1.93
3	6	680	3.90	0.308	0.31
4	7.15	500	4.9350	0.2771	1.345

Table I. Loading conditions, mass and loading ratios for the four samples.

V. NEUTRON EMISSION AFTER LOADING TI WITH DEUTERIUM

Neutron emissions from samples 2, 3 and 4 were monitored beginning with the moment the Deuterium reached the Titanium surface for samples 2 and 4, and starting 5 hours after that for the sample 3. The temperatures of the samples decreased as the reactor was losing heat in air. The samples were not subject to any other temperature variation during this type of experiment. Results are presented in Table II, where No. n emissions is the number of records that are above the background with more than 3 σ, e/t is the ratio of the total emission time to the total experiment time, R is the average counting rate and B is the average background, where both R and B are in counts for 10 minutes.

Sample	No. of records	No. n. emissions	e/t, %	$(R - B)/\sigma$
2	102	3	2,9	0,2
3	110	3	2,7	1,1
4	121	16	13	1,64

Table II. Results of the post-Deuterium loading neutron emission.

The most relevant, in respect to neutron emission, was the run conducted with sample 4 and the variation of the neutron counts during the experiment is presented in Figure 1. An interesting feature of the neutron emission is that it occurred randomly and in bursts throughout the experiment.

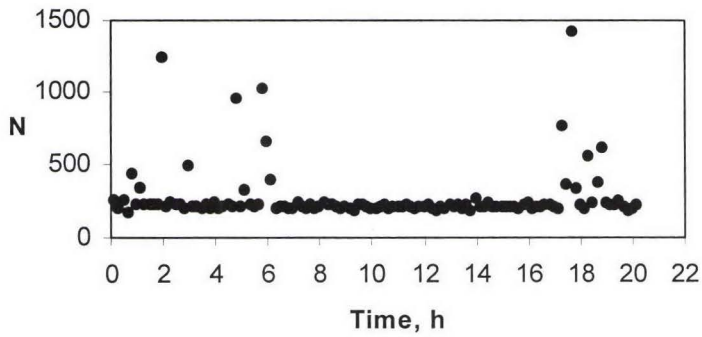

Figure 1. Neutron counts (for 10 minutes) after loading Titanium with Deuterium.

The average background was 225.8 neutrons for 10 minutes, with σ=15. The high values appeared both isolated and as groups over time intervals of 30 to 40 minutes. Another interesting feature of the results is that the average counting rate is higher than the background and for the last experiment with as much as 1.64σ.

VI. NEUTRON EMISSION DURING TEMPERATURE VARIATION BETWEEN 20 ^{o}C AND 700 ^{o}C

One run was conducted for samples 1 and 2 and three runs for the sample 3. Sample 3 was the sample that was loaded at a lower loading ratio to enable it to absorb Deuterium during these experiments. The results of the five runs are presented in Table III, the header being the same that of Table II. It shows that e/t has values considerably above 0.7%, which was the highest value found during the background monitoring.

Sample	No. of records	No. n. emissions	e/t, %	(R – B)/ σ
1	110	2	1.8	0.83
2	25	8	32	2
3	100	26	26	2.5
3	127	13	10.2	162
3	162	16	3.7	0.12

Table III. Neutron emission as a consequence of temperature variation between 20 ^{o}C – 600 ^{o}C.

The first sample was heated and maintained at 700 ^{o}C for 2 hours and cooled slowly to 20 ^{o}C. The pressure inside the reactor was 1 MPa. The second sample was heated and maintained at 700 ^{o}C for 3 hours and cooled rapidly to 20 ^{o}C in 3 minutes; the Deuterium pressure in the reactor was 1 MPa. The third sample was heated and maintained at 600 ^{o}C for 6 hours and cooled slowly to 20 ^{o}C; the initial pressure was 2 MPa and was

not monitored during the other runs. The fourth sample was heated and maintained at 670 °C for 3.5 hours and cooled slowly to 20 °C.

The results presented in Table III show a high e/t ratio, close to 1/3 for sample 2 and an average counting rate higher than the background, especially for sample 3, which are a good indication of neutron emission during the temperature variation experiments.

VII. NEUTRON EMISSION DURING TEMPERATURE VARIATION BETWEEN 293 AND 77 K

This type of experiment consisted of monitoring the neutron emission from Deuterided titanium samples during rapid temperature decrease produced by immersing the samples in liquid Nitrogen.

The first experiment involved sample 1 inside the closed reactor. The reactor was placed near the detector and liquid Nitrogen was poured over it. After the temperature decreased, the reactor was completely covered with liquid Nitrogen and it was maintained at 77 K for 2 hours, then it was extracted and heated slowly to 20 °C. Then immersing was repeated and the Nitrogen evaporated slowly. Neutron emission was monitored for 24 hours.

During the second run sample 1 alone was cooled very rapidly to 77 K by simply dropping it in liquid Nitrogen near the neutron detector. The same procedure was used for sample 2. The results of the data analysis for these three experiments are presented in Table IV, header having the same meaning as in Tables II and III.

Sample	No. of records	No. of emissions	e/t, %	$(R - B)/\sigma$
1	140	2	1.4	0.014
1	22	7	31.8	3.6
2	146	30	21	3

Table IV. Neutron emission during rapid temperature decrease.

During the experiment performed with sample 2 the average background was 206. A sequence of neutron emissions occurred when the liquid Nitrogen evaporated and the temperature of the sample was rising slowly. These sequences, located after the burst of 4821 recorded neutrons and detected 18 hours after the immersion, are presented in Figure 2.

VIII. DISCUSSION

Data from experiments described in this paper was analyzed to check if their distribution is a Gaussian one, as described in Section III. The theoretical and experimental standard deviation was computed for all the experiments performed with samples 2,3 and 4 and results are 289%, 33%, 407%. These values are considerably larger then 8%, which was the highest value found for the background. Therefore it can be concluded [7] that the Gaussian distribution distortion is caused by the neutron emission of the sample.

These experiments performed on TiD_x samples under non-equilibrium conditions confirm the results reported in many other experiments of examining neutron emissions from certain metals highly loaded with Deuterium, [8] - [10]. No other experimental variable related to the processes that accompany the loading of certain metal samples with hydrogen isotopes, like power excess, reported in many experimental papers [1] - [5], was monitored during these experiments.

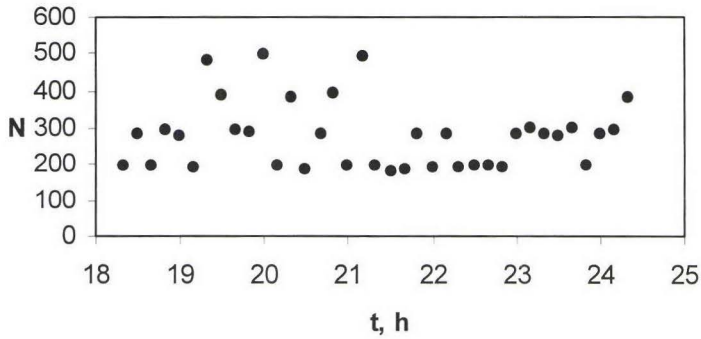

Figure 3. A sequence of neutron bursts during slow temperature increase from 77 K

ACKNOWLEDGEMENTS

I am especially indebted to Drs. Alexandru Biris, Iosif Chereji and Peter Gluck of I.T.I.M. Cluj-Napoca, for the fruitful discussions direct help.

REFERENCES

1. M. Fleischman, S. Pons, "Electrolitically Induced Nuclear Fusion of Deuterium", J. Electroanal. Chem., 261, 301, 1989.
2. Proc. ICCF-3, October 21 – 25, 1992, Nagoya, Japan.
3. Proc. ICCF4, December 6-9, 1993, Lahaina, Maui.
4. Proc. ICCF5, Monaco, April 9-13, 1995.
5. E. Storms, "Critical Review of the Cold Fusion Effect", Journal of Scientific Exploration 10, June 1996.
6. Shirokov Yu.M., N.P.Yudin, NUCLEAR PHYSICS vol. II, MIR Publishers, Moscow, 1982.
7. Ciorăscu F., Oncescu M., "Detection and Measurement of Nuclear Radiation, Romanian Academy of Sciences Press, 1964.
8. M. Alguero, J.F. Fernandez, F. Cuevas, C. Sanchez – "An Interpretation of Some Postelectrolysis Nuclear Effects in Deuterated Titanium", Fusion Technology 29, 390, 1996.
9. F. Celani, A. Spallone, F. Croce, L. Storeli & all, "Search for Ennancement of Neutron Emission from Neutron Irradiated, Deuterided, High – Temperature Superconductors in a very Low Background Environment", Fusion Technology 22, 181, 1992.
10. M. Yagi, Y. Shiokawa, S. Suzuki & all, - "Measurement of Neutron Emission from a Ti-D_2 System", J. Radioanal. Nucl. Chem. Letters 137 /6/, 411, 1989.
11. D. Chicea, D. Lupu, "On Low Intensity Neutron Emission from Tid_x Samples under Non-Equilibrium Conditions", Accepted to be published in Fusion Technology, January 2001.

Conference Proceedings Vol. 70
"ICCF8"
F. Scaramuzzi (Ed.)
SIF, Bologna, 2000

APPLICATION OF CR-39 PLASTIC TRACK DETECTOR FOR DETECTION OF DD AND DT-REACTION PRODUCTS IN COLD FUSION EXPERIMENTS

Roussetski A.S.

P.N.Lebedev Physical Institute, Russian Academy of Sciences
53, Leninsky prospect, 117924, GSP, Moscow, Russia
E-mail: rusets@x4u.lebedev.ru

ABSTRACT

The results of application of CR-39 plastic track detector in Cold Fusion experiments are presented. According to the calibration it is shown, that this detector registered not only dd-fusion reaction products, but also dT ones. The procedures for identifying different particles of dd and dT-reaction are recommended. According to these procedures the possible levels of dd and dT-reactions in different experiments have been estimated.

1. INTRODUCTION

The problems of identification of different particles and background / foreground separation are very important in Cold Fusion experiments. CR-39 plastic track detector, which is used for registration of heavy charged particles, is very convenient instrument for detection not only dd-fusion reaction products:

$$d + d \rightarrow n\ (2.45\ MeV) + He\text{-}3\ (0.82\ MeV) \quad (\sim 50\%) \qquad (1)$$

$$d + d \rightarrow p\ (3.02\ MeV) + T\ (1.02\ MeV) \quad (\sim 50\%) \qquad (2)$$

but also dT ones:

$$d + T \rightarrow n\ (14.01\ MeV) + He\text{-}4\ (3.5\ MeV) \qquad (3)$$

This detector has characteristic response to every type of particles from reactions (1) – (3). Charged particles are registered directly and neutrons – through the secondary recoil particles ore nuclear reactions. Particle tracks on detector became visible after etching and are investigated by microscope technique. The goal of present work is studying of CR-39 detector response to different types of particles from reactions (1) – (3) in different conditions of experiment.

2. EXPERIMENTAL METHODS

2.1. CR-39 detector

CR-39 plastic track detector represents a $C_{12}H_{18}O_7$ polymer with density 1.3 g/cm^3. In this work we used CR-39 produced by Fucuvi Chemical Industry Co., (Japan) in 1996. After exposition the detector was etched in 6N NaOH solution at 70°C during 7 h. After the etching charged particle tracks became visible and can be investigated by microscope.

As it is known, the main parameter of track detector is the ratio of etching rates in and outside track (v_T/v_B). This ratio is the function of ionization energy loss (stoping power, dE/dx). Track diameter is connected with this ratio by parametric equation system [1]. The dependence of track diameter from dE/dx gives a possibility to identify a type of particles. The critical angle of registration ($\theta_c = \arcsin(v_B/v_T)$) is also an important characteristic. θ_c is the minimum angle of particle incidence on the detector when track formation is possible. It is easy to shown, that the detection efficiency for a given type of particles is determine by the relation [2]:

$$\eta = 1 - \sin\theta_c \qquad (4)$$

2.2 DD-calibration

The calibration of CR-39 detectors by dd-reaction products has been carried out by low-energy high-current generator in the Laboratory of Nuclear Science of Tohoku University (Sendai, Japan) [3]. Deuteron beam with primary energy of 10 keV bombarded the TiD_2 target. The low energy of primary deuterons allows to get dd-fusion products with minimum deviation in their energy. CR-39 detector (3x1.5 cm^2) was placed at the distance ~4 cm from interaction point.
After the exposition the detector was etched and investigated by MBI-9 microscope. The investigation of tracks was carried out on square ~1 cm^2 in different points of the detector. The distribution for a number of tracks versus their diameters is shown in fig. 1. There are three peaks on this distribution. According to the dependence of track diameter from dE/dx (the higher dE/dx, the

larger track diameter) it is possible to suppose, that the peak in the region Ø ~ 5 μm corresponds to protons (E_p ~ 3 MeV), the peak in the region ~ 6.4 μm – to tritons (E_T ~ 1 MeV), and the peak in the region ~ 7.2 μm with long "tail" to ~ 10 μm – to He-3 nuclei ($E_{He-3} \leq 0.8$ MeV). Strong dispersion of the third pike may be explained by the fact that He-3 nuclei flied from different depth of target have energy dispersion caused by large ionization loss.

The results of calibration shown, that under conditions when dd-fusion take place in thin (< 0.5 μm) surface layer of the target, the charged particles from reactions (1) and (2) can be reliably detected and identified by CR-39 track detector.

2.2. DT-calibration

To investigate the CR-39 response to He-4 nuclei the detector was irradiated by α- particles from Pu-239 and Ra-226 sources through different Al foils. The dependence of track diameter from energy of α-particles is shown in fig. 2.

In real conditions of experiment when dT-fusion takes place in thick sample, α-particles from reaction (3) may have energies from 0 to 3.5 MeV because ionization loss. Thus, the investigation of reaction (3) yield by α- particles is difficult.

DT-neutrons interact with detector nuclei (C,O,H) and produce different tracks from recoil particles or nuclear reaction products. One of the neutron interaction in CR-39 detector is inelastic scattering on C-12 nucleus caused its decay into three α-particles:

$$n + C\text{-}12 \rightarrow n' + 3\alpha \qquad (Q = -7.37 \text{ MeV}) \qquad (5)$$

The cross section of reaction (5) is ~ 190 mb at E_n = 14.5 MeV, the threshold of neutron registration in CR-39 by this reaction is ~ 10 MeV. The presence of three α-particle tracks outgoing from single point allows to separate these reactions from other neutron interactions with CR-39 nuclei. The efficiency of dT-neutron registration in CR-39 detector was investigated in [4].

The irradiation of Cr-39 detectors was carried out with dT-neutron source of Rare Metal Industry Institute (GIREDMET, Moscow)[5]. The dT-neutrons were generated in TiT_2 target bombarded by the 350 keV deuteron beam. The density of neutron flux at the target chamber was $4x10^{10}$ n/cm^2/s. The CR-39 detectors were placed at a distance of 31 cm from the target. Both usual CR-39 detectors, and detectors with 60 μm polyethylene radiator were used. The detectors were oriented at five different angles (0°, 30°, 45°, 60°, 75°) to the neutron flux. The exposure time was 5 s. Thus, the neutron fluence at the detector plane was ~ $2x10^8$ n/cm^2.

After the exposition the detectors were etched and investigated by optical microscope. The microphotographs of several 3α-events are presented in fig. 3. We can see many different pictures of this events depending on the energy transmitted to C-12 nucleus and direction of α-particle emission.

The mean values of the detection efficiency for dT-neutrons by reaction (5) (for five different directions of the neutron flux) were estimated as $(4.7 \pm 0.6)x10^{-7}$ and $(1.2 \pm 0.1)x10^{-6}$ for detector without and with radiator respectively. The increase in the efficiency for the detector with radiator is caused by the detection of 3 α-particles from reaction (5) that takes place not only in etched layer (~10 μm) but also in the radiator layer near detector surface.

The investigation of small yields of dT-reaction in Cold Fusion experiments may be very useful, because the background flux of neutrons with energy more than 10 MeV on the earth surface is negligibly small. The measurements showed that the density of background 3α-events in CR-39 detector not exceed one per few cm^2. It allows to carried out very long expositions of detectors at very low background.

3. RESULTS AND DISCUSSION

3.1. The measurement of dd-reaction yield in Pd/PdO deuterated heterostructures

The PdO/Pd/PdO and PdO/Pd/Au samples were prepared in the Institute of Physical Chemistry, Russian Academy of Sciences from 30-60 μm Pd foils by the method described in [6]. This samples were deuterated by electrolysis in 1M NaOD solution in D_2O. The current density was ~20 mA/cm^2, the duration of electrolysis – 5-20 min. After the electrolysis the sample was washed by pure D_2O and dryed by filter paper. Then, the sample was placed on CR-39 detector and compressed between two plates by screw. The sample was heated to ~50°C to stimulate the desorption of deuterium. The time of one cycle of measurements was 1-2 h. Then the sample was deuterated again and the cycle was repeated. The full time of exposition was 20 h.

Then the detector was etched and investigated by MBI-9 microscope. As it was noted, the investigation of yields for reaction (1) and (2) from thick samples is difficult, because charged

particles come to detector with large energy spread and their tracks have different diameters. The accurate estimation may be only for dd-reactions take place in thin surface layer. So we used the following method for estimations. We chouse only events when track of proton (E_p~ 3 MeV, Ø ~ 5 μm) spaced near (~15 μm) the other track Ø ~6-7.5 μm (triton, E_T ~ 1 MeV ore He-3, $E_{He-3} \leq 0.8$ MeV). As you can see in fig. 2, tritons and He-3 nuclei have close track diameters and their distributions can be intersected. This disposition of two tracks may be accidental or it may be caused by presence of some zones in the sample with high concentration of D, where dd-fusion is more probable. The registration efficiencies of this events we estimated by (4), taking into account that critical angles for proton (E_p ~3 MeV), triton (E_T ~1 MeV) and He-3 (E_{He-3} ~0.8 MeV) are ~60°, ~40° and ~5°, respectively.

For the detector contacted with deuterated sample the track density of events, satisfied the criteria mentioned above, is estimated as (24.0 ± 3.4) cm^{-2}. For the background detectors contacted with unloaded sample and the sample loaded by hydrogen it was (4.0 ± 1.4) cm^{-2}. Thus, the density of double tracks caused by "coincidence" (not in time but in space) of products of reactions (1) and (2), taking place in thin (< 0.5 μm) layer of sample, is (20 ± 4) 1/cm^2. For the exposure time 20 h the mean flux of dd-fusion reactions may be estimated as $(2 - 6)\times10^{-3}$ s^{-1} into 4π solid angle per 1 cm^2 of the sample. This value is in good agreement with the result of measurements of reaction (2) yield carried out by Si SSB detector – $(3.6 \pm 1.0)\times10^{-3}$ s^{-1} into 4π solid angle [7].

3.2.The measurement of dd-reaction yield in glow discharge of D_2

The CR-39 detector was also used in the measurements of dd-reaction yield in glow discharge of D_2 with Pd, Ti and Nb cathodes[6]. The detectors were placed at the distance of ~3 cm from the cathode. The detectors with different covers were used to prevent the irradiation by ultraviolet rays. The control experiments were carried out in glow discharge of H_2. The mean flux of dd-protons during the long-time exposition (~10 h) was estimated as (0.03 – 0.18) s^{-1} into 4π solid angle per 1 cm^2 of the cathode. These results are presented in more detail at this conference (A.Karabut, A.Lipson, A.Roussetski).

3.3.The measurement of dT-reaction yield in deuterated Pd/PdO heterostructures

In this experiment we used Au/Pd/PdO and PdO/Pd/PdO samples with a thickness of 8, 20, 40, 60 μm and dimensions - 2x4 cm^2. The loading of samples with deuterium and the expositions of detectors were carried out by the procedure mentioned above, except the thermostimulation of D_2 desorption. The exposure time for CR-39 detectors was 7-72 h. Hydrogenated samples were used in background measurements. After the exposition, the detectors were etched in standard conditions. The investigation of tracks was carried out by a microscope supplied with Hitachi video-system in the NHE-laboratory, Sapporo (Japan).

We look for events with characteristic disposition of three α-particle tracks directed to a single point (3α-events). These events corresponded to decays of C-12 nucleus in CR-39 material into 3α-particles caused by high-energy neutron (E_n> 10 MeV). It was scanned ~ 30 cm^2 of detectors both in background and in foreground measurements. The mean track density of 3α-events was in foreground $\langle n_{3\alpha f} \rangle = (0.81 \pm 0.16)$ cm^{-2}, in background - $\langle n_{3\alpha b} \rangle = (0.20 \pm 0.09)$ cm^{-2}. Taking into account the exposure time we get the mean value of 3α-event flux $\langle n_{3\alpha} \rangle = (1.2 \pm 0.3)\times10^{-6}$ cm^{-2}s^{-1}. If we know the registration efficiency for dT neutrons by reaction (5), we can to estimate the mean dT neutron flux emitted from deuterated samples. This value was estimated as $n_n \leq 1$ n/s/cm^2. We need to note, that to explain this flux x of dT-neutrons we need to suppose the production $10^2 - 10^5$ tritons/s/cm^2 with energies from few keV to few MeV. This value is more higher than yield of tritons from dd-reactions. So there is ,at least, two explanations for effect of 3α.-events

(1) The emission of dT-neutrons as a result of production of fast tritons in deuterated samples by unknown channel.
(2) The emission of high-energy neutrons (E_n > 10 MeV) resulted from some unknown nuclear reactions. These processes may be 3d and 4d fusion reactions predicted by A.Takahashi [8].

4. CONCLUSION

Thus, it is established that CR-39 track detector can to detect all particles from reactions (1) - (3). This detector can be successfully used in long-time experiments on Cold Fusion.

In conclusion the author want to express the appreciation to Dr. A.Lipson (Institute

of Physical Chemistry, Moscow) for his help during all stages of the experiments and fruitful discussions of problem. I also very thank to Prof. J.Kasagi (Tohoku University, Japan) for his help in dd-calibration on the deuteron beam, and to Dr. N.Asami (Japan) for the possibility of microscope measurements in the NHE-laboratory. I am appreciative to Dr. A.Andreev (GIREDMET, Moscow) for the help in irradiation of detectors by dT-neutrons. I am very grateful to Drs. A.Marenny, N.Nefedov and V.Kushin (Moscow) for the help in preparation of CR-39 detectors and the scientific consultations.

References

1. Samogyi G., Shalay S.A. Nucl. Instr. And Meth., **109**,(1973), N 2, 211.
2. R.L.Fleisher, P.B.Price, R.W.Walker. Nuclear Tracks in Solids. Principles and Applications. University of California Press, 1975, v.1.
3. H.Yuki, T.Sato, T.Otsuki et al. J. Phys. Soc. Jpn. **66**, (1997) 73.
4. Marenny A.M., Nefedov N.A., Roussetski A.S. Kratkie Sobshenia po Fizike FIAN (Bulletin of Lebedev Physics Institute) **6**, (1998) 42.
5. Andreev A.V., Baryt I.J., Varych O.M. Atomnaia Energuia (Atomic Energy) **66**(2), (1989) 134.
6. A.G.Lipson, B.F.Lyakhov, B.V.Deryaguin, D.M.Sakov. Sov. Tech. Phys. Lett. **18**(10), (1992) 673.
7. A.G.Lipson, B.F.Lyakhov, A.S.Roussetski et. al. Fusion Technology. 2000. In press.
8. A.Takahashi. Fusion Technology, **26**(4T), (1994) 451.

Figure captions

Fig. 1. Distribution of track diameters of dd-fusion reaction products in CR-39 detector etched in 6N NaOH solution at 70°C during 7 h.
Fig. 2. Dependence of α-particle track diameter from their energy for CR-39 detector etched in 6N NaOH solution at 70°C during 7 h.
Fig. 3. Microphotographs of 3α-events in CR-39 detector exposed to dT-neutrons.

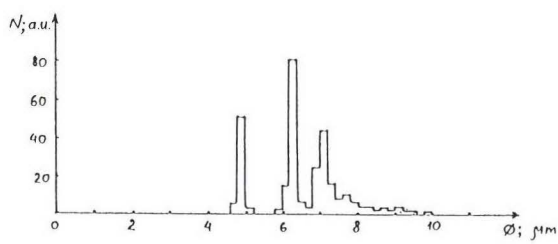

Fig. 1.

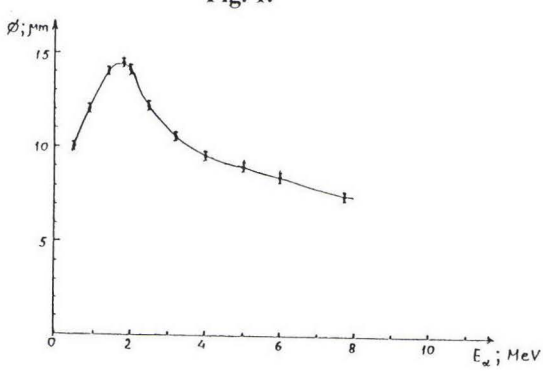

Fig. 2.

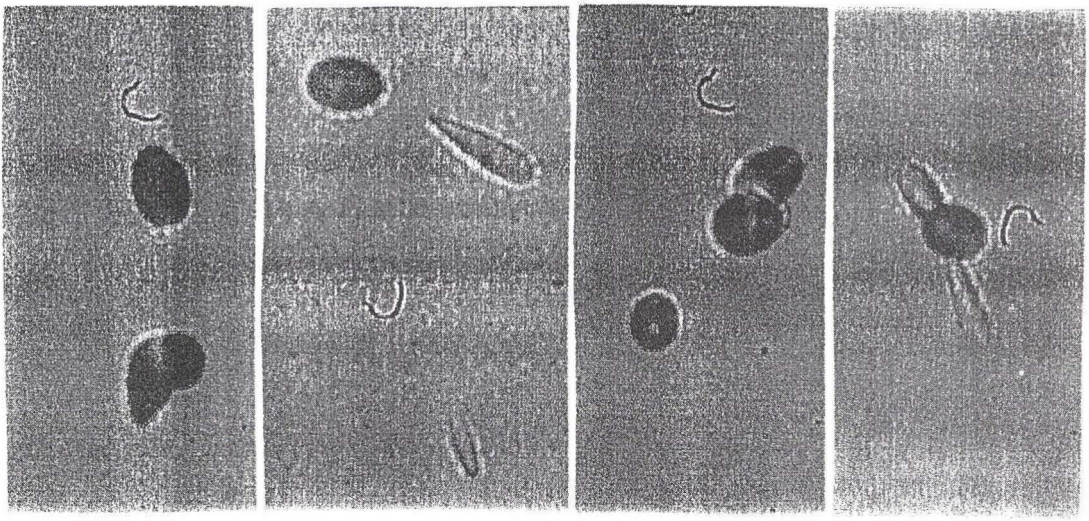

Fig. 3.

Conference Proceedings Vol. 70
"ICCF8"
F. Scaramuzzi (Ed.)
SIF, Bologna, 2000

REGISTRATION OF SUPERFLUOUS HEAT AT SORBTION-DESORBTION OF HYDROGEN IN METALS

V.A.Romodanov, *N.I.Khokhlov, **A.K.Pokrovsky

StateRI SIA"LUTCH", Zheleznodorozhnaya 24, Podolsk, Moscow reg. 142100. RUSSIA. Tel.:095-137-9258. Fax.:095-137-9384. E-m.:luch@atis.dhtp.kiae.su
* StateSC RF "Karpov SRPCI", Vorontsovo pole 10, Moscow, 103064. RUSSIA.
**SDL SRC "TENEKS", Volzhskiy boulevard b.8, h.1. Moscow, 109518. RUSSIA.

ABSTRACT

Emergence of an excess heat which can arise at interaction between hydrogen isotopes and a heated metal membrane with various covers has been investigated. The covers of these membranes were both continuous and separate on the enter or exit side. It is shown, that at desorbtion of hydrogen from hydride-forming metals with various continuous covers an excess heat generation was observed. The same structures can absorb the excess heat at their saturation with hydrogen.

The phenomenon of the excess heat generation which can arise in passing of hydrogen through the membrane with a cover on the exit side and adsorbtion of the excess heat in passing of hydrogen through the membrane with a cover on the enter side has been discovered. It is established, that, the amount of generated or absorbed excess heat in passing of hydrogen through the asymmetrical membrane was increased with increasing hydrogen flow.

1. INTRODUCTION

Emergence of both nuclear and thermal effects at transfusion of hydrogen isotopes through some metals with radiation-stimulated and thermal activation was shown earlier in [1-4]. One of the most interesting facts was the detection of a zone with maximum temperature ahead of glow discharge area for revolving of a sample loaded in hydrogen. That fact visually indicated an existence of anomalous excess heat at low-energy interaction of hydrogen isotopes with a solid [5]. The obtained results permited to determine new demands necessary for excess heat generation emerging at interaction of hydrogen isotopes with a solid.

The present work is devoted to the study of a nature of emerging excess heat generation and new effects, appearing at interaction of hydrogen isotopes with any kind of metals and environment during transfusion of hydrogen through the solid compositions.

2. EXPERIMENTAL DESIGN AND PROCEDURE

The technique, which is similar to the discribed one in [5], was used for experiments on sorbtion-desorbtion of hydrogen in metals and complex samples, but for the membrane experiments there was used the technique discribed in [4]. In all the cases the regime thermo-activation was used only. The scheme of sorbtion-desorbtion experiments is presented in Fig.1.

Sample 3, which is a gang slices 0.5-1 mm in thickness, 30x30 mm in size, about 30-50 mm in package breadth in vacuum chamber 1. Sometimes the sample was made as a spiral or zigzag with maximal sizes up to 50 mm. The samples were made of vanadium or niobium of technical purity (the total contents of impurities did not exceed 1%), and they had weight to 100 g. Chromel-alumel thermocouples 4 were placed inside the samples. Temperature changes within the range of 300-1600 K were obtained due to changes of supplied power to the molybdenum heater. The chamber was filled by hydrogen up to a pressure of $(20-100)\cdot 10^3$ Pa. The technique implied that during about 10 s a certain power of the heater was installed and a rate of changing sample temperature was registrated depending on time for both temperature increase and its decrease. The absolute error for of tempera-

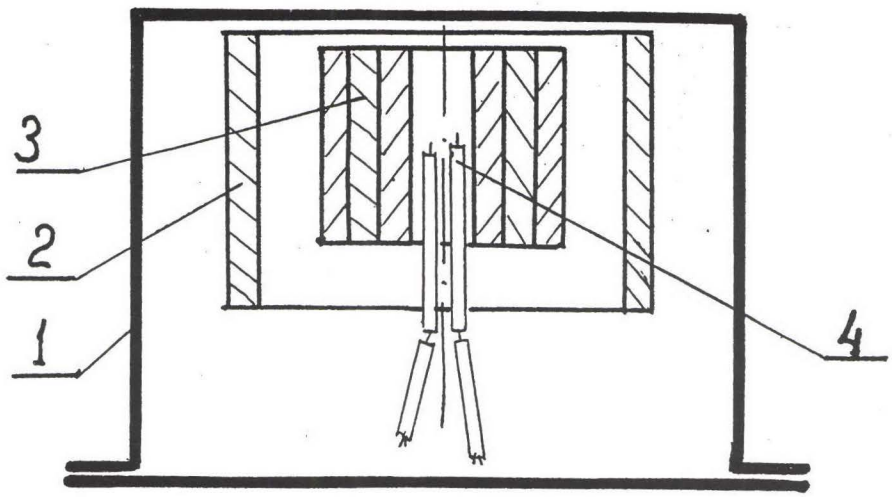

Fig.1. The scheme of experiments on sorbtion-desorbtion of hydrogen.
1-vacuum chamber; 2-heater; 3-sample; 4-thermocouple.

ture measurements was not worse $\pm$5%, and relative $\pm$0.3%.

A new equipment system was used for the membrane experiments, a unit of it is presented in Fig.2. Metal sample 3 0.01-1 mm in thickness and 60 mm in diameter was plased into molybdenum tank 2 and pressed by ring 6 with the help of clamps 4 and bolts 5. All the unit was placed in the vacuum chamber and heated up by the resistive heater made of molybdenum. A temperature of the sample was changed in the range of 300-1100 K. For monitoring temperature three thermocouples 1 were pressed to the sample, in so doing the absolute error of membrane temperature measurements was not worse than $\pm$10%, and the relative one was $\pm$0,5%. The membrane samples were made of sheets of vanadium, niobium, tantalum, titanium etc. Thin (0.01-50 microns) covers with specific porosity were created on some samples. Those covers were applied to one side or to both sides together. Outside and inside the tight sample we could create both vacuum 10^{-2}-10^{-4} Pa and a pressure of hydrogen isotopes of $(0.1\text{-}100)\cdot 10^{3}$ Pa. For experiments we used a nature mixture of hydrogen isotopes with concentration $1.5\cdot 10^{-2}$% of deuterium in protium (ordinary hydrogen) and 95% of deuterium with 5% of protium (technical deuterium).

The technique of the experiments was consisted in that at the beginning we set the certain membrane temperature for evacuation from two sides of the membrane, and then we made fast filling of hydrogen up to the specific pressure under one side of the membrane. In certain conditions emergence of a step on the dependence of temperature versus time is possible, and the temperature can be both increased and reduced.

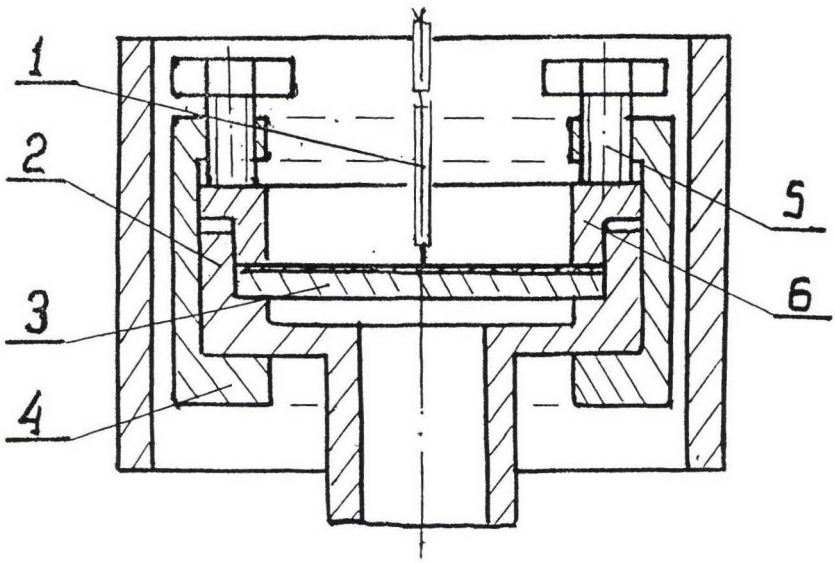

Fig.2. The scheme of a unit for membrane experiments.
1-termocouple; 2-tank; 3-membrane; 4-clamps; 5-bolts; 6-ring.

3. RESULTS

In Tab.1 the parameters values of a number of experiments on sorbtion-desorbtion for vanadium samples with thin copper cover are given. From this table we notice, that maximum temperature changes because of excess heat generation have achieved 50-75 K. An example of dependence of a temperature change versus time for sorbtion-desorbtion experiments, for a vanadium spiral sample with copper cover about 20 nm in thickness, is shown in Fig.3. Here we can see, that the desorbtion of previously saturated hydrogen in vacuum, hydrogen and ammonia with water has noticeable temperature peaks. In many cases we observed gently sloping return peaks, which were considerably smaller in magnitude but more long (about 2 hours) in time, on the plot of temperature changing at cooling of the sample, that pointed to absorbtion of heat at cooling of the sample and sorbtion of hydrogen. On the vanadium and niobium samples without covers the temperature peaks at desorbtion did not exceed 5-10 K, and usual processes of hydrogen sorbtion-desorbtion gave the noticeable shelfs of heat absorbtion at hydrogen desorbtion and heat generation at hydrogen sorbtion on the temperature curve.

The preliminary experiments with a passage of hydrogen through a membrane have shown, that if the membrane is pure on both sides or there are identical covers on them, then the membrane temperature drops a little for hydrogen passage, because of cooling by more cold gas. If the thin cover is applied to the membrane side, through which the hydrogen enters, the temperature considerably drops, showing, that is the membrane is cooled much more, than from hydrogen flow associated with hydrogen heat capacity. If hydrogen is passed through the membrane with the exit side cover, its temperature it will be increased, and a value of the temperature increasing is determined by a value of hydrogen flow through the membrane (Fig4).

Some results on measurement of additional generation or absorption of excess heat emerging for passage of hydrogen through the niobium membrane with nickel cover on one of sides are shown in Tab.2. The maximum

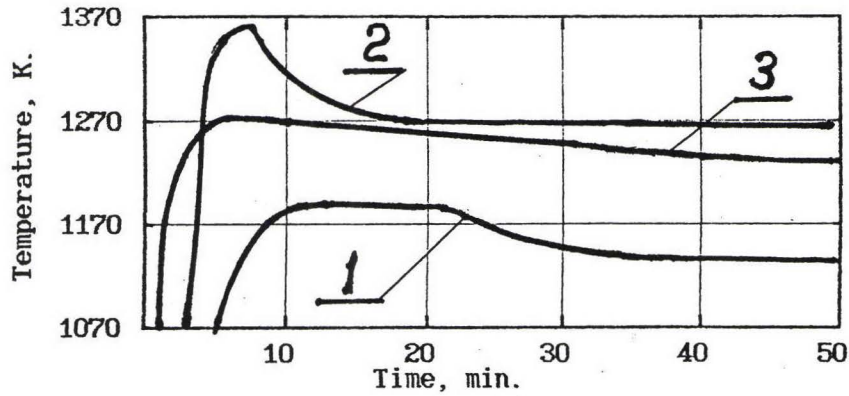

Fig.3. Dependence of changind sample temperature versus time for sorbtion-desorbtion experiments with vanadium sample(V-0.4 mm+ Cu-20 nm).

1-vacuum; 2-hydrogen, 40000 Pa; 3-NH_3 + H_2O, 15000-28000 Pa.

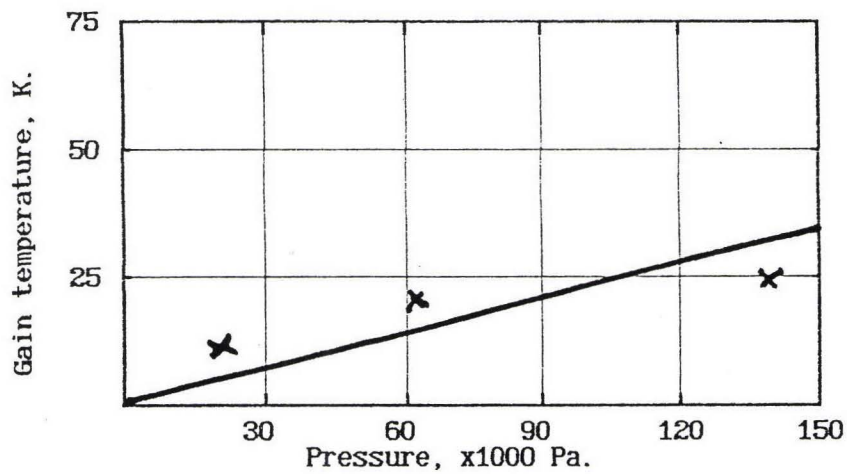

Fig.4. Dependence of membrane temperature increase versus hydrogen flow.

Table 1.

Parameters of experiments on measurement of excess temperature for vanadium sample with copper cover (V–0.4 mm+Cu–20nm)

Environmental	Pressure	Current	Temperature	Excess temperature	Time of preliminary loading	Summary time of excess pike	Time for maximum pike	Quantity of excess heat
	Pa x 1000	A	K	K	h	min	min	arbitr. units
H	80	1400	1180	20	18	73	6	36
H	80	1400	1190	20	6	63	7	24
H	80	1400	1190	20	14	87	7	85
H	80	1400	1170	19	21	67	10	52
H	80	1400	1190	18	2	30	4	-
NH_3 + H_2O	15-28	1350	1200	33	96	53	7	48
Vac.	10^{-6}	1200	1140	42	47	53	12	46
Vac.	10^{-6}	1150	1110	12	2	-	13	-
Vac.	10^{-6}	1200	1140	12	3	40	10	-
H	40	1350	1240	75	17	33	4	20

Table 2.

Parameters of membrane experiments on measurement of excess heat for niobium sample with nickel covers

Sample	Pressure in sam volume	Pressure in ch.	Temperature	Temper. difference	Hydrogen flow	Excess power	Specific power
	$x10^{-3}$ Pa	$x10^{-3}$ Pa	K	K	Mol/s	W	eV/atom
NbO.2+	134	10^{-6}	495	10	$2\cdot10^{-7}$	1.4	38
NiO.025	142	10^{-6}	770	27.5	$1\cdot10^{-6}$	4.2	22
Ni in	137	10^{-6}	830	25	$2\cdot10^{-6}$	3.6	10.5
chamber	148	10^{-6}	985	7.5	$3\cdot10^{-6}$	1.1	2
NbO.2+	142	10^{-6}	485	-2.5	$1\cdot10^{-7}$	-0.4	-
NbN-	162	10^{-6}	680	-12.5	$3\cdot10^{-6}$	-1.9	-3.1
20HM in	153	10^{-6}	800	-2.5	-	-0.4	-
v. samp	155	10^{-6}	980	-17.5	$5\cdot10^{-6}$	-2.6	-2.7
NbO.1+ NiO.025	146	10^{-6}	970	-5	$3\cdot10^{-6}$	-0.4	-0.6
Ni in v sample	10^{-4}	75	1020	+16.2	$1\cdot10^{-5}$	+1.2	+0.7
NbO.2+	151	10^{-6}	535	7.5	$3.5\cdot10^{-7}$	1	15.3
NiO.025	154	10^{-6}	670	25	$1.3\cdot10^{-6}$	3.5	13.7
Ni in	144	10^{-6}	855	12.5	$6.9\cdot10^{-6}$	1.8	1.4
chamber	147	10^{-6}	930	15	$2.6\cdot10^{-5}$	2.2	0.4

flow of excess heat achieved 3-5 W for the optimum temperature of 700-800 K. Specific values of excess heat in relation to passed atoms of hydrogen were increased at a flow dininution (lowering of membrane temperature) and they achieved several tens electron-volt per atom (0.4-38 eV/atom). It was noted, that both the generated magnitudes of excess heat and absorbed ones for return hydrogen flow had the comparable magnitudes.

4. DISCUSSION

The new phenomenon which consists in generation of excess heat at passing of hydrogen isotopes through the membrane with a cover on the exit side and in absorbtion of excess heat at passing of hydrogen isotopes through the membrane with a cover on the enter side has been discovered. The indicated covers change not only the kinetics of a hydrogen penetration through the membrane, but also the energetics of the processes. The phenomenon is not limited in time and, taking into account the results on sorbtion-desorbtion, is exhibited as for hydrogen passage through the membrane into vacuum, so also into various mediums, for example, hydrogen or ammonia and water. The evaluations of the spesific energy release do not give an unequivocal answer about a nature of the mechanism of discoveried phenomenon yet. Nevertheless, a level of some tens electron-volt per atom of hydrogen allows to hope for a reality of nuclear models too. It is not presented while the answer about a reason of convertibility of excess heat generation or its absorbtion at changing hydrogen flow direction through the asymmetrical membrane.

5. CONCLUSION

5.1. It has been shown, that for hydrogen desorbtion from hydride-forming metals with various continuous covers the generation of excess heat is observed. The same structures can absorb excess heat at their saturation by hydrogen.

5.2. The phenomenon of the generation of excess heat at passing of hydrogen through the membrane with a cover on the exit side and the absorbtion of excess heat at passing of hydrogen through the membrane with a cover on the enter side has been discovered.

5.3. It has been established, that the amount of generated or absorbed excess heat at passing of hydrogen through the asymmetrical membrane is increased with increase in hydrogen flow and has the optimum range of temperature for maximum values ~700-800 K. The specific amount of generated excess heat increases for reduction of hydrogen flow (diminution of temperature) and its maximum value for membrane Nb-0.1mm + Ni-0.025mm achieved almost 40 eV/atom (0.4-38 eV/atom) for lower temperatures (~500-700 K).

REFERENCES

1. V.A. Romodanov, V. Savin, Ya. Skuratnik and Yu. Timofeev. Frontiers of Cold Fusion. Proceedings of the ICCF3. Nagoya, Japan. Ed.by H. Ikegami. Universal Academy Press Inc., Tokyo, Japan,1993, p. 307-319.

2. V. Romodanov, V. Savin, Ya. Skuratnik, V. Elksnin. Proceedings. ICCF4.Hawaii. TR-104188-V3, EPRI, 1994, p. 15(1-15).

3. V.A.Romodanov, V.I.Savin, Ya.B.Skuratnik. Progress in New Hydrogen Energy. Proceedings ICCF6. Japan. Ed. by M.Okamoto. Publiched by NEDO. IAE. Tokyo, Japan, 1996, V.2, p. 585 - 589.

4.Vitaliy A.Romodanov, Valeriy I.Savin, Yakov B.Skuratnik, at all. Proceedings ICCF7. Canada. Ed. by G.Miley. Publiched by ENECO, Inc. Salt Lake Sity, Utah, USA, 1998, p. 319-324.

5.Vitaliy A.Romodanov, Valeriy I.Savin, Yakov B.Skuratnik, at all. Proceedings ICCF7. Canada. Ed. by G.Miley. Publiched by ENECO, Inc. Salt Lake Sity, Utah, USA, 1998, p. 325-329.

Conference Proceedings Vol. 70
"ICCF8"
F. Scaramuzzi (Ed.)
SIF, Bologna, 2000

GENERATION OF TRITIUM FOR DEUTERIUM INTERACTION WITH METALS

V.A.Romodanov, *Ya.B.Skuratnik, **A.K.Pokrovsky

StateRI SIA"LUTCH", Zheleznodorozhnaya 24, Podolsk, Moscow reg. 142100. RUSSIA. Tel.:095-137-9258. Fax.:095-137-9384.E-m.:luch@atis.dhtp.kiae.su
* StateSC RF "Karpov SRPCI", Vorontsovo pole 10, Moscow, 103064. RUSSIA.
**SDL SRC "TENEKS", Volzhskiy boulevard b.8, h.1. Moscow,109518. RUSSIA.

ABSTRACT

Reserch on tritium generation for interaction of hydrogen isitopes with a solid in conditions of thermal activation both in stationary conditions, and in dynamic mode at transfusion of hydrogen isotopes through the heated membranes has been made.

It has been estabiliched that a long endurance (26750 h) of hydrogen in metal, heated up to 820 K does not result to tritium generation. An accumulation of tritium in hydrogen and deuterium passing through the heated metal membranes has been fixed. A specific rate of tritium accumulation in deuteriums is almost three times greater than a rate of its accumulation in hydrogen, that testifies to a possibility of tritium generation in deuterium not only due to its before accumulated release, but due to nuclear reactions.

1. INTRODUCTION

Tritium takes a special place in research on products formed as a result of low-energy nuclear reactions. In the environment it is six order less, than 4-helium, and the sensitivity of the equipment recording beta-radiation is much higher than the sensitivity of mass-spectrometers. So, when we try to find a correspondence between generation of excess heat and nuclear products, the tritium generation research should be preferred. Earlier we detected tritium generation and excess heat at transfusion of hydrogen isotopes through the metal membrane both in conditions of glow discharge, and of thermal activation [1-4]. However, it is not clear yet, what part of tritium generation is connected with releasing tritium, accumulated in the environment before, and what part is connected with nuclear reactions. The present work is devoted to study tritium generation for interaction of hydrogen isotopes with metals at transfusion of isotopes through the membrane.

2. EXPERIMENTAL DESIGN AND PROCEDURE

Hypothesis for reallity of nuclear reactions with tritium generation in stationary conditions [3] for interaction of nature mixture hydrogen isotopes ($1.5 \cdot 10^{-2}$% of deuterium in protium) with heated metals in conditions of long experiment was checked up in the tight system, Fig.1.

Sample 3 made of zirconium hydride with stoichiometry closed to ZrH_2 was placed in to the reactor 2 with oxidizing atmosphere 4. The oxidizing atmosphere hindered release of hydrogen from hydride zirconium in the heated condition. The reactor was heated up by resistive heater 1, in which a temperature of the sample (750-820 K) was supported for 26750 h. After endurance of the sample, it was taken out of the reactor. Trial parts of 0.4-0.5 g were broken off the sample then. Then the parts of hydride zirconium were dissolved in 5 ml of concentrated sulfuric acid. The trial parts were dissolved approximately by 90% for 2 hours at 360 K. The residual part of the test was washed, dried and weighed. During dissolution of the test the selected hydrogen was mixed with the air and burned on the incandescent spiral in the cylindrical furnace. Water from the burning was freezed in the cooled trap at a temperature of 260-270 K. Then 0.2 ml of the derivated water were entered in to liquid scintillator ZHS-8 and the content of tritium was measured on installation Beta-2. The

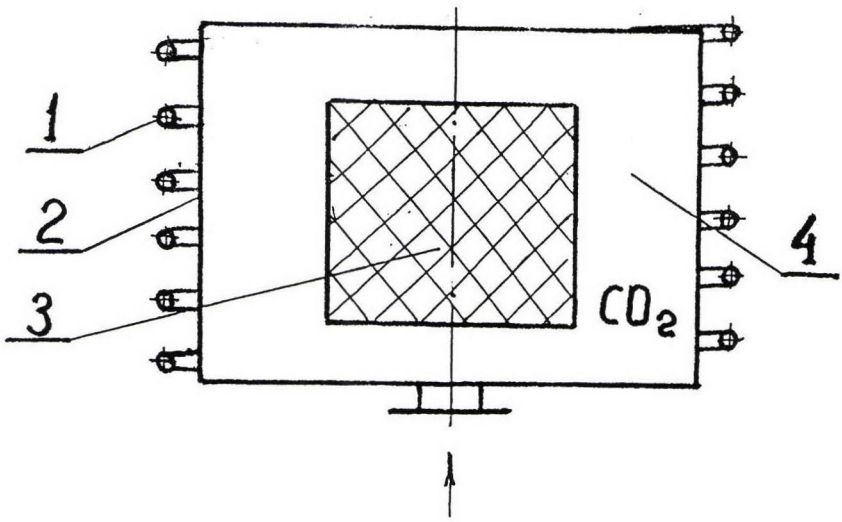

Fig.1. The scheme of experiment on interaction of hydrogen with metals in stationery conditions.
1-resistive heater; 2-reactor; 3-sample; 4-medium oxidizing.

efficiency of measurements of beta-particles in the mode of measuring the test was 28% according to measurement standarts VNIIFTRI. Weighing of the exemplars was conducted on the analytical balances to $1x10^{-4}$ g accuracy.

The experiments on research in tritium generation for passing of hydrogen isotopes through the membrane were conducted on the installation circumscribed in [5]. The addition implied that gas passed through the membrane and evacuated by a pump was collected in a rubber cushion and then burned and analyzed on tritium by the scintillation technique circumscribed above. Niobium and tantalum slices 0.02-0.2 mm in thickness and 60 mm in diameter were used as the membranes. For experiments we used a mixture of hydrogen isotopes with concentration 0.015% of deuterium in protium (ordinary hydrogen) or 95% of deuterium with 5% of protium (technical deuterium). Gas, passing through the membrane was collected during 3-7 h.

3. RESULTS

The results on research in the content tritium of zirconium hydride after a long endurance are presented in Tab.1. It is visible, that the difference in the gain of activity of the tests was made 7% (from the initial state to the state after long endurance with zirconium hydride heating). For the general error of the technique of $\pm$ 50% it is possible to consider such changing as not essential and to make the conclusion, that the long endurance in the heated condition of hydrogen in the metal lattice does not result in tritium generation.

The results on research in the tritium content after passing of hydrogen isotopes through the membrane in the thermal activation condition are represented in Tab.2. It is shown, that the tritium generation rate

Table 1

Activity of zirconium hydride before and after long endurance in heated conditions (26750 h, 750–820 K)

Material	Weight	Activity backgr.	Activity backgr. middle	Probe activity	Probe activity middle	Gain activity	Gain activity
	mg	pulse/100s	pulse/100s	pulse/100s	pulse/100s	pulse/100s	Bk
ZrH_2 background	502	55 59 49 53 51	53.4	65 72 69 63 70	67.8	14.4	0.58
ZrH_2 after endurance	487	69 51 57 50 52	55.8	61 80 72 64 69	69.2	13.4	0.54

in dynamic mode achieved $10^7 - 10^8$ atom/s, in so doing tritium occurred both in hydrogen and in deuterium. The tritium genereton rate in deuterium approximately three times greater than its value for hydrogen.

4. DISCUSSION

For long endurances hydrogen in zirconium hydride was in the closed volume and did not exchange with the environment. So, for the minimum difference in activity of hydrogen extracted from the initial sample and after long endurance with heating it is possible to state, that the presence of hydrogen in the heated up solid does not result in nuclear reactions and generation of tritium.

The pressurization of hydrogen and deuterium through the niobium and tantalum membranes has significantly increased the initial activity of purged gas, and the tritium generation rates were compared with the obtained ones earlier in glow discharge [1]. If it is granted that the tritium generation rate, obtained on hydrogen, in the given system is associated with the release of the tritium, accumulated in the environment before, so about half of tritium generation rate in the deuterium ($\sim 2 \cdot 10^7$ atom/s) can be associated with the nuclear reactions.

5. CONCLUSION

5.1. It has been istablished, that the long endurance of hydrogen (26750 h) in the lattice of zirconium for isothermal conditions (750–820 K) does not result in tritium generation.

Table 2.

Results of research on tritium generation in membrane experiments for passing of hydrogen isotopes

Membrane	Gas	Volume	Temperature	Pressure in vol. sample	Pressure in chambers	Time	Tritium generation rate	Specific tritium gener. rate	Rate relation
		l	K	$x10^{-3}$ Pa	$x10^{-3}$ Pa	h	at/s	at/ s·l	V_D/V_H
Ta0.1+ 4Nb0.03	H_2	10	850	55	10^{-6}	6	$2.4 \cdot 10^7$	$2.4 \cdot 10^6$	-
Ta0.1+ 2Ta0.02	D_2	10	690		10^{-6}	3	$8.9 \cdot 10^7$	$8.9 \cdot 10^6$	3.7
5Ta0.02	D_2	10	850	100	10^{-6}	5	$7.6 \cdot 10^7$	$7.6 \cdot 10^6$	3.2

5.2. It has been shown, that the tritium accumulation in the hydrogen and deuterium passed through the heated up metal membranes testifies to a possibility of tritium generation. In case of tritium generation in deuterium it is hoped that it occurs not only due to its accumulation in the environment earlier, but also as a result of nuclear reactions.

REFERENCES

1. V.A. Romodanov, V. Savin, Ya. Skuratnik and Yu. Timofeev. Frontiers of Cold Fusion. Proceedings of ICCF3. Japan. Ed. by H. Ikegami. Universal Academy Press Inc., Tokyo, Japan, 1993, p. 307-319.

2. V.A.Romodanov, V.I.Savin, Ya.B.Skuratnik. Progress in New Hydrogen Energy. Proceedings of ICCF6. Japan. Ed. by M.Okamoto. Publiched by NEDO, IAE. Tokyo, Japan, 1996, V.2, p. 585 - 589.

3. Vitaliy A.Romodanov, Valeriy I.Savin, Yakov B.Skuratnik at all. Proceedings of ICCF7. Canada. Ed. by G.Miley. Publiched by ENECO, Inc. Salt Lake Sity, Utah, USA, 1998, p. 319-324.

4. Vitaliy A.Romodanov, Valeriy I.Savin, Yakov B.Skuratnik at all. Proceedings of ICCF7. Canada. Ed. by G.Miley. Publiched by ENECO, Inc. Salt Lake Sity, Utah, USA, 1998, p. 325-329.

5. V.A.Romodanov, N.I.Khokhlov, A.K.Pokrovsky. Registration of Superfluous Heat at Sorbtion-Desorbtion of Hydrogen in Metals.
Presented on ICCF8, 2000.

Conference Proceedings Vol. 70
"ICCF8"
F. Scaramuzzi (Ed.)
SIF, Bologna, 2000

Erzion Discovery in Cosmic Rays and its Possible Great Role in Nature in Framework of Erzion Model of Cold Nuclear Transmutation

Bazhutov Yu.N.

State Technical Univercity (MADI)
P.O.Box 169, 105077 Moscow, Russia
E-mail: bazhutov@erzion.madi.ru

ABSTRACT

With help of telescope (DOCH-4) of two coaxial scintillation detectors located vertically on the surfase of the Earth it was discovered new stable single charged particles with mass $M=(175 \pm 25)$ GeV/c^2 during 106 hours. Their intensity in cosmic rays on the Earth surface is $J=(1.8 \pm 0.4).10^{-6}$ $cm^{-2}sr^{-1}s^{-1}$ (at E<6 GeV, P<50 GeV/c). The discovered particles characteristics are in full correspondence with our phenomenological predictions, with our previous experimental results and with the prediction of "mirror" model for the existing of stable heavy hadrons (Erzions), hypothetical catalysts of Cold Nuclear Transmutation. Erzion existence in Nature can give principle explanation for many problems in Astrophysics, Geophysics, Cosmic Ray Physics. The same important role Erzion can play in new pure Nuclear Energetics and Technology (radioactive wastes utilization, cheap production of some chemical elements and isotopes etc.).

INTRODUCTION

The hypothesis about new penetrating stable heavy hadrons [1,2] was proposed to explain the anomalous slope of cosmic muon energy spectra [3,4,5]. Many of the characteristics of the hypothesized hadrons (mass, charge, lifetime, intensity, nuclear interaction mode, interaction and absorption paths) were predicted phenomenologically to harmonize the very copious anomalous and ordinary experimental cosmic ray data and to make them consistent. There are many different experiments in cosmic rays which indicate on existence of stable heavy particles [6-15], but there are no any simple and correct proofs until now. Later, we made attempts to find them experimentally [16-21] and to construct a model that would offer a theoretical support to their long lifetime ($\tau > 10^{-5}$ s), given their very high mass (M > 30 GeV/c^2). Now Standart models [25] fail to explain such long time for heavy elementary particles in term of weak interaction. The pioneer attempts were made using the supersymmetrical model [22], but the use of the «mirror» model U(1)xSUl(2)xSUr(2)xSU(3) [23-24] proved to be more successful. This model [23,24,30] appeared to explain not only cosmic rays anomalous results , but the same new great discovery in Physics - Cold Nuclear Fusion [31]. In framework of this «mirror» model Erzion - hypothetical heavy hadron - is meson doublet (E^0,E^-) and consists of heavy untiquark (U*) and usual quark (u), or (d) [E^0=(U*,u), E^-=(U*,d)]. With nuclei it can create only one erzion-nucleus: Enion [E_n=(U*,u,u,d,d)],

which can dissociate as to neutral pare of particles (E^0,n), as to charged pare (E^-,p) with different coupling energy. Such way Erzions (Enions) can provide Erzion-nuclear catalysis due to nucleon exchange reactions with great cross-sections or great frequency (~THz) in solid state materials.

ERZION DISCOVERY IN COSMIC RAYS

The theoretical ideas about the structure of hypothetical heavy hadrons, given a better understanding of their interaction mode, have permitted the heavy hadron search experiments to be designed more consistently on the basis of the purpose-oriented underground facility of the Institute of Nuclear Physics of the Moscow State University (40 m.w.e., $S\Omega \sim 10^3$ cm^{2}sr). The facility has operated for ~200 hours and detected three appropriate events of the sought particles ($J_E \cong 4 \cdot 10^{-8}$ cm^{-2}sr^{-1}c^{-1}) [18-19].

For different reasons, unfortunately, the experiments with the second and third generation equipment [20-21], which was cheaper and simpler in use, have failed to yield any positive results. In this work it has been realized the simplest fourth-generation equipment to search for stopped heavy charged particles in cosmic rays. The experimental facility is a vertical telescope composed of a pair of coincidence-mode scintillation detectors (SD) (see Fig.1). The upper detector, SD1, is a thin CsI crystal (Ø63x0.35 mm^2) coupled to a FEU-110 photomultiplier; the lower detector, SD2, is a thick NaI single crystal (Ø150x100 mm^2) coupled to a FEU-49 photomultiplier. High voltage is supplied from a BNV3-0,5 source to FEU-110, and from the SBS-50M analyzer chip (see below) to FEU-49 (see Fig.1).

The two crystals are spaced 50 mm coaxially apart, so the telescope aperture is $S\Omega \cong 30$ cm^{2}sr. The pulses from either SD-s are recorded (see Fig. 1) with a C8-17 dual-trace memory oscilloscope with the coincidence time 0,5 μs. Besides, the telescope was adjusted and monitored to check on its proper performances by recording the pulses also from SD2 with a «Greenstar» Co-made SBS-50M multichannel (8192 channels) analyzer chip built into an IBM-PC, as well as with an AI-1024 multichannel analyzer (SD1).

The expected correlations of the SD1 and SD2 pulse amplitudes (A_1 and A_2) were calculated using the Bethe-Bloch and Bragg curves and the path-energy functions plotted for singly-charged particles of different masses (1, 10, 150, 200, 1000 GeV/c^2) on the basis of the similar curves for protons in different media [26,27,28] (see Fig.2). The A_1 and A_2 values are presented in their normalized form in units of the amplitudes that are most probable to occur in the differential spectra of amplitudes induced by separate relativistic cosmic muons in either of the SD-s (μ_1, μ_2).

During 106 hours of its operations, from July 6 to 30, 1999, given the event selection thresholds $A_1 \geq 1\mu_1$ (events intensity $3 \cdot 10^{-3}$ s^{-1}) and $A_2 \geq 10\mu_2$ (events intensity 0,1 s^{-1}), the telescope detected 23 events in which the

amplitudes A_1, and A_2 were observed simultaneously. Fig.2 shows the events together with the theoretical curve for protons and hypothetical singly-charged heavy particles with masses of 10, 150, 200, and 1000 GeV/c^2. The calculations were made assuming that the non-relativistic hadrons loose their energy for ionization only, so their nuclear interactions can be disregarded, i.e., they behave lepton-like. In accordance with the Pearson fitting criterion [27], almost all of the experimental points (except for three) are within the confidence domain of two curves calculated for singly-charged heavy particles with mass of 175 GeV/c^2, namely χ^2=0.95 . The fact is of great importance that the falling branches of the two curves adjoin the points corresponding to the particle stoppages inside SD2 and permitting the mass of a sought particle to be estimated reliably. From the condition of the particles being non-relativistic (V<0.3 c) and allowing for the telescope dimensions (l=d+h=15 cm) it follows that their lifetime τ must be longer than their flight time in the telescope(t=l/v); hence $\tau_E > 1.5 \cdot 10^{-9}$ s. During the 106 hours-long experiment, 20 particles were detected. The recorded particle mass is M_E=175±25 GeV/c^2, the particle ionization A>10μ ($E_E \leq$ 6 GeV, $P_E \leq$ 50 GeV/c) proved to be increased, and the particle intensity is J_E = N / S·Ω·T $\cong$ 20 / (106·3600·30) = =(1.8±0.4) $\cdot 10^{-6}$ [$cm^{-2}sr^{-1}s^{-1}$], which is in a good agreement with the expected intensity [1,2] and does not contradict three «appropriate» events recorded at 40 m.w.e. underground (see the above explanations). Meanwhile, all three «appropriate» events were of negative charges as recorded by the magnetic spectrometer, just what follows from the Erzion model of the hypothetical particles [23,24].

ERZION ROLE IN NATURE

As it was noted earlier Erzion model (EM) was created not only for interpretation of abnormal results in cosmic rays but the same for interpretation of Cold Fusion results. Such way EM must solve these problems but in future it turns out that EM can solve a lot of another problems. Let us look through some of them.

EM can give principle explanation for many problems in Astrophysics and Geophysics. The most global from them is the problem of dark matter in Universe. It was solved on principle in article [24] due to such fact that neutral Erzion in EM may be absolute stable particle and mustn't create coupled state with nuclei although it is hadron. EM can also solve the Solar Neutrino problem as it was done in [34] with supposition that in almost all Solar volume Erzion catalysis nuclear reactions are running with Erzion density about 100 cm^{-3}. In this case Erzion nuclear catalysis provides 70% of energetic Solar balance and only 30% is due to thermonuclear cycle. And because of in Erzion nuclear catalysis neutrino is almost absent its flux is three time less. Excess Jupiter energetic disbalance has the same decision [34] due to Erzion nuclear catalysis running in only 10^{-5} of Jupiter mass where the temperature is enough (~10^5K) to stay Enion free from nuclei capture and density is the same as in Solar (100cm^{-3}). The problem of catastrophic reducing of Li,Be,B contents in the Solar and Earth matter was solved in [34] due to such fact that in EM these elements are the best fuel. The similar interpretation has the problem of C^{13} isotope disbalance in some diamonds [35], where C^{13} is best fuel and C^{12} is best Enion donor and at some conditions (high temperature and pressure) such Erzion

catalysis reactions can run. The excess He^3 and T isotopes in Volcano products has the same interpretation [34] of running such Erzion cycles inside of Earth. The Ball-lightning nature had its decision in framework of EM too [35] . At some conditions (lightning discharge to tree) Erzion nuclear catalysis can be started in organic and air matter and due to enough Erzion density and temperature inside this plasma may be continued rather long up to 100s in plasma volume up to $1000cm^3$ with power up to 1MW.

Some Cosmic Rays problems can be solved in framework of Erzion model too.

Erzion hypothesis has appeared to explain the abnormal muon energy spectrum [1]. Such way this problem has been decided due to EM. More over, as Erzion consists of usual quark (u,d) and heavy (U*) antiquark, it must take part in 2-component inelastic strong nuclear interaction : interaction by usual quark with usual cross-section but with small inelasticity coefficient or interaction by heavy antiquark with very small cross-section and with inelasticity coefficient equal to 1. Due to such interaction in Cosmic Rays there are appeared events with long-length hadron cascades [8,15] and with large across momentums in cascades at high energy [28,29]. Due to rather heavy Erzion mass and its penetrating feature there are appeared delayed particles in Air Showers [10,11,14]. The problem of high energy neutral particles flux from local space sources [36] couldn't be decided because stable neutral hadrons are absent in Standart Model of Elementary Particles but Erzion is the same particle and can solve this problem too [34].

The same important role Erzion can play in Applied Science and Future Technology due to Erzion Catalysis Model of Cold Nuclear Transmutation. As it was shown in introduction Erzion-nuclear catalysis due to nucleon exchange reactions with great cross-sections (or great frequency ~THz) in solid state materials can provide in principle creation of new energy-capacious, ecology-pure and technology-simple nuclear energetics [24,35,37,38]. But for such creation we must study all Erzions features and its interactions features. In such cold exothermic nucleon exchange reactions only more coupled nuclei are formed. And because all radioactive nuclei are not more coupled then stable in such reactions due to Erzion catalysis almost always radioactive nuclei must transmutate to stable nuclei. Such way there are solved the problem of principle and radical radioactive wastes utilization [39,40]. More over, in framework of such Erzion catalysis nuclear reactions we can provide cheap production of some chemical elements and isotopes [39] (gold for example) etc.

CONCLUSION

There are discovered a new species of stable heavy singlecharged particles in cosmic rays (*Erzions*) whose parameters are: mass M_E = (175±25) GeV/c^2, intensity in cosmic rays on the Earth surface J_E = $(1.8\pm0.4)\cdot10^{-6}$ $cm^{-2}sr^{-1}s^{-1}$ at $E_E \le 6$ GeV and $P_E \le 50$ GeV/c, lifetime $\tau_E > 1.5\cdot10^{-9}$ s. The events recorded [32,33] are quite in agreement with our phenomenological predictions, with the earlier experimental results of searching for the hypothetical particles, and with the predictions of the «mirror» model that offers a theoretical support to the feasibility for the hypothetical stable heavy hadron (*Erzions*) to exist actually.

Erzion existence in Nature has great significance. It can give principle explanation for many problems in Astrophysics, Geophysics, Cosmic Ray Physics. The same important role Erzion can play in new pure Nuclear Energetics and Technology (radioactive wastes utilization, cheap production of some chemical elements and isotopes etc.).

The author is indebted to Drs. L.A.Mikaelyan, V.S.Murzin, B.A.Khrenov, L.G.Sapogin, A.F.Perekalski, N.I.Khokhlov, S.N.Yashin, D.S.Baranov, A.M.Frolov, V.G.Grishin for their assistance and support and to Drs. I.V.Goryachev, V.P.Koretsky, E.V.Pletnikov and V.P.Levitsky for their help in preparing the work for publication.

REFERENCES

1. Yu.N.Bazhutov et al. Izv. Akad. Nauk SSSR, ser. Fiz., **46**, 2425 (1982).
2. Yu.N.Bazhutov. Ph.D. Thesis, Moscow (1984).
3. Yu.N.Bazhutov, G.B.Khristiansen et al. Proc. 16-th ICRC, Kyoto, **10**, 24 (1979).
4. Yu.N.Bazhutov, G.B.Khristiansen et al. Proc. 17-th ICRC, Paris, **7**, 59 (1981).
5. Yu.N.Bazhutov et al. VANT, ser. Exp. Tech. in Physics, **26(5)**, 24 (1985).
6. G.R.Alcock, R.C.M.Yock et al. Proc.13-th ICRC, Denver, **3**, 2106 (1973).
7. P.N.Bhat, S.C.Tonvar et al. Proc. 16-th ICRC, Kyoto, **13**, 8-13 (1979).
8. A.I.Demiyanov et al. «Nuclear-cascade process in c.m.», Moscow, Nauka, (1977).
9. V.V.Avakyan et al. VANT, ser. Exp. Tech. in Physics, **25(4)**, 77-80 (1985).
10. H.Sakujama, N.Suzuki et al. Proc. 20-th ICRC, Moscow, **9**, 181-188 (1987).
11. H.Sasaki, S.Sato, A.Nioshioka et al. Proc. 20-th ICRC, Moscow, **6**, 366-369 (1987).
12. S.G.Baiburina et al. Izv. Akad. Nauk SSSR, ser. Fiz., **53 (2)**, 277-279 (1989).
13. V.S.Aseikin et al. Izv. Akad. Nauk SSSR, ser. Fiz. , **53(2)**, 307-310 (1989).
14. G.K.Garipov et al. Izv. Akad. Nauk SSSR, ser. Fiz., **55(4)**, 682-685 (1991).

15. S.B.Shaulov. Izv. Akad. Nauk SSSR, ser. Fiz. , **57(4),** 25-28 (1993).
16. Yu.N.Bazhutov. Proc.18-th ICRC, Bangalore, **11**, 24 (1983).
17. Yu.N.Bazhutov, V.I.Kovalev et al. Inventor's Certificate, **4171305** (1988).
18. A.V.Abramov, Yu.N.Bazhutov et al. Proc. All-Union CRC, Alma-Ata, **1**, 101 (1989).
19. A.V.Abramov, Yu.N.Bazhutov, Yu.L.Spiridonov. « FPINVOF », CRIMB, 53 (1990).
20. Yu.N.Bazhutov, G.M.Vereshkov. Preprint No.**2** , CRIMB (1990).
21. Yu.N.Bazhutov, V.P.Koretsky et al. Proc. 24-th ICRC, Rome, **1**, 1056 (1995).
22. Yu.N.Bazhutov, G.M.Vereshkov et al. Proc. All-Union CRC, Alma-Ata, **1**,103 (1989).
23. Yu.N.Bazhutov, G.M.Vereshkov. Preprint No.**1** , CRIMB (1990).
24. Yu.N.Bazhutov, G.M.Vereshkov, V.I.Cuksa. Proc.RCCFNT-3, Moscow, 157 (1996).
25. L.B.Okun. «Leptons and Quarks», Nauka, Moscow (1981).
26. «Physical Units». ed. by I.S. Grigoriev, Energoatomizdat, Moscow, 1141 (1991).
27. V.I.Kalashnikova et al. «Elementary Particles Detectors», Nauka, Moscow, 16 (1966).
28. S.Hayakawa. «Physics of Cosmic Rays», Moscow, Mir, **1**, 105 (1973).
29. V.S.Murzin. «Introduction into Cosmic Ray Physics», Atomizdat, Moscow (1979).
30. Yu.N.Bazhutov, G.M.Vereshkov et al. «FPINVOF», CRIMB, 67 (1974).
31. M.Fleischmann, S.Pons, M.Hawkins. Journ. Electroanal. Chem., **261**, 301 (1989).
32. Yu.N.Bazhutov. WWW.XXX.LANL.GOV/List/Hep-ex/9908053.
33. Yu.N.Bazhutov. VINITI, N2872-B99, Moscow (1999).
34. Yu.N.Bazhutov. Proc. ICCF-4, Hawaii, **4,** 25-1 (1993).
35. Yu.N.Bazhutov. Proc. ICCF-6, Sapporo, **1**, 396 (1996).
36. Yu.N.Bazhutov et al. VANT, ser. Exp. Tech. in Physics, **33(2),** 45 (1985).
37. Yu.N.Bazhutov et al. Proc. Conf. «Physics & Conversion», Kaliningrad, 141 (1991).

38. Yu.N.Bazhutov, G.M.Vereshkov. Proc. ICCF-4, Hawaii, **4**, 8-1 (1993).

39. Yu.N.Bazhutov, V.P.Koretsky, A.B.Kuznetsov. Proc. ICCF-4, Hawaii, **4,** 27-1(1993).

40. Yu.N.Bazhutov, V.P.Koretsky. Proc. ICCF-6, Sapporo, **1**, 392 (1996).

Conference Proceedings Vol. 70
"ICCF8"
F. Scaramuzzi (Ed.)
SIF, Bologna, 2000

REPRODUCIBILITY OF EXPERIMENTS IN GLOW DISCHARGE AND PROCESSES ACCOMPANYING DEUTERIUM IONS BOMBARDMENT

Irina Savvatimova
Scientific Industrial Association "Lutch"
24, Zhelesnodoroznaya St., 142100 Podolsk, Moscow Region, Russia

ABSTRACT

The problems of reproducibility of experiments in glow discharge (GD) and electrolysis are considered. The difficulty in estimation of nuclear and non-nuclear processes contribution in isotopic and elemental composition change in material irradiated by ions is noted.

The post-experimental charged particles flow from samples in Deuterium GD was measured. The current ranging ~ 10^{-6}A·см$^{-2}$ - ~10^{-13}A·см$^{-2}$ was registered in the first 1-3 post-experimental minutes for different materials (Pd, Pd alloys, Ag and Mo) and experimental parameters. The emissions duration lasted 30-100 minutes and depended upon experimental parameters.

Analysis of tracks on X-ray films placed inside and outside of a metal GD chamber has shown existence of tracks varying from several to tens of millimeters. The tracks were of various shapes: round and curvilinear, and also rotating including double spirals.

PROBLEMS of REPRODUCIBILITY

The problem of why researchers get different effects in similar experimental conditions in electrolysis and in gas GD experiments attracts a lot of attention. All "pro" and "against" are not clear yet. However the questions of the surface preparation [1], configuration and surface topography [1], the contribution of preferably lighter elements sputtering from the surface, and also the contribution of chemical sputtering seems no less important.

The following processes influence the surface isotopic and elemental composition change in the course of ion bombardment: 1- preferential sputtering of lighter isotopes; 2 - diffusion separation; 3 - concentrations gradient; 4 - mechanical stresses gradient; 5 - implantation of elements from the device parts and from gaseous environment. However, the experimental data and calculations supplied by numerous researchers show that the change of surface composition in binary alloys for ~ 0,5-5 keV energies were small and were kept within the limits of measurement errors. The change of isotopic surface composition during ionic bombardment resulting from mass distinction and surface connection energy for pure metals is insignificant. The preferential sputtering – isotope separation with energies < 1 keV is equal or < 10 %, for isotopes with masses of ~100 it amounts to~ 0,003 %[2].

The influence of hydrogen on anomalies of processes should be taken into account. Among them are enhanced diffusion, interaction of hydrogen complexes with different types of structural defects, accelerated transport of impurities along dislocations and fastening of impurities (including gas impurities) on the defects [3].

It is known that irradiation of materials by low-energy ions is accompanied by such physical processes at the atomic level which proceed simultaneously: knocking of atoms from the crystal lattice nodes, sputtering and re-precipitation of atoms. And the resulting formation of vacancies and interstitions, their clusters, and also of separate dislocations, dislocation loops,

grids and dislocations and pores accumulation is going on. Sputtering on the defects leads to changes in surface topography, formation of cones, salients, "whiskers". It can also bring about changes in local current density, microarcing and microexplosions on the "tips" and other defects.

The microarcs and microexplosions, in turn, can be by a reason of high cramping and pulling stresses in microvolumes of the surface layers as result of the fast instantaneous melting and hardening in these microvolumes. The stresses can result to dislocation formation and to intensification of diffusion processes, to acceleration of the transport of impurities along dislocations at hundreds and thousands times and can give the redistribution of impurities.

POST GD MEASUREMENT of NEGATIVE PARTICLES FLOW from the CATHODE SAMPLES

The effect of " life after death " (as M. Fleischmann had called it in his paper " The Heat after Death " [4].) can also be registered for negative charged particles from sample exposed to deuterons after GD switch off. " Life after death " was confirmed in the papers published earlier on glow discharge investigations (ICCF2 — ICCF7 and the 1-7th Russian Conferences on Cold Fusion and Cold Nuclear Transmutation and also in others publications). The authors noted that X-ray films after contact with samples exposed to Hydrogen and Deuteron in GD became black too [5]. It was assumed that the blackening resulted from β-emissions. This kind of emissions was also registered in 15 minutes after removal of samples from the discharge chamber. The "hot points" on the upper Pd samples were observed for the first 2 hours of the exposure.

Some data on charged particles registration from cathode samples after the GD switch off are presented, the measurements having been taken in ~1-2 minutes.

The measurement of charged particles flow was carried out with the help of U5-6 electrometric amplifier. The electrometric amplifier is designed for measurement of positive or negative charged particles flow (for stationary and slowly changing currents) within the range of $1 \cdot 10^{-13}$ - $1 \cdot 10^{-6}$ A. U5-6 amplifier operates on the principle of small currents measurement in accordance with the number of voltage drops on the fixed resistance ($1 \cdot 10^{12}$; $1 \cdot 10^{10}$; $5{,}1 \cdot 10^{6}$ Ohm). There are three overlapping ranges for current measurement: I - ranging ~$1 \cdot 10^{-13}$ - $1 \cdot 10^{-10}$ A; II - ranging ~$1 \cdot 10^{-12}$ - ~$1 \cdot 10^{-8}$ A; III – ranging ~ $1 \cdot 10^{-9}$ - ~$2 \cdot 10^{-5}$ A. The measurement error of the first range amounted to ~10 %, the second and the third ±5 %, correspondingly. The peak value for low-frequency fluctuations voltage corresponds to noise for each range: I ~ $3 \cdot 10^{-15}$-$5 \cdot 10^{-16}$A, II ~$1 \cdot 10^{-13}$ -$2 \cdot 10^{-14}$A, III < $1 \cdot 10^{-11}$ A.

The samples were of 20 mm in diameter, ~100 μkm in thickness and the exposure area of 1 cm^2. The operating gas used was Deuterium. The chamber pressure was down to 10^{-4} Torr and up to 5-15 Torr when filled with gas. The samples were exposed to irradiation at 30-300 mA current, 50-1100 Volts voltage, the time duration ranging 1,5-4 hours. The charged particles measurement system calibration was carried out on a tritium target placed instead of a sample in the vacuum discharge chamber. The electrometer showed a current ~ $5 \cdot 10^{-11}$À from a tritium target from ~1cm^2 area with radioactivity ~ $4{,}1 \cdot 10^{9} cm^{-2} c^{-1}$ in vacuum ~$1 \cdot 10^{-4}$ Torr. It means that β-emission after ten minutes post-irradiation was usually $<10^{7} cm^{-2} c^{-1}$.

The post-irradiation sample current measurement diagram is given in Fig. 1

The duration of the emission varied by two or three times and the registration duration amounted to ~ 30-100 minutes. The current within first minutes was usually the biggest. However some samples showed weak current within the limit of electrometer sensitivity threshold. It depended upon the following parameters: current density at the first stage (during loading), quantity of loaded Deuterium at this stage, cathode temperature and less dependence from Voltage. The emission current for various Pd samples ranged $\sim 1 \cdot 10^{-6}$ - $\sim 2 \cdot 10^{-13}$A and was dependent upon the parameters of the process. The tendency to increase current for Pd during gas evacuation from 10^{-1} to 10^{-3} Torr was observed. Current was changed from $9.7 \cdot 10^{-7}$ to $1,2 \cdot 10^{-6}$ in the course of 80 minutes. Current from Ag sample increased by ~20 %(to $\sim 1,2 \cdot 10^{-6}$ A) in the course of 15 minutes of gas pumping-out of deuterium from $1 \cdot 10^{-1}$ Torr to $1 \cdot 10^{-4}$ Torr and was decreased to $\sim 10^{-14}$A. One hour post-irradiation β-emission was always $< 10^{6}$ $cm^{-2}c^{-1}$. So, 10^{-13}A correlate with $10^{7} cm^{-2}c^{-1}$β-emission. It is good conformed with Fig.4[5].

In PdPtW alloy the current was increased by ~ 2 times for 20 minutes after GD switch off (up to $\sim 4 \cdot 10^{-5}$A). The unstable short-term increase of emission current on PdPtW for the first 1-2,5 minutes after the GD switch off was noted. The current after GD switch off decreased by $\sim 5 \cdot 10^{-6}$A - $\sim 4 \cdot 10^{-7}$A, and then increased up to $\sim 1 \cdot 10^{-6}$A. The emission current was lower by $\sim 10^{-5}$-10^{-7} times when the cathode temperature was higher by 10-20^0 in the course of the experiment (for example, $\sim 10^{-7}$A and $\sim 10^{-13}$A). Some data on current from samples 2 minutes after GD switch off are given in Fig. 2. The post-experimental current did not diminish with drop of temperature by 100 -150 °C. It was not the current of a thermo-ionic emission because for Pd and Mo at temperature 500 °C it amounts to $\sim 10^{-21}$ and $\sim 10^{-23}$ $A \cdot cm^{-2}$, accordingly. With temperature drop the current of a thermo-ionic emission impinges. The correlation of quantity and duration of current after the GD switch off versus a plasticity and brittleness of a material sample is not observed, therefore it was assumed, that the current does not result from the stress electronic emission.

STUDY of the TRACKS ON X-RAY FILMS.

The method for X-ray films blackening estimation for registered radiation was also applied. The X-ray films with a series of the screens (metallic and organic) inside and outside of the GD chamber were used. We observed the blackening of X-ray films, the diffraction spots and the tracks of unusual shape. The tracks on X-ray films placed inside the GD chamber were spaced at 350 mm from the samples and were similar to the tracks in (Wilson) expansion chamber and in the bubble chamber. The aggregate of paths with regard to the black specks, some rectilinear, some curvilinear, some as though from tracks of the particles refracted by the strong electric field. Sometimes these tracks reminded tracks from " of impinging stars" or comets. The clearly visualized spiral tracks were most unusual. These tracks had sizes ranging from one to tens of millimeters. Such tracks were observed on x-ray films inside the chamber at a distance of 300-350 mm from the cathode and outside the stainless steel chamber with ~ 5 mm thick walls (Fig.3).

Similar tracks were observed by Takaaki Matsumoto. He termed them "artificial ball lightnings", which can be initiated by cold fusion processes [8]. We also observed the spiral tracks with dimensions up to several tens of millimeters. The coils of the spiral were of varying brightness. These tracks are shown on Fig.3. A lot of small tracks look as separate zigzags, irregular tracks. It is impossible to explain the spiral and zigzag tracks as resulting

Fig.1

The post-irradiation sample current measurement diagram after Glow Discharge switch off Left-irradiation diagram; right-post-irradiation measurement (1-vacuum chamber, 2-sample, 3-amplifier-electrometer)

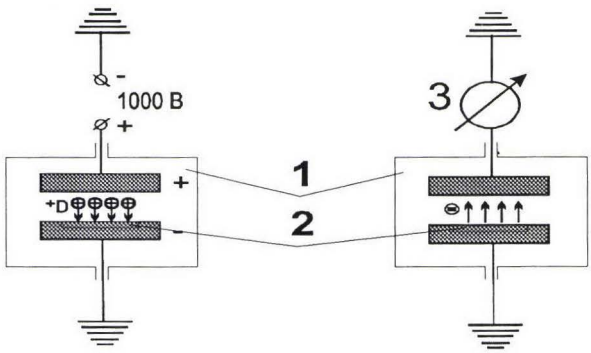

Fig.2

Current from samples "in situ" after two minutes Glow Discharge switch off, $A \cdot 10^{-14}$ (1-17- number of the samples: #1-5 Pd; #8 - PdRu; #9 - Ag; #10-11 PdPtW; #12 - PdNi; #13-14 - Cu-Pd; #16-17 Mo)

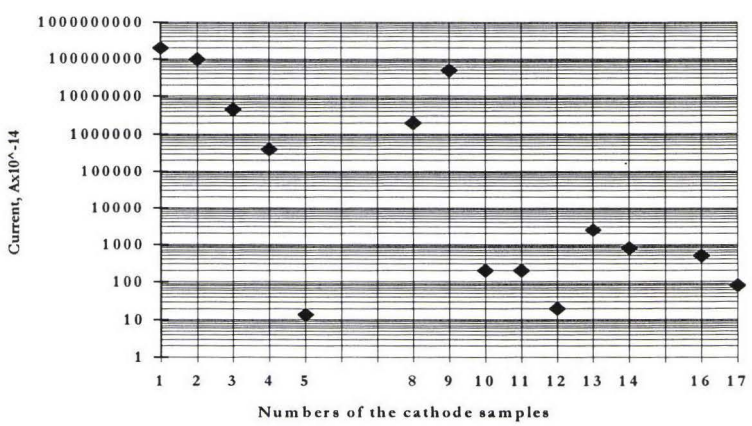

Fig.3
The unusual traces on x-ray film outside (A, B) and inside vacuum chamber after deuteron irradiation in Glow Discharge (C)

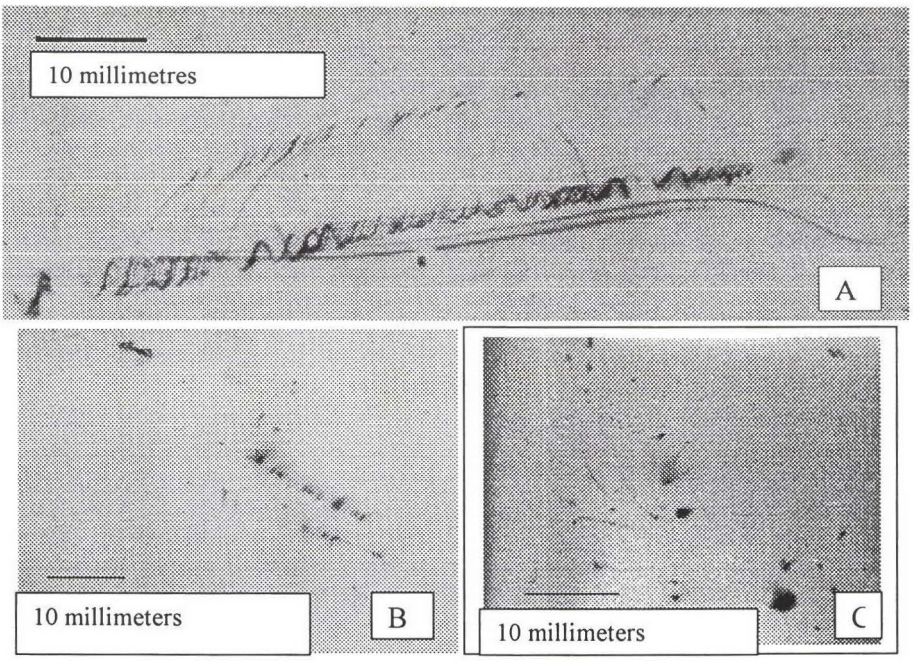

Fig.4

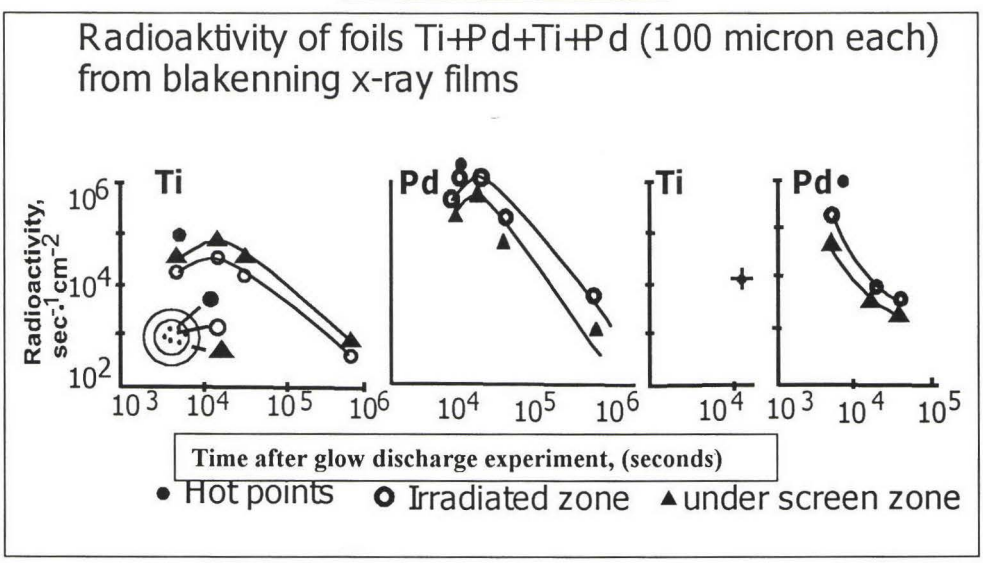

from the ion bombardment or as the flaws of the x-ray films. Similar effects were absent from the x-ray films - witnesses placed at a distance of several meters from the GD chamber. Maximum tracks on x-ray films (for films exposed inside and outside the GD chamber) for maximum isotopic and chemical changes were observed.

DISCUSSION

It is difficult to share the contribution of nuclear and atomic processes in balance of measurements for mass (chemical) composition change, heat measurement and energy which is carried away with radiation. However even the most accurate measurements can not describe all apparent processes going on simultaneously on GD cathode fully enough.

Here are possible reasons for non-identical reproducibility of experiments in GD resulting from stochasticity: 1. formation of various structural defects for every experiment: vacancies, interstitions, its clasters, voids and pores, inter-weavings, separate dislocations, segregation and nets of dislocation, hydrogen - vacancy complexes; 2. preferential sputtering on structural defects of a crystal lattice; 3. preferential accumulation of deuterium on defects of crystal lattice during ion implantation; 4.separation of elements with various mass number; 5.shaping of craters in places of micro-arcs and micro-explosion formation; 6. change of surface topography, formation of whiskers and cones. The processes (1-6) are going on at the atomic level.

The following facts result from nuclear reaction: 1) the local blackening of X-ray films in contact with samples irradiated by deuterium ions in GD is consequence of "the hot points "- the local nuclear reactions (Fig.4), and the radioactive isotope formation[5, 9]; 2) the tracks of various shape on X-ray films inside and outside the GD chamber can proceed from effect from different particles from nuclear reactions; 3)formation of local micro-segregations of impurities and "new" elements (chemical elements); 4) detection of dot aggregates of impurity elements on mass-spectra and distinction of mass-spectra in initial samples before and after experiments can also result from nuclear reactions.

A non-uniform blackening, "hot points" on the x-ray films from ion irradiated samples is the certificate of stochasticity of nuclear reactions and impossibility to receive identical effects on change of elemental and isotopic composition and heat effects. It was suggested that these local processes were fusion and fission of low energy nuclear reactions [5 - 7, 9,10].

For experiments in electrolysis all the above processes are relevant but at more local volumes of gas bubbles on the cathode. Such processes as micro-explosions, micro-arcs occur both in electrolysis and in ion bombardment. This leads to the instability of the process.

These processes in the surface layers can result from: the pressure in micro-pores, generated during irradiation of metals by low-energy ions (of Hydrogen and Deuterium) with high-density of ion current can achieve tens and hundreds kg/cm^2; the delay of micro-pores and output of protons, the change of surface topography irradiated by ions, shaping of cones and other outgrowths on the cathode. It can also lead to change of electron subsystem in a crystal lattice. The local changes in electric and magnetic fields can influence nuclear processes more delicately, can serve as a trigger mechanism for this phenomena and stimulate the phenomena on the nuclear level.

Let's assume that occurrence of "new" elements and change of isotopic composition resulted only from ionic bombardment (for example, preferential sputtering of light elements).

In this case maximal effects "new" elements occurrence and isotopic composition change after Hydrogen, Deuteron and Argon irradiation of samples in identical condition should be in the samples exposed to heavy Argon ions. However the maximum isotopic effects after Deuteron irradiation of Pd are observed. It was published earlier (the ICCF6) . These changes were presented quantitatively in a row: Deuterium / Hydrogen / Argon with ratio ~ (6-10) / (2-4) / 1 by x-ray microprobe analyses[_6].

CONCLUSIONS

1.The processes in GD experiments are stochastic and accompanied by formation of various defects, "hot points" with localized isotopic and elemental structure changes and are not equally reproducible. Only special structure and design could contribute to solving of the problem.

2. The charged particles emission from the samples exposed to Deuterium after GD current switch off show: the maximum value for Pd and Pd with small addition of refractory metals. The increase of current emission and its duration with decrease of residual gas pressure at discharge chamber can determine the charged particle current as β emission.

3. Tracks on X-ray films accompanying deuterium bombardment depended upon the exposed materials and parameters of process. There are more tracks for experiments with increasing new elements on the cathode surface.

The stochasticity of nuclear reactions, the impossibility to receive identical results on change of elemental and isotopic composition and heat effects testify to the necessity of the process further study. The impossibility to explain some parties of the phenomenon, to connect all verges of process and to count the complete energy balance probably will show necessity of the more profound research of this phenomenon.

ACKNOWLEGEMENTS

The author expresses the gratitude to Organization Committee for possibility of the presentation of this work on ICCF8 and to Corresponding Member of Russian Academy Fedik I.I., to Prof. Babad-Zakrapin A.A., to Prof. Rodionov B.U. for interest to this research and its discussion.

REFERENCES:

1.G.Preparata, F.Scaramuzzi, A. De Ninno, E. Del Giudice in Reports of ICCF8, 2000
2.Scuttering of solid by ion bormbardment,R.Berish, Berl.-N.Y.-Tok.,"Spr.Verl"1985, 488
3.A.Babad-Zakhrapin, I. Savvatimova et al."Atomic Energy"Moscow V48, 2,(1980)P.98.
4.S. Pons, M. Fleishmann Heat after death. Trans. Fusion Technology, Dec.(1993), P.101
5.I. Savvatimova et al., Radioactivity of the cathode samples..,ICCF5, Monaco,1995, p.209
6.I. Savvatimova et al. Transmutation Phenomena in the Pd... ICCF6. Japan,1996, P.575.
7. A. Karabut, Ya. Kucherov, I. Savvatimova, Nuclear product ratio for glow discharge in deuterium. Physics Letters A, 170, P. 265-272 (1992).
8. T. Matsumoto, Steps to the Discovery of Electro-Nuclear Collapse. Collected Papers (1989- 1999) Sapporo 060-0813. Japan .2000. 289P.
9. I. Savvatimova, Ya. Kucherov and A. Karabut, "Cathode Material Change after Deuterium Glow Discharge Experiments," Trans.of Fusion Technology", Dec.1994, P.389.
10. I. Savvatimova Transmutation at cathode materials in GD... ICCF-7, 1998, 342-350.

CHAPTER 6.

EXPERIMENTS WITH STIMULATION: ENERGETIC PARTICLES, E.M. – RADIATION, ULTRASOUNDS

Conference Proceedings Vol. 70
"ICCF8"
F. Scaramuzzi (Ed.)
SIF, Bologna, 2000

NUCLEAR TRANSMUTATION IN DEUTERED PD FILMS IRRADIATED BY AN UV LASER

Castellano[a], M. Di Giulio[a] M. Dinescu[b],
V. Nassisi, A. Conte and P.P. Pompa.

Department of Physics, University of Lecce,
I.N.F.N., C.P. 193, 73100 Lecce-I.
Tel. 832 320495 Fax. 832 320505 E-Mail Nassisi@le.infn.it

a) Department of Material Science, INFM
b) IFA, NILPRP, PO Box MG-16, RO 76 900, Bucharest V, Romania

ABSTRACT

Nuclear transmutation results in palladium films loaded with deuterium gas and processed by an excimer laser are reported. Vacuum evaporation was utilised to obtain palladium films on Si wafers. The films were inserted in chambers with deuterium gas at a variable pressure up to 5 bar. During the UV laser processing the maximum irradiating energy density was lower than 50 mJ/cm^2 in order to avoid the ablation of the palladium films. The samples were analysed by a scanning electron microscope and an electron probe microanalyzer. After the experiments, we found that the Pd films was modified. They presented many cracks and bubbles with very sharp edges. In the bubbles the transmutation of elements was observed.

INTRODUCTION

In the past, experiments were performed in Applied Electronics Laboratory of Lecce University devoted to investigate the "cold fusion" phenomenon as a potential new energy source[1]. Later on, we concentrated our attention upon nuclei transmutation which seemed to be either a reproducible phènomenon or an interesting result of nuclear physics.

Several "cold fusion" experimental results have reported the generation of new elements by Pd nuclei transmutation utilizing Pd samples as bulk and films[2-5]. The elements found out by the EDX microanalysis on the samples used in the first experiments were at first attributed to contamination, as no particular care had been made for the samples preparation before putting them inside the chambers. In this work, in order to exclude the contamination and to study the effect of the transmutation, the chambers have been accurately prepared and the samples were obtained by evaporating palladium on Si wafers. In this way, depositing Pd film of different thickness, we wanted to study the transmutation of elements as a function of the Pd film thickness and of the D_2 pressure. Gas loading was also accurately carried out in order to reduce

contamination. Measurements of X and gamma emission and other particles have been also performed by other authors [6, 7].

We studied also the transmutation of elements versus the Pd film thickness and the D_2 pressure applied during the loading process. The maximum new element density was found on the film of greatest thickness.

EXPERIMENTAL APPARATUS

We realized the films by thermal evaporation of palladium wire (99.95% purity) from a W boat on Si (100) wafers as substrate. The evaporating chamber was evacuated by a diffusion pump up to a residual pressure below $1 \cdot 10^{-5}$ Pa. At about 1 cm below the substrates a sliding mask was placed. In this way, during the deposition the mask was moved in order to deposit films of three different thickness in the same deposition run. The substrates were cut and their area was about $1 cm^2$. They were cleaned by an ultrasonic bath in acetone.

The reaction chambers were stainless steel cylinders having an internal diameter of 4 cm and a length of 20 cm. Before performing the experiments, the chambers were accurately washed with acetone and fluxed with nitrogen. Two quartz windows were placed at the two extremities of each chamber to allow the inside access for the UV laser beam. They were evacuated by means of a turbomolecular vacuum pump and filled with deuterium from gas bottles. Laser processing was performed after injecting D_2 gas inside the chamber.

The laser utilized was a home made XeCl excimer laser (λ= 308 nm) [8]. The UV light favors multiphoton absorption processes, which localize the gas atoms within the Pd host crystal [9]. The laser beam was led into the chamber after the D_2 loading process by a focalizing lens (L) and a set of neutral density filters. The experimental apparatus is shown in Fig. 1. The laser energy density was varied by changing the lens position and the neutral density filter.

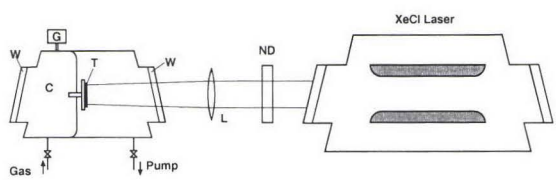

Fig.1: Experimental setup for laser irradiation. C: Loading chamber; ND: Neutral density filters; T: Target, W: windows; G: Pressure Gauge.

EXPERIMENTAL RESULTS AND DISCUSSION

Utilizing the evaporating device described above, we produced Pd films of 16, 35, 50, 83, 90, 106, 125 and 141nm on silicon wafers. The thickness was measured by a Tencor Alpha Step 200 stylus profilometer with an accuracy of about 5%. One or two samples were placed inside of each chamber, where the pressure of the deuterium was raised to 2.4 or 5 bar. After one week of D_2 loading some samples were irradiated with laser in order to create layers and to

localize the gas atoms inside the palladium. Laser fluence was very low to avoid palladium ablation. Thicker films were irradiated with 50 mJ/cm^2, while lower energy densities were applied to Pd films having a lower thickness. The irradiation consisted in 400 shots at a laser repetition rate of 1 Hz and the process was repeated 4 times weekly. The total laser shots applied were 1600.

A few samples were closed in a chamber and taken into contact with air.

After about 5 weeks the chambers were open and the samples were analyzed by a scanning electron microscope (SEM) and by an Energy Dispersive X ray Spectroscopy (EDX) for studying the surface morphological aspect and the chemical composition. All samples processed with D_2 shown many cracks and bubbles with very sharp edges while the samples taken into contact with air did not present any morphological modification. This points out that the D_2 concentration is the cause of the morphological modification.

The cracks found were distributed over the whole area and the distance among the bubbles, whose external dimensions were about 2 μm, increased as the film thickness increased. Generally the bubbles were created near to the cracks, see Fig. 2. This result indicates that the formation of the bubbles is tied to the formation of the cracks. The EDX spectrum recorded on the bubble presented many new elements: Sn, Ag, Na, Mg, S, Cl, K, Fe, Ni, Zn, Al, P, Ca, La, Ce, Cr, Ga, F, Ti and Cu. Considering only the elements having a concentration higher than 5% we plotted the number of elements found as a function of the Pd thickness, as Fig. 3 shows. One can see that the number of elements increases as the film thickness increases. There are four films showing a big number of elements (Table 1) and the maximum was obtained with the sample loaded with 2.4 bar and without laser action (case A) and with the sample loaded with 5 bar and processed with laser beam (case D).

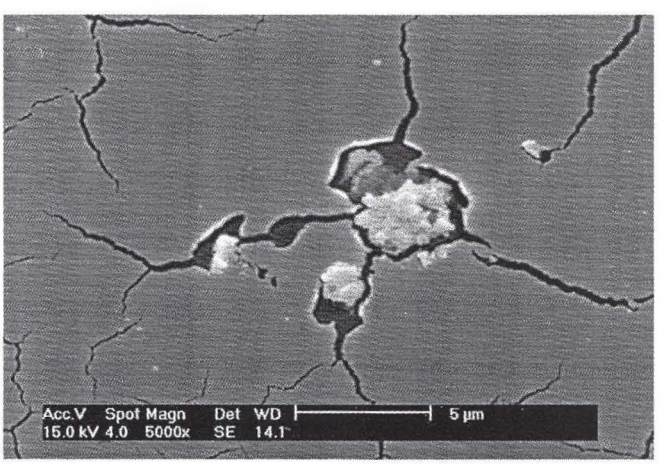

Fig. 2: SEM micrograph of a modified Pd film.

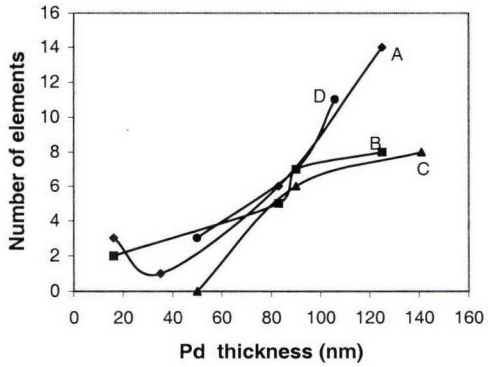

Fig.3: New element number as a function of the Pd film thickness loaded with palladium. A) sample loaded with 2.4 bar; B) sample loaded with 2.4 bar and processed with laser, C) sample loaded with 5 bar and D) sample loaded with 5 bar and processed with laser.

	Film thickness	D_2 pressure	New elements
Case A no laser action	125 nm	2.4 bar	Fe, Ni, Zn, Na, Mg, Al, P, S, Ca, Cl, K, La, Ce, Cr.
Case B laser action	125 nm	2.4 bar	Na, Mg, Al, P, S, Cl, Ca, Ga.
Case C no laser action	141 nm	5.0 bar	Na, Al, S, Cl, K, Ca, Fe, Ga.
Case D laser action	106 nm	5.0 bar	Na, Al, S, Cl, K, Ca, Fe, Ni, Zn, Cu, Sn.

Table 1. Global results related to A, B, C and D cases.

It is possible to suppose that these results are due to nuclear transmutations and they could be provoked by phonons and plasmons generated inside the crystal[10,11]. In the A case the deuterium concentration is low and it can induce low energy phonons, while in the D case the deuterium concentration is high and as a consequence high energy phonons could be formed. These last two conditions allow to get many elements in the film. Fig. 4a and 4d show the element concentration on atomic number of the elements found on sample A and D, respectively. The elements found are centered at 15, 28 and 58 atomic number for A case and 20, 28 and 50 atomic number for the D case. These two cases present a high element concentration. Fig. 4b and 4c show the element concentration on atomic number of the elements found on sample B and C, respectively. The elements found are centered at 13, 20 and 31 atomic number for B case and 11, 17, 20 and 26 atomic number for the C case.

These last two cases present a low concentration likely due to a lower phonon and plasmon energy the low deuterium loading.

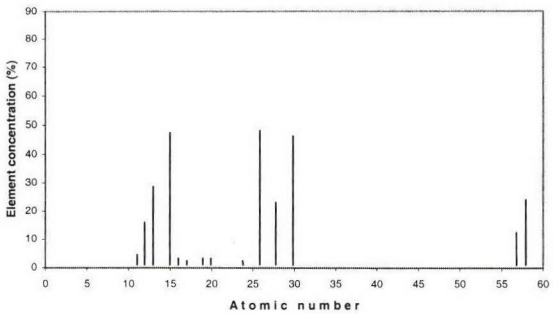

Fig. 4a: Plot of the percentage of the elements found in the bubbles as a function of the atomic number. Data related to A case.

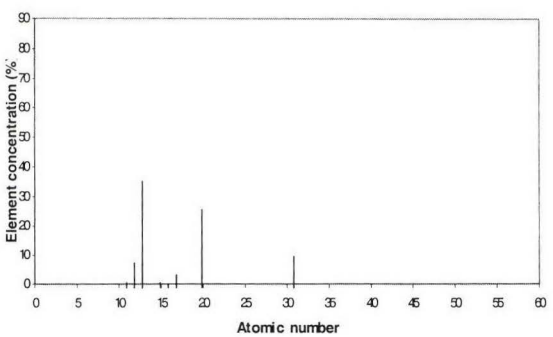

Fig. 4b: Plot of the percentage of the elements found in the bubbles as a function of the atomic number. Data related to B case.

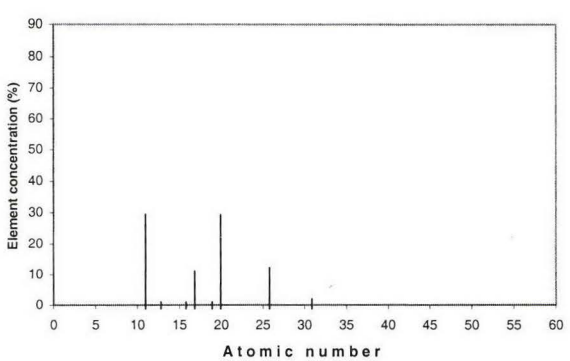

Fig. 4c: Plot of the percentage of the elements found in the bubbles as a function of the atomic number. Data related to C case.

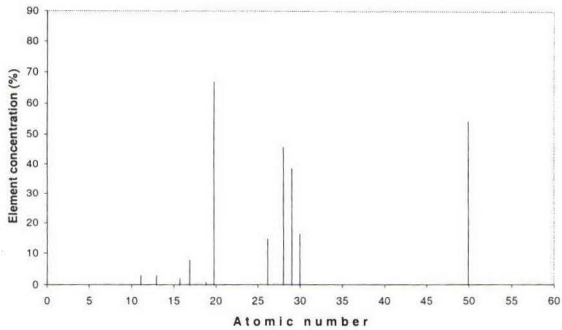

Fig. 4d: Plot of the percentage of the elements found in the bubbles as a function of the atomic number. Data related to D case.

We performed measurements on Pd films taken into contact with air. These samples did not present transmutation of elements and the surface conductivity was lower than the one of the film loaded with deuterium.

REFERENCES

[1] V. Nassisi, *Transmutation of elements in saturated palladium hydrides by an XeCl excimer laser,* Fusion Technology **33**, 468-475(1998).

[2] G. Miley, *Nuclear reaction in palladium hydrogen system*, Proc. of II International Low Energy Nuclear Reaction Conference, (1996)

[3] T. Mizuno, *Reaction products induced by isotopic changes of electrolysis*, Infinite Energy, 4, 9, (1996)

[4] G. Miley, *Product characteristics and energetics in thin-film electrolysis experiments*, Proceedings of VII International Conference on Cold Fusion, 241 (1998)

[5] S.Z. Wang et Al., *The evidence of nuclear transmutation phenomena in Pd-H system using NAA (Neutron Activation Analysis*), Proceedings of VII International Conference on Cold Fusion, 259 (1998).

[6] Y. Iwamura, T. Itoy, N. Gotoh and I. Toyod., *Detection of anomalous elements, X - ray, and excess heat in a D_2-Pd system and its interpretation by the electron -induced nuclear reaction model,* Fusion-Technology, **4**, 476 (1998)

[7] S. Focardi et al., *Neutron emission in Ni-H systems,* Il Nuovo Cimento, Vol.112 A, N. 9, pp.921-930 (1999).

[8] V. Nassisi, Experimental Studies of a XeCl Laser with UV Preionization Perpendicular and Parallel to the Electrode Surfaces; *Appl. Phys.* **B** 53, 14 (1991).

[9] T.Sugii, T. Ito and H. Ishikawa, *Excimer laser enhanced nidridation of silicon substrates,* Appl. Phis. Lett., **45**, 966 (1984).

[10] G. Stoppini, Nuclear processes in hydrogen loaded metals, *Fusion Technology*, **34**, 81 (1998).

[11] F.Frisone, Probability of deuteron-plasmon fusion at room temperature within microcracks of crystalline lattices with deuterium loading, (These Proceedings).

Conference Proceedings Vol. 70
"ICCF8"
F. Scaramuzzi (Ed.)
SIF, Bologna, 2000

Sono implantation of hydrogen and deuterium from water into metallic fine powders

Yoshiaki ARATA and Yue-Chang ZHANG

Cooperation Research Center for Science and Technology, Osaka University
2-1 Yamadaoka, Suita, Osaka, 565-0871, Japan

ABSTRACT : We observed the production of hydrogenated/deuterated metallic fine powders when various metals (Ti, Fe, Pd, Ag, Ta, Pt and Au) were irradiated in normal and heavy water by ultrasonic waves. Mass analyses of remnant metal powders revealed substantial amounts of sono-implanted deuterium (D-implantation) was found to be much stronger than the implanted hydrogen (H-implantation).

1. INTRODUCTION

It is well know that both cavitation and decavitation are generated in an ultrasound filed and many bubbles are simultaneously induced there, moreover the intense "imploding bubble" take place a violent imploding shock wave which will make effectively a peculiar reaction with materials.[1)-14)] Thus, Their application fields were widely developed as the "sono-chermist", for instance, "solid-processing" and "liquid-processing" were performed widely.[5), 6)]

Consequently, using a powerful supersonic wave with high energy density, a violent imploding "sono bubble" can be produced. Concentrating this energy , an ultra high energy density zone will occur inside the bubble. When these "sono bubbles" collide with any solid within the H_2O/D_2O liquid, an enormous implantation of hydrogens/deuteriums come into the solid as a "sonoplasma-cluster' with high energy density of protons/deuterons. This event should be called "sono implantation', and when it is strongly generated, an intense "latticequake"[15)] generates locally within a host lattice and a highly hydrogenated/deuterated solid can be easily made in an extremely short period.[16), 17)]

We observed sono dissociation of H_2O and D_2O in the presence of metallic foils of Ti, Fe, Pd, Ag, Ta, Pt and Au, and the production of hydrogenated/deuterated metallic fine powders when these metals were irradiated in normal and heavy water by ultrasonic wave. Mass analyses of remnant metal powders revealed substantial amounts of sono-implanted hydrogen and deuterium. The D-implantation in D_2O was found to be much stronger than the H-implantation in H_2O. This provides a new method of "sono implantation" of hydrogen and deuterium into metallic fine powders.

By the way, we have emphasized[18),19)] that production of the high hydrogenated/deuterated

bulk metal is extremely difficult under usual electrolytical method and high pressure method, etc. To overcome such difficulty, we developed a new system using sono implantation-effect and as a results, a highly hydrogenated/deuterated bulk metal can be easily made in an short period. Particularly, the deuterated was much stronger (about one order) than the hydrogenated.

2. EXPERIMENT

The present experiment was carried out as follows: we applied ultrasonic waves to an enclosed vessel in which working liquids (normal water and heavy water) were placed together with metallic foils, as shown in Fig.1. The working gases were H_2/D_2 (or H_2O/D_2O), N2 and inert gases (Ar, He, Ne, Xe). The vessel was evacuated for the purpose of degassing the working liquids. The metallic foils, initially placed in the vessel, had sizes of 1-2 mm × 1-2 mm × 0.1mm. An ultrasonic wave of about 300 W was applied, using a sono-generator of 600 W and 19 kHz (cf. fig.1). Then, the foils gradually broke up into smaller pieces and finally powdered after 20 hrs of irradiation. The metallic fine powders thus produced (hereafter called "sono-powders") were taken out of the vessel and enclosed in a high-vacuum chamber for mass analyses. The size of the powders distributed in the range of 10-100 μ m in diameter. Hereafter, we designate the combinations of the metal X in a working liquid of H_2O and of D_2O as $[H_2O]$-X and $[D_2O]$-X, respectively.

The mass analyses for sono-powders were performed by using a quadrupole mass spectrometer system, which was composed of three parts: a sample vessel, a Ti getter pump and a quadrupole mass spectrometer (QMS). The vacuum chamber united with these three parts (total volume of 5,000 cc) had been kept at a high vacuum of 10^{-9} Torr before a sample of about 20 mg was mounted. It was further evacuated to 10^{-9} Torr for 20 h, and the chamber was closed, but kept evacuated by the getter pump. Then, the sample was heated inside a very small holder made by a Ta tube and the evaporated gasses from the heated sample were analyzed by the QMS. Chronological changes of the intensities of all the relevant mass species were measured on each sample with the QMS.

As the results, Fig. 2 demonstrates the "sono implantation" for many kinds of metals. Using mass spectrometer "QMS", the "sono implantation-effect "of deuterium is indicated by detecting intensity of D_2, DH, D_2O and DHO which are reacted compounds of deuterium discharged from heating samples of metals. These compounds are main parameter showing the intensity of implantation of deuterium ("implantation parameter") and provide a real evidence of deuterizing for metals.

Figure 3 shows typical examples of the time evolution of logarithmic intensities of mass species of particular interest on the Ta-holder, [Virgin]-Au (Au powders of about 50 μ m immersed in D_2O for 20 hrs without ultrasonic irradiation), $[H_2O]$-Au , and $[D_2O]$-Au.

Figure 4 shows the QMS intensities of M=1 to M=50 components recorded at 1 min after heating in the case of Au. The black bars are for [Virgin]-Au, the oblique line bars for $[H_2O]$-Au and the open bars for $[D_2O]$-Au. The unit current 10^{-10} A corresponds to 3×10^{-7} cc @STP.

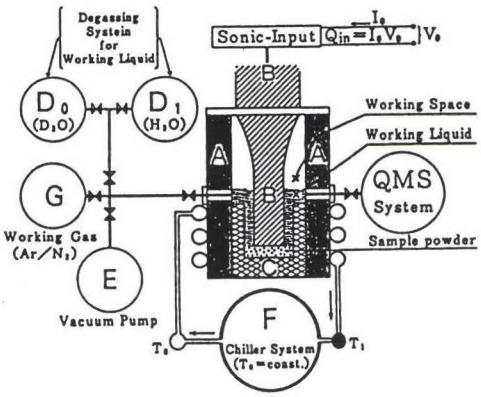

Fig.1 Schematic view of the irradiation vessel used for the present experiment

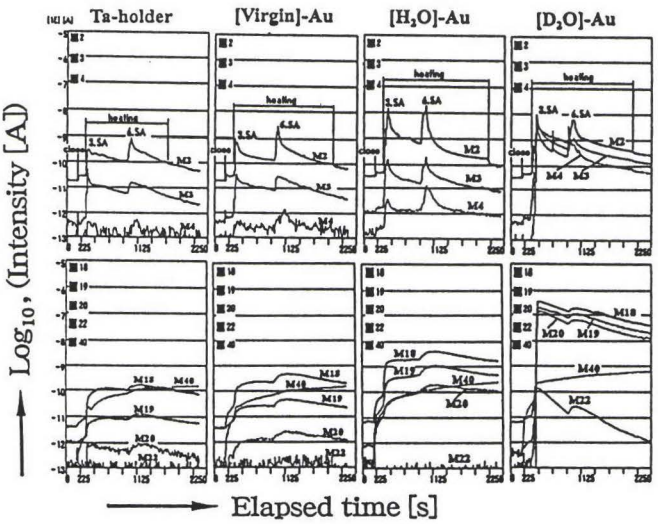

Fig.3 Chronological changes of QMS intensities of relevant masses, measured on Ta holder, [Virgin]-Au, [H2O]-Au, and [D2O]-Au.

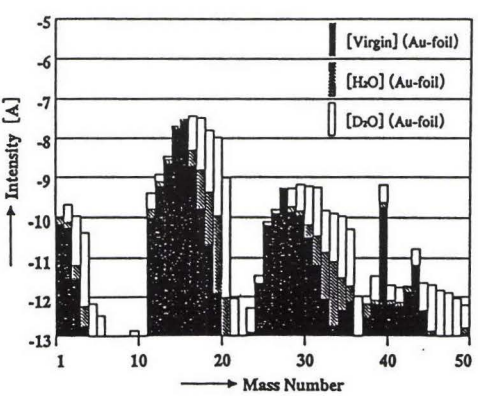

TABLE I. Net intensities of relevant mass species in [Virgin]-Au, [H_2O]-Au, and [D_2O]-Au. The molecular species (together with their intensities in A in parentheses) are presented. In the columns of [H_2O]-Au and [D_2O]-Au, the intensities are background-subtracted values: [H_2O]-[Virgin] and [D_2O]-[Virgin], respectively.

Mass	[Virgin]-Au	[H_2O]-Au	[D_2O]-Au
1	H (8×10^{-11})	H (1×10^{-11})	H (−)
2	H_2 (5.5×10^{-11})	H_2 (2.2×10^{-11})	D (1.7×10^{-10})
3	DH (3×10^{-12})	DH (5×10^{-12})	DH (1×10^{-10})
4	D_2 (1.5×10^{-13})	D_2 (5.3×10^{-13})	D_2 (5.0×10^{-11})
16	CH_4 (2.2×10^{-8})	CH_4 (1.8×10^{-8})	CH_4 (1.0×10^{-8})
17	HO (1.9 ± 10^{-9})	HO(3.0×10^{-9})	CH_3D (3.8×10^{-8})
18	H_2O (1.8×10^{-10})	H_2O (1.4×10^{-9})	DO (3.6×10^{-8})
19	HDO (2.1×10^{-11})	HDO (2.3×10^{-10})	HDO (1.8×10^{-8})
20	D_2O (1.3×10^{-12})	D_2O (1.1×10^{-10})	D_2O (1.1×10^{-8})

Fig. 4 Observed QMS intensities of mass numbers of M=1-M=50 in [Virgin]-Au(black bars),[H2O]-Au (oblique line bars) and [D2O]-Au(open bars). In other words, sono-implanted H/D atoms emitted from the heated powers constitute molecules of hydrides/deuterides dispersed in all oblique line bars and open bars, respectively.

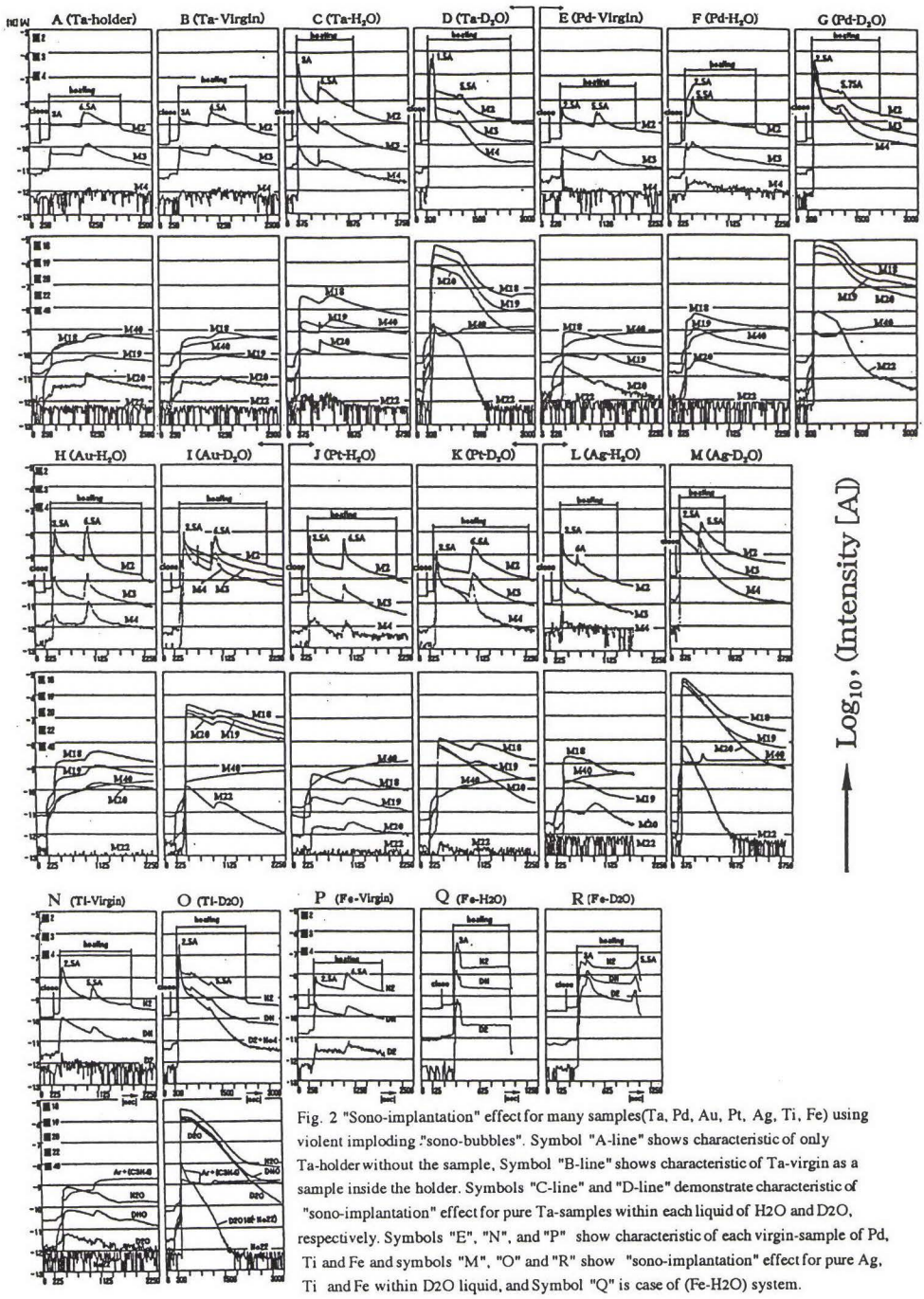

Fig. 2 "Sono-implantation" effect for many samples(Ta, Pd, Au, Pt, Ag, Ti, Fe) using violent imploding "sono-bubbles". Symbol "A-line" shows characteristic of only Ta-holder without the sample, Symbol "B-line" shows characteristic of Ta-virgin as a sample inside the holder. Symbols "C-line" and "D-line" demonstrate characteristic of "sono-implantation" effect for pure Ta-samples within each liquid of H2O and D2O, respectively. Symbols "E", "N", and "P" show characteristic of each virgin-sample of Pd, Ti and Fe and symbols "M", "O" and "R" show "sono-implantation" effect for pure Ag, Ti and Fe within D2O liquid, and Symbol "Q" is case of (Fe-H2O) system.

[Virgin]-Au includes not only the molecules evaporated from the sample of Au itself but also all the contaminants from the wall of the heating devices and the closed vacuum chamber. They contain large amounts of M=1 (H), 2 (H_2 and D), 12 (C), 13(CH), 14(CH_2),15 (CH_3), 16 (CH_4), 17 (HO) and 18 (H_2O). There was no significant change of the intensities, when the virgin Au powders were immersed in water without ultrasonic irradiation. They constitute background for [H_2O]-Au and [D_2O]-Au. The observed net intensities of the most relevant masses are presented in Table 1.

First, we observe a significant amount of M=4 component (uniquely identified as D_2) in [D_2O]-Au. There was no such component in [Virgin]-Au, Au fine powders immersed in heavy water under a similar condition but without ultrasonic irradiation. Therefore, we conclude that the fine powders of [D_2O]-Au were highly deuterated in the process of ultrasonic irradiation. This striking phenomena can be called sono-implantation of deuterium (or D-implantation) from D_2O.

Evidence for corresponding sono-implantation of hydrogen (H-implantation) can be obtained from the intensity of M=2 (assigned to H_2), although the net M=2 component was very much masked by the high contamination level of M=2, as shown by [Virgin]-Au in Fig.3. As a result, Fig.3 demonstrates that the sono-implanted H and D atoms emitted from the heated powders constitute the molecules of hydrides/deuterides dispersed in all oblique-line and open bars, respectively, and the intensities of these molecules in open bars are much higher than that of oblique-line bars. It means that D-implantation is much stronger than the H-implantation. For further details, we describe these events in Table 1. The ratio of the degree of D-implantation to H-implantation can be expressed as

$$F\left(\frac{D+D_2}{H+H_2}\right)=\frac{I_{M2+M4}([D_2O]-Au)}{I_{M1+M2}([H_2O-Au)}\sim 7. \qquad (1)$$

Namely, the implantation power in [D_2O] is by an order of magnitude larger than that in [H_2O]. Furthermore, the QMS spectra of [D_2O]-Au showed significant amounts of DO and D_2O, and the [H_2O]-Au sample also showed some net HO and H_2O beyond the background. The QMS intensities of these molecules are much stronger than those from [Virgin]-Au (metallic fine powders immersed in the respective water without ultrasonic irradiation). Thus, it is clear that the abundant production of these molecules from [H_2O]-Au and [D_2O]-Au originated from the sono-implantation of hydrogen and deuterium.

Since the presence of O as a form of DO or D_2O inside the metal powders is unlikely, the detected M=20 component is supposed to originate from sono-implanted D's, which are emitted during heating and recombined with O into DO or D_2O (and M=19 (DHO)) either at the surface of the fine powders or in the vacuum chamber. In other words, only a part of the whole sono-implanted D may have been detected as the M=4 fraction, and most of the remainder may have contributed to the DO and D_2O components. Thus, the intensities of DO and D_2O give another good signature for sono-implantation of deuterium. We notice a distinct difference between [H_2O]-Au and [D_2O]-Au:

$$F(\frac{DO+D_2O}{HO+H_2O}) = \frac{I_{M18+M20}([D_2O]-Au)}{I_{M17+M18}([H_2O]-Au)} \sim 10. \qquad (2)$$

As in the cases of D + D_2 and H + H_2 (see equ.(1)), it is concluded that the effect of ultrasonic irradiation in [D_2O]-Au is much stronger than that in [H_2O]-Au.

Another example for such recombined D-molecules is seen in the large abundance of the M=17 component in [D_2O]-Au, which has to be assigned to CH_3D. The CH4 molecule is the most abundance contamination, as seen as M=16 in [Virgin]-Au in Fig.3. The M=17 component in [D_2O]-Au is interpreted as being the result of recombination of sono-implanted deuterium with the background CH_4.

Consequently, it is very important conclusion that the D-implantation is much stronger than the H-implantation in general. More detailed information will be obtained in other paper. [16),17)]

REFERENCES

[1] K.S. Suslick, Science 247, 1439 (1990).

[2] Sonochemistry, edited by T.J. Mason (Cambridge, U.K., 1990).

[3] B.P. Barber and S.J. Putterman, Nature (London) 352, 318 (1991).

[4] D.F. Gaitan, L.A. Crum, C.C. Church and R.A. Roy, J. Acoust. Soc. Am. 91, 3136.(1992)

[5] N.W. Grinstaff, A.A. Crichowals, S.B. Choe and K.S. Suslick, Ultrasonics 30, 168 (1992)

[6] K.S. Suslck, Yearbook of Science and the future, Encyclopedia Britannica, Inc., 130 (1994)

[7] R.G. Holt, and D.F. Gaitan, Phys. Rev. Lett. 77, 3791 (1996).

[8] W.C. Moss, D.B. Clarke, J.W. White and D.A..Young, Physics letters A211, 69 (1996).

[9] L.A. Crum and T.J. Matual, Science 276,1348 (1997).

[10] W.C. Moss, D.B. Clarke and D.A. Young, Science 276, 1398 (1997).

[11] D. Lohse and S. Hilgenfeldt, J. Chem. Phys. 107, 6986 (1997).

[12] T.J. Matula and L.A. Crum, Phys. Rev. Lett. 80, 865 (1998).

[13] J.A. Ketterling and R.E. Apfel, Phys. Rev. Lett. 81, 4991 (1998).

[14] S. Hilgenfeldt, S. Grossmann and D. Lohse, Nature 398, 402 (1999).

[15] Y. Arata and Y.C. Zhang, J. High Temperature Soc., Japan 23 (Special volume), 1 (1997).

[16] Y. Arata and Y.C. Zhang, Proc. Japan. Acad., 74B, 201 (1998).

[17] Y. Arata and Y.C. Zhang, Appl. Phys. Lett. 76, 2472 (2000).

[18] Y. Arata and Y.C. Zhang, Proc. Japan. Acad. 75B, 71 (1999).

[19] Y. Arata and Y.C. Zhang, Japan. Appl. Phys. 39, part.1, 7A (2000).

Conference Proceedings Vol. 70
"ICCF8"
F. Scaramuzzi (Ed.)
SIF, Bologna, 2000

The Cavitation Micro Accelerator

Roger Stringham

First Gate Energies 2166 Old Middlefield Way, Mountain View, CA 94043, USA

Abstract

Experimental evidence gathered over a period of several years combines some new with old data which together create an effective model. The analytical results of acoustically cavitating D_2O in the presence of metal foils progress in a unique sequence of events. The implantation of a dense plasma into a metal surface is followed by the interaction of transient deuterons in that metal lattice. In this very dense transient deuteron environment, single or cluster events occur deep in the lattice. This is where the production of He and T, and perhaps transmutation occurs with some of these products expelled into the D_2O. The interaction events release large amounts of heat that radiate towards the lattice surface, with the ultimate vaporous expulsion of metal ejecta. These products are found in the analyses of reactor gases where other products remain in and on the foil or in the metal debris. FE SEM photos reveal microscopic surface vents of various sizes. These serve as paths for ejected vaporous metal and gases from the interior of the foil. A path is proposed to explain the analytical results such as excess heat, nuclear products of T and He and their connection to surface vents. The measurement found no long range radiation during and after reactor runs.

Introduction

The sonalysis of D_2O or H_2O produces TCBs, transient cavitation bubbles, and in association with a 5x5cm and 100 μm thick target foil, a fascinating sequence occurs. The interaction between the pseudo-adiabatic bubble collapse and the rapid heat evolution in the metal lattice is shown via FE SEM (field emission scanning electron microscope) photos. The FE SEM of the target foil shows millions of high energy events ranging from 10^{-13} to 10^{-5} J. We would like the model to show that the sequence of bubble jet plasma input, high energy events and the ejecta output are connected. It is known that collapsing TCBs and their generated high density plasma jet are monoenergetic as shown by bubble physics [1,2,3,4]. The produced bubble jets consist of a high density and low energy plasma whose content is and unidirectional and serve as the input energy into the target (10^{-8} J). See *figure* 1. The target surface, where the bubble jet plasma implants deuterons into the lattice, is a unique transient, localized, and dense deuteron environment. The implanted deuterons diffuse quickly, in a few picoseconds, into and through the lattice. Few deuterons remain in the lattice [5] but do leave a permanent lattice distortion, measured by xray diffraction, shows a lattice expansion of over 5% in volume [6]. The deuterons find their way deep into the target by localized lattice melts via dense implanting plasma or by channeling

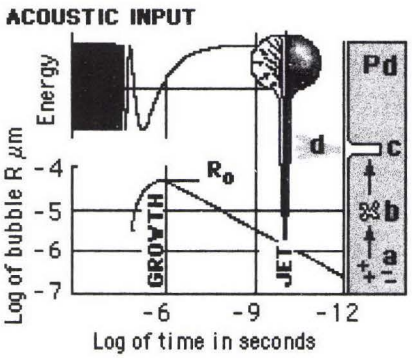

Fig. 1 The log log plot of the acoustic energy input examines the detail of one acoustic cycle, which is the lifetime of a TCB (at 40 kHz and 25 µ sec.). The radius of the TCB grows isothermally to Ro, the maximum radius of 40 µm, then collapses pseudo-adiabatically, less than a micro second. A Jet plasma implants the Pd target, **a,** implanting deuterons into the foil. In the picosecond time frame a fusion event or events, **b**, occurs. The radiating heat produces vaporous metal ejecta, **d**, at the vent sites **c.** The FE SEM photos of the target surface show an energy population distribution via vent sizes.

of the metal grains. The heat-creating events, deep in the lattice, immediately after implantation are responsible for the variable vent size population. The size of the vent depends on the magnitude, the number, and the type of hot lattice events. The time line for one 40 kHz acoustic cycle, *figure* 1, shows the isothermal growth, the TCB collapse, the plasma jet lattice implant, the transient deuterium and the electron lattice population. The hot events occur in the lattice followed by the expulsion of the vaporous ejecta, and the target vent sites. These vent sites vary in size from 25 to 5000 NM in diameter, *figure* 2. The evidence for nuclear events relates to the energy required to produce the vents. Examination of the SEM photos of the target surface shows no evidence of the monoenergetic jet plasma impacts other than maybe some surface melting. The ejected mass from the vents is target metal, called ejecta, and usually is expelled from the vents as metal vapor at several thousand degrees K. In addition to the micro-vent formation, there are also the gaseous products of T and He found in reactor gases analyzed by MS [7]. These products are probably linked to the ejecta and vent site population. The foils that have a large grain structure are quickly destroyed, in some cases in minutes, [8] by the activity of the TCBs at 10 watt acoustic input levels. The small grained targets may last for months and appear to suffer only the more traditional TCB cavitation damage.

Apparatus

A brief description of the apparatus and the overall process follows. The TCBs are formed in a sealed piezo driven reactor which cavitates 15 ml D_2O surrounding a 100 µm thick target foil. The reactor volume configuration is 6 cm in diameter and .5 cm in thickness. The acoustic field is unfocused and spread evenly in the D_2O. The reactor is pressurized with several atmospheres of Ar. In an acoustic cycle those bubbles that are of the resonance size are driven by three controlling parameters of the reactor; pressure, temperature, and acoustic input. The small bubbles grow isothermally in the negative pressure portion of the acoustic cycle and acquire new mass in the form of vaporous D_2O [9]. As this acoustic cycle progresses to its positive pressure mode, the bubble collapses violently and pseudo-adiabatically in less than a µ second. In the last stages of the TCB collapse the dissociated contents of the bubble form a jet plasma of low energy and high density deuterons [10,11]. From these collapsing bubbles near and on the target, the jet

plasma implants its deuteron content into the target lattice [12]. The estimate of the number of deuterons in the jet is 10^9 with the particle energy of about 25 eV [13]. These particles of similar energy and direction are accelerated coherently, impacting the target foil. The impact is not that of an ion beam but of a dense plasma [14]. The expected target input of narrow plasma implant energy and the very broad output of the vent site population should show different distributions.

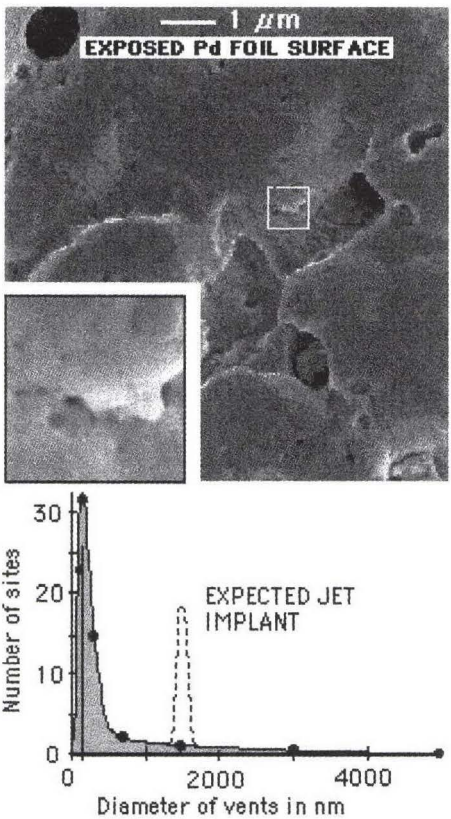

Fig. 2 A typical surface of a Pd foil (Pd #2 (SRI)) showing the size range of the vent population. In the graph of these vents, the expected population at 1500 nm of the jet implant on the surface of the Pd foil was not observed.

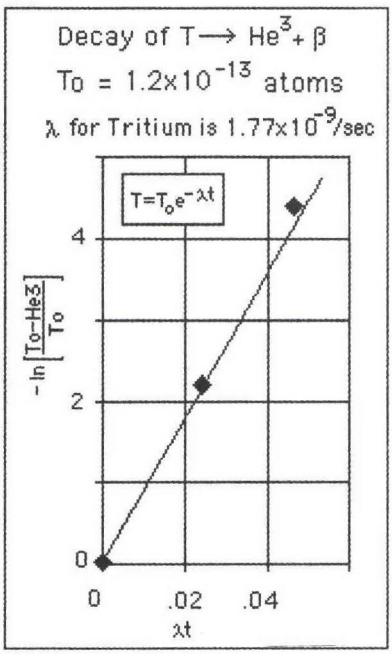

Fig. 3 T was present in a gas sample collected at the end of a LANL Ti foil run. Several MS determinations found a temporal increase of He-3 concentration in the 50 cc volume sample volume. The decay product of T, He-3, increased at a rate that relates to the disintegration constant, λ, for T. The three points were measured assuming no He-3 at 0 time. The other two points were measured after 136 and 281 days. The line is the decay of T. The error in these measurements are less than 5%.

The estimated vent energy ranges from 10^{-13} to 10^{-5} Joules. The expected implantation maximum at 10^{-8} J is not found. The energetic intermediate process occurring in the foil causes rapid heating from an event or events whose source is deep in the foil. The heat pulse expands and as it nears the surface there is an expulsion of vaporous ejecta which is responsible for the vent site formation, *figure* 2 & 4. The impact of the jet plasmas which implant on both surfaces of the target (an area of about 30 cm^2 of foil) showed, via FE SEM photos, no obvious implantation melt spots from the jet plasma but we do see many of the

vent sites. It is of interest to speculate on micrometeor impact events comparing them to the vent sites and jet plasma impacts and their differences. The densities and the velocities of the jet plasma are similar to micrometeor impact events. Some micrometeor surface impacts are found when analyzing the FE SEM photos and result in 100 μm diameter depressions in the target foil. See *figure* 4 -1. On the other hand a high density plasma jet has the ability to accelerate through water as shown in photos and in a like mode penetrate deep into the solid phase target lattice [15]. Large grained metal lattices may provide an opportunity for deuteron channeling [16].

Observations

Plasma impacts and vent sizes are not directly connected. This is determined from the energy distribution of the ejecta that is expelled from the vent site population. See figure 2. The energy of the jet plasma implant is 10^{-8} and is expected to be confined to an observable footprint of close energy distribution (the dotted peak in *figure* 2 and contrasted to the deep vent in *figure* 4). The impact of the jet plasmas, which are spread over both sides of the target surface area are shown in FE SEM photos. No obvious plasma jet implantation melt spots on the foil surface from the jet plasma have been observed, but we do see a wide size distribution of vent sites. The discovery of the vent population with a size distribution range from 25 to 5000 NM in diameter fits a typical statistical distribution [17]. The energies from events which create vents can be related to a single 20 MeV event or a multi event occurring deep in the lattice. The FE SEM photos of the surface of fine grained Ti foils are of equal interest and different from the Ag and Pd target foils. The most impressive are the mass spectrometry measurements of the reactor gas products over a Ti foil exposed to cavitation in D_2O for 12 hours. About 1% of the collected sample is used in each analysis and, over a period of a year, showed an increasing amount of He-3 gas, a decay product of T. The T was analyzed, from a 50 cc gas sample collected at the end of the run, several times over a period of a year. As the He-3 concentration grew in the sample volume, three measurements starting at day 0, day 136 and day 281 [7] were made. The analyses for He-3 establishes a disintegration constant, λ, close to T [18]. *figure* 3.

Conclusions

The jet that implants high density deuterons into the target lattice, produces for an instant an environment that screens them from their repulsive coulombic forces. The very high momentary deuteron density, and a super loading, in a small volume of the target lattice is responsible for the hot events. The implanting plasma has the following characteristics; a density of 3 to 10 gm/cm^3, an energy of 16 to 25 eV, a magnetically pinched diameter of 0.2 μm, a length of 1 μm, and a population of 10^9 deuterium ions in a multi-bubble system. The jet plasma's acceleration path passes through and out from the bubble surface producing shock waves in the water [19]. The dense plasma constrained by a pinch effect, a unique chunk of matter, is a self-contained bundle during its several picosecond lifetime. In the TCB collapse process, those particles that are not moving towards the bubble center are lost to the surrounding water. Only 1 in 10,000 deuterons are left to be part of the jet plasma leaving about 10^9 deuterons in the plasma. At these low energies, a deuteron ion beam's range in target metals is in the order of 0.1 nm and electrons 1 nm [20].

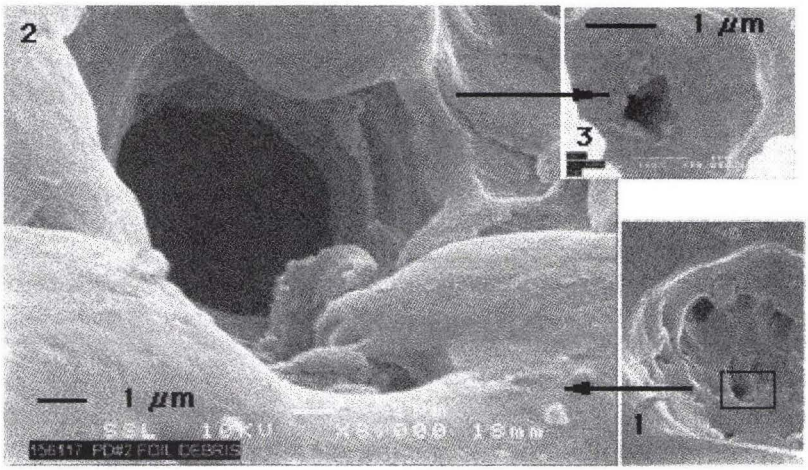

Fig. 4 shows a large complex vent site (follow the sequence **1, 2, 3)** in a piece of debris from a 100 μm thick Pd target foil 5000 nm in diameter and a calculated ejecta energy of 10^{-6} J. **1** shows the location of the vent in a 100 μm eroded microcrater. **2** is peering into the vent site that exhibits smooth walls and curious details which include symmetric rings near the bottom and an irregular (hedge hog) 500 nm hole at the bottom of the vent. **3** is the detail of the bottom hole that may be the site of the initial nuclear events and a calculated ejecta energy of 10^{-9} J. (This is an initial interpretation of this site).

The very high densities of these plasmas, compared to ion beams, are 10^{10} more dense [14]. The photos of bubble jets that accelerate in water [9,15] lead one to expect more penetration into the foil, so the very high density deuterium plasma implants deeper into the target lattice than the deuterium ion beam because of the characteristic fluid like properties of dense plasmas. The deuterons may chase the plasma electrons into the lattice via coulombic attraction, coupled and channeling in the large lattice crystals. This picture is not clear, but the superloading of a small volume of the target lattice with 10^9 close packed coherent deuterons, lasting a few picoseconds, presents a good environment for nuclear events. The transient, high density coherent deuterons in the lattice present an alternate channel for energy removal in the form of heat rather than in long range radiation [21].

Summary

The rapidly evolving events, at the end of one acoustic cycle, described in the paragraphs above lead to a very unique environment where there is for a picosecond, in the lattice, a local concentration of deuterons perhaps a 100 times the metal lattice atoms. The electrons penetrated deeper into the lattice than the deuterons creating a transient charge separation in the superloaded lattice. The superloaded lattice does have a time presence in the foil providing environments for interaction between deuterons and other particles. The mechanisms for a high density, non-radiative fusion process are not known but a very small unique transient environment, as described here, is present for each bubble on the target foil. The one picosecond time-frame for the duration of this unique and transient deuterium, superloaded lattice is where nuclear events can occur, favoring the internal conversion electrons and heat rather than gamma emission. This is a tentative explanation for not

finding gamma radiation [18]. The TCB micro-accelerator produces a high density jet plasma which implants the lattice target with transient deuterons. An environment where hot events occur, that produce heat and vaporous metal, which escapes the lattice through vent sites as ejecta. The vents, a residual of these events, are shown in the FE SEM photos. The gaseous products formed escape with the vaporous metal ejecta from the vents into the D_2O. The cavitation exposed foils of Ti and Pd produce T and He with no long range radiation. Various types of target foils experience similar heat producing interactions with the implantation of high density plasmas [22]. Other contributing factors to the bubble accelerator are the induced foil resonance, the high pressure Ar reactor operation, acoustic pulsing and the pinch effect in the jet, as deuterons are accelerated as a high density plasma into the lattice.

Acknowledgments for the use of the SRI laboratory and facilities are due; Fran Tanzella and Michael McKubre, who support calorimeter studies of metal foil cavitation using a reactor built by Scott Little [23]. We appreciate Kip Wallace's unique design of a feedback oscillator which drove the acoustic piezos in the reactor, and Dick Raymond for all his time, help and support over the years.

References

[1] T. S. Lundgren and N. N. Mansour; *J. Fluid. Mech.*; vol. 224, 177-196 (1991).
[2] M. S. Plesset and R. B. Chapman; *J. Fluid. Mech.*; vol. 47 (part 2); 283-290 (1971).
[3] T, B. Benjamin and A. T. Ellis; *Phil. Trans. R. Soc. A*; 260 (1966).
[4] J. P. Best; *J. Fluid. Mech.*; vol. 251; 79-107 (1993).
[5] Ed Storms gravametric analysis of cavitation exposed foils indicate that there was no measurable weight change. Therefore there was no permanent deuterium loading of the Pd foils, (1998).
[6] George Chambers of NRL in 1994 examined cavitation exposed and unexposed Pd foils using xray diffraction and noted the permanent stretching of the Pd lattice (1995).
[7] Brian Oliver of DOE performed the helium three analyses measurements. His methodology involved removing any hydrogen species before each analysis (1994 -5).
[8] Some large grained Pd foils from Ithaca were run in the SRI laboratories in 1995. In several cases only 25% of the foil remained after exposure to cavitating D_2O for less than 25 minutes (1994 - 8).
[9] W. Lauterborne and H. Bolle; *J. Fluid. Mech.*; vol. 72, 391 (1975).
[10] L. A. Crum; *J. Acoustic Soc. Am.*; vol. 95, 559-561 (1994).
[11] W. C. Moss, D. Y. Young, J. A. Harte, J. L. Levatin, B. F. Rozsnyai, G. B. Zimmerman, and I. H. Zimmerman; *Phys. Rev. E*; vol. 59, 3, 2986 (1999).
[12] Video taped observations of Pd foils, with large grain structure show, when cavitating D_2O or H_2O, a rapid and permanent swelling of the lattice. This swelling corresponds to more than a 5% increase in the lattice volume. Transient loading of the metal lattice was observed in Pd and Ag foils (1994 - 5).
[13] The 25 ev is based on the cavitation dissociation of D2O. Our experience and others have shown that cavitating D2O at 1 atm. pressure produces DH, D_2, O_2 and DOOD where 16ev are required to dissociate D2O. Doubling the external pressure will effectively double the bubble energy density (1991 - 6).
[14] F. Okuyama, H. Tsujimaki; *Surface Science*; vol. 382, L700-L704 (1997). --- H. Yuki, T.Satoh, T. Ohtsuki, T. Yorita, Y. Aoki, H. Yamazaki, J. Kasagi; *ICCF-6 Japan*; 259 (Oct. 13-18 1996).
[15] Y. Tomita and A. Shima; *Acoustica*; vol. 71; 161-171 (1990).
[16] *McGraw- Hill Encyclopedia of Physics*, Second edition; Channeling ion-solid interactions; 612 (1993).
[17] A skewed χ^2 distribution with 4 degrees of freedom gives a good fit (2000).
[18] Experiments and radiation measurements at LANL with the help of T. Claytor and D. Tuggle (1995).
[19] A K. R. Weninger, P. G. Evans, and S. J. Putterman; *Phys. Rev. E*; vol. 61, 2, R1020 (2000).
[20] J. Kantele; *Nuclear Spectrometry*; Academic Press; (1995).
[21] Y.E. Kim, A. L. Zubarev; *Proceedings of ICCF-7*; 186-191 (1998)
[22] R. Stringham; *IEEE Ultrasonic Symposium*, Sendai, Japan, vol. 2, 1107 (Oct. 5-8 1998).
[23] Work in progress - SRI calorimetry of anomalous heat via a cavitation process (May 2000)

Conference Proceedings Vol. 70
"ICCF8"
F. Scaramuzzi (Ed.)
SIF, Bologna, 2000

Low Energy Nuclear Fusion Reactions in Solids

J. Kasagi, H. Yuki, T. Baba and T. Noda
Laboratory of Nuclear Science, Tohoku University, Mikamine, Sendai 982-0826, Japan

Abstract

The DD fusion reactions in various materials have been studied, and enhancements in the rate of the D(d,p)T fusion reaction over the Gamow function were clearly seen in the materials. Of particular interest is the fact that the reaction rate of the D+D reactions at 2.5 keV in PdO is 60 times (and in Pd 10 times) larger than in Ti, and the deduced screening energy amounts to 600 eV (300 eV). Furthermore, the subsequent study on the Li+d reactions showed large screening energy as 1.7 keV, again, in Pd metal. These cannot be explained by bound-electron screening which may give at most an energy of 20 eV for the DD reaction and of 0.3 keV for the Li+d reaction, but suggests the existence of an additional, and important, mechanism. Perhaps there is a fluidity of deuterons in metals that also reduces the Coulomb barrier between the fusing nulcei.

1. Introduction

It has been pointed out that there should be two miracles in order to realize the cold fusions; (1) a tremendous reduction of the Coulomb barrier between two deuterons fusing in metals, and (2) branching ratios of the reaction channel are completly different from those known for the normal DD fusions. It might be possible to see a glimpse of such extraordinary phenomena as a precursor of cold fusion, if exists, when one studies fusion reactions with higher energies but in a different condition such as in solids. As reported at the ICCF6[1] and ICCF7[2], we have started a series of measurements of the D(d,p)T reactions in solids with bombardment energies far below the Coulomb barrier, in order to see the possibility of (1).

In nuclear reactions with normal targets, the cross sections at very low energies have already been known to be somewhat larger than those of bare nuclei without electrons: This is explained by the electron screening effect and is described quantitatively by the screening energy U_S. However, the reactions concerned here are in different environments from the ordinary condition, since target nuclei are embedded in another material and the number density of target nuclei is nearly equal to that of the host atoms. We have developed a method to measure the reaction rates of such reactions with low-energy deuterons, and have performed a series of measurements on D+D reactions in various materials.

The screening potential for DD fusions in a metal was first deduced in Ti by measuring the proton yield in the D(d,p)T reaction.[3] The result, U_S = 19 +- 12 eV, was almost the same as for the gas target. However, a strikingly large value of 600 eV was obtained for the DD fusions in PdO as reported in ICCF7[2], although the result was preliminary that time. We have continued the measurements of DD fusions in various metals to find the mechanism of the enhancement as well as to look for more favorable metal. Recently, the investigation on the Li+d reactions in various metals has also strated.

In the present work, we report on a series of the temperature controled measurements of the D(d,p)T reactions in PdO, Pd, Fe, Au and Ti for $2.5 < E_d < 10$ keV, and the first result of the Li+d reaction in Pd for $30 < Ed < 75$ keV.

2. Experimental Procedure

The measurements were performed using a low-energy ion beam generator[3]. For the DD fusions, the generator was operated in the deceleration mode and deuteron beams with energies lower than 25 keV were bent by a charge filter magnet placed just after the decelerator (or accelerator) electrode, in order to reject neutral beams. For the Li+d reactions, the generator was operated in the acceleration mode and deuteron beams with energies from 25 to 80 keV were used to bombard the target. The beams were collimated so as to fix the beam position and size; the beam spot on the target was 4 mm in diameter.

Targets used for the DD fusion reactions were foils of Ti, Fe, Pd, Au and PdO/Pd/Au. Commercially available metalic foils of Ti, Fe, Pd and Au with thickness of 0.2 to 1 mm were annealed in vacuum at about 800 ^{o}C for several hours. The PdO/Pd/Au foil was prepared in such a way that a rolled Pd foil with thickness of 40-50 μm was annealed in an oxygen flame at about 1000 ^{o}C and Au was electrochemically deposited on one side of the foil. The PdO surface side was bombarded and the thickness of PdO layer measured by the SEM technique was about 30 nm. The target used for the Li+d reactions was a foil of the Pd-Li alloy, whcih was prepared by Sakamoto by arc melting Pd and Li as as described in ref. [5].

The targets were cooled during the bombardments by liquid nitrogen and the temperature of the foil surface was monitored by a thermocouple. The total dose of the deuteron beam was deduced from the electric current on the target, with a small correction for secondary electron emission.

In order to detect charged particles, protons emitted in the D(d,p)T reactions and α-particles in ^{6,7}Li(d,α)^{4,5}He reaction, a ΔE-E counter telescope consisting of two Si surface barrier detectors was used: The front face of the ΔE detector was covered with a thin Al foil to prevent electrons and scattered deuterons from hitting the detector. The telescope was placed at 2 cm from the target and at 90^{o} to the beam direction. Requiring a coincidence between the ΔE and E detectors completely eliminated electrical noise and enabled unambiguous identification of protons and α-particles from the D(d,p)T and Li(d,α) reaction, respectively.

In the D(d,p)T reactions, the proton yield is proportional to the number of projectiles and targets as well as the reaction cross section. In the present case, deuterons impinging upon the metal play a dual role, projectiles and targets of the reaction. Since the fusion enhancement factors we seek are obtained from only the energy dependence of the proton yield, it is not necessary to know the absolute number of targets. But it is necessary to keep that number reasonably constant as the deuteron energy is varied. Hence, a method for controling the number of target deuterons had to be developed.

We have measured the proton yield from the D(d,p)T reaction in our targets under various conditions and deduced the dependence of the number of targets on the deuteron dose, metal temperature and beam current. The important result concerning the number of the target deuterons during the bombardment is the fact that the number of the target deuterons increases when the metal foil does not contain deuterium initially and at a certain fluence reaches saturation. The saturation number of deuterons depends strongly on both the host metal and on the temperature, as shown in Fig. 1. The measurements of the excitation function of the D(d,p)T reaction in metal have been carried out by controling and monitoring the number of the target deuterons as follows.

Prior to the measurement, the metal foil was bombarded by 10-keV deuterons with a beam current of 60 μA until the proton yield together with the temperature of the metal becomes constant. This basically ensures the saturated condition on the deuterium concentration at the equilibrium

temperature; we always confirmed that proton emission rate converged to nearly same number whether initially the foil contained no deuterons or was full of them. At other bombarding energies, the beam current must be adjusted so as to keep the input power (and, hence, the temperature) constant; the temperature of the target was always monitored. In this way, the number of target deuterons was hold constant during the measurement. Nevertheless, the proton yield at 10 keV was measured at frequent intervals to verify this constancy. During the accumulation of the data at 2.5 keV, for example, such measurements were carried out more than ten times (a few minutes at 10 keV, a few hours at 2.5 keV, again and again). The proton yield is, then, always divided by the yield at 10 keV measured just before and after the run. This procedure of normalization gives the relative reaction rate as a function of the bombarding energy.

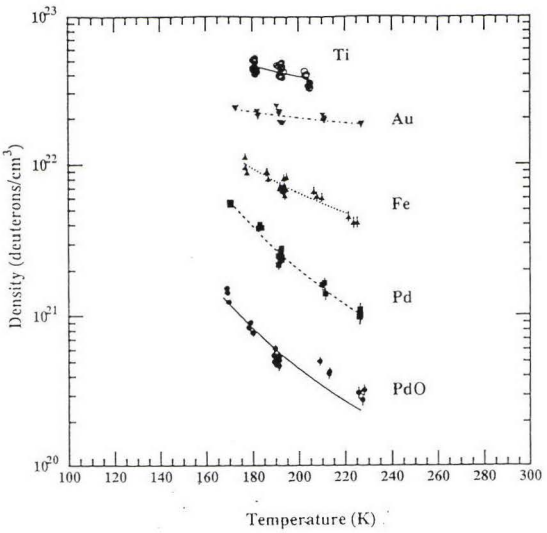

Fig. 1 Saturation density of deuterons versus target temperature.

For the Li(d,α)He reactions in Pd, we measure the excitation function in a similar manner as described above: we kept the teperature of the target nearly constant by adjusting the beam intensity and checked the number of Li in Pd by the frequent measurements of α-paricle yields at 75 keV. Then, the yield at each bombarding energy was normalized to that at 75 keV.

3. Results

In the upper half of Fig. 2, plotted are the relative yields of the D(d,p)T reaction in metals against the bombarding energy. Figure 2(a) shows results of two independent measurements for PdO, Fig. 2(b) results for Pd and Fe, and Fig. 2(c) for Au and Ti. The yields decrease very rapidly as the bombarding energy decreases. However, it is clearly seen that the yield at lower energies very much depends on the host metal; the largest yield is observed in PdO followed by Pd, Fe, Au and Ti, in order.

Since the projectile deuterons are slowed down in the metal and the reactions can occur until the deuteron stops, the observed proton yield Y_p at the bombarding energy E_d is the integrated one down to the zero energy (thick target yield). We estimated a standard thick target yield by using the reaction cross sections parametarized by Bosh and Hale[5] and the stopping cross sections by

Anderson and Ziegler[6]. The solid line in Fig. 2 indicates the calculated standard thick target yield corresponding to the bare D+D reaction, *i. e.*, without any enhancement of the reaction rate. As seen, the standard calculation without any enhancement completely fails to explain the data at the lower energies, especially for PdO, Pd and Fe.

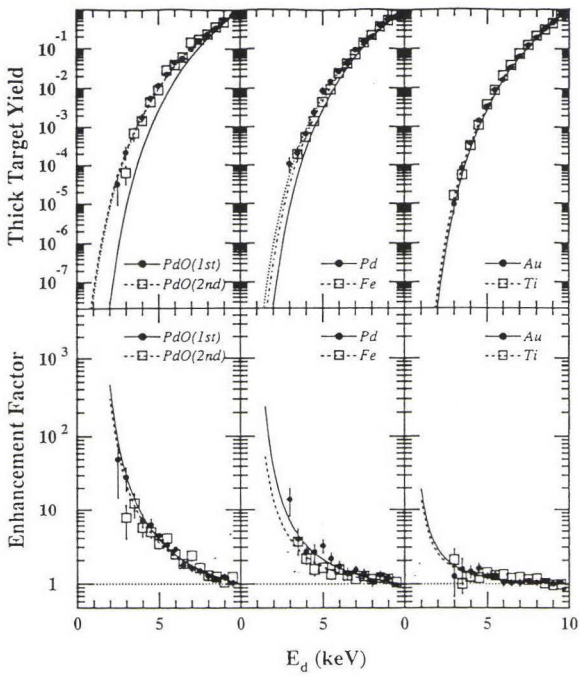

Fig. 2 Relative yields of the D(d,p)T reaction in metals against the bombarding energy. In the lower part, the ratios of the experimental yield to the standard calculation are shown.

In the lower part of Fig. 2, we plot the ratio of the experimental yield to the standard calculation (no enhancement) in order to make comparisons more clearly. As seen, the reaction rate in PdO is enhanced very much, about 50 times larger than the standard at E_d = 2.5 keV. On the other hand, the deduced enhancement is very small for Au and Ti.

Since the fact that the enhancement increases as the bombarding energy decreases is a feature of the reaction characterized with a screened Coulomb potential[7], we have naively attempted to parameterize the enhanced reaction rate by a screening potential (U_s) which reduces the Coulomb barrier between two deuterons.

We calculated thick target yields for various values of U_s as described in [3], and determined the values of U_s to give the best fits to the enhancement factor data. These fits are shown by the curves in Fig. 2. The results are U_s = 600 +- 20, 310 +- 20, 200 +- 15, 70 +- 10 and 65 +- 10 eV, respectively, for PdO, Pd, Fe, Au and Ti. Since the screening energy caused by electrons in metal is only several tens of eV [8], the values obtained for PdO, Pd and Fe are extraordinary large; especially 600 eV for PdO.

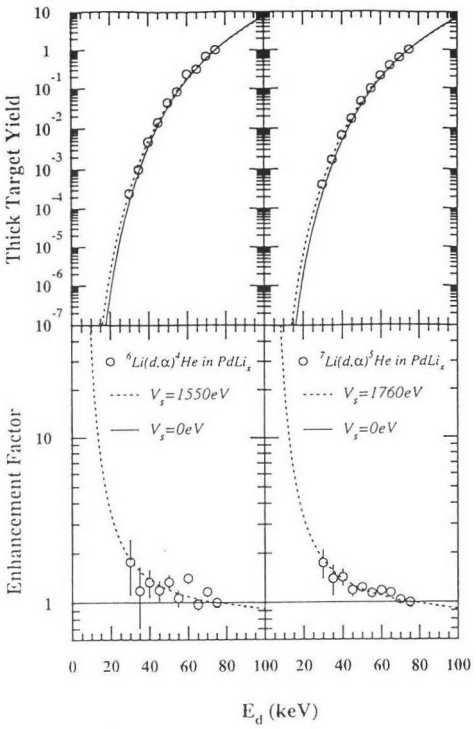

Fig. 3 Relative yields of the $^{6,7}Li(d,\alpha)^{4,5}He$ reaction in Pd against the bombarding energy. In the lower part, the ratios of the experimental yield to the standard calculation are shown.

In Fig. 3, we show results of the $^{6,7}Li(d,\alpha)^{4,5}He$ reaction in Pd. Solid lines show the standard thick target yield corresponding to the bare Li+d reaction, *i.e.*, without enhancement. Again, significant enhancement can be seen at low energy. We deduced the values of U_s to give the best fits to the enhancement factor data. These fits are shown by the dotted curves in Fig. 3. The results are U_s = 1.55 +- 0.40 and 1.76 +- 0.30 keV, respectively, for the $^6Li(d,\alpha)^4He$ and $^7Li(d,\alpha)^5He$ reactions in Pd. Since the screening energy due to the bound electrons is only about 0.3 keV, these values in Pd are really large.

4. Discussion and conclusion

Since the screening potential caused by electrons in metal is only several tens of eV [17] for the DD fusion case, the presently deduced values for PdO, Pd and Fe can never be due to the electron screening alone. Of particular interest is the existence of a strong correlation between the screening potential and the deuteron density in metal during the bombardment, as shown in Fig. 4, where the deduced screening potentials are plotted against $(density)^{-1}$. The deuteron density during the bombardment is an index of the fluidity of deuteron; it might be proportional to the inverse of the density. Thus, we infer that for the nuclear reactions in solids at very low energies there exists a significant screening mechanism, the effect of which increases drastically with an increase of the fluidity of deuteron in metal, in addition to the electron screening known previously.

The diffusion constants of deuteron for ordinary condition at T = 300 ^oK are $\sim 5 \times 10^{-7}$, $\sim 4 \times 10^{-5}$ and $\sim 3 \times 10^{-13}$ cm^2s^{-1} in Pd, Fe and Ti, respsctively.[18] Enhanced deuteron diffusivity has

also been reported under stress and under deuteron implantation. Although the mechanism to increase the diffusion is not understood completely, the diffusion constant can easily be changed under such special conditions. In the present work, thus, it is said very roughly that large diffusivity of deuteron results in low deuteron density.

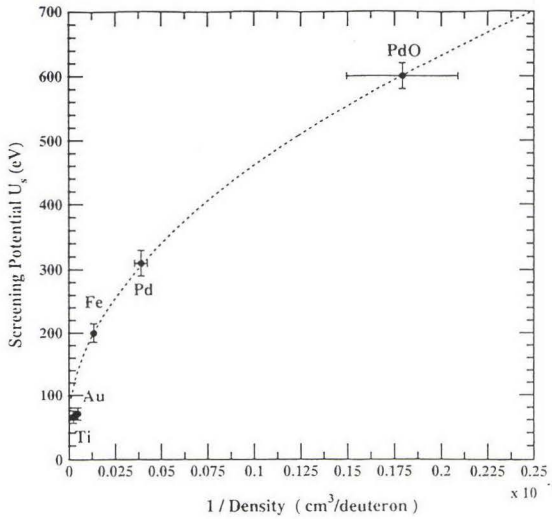

Fig. 4 Deduced screening energy for DD in solids versus (deuteron density)$^{-1}$.

It is most important in this work that the DD fusion and the Li+d reactions can be enhanced extraordinarily when the reaction occurs in a particular host material such as PdO and Pd. The anomalously large screening potential clearly indicates the exsistence of a new mechanism to enhance the reaction rate.

Moreover, if the reaction cross section can be extrapolated to thermal energies with the same screening energy and with the deuteron density of 1.2 x 10^{21}/cm^3, then one can presume the DD fusion rate to be > 10^7 sec^{-1}cm^{-3} at room temperature. For the Li+d reaction case, however, the reaction rate would be about 10^{-4} sec^{-1}cm^{-3}.

The authors would like to thank Prof. Sakamoto and Dr. Lipson for preparing the PdLi and PdO/Pd/Au targets to be bombarded.

References

[1] H. Yuki et al., Proc. of ICCF6 (1996), Vol. 1, p. 259.

[2] H. Yuki et al., Proc. of ICCF7 (1998) p. 180.

[3] H. Yuki *et al.*, J. Phys. Soc. Japan 66, 73 (1997); J. Phys. G. 23, 1459 (1997).

[4] Y. Sakamoto et al., Z. Phys. Chem. 173, 235 (1991).

[5] H.S. Bosch and G.M. Hale, Nucl. Fusion 32, 611 (1994).

[6] H.H. Anderson and J.F. Ziegler, Hydrogen Stopping Powers and Ranges in All Elements (Pergamon, New York, 1977).

[7] H.J. Assenbaum, K. Langanke and C. Rolfs, Z. Phys. A237, 461 (1987).

[8] S. Ichimaru, Rev. Mod. Phys. 65, 255 (1993).

Conference Proceedings Vol. 70
"ICCF8"
F. Scaramuzzi (Ed.)
SIF, Bologna, 2000

PRODUCTION OF HIGH ENERGY CHARGED PARTICLES DURING DEUTERON IMPLANTATION OF TITANIUM DEUTERIDES

N. Kubota, A. Taniike and A. Kitamura.

Department of Nuclear Engineering, Kobe University of Mercantile Marine
Fukae-minamimachi 5-1-1, Higashinada-ku, Kobe 6580022 Japan

Abstract Implantation experiments using 300-keV deuteron beams are performed to study the 3-body reaction in metal deuterides with full use of *in situ* analyses of the target. The ΔE-E telescope and the angular correlation measurements of the reaction products are made for TiD_x samples prepared with various methods. A portion of the α-particle spectra with a yield ratio of 10^{-7} to D(d,p) protons, which is difficult to explain by reactions with impurities and the sequential reactions, is ascribed to the $3D \rightarrow \alpha + p + n$ channel.

Keywords TiD_x, implantation, 3-body reaction, ΔE-E telescope

1. Introduction

Three-body nuclear reactions, $D + D + D \rightarrow \alpha + p + n + 21.6$ MeV [1], $\alpha + d + 23.8$ MeV [2] and $t + {}^3He + 9.6$ MeV [3], have been claimed to take place with greatly enhanced rates during deuterium implantation of titanium deuterides. The α-particle yield of the α-p-n channel, for example, exceeded the theoretically evaluated value taking account of effects of electron screening [4] by 12 orders of magnitude. Theoretical models such as the formulation based on the optical theorem [5] and the multibody fusion model [2] have been presented to explain the observed enhancements from refined points of view. However, the angular correlation of the reaction products have never been confirmed yet. Moreover, it is curious that these reactions have never been observed to occur simultaneously, since the branching ratio of the final states seems to be of the same order of magnitude.

We are studying the reaction probability under various conditions of the beam and

the target to clarify the phenomena. In these experiment, ΔE-E coincidence method is employed to simultaneously measure the mass and the energy of the reaction products with special attention to helium isotopes, and the angular correlation of reaction products is also examined. After implantation experiments, these samples are analyzed *in situ* using Elastic Recoil Detection Analysis (ERDA), Nuclear Reaction Analysis (NRA) and/or Rutherford Backscattering Spectroscopy (RBS) by proton [6].

2. Experimental procedure

A schematic of the experimental set-up is shown in Fig.1. The target chamber is evacuated by a turbo-molecular pump to a base pressure of 5×10^{-5} Pa. 300 keV deuteron beams from Pelletron 5SDH-2 accelerator bombard a target with the incident angle of 30° through an aperture of 2.4 mm in diameter. The typical current density is 13 μA/cm^2. A positive bias of 240 V is applied to the target to absorb secondary electrons from the target sample.

The ΔE-E telescope is used for simultaneous measurement of the mass and the energy. A pair of solid state detectors (SSDs) with the depletion layer thickness of 20 μm and 500 μm is prepared around the target for detection of ΔE and E, respectively. The solid angle is defined to 4.3×10^{-5} sr by an aperture of 7 mm in diameter. Output signals from each SSD are analyzed with a dual multi-channel analyzer (DMCA) with a coincidence time of 2.4 μs, to measure the mass and the energy simultaneously.

On the other hand, angular correlation of the reaction products, α and d, or t and ^{3}He, is measured with two SSDs positioned oppositely with respect to the target. One is the ΔE-SSD used for the telescope and the other is SSD#3 whose depletion layer is 500 μm thick. Then a ΔE-E anti-coincidence circuit is prepared to reject possible chance

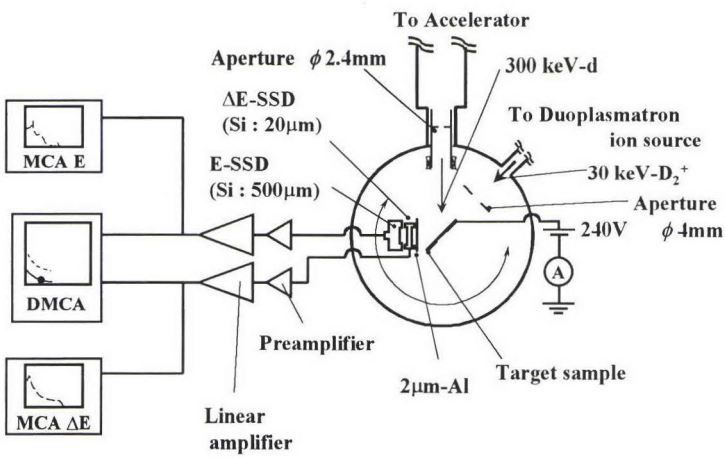

Fig.1. Experimental set-up of the ΔE-E system.

coincidence caused by the D(d,p) protons. The output signals from the anti-coincidence circuit gate the angular correlation measurement.

All SSDs have been calibrated for energy using an ^{241}Am alpha source. Thin aluminum films with 2-μm thickness are mounted on all SSDs to shield thermal radiation from the target heated by the beam.

Three kinds of samples are prepared; 300-1000 μm thick as-received titanium films, 5-1000 μm thick titanium films deuterated by means of gas phase loading and those by ion implantation with 30-keV molecular deuterium ion beams. Some of the gas loaded samples are coated with 100-nm thick aluminum layer, which is expected to suppress deuterium loss caused by the beam heating.

3. Results and discussion

A typical spectrum observed on the DMCA after 300-keV deuteron implantation of an as-received sample of Ti up to a fluence of 4×10^{18} cm^{-2} is shown in Fig.2. The horizontal and vertical axes show the energy measured at the E-SSD and the ΔE-SSD, respectively. The D(d,p)T protons appearing around (E, ΔE) = (2.6, 0.4) MeV predominate in the spectrum. Protons originating in (d,p) reactions with carbon, nitrogen and/or oxygen on/in the target are also distinguishable. For example, small peaks at (2.3, 0.4) MeV and (8.1, 0.2) MeV correspond to the ^{12}C(d,p)^{13}C and ^{14}N(d,p$_0$)^{15}N (Q = 8.6 MeV) reaction, respectively. The impurity carbon is mainly introduced on the surface of the target during ion irradiation. Nitrogen and oxygen are easily introduced in/on the Ti as impurities.

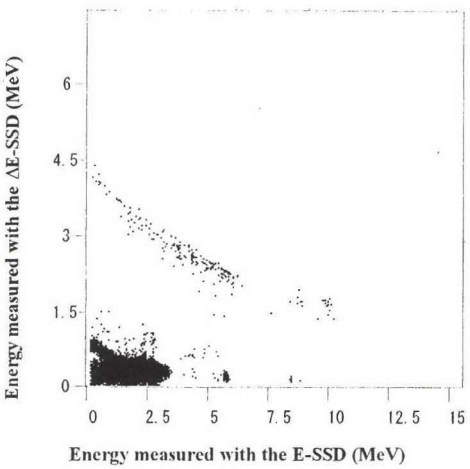

Fig.2. ΔE-E scatter plot of signals measured at 90° during 300-keV-d implantation of the as-received sample.

A distinct trace of α-particles is observed in the energy range from 4.4 to 1.5 MeV on the ΔE-SSD and from 0 to 10.0 MeV on the E-SSD. The α-particles produced by the 3D reactions lie in this energy region and might be hidden in the trace. The total energy spectrum of only α-particles deduced from the DMCA spectrum is shown in Fig.3, and labeled as (a). For comparison a similar spectrum (b) obtained for a gas-loaded $TiD_{1.6}$ sample implanted with 300-keV deuterons up to a fluence of 9×10^{18} cm^{-2} is also shown

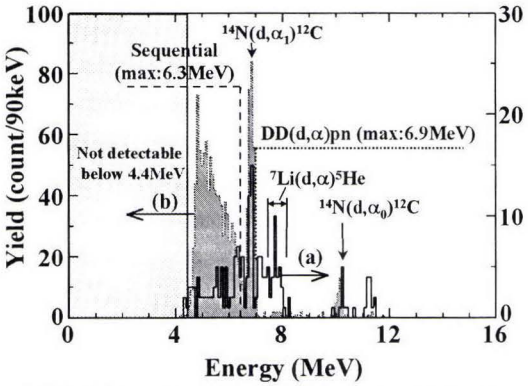

Fig.3. Comparison of α particle spectra obtained with 90-degree ΔE-E telescope.

with shading. The α-particles with energies below 4.4 MeV are lost by the ΔE-E coincidence filtering. The peaks at 6.8 MeV and 10.2 MeV correspond to the α-particles originating in the $^{14}N(d,\alpha_1)^{12}C$ reaction (Q = 9.1 MeV) and $^{14}N(d,\alpha_0)^{12}C$ reaction (Q = 13.6 MeV), respectively. Subtracting the 6.8 MeV peak, a hump remains between 4.4 and 8.4 MeV in the spectrum (a), the yield of which was found to be almost independent of the fluence of the 300-keV deuteron beam. The spectral shape above 6.3 MeV differs from that of α-particles emitted via sequential reactions; D(d,t)p followed by D(t,α)n together with D(d,^{3}He)n followed by D(^{3}He,α)p. The energy spectrum of the latter has been calculated, and is found to be in fair agreement with the spectrum (b) with the maximum energy indicated by the dashed line.

The reactions which could be induced by the present low-energy deuterons with a reasonable cross section and emit α-particles observed in this energy region are the $^{7}Li(d,\alpha)^{5}He$ and the $^{17}O(d,\alpha)^{15}N$ reaction. If the latter were responsible for the hump (a), the more abundant isotope ^{16}O must exist with the approximate areal density of $2\times10^{16}/cm^2$ which is equivalent to 10 monolayers or more. And this amount of ^{16}O should have produced more than 10^4 counts of 1.0-MeV protons via the $^{16}O(d,p_0)^{17}O$ reaction, which we can not recognize. Then the α-particle spectrum from 6.3 to 8.4 MeV in (a) cannot be explained by the oxygen contamination alone.

We ascribe it mostly to the $^{7}Li(d,\alpha)^{5}He$ and the $^{7}Li(d,2\alpha)n$ reaction, although we don't know the cross section of the reaction. The former produces 7.8 MeV α-particles after passing through the Al shield foil, while the latter produces α-particles with a continuum energy spectrum below 8.2 MeV through the Al foil. The reason why we don't have a sharp peak at 7.8 MeV is the uncertainty in the mass of the ground state of the ^{5}He nucleus. The FWHM uncertainty of about 1.2 MeV [7] is calculated to result in the dispersion of ±0.4 MeV in the energy of the α-particles emitted from the $^{7}Li(d,\alpha)^{5}He$ reaction, accounting for the broad hump from 7.0 to 8.4 MeV in (a). It is not surprising that the counterpart of the α-particle, ^{5}He with energy around 6.1 MeV, have never been measured simultaneously, since the ^{5}He travels only about 10 fm during its life time. The α-particle energy was observed to decrease with increasing detection angle, as is expected for the $^{7}Li(d,\alpha)^{5}He$ reaction.

The existence of ^{7}Li has been confirmed by means of the $^{7}Li(p,\alpha)^{4}He$ NRA. The depth profile of ^{7}Li density deduced from the α-particle spectrum is shown in Fig.4. The cross section has been cited from ref.[8]. Although the estimated resolution of 530 nm is rather poor and the cross section does not allow the analysis beyond 3 μm, the profile indicates that the as-received Ti contains lithium as an impurity with concentration exceeding 1 ppm.

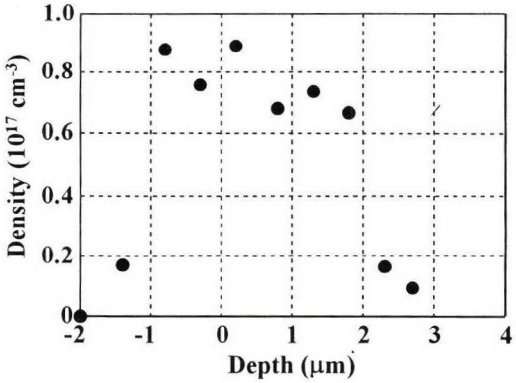

Fig.4. Depth profile of the ^{7}Li density in the as-received Ti.

There might be hidden the α-particles from the $3D \rightarrow d + \alpha$ and $3D \rightarrow n + p + \alpha$ reactions. In the former case the partner products, 15.9 MeV deuterons, should be measured together with the 8.0 MeV α-particles. Unfortunately, both of the deposition energies of the deuterons, 0.2 MeV in the ΔE-SSD and 5.6 MeV in the E-SSD, are not high enough to be separated from other peaks. Moreover, since carbon has been identified in the spectra, it is possible that the 15.9-MeV deuterons are hidden by the contour of 5.8 MeV protons from the $^{13}C(d,p)^{14}C$ reaction on the ΔE-E plot.

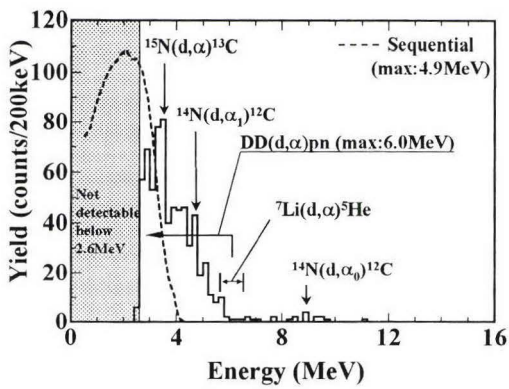

Fig.5. The total energy spectrum of α-particles during the 300-keV-d implantation of a $TiD_{1.8}$ implanted with 30keV-D_2^+ up to a fluence of $2.1 \times 10^{19}/cm^2$.

The angular correlation was then measured to separate the α-d channel products from other reaction products using the detector pair placed oppositely to each other with respect to the 300-μm-thick as-received target. However, no coincidence between the deuteron and the α-particle was observed up to a fluence of $4\times10^{18}/cm^2$.

This result does not always exclude the possibility that the α-particles through the α-p-n channel of the 3D reaction are hidden, which are expected to form a broad continuum from 6.9 MeV down to 0 MeV. To separate the α-particles produced at different depth,

the measurement of the α-particles are made at 90° behind the 5-μm-thick Ti implanted with 30-keV-D_2^+. The result is shown in Fig.5. The broken line shows the calculated spectrum of α-particles emitted through the sequential reactions. The α-particles from the α-p-n channel are expected to appear below 6.0 MeV. We could attribute the portion of the spectrum between 5.0 and 5.5 MeV to the α-p-n channel. The maximum ratio of the α-particle yield to that of the proton from the D(d,p)t reaction reaches 10^{-7}, which exceeds the theoretically evaluated value taking account of effects of electron screening [4] by 11 orders of magnitude.

The 3D → t + ^{3}He reaction is also expected. However, we could not identify the ^{3}He peak in the DMCA, and the 4.8-MeV tritons, if any, are difficult to identify, since the energies of 0.7 MeV and 4.0 MeV deposited in the ΔE-SSD and the E-SSD, respectively, lie in the pile-up spectrum of D(d,p) protons.

4. Conclusions

The α-particles except those originating in deuteron induced reactions with impurities and the sequential reactions have been observed in the energy range from about 5 MeV to 8 MeV for the gas-loaded sample and the as-received sample. The result of NRA using the ^{7}Li(p,α)^{4}He reaction, together with the absence of the coincident partner, as well as the dependence of the yield on the deuteron fluence, suggests that the portion of the spectrum from 7.4 to 8.1 MeV can be ascribed to the α particles originating in ^{7}Li(d,α)^{5}He reaction. For the 5-μm thick sample implanted with the 30-keV-D_2^+ beam, α-particles have been observed in the energy range from 5.0 to 5.5-MeV with a yield ratio of 10^{-7} to the D(d,p) proton. We speculate that these are the α-particles from the 3D → α + p + n channel.

References

[1] J. Kasagi et al., J. Phys. Soc. Japan, 64 (1995)777

[2] A. Takahashi, T. Iida, H. Miyamaru and M. Fukuhara, Fusion Technol., 27 (1995)71

[3] A. Takahashi, K. Maruta, K. Ochiai and H. Miyamaru, Fusion Technol., 34 (1998)256

[4] S. Ichimaru, Rev. Mod. Phys., 65 (1993)255

[5] Y. E. Kim and A. L. Zubarev, Proc. ICCF5 (1995)293

[6] N. Kubota, A. Taniike, Y. Furuyama and A. Kitamura, Nucl. Instrum. & Meth. B, 149 (1999)469

[7] F. Ajzenberg-selove, Nucl. Phys. A, 413 (1984)1

[8] A. Sagara and K. Kamada, Nucl. Instrum. & Meth. B, 34 (1988)465

Conference Proceedings Vol. 70
"ICCF8"
F. Scaramuzzi (Ed.)
SIF, Bologna, 2000

NUCLEAR PHENOMENA IN P+TI^2H_X EXPERIMENTS

TIESHAN WANG[1], YONGTAI ZHU[1], ZHIGUO WANG[1], SONGLIN LI[1]
AND SHIKUI ZHENG[2]

1. Institute of Modern Physics, Chinese Academy of Sciences, *Lanzhou 730000, P. R.China*
2. Nuclear Power Institute of China, Chengdu 610041, P. R. China

A series of charged particle products were observed in the intensive proton beam bombarding deuterated titanium target (Ti^2H_x) experiments. Most of the charged particle products were identified as charged particles with alpha features. Most of the products were from the sub Coulomb barrier nuclear reactions between proton and impurity nuclei, but some of the products are difficulty to be interpreted by known nuclear reaction. There might be some other physical process occurred in the experiments, however, whether it is a kind of nuclear process is not yet confirmed.

1. INTRODUCTION

The interaction between protons and various kinds of matter have been studied for over half a century [1-9]. However, the nuclear reaction induced by protons with energies of only a few hundreds keV has not yet been well studied, since very few reactions have been predicted by theoretical analysis [1,4]. Therefore, experimental data in the energy region lower than 500 keV are rare [5,6]. Some laboratories engaged to study in the energy region for nuclear astrophysical etc. purposes [5-7]. Following the p+Ti^2H_x experiment done by OKTAVIAN laboratory, Osaka University, Japan, Some charged-particle products were also observed in our 60-330 keV proton implantation experiments [9]. There must be some sub-Coulomb barrier proton reactions occurring in the implantation process. Moreover, three of the reaction products in p+Ti^2H_x experiment are charged particles, which exhibits the features of alpha particles. Thus the problem becomes very complex, because the alpha particle cannot be directly produced from the bombarding nucleus (proton) and the major target nucleus (deuteron). These experimental phenomena can always be observed clearly and are always reproducible.[9] Here, a series of experimental studies on these phenomena are reported.

2. EXPERIMENTAL PROCEDURE

Experiments were done with a Cockroft-Walton accelerator. The schematic view of

the experimental system is shown in Fig. 1.

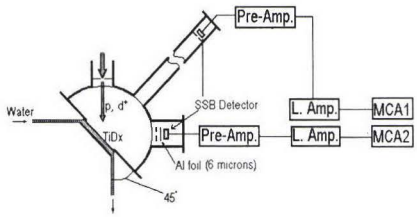

Fig. 1 schematic view of the experimental system

The proton beam was very pure (purity >99.9%) after going through a magnetic analyzer. Charged particle spectra were detected by two Si(Au) solid state detectors (SSDs) of about 450 microns in thickness. They were placed at 90° and 135° in the laboratory system to the proton beam direction, respectively. A ΔE+E telescope was also installed at 90° . All the experimental data were obtained with the detector at 90° , and the measurement at 135° was for checking the angular dependence of the reaction products. The detection solid angles were about $7x10^{-4}$ sr. The Ti^2H_x target was a $2mg/cm^2$ deuterated titanium layer on a 0.2 mm molybdenum substrate, which was prepared in China Atomic Energy Institute by special gas loading method. The amount of the loaded deuterium was estimated by the difference of deuterium gas pressure in the chamber before and after the loading process. Hence, the loading ratio of deuterium to titanium was therefore determined by the amounts of deuterium and titanium. The backside of the target was directly cooled by high-pressure water during the experiment, and it could bear over 1 kw ion beam bombarding. The ion beam current was directly measured from the target, thus the measured value could be higher than the real ion beam current, on considering the secondary electron effect. The charged particle detection system was calibrated with a Thc-Thc' standard alpha source, which contains two kinds of alpha particles with energies 6.15 MeV and 8.78 MeV, respectively. The energy uncertainty in the experiment could be less than 200keV.

3. EXPERIEMNTAL PHENOMENA

A. Charged-particle products

Different kinds of charged particles were observed, their energies can be about 3.0, 3.9, 5.6 and 8.4MeV. A typical charged particle spectrum is shown in Fog. 2.

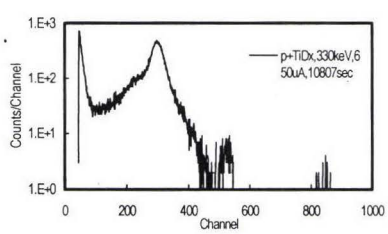

Fig. 2. A typical charged particle spectrum in $p+Ti^2H_x$ experiment.

Proton energy: 330 keV,; beam current: 1.10 mA; measure time: 1000 s; dead time: ≤ 0.2%; Target: Ti^2H_x . The atomic ratio is $x=^2H/Ti \geq 1.6$; and a 6 μm aluminum foil is set in front of the detector.

The peak with about 3.9 MeV had very high intensity. The maximum reaction rate in the experiment reached to over 10^5 r/s at the 324 keV and 1.2 mA proton beam bombardment.

B. Identification of the charged particle products

Identification experiments were done with both ΔE+E coincidence and absorption methods. A typical two-dimensional charged particle spectrum is shown in Fig 3.

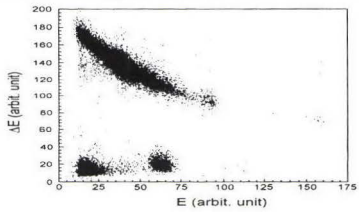

Fig. 3. A two-dimensional charged particle spectrum in p + Ti^2H_x experiments.

D(d,p)T secondary reaction induced by the recoiled deuteron. The other three At least four kinds of charged particles are shown in Fig. 2. One is the 3.0MeV proton from the kinds of charged particle products are located in the alpha (or ^{3}He) zone and their energies are 3.9, 5.6 and 8.4 MeV, respectively.

It is very difficulty to identify whether the products are ^{4}He or ^{3}He due to the limitation of resolution of the detector telescope system. Therefore, the absorption method is applied to the study of the feature of energy loss in the charged particle products. There is only the shift of peak position but no other difference on the feature of the spectra, when aluminum, nickel and titanium foils with the similar thickness were used. Thus, the unknown peaks are from energetic particles, and the reactions are true proton beam-target effect, not from indirect reaction occurring between scattered protons and the screen foil. The dependence of energy loss on aluminum foil thickness is shown in Fig. 4.

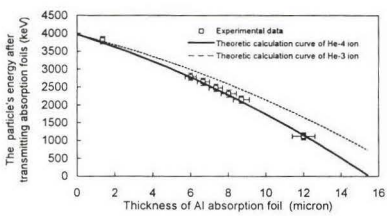

Fig. 4. Comparison of the experimental energy loss data measured by changing thickness of aluminum screen foils and the theoretical energy-loss curves of ^{3}He and ^{4}He ions in aluminum.

It is clearly shown in Fig. 4 that all the experimental data are located on the theoretical energy-loss curve for alpha particles. Thus, the unknown particle with 3.9 MeV is identified to be an alpha particle but not ^{3}He particle. The original energy of the particle has been easily determined as 3.9 MeV by extrapolating the energy loss curve.

C. Energy dependence of the reaction rate

Energy dependence of the reaction has been studied in our experiment. The primary excitation curve of the reaction is shown in Fig. 5.

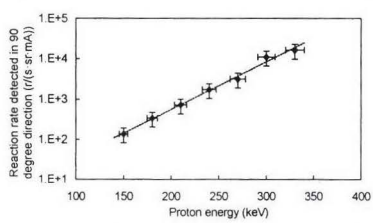

Fig. 5. Energy dependence of the detected unknown reaction rate.

The angular distribution was checked by the measurement made at 90° and 135° The difference of the reaction rates in both directions was difficult to be identified in the

uncertainty of the measurement. It was observed that the peak positions did not change significantly while the proton energy was changed from 150 to 330 keV. This implies that the reaction product energies are not evidently energy-dependent in this energy region, since the kinetic energy of the protons was much less than the Q value. Thus, we may estimate roughly the reaction rate with the experimental data measured in the 90° direction. The fitted curve of the experimental data in Fig. 5 is linear in semi-logarithmic coordinates. This means that the reaction rate grows exponentially with the increase of proton energy.

D. Impurity analysis

X-ray photoelectron spectroscopy (XPS) and gas mass spectroscopy (GMS) methods were used to analyze the elements of the target. The contents of the impurity elements are listed in Table 1. The major impurity elements are carbon and oxygen. The ratio of nitrogen is less than 3 percent. Although the elements of silicon, sulfur, sodium, chlorine, calcium etc. are also observed within very tiny ratio.

Table 1. Quantification ratios of the impurity elements measured by XPS

Peak	Center	Peak area	% (normalized)
C 1s	285.00	1070560	77.36
O 1s	532.58	87756	17.47
N 1s	399.62	9285.8	2.67
Na 1s	1071.98	7862.6	0.895
Si 2p	102.58	910.46	0.351
S 2p	168.84	1751.8	0.392
Ca 2p	347.94	1591.1	0.178
Cl 2p	199.16	866.70	0.129

E. Other background experiments

Some comparison experiments were done with targets of titanium alloy, titanium on molybdenum substrate, molybdenum and stainless steel etc.. There were only some counts of charged particle products located in the interesting energy range. The reaction rate was at least four orders lower than in that p+Ti^{2}H$_x$ experiment.

4. DISCUSSIONS AND CONCLUSIONS

These reactions cannot be a direct reaction between a proton and a deuteron, because the product is alpha particle, whose mass is higher than that of a proton plus a deuteron, therefore, this cannot satisfy the basic principle of energy-mass balance. However, the phenomenon was observed clearly in our experiment. There must be some sub-Coulomb barrier reactions between the proton and nuclei, of which the experimental target material other than deuterium consists.

Another major target constituent is titanium nuclei. All the Q values of the possible reactions between proton and titanium are negative [1], thus, there is no possibility for these reactions to occur in low energy protons implantation experiments.

The possibility of any reaction occurring between proton and impurity nuclei in the target is therefore considered. The possible impurities in the target are tritium, helium,

carbon, nitrogen, oxygen and some other elements. The reactions with energetic alpha product that occur between a proton and the above possible impurity nuclei are [11,2,7,81]:

$^{15}N + p \rightarrow {}^{12}C + \alpha + Q(4.966MeV)$ (1)

$^{17}O + p \rightarrow {}^{14}N + \alpha + Q(1.191\ MeV)$ (2)

$^{18}O + p \rightarrow {}^{15}N + \alpha + Q(3.979\ MeV)$ (3)

Among these three reactions, the energies of alpha products from reactions (1) and (3) are 0.926 and 3.14 MeV, respectively; they are much less than the experimental data, hence, these reactions have no effect in the interpretation of experimental results. Reaction (2) seems to be the only candidate, due to the alpha product with 3.73MeV energy[7]. However, the natural abundance of ^{15}N is only 0.366%. If its reaction cross section is not above 1 barn, its reaction rate under our experimental condition should be a few orders lower than that of the detected events (once reached 10^5 r/s)[7,9,10]. According to the impurity analysis results obtained by XPS and GMS methods, the amount of the nitrogen was far from enough to be applied to the interpretation of the experimental phenomena, unless the reaction cross section is larger than a barn, which is impossible according to the theoretical prediction.

Some other nuclear reactions with alpha product between proton and light nuclei, e.g., $^6Li(p, \alpha)^3He$+4.018MeV, $^7Li(p, \alpha)^4He$+17.36MeV, $^9Be(p, \alpha)^6Li$+2.126MeV, $^{10}B(p, \alpha)^7Be$+1.146MeV, $^{11}B(p, 2\alpha)^4He$+8.682MeV, $^{11}B(p, \alpha)^8Be$+8.59MeV, $^{19}F(p, \alpha)^{16}O$+8.11MeV and $^{27}Al(p, \alpha)^{24}Mg$+1.601MeV are also considered. They are also not the suitable candidate reactions for the 3.9MeV alpha product. The $^{11}B(p, \alpha)^8Be$+8.59MeV, $^{19}F(p, \alpha)^{16}O$+8.11MeV, $^7Li(p, \alpha)^4He$+17.36MeV might be used to interpret the high energy alpha particle products, but no significant impurities of ^{11}B, ^{19}F and ^7Li were found in the target by the element analysis.

T(d, n)^{4}He reaction has been considered too, because there might be some tritium in the target from the reaction product of D(d, p)T reaction. However, this is already a sub-secondary reaction, and the alpha particle from T(d, n) ^{4}He reaction has only 3.5 MeV energy, lower than the unknown particle's energy, thus it could not be the suitable interpretation. In addition, the experiment done with a fresh target without any tritium displayed the same phenomenon. Thus this possibility is also excluded.

Since there is not any convinced interpretation according to the known nuclear reactions between the proton and possible target nuclei, this reaction is considered anomalous. Some proposals are brought out.

Firstly, $D + {}^3He \rightarrow {}^4He + p + (18.89\ MeV)$ secondary reaction is considered, because deuteron and helium-3 produced by the $D + p \rightarrow {}^3He + \gamma$ (5.5 MeV) reaction can receive energy by the recoiling of proton and may react each other in the target material. In the above process, the alpha particle with 3.8 MeV energy and proton with 15.09 MeV should be produced. If this reaction occurs, a peak should appear at around 2.2 MeV, which correspond with the energy loss of 15.09 MeV proton in a 450 μm Si detector. However, we have detected only the alpha particle with about 3.9 MeV without significant peak around 2 MeV. Therefore, this interpretation is also not very convincing.

The neutron reactions, e.g., n+Mo reactions, are also considered. However, the possible neutrons are from D-D secondary reaction, which was observed in less than 10^2

n/s in the experiment. Only a few nuclear reactions can be induced by D-D neutron, and the cross section should be very small. Therefore, the neutron could not play any meaningful role.

Multi-body reaction is also considered, even though the reaction cross section of three-body reaction is considered as over 30 orders lower than two-body reaction based on theoretical prediction [11]. Because the atomic ratio of deuterium to titanium can reach up to 2.0, there is more than one deuterium in each lattice cell of titanium crystal. When the shell electron of deuterium is captured, the deuterium in titanium exists as deuteron (bare nucleus). Two or more deuterons exist in plasma state with very high density inside lattice. In this case, bombarding proton is supposed to react with two or more bounded deuterons in such an experimental condition. [5] One of the proposed reaction is p + 2D $\rightarrow$ ^{4}He + p + Q (23.8 MeV). In this process, an alpha particle with 4.7 MeV and a proton with 19 MeV should be produced. The same problem is that no 19.1 MeV proton was detected in our experiment. Also the alpha particle energy from p+2D reaction is higher than the energy detected in this experiment. So, this proposal is also not convincing.

Therefore, the origin of this reaction is still unclear. The ^{15}N(p, α)^{12}C reaction seems to be the most possible candidate, but the amount of nitrogen in the target is far from enough to be used to support this assumption[10], unless the cross section of ^{15}N(p, α)^{12}C is enhanced significantly. Whatever the kind of nuclear reaction is, it must be a reaction under the Coulomb barrier. Because the bombarding nucleus is a proton with very low energy, this reaction might play some roles in nuclear astrophysics (solar physics) and the application of fusion energy.

5. ACKNOWLEDGMENTS

This Project is supported in parts by the National Natural Science Foundation of China (contract no.19845002), the special fund from the president of the Chinese Academy of Sciences and also the special fund from the Institute of Nuclear Power of China. The first author would like to thank Prof. A. Takahashi, Osaka University Japan, for his helpful discussion and information.

References:

1. F .E. Cecil, D. Ferg and H. Liu et al., Nuclear Physics A539(1992) 75-96
2. F. K.McGowan and T. Milner, Atomic Data and Nuclear Data Tables Vol.18 No. 1 (1976), p.8-119
3. X. T. Lu, Z. C. Chen and J. G. Chen, Handbook of nuclear data (in Chinese), Press of Atomic Energy (1981), pp. 6-21
4. G. Battistig, G. Amsel and E. d'Artemare, Nucl. Ins. & Meth.B66 (1992) 1-10
5. E. Ray, R.Kirsch, H.H. Mikkelsen et al. Nucl. Ins. & Meth. B. 69, 133-141 (1992).
6. M. Youn. H. T. Chung and J. C. Kim et al., Nuclear Physics A 533 (1991) 321-332
7. C. Rolfs and S. Rondney, Nuclear Physics A235(1974) 450- 459
8. H. Lorenz-Wirzba, C. Rolfs and W. S. Rodney, Nucl. Physics a313(1979) 346-362
9. T. S. Wang, Y. T. Zhu, Z.G. Wang et al., Proc. of ICACS-18, Odense, Denmark, Aug. 1999, p168
10. M. Soltani-farshi, H. Baumann, B. Baretzky et al. MER Syp. Proc. 513(1998), 203-208
11. A. Takahashi, K. Maruta, K. Ochiai etc., Fusion Technology, 34, 11: 2734 (1998).

Conference Proceedings Vol. 70
"ICCF8"
F. Scaramuzzi (Ed.)
SIF, Bologna, 2000

STUDY OF THE DEUTERATED TITANIUM TI^2H_X SAMPLE BY USING NUCLEAR REACTION ANALYSIS (NRA) AND MATERIAL ANALYSIS METHODS

TIESHAN WANG[1], Baowei DING [1], ZHIGUO WANG[1], SHIKUI ZHENG[2], YOURONG JIANG[2] AND WEIDONG LI[2]

1. *Institute of Modern Physics,* Chinese Academy of Sciences, *Lanzhou 730000, P. R.China*
2. *Nuclear Power Institute of China, Chengdu 610041, P. R. China*

Titanium is one of the best hydrogen loading material. The predicted maximum loading ratio of hydrogen in titanium may reach to 2.0. In this work, a titanium layer on molybdenum substrate was deuterated with the atomic ratio $X=^2H/Ti \geqslant 1.6$. The distribution of deuterium in the Ti^2H_x sample was studied with D(d, p)T reaction. The change of the surface topography and microstructure of the sample before and after loading was observed by using of Scan Electron Microscopy (SEM). The surface segregation of samples after deuteron bombardment was also observed. A fluctuant-increasing trend of the deuterium density in titanium target was detected in the deuteron implantation experiments, which indicated a suddenly explosion (segregation) or fast diffusion of deuterium in titanium. Significant amount of nitrogen contamination was found in the Ti^2H_x sample by Nuclear Reaction Analysis (NRA) analysis, which indicated that the Ti^2H_x structure might have the feature to trap nitrogen from air. The nitrogen contamination in Ti^2H_x made significantly influence to increase the atomic ratio $X=^2H/Ti$.

1. INTRODUCTION

The embrittlement phenomena can be induced by the ingression of hydrogen in materials, sine the different contents and distributions of hydrogen in solids may affect significantly the mechanical and chemical characteristics of materials [1-6]. Study of hydrogen behaviors, including the accumulation and diffusion of hydrogen in solids and the segregation, changes of nano- and macro-mechanical characteristics of materials etc. are very essential to understand the embrittlement and corrosion. A lot of work was brought out [1-12]. However, studies of hydrogen behaviors under some e extreme condition and some new materials are insufficient. Titanium and its alloys are widely applied, due to their good chemical stability and mechanical features. Titanium is also

one of the best hydrogen loading metal. The predicted maximum loading ratio of hydrogen in titanium may reach to 2.0. Therefore, the fundamental study of hydrogen behaviors in titanium and its alloys are very essential for the new material research and engineering applications [1-3, 6-12]. In this work, some preliminary studies on the pure titanium are brought out.

2. LOADING THE HYDROGEN INTO TITANIUM SAMPLES

Gas loading, ion beam implantation and electrolysis three methods are usually used to loading hydrogen in to metals. However, the loading ratio (H/Ti) in electrolysis method is very difficult to be controlled. So, the gas loading and implantation methods were used in this work. Since the hydrogen isotopes have the same chemical and mechanical features, instead of hydrogen, deuterium was applied in order to study its diffusion and distribution with nuclear reaction analysis method.

2.1 Gas loading

The sample for gas loading was a thin titanium layer formed on the molybdenum substrate by sputtering technology. The sample was put in a vassal with deuterium gas, and the titanium layer was deuterated with changing temperature. The loading ratio was determined by the change of the deuterium gas pressure before and after the loading process. The atomic loading ratio (D/Ti) can be larger than 1.6 in this work.

2.2 Ion beam implantation

Deuteron implantation experiments were performed in a 600KV high voltage accelerator. The deuteron beam was analyzed after acceleration, then implanted into a titanium sample. The ion beam energy and density were 300keV and 125 μ A/ cm^2. D(d,p)T reaction was used to monitor the deuterium density in sample. The charged particles emitting from D-D fusion during the implantation were detected by a Si(Au) detector and data acquire system. The diffusion and accumulation of deuterium in sample may be indicated by the change of D-D fusion yields.

3. RESULTS AND ANALYSES

3.1 Topography of the titanium deuterides

The change of titanium nano-structure was observed with scan electron microscopy (SEM) technology (fig.1).

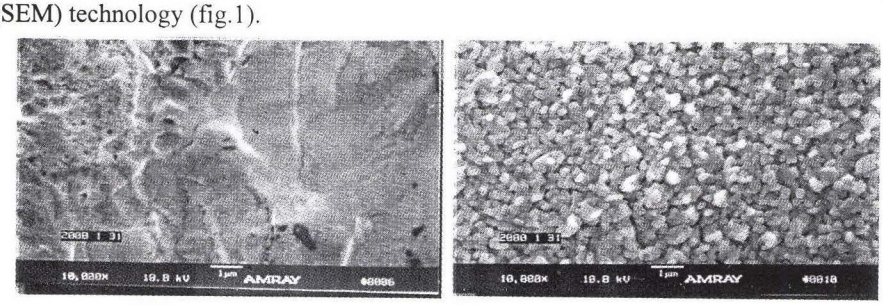

Fig. 1 Topographies of the Titanium sample before (left) and after (right) loading deuterium (x10,000)

The titanium deuteride was observed in fig.1, and the metal structure cracked into powder, while the loading ratio (D/Ti) was larger than 1.4; And quite symmetrical crystal grain were formed while the loading ratio was larger than 1.6. The sizes of titanium crystal grains are between 100nm and 500nm. It was found that the metal crystal cracked into nano crystal grains with very clear-cut boundary, while the loading ratio was larger than 1.6, and the metal crystal just partly cracked into nano crystal grains, while the ratio was between 1.4 and 1.6.

3.2 Accumulation of deuterium in titanium during deuteron implantation

The accumulation and diffusion of hydrogen in titanium metal were studied qualitatively by using D-D fusion reaction analysis. The average deuterium density in the titanium target was directly corresponding to the D-D reaction yield induced by each implanted deuteron, while the deuterium distribution in target and the deuteron beam parameters were same. The experimental curve obtained in the deuteron beam implantation with constant parameters is in fig.2.

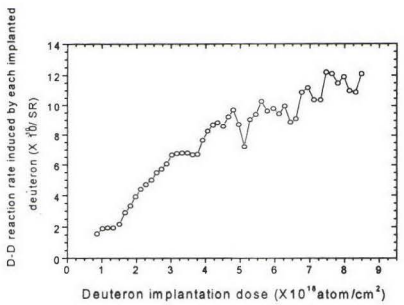

Fig.2 D-D reaction yield vs. deuteron implantation dose on titanium

A fluctuant-increasing trend of the deuterium density in titanium target is shown in the curve of fig.2. At some points, there are significant decreases before next increase. The higher of the implantation dose is, the more frequent of fluctuates is. Fluctuate of D-D fusion yield directly corresponded to the density change of target deuterons in target, which was related with the accumulation and diffusion of deuterium in target. Each fluctuate might indicate an event of deuterium escape from the reaction zone, and the next increase was just a new accumulation process. A saturated trend is also shown in the fig. 2, but the maximum loading ratio (D/Ti) was less than 1.6.

3.3 Damages of the sample after implantation

Serious damages of the sample surface were observed by using of SEM. The surface topographies of the sample before and after implantation are shown in fig.3.

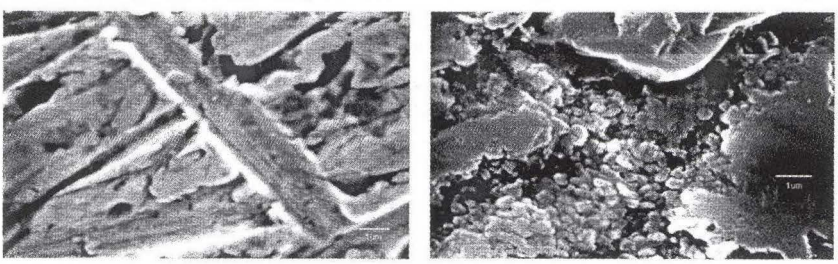

Fig.3 comparison of topographies before (left) and after (right) bombarding (x10,000)

Many segregation layers are shown in the fig.3. A lot of crystal grains with the size of few hundreds nano-meters were formed under the surface. However, the crystal grains are round like

beans.

3.4 Anomalous nitrogen contamination

Significant contamination of nitrogen in sample was found in experiments. The contents of nitrogen-15 in different metal samples were determined with the $^{15}N(p, \alpha)^{12}C$ nuclear reaction analysis (NRA). The results are listed in table 1.

Table 1. Content of ^{15}N in different samples (NRA results)

Samples	^{15}N density (atom/cm^2)
Used Ti^2H_x	4×10^{16}
Fresh Ti^2H_x	1×10^{16}
Ti	2×10^{14}
Mo	3×10^{14}
TiMo	6×10^{14}

Comparing to other metal samples, the nitrogen contamination in Ti^2H_x samples is about two orders higher, and the amount of ^{15}N in used Ti^2H_x sample is four times of the amount in fresh Ti^2H_x. This result indicated that the Ti^2H_x sample has strong ability to trap nitrogen from air, the longer of the sample stored in air, the more nitrogen contamination accumulated in Ti^2H_x sample. The nitrogen contamination might relate with the titanium hydride structure, but the ingression of nitrogen might affect the deuterium loading ratio in titanium.

4. CONCLUSIONS

The crystal nano-structure is changed evidently, while deuterium ingress into titanium; cracks were observed, while the deuterium loading ratio was larger than 1.4; and the titanium metal was completely cracked into crystal grains with the size of a few hundred nano-meters, while the deuterium loading ratio was larger than 1.6. However, the shape of crystal grains formed by deuteron beam implantation method is different from the grains formed by gas loading method. The loading ratio is larger in case of gas loading, comparing to the implantation method. The larger of the loading ratio is, the finer of the crystal grains are. This phenomenon may be applied to prepare nano-size titanium hydride powder.

The deuterium density in titanium target changed abruptly during the implantation process, it implies a suddenly explosion (segregation) or fast diffusion of deuterium in titanium. This phenomenon is not yet observed before.

Ti^2H_x has strong ability to trap nitrogen from air, comparing to titanium, stainless steel and molybdenum etc. metals. The amount of nitrogen contamination might reach to the comparable level to the deuterium in titanium. It may make significant influence for the charge of deuterium in titanium.

5. ACKNOLEDGEMENT

This work is partly supported by the Special fund of the Chinese Academy of Sciences and the Special fund of the Nuclear Power Institute of China.

We are grateful to Pingzhi WANG and Jiyuan HAO who have operated the accelerator for the experiments.

References:

1. B. S. Yilbas, A. Coban, R. Kaharaman, Hydrogen Embrittlement of Ti-6Al-4V Alloy with Surface Modification by TiN Coating. Int. J. Hydrogen Energy (UK), Vol.23, No.6, p.483-9(june 1998).
2. E. Berhadsky, A. Klyuch, M. Ron et al., Hydrogen Absorption and Desorption Kinetics of $TiFe_{0.8}Ni_{0.2}H$, J. Hydrogen Energy (UK), Vol.20, no.1, p.29-33 (Jan1995).
3. N. E. Lo Biondo, R. R. Aharonov, R. P. Fontana, An Investigation of the properties of Ti-C:H Films. Surf. Coat. Technol., Vol.94-95, No.1-3,p.652-7(Oct.1997).
4. B. Li, K. Griffiths, C. S. Zhang et al. The Interaction of D2O with Zr(0001) at 80 K, Surf. Sci. 370(2-3):97-112, (1997) Jan 10.
5. C. S. Zhang, B. Li, P. R. Norton et al. The Initial Stages of Interaction of Hydrogen with the Zr(10(1)Over-Bar0) Surface, Surf. Sci. 346(1-3):206-221, (1996) Feb 1.
6. P. Scardi, M. Leoni, R. Chechetto, Residual Strain in Deuterated Ti Alloys. Mater. Lett. (Netherlands), Vol.36, No.1-4, p.1-6 (July 1998).
7. H. Y. Zhu, J. Wu, Q. D. Wang, Reaction Behavior of TiFe Hydride, J. Alloys Comp. (Switzerland), Vol.215, no.1-2, p.91-5 (Nov.1994).
8. J. Choboy, A. Marcelli, L. Bozukov et al. Effect of Hydrogen Absorption on the Cerium Electronic State in CeFeTi, Phys. Rev. B, Condens. Matter (USA) Vol.51, no.14, p.9005-14 (April 1995)
9. A. Takasaki, Y. Fuyuya, K. Ojima et al., Hydride Dissociation and Hydrogen Evolution Behaviour of Electrochemically Charged Pure Titanium, J. Alloys Comp. (Switzerland), Vol.224,no.2, p.69-73 (July 1995)
10. Takasaki, Y. Fuyuya, K. Ojima et al., Hydrogen Evolution from Cathodically Charged Two-Phase (Ti_3Al+TiAl) Titanium Alminides, J. Alloys Comp.(Switzerland), Vol.224, no.2, p.299-304(july 1995)
11. A. A. Popov, N. G. Rosina, N. I. Kardomina et al. A study of the Cause of Hydrogen Embrittlement of Titanium Alloys on Depositing and Removing Protective Coatings, Russ. Metall. (USA), no.5, p.106-9(1994)
12. Kagawa, Absorption of Hydrogen by Vanadium-Titanium Alloys, Rep. Fac. Eng. Nagasaki Univ. (Japan), Vol.25, p.233-9 (July 1995).

Conference Proceedings Vol. 70
"ICCF8"
F. Scaramuzzi (Ed.)
SIF, Bologna, 2000

ANALYSIS OF EXPERIMENTAL RESULTS ON EXCESS HEAT POWER PRODUCTION, IMPURITY NUCLIDES YIELD IN THE CATHODE MATERIAL AND PENETRATING RADIATION IN EXPERIMENTS WITH HIGH-CURRENT GLOW DISCHARGE

Karabut Alexander B.
SIA LUCH, 142100, Moscow region, Podolsk, Zheleznodorozhnaja Str. 24, Russian Federation.

Abstract

So far a considerable collection of results on Excess Heat registration, the cathode material impurity nuclides yield (with changed natural isotopes ratio) and generation of high-energy penetrating radiation (fast electrons, X-ray and gamma emissions) has been accumulated in experiments with high-current Glow Discharge.

Analysis of these results allows one to assess possible basic processes going on in the cathode material exposed to high-current Glow Discharge (GD).

1. Experimental

Excess Heat power production [1] presents results on Excess Heat power production up to several tens W with Efficiency up to 150% and even higher.

Excess Heat values depend upon the cathode material and the plasma-forming gas being used. The highest Excess Heat value (up to 4.0 MJ) obtained on one of the cathode samples exposed to Glow Discharge operation for a long time duration (up to 150 hours) assumedly points out that the said energy is nuclear origin.

Yield of impurity nuclides with altered (by several tens of times) natural ratio of elements isotopes. Proceeding from the assumption that the registered Excess Heat [1] results from going on nuclear reactions [2] the impurity yield content in the cathode samples material was analysed before and after the experiments with the high-current Glow Discharge device [1]. The following procedures were used: spark mass spectrometry, secondary ion mass spectrometry, secondary neutral mass spectrometry. Those were used for analysis of impurity nuclides in the cathode samples material before and after the experiment. The difference in impurity elements content before and after the experiment was defined as the yield of impurity elements in the course of the experiment. Impurity elements with masses by approximately two times less than that of Pd and the ones with their masses close to that of Pd have been registered in 100 nm thick surface layer in quantities up to several tens %. The main recovered impurity nuclides (with more than 1% content) are ^{7}Li, ^{12}C, ^{15}N, ^{20}Ne, ^{29}Si, ^{44}Ca, ^{48}Ca, ^{56}Fe, ^{57}Fe, ^{59}Co, ^{64}Zn, ^{66}Zn, ^{75}As, ^{107}Ag, ^{109}Ag, ^{110}Cd, ^{111}Cd, ^{112}Cd, ^{114}Cd (Fig.1). The total content of these impurities amounts to 10^{17}, the experiment duration being up to $2x10^{4}$ sec. The observed change of natural isotope ratio for these impurity nuclides is up to several tens of times, some main isotopes of impurity elements (with high natural abundance percentage) being absent. The following isotopes were registered as being absent: ^{58}Ni, ^{70}Ge, ^{73}Ge, ^{74}Ge, ^{113}Cd, ^{116}Cd. These peculiarities are also registered within 100nm thick surface layer (Fig.2), the observed natural Pd isotopes ratio of the sample being changed (Fig.4).

The said results obtained by various methods show good agreement with each other and are 100% reproducable.

Gamma emissions registration was carried out with the help of Ge-Li detector and the multi-channel spectrum analyzer. The detector was placed into 10 mm thick lead chamber together with the GD device. Gamma emissions ranging 0.1 - 3 MeV were observed when the Glow Discharge was on and in the course of 8 days after the discharge current switch off. When using cathodes of various materials it was observed that after the discharge current

switch off the induced gamma emissions value grows proportional to the increase of deuterium ions dose received by the cathode from the discharge plasma (fig.6). In spectra registered for one and the same Pd cathode sample in the course of 8 days after the discharge current switch off (Fig.5) groups of radioactive nuclides were discovered, their semi-decay period ranging from 1 to 6-7 days (Fig.7).

The induced gamma activity range included areas exceeding the uniform spectrum (continuum) and separate lines imposed upon them. In these conditions the excess of gamma-line area over the background was of a small value (δ=2.5-5). The meaning of δ for the continuum was equal to 8-10 (δ=8-10). The gamma spectra obtained when the Glow Discharge was on and after the Discharge current switch off were processed with the help of a data-base [2] to compare the gamma-lines of irradiating nuclides. The analysis showed neutron-excessive nuclei with masses ranging from A=16 to A=136, resulting in formation of β-radioactive decay chains, to be the source of gamma emissions. Given below is an example of such a chain for an atomic mass of A=102. All the gamma lines presented in this chain were registered in the experiment.

$$\overset{\text{n,(31\%)}}{\underset{\beta^-,32\text{ms}}{}}\ {}^{101}\text{Rb} \longrightarrow \overset{\text{n,(2,37\%)}}{\underset{\beta^-,118\text{ms}}{}}\ {}^{101}\text{Sr} \longrightarrow \overset{\text{n,(1,94\%)}}{\underset{\beta^-,448\text{ms}}{}}\ {}^{101}\text{Y} \longrightarrow \underset{\beta^-,2.1\text{ s}}{}\ {}^{101}\text{Zr} \longrightarrow \underset{\beta^-,7.1\text{s}}{}\ {}^{101}\text{Nb} \longrightarrow \underset{\beta^-,14.61\text{m}}{}\ {}^{101}\text{Mo} \longrightarrow \underset{\beta^-,14.22\text{m}}{}\ {}^{101}\text{Tc} \longrightarrow {}^{101}\text{Ru}$$

The total quantity of radioactive atoms (Fig.8) was determined taking into account the gamma-lines area, the detector efficiency and the quantum output value. The main contribution to gamma emissions (radioactive nuclides impurity yield up to 10^5 of atoms) was made by beta-radioactive chains with masses A=16; 17; 23; 30; 46; 47; 51; 54; 55; 58; 63; 64; 71; 75; 80; 84; 92; 97; 99; 100; 101; 102; 103; 104; 105; 106; 107; 108; 109; 110; 118; 123.

Experimental results on nuclear products registration show that presumably there exists a certain mechanism for conversion of low-energy (hundreds of eV) initial excitation from electric discharge into high-energy processes. The X-ray emissions may serve as a testimony for the existence of such a mechanism.

The X-ray emissions registration was carried out on modified GD device. The X-ray emissions were allowed to escape from the GD area through a number of holes bored in a flat anode body. X-ray film, Al-oxide-based thermo-luminescent detectors (TLD) and thick-film nuclear emulsion were used to register the said emissions. The picture of anode-cathode area left by the X-ray irradiation upon the X-ray film or nuclear emulsion was obtained with the help of obscure chamber covered by 0.015 mm thick berillium filter. TLD-based seven-channels spectrometer with berillium filters of varying thickness was used to estimate the emissions spectrum constituents. The X-ray pictures show that it is the anode walls and the central cathode area which irradiate the emissions of highest intensity. The overall X-ray irradiation dose for 6 hours of the experiment amounted to 5000 Roentgen. Registration results obtained by the seven-channels spectrometer (Fig.9) allow to single out spectrum areas with energy of 1.5 and 2 keV. There are areas of intensified registered irradiation, which imply presence of harder irradiation constituents. Pd-D system results in 10-15 times more intensive irradiation, than W-H and T-H systems, correspondingly. The procedure for analysis of photo-electrons tracks (counting of darkened grains) obtained upon the nuclear photo-emulsion using the obscure chamber was also used in the experiment for defining x-ray emissions spectrum. These results show more intensive (high-energy up to 30 keV) X-ray irradiation (Fig.10).

2.Experimental Results and Discussion

The following processes may lead to initiation of nuclear reactions:

1. Deuterium ions acceleration in the Glow Discharge near-cathode area to energies of several hundred eV.

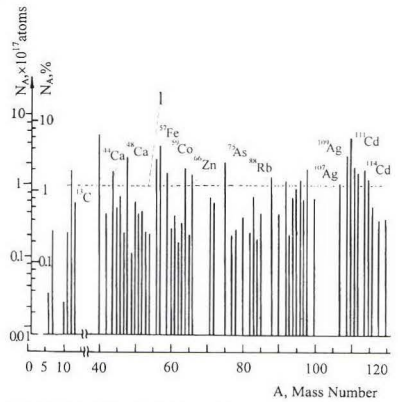

Fig.1. Post-Glow Discharge impurity yield in Pd cathode.

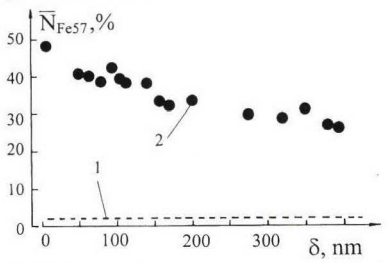

Fig.3. 57Fe and 56Fe isotopes ratio change in Pd cathode superficial layer. 1-natural ratio, 2-after Glow Discharge.

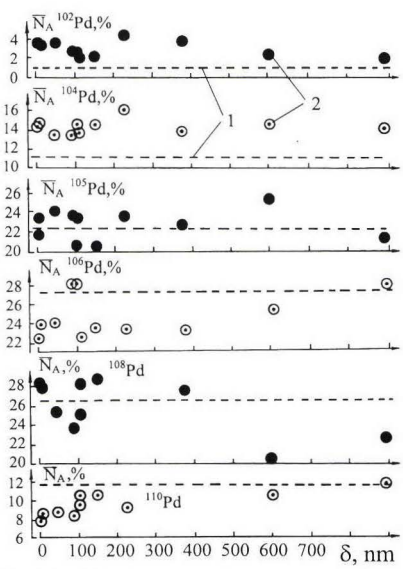

Fig.4. Post- Glow Discharge Pd isotopes ratio change in Pd cathode superficial layer.

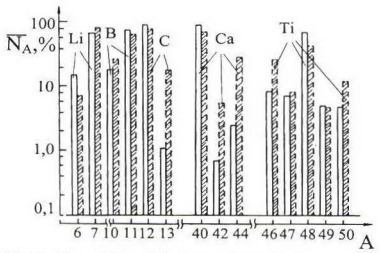

Fig.2a. Post- Glow Discharge impurity isotopes ratio change (in comparison to the natural abundance) in PD cathode.

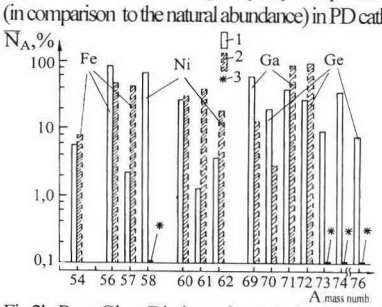

Fig.2b. Post- Glow Discharge impurity isotopes ratio change (in comparison to the natural abundance) in PD cathode.

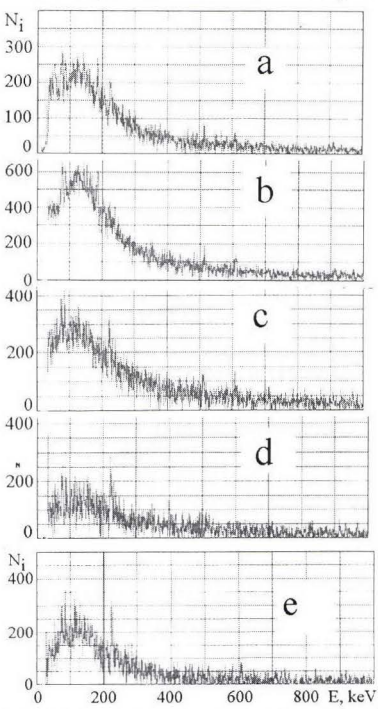

Fig.5. Post- Glow Discharge induced gamma-emissions spectra, a-During Glow Discharge operation (τ = 23000 sec.); b-1day later, c-2 days later, d- 6 days later, e-8 days later (b-e - τ = 60000 sec.).

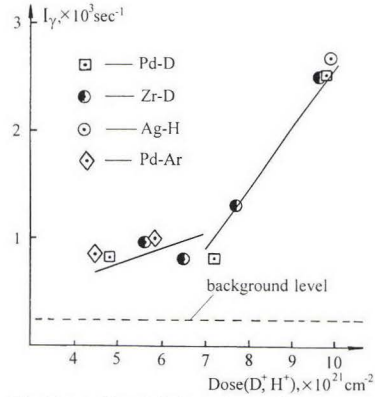

Fig.6. Post- Glow Discharge induced gamma-emissions intensity versus deuterium ions dose in the cathode.

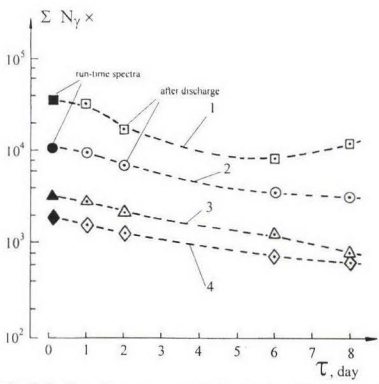

Fig.7. Induced gamma-emissions intensity change (total number of events within specified energy range) for different spectrum areas. 1) 100 - 150 keV energy range, 2) 300 - 350 keV energy range, 3) 650 - 700 keV energy range, 4) 1100 - 1150 keV energy range.

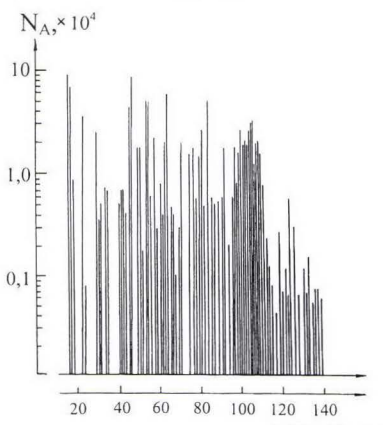

Fig.8. Total quantity of radioactive nuclides in post-GD Pd cathode.

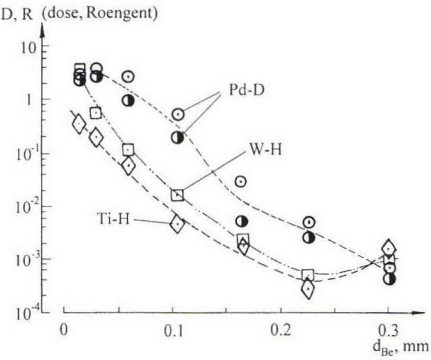

Fig.9. X-ray emissions dose absorbed by TLD behind Be filters of various thickness.

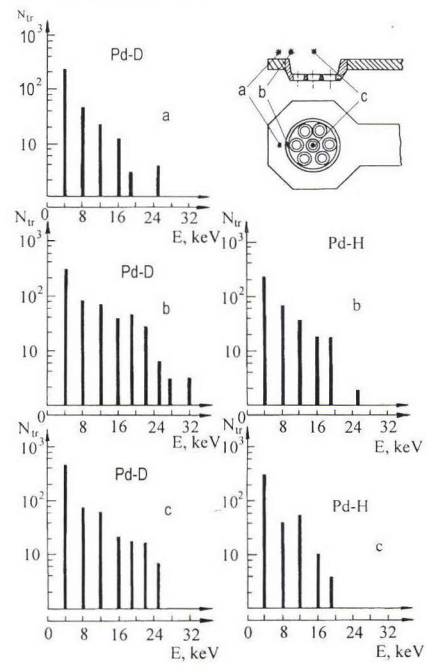

Fig.10. X-ray emissions spectra obtained by procedure of tracks registration in nuclear photo-emulsion using the obscure chamber. Pd-D system. a- plasma area, b- anode wall, c- cathode central part. Pd-H system. b- anode wall, c- cathode central part.

2. Non-resilient processes of deuterium ions collision with the crystal lattice ions (Pd^{4+} ions for Palladium). Under these conditions the electron frame is displaced relative to nucleus and a dipole or optic polar phonon is formed. The initial optic polar phonons frequency is $\omega_{op} = 2\pi \cdot \times \nu$, where $\nu = W_{op}/2\pi \times h$. At energies W=1keV $\omega_{op} = 0.95 \times 10^{19}$ sec^{-1} which is higher than the plasma frequency $\omega_p = (1.3\text{-}2.5) \times 10^{16}$ sec, plasmones are not produced and there is no compensation for the arising spatial division of charges. These processes cross-section related to non-adiabatic transition is determined according to Massey criterion:

$\xi = \Delta E \times a \times 2\pi/(h \times v)$.

Here $\Delta\mathbf{E}$ represents the bombarding deuteron energy variation, **a** stands for the area dimension, where the adiabatic wave function is essentially changed, **h** is the Plank constant, **v** shows the relative deuteron velocity. For $\Delta\mathbf{E}$ = 0.07-1.5 keV (the discharge conditions) the Massey criterion $\approx$ 1 and the non-resilient processes cross-section for optic polar phonons formation becomes close to gaso-kinetic one.

3. The local electric field intensity $\mathbf{E_{loc}}$ resulting from the displacement of both the electron shell and the nucleus is characterized by a very big value because the distance between the electric charges is very small. At the said electric field frequency being higher than plasma frequency the electric induction value is close to zero. The electric field intensity is identified by the number of dipoles being formed. The macroscopic electric field intensity $\mathbf{E_a}$ builds up with the increase in the number of atoms $\mathbf{n_a}$ assuming the state of polar phonon excitation (the dipoles number): $\mathbf{E_a} \sim n_a \cdot E_{loc}$.

At big values of macroscopic electric field intensity $\mathbf{E_a}$ the largest share in the distribution of energy is taken by non-linear (anharmonic) occurrences The medium dynamic polarization can be represented as follows: $P=\varepsilon_0 \cdot (\chi_1 E_1 + \chi_2 E_1^2 + \chi_3 E_1^3 + ...)$

Here **P** denotes environment polarization, χ_1, χ_2, χ_3.. stand for non-linear media susceptibilities. The intensity of non-linear processes is determined by the following members: $\chi_2 \mathbf{E_1}^2$, $\chi_3 \mathbf{E_1}^3$,... In the general case χ_2, χ_3 susceptibilities are defined by the kind of material, type and state (physical parameters) of the crystal lattice.At big concentration of initial optic phonons (high charge current density) non-linear unharmonic processes start playing their essential part. Presumably, processes of the 3-rd and the 4-th order begin.

$$h\omega_{1\,in} + h\omega_{2\,in} \rightarrow h\omega_3 \quad \text{and } \omega_1 < \omega_3 > \omega_2$$

$$h\omega_{1\,in} + h\omega_{2\,in} + h\omega_{3\,in} \rightarrow h\omega_4 \quad \text{and } \omega_1 < \omega_4 > \omega_2,\ \omega_4 > \omega_3$$

These expressions mean that two ($h\omega_{1\,in}$, $h\omega_{2\,in}$) or three primary phonons are combined and formed into one $h\omega_3$ or $h\omega_4$, the frequency and energy of the newly formed phonons being bigger $W_{op} = h\omega_{op}/4\pi^2$. In this way out of a big number of primary phohons with energies of 0.07 - 1.5 keV a small number of high energy phonons (up to tens and hundreds keV) is formed. The primary phonons energy spectrum is displaced in the direction of bigger values. As this takes place the Pd crystal lattice is "cold" $(300\text{-}400^0)$ K, Pd ions are located at the lattice points and perform oscillations, corresponding to this temperature. Deuterium ions are also spatially fixed between Pd ions. But Pd ions are in a state of optic polar oscillatory excitation with energy up to tens and hundreds keV (Fig. 11). An environment with non-equillibrium excitation of one of its energetic states (similar to isomers nuclei) is formed. It is known that the rate of nuclear reactions of spontaneous fission for nuclear isomers is bigger by 10^{23} - 10^{26} times [3].

4. At densities corresponding to those of solids and energies of several tens keV the intensity of nuclear reactions is high enough.

The following types of nuclear reactions of transmutation resulting in formation of stable nuclides are possible:

$A + mB \rightarrow [AB]^*$ 1) $[AB]^* \rightarrow F + Heat$

2) $[AB]^* \rightarrow C^* + D^* \rightarrow C + D + Heat$

Where **A** stands for Pd or other element nucleus; **B** represents deuterium or hydrogen; **[AB]*** is a short-lived intermediate compound nucleus; **m-1,2,3 .., C*, D*** denote nuclear isomers of nuclides with masses less than that of Pd; **C,D** are stable nuclides; **F** stands for a nuclide with a mass more than that of Pd. At first a composite compound-nucleus in excited state is formed. Then one of the two possible modes is realized: 1) the compound nucleus may lose its excitation and form a stable nucleus of a heavier than Pd element; 2) the compound nucleus may split into two nuclei fragments with masses less than that of Pd. In so doing the two nuclei should be in excited isomer state (experiments show that the nuclear reactions energy is not produced in the form of nuclear fragments kinetic energy).

The possible types of nuclear transmutation reactions (2), which may be considered in the course of analysis of experimental results, are the following:

$^{105}Pd \rightarrow [Pd]^* \rightarrow {}^{48}Ca + {}^{57}Fe + 15.976$ MeV;

$^{105}Pd + {}^{2}D \rightarrow [Pd;D]^* \rightarrow {}^{107}Ag + 13.124$ MeV;

$^{104}Pd + {}^{2}D \rightarrow [Pd;D]^* \rightarrow {}^{13}C + {}^{93}Nb + 7.824$ MeV

$^{108}Pd + 2{}^{2}D \rightarrow [Pd;2D]^* \rightarrow {}^{112}Cd + 27.332$ MeV

$^{104}Pd + 2{}^{2}D \rightarrow [Pd;2D]^* \rightarrow {}^{44}Ca + {}^{64}Ni + 45.44$ MeV

The nuclear reaction value being assumed as 10-15 MeV per an atom of nuclear product, the heat energy value registered per a cathode sample (1) shows good agreement with the quantity of discovered stable nuclides impurity yield (2).

The following types of nuclear reactions of transmutation accompanied by formation of radioactive nuclides are possible:

$A + mB + xe^- \rightarrow [AB]^{**}$ 3) $[AB]^{**} \rightarrow F^* + Heat$

4) $[AB]^{**} \rightarrow C^{**} + D^{**} \rightarrow C^* + D^* + Heat$

Where **A** is Pd or other element nucleus; **B** stands for deuterium or hydrogen; $\mathbf{e}^-$ denotes an electron; **[AB]**** represents an intermediate short-lived neutron excessive compound-nucleus; **m=1,2,3..., x=1,2,3..., C**** shows neutron excessive nuclear isomers of nuclides with masses less than that of Pd; **C*, D*** are neutron excessive nuclides; **F*** stands for a neutron excessive nuclide with a mass bigger than that of Pd.

5. The last stage of the process is conversion of nuclear reaction energy into heat. Presumably, relaxation of the compound nucleus or nuclear isomers excited state proceeds by multi-stage transitions, with the energy transfer to all the atoms of macro-monocrystal (up to 10^8) at each transition stage by multi-phonon processes.

Acoustic phonons (resilient sound-wave) interact with all the macro-monocrystal atoms in the course of one nuclear isomer transition stage converting this energy into energy of crystal lattice heat oscillations.

References

1. A.B.Karabut, "Excess Heat Registration in High Current Density Glow Discharge", Proceedings of the Sixth Conf. on Cold Fusion, Vol.2, October 13-18, 1996, Japan, p.463.

2. Table of Isotopes, 8th Edition, Editor: V.S.Shirley, 1996, by John Wiley & Sons, Inc.

3. Muhkin, Experimental Nuclear Physics, Moscow, Energoatomisdat, 1993.

Conference Proceedings Vol. 70
"ICCF8"
F. Scaramuzzi (Ed.)
SIF, Bologna, 2000

CORRECT MEASUREMENT of DD - REACTION YIELD and X – RAY in a HIGH – CURRENT DEUTERIUM GLOW DISCARGE OPERATING at 0.85 - 1.20 kV VOLTAGE APPLIED

A.B. Karabut[1], A. G. Lipson[2], A.S. Roussetsky[3].

[1] Scientific Industrial Association "Lutch", Podol'sk, Moscow region 142100 Russia
[2] Institute of Physical Chemistry of RAS, Moscow 117915 Russia
[3] Lebedev Physics Institute of RAS, Moscow 117924 Russia

Abstract

Charged particles (3.0 MeV protons) emission and a soft X–ray radiation that may accompany DD–reaction in high current deuterium glow discharge at nominal operating voltage applied U = 0.85 – 1.20 kV have been measured using CR–39 and thermoluminescent solid-state detectors. It has been established that in the deuterium glow discharge with Pd, Ti or Nb cathodes at nominal voltage U < 1.2 kV the anomalous (in terms of voltage applied) yields of DD–reaction (3.0 MeV protons), emission of long-range alpha-particles and X-ray having short-wave edge of 2.5 keV is observed. The data on DD – reaction yields and a soft X-ray can be naturally explained by the assumption that some effective accelerating voltage $<U_{eff}>$ = 2.5 kV is generated in the discharge, exceeding by more than 2 times the nominal voltage applied. The yields of DD–reaction in a glow discharge for Pd and Ti cathodes have been estimated, taking into account their loading ratios x = D/Me : $\lambda_{DD} = 3.4*10^{-17} s^{-1}$/DD – pair (x = D/Pd = 0.09) and $\lambda_{DD} = 1.1 * 10^{-18} s^{-1}$/DD – pair (x = D/Ti = 1.43), respectively.

1.Introduction

Earlier it was established [1,2] that in experiments with the deuterium glow discharge on Pd cathodes the effects of isotopic content change and nuclear emissions sometimes accomanied by Excess Heat generation are observed

Proceeding from the above, the aim of the present work is to achieve a correct measurement of DD-reaction yield and X-ray emissions (the so-called Lattice Induced Nuclear Processes "LINP") in the deuterium glow discharge with Pd and other (Ti, Nb, Ta) cathodes, operating within 850 - 1200 V applied voltage range. In order to prevent errors associated with the electromagnetic noise separation the detection of radiation was carried out by electronic free solid-state detectors: CR-39 plastic track detectors for charged particles and Al_2O_3-based thermo-luminescent dosimeters.

2. Experimental

The procedures of charged particles and X-ray detection have been carried out in-situ in vacuum chamber during the GD operation. The power supply used allowed to obtain a stable GD with deuterium pressure ranging P = 5.0 - 8.0 mm Hg. At a mean discharge current I equal to 50 mA its maximal value did not exceed 200 mA and the discharge voltage could be varied within the range of 850 - 1200 V. No high current (voltage) pulsation with resolution of 10 ns had been observed during the discharge operation.

The block–diagram of the glow discharge device (GDD) is presented in Fig.1. The distance between the massive Mo anode and the removable cathode (thickness h = 0.01 cm, effective area S = 0.64 cm^2) amounted to 5.0 mm. During the GD operation the glow was spread upon the whole of the cathode area, therefore the discharge operational regime used can be considered as "anomalous" [4]. In order to detect radiation resulting from the GD operation several holes were drilled out in the anode. Behind the said holes (at the back of the anode) corresponding solid-state detectors were placed. The employed background measurements

included data obtained with the help of similar electrodes used in hydrogen GD and also data on detectors exposure upon the outside wall of the GD.

To detect charged particles CR–39 purified plastic track detectors (Fukuvi Chemical Industry, Japan) have been used. The yield of D(d,p)T reaction from TiD_2 target exposed to bombardement with a 10 keV deuteron beam has been used for calibration experiment. As is shown in Fig. 2 a, the track spectrum obtained allows to distinguish each DD–reaction charged product: 3.0 MeV protons (track diameter ranging 5.0–5.5 μm), 1.0 MeV tritons (6.0–7.0 μm) and 0.8 MeV He-3 (7.5–10.0 μm). CR–39 detectors calibration by alpha–particles has been carried out by standard α-sources, their energies ranging 4.0–7.7 MeV, with a subsequent approximation of tracks diameters to higher energies.

In order to prevent the cathode (anode) material sputtering onto the CR-39 surface and also to avoid influence of deuterium plasma and its UV–radiation, the detectors were covered with 11–33 μm thick Al foil. In this case the protons track diameters have been estimated taking into account the energy losses in Al foil (~ 0.3 MeV/11 μm Al). At the same time the sreening of CR–39 detectors with 11 μm thick Al foil resulted in the total absorption of 1.0 MeV tritons and 0.8 MeV He-3 in the foil.

To estimate the mean energy of the soft Bremsstrahlung in the GD and to measure its intensity, thermo–luminescent detectors (TLD) based on Al_2O_3 crystals were used with a set of 15–300 μm thick Be–foils (2.78 – 55.5 mg/cm^2) placed between the anode and TLD. In each GD experiment a total of 7 TLD (5mm diameter and 1mm thick) were exposed simultaneously, each being placed at 70 mm distance from the anode. TLD calibration procedure has been carried out with Cu K_α - X–ray radiation. It was established that the absorbed dose of 10 mGy corresponds to photo–current integral of Ip=11.0 ± 1.0 μC at the TLD self – efficiency of $\varepsilon_0 \sim 0.3$.

3.Experimental Results and Discussion

Experiments on charged particles detection showed that per each cathode used (Pd,Ti, Nb) (with the exception of Ta) the statistical significant yield of 3.0 MeV protons (from D(d,p)T reaction) and high-energy alphas (Eα > 8.0 MeV) was registered. In the control (blank) experiments with Pd cathode in hydrogen the tracks number ranging of 5.0–5.3 μm corresponding to 2.7 MeV protons (taking into consideration energy losses into 11 μm thick Al foil) did not exceed the similar value obtained during CR–39 detector long-time exposure on the outside wall of the discharge chamber during the GD operation (Fig.3). Proceeding from this point, in further experiments with deuterium the control Pd cathode (blank) experimental data has been used as a background. The typical spectrum of charged particles (protons), passed through the 11 μm Al foil in the course of CR-39 exposure in the deuterium GD Pd-cathode experiment is presented in Fig.3. In case of Ti–cathode application the yield of 3.0 MeV protons at τ = 10 h exceeds similar value for Pd by about 2.5 times. It should be noted that the decrease in the discharge voltage (from 1190 to 850 V) does not lead to change in DD–reaction yield for the Ti–cathode. This is rather unexpected because within the indicated deuteron energy range the decrease by 1.4 times in the accelerating voltage would result in DD–reaction yield drop by 6 orders of magnitude or more. Hence, one arrives at a paradoxical conclusion: DD – reaction yield in the glow discharge of the said type is independent from the potential difference applied between the cathode and the anode.

At the same time, the Nb–cathode DD – protons yield is by about 2 times less than the Ti one and close to that of Pd–cathode at τ < 10 h. However, with Ta–cathode the emission of 3.0 MeV protons is, in fact, absent (Fig.3). It should be noted that the intensity of the cathode material sputtering sharply decreases in case of Pd, Ti, Nb, Ta.

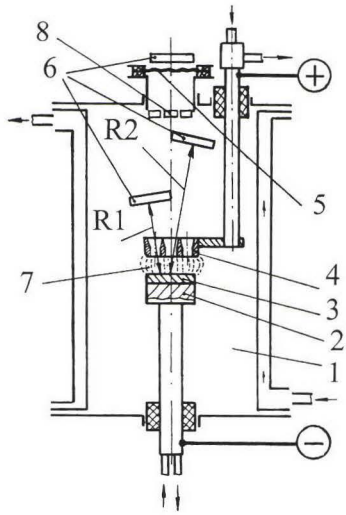

Fig.1 Experimental glow discharge device.
(1) vacuum chamber; (2) cathode holder;
(3) cathode sample; (4) anode;
(5) Be window; (6) CR –39 detectors;
(7) glow discharge area; (8) TLD

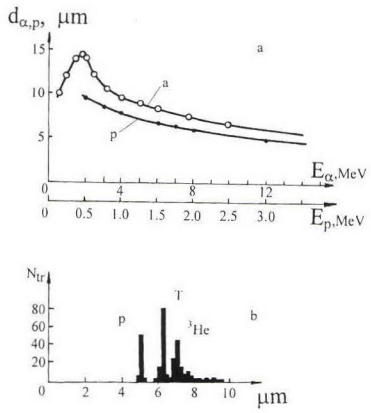

Fig. 2. a - Calibration spectrum of alpha and proton - particles: track diameter vs. Alpha and proton - particle energy. **b -** Calibration spectrum of the charged DD - reaction products vs. thei CR - 39 track diameter, obtained during 10 keV deuteron bombardment of TiD_2 target and their microphotographs.

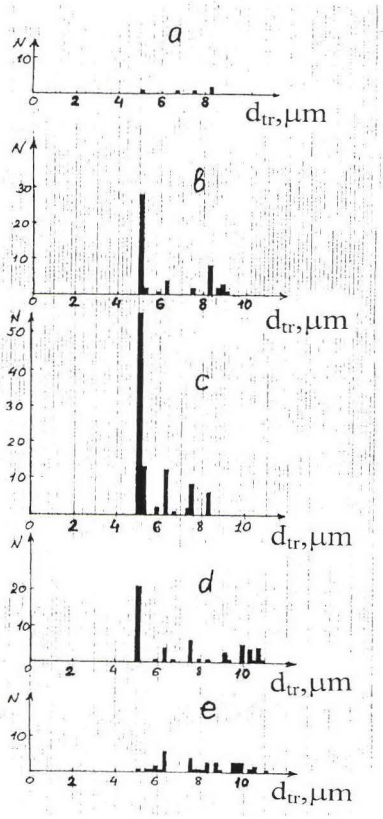

Fig.3. Typical charged particle spectrum of CR - 39 track detector covered with 11 μm Al - film. CR-39 area= 1.25cm^2. Distribution of charged particle track diameter obtained for CR – 39 track detectors covered with 11 μm Al - film exhibited upon the glow discharge operation: a-Ta – cathode, D2 , <U>= 1180 V, <I>= 57.4 mA, τ = 8 h; b-Nb – cathode, D2, <U>= 1150 V, <I>= 66.0 mA, τ = 10h; c-Ti – cathode, D2, <U>= 1190 V, <I>= 60.0 mA, τ = 10 h; d-Pd – cathode, D2, <U>= 1156 V, <I>=52.6 mA, τ = 10 h; e-Pd – cathode, H2, U>= 1160 V, <I>= 63.0 mA, τ = 5.5 h.

Experiments also showed that for Pd, Ti and (with less statistics) Nb – cathodes used, besides the 3.0 MeV proton tracks left on exposed CR–39 detectors covered with Al foil, characteristic alpha–particles tracks were observed with densities dependent upon the cathode material used and the discharge duration time τ. As seen from Fig.3 the maximum emissions intensity for long–range α-particles has been obtained for Ti–cathode cases at U = 850 V. Moreover, as it was already mentioned [6], in experiments with hydrogen long-range α–particles are detected with the same intensity as is the case with deuterium .

In order to compare the measured glow discharge DD – reaction cross - section to the standard one (Bosch & Halle parametrization [8]), the normalization procedure of D-D-protons yield obtained to the similar yield at Ed = 10 keV (in accelerator experiment [5]) for Pd and Ti has been carried out, with regard to their real temperatures in GD. Total data concerning DD-reaction yield for Pd and Ti (including x = D/Me, evaluated with (1) and by measurement of D –pressure change in discharge) is given in Fig.3. Fig.5, in its turn, represents the dependences of a relative D(d,p)T-reaction yield normalized to the yield at E_d = 10 keV obtained in [5].The continuous curve shows the standard DD-reaction cross-section drop proportional to deuterons energy decrease without any enhancement. For Pd case the significant yield deviation from the standard curve (enhancement) is satisfactorily described by screening potential Us = 250 eV. In the Ti case this deviation is rather small U_s ~ 20eV and close to that for deuterium gas target (U_s = 25 ± 5 eV) [9]. The yields values, obtained in GD experiment $Y(x) = \Delta n_p / I$ (where Δn_p is a proton yield, I stands for a discharge current), normalized to the corresponding values Y(10 keV) and calculated by (1) are plotted by circles (points) in Fig.5 with regard to measurement errors and in accordance to nominal discharge voltage.

If the assumed GD higher effective accelerating voltages are true, then during the deceleration of the electron component upon the anode the X- ray (continuous spectrum) Bremsstrahlung should be observed with approximately the same $<U_{eff}>$ value as for the DD-reaction (Fig.5).

Fig.6 represents the dependence of falling and transmitted radiation ratio detected by TLD versus Be-absorber thickness. Thus, we can certainly say that radiation detected by TLD with a set of Be - foils is a soft X - ray Bremsstrahlung. Indeed, the curve in Fig.6 could be satisfactorily defined by the X-ray absorption Law [10]: $I_m/I_0 = \exp(-\mu_m * h)$, where I_m stands for the transmitted radiation, I_0 represents the falling radiation, h is the absorber thickness (g/cm^2), provided the mass absorption coefficient is $\mu_m = 170\ cm^2/g$.

Intensity maximum energy position is E_x = 1.68 keV. Then the meaning of the X–ray tube accelerating voltage (the gap between Pd cathode and Mo anode) corresponding to short - wave edge of Bremsstrahlung with the maximum intensity E_x = 1.68 keV, should be 1.5 times higher and should amount to U = 2.52 kV. Similarly, the accelerating voltage value was determined in 10 independent experiments on X-ray absorption in Be-foils using a Pd - cathode. The obtained mean values for X-ray parameters amounted to $<E_x>$ = 1.65 ± 0.13 keV and $<U_{eff}>$ = 2.50 ± 0.20 kV. Comparison of mean <Ueff> value obtained from X-ray absorption data with that, calculated on the basis of DD - reaction yield (Fig.3), shows they are in good agreement.

The following results on intensity estimation of the X-ray emissions generated in the GD with Pd cathode were obtained. In accordance with the TLD calibration data, the mean detected X-ray dose power P value was $P = 6.3*10^{-5}$ erg/s*cm^3. Then, the number of X-ray quanta is equal to $N_x = 8*10^8\ s^{-1}$ in 4 π solid angle. The said N_x value corresponds to the electron beam current density $J_e = 1\ \mu A/cm^2$. Thus, the current density of fast electrons with 2.5 keV mean energy, causing the a soft X–ray in the glow discharge with nominal voltage

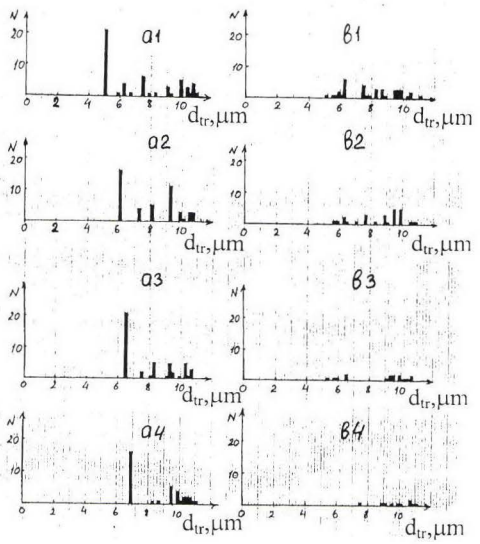

Fig.4. Distribution of charged particle spectrum (CR-39 track detector coating Al and polyethylene PE films diferent thichness) after exhibition in deuterium and H_2 glow discharge with Pd-cathode. a1 – Al 11μm, D2, t_{exp}10h; b1 – Al 11μm, H2, t_{exp}5.5h; a2 – Al 11μm + PE 60μm, D2, t_{exp}10h; b2 – Al 11μm+PE 60μm, H2, t_{exp}5.5h; a3 – Al 22μm + PE 60μm, D2, t_{exp}10h; b3 – Al 22μm+ PE 60μm, H2, t_{exp}5.5h; a4 – Al 33μm + PE 60μm, D2, t_{exp}10h; b4 – Al 33μm+PE 60μm, H2, t_{exp}5.5h;

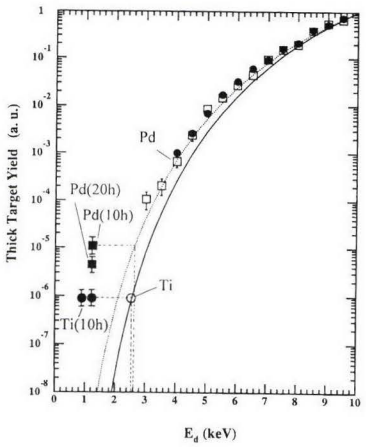

Fig.5. Thick target yield of D(d,p)T reaction normalized to E_d = 10 keV : bare yield (solid curve); the yield for Pd target at T = 190 K [5], (solid squares). The dashed curve is a parametriztion of the experimental Pd yield with screening potential Us = 250 eV. The experimental yields obtained in glow dischrge and normalized to E_d = 10 keV for Pd and Ti - cathodes are presented in a point form in accordance to nominal discharge voltage and operating time used. $<U_d>$ - effective accelerating voltage; Pd (10h): $<U_d>$= 2.6±0.1 kV, x=D/Pd=0.9; Ti (10h): $<U_d>$= 2.5±0.1 kV, x=D/Ti=1.43; Pd (20h): $<U_d>$=2.5±0.1 kV.

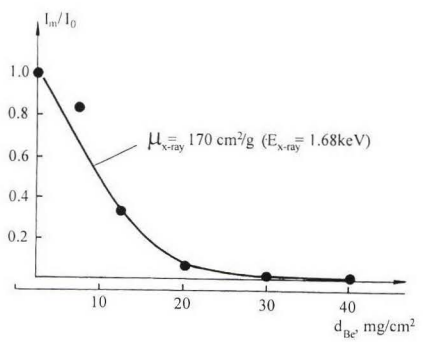

Fig.6. Ratio between a falling and transmitted through Be foil obtained radiation dependence versus Be – absorber thickness ($I_m/I_0 = \exp(-\mu_m * h)$, where I_m - transmitted, I_0 - falling radiation, h – absorber thickness (g/cm²) in the condition that mass absorption coefficient is μ_m = 170 cm²/g).

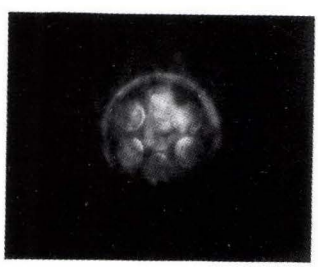

Fig.7. X-ray image of the anode - cathode area with obscure chamber (d = 0.1 mm) using 15 micron hick Be filter.

of 1.2 kV between the cathode and the anode, amounts to only $\sim 10^{-5}$ part of the total discharge current. It should also be noted that the Bremsstrahlung with similar parameters has been observed during the GD operation with Pd - cathode in hydrogen.

4.Conclusions

Therefore, it was found that in high current deuterium glow discharge at nominal voltage U < 1.2 kV the anomalous (in terms of voltage applied) yields of DD-reaction, emission of long-range alpha-particles and X-ray with a short- wave edge Ex = 2.5 keV is observed.

Yields of DD - protons obtained and estimation of deuterium concentration in Pd and Ti cathodes allow to evaluatethe absolute DD – reaction yields in glow discharge per DD - pair:

$$\lambda_{DD} = 2\Delta n_p / N_D (R_D/h),$$

where Δn_p is the difference between the experimental proton yield in the glow discharge and the background, N_D stands for the mean deuterium concentration in the cathode during the discharge operation , R_D represents a stopping range for 2.5 keV deuterons in the cathode used, h is the cathode thickness.

a) Pd - cathode: $\Delta n_p = 0.078$ p/s (at t = 10h) , $R_D = 1.5*10^{-6}$ cm [12]; for x = D/Pd = 0.09, $N_D = 3.9*10^{19}$ at.D/Pd - cathode, h = 0.01 cm and $\lambda_{DD} = 3.4*10^{-17} s^{-1}$/DD - pair.

b) Ti - cathode: $\Delta n_p = 0.18$ p/s (t = 10h), $R_D = 5*10^{-6}$ cm [12]; for x = D/Ti = 1.43, $N_D = 6.2*10^{20}$ at.D/Ti - cathode, h= 0.01cm and $\lambda_{DD} = 1.1 * 10^{-18} s^{-1}$/DD - pair.

As seen from the above estimations the λ_{DD} value for Pd - cathode is by 30 times higher than for Ti case, regardless of bigger protons yield for Ti at the same discharge voltage (Fig.3). This estimation is made with regard to the relative DD - reaction yields (normalized to 10 keV yield) obtained in our experimentation and in the accelerator experiments [5].

It should also be noted that λ_{DD} values, defined according to (3) are by 5 - 6 orders of magnitude above the "Jones level" [3], that is observed usually for nuclear processes induced by crystalline lattice at room temperatures. However, the yields obtained still remain at least by 6 orders lower than the values claimed necessary for production of DD - reaction excess heat power. Therefore, it is possible to conclude that the effect of excess heat power production in deuterium glow discharge is not related to DD – reaction enchancement upon the cathode surface.

References

A.B. Karabut, Ya. A. Kucherov, I.B. Savvatimova: Fusion Tech., 20(4), 924 (1991).

2. A.B. Karabut, Ya. A. Kucherov, I.B. Savvatimova: Phys. Lett. A 170, 265 (1992).

3. A. G. Lipson, B.F. Lykhov, A.S. Roussetsky et al.: Fusion Tech., (2000) in press.

4. E.P. Velikhov, A.S. Kovalev, A.T. Rakhimov: "Physical Phenomena in a Gas Discharge Plasma" (in Russian), Nauka, Moscow, 1987.

5. H. Yuki, J. Kasagi, A.G. Lipson et al.: JETP Lett, 68(11),823 (1998).

6. R. Taniguchi: Trans. Fusion Tech., 26 (4T), 186 (1994).

7. A.G. Lipson, B.F. Lyakhov, A.S. Roussetsky, N. Asami: Abstracts of ICCF-8, May 21-26, Lerici, Italy.

8. H.S. Bosch and G.M. Halle: Nucl. Fusion, 32, 611 (1994).

9. U. Griefe, F. Gorris, M. Junker et al.: Z. Phys. A 351, 107 (1995).

10. M. A. Blokhin: "Physics of X - rays", 2-nd ed. (in Russian), Gostechtheorizdat, Moscow, 1957.

11. F.G. Baksht and V.G. Yuriev: Sov. Tech. Phys.49(5), 905 (1979).12. H.H. Andreson, J.F. Ziegler:"Hydrogen Stopping Powers and Ranges in All Elements", Pergamon Press, New York, 1977.

Conference Proceedings Vol. 70
"ICCF8"
F. Scaramuzzi (Ed.)
SIF, Bologna, 2000

Anomalous Heat Evolution of Deuteron Implanted Al upon Electron Bombardment Ⅳ

-Trial to Observe the Nuclear Reaction-

Kohji Kamada,Yoshio Katano(*),Nariaki Ookubo(**)and IsaoYoshizawa(**)

The Wakasa Wan Energy Research Center,Nagatani, Turuga, Fukui, 914-0192 JAPAN
(*) Japan Atomic Energy Research Institute, Tokai,Ibaraki, 319-1195 JAPAN
(**) Ibaraki University, Mito, Ibaraki, 310-0056 JAPAN

1.Introduction

In the previous papers (1,2,3) one of the authors (K.K) has reported the anomalous heat evolution in the surface layer of 12.5 keV deuteron implanted Al metal on 175 keV electron bombardment in transmission electron microscope. The hydrogen implantation, on the other hand, did not show the melting under the same experimental conditions. The heat evolution was manifested by a melting and eventual re-crystallization of the surface layer, which was observed in- situ in the electron microscope during the observation. Though various melting mechanisms of the surface were proposed so far, all of them could not explain it adequately judging from the experimental results described in (1) and (2). However, the one mechanism, which we could not properly estimate, was the nuclear reaction. The passage of many energetic particles, due to the d-d reaction, through the surface layer in a limited short time can possibly explain the melting as described in (1) and (2). However, for this mechanism to be effective the d-d nuclear reaction must be assumed taking place in a very low energy region. The main aim of the present paper is to try to observe the neutron from the reaction using recently developed n:γ discrimination system using the pattern recognition of radiation pulses (4). At the same time, the confirmation of the previous observations was also aimed, observing the melting on the electron bombardment of the deuterium implanted Al as before, using different facilities and by different experimental staffs. The previous results were certainly confirmed, as shown in Fig.1.

The result of the radiation measurements was rather unexpected. That is, in spite of the melting, neutron emission was not observed. Therefore, the origin of the heat evolution should be looked for in other kind of mechanisms. And, more unexpectedly, the X-ray emission of energy less than roughly 400keV was observed when the specimens filled with

bubble structure was bombarded with the electron beam. The bubble structure, however, did not show the melting as reported in the previous papers (1) and (2).

However in this paper, we leave the details of the experimental procedures and results to a recent paper (3). Instead, we summarize the so far proposed mechanisms and discuss why they can not explain the melting. Further we discuss that the melting is due to an excess heat generation, though its mechanism is not fully understood at present.

2. Experimental results.

The experimental procedures are the same with those described previously and we leave the details to those described in (1) and (2). The differences from these papers are that we used 15 keV, instead of 12.5 keV, d^+ ions for the implantation and 200 keV, instead of 175 keV, electron beam for the electron microscopic observation as described in (3).

Typical examples of the bubble structure and the tunnel structure are shown in Fig.1. The latter shows the transformation from single crystalline to polycrystalline material after the melting.

The results of the radiation measurements are shown in Figs.2 and 3. These are rise time spectra observed in-situ during the electron microscopic observations. We leave the details of concomitantly measured pulse height measurements, from which we estimated the energy of radiation, to (3).

Experimentally, the radiation was measured by liquid scintillator, NE-213, with a n-γ discrimination circuit, developed recently in our laboratory (4). The amount of the radiation emitted from the deuterium coagulation upon the electron bombardment was determined by subtracting the background spectrum from the spectrum taken on the deuterium implanted Al specimens. The background was measured separately using the non-implanted Al specimens on electron bombardment. Each spectrum was the average of 3 to 5 independent measurements. The error estimation was performed taking into account of the error propagation due to the averaging and the subtraction of background (3). Thereby, we could conclude that the credible amount of radiation well exceeding the detection limit being measured in the case of bubble structure, and vice versa, credibly no emission in the case of the tunnel structure.

3.Conceivable Mechanism of the Melting

In the present experimental situations, we can conceive several mechanisms for the melting of the surface area of Al. Followings are those mechanisms, and the reasons why they are not acceptable as the mechanisms of the present melting.

1) "Since the depth where the deuteron is implanted is less than that of proton with the same energy, the heat capacity of the surface region is smaller for the deuteron case than the proton. So the deuteron implanted case is easier for the melting to take place than proton implanted case."

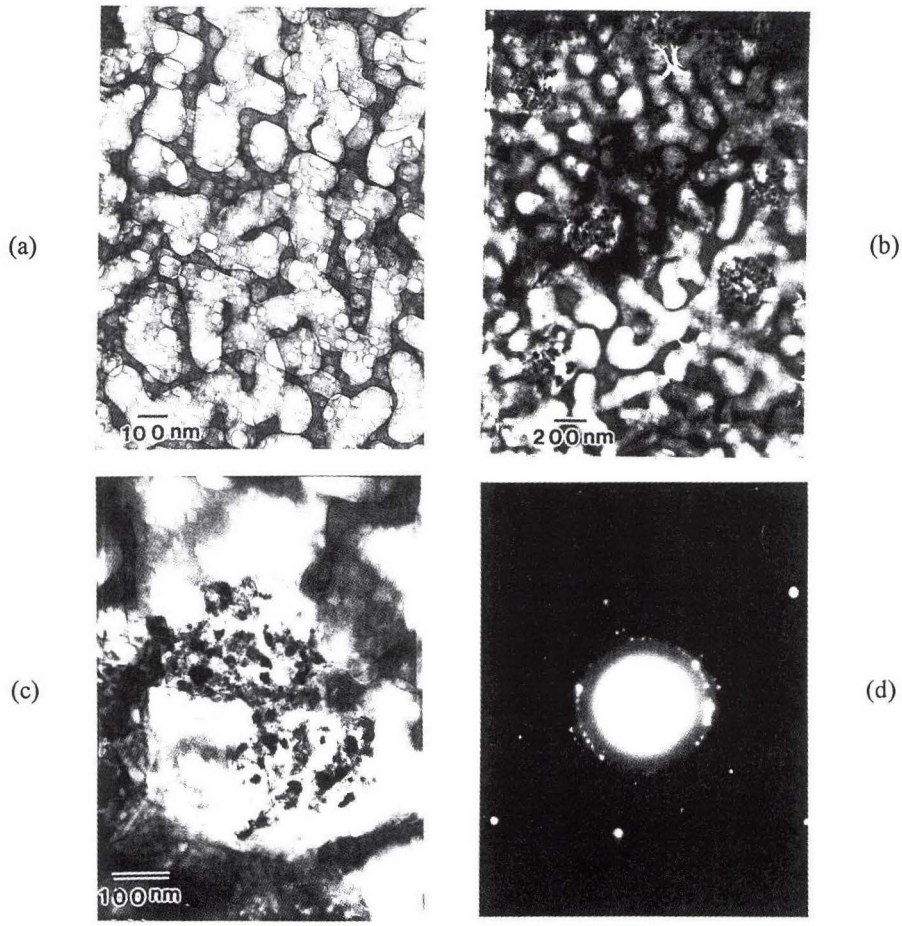

Fig. 1. Transmission electron microgram of the tunnel structure observed in the group of specimens from which any kind of radiation emission was not observed.

Polycrystalline structures, seen as speckled areas, are observable, which appeared during the observation.

The scales of the micrograms are: (a) 500 nm, (b) 200 nm, (c) 100 nm, and (d) is a typical diffraction pattern including one speckled area.

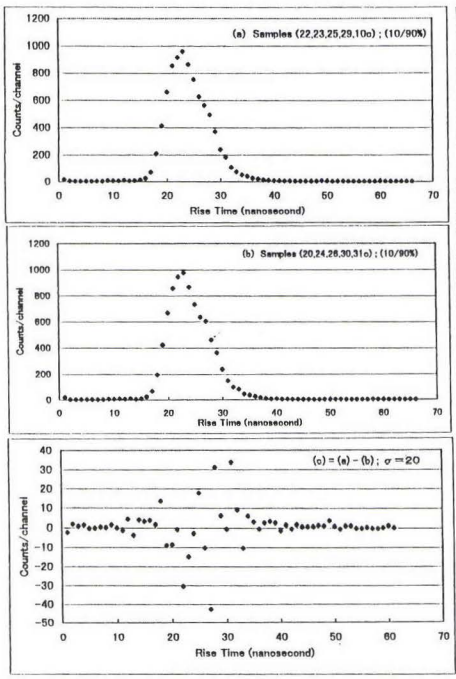

Fig.2

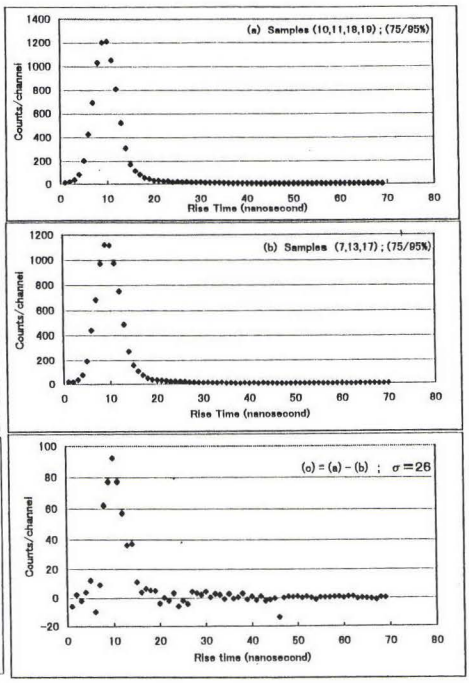

Fig.3

Fig. 2, Average rise time distributions of five deuteron implanted specimens (a), five background measurements with electron beam (b), and the difference between them (c). Rise times were measured between 10% and 90% of the pulse height. These specimens contain the tunnel structures, and, at the least, 34 speckled areas were observed in all specimens.

Fig. 3, Average rise time distributions of the four deuteron implanted specimens (a), three background measurements with electron beam (b), and the difference between them (c). Rise times were measured between 75 and 95% of the pulse height. These specimens contain only the bubble structures.

Experimentally, in Al, both proton and deuteron precipitate at the depth of the maximum energy loss, namely at the depth where lattice defects formation actually takes place. This was already confirmed using Elastic Recoil Detection (ERD) analysis by one of the author (K.K), and confirmed that both proton and deuteron precipitate at almost the same depth within experimental error. Therefor, the above statement can not be the mechanism of the surface melting.

2) "Thermal insulation of the surface layer due to the hydrogen or deuterium precipitation."

This is common for both proton and deuteron implantation, so can not make the difference. Moreover, thermal conductivity of the hydrogen and deuterium precipitation are lower for lower internal pressure or, as a natural consequence, for lower density. However, experimentally, the melting can not be observed when the implanted specimens are left at room temperature for several hours, during which the implanted deuterium diffuse out of the specimens, consequently lowering the internal pressure. Therefor, the insulation of the surface region does not make easier for the melting. Conversely this fact means that the melting strongly depends on the deuterium density in the tunnel structure.

3) "Stored energy due to the deuteron injection is released by the electron bombardment."

This is also contradictory to the observations. In our experiment, however, we need rather narrow range of optimum implantation of deuteron, namely around $4x10^{17} d^+ / cm^2$, to observe the melting. Below and above this range the melting does not take place. Usually the stored energy is proportional to displacement per atom (dpa) due to the injected charged particles. Therefor, if the stored energy is responsible to the melting, higher implantation must be easier for the melting in contradictory to the observations. In the above statement, temperature rise due to the beam heating must be responsible for the release of the stored energy. However, empirically the temperature rise during the implantation is higher than that of during the electron microscopic observations. This is presumably due to the small stopping power of electron in contrast to that of deuteron. So the release of the stored energy due to the electron bombardment can not be acceptable as the mechanism of the melting.

4) "Decrease of melting point due to the thickness of Al."

The decrease of the melting point is usually discussed theoretically in metal powder of diameters less than 10 nm、and observed experimentally in Pb. In Al similar behavior with Pb is expected theoretically. However, the present specimens are of wedge type, so the decrease of the melting point is hard to imagine. And, moreover, at the very edge of the wedge type specimen, where may be very thin around 10 nm, we can not observe any

bubbles or tunnel structures. It means that deuterium is not contained in this region. Of course the melting was never observed there.

5) "Transformation of Al from single crystalline to polycrystalline form by the plastic deformation due to local heating or by deuterium gas pressure on the beam heating."

In the present experiment, we have never observed the plastic deformation around the melted regions. In Al, around room temperature, such kind of solid-state transformations has never been observed. Plastic deformation never transform single crystal into polycrystalline form.

4. Excess energy consideration

Since the nuclear reaction is not taking place in the deuteron implanted Al, the only energy given to the Al specimen under observation with electron microscope is the energy loss of the electron beam getting through the Al specimen. Main energy loss of high energy electrons through material is that of due to plasmon excitation in the materials. Assigning both hydrogen and deuterium aggregates as insulators, the plasma excitation can be neglected in both of them. Even if we assumed the presence of free electrons in them, we can not find any reason that the plasma frequency is different in the both. Another important energy loss is phonon excitation or ionic plasma excitation. However, the energy of the ionic plasma should be lower in the deuterium aggregate than in the hydrogen, since the plasma frequency ω is proportional to the inverse root of the atomic mass, i.e. $M^{-1/2}$. And, further, both electron excitation and ionization give the same energy loss for both hydrogen and deuterium aggregates.

Altogether, the energy loss of the electron beam through the deuterium implanted Al is smaller, though a little amount, than that of through the hydrogen implanted Al.

It means that the melting observed in the deuteron implanred specimens is due to some excess energy, which is not yet fully understood in this paper.

Literatures

(1) K.Kamada,H.Kinoshita nd T.Takahashi; Jpn.J.Appl.Phys., 35, 738 (1996).

(2) K.Kamada, H.Kinoshita, H.Takahashi and H.Kakihana; J.Atom.Energ.Soc.Japan38, 143 (1996); (in japanese).

(3) K.Kamada, Y.Katano, Y.Enokido, N.Ookubo and I.Yoshizawa; to be published in "Radiation Effects and Defects"

(4) K.Kamada, U.Enokido and S.Ogawa; Nucl. Inst. Meth. In Phys. Res. A426, 633 (1999).

CHAPTER 7.

THEORIES

Conference Proceedings Vol. 70
"ICCF8"
F. Scaramuzzi (Ed.)
SIF, Bologna, 2000

A SIMPLE MODEL OF THE "CÖHN-AHARONOV" EFFECT IN A PECULIAR ELECTROLYTIC CONFIGURATION

M. Cola(**), E. Del Giudice(*), A. De Ninno(**), G. Preparata(°)

(**)ENEA- Via Enrico Fermi 45, 00044 Frascati, Italy
(*) INFN- Via Celoria 16, 20133 Milano Italy
(°) deceased the 24th April 2000

INTRODUCTION

All the investigations on cold fusion [1] in the last decade have pointed to the dependence of this fascinating and elusive phenomenon upon the concentration of deuterium into the palladium matrix; namely the phenomenon occurs when the stoichiometric ratio *D/Pd* exceeds one. However, reaching this critical threshold is not at all an easy task and just this circumstance could be at the root of the difficulties met by many groups when trying to reproduce the phenomenon. Understanding the dynamics of loading has required a detailed consideration of the properties of the *D-Pd* system, which remains a partially explored system.

So far it has been well understood [2] that hydrogen (and its isotopes) can be present in the Pd lattice in two phases.

i) The α phase where hydrogen atoms are interspersed in the metal matrix as the components of a gas. At room temperature the α phase exists for $x \leq 0.02$.

ii) the β phase where hydrogen atoms are confined in small regions in the lattice volume, around the so called octahedral sites (see Fig.1). At room temperature the β phase exists for $x \leq 0.7$.

It has been discovered [3] that when $x \approx 0.7$ at room temperature hydrogens migrate to the tetrahedral sites of the lattice. Is this the evidence of a transition to a new phase? During the last years, Mengoli and his group in Padua [4] have shown that the diffusion coefficient D of the hydrogen into Pd exhibits a discontinuity at $x \approx 0.7$. On the other hand Dandapani and Fleischmann [5] have found a long time ago that at high loading, when $x > 0.7$, hydrogen enters a new configuration, characterised by shift from the localized state of the β-phase to a state where the atoms perform wide oscillations into shallow potential wells.

All these features point to a new phase of the *H(D)-Pd* system, which has been named γ phase.

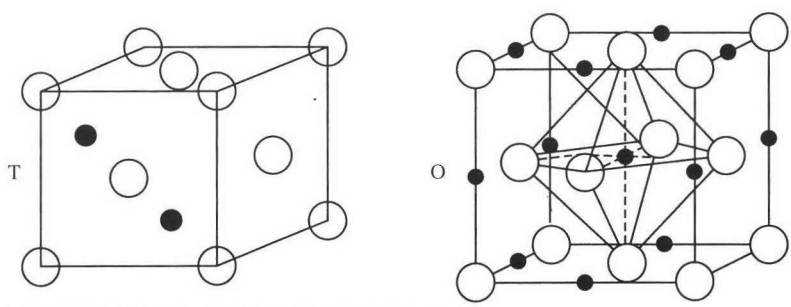

Fig.1 - Pd-H (D) lattice. Octahedral and tetrahedral sites.

A QED DESCRIPTION OF THE H-PD SYSTEM

It is well known [6] that hydrogen dissolves in the Pd-lattice in ionic form. This feature cannot be accounted for in the frame of conventional solid state physics, since it demands the existence of potential wells deeper than *30 eV* at the sites where hydrogens settle. This feature has been explained in the frame of quantum electrodynamics (QED) [7,8]; let us summarise the main points:

1 the *d*-electrons of *Pd* are able to perform coherent plasma oscillations, so that stationary electron clouds appear at selected points in the lattice. The size of the coherence domains of the electron plasma is about *400Å*;

2 these clouds produce potential wells about *40 eV* deep;

3 these wells are able to ionise *H(D)* molecules, whose electrons mix with the lattice electrons, whereas the nuclei form a plasma.

The problem of the localization of *H(D)* nuclei in the *Pd* lattice has been analysed in the QED framework [9] and the profile of the potential V as a function of the distance from the octahedral sites (fig.2) and the tetrahedral sites (fig.3) has been derived. As a consequence it has been possible to draw the curves of the chemical potential μ for D as a function of the stoichiometric ratio x (Fig. 4) in the two cases where hydrogens settle in the octahedral sites (β phase) and in the tetrahedral sites (γ phase). In order to derive the chemical potentials we choose the values of the parameters so to ensure that the two curves cross each other at the reasonable value of $x = 0.7$.

The feature 3) is at the root of the onset of coherence in the *H(D)* plasma oscillations in the γ-phase [7,8,9]. On consequence the *H(D)*'s form a quantum coherent state (described by a unique wave function) in the *Pd* lattice; the size of the coherence domains whose size is estimated [6] as a few microns. Coherence of *H(D)* in the γ–phase is just the basis of the "Cöhn-Aharonov effect".

In the 1950's D. Böhm and Y. Aharonov [10] showed that in a physical system described by a unique wave function (not, as usual, by a mixture of individual wave functions, one for each component) externally applied electromagnetic potentials enter into the wave-function phase where they add to the chemical potential [10]. This

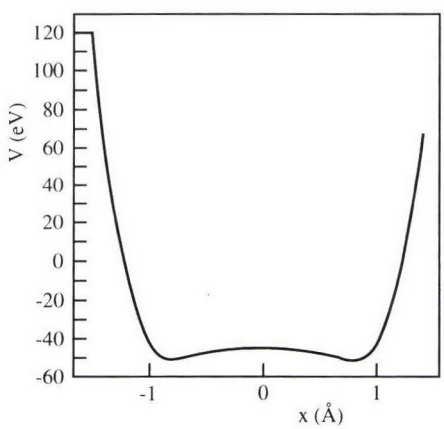

Fig. 2 - Potential well in octahedral sites

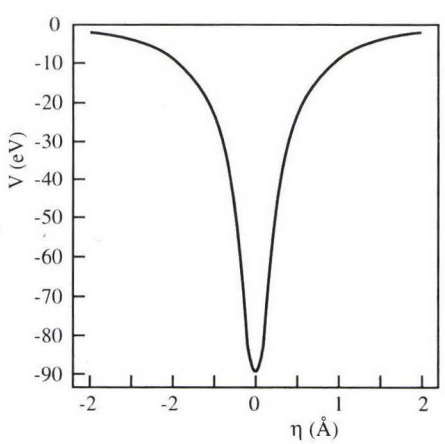

Fig. 3 - Potential well in tetrahedral sites

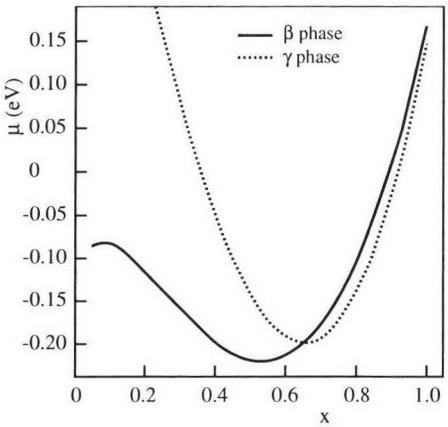

Fig. 4 - Chemical potential μ for D in PD. Continuous curve is μ for β phase; dashed curve is for γ phase.

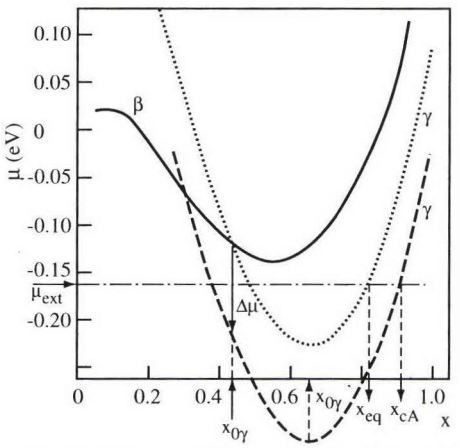

Fig. 5 - Influence of the negative electric potential V on the chemical potential μ

effect, which has also received an experimental verification [11] has been applied to the ensemble of *H(D)*'s in *Pd* by Preparata in 1993; an externally applied potential V would thus shift the chemical potential μ in Figs. 4 and 5 by an amount

(1) $$\Delta\mu = Z^{*}eV$$

where $Z^{*}e$ is the effective (screened) electric charge of the hydrogen nuclei in the γ phase. Since Cöhn has been the discoverer of the ionic form of *H(D)* present in the *Pd* lattice, this effect has been christened jokingly by Preparata as "Cöhn-Aharonov effect".(*) In Fig. 5 we show how the intersection of chemical potentials of the β and γ phase is changed by eq. (1) when we apply a negative electric potential. It is apparent that the system reaches its equilibrium at a value $x_{ca} = x_{eq} + \delta x$, where δx is proportional to the applied potential. Therefore if we apply a negative potential when the system reaches $x = x_{\beta\gamma-\text{trans}} \equiv x_0$, a flow of hydrogens would enter the *Pd* lattice, proportional to $\Delta\mu$ of eq. (1). This flow current j_{ca} adds up to the electrolytic current.

Introducing the diffusion equation

(2) $$j_{ca} = -M\left(\frac{n}{V}\right) grad\mu$$

it is possible to derive the equation

(3) $$j_{ca} = j_{el}\frac{\mu(x_0) - \mu(x)}{\mu(x_{ca}) - \mu(x_0)}.$$

In eq. (2) M is the mass of the Hydrogen, n/V is its density. The total flow

---

(*) Following the death of our friend Giuliano Preparata, we propose that, from now on, the C.A. effect be rechristened "the Preparata effect".

(4) $$j = j_{el} + j_{ca} = j_{el} \frac{\mu(x_{ca}) - \mu(x)}{\mu(x_{ca}) - \mu(x_0)}$$

vanishes when $x = x_{ca}$.

We note that hydrogen is not attracted into the *Pd* lattice by the longitudinal electric field generated by a negative applied voltage (electromigration), but by the transverse effect produced by the depression of the chemical potential inside the lattice. The verification of this enhanced loading should be evidence for the existence of coherence in the ensemble of hydrogens. Of course, the applied voltage, apart from the above quantum effect, produces also a current across the cathode, according to the Ohm's law, which will disrupt coherence through the Joule heating effect. Therefore in order to gain a net enhancement of the loading in an electrolytic cell, we need a cathode having a very large internal resistance. Massive cathodes have actually quite a low resistance, so that we should use one dimensional cathodes, having a very small cross section and a large length.

EXPERIMENTAL CHECKS

We present in this paragraph an experimental verification of this quantum effect. We compare the loadings of a thin *Pd* plate and of a strip of *Pd* deposited on an inert surface under identical electrolytic regime. The experimental layout is described in a paper [12] presented at this Conference. The loading is estimated by measuring the ratio of the electrical resistances R/R_0 (where R_0 is the resistance of the empty palladium matrix) which is connected to the loading through the well known Baranowskii curve (R/R_0 vs x), valid for an homogeneously loaded sample. The presence in our case of the Cöhn - Aharonov effect should in principle modify this curve as we show below. In Figs. 6 and 7 we plot R/R_0 as a function of time, for the loading of the plate and of the bustrophedic configuration respectively. On the same figures the current intensity too is represented. It is possible to see that when the current is switched off $R(t)/R_0$ exhibits opposite behaviours in the two cases. In the thin plate $R(t)/R_0$ decreases so that we can infer that the plate is still in the β-phase since the system is described by a point on the left-hand side

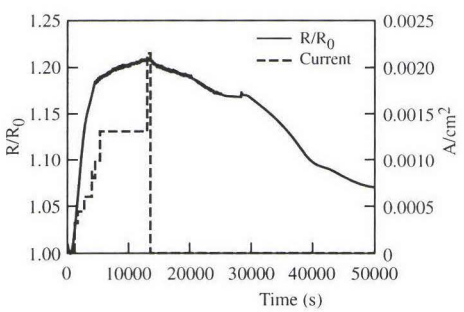

Fig. 6 - Hydrogen loading of a Pd plate sputtered on Vycor glass.

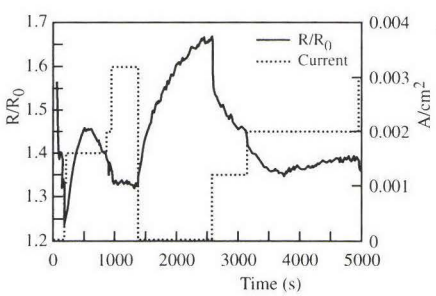

Fig. 7 - Deuterium electrolytic loading of a Pd "bustrophedic" film sputtered on Vycor glass. The resistance of this specimen was about 2000 Ohm.

of the Baranowski curve and $x < x_0$. On the other hand in the bustrophedic case $R(t)/R_0$ increases when removing the power supply and this is the proof that the physical system is described by a point on the right hand side of the Baranowski curve.

We can conclude that the C.A. effect has been qualitatively verified.

It is interesting to see that both in the thin plate and in the bustrophedic configuration the system does not reach the Baranowski peak value of $(R(t)/R_0)$=1.8 for hydrogen, $(R(t)/R_0)$=2 for deuterium. A thorough discussion of the origin of this phenomenon will be given elsewhere. Here we limit ourselves to an intuitive argument. The peak value of $R(t)/R_0$ occurs at the value of x where the chemical potential curves of the β and γ phases intersect. When the depth of the *Pd* sheet is smaller than the size of the coherence domain of the *Pd* electrons, coherence of electrons will be hampered; since the depth of the potential wells at the sites depends just on the coherence, we will obtain shallower wells. In ref. [9] it has been shown that in the β phase the electron oscillations are spherical, whereas in the γ phase are linear. Thus thin sheets produce shallower wells in the β phase, whereas the wells in the γ phase are unchanged. As a consequence the chemical potential of the β phase is increased, whereas the chemical potential of the γ phase is left unchanged (see Fig. 8). The intersection between the curves is thus shifted to a smaller value of x, which corresponds, according to the Baranowski curve, to a smaller value of R/R_0. Defects in a large crystal act just as limiting surfaces, so that the distance between such defects is a decisive factor for the value of R/R_0.

The above prediction has found an experimental support: in reference [13] the peak value of R/R_0 has been measured as a function of the depth of very thin *Pd* specimens.

It is interesting that for depths smaller than *500 Å* the peak value decreases. As a matter of fact in our plates and strips linear defects normal to the external surface have been detected and their average mutual distance is about *180 Å*, less than one half of the size in a perfect crystal.

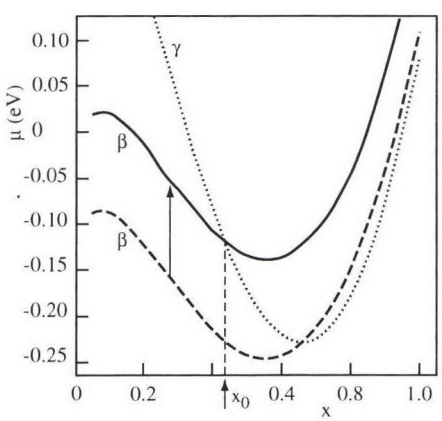

Fig. 8 – Effect of the wells shallower in β phase due to the srinking of one dimension of the coherence domain

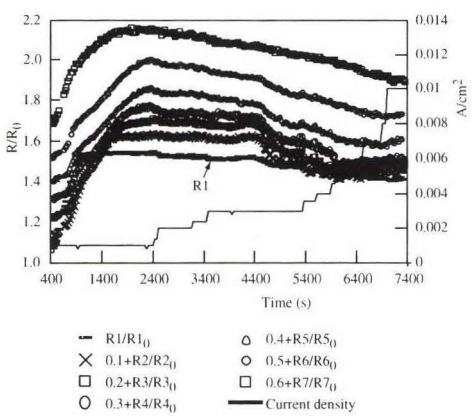

Fig. 9 - Hydrogen loading of a bustrophedic configuration. See details in ref. [12]

For a quantitative analysis of this effect we have analysed the time variation of R/R_0 during an electrolytic experiment (see Fig.9) in a cell with a one-dimensional cathode (a bustrophedic deposition). The cell potential Vac has been applied between the anode and one end of the cathode whereas the potential of the other end has been left free to float. In this way a potential

$$V(z) = -\frac{V_{ac}}{\cosh(\xi L)}\cosh[\xi(L-z)] \tag{5}$$

appears at the cathode, where z is its curvilinear coordinate, L is its total length and $\xi^2 = \frac{\rho_c}{\rho_{el}}\frac{1}{\delta d}F$. F is a factor which accounts for the cell geometry, δ and d are the cathode thickness and width and ρ_c and ρ_{el} are the electrical resistivities of cathode and electrolyte respectively. Equation (5) is the solution of the electrostatic equation for the cell. This potential acts as a source of the CA effect; no additional voltage is applied to the cathode which is divided into seven sectors in order to follow the loading along the total lenght.

In Fig. 9 we show the experimental graph of R(t)/Ro for each sector. We can analyse this graph as follow: initially the system is in α–β phase so that we have the equation

$$\dot{x}(z) = \frac{1}{\delta n_{Pd}} j_{el}(z) = k(z)\,. \tag{6}$$

When the loading reaches the value x_0 in equation (6) j_{el} is replaced by the value in equation (4) so that

$$\dot{x}(z) = k(z)\frac{\mu_\gamma(x_{ca}) - \mu_\gamma(x)}{\mu_\gamma(x_{ca}) - \mu_\gamma(x_0)}\,. \tag{7}$$

We approximate the chemical potential $\mu_\gamma(z)$ by the quadratic expansion

$$\mu_\gamma(x) = \mu_\gamma(x_0) + a(x - x_{0\gamma})^2 \tag{8}$$

(see Fig. 8) so that equation (7) becomes

$$\dot{x}(z) = k(z)\frac{(x_{ca} - x_{0\gamma})^2 - (x - x_{0\gamma})^2}{(x_{ca} - x_{0\gamma})^2 - (x_0 - x_{0\gamma})^2}\,. \tag{9}$$

The dependence on the constant a is automatically cancelled in the derivation. The solutions of equations (6) and (9) are

$$x = k(z)t \qquad t \le t_0(z) \tag{10}$$

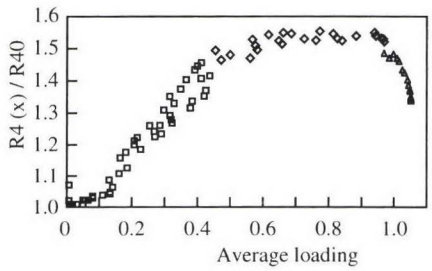

Fig. 10 The dependence of R/R0 upon the concentration x as emerging from the theoretical treatment of the experimental data shown if fig. 9

$$x = \frac{2x_{0\gamma} - x_{ca} + x_{ca} A e^{\lambda(z)[t-t_0(z)]}}{1 + A e^{\lambda(z)[t-t_0(z)]}} \qquad t > t_0(z) \tag{11}$$

where $t_0(z) = \frac{x_0}{k(z)}$, $\lambda(z) = Bk(z)$, $A = \frac{x_{ca} + x_0 - 2x_{0\gamma}}{x_{ca} - x_0}$, $B = \frac{2(x_{ca} - x_{0\gamma})}{(x_{ca} - x_0)(x_{ca} + x_0 - 2x_{0\gamma})}$.

We are now in a position to analyse the graph of figure 9.

1. For $t < t_0$ the experimental curve is well fitted by the linear approximation in eq. (10). This behaviour corresponds to the α–β phase that exists for $x \leq x_0$.
2. At the time t_0 when the experimental and the Baranowski curves start to diverge, at $x = x_0$, we can assume that the C.A. effect becomes evident.
3. For $t > t_0$ the loading $x(t,z)$ is given by eq.(11)
4. For each sector we take a z-average $\bar{x}(t)$ of the function $x(t,z)$ thus obtaining $\bar{x}(t)$ from eq. (10) and (11).
5. We can now invert $\bar{x}(t)$ and obtain $t = t(\bar{x})$
6. We introduce $t = t(\bar{x})$ in the experimental curve $R(t)/R_0$, obtaining finally a Baranowski type *R(x)* curve in presence of the C.A. effect as is shown in fig. 10.

We obtain for every sector $x_{ca} \approx 1$, whereas a plate with the same thickness usually is loaded up to $x \approx ..0.6$ we therefore have $\delta x \approx 0.4$ which correspond to (see Fig 8) $\delta\mu \approx 0.3eV$. Since the potential loss in the cathode is of the order of 1.4 volt, eq (1) tells us that $z^* \approx 0.2$, which compares well with the generally accepted estimates of z^* at high loading.

Direct measurements of x will began shortly in order to provide an independent assessment of the above theoretical derivation. A more detailed exposition of the topics presented in the present preliminary paper will be published in due course.

In conclusion it appears that the C. A. effect provides a means to achieve high loadings thereby reducing the irreproducibility of the cold fusion experiments.

REFERENCES

[1] See the Proceedings of the previous ICCF's.
[2] *G. Alefeld and J. Volkl*, "Hydrogen in metals" vol. I, II; Springer-Verlag (1978).
[3] *G. Bambakidis et al.*, Phys. Rev. **177** (1969) 1044.
[4] G. *Mengoli et al*, J. Electroan. Chem. **350** (1993) 57.
[5] *B. Dandapani and M. Fleischmann*, J. of Electroan. Chem. **39** (1972) 323.
[6] *A. Cöhn*, Z. Elektrochem., **35** (1929) 676.
[7] *G. Preparata*, "QED Coherence in Matter"; World Scientific (1995).
[8] *M. Fleischmann, S. Pons and G. Preparata*, Il Nuovo Cimento **107A** (1994) 143.
[9] *F. Taddei*, Doctoral Thesis, University of Milan (1994). A paper on this subject is in preparation.
[10] *Y. Aharonov and D. Böhm*, Phys. Rev. **115** (1959) 485.
[11] For a review, see the book of *M. Peshkin and A. Tonomura*, "The Aharonov-Böhm effect" Lecture Notes in Physics n° 340; Springer-Verlag (1989).
[12] *E.Del Giudice, A. De Ninno, A. Frattolillo, G.Preparata, F. Scaramuzzi, A. Bulfone, M. Cola, C. Giannetti,* this Conference
[13] *M. Nicolas, L. Dumoulin and J. P. Burger*, J. Appl. Phys. **60**, (1989) 3125

Conference Proceedings Vol. 70
"ICCF8"
F. Scaramuzzi (Ed.)
SIF, Bologna, 2000

COHERENCE in COLD and HOT FUSION

---Nuclear Physics for Nuclear Fusion---

Xing Z. Li, Ming Y. Mei, Jian Tian, Dong X. Cao, and Chong X. Li
Department of Physics, Tsinghua University, Beijing 100084, China

ABSTRACT The nuclear fusion data for deuteron-triton resonance near 100 keV are found to be consistent with the selective resonant tunneling model. It shows that the resonance mechanism selects not only the energy level, but also the damping rate (nuclear reaction rate). When the Coulomb barrier is thin and low, the resonance selects the fast reaction channel; however, when the Coulomb barrier is thick and high, the resonance selects the slow reaction channel. This mechanism might open an approach towards fusion energy with no strong nuclear radiation.

LAWSON CRITERION MODIFIED ?

Plasma physics developed rapidly in the past 40 years due to the research and development for the controlled nuclear fusion devices. Plasma physics and nuclear fusion have been so closely related that some journals and institutions are named by plasma and fusion together. However, the overwhelming dominance of plasma physics attracted most of the theoretical effort in magnetohydrodynamics and kinetics, in turbulence and chaos, in instabilities and

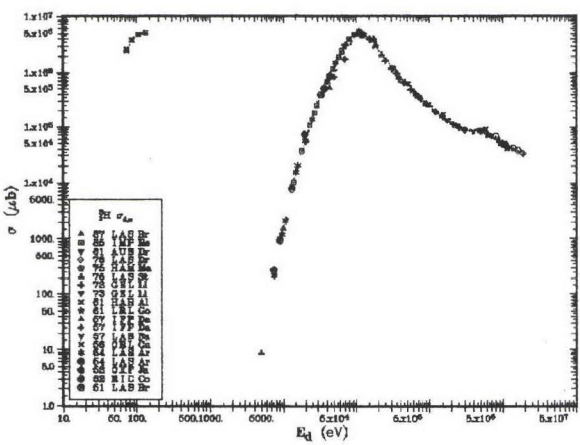

Fig.1 The deuteron plus triton fusion cross section showing an unexpected bump in cross-section near 100 eV from NNDC data before October, 1999[1]

transport ..... Unfortunately, nuclear physics was almost neglected. The unawareness of the nuclear physics was so evident that a set of seemingly good data was totally ignored for more than three years. The National Nuclear Data Center at Brookhaven National Laboratory has been so kind to provide the nuclear data to the scientists in the whole world free of charge. A set of data for d+t fusion cross-section was cited there in 1996.[1] It clearly showed that a jump in cross-section existed near 100 eV (Fig.1), the cross-section

at this jump was about 5 barns. If this set of data were true; then, the Lawson criterion[2] should have been much more favorable than that in 1957. Figure 2 shows the modified Lawson criterion with consideration of this set of new data. The upper curves show the necessary $n\tau$ at certain T_i for ignition, and the lower curves show the necessary $n\tau$ for an effective energy source.($n\tau$ is the product of plasma density and the confinement time; T_i is the ion temperature). The right hand side of Fig.2 is almost the same as the original Lawson

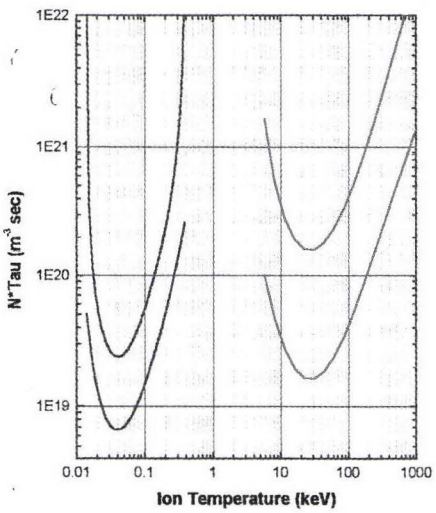

Fig.2 The modified plot for Lawson criterion if the unexpected bump in cross-section near 100 eV was true.

criterion, but the left hand side of Fig.2 considers the new set of fusion cross section data near 100 eV. It seems that $(n\tau) < 10^{19}$ m^{-3}·sec and $T_i < 100$ eV are enough to be an effective energy source. If this was true; then, the small spherical torus in UK, START, should have achieved this requirement already. However, no one noticed this mistake until the physics of resonant tunneling was revisited recently.

SELECTIVE RESONANT TUNNELING

In most of the literatures, resonant tunneling of the Coulomb barrier for the nuclear reaction was treated as a two-step process. That is tunneling first; then, decay. The tunneling probability was calculated in an over-simplified one-dimensional model [3], and the decay was assumed to be independent of the tunneling process. Nevertheless, this is not true in the case of the light nucleus fusion. In reality, when the wave function of the projectile penetrates the Coulomb barrier, it will reflect back and forth inside the nuclear well. This reflection inside the nuclear well is totally neglected in the one-dimensional model where the wave has no reflection as long as it penetrates through the barrier.(In the case of α-decay, the outgoing α-particle will have no reflection after penetrating the Coulomb barrier even if in 3-dimensional model [4]). Indeed this reflection is essential for the resonant penetration into the center of nuclear well through the Coulomb barrier. Secondary, the decay of the penetrating projectile will terminate the motion of bouncing back and forth inside the

nuclear well. If nuclear reaction happens quickly; then, the wave function will have no time to bounce back and forth. That is: the short lifetime of the penetrating wave may not allow enough bounce motion to build-up the wave function in terms of constructive interference inside the nuclear well. In a word, the tunneling and the decay in the light nucleus fusion should be combined together as a single-step process. Tunneling and decay are no longer independent.

It has been shown that an imaginary part of potential inside the nuclear well is a good way

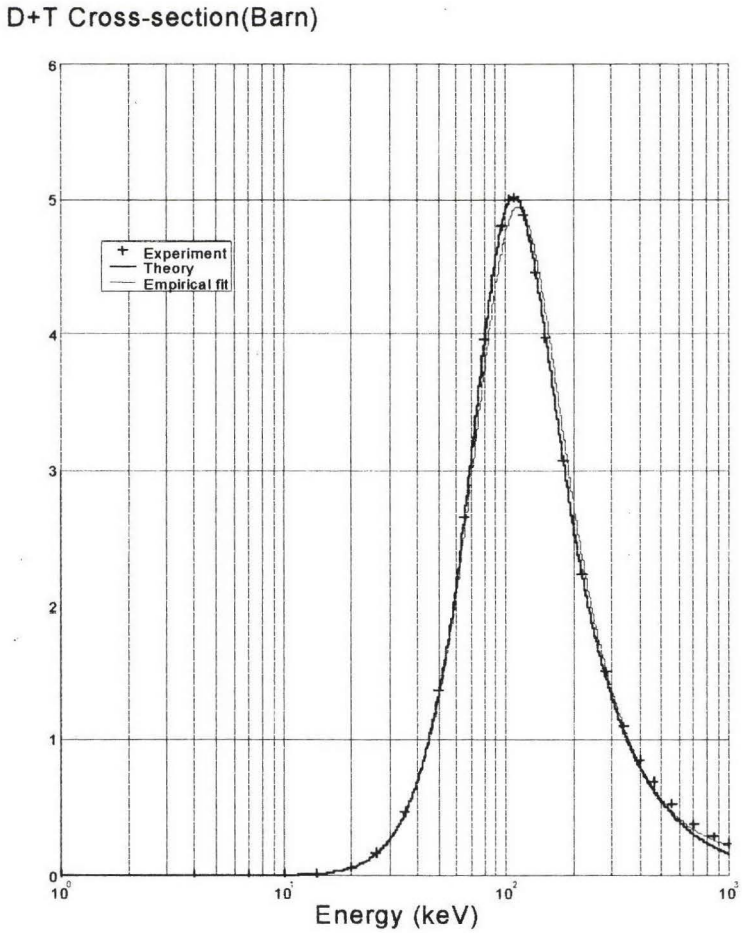

Fig.3 The comparison between the experimental data (cross) and the theoretical calculation based on the selective resonant tunneling model (solid line). The thin line shows the result of 5-parameter empirical formula.

to consider this lifetime effect on the resonance. A complex nuclear potential is proposed to describe this resonant tunneling effect for sub-barrier fusion in a 3-dimensional model for wide range of the energy of the projectile [5-7]. In that 3-dimensional calculation, we

introduced a new pair of parameters: the real and the imaginary parts of the cotangent of phase shift, i.e.

$$\cot\delta_0 = W_r + iW_i, \tag{1}$$

Thus, the fusion cross section for s wave will have a simple expression as

$$\sigma_r^{(o)} = \frac{\pi}{k^2}\frac{(-4W_i)}{W_r^2 + (W_i - 1)^2}. \tag{2}$$

W_r and W_i may be expressed as the function of two other parameters: i.e. the real and the imaginary parts of the nuclear potential U_{1r} and U_{1i},

$$W_r = \theta^2\left\{\frac{a_c}{a}\frac{z_r\sin(2z_r) + z_i\sinh(2z_i)}{2[\sin^2(z_r) + \sinh^2(z_i)]} - 2\left[\ln\left(\frac{2a}{a_c}\right) + 2C + h(ka_c)\right]\right\}, \tag{3}$$

$$W_i = \theta^2\left\{\frac{a_c}{a}\frac{z_i\sin(2z_r) - z_r\sinh(2z_i)}{2[\sin^2(z_r) + \sinh^2(z_i)]}\right\}. \tag{4}$$

Here $1/\theta^2$ is the famous Gamow penetration factor,

$$\theta^2 = \frac{1}{2\pi}\left[\exp\left(\frac{2\pi}{ka_c}\right) - 1\right]. \tag{5}$$

It is a function of incident energy E only, because $k^2 = (2\mu/\hbar^2)E$, and $a_c = \hbar^2/(Z_1Z_2\mu e^2)$ is a constant(the Coulomb unit of length). Here μ is the reduced mass, Z_1 and Z_2 are the charge number for the colliding nuclei, respectively; e is the electrical charge of a proton, $\hbar$ is the Planck constant divided by 2π. A complex number z is defined as $z = k_1a \equiv k_{1r}a + ik_{1i}a \equiv z_r + iz_i$. $k_1^2 = (2\mu/\hbar^2)(E - U_{1r} - iU_{1i})$ is the wave number inside the nuclear well. a is the radius of the nuclear well. $a = a_0(A_1^{1/3} + A_2^{1/3})$. A_1 and A_2 are the mass number for the colliding nuclei, respectively. a_0=1.746 fm to give the correct diameter for deuteron (4.4 fm)[8]. C=0.577...is Euler constant. h($k\,a_c$) is related to the logarithmic derivative of Γ function :

$$h(x) = \frac{1}{x^2}\sum_{n=1}^{\infty}\frac{1}{n(n^2 + x^{-2})} - C + \ln(x) \tag{6}$$

Equation (2) is different from the traditional expression for the cross-section of a resonance. It does not use any Taylor expansion; therefore, it may be applied to a wide range of energy as we will see later. When this model was applied to the d+t fusion cross section near 100 keV, it was a surprise to see the good fit between the theoretical calculation and the experimental data points. There are only two adjustable parameters U_{1r} and U_{1i} in this model. We may adjust them to meet the resonance peak (5.01 Barns at 110 keV); then, it will reproduce the experimental data covering the range of energy from 400 eV to 500 keV. Fig.3 depicts the experimental data points (in cross), and the results from the selective resonant tunneling model (solid line) with a square well of U_{1r}=-47.33 MeV, and U_{1i}=-115.25 keV. As a comparison we draw the curve (thin line) using the empirical formula in the NRL handbook for plasma formula[9]. We can see that our calculated results agree better than the empirical formula at the resonance. The complicated empirical formula needs five parameters to fit these data points.

SUPPRESSION OF NEUTRON EMISSION

This surprisingly good agreement with experimental measurements encourages us to further explore the physical meaning involved in this model. Eq.(2) tells that a resonance will appear at W_r=0. However, there is another requirement for W_i as well. W_i must be in the order of (-1) to see a resonance at the point where W_r=0. When W_i approaches zero or much less than (-1), it is hardly to see any resonance peak there [7]. As we mentioned above, this is just the meaning of selectivity in reaction rate (damping rate), because W_i is directly related to the imaginary part of the nuclear potential well (i.e. the lifetime of penetrating wave). Eq.(4) shows that z_i must be in the order of $1/\theta^2$ to make $W_i \approx -1$. Indeed, the physical meaning of z_i is the ratio of the flight time to lifetime of the penetrating wave inside the nuclear well, because

$$z_i \equiv k_{1i}a = \left| \frac{\mu a}{k_{1r}\hbar^2} U_{1i} \right| = \left| \frac{\frac{a}{k_{1r}\hbar/\mu}}{\hbar/U_{1i}} \right| \approx \frac{\tau_{flight}}{\tau_{life}} \approx O(\theta^{-2}) \qquad (7)$$

Now lets go back to Fig.1 and see if it could be true to have a jump in cross-section with neutron emission at the energy of about 100 eV. At such a low energy, it should be a resonance. Since $\theta^2 >> 1$; therefore, the resonance should select the channel with

$$\tau_{life} = O(\theta^2 \tau_{flight}) >> \tau_{flight}. \qquad (8)$$

However, the neutron emission happens in a channel where strong nuclear interaction plays key role, and gives a lifetime in the order of flight time. This channel would never be in resonance with the penetrating projectile at low energy. In this sense, we started to suspect the truthfulness of this piece of data. We checked further the height and the width of this resonance near 100 eV. Fig.4 shows schematically that the peak height of an assumed resonance should be getting higher and higher, and its width should be getting narrower and narrower when the energy of the resonance is getting lower and lower. This can be expected from eq.(2) where the k^2 in the denominator is getting smaller for the lower energy E. The width of the resonance Γ is determined by

$$\Gamma = \left| \frac{(W_i - 1)}{\frac{\partial W_{1r}}{\partial E}} \right|_{resonance} \approx O(\theta^{-2}). \qquad (9)$$

This width should become very small when the energy of injected projectile approaches to 100 eV, because the Gamow factor diminishes quickly. However, Fig.1 shows a resonance with almost same peak cross section as that of 100 keV resonance, and its width is clearly too broad to be consistent with this resonant tunneling model.

Fortunately, in October, 1999, this mistake was corrected by NNDC. This is the first time to correct a piece of experimental data based on the selective resonant tunneling model.

IDENTIFICATION OF A LOW ENERGY RESONANCE

Now let us ask a question, if there is a resonance at even lower energy; then, how can we identify this resonance? It must have no neutron emission, or gamma radiation, because the thicker and higher Coulomb barrier will require an even longer lifetime state for such a low energy resonance. The state, which emits neutron or gamma, is a short lifetime state, because the strong interaction or electromagnetic interaction is too strong to have a long

lifetime state. Then, the usual nuclear technology for neutron or gamma radiation is no longer applicable to detect this low energy sub-barrier resonance. The calorimetric technology in chemistry turns out to be the better choice, because the energy released in a nuclear reaction is always there. If there is any energetic charged particle as a nuclear product, we may use the nuclear track detector; or we may detect the helium directly. If we are able to identify such kind of low-energy resonant tunneling; then, this is a fusion

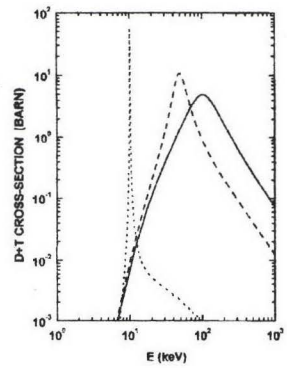

Fig.4 The shape of d+t fusion cross section predicted by the selective resonant tunneling model for the low energy resonance (if any).

reaction without strong nuclear radiation.
In conclusion, the nuclear physics for sub-barrier fusion provides a new approach towards nuclear fusion energy with no strong nuclear radiation.

Thanks to Professors H. Hora and S. Mercurio for their suggestions to improve this work. This work is supported by State Commission of Science and Technology (#1997567), Natural Science Foundation of China (#19645005), and Fundamental Research Fund of Tsinghua University. This proceedings' paper is finalized at University of Bologna with a grant from ICTP TRIL program with Professor S. Focardi.

REFERENCES

[1] Data retrieved from the CSISRS database World Wide Web site, file EXFOR C0023001, dated Feb. 27, 1996. Plot produced using the code BNL 325, written by C. L. Dunford, National Nuclear Data Center, Brookhaven National Laboratory.
[2] J. D. Lawson, Proc. Phys. Soc. (London) B 70 (1957) 6.
[3] G. Gamow , Phys. Rev. 53 (1938) 598.
[4] G. Gamow , Zeits. f. Physik. 51 (1928) 204.
[5] X. Z. Li, Czechoslovak Journal of Physics, 49 (1999) 985.
[6] X. Z. Li, C. X. Li and H. F. Huang, Fusion Technology, 36 (1999) 324.
[7] X. Z. Li, J. Tian , M. Y. Mei and C. X. Li, Phys. Rev. C 61 (2000) 024610.
[8] H. Feshbach, Theoretical Nuclear Physics, John Wiley & Sons, Inc. (New York) 1992, p.488.
[9] D. L. Book, NRL Plasma Formulary, NRL Publication 177-4405, Naval Research Laboratory, (revised 1990) p.44.

Conference Proceedings Vol. 70
"ICCF8"
F. Scaramuzzi (Ed.)
SIF, Bologna, 2000

A UNIFIED MODEL FOR ANOMALIES IN METAL DEUTERIDES

PETER L. HAGELSTEIN

Research Laboratory of Electronics
Department of Electrical Engineering and Computer Science
Massachusetts Institute of Technology
Cambridge, MA

Introduction

There have been numerous reports of observations of anomalies in metal deuterides during the past eleven years. The anomalies that we recognize for the purposes of the present discussion include: low-level neutron emission; fast ion emission; gamma emission; the Kasagi effect (3-body ddd-fusion reaction); excess heat and correlated slow ^{4}He emission; slow tritium production; and lattice-induced radioactivity. Many of these effects are under discussion in other papers that were presented at ICCF8. For many years we have sought physical mechanisms that might provide a theoretical explanation for these anomalies. During the past 2-3 years, our efforts have led to a unified picture that appears to provide mechanisms systematically for all of these anomalies. In this conference proceeding, we will provide an overview of the general approach, the basic model, and the relevant physical mechanisms.

We note that there have been a number of reports of observations of a massive transmutation effect that would involve reactions that increase the nuclear mass of the host metal. This effect is not included within the model under discussion.

Overview of the Model

The premise of the model is that nuclear reactions in the lattice can take place, and that the lattice must be included in the physical description. There exists well-studied models for fusion reactions in free space, which we must generalize to include lattice effects. When the nuclei and lattice are described together within the basic formulation, we find that the lattice phonon degrees of freedom mix with the microscopic

nuclear degrees of freedom. This coupling comes about at a very fundamental level as a consequence of the natural separation of microscopic position coordinates into center of mass coordinates, relative coordinates and internal coordinates.

While it comes as no surprise that phonons might play a role in a fusion reaction between deuterons within a lattice, our intuition suggests strongly that any such interactions can have only a small impact on the physics of the reaction. In fact the model under consideration can be used to quantify just how small the effect of the lattice is on all first order reaction processes. The exchange of a single phonon would not be expected to cause much change in the dynamics of a dd-fusion reaction involving exit channels with product nuclei separating with several MeV of relative energy. The new theory is consistent with this expectation.

However, there exists the possibility of new second order effects when the lattice is involved. For example, a reaction might occur at one site where phonon exchange takes place with a highly excited phonon mode. A second reaction might take place at a different site, again with phonon exchange with a highly excited mode. While the effect of phonon exchange for all first order processes is arguably negligible, at second order the situation can be very different. Within a second order process, it may be the case that energy conservation is apparently violated for each individual process, but rigorous energy conservation must be required for the two-step second order process. When phonon exchange with the lattice occurs, we must consider the possibility that an exothermic fusion reaction occuring at one site might be coupled with some other endothermic process at a different site.

The consequences of this are enormous, and the theory that results appears to coincide with many of the experimental observations. The most important second order site-other-site process of this sort is the "null" reaction, in which a fusion of two deuterons to a ^{4}He nucleus at one site is coupled to a dissociation of a ^{4}He nucleus at another site. In such a reaction, no new products are formed. The only effect of such a process is to exchange excitation between two sites. One finds that the (E2) microscopic selection rules for this can be satisfied through phonon exchange. One also finds that this process can be greatly enhanced when many sites are involved. One consequence of this process is that the probability of deuterons being found close together increases greatly (when the helium dissociates, the resulting deuterons are born close together). In the simplest case, these deuterons can react to make neutrons and other dd-fusion products. If significant phonon exchange occurs, then the two deuterons will have significant relative angular momentum, which can exclude the conventional dd-fusion reaction channels. In this case, they may remain together with significant probability. There presence can be detected then through a 3-body reaction when fast (100 keV) deuterons are incident. This appears to lead naturally to the Kasagi effect. [1]

The close coupling of the phonons and deuterons that occurs in such a process leads to a strong mixing of the phonon and nuclear degrees of freedom. Under these conditions, phonon dissipation will lead to a loss of nuclear energy from the coupled system, because the degrees of freedom are mixed. The ash from this process will be ^{4}He, produced in place with no kinetic energy, as is observed. The same basic mechanism also applies to tritium production, where the associated "null" reaction is two deuterons reacting to produce a slow proton and tritium pair at one site, and the inverse process occurs at a different site. Fast charged particles can result when a fusion at one site is coupled to lattice-induced particle ejection at another site. For example,

alpha particles and other low mass ejecta can be ionized from high-Z nuclei within the lattice through "electrostatically" mediated phonon exchange, as the second part of a two-step second order process where the energy is provided by a fusion reaction as a first step. There exist reports of such an effect. [2] The lattice-induced radioactivity seen by Wolf would result from a process in which the initial fusion were mediated by a 70-phonon exchange process, with each of the phonons dissipating their energy in a roughly 350 KeV weak-interaction decay channel.

The model also predicts a proton-deuteron reaction pathway, involving ^{3}He final states. While the possible existence of such a pathway has been noted by many, it has usually been assumed that any associated anomalous reactions would proceed at a rate proportional to the overlap probability, which is orders of magnitude greater for the proton deuteron system. Null reactions involving protons and deuterons would lead to a large increase in the associated probability at short range, which would be qualitatively similar to the situation for deuteron-deuteron reactions. Consequently, a heat effect involving the proton-deuteron pathway would likely be limited by phonon dissipation effects, and not by the overlap probability of the associated molecular system as has been often conjectured. If the light water heat experiments are conjectured to be the consequence of proton-deuteron reactions, then it would be sensible to assay for ^{3}He as a possible ash. The present model supports this conjecture.

Including Lattice Effects in the Basic Formulation

Most theoretical papers on the dd-fusion reaction have made use of the resonating group method or the R-matrix method. Consequently, we wish to generalize these methods to include lattice effects. The resonating group method [3] assumes a total wavefunction Ψ_T of the form

$$\Psi_T = \sum_j \Phi_j F_j \tag{1}$$

where the internal nuclear states are included in Φ_j, and where F_j is the channel separation factor. The internal nuclear states are presumed to be fixed, and the channel factors are determined from a solution of the coupled-channel equations

$$E F_j = \langle \Phi_j | H | \Phi_j \rangle F_j + \sum_k \langle \Phi_j | (H - E) | \Phi_k F_k \rangle \tag{2}$$

In all cases, the wavefunctions must be properly antisymmetrized (a requirement not made explicit by the abstract formulation presented here).

The channel separation factor F_j is a function of the relevant relative mass coordinate(s) between the center of mass coordinates of the constituent nuclei in the jth channel. As the center of mass coordinates of the constituent nuclei also occur in a lattice description, we can generalize the resonating group method to include lattice effects simply by replacing the separation channel factors with lattice channel factors. Consequently, we generalize the resonating group method by using an initial wavefunction of the form

$$\Psi_T \;=\; \sum_j \Phi_j \; \Psi_j \tag{3}$$

where Ψ_j now includes the center of mass coordinates for the reacting nuclei associated with channel j, and also the center of mass coordinates for the other nuclei in the lattice. Assuming equivalently that the internal nuclear states Φ_j do not depend on the relative separation, the lattice channel functions can be determined from a solution of the lattice multi-channel equations

$$E\;\Psi_j \;=\; \langle \Phi_j | H | \Phi_j \rangle \; \Psi_j \;+\; \sum_k \langle \Phi_j | \; (H - E) \; | \Phi_k \Psi_k \rangle \tag{4}$$

These equations can serve as the starting point for modeling anomalies in metal deuterides. We note that a similar generalization of the R-matrix method to include lattice effects is completely straightforward. The total lattice wavefunction in this case can be developed using lattice channel factors $\Psi_T = \sum_j c_j \Phi_j \Psi_j$, and then an appropriate eigenvalue equation for the amplitudes c_j can be developed.

Interaction between Two Sites

We can extend the analysis to include coupling between reactions at different sites. For simplicity, we consider the case of two sites here. The "null" reaction of interest can be written as

$$(d+d)_a \;+\; (^4He)_b \;\longleftrightarrow\; (^4He)_a \;+\; (d+d)_b \tag{5}$$

To model this, we assume a total wavefunction of the general form

$$\Psi_T \;=\; \sum_j \sum_n \; \Phi_j^a \; \Phi_j^b \; \phi_n \; \Psi_{j,n} \tag{6}$$

The internal nuclear states at site a are included in Φ_j^a, and the internal states at site b are included in Φ_j^b. We assume a highly excited delocalized phonon mode with n phonons present, modeled by ϕ_n. The rest of the lattice wavefunction is modeled by the lattice channel function $\Psi_{j,n}$. The relevant two-site coupled lattice channel equations are of the form

$$E\;\Psi_{i,n} \;=\; \langle \Phi_i^a \Phi_i^b \phi_n | H | \Phi_i^a \Phi_i^b \phi_n \rangle \; \Psi_{i,n} \;+\; \sum_{j,n' \neq i,n} \langle \Phi_i^a \Phi_i^b \phi_n | \; (H - E) \; | \Phi_j^a \Phi_j^b \phi_{n'} \Psi_{j,n'} \rangle \tag{7}$$

No interesting new effects are present at first order. We can eliminate intermediate states to obtain a second order model

$$E\;\Psi_{i,n} \;=\; \langle \Phi_i^a \Phi_i^b \phi_n | H | \Phi_i^a \Phi_i^b \phi_n \rangle \; \Psi_{i,n}$$
$$+ \sum_{j,n' \neq i,n} \sum_{k,n'' \neq j,n'} \frac{\langle \Phi_i^a \Phi_i^b \phi_n | \; (H - E) \; | \Phi_j^a \Phi_j^b \phi_{n'} \; \langle \Phi_j^a \Phi_j^b \phi_{n'} | \; (H - E) \; | \Phi_k^a \Phi_k^b \phi_{n''} \Psi_{k,n''} \rangle \rangle}{E - E_{j,n'}} \tag{8}$$

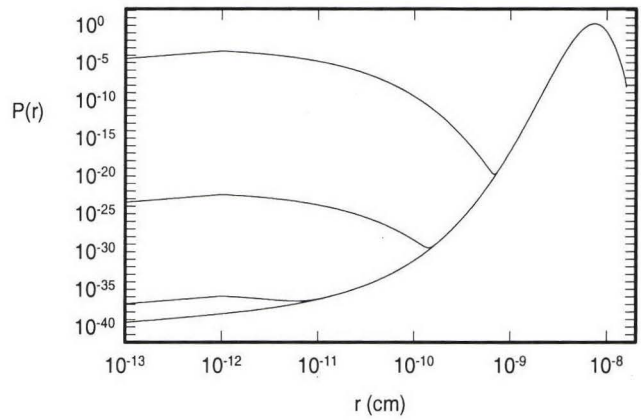

Figure 1: Model computation of the probability amplitude for the ^{5}S channel assuming 2-phonon exchange. One observes the effect of a source term near the origin for different coupling strengths.

This equation can then be used to understand the coupling of a reaction at site a with its inverse at site b. If we focus on the local probability amplitudes for relative separation at each of the two sites, we obtain coupled equations, one of which is given by

$$
\begin{aligned}
E\,\psi_{a,n}(\overline{\mathbf{R}}_1,\overline{\mathbf{R}}_2) \;=\; & \left[-\frac{\overline{\nabla}_1^2}{2M_1}-\frac{\overline{\nabla}_2^2}{2M_2}\;+\;V_{lat}(\overline{\mathbf{R}}_1)\;+\;V_{lat}(\overline{\mathbf{R}}_2)\;+\;V_{nn}(\overline{\mathbf{R}}_1,\overline{\mathbf{R}}_2)\right]\psi_{a,n}(\overline{\mathbf{R}}_1,\overline{\mathbf{R}}_2) \\
& +\;\sum_{n'\neq n}\frac{\langle\Phi^a_{dd}|\;V_{nn'}\;|\Phi^a_{He}\,\langle\Phi^b_{He}|\;V_{n'n}\;|\Phi^b_{dd}\,\psi_{b,n}(\overline{\mathbf{S}}_1,\overline{\mathbf{S}}_2)\rangle\rangle}{\Delta E\;-\;(n'-n)\hbar\omega_0} \\
& -\;\sum_{n'\neq n}\frac{\langle\Phi^b_{He}|\;V_{nn'}\;|\Phi^b_{dd}\,\langle\Phi^a_{dd}|\;V_{n'n}\;|\Phi^a_{He}\,\psi_{b,n}(\overline{\mathbf{S}}_1,\overline{\mathbf{S}}_2)\rangle\rangle}{\Delta E\;+\;(n'-n)\hbar\omega_0}
\end{aligned}
\tag{9}
$$

For transitions between orthogonal channels, the nuclear and Coulomb interaction appears through

$$
V_{n,n'}\;=\;\langle\phi_n|(H-E)|\phi_{n'}\rangle \tag{10}
$$

We see in the first line of equation (9) a two-body problem for the two deuterons at site a, which is essentially the molecular D_2 problem in an external potential. This problem is written in terms of the residual local position variables $\overline{\mathbf{R}}_1$ and $\overline{\mathbf{R}}_2$, which are the true position variables minus the contribution of the excited phonon mode (see Ref [4]). The second and third lines include source terms due to the dissociation of the ^{4}He nucleus at site a. This dissociation comes about as part of a the second order null

reaction, in which a fusion at one site is coupled to a dissociation at another site. There exist some technical issues regarding the denominator of the second summation which are important but suppressed in this discussion. Two deuterons that are produced close together can either tunnel or interact, thereby destroying the relative symmetry of the two channels. This effect reduces significantly the destructive interference between the two possible intermediate pathways, and increases the effects under discussion.

In Figure 1, we illustrate the essential physics contained in this model in a computation of the probability amplitude for the separation between the two deuterons assuming a molecular D_2 potential, and injection of probability amplitude at 10 fermis. The source term is linear in the number of sites that participate in phase. We have illustrated results for different coupling strengths (ie. different number of sites and different phonon interaction strengths).

Discussion

The discussion above indicates that second order coupling between reactions at two sites is expected when the lattice is included in the initial formulation of the nuclear problem. For the S-wave example illustrated in the last section, we require two-phonon exchange to satisfy the microscopic selection rules. This kind of effect would lead to neutron emission, since the deuterons at close range would run into each other occasionally and react. If more than 25 phonons are exchanged, then a strong inhibition of the normal dd-fusion channels occurs. In this case, a very large amount of probability amplitude could accumulate at short range, which would be observable in a Kasagi-type of experiment. The approach outlined here can be applied uniformly to neutron emission as well as to the Kasagi effect. Inclusion of phonon dissipation in the model leads to heat and helium production.

It remains to be proven experimentally that the Kasagi effect is due to a 3-body reaction (this will probably require a coincidence measurement of the proton and alpha particle). If it proves to be due to ddd-fusion, then the model outlined here may provide the only possible explanation. The experimental result could then be interpreted in proving that energy could be exchanged through the lattice between reactions at different sites. In our view, this is ultimately the basis for understanding all of the anomalies.

References

[1] J. Kasagi, T. Ohtsuki, K. Ishu and M. Hiraga, *J. Phys. Soc. Japan* **64** 777 (1995).

[2] F. E. Cecil, H. Liu, D. Beddington and C. S. Galovich, AIP Conf. Proc. **228** page 383 (1990).

[3] J. A. Wheeler, *Phys. Rev.* **52** 1107 (1937).

[4] P. L. Hagelstein, *Phil. Mag. B* **79** 149 (1999).

Conference Proceedings Vol. 70
"ICCF8"
F. Scaramuzzi (Ed.)
SIF, Bologna, 2000

ELECTRON SCREENING IN METAL DEUTERIDES

K. P. SINHA and PETER L. HAGELSTEIN

Research Laboratory of Electronics
Department of Electrical Engineering and Computer Science
Massachusetts Institute of Technology
Cambridge, MA

Introduction

Experimental evidence in support of anomalies in metal deuterides has accumulated during the past decade. These anomalies include neutron emission, fast (MeV) charged particle emission, excess power generation and correlated ^{4}He production, tritium production and induced radioactivity. As yet, there is no consensus on a theoretical explanation for these effects. Prior to the introduction of any new physics that pertain specifically to the anomalies, one would like to have a basic understanding of the deuteron-deuteron interaction at close range due to conventional solid state effects. In this work we examine the general issue of electron screening between deuterons in a metal deuteride.

Screening and Recent Accelerator Experiments

In the case of molecular D_2, the screening between the deuterons is a consequence of the change of the electronic energy due to modifications in the electronic orbitals as a function of the deuteron separation. Within the framework of the Born-Oppenheimer approximation, this effect can be included as an effective potential in addition to the Coulomb repulsion between the deuterons. For example, when a fast deuteron collides with a stationary deuteron, electron screening should occur in much the same way as in the D_2 molecule. This should produce an increase in the fusion probability over the theoretical ion-ion calculation (with an unscreened Coulomb barrier) that will be most noticeable at low incident energy. Experiments involving keV deuterons incident on molecular deuterium gas targets give an increase in the fusion rate at low energy over

the theoretical ion-ion calculation that is consistent with such a screening mechanism [1,2]. The experimental data are fit to a screening energy U_S, which for D_2 gas targets is found to be about 25 eV. The corresponding screening length D_S is related by

$$D_S = \frac{e^2}{U_S} \tag{1}$$

In this case, the associated screening length is on the order of a Bohr radius. Similarly, keV deuterons incident on TiD targets show a low energy behavior consistent with a screening that is weaker than for molecular targets. The associated screening energy is 19 eV (with a screening length $D_S = 0.75$ Å).

Experiments in other metal deuterides show a much stronger relative enhancement in the fusion yield at low energy, which has been conjectured to be indicative of a much stronger electron screening effect. For example, In YbD, the screening energy is 60 eV ($D_S = 0.24$ Å). In PdD, the experimental result is consistent with a screening energy of 250 eV ($D_S = 0.058$ Å). We note that a screening length that is less than 0.1 Å is extremely small. It is hard to understand theoretically what physical mechanism could be responsible for such strong screening.

As PdD has been involved in experiments yielding anomalies such as neutron emission and excess heat, it would be natural to imagine that there might exist some physical mechanism that is capable of producing anomalously large screening in PdD. A recent computation by Ichimaru has indicated that large screening effects should be present in PdD near room temperature [3]. Consequently, we have been motivated to examine the issue of screening in metal deuterides, in order to understand whether there can exist a greatly enhanced screening effect.

A Naive Approach to Screening

In the simplest possible picture, the screening between two deuterons in a metal deuteride depends primarily on local electrons that are bound (in a local molecular sense), and somewhat less on more distant electrons through a polarization effect. In a naive view, one might postulate that the interaction between the deuterons at short range was of the form

$$V_{ij} \sim \frac{q_i q_j}{\epsilon} \frac{e^{-R/D_S}}{R} \tag{2}$$

At close range, the interaction is pure Coulombic; at longer distances the interaction is screened exponentially. The effect of polarization in this naive picture is taken into account through the introduction of a dielectric constant. In the computation of Ichimaru, polarization effects were accounted for through the introduction of a constant dielectric constant ϵ. Ichimaru estimated this dielectric constant to be on the order of 1.25 in PdD. Such a relatively high dielectric constant has a very large impact on the deuteron-deuteron overlap probability. There is reason to be concerned about the use of a constant dielectric constant in this application, as it is unlikely that there exists a uniform dielectric background medium when the two deuterons are closer together than the screening distance D_S.

An Improved Model

In order to include the effects of both local and distant electrons on the deuteron-deuteron interaction at short range, we are considering a model that seeks to include both effects explicitly. Local bound electrons can be modeled in the Born-Oppenheimer approximation through the use of an effective electronic potential. When the two deuterons are close, the local ground state electronic orbitals are compact and mismatched in energy from the surrounding orbitals of the host metal. In this case, we expect the effective potential to be close to the equivalent molecular problem. The dielectric response of the electrons at all other sites can be included using a form of linear response theory. One deuteron produces an electrostatic field that polarizes nearby electronic orbitals. The induced electronic polarization then produces a field that effects the second deuteron. The overall effect of the polarization is to cause a screening; however, the strength of this screening is diluted to some degree since the orbitals are relatively distant. Such a model should account for polarization effects much better than using a local dielectric constant as described in the naive model above.

A Hamiltonian that implements this type of model can be written as [4]

$$\begin{aligned} H = & \frac{|\mathbf{P}_1|^2}{2M_1} + \frac{|\mathbf{P}_2|^2}{2M_2} + \frac{q_1 q_2}{|\mathbf{R}_1 - \mathbf{R}_2|} + E_e(|\mathbf{R}_1 - \mathbf{R}_2|) + V_{lat}(\mathbf{R}_1) + V_{lat}(\mathbf{R}_2) \\ & + \sum_m \left\langle \frac{q_1 e}{|\mathbf{R}_1 - \mathbf{r}_m|} \left[E - H_0 \right]^{-1} \frac{q_2 e}{|\mathbf{R}_2 - \mathbf{r}_m|} \right\rangle \\ & + \sum_m \left\langle \frac{q_2 e}{|\mathbf{R}_2 - \mathbf{r}_m|} \left[E - H_0 \right]^{-1} \frac{q_1 e}{|\mathbf{R}_1 - \mathbf{r}_m|} \right\rangle \end{aligned} \tag{3}$$

The first line of this Hamiltonian includes essentially the molecular D_2 problem in the metal lattice environment. The second two lines includes polarization effects with electrons centered at neighboring atomic sites. The summation over index m includes the different electronic orbitals at those neighboring sites. The expectation value is taken over electronic states.

It is possible to apply this model systematically to the different metal deuterides in order to understand screening effects. Two features of the model are obvious that are nearly independent of the host metal deuteride. One is that when the two deuterons are close, the underlying model becomes very much like the molecular D_2 problem, independent of the metal. Another is that it is apparent that polarization effects due to relatively distant electronic orbitals will give rise to essentially no screening effect between deuterons at short range. This is in contrast to the model of Ichimaru.

Dependence of the Dielectric Response on Deuteron Separation

A major focus of the model is to understand the dielectric response of the metal deuteride under conditions when the two deuterons are close together. It is possible to use a Taylor series expansion based on the center of mass and relative coordinates

$$\mathbf{R}_1 = \mathbf{R}_{cm} - \frac{1}{2}\Delta\mathbf{R} \tag{4}$$

$$\mathbf{R}_2 = \mathbf{R}_{cm} + \frac{1}{2}\Delta\mathbf{R} \tag{5}$$

in order to understand the physical content of the polarization terms. Keeping terms to second order in the separation $\Delta\mathbf{R}$ leads to an expression of the general form

$$V_{pol} = V_0 + \Delta\mathbf{R} \cdot \mathbf{M} \cdot \Delta\mathbf{R} \tag{6}$$

The polarization potential is made up of a constant solution energy offset V_0 that depends on the center of mass position $\mathbf{R}_{cm}$, and a term that is quadratic in the separation $\Delta\mathbf{R}$ where $\mathbf{M}$ is a function of $\mathbf{R}_{cm}$. The detailed evaluation of the terms that appear in this kind of analysis has been carried out and submitted for publication elsewhere[5].

Discussion

The simplest possible model for screening between deuterons in a metal deuteride must include local orbital effects and polarization effects. When the two deuterons are close together, the local electronic orbitals are essentially molecular D_2 orbitals. In TiD, one is tempted to conclude that the local molecular picture extends to distances on the order of a Bohr radius or more. Polarization effects are weak when the deuterons are close, independent of the host metal. In PdD, the outer electronic orbitals of the Pd atoms mix with the $1s$ orbitals of the D atoms when the deuterons are far apart due to a near resonance in the energies of the orbitals. While this complicates the picture, the relevant screening length associated with such mixed orbitals cannot differ by a factor of 10 as would be required to account for the apparent experimental results. The screening length due to such mixing may decrease by about a factor of 2 from the molecular case as has been estimated by Ichimaru and colleagues.

So we are left with an apparent dilemma in accounting for the experimental results in PdD, while TiD seems to be consistent with the general picture described here. The situation becomes further confused relative to the anomalies, as the deuterides of both titanium and palladium appear to give rise to anomalies. To sort out the various issues, we need to be somewhat more precise in our arguments. We must distinguish between the static problem and the collision problem as being potentially different fundamentally in principle. In the case of the static problem, we must also distinguish between three different local environments.

We first consider the collision problem, which gives an apparent screening effect that seems to be impossibly large. The presence of screening is deduced based on a relative increase in the fusion yield at low energy as compared to the theoretical ion-ion collision problem. Hubler (private communication) has suggested that the experimental measurements may be susceptible to an artifact involving a nonuniform deuterium concentration gradient near the surface. If the outer 100 Å of the target near the surface had a higher density of deuterium, then the yield would be larger for the lower beam energy since the range of the deuterons is much shorter at 3 keV than at 10 keV.

Such an effect would give an apparent increase in the low energy yield, but would not be a screening effect. Kasagi has indicated that he measures this profile, and thereby guards against such an artifact (private communication). Nevertheless, due to the theoretical implications of the result, some way needs to be found to be sure that experimental artifacts are not present. For example, in the unlikely event that the deuterons should somehow channel in the intersticies between the Pd atoms preferentially at low energy, then the apparent relative yield would increase at low energy. It is not believed at present that this can happen.

One possible route to accounting for the low energy enhancement might be to consider atomic recoil during the collision event. For example, suppose that the incident deuteron accelerated the stationary deuteron so that it moved much closer to a neighboring Pd nucleus. The screening length in this case could be very much shorter if a more strongly bound Pd orbital (for example, an M-shell orbital) were involved in the screening. In the absence of a detailed analysis of the effect, this appears to be the only way that a screening length less than 0.1 Å could possibly occur. If such a mechanism were the answer to the dilemma, it would not apply to the screening between two nearly static deuterons in the lattice since they would never be found together near an inner Pd electron orbital.

If we focus now on the static problem, we find immediately that there is a question as to what conditions lead to significant tunneling. Three different situations might occur. Two deuterons could be at neighboring sites, and perhaps meet half-way in between. Alternatively, a deuteron from one site could be thermally excited to go into a neighboring site that is already occupied. Finally, it may be that there is a nearby host metal vacancy, so that it becomes much easier for two deuterons to approach. The latter two cases produce the largest tunneling probabilities, and are consequently the most interesting in the consideration of anomalies. In both cases, the local center of mass will likely be near a local potential minimum, and the confining potential will be approximately quadratic. The molecular approximation with minor modifications ought to be a good first approximation in both cases. Deviations from this will be due to orbital mixing with the metal atoms, which is strongest when the orbital align in energy such as in the case of Pd or Ni.

Other Effects

The discussion above has focused on the screening problem assuming a static lattice model. We note that phonons are present, and that it is possible for the interaction between the phonons and the electrons to introduce further complications. Electron exchange between the deuteron orbitals in the molecular case is understood, but one wonders about the situation when strong mixing between the hydrogen orbitals and the metal orbitals occurs. We note also that anomalies in metal deuterides appear to be correlated with conditions under which either an electron current density or ion flux density is present. An electron current will entail a minor modification of the local electron orbitals. An ion flux will be associated with an increase in the optical phonon excitation, which will produce a larger overlap probability.

References

[1] H. Yuki et al, *Proc. ICCF6* p. 259 (1996).

[2] J. Kasagi et al, *Proc. ICCF7* p. 180 (1998).

[3] S. Ichimaru, *Rev. Mod. Phys.* **65** 255 (1993).

[4] K. P. Sinha and P. L. Hagelstein, *RLE 1999 Annual Report.*

[5] K. P. Sinha and P. L. Hagelstein, submitted to *Phys. Rev. B.*

Conference Proceedings Vol. 70
"ICCF8"
F. Scaramuzzi (Ed.)
SIF, Bologna, 2000

Ultra Low-Energy Nuclear Fusion of Bose Nuclei in Nano-Scale Ion Traps

Yeong E. Kim and Alexander L. Zubarev
Purdue Nuclear and Many-Body Theory Group
Department of Physics, Purdue University
West Lafayette, Indiana 47907, U.S.A.

Abstract: Our recent theoretical investigation on nuclear fusion of integer spin nuclei confined in an isotropic ion trap is described. Solutions of the ground state for charged bosons trapped in the isotropic harmonic oscillator potential are calculated using the equivalent linear two-body method for many-body problems, which is based on an approximate reduction of the many-body Schrödinger equation by the use of a variational principle. Using the ground state wave function, we derive theoretical formulae for rates of nuclear fusion for Bose nuclei confined in ion traps. Our formulae show that the fusion rate does not depend on the Coulomb barrier penetration probability but instead depends on the probability of the ground-state occupation, which is expected to increase as the temperature decreases. Numerical estimates for deuteron-deuteron fusion rates are presented for the case of deuterons trapped in metal powders. Experiments for proof of the principle are suggested to test our theoretical predictions.

1. Introduction

Since the 1989 announcements [1,2] of nuclear fusion at room temperature in D_2 loaded palladium (Pd) and titanium (Ti) cathodes in electrolytic cells containing heavy water (D_2O), there have been persistent claims of observing cold fusion (CF) phenomena. However, most of the reported experimental results are not reproducible. A few notable exceptions are the recently published work by Arata and Zhang [3-5], Bush et al. [6-8], Miles and Bush [9], Case [10], and Stringham *et al.* [11]. We suggested [12] that CF phenomena may be due to the Bose-Einstein condensation of deuterons.

In this paper, we investigate theoretically different aspects of the properties of identical integer-spin nuclei ("Bose" nuclei) confined in ion traps by approximating the ion trap with an isotropic harmonic oscillator potential for simplicity. We report the results of our theoretical investigation on the feasibility of nuclear fusion in such setups ("ion-trap nuclear fusion") using the recently developed equivalent linear two-body (ELTB) method for many-body problems [13]. The ELTB method is based on an approximate reduction of the many-body Schrödinger equation by the use of a variational principle.

2. Anomalous Ultra Low-Energy Nuclear Fusion

Recently, Arata and Zhang [3-5] observed anomalous production of both heat and helium-4 (^{4}He) from their electrolysis experiments. A Pd metal cylinder containing Pd fine particles was used as a cathode in the electrolysis of heavy water (D_2O). No other nuclear ashes or radiation were observed. The anomalous heat was not observed in the electrolysis of water (H_2O) in the control experiment [3].

A similar anomalous result, producing both heat and ^{4}He but no nuclear ashes nor radiation was also observed by Bush et al. [6-8], Miles and Bush [9], and Case [10]. In Case's experiment [10], gaseous D_2 (at 1-3 atm) was introduced in a catalysis container consisting of activated carbon coated with a platinum-group metal (Pd, Pt, Ir, and Rh), operating at 130-300°C.

The experimental results [3-11] suggest the following radiationless nuclear reaction,

$$d + d \rightarrow {}^4He, (Q = 23.848MeV), \tag{1}$$

as the explanation of CF. However this reaction cannot occur in free space since it violates momentum conservation. However, the above reaction (1) can occur if it takes place in a many-body quantum state consisting of many deuterons (Bose-Einstein condensation [12] "coherent quantum (CQ) state" [14,15]) because the CQ state can absorb the recoil momentum thus satisfying momentum conservation.

3. Ground-State Solution

In this section, we consider N identical charged Bose nuclei confined in an ion trap. For simplicity, we assume an isotropic harmonic potential for the ion trap to obtain order of magnitude estimates of fusion reaction rates. The Hamiltonian for the system is then

$$H = -\frac{\hbar^2}{2m}\sum_{i=1}^{N}\Delta_i + \frac{1}{2}m\omega^2\sum_{i=1}^{N}r_i^2 + \sum_{i<j}\frac{e^2}{\mid \mathbf{r}_i - \mathbf{r}_j \mid} \tag{2}$$

where m is the rest mass of the nucleus. In order to obtain the ground-state solution, we will use the recently developed method of equivalent linear two-body (ELTB) equations for many-body systems [13,14].

For the ground-state wave function Ψ, we use the following approximation [14]

$$\Psi(\vec{r}_1, ...\vec{r}_N) \approx \tilde{\Psi}(\rho) = \frac{\Phi(\rho)}{\rho^{(3N-1)/2}}, \tag{3}$$

where

$$\rho = \left[\sum_{i=1}^{N} r_i^2\right]^{1/2}. \tag{4}$$

In reference [13] it has been shown that approximation (3) yields good results for the case of large N.

By requiring that $\tilde{\Psi}$ must satisfy a variational principle $\delta\int\tilde{\Psi}^*H\tilde{\Psi}d\tau = 0$ with a subsidiary condition $\int\tilde{\Psi}^*\tilde{\Psi}d\tau = 1$, we obtain the following Schrödinger equation for the ground state wave function $\Phi(\rho)$

$$[-\frac{\hbar^2}{2m}\frac{d^2}{d\rho^2} + \frac{m}{2}\omega^2\rho^2 + \frac{\hbar^2}{2m}\frac{(3N-1)(3N-3)}{4\rho^2} + V(\rho)]\Phi = E\Phi, \tag{5}$$

where [13]

$$V(\rho) = \frac{N(N-1)}{\sqrt{2}\pi}\frac{\Gamma(3N/2)}{\Gamma(3N/2-3/2)}\frac{1}{\rho^3}\int_0^{\sqrt{2}\rho}V_{int}(r)\left(1-\frac{r^2}{2\rho^2}\right)^{(3N/2-5/2)}r^2\,dr \tag{6}$$

For $V_{int}(r) = e^2/r$, $V(\rho)$ reduces to [13]

$$V(\rho) = \frac{2N\Gamma(3N/2)}{3\sqrt{2\pi}\Gamma(3N/2-3/2)}\frac{e^2}{\rho}. \tag{7}$$

Instead of the variable ρ in the Schrödinger equation (12), we introduce a new quantity $\tilde{\rho}$ defined as

$$\tilde{\rho} = \sqrt{\frac{m\omega}{\hbar}}\rho. \tag{8}$$

Substitution of Eq. (7) into Eq. (5) leads to the following equation

$$\frac{\hbar\omega}{2}[-\frac{d^2}{d\tilde{\rho}^2} + \tilde{\rho}^2 + \frac{(3N-1)(3N-3)}{4\tilde{\rho}^2} + \frac{\tilde{\gamma}}{\tilde{\rho}}]\Phi = E\Phi, \tag{9}$$

where

$$\tilde{\gamma} = \alpha\sqrt{\frac{mc^2}{\hbar\omega}}\frac{4N\Gamma(3N/2)}{3\sqrt{2\pi}\Gamma(3N/2-3/2)} \tag{10}$$

with $\alpha = e^2/(\hbar c) \approx 1/137$. The ground state solution of Eq.(9) has been obtained in the following form

$$\Phi(\tilde{\rho}) = \sum_i c_i \tilde{\rho}^{\frac{3N-1}{2}} e^{-(\tilde{\rho}/\alpha_i)^2/2}, \tag{11}$$

where c_i are determined from Eq.(9) [14].

3. Imaginary Part of the Fermi Potential for Nuclear Interaction

In order to parametrize the short-range nuclear force, we use the optical theorem formulation of nuclear fusion reactions [16]. The total elastic nucleus-nucleus amplitude can be written as

$$f(\theta) = f^c(\theta) + \tilde{f}(\theta), \tag{12}$$

where $f^c(\theta)$ is the Coulomb amplitude and $\tilde{f}(\theta)$ can be expanded in partial waves

$$\tilde{f}(\theta) = \sum_l (2l+1)e^{2i\delta_l^c} f_l^{n(el)} P_l(\cos\theta). \tag{13}$$

In Eq. (13), δ_l^c is the Coulomb phase shift, $f_l^{n(el)} = (S_l^n - 1)/2ik$, and S_l^n is the l-th partial S-matrix for the nuclear part. For low energy we can write [16]

$$Im f_l^{n(el)} \approx \frac{k}{4\pi}\sigma_l^r,$$

where σ_l^r is the partial wave reaction cross section. For the dominant contribution of only s-wave, we have

$$Im f_0^{n(el)} \approx \frac{k}{4\pi}\sigma^r, \tag{14}$$

where σ^r is conventionally parameterized as

$$\sigma^r = \frac{S}{E}e^{-2\pi\eta}, \tag{15}$$

$\eta = \frac{1}{2kr_B}, r_B = \frac{\hbar^2}{2\mu e^2}, \mu = m/2$, and S is the S-factor for the nuclear fusion reaction between two nuclei.

In terms of the partial wave t-matrix, the elastic scattering amplitude, $f_l^{n(el)}$, can be written as [16]

$$f_l^{n(el)} = -\frac{2\mu}{\hbar^2 k^2} < \psi_l^c \mid t_l \mid \psi_l^c >, \tag{16}$$

where ψ_l^c is the Coulomb wave function.

Introducing a new quantity U as the imaginary part of t_0,

$$U = Im(t_0), \tag{17}$$

we have

$$\frac{k}{4\pi}\sigma^r = -\frac{2\mu}{\hbar^2 k^2} < \psi_0^c \mid U \mid \psi_0^c > . \tag{18}$$

For our case of N Bose nuclei, to account for a short range nature of nuclear forces between two nuclei, we introduce the following Fermi pseudo-potential $V^F(\vec{r})$,

$$ImV^F(\vec{r}) = -\frac{A\hbar}{2}\delta(\vec{r}), \tag{19}$$

where the short-range nuclear force constant A is determined from Eqs.(15) and (18) to be [14]

$$A = \frac{2Sr_B}{\pi\hbar}. \tag{20}$$

We note that Eq.(20) above relates the short-range nuclear force constant A to experimentally extracted value of the S-factor S in Eq.(15). The S-factor is a nuclear force strength factor (or coupling constant) independent of Coulomb force contribution which is parameterized by the Gamow factor $e^{-2\pi\eta}$ in Eq.(15). The values of the S-factor have been extracted from low-energy nuclear reaction cross-section using Eq.(15).

For a many Boson (deuteron) system, the two-body Coulomb wave function ψ_o^c in Eq.(18) is no longer applicable, and hence the Gamow factor $e^{-2\pi\eta}$ is not also applicable. Therefore we must now use an eigenstate solution Ψ (or Φ) of the many-body Hamiltonian, Eq.(2), which includes all pair-wise Coulomb interactions between deuterons. In the following section, we derive the fusion rates for many deuterons confined in a trap.

4. Fusion Rates

For N identical Bose nuclei confined in an ion trap, the nucleus-nucleus fusion rate is determined from the trapped ground state wave function Ψ as

$$\tilde{R} = -\frac{2}{\hbar}\frac{\Sigma_{i<j} < \Psi|ImV_{ij}^F|\Psi >}{< \Psi|\Psi >}, \tag{21}$$

where ImV_{ij}^F is the imaginary part of the Fermi potential given by Eq.(19).

The substitution of Eq.(3) into Eq.(21) yields [14]

$$\tilde{R} = \frac{AN(N-1)\Gamma(3N/2)}{2(2\pi)^{3/2}\Gamma(3N/2-3/2)}\frac{\int_0^\infty \Phi^2(\rho)\frac{1}{\rho^3}d\rho}{\int_0^\infty \Phi^2(\rho)d\rho}. \tag{22}$$

For large N, we use an approximate solution for $\Phi(\rho)$ (see Eq.(11))

$$\Phi(\rho) \approx \tilde{\rho}^{\frac{3N-1}{2}} e^{-(\tilde{\rho}/\alpha_t)^2/2} \tag{23}$$

where $\alpha_t = (\zeta/3)^{1/3}, \zeta \approx 2\sqrt{mc^2/2\pi\hbar\omega}\alpha N$, and $\tilde{\rho} = \sqrt{m\omega/\hbar}\rho$.
Using Eq.(23), we obtain from Eq.(22)

$$R_t = \Omega B N \omega^2, \tag{24}$$

where

$$B = \frac{3A}{8\pi\alpha}(\frac{m}{\hbar c}), \tag{25}$$

and Ω is the probability of the ground state occupation,

The average size $<r>$ of the ground-state for Bose nuclei confined in a trap can be calculated using the ground-state wavefunction, Eq.(23), and is related to ω by the following relation for the case of large N,

$$\omega^2 = \sqrt{\frac{3}{4\pi}}\alpha\left(\frac{\hbar c}{m}\right)n_B, \tag{26}$$

where $\alpha = e^2/\hbar c.$ and $n_B = N/ < r >^3$ is Bose nuclei density in traps. In terms of n_B we can rewrite R_t, Eq.(24), as

$$R_t = \sqrt{\frac{3}{4\pi}}\Omega B\alpha\left(\frac{\hbar c}{m}\right)Nn_B \quad . \tag{27}$$

For the case of multiple ion traps in a metal with each trap containing N Bose nuclei, we define a trap number density n_t (number of traps per unit volume) as $n_t = n_B/N =< r >^{-3}$. where N is the average number of Bose nuclei in a trap. For this case, the total ion-trap nuclear fusion rate R per unit time and per unit volume can be written as

$$R = \sqrt{\frac{3}{4\pi}}\Omega B\alpha\left(\frac{\hbar c}{m}\right)n_t Nn_B \quad . \tag{28}$$

We note a very important fact that both R_t and R do not depend on the Gamow factor in contrast to the conventional theory for nuclear fusion in free space. This is consistent with the conjecture noted by Dirac [17] and Bogolubov [18] that boson creation and annihilation operators can be treated simply as numbers when the ground state occupation number is large. This implies that for large N each charged boson behaves as an independent particle in a common average background potential and the Coulomb interaction between two charged bosons is suppressed. Furthermore, the rates R_t and R are proportional to Ω which is expected to increase as the operating temperature decreases. Since n_B is nearly constant and $n_t = n_B N^{-1} = <r>^{-3}$ in Eq.(28), and the average distance between nearest two deuterons is $n_D^{-1/3} \approx 2.45$Å, the nuclear fusion rate per unit volume, R, given by Eq.(28) is proportional to n_B^2. This implies that R can be made larger by increasing the deuteron density. Since metal powders or blacks can provide larger total surface area, they are more desirable and efficient systems for achieving steady high density states of deuterons in cluster-traps than bulk metals. This may explain why Arata and Zhang observe a larger effect and can reproduce their former results consistently using Pd blacks (powders) of $<r>\approx$ 40nm while others have experienced difficulties in attaining reproducible results. However, N decreases as $<r>$ decreases, and the CQ state may not be achieved with a much smaller value of N. Furthermore, Eq.(28) also becomes inaccurate as N becomes smaller.

5. Application to Deuteron-Deuteron Fusion

5.1 Multiple-Trap Experiment

For deuteron-deuteron (DD) fusion via reactions $D(d,p)T$ and $D(d,n)^3He$ the S-factor is $S = 110keV\text{-}barn$ and hence we find from Eq.(20) the nuclear rate constant to be

$$A \approx 1.5 \times 10^{-16} cm^3/sec, \tag{29}$$

and from Eqs.(25) and (29), we have

$$B = 2.6 \times 10^{-22} sec. \tag{30}$$

In order to apply our theoretical results for R_t and R, Eqs.(27) and (28), to the results of Arata and Zhang [3-5], we assume a transient situation in which a constant net (in and out) flux of deuterons is maintained across the surfaces of each Pd atom cluster so that deuterons inside the cluster are mobile while maintaining a constant density of $n_D \approx n_{Pd}$, i.e., each Pd atom cluster acts as an effective trap for deuterium ions ("cluster-trap").

For the experiments by Arata and Zhang [3-5], $3g$ of Pd blacks (powders) consisting of $\sim$ 40 nm average size clusters was used. $3g$ of Pd blacks contain $\sim 1.7 \times 10^{22}$Pd atoms ($\approx 3g \times (6 \times 10^{23})/106.4g$ where 106.4g is a molar weight of Pd). Since the volume density of Pd metal is 12.02 gcm^{-3}, the number density of Pd atoms is $n_{Pd} \approx 6.8 \times 10^{22} cm^{-3}$. Since they achieved a high deuteron density of $n_D \approx n_{Pd}$ ($n_D = n_B$), we have $n_D \approx 6.8 \times 10^{22} cm^{-3}$ and also $N_T \approx 1.7 \times 10^{22}$ D atoms in 3g of Pd blacks. For a cluster of $<r> \approx 40nm (= 4 \times 10^{-6} cm)$ size, it contains $N = n_D <r>^3 \approx 4.35 \times 10^6$ D's. We note that $N <r>^{-3} = n_D$ in Eqs.(27) and (28), and the average distance is $n_D^{-1/3} \approx 2.45$Å between nearest two deuterons.

Using the above numerical values, we have from Eq.(27)

$$R_t = \Omega B(10^{34}) sec^{-2} \text{ per cluster-trap}, \tag{31}$$

where B is given in units of seconds. From Eq.(28) with $n_t = n_D/N = < r >^{-3} = 1.56 \times 10^{16} cm^{-3}$, we obtain for the DD fusion rate

$$R = n_t R_t = \Omega B(1.56 \times 10^{50}) sec^{-2} cm^{-3}, \tag{32}$$

with B given in units of second.

For DD fusion via reactions $D(d,p)T$ and $D(d,n)^3He$, $B = 2.6 \times 10^{-22} sec$ (see Eq.(30)), and hence we obtain from Eq.(31),

$$R_t = \Omega(2.6 \times 10^{12}) sec^{-1} \text{ per cluster-trap}, \tag{33}$$

and from Eq.(32),

$$R = \Omega(4 \times 10^{28}) sec^{-1} cm^{-3} . \tag{34}$$

For reaction (1) occurring in the coherent quantum state (CQS), the cross-section ($\sigma_{CQS}(dd \rightarrow {}^4He)$) for reaction $dd \rightarrow {}^4He$ may be larger than that of reactions, $D(d,p)T$ or $D(d,n)\ {}^3He$. If the effective S-factor for $\sigma_{CQS}(dd \rightarrow {}^4He)$ happens to be larger than those for $\sigma(D(d,p)T)$ and $\sigma(D(d,n)\ {}^3He)$, it can provide a theoretical explanation of the anomalous effect [3-11].

If the predominant production of T over ${}^4He$ or ${}^3He$ as claimed previously by many is definitively confirmed in future experiments, we need to investigate other possible many-body effects and mechanisms such as possible modification of the S-factors in different reaction channels due to many-body nature of the system.

For DD fusion via reaction (1), the experimental results [3-11] indicate that the S-factor for reaction (1) is greater by at least 10^6 than that for reactions $D(d,p)T$ and $D(d,n)^3He$ implying $B = 2.6 \times 10^{-16} sec$ for this reaction. Using this value of B in Eqs.(31) and (32), we obtain for reaction (1),

$$R_t^{^4He} = \Omega(2.6 \times 10^{18}) sec^{-1} \text{ per cluster-trap}, \tag{35}$$

and

$$R^{^4He} = \Omega(4 \times 10^{34}) sec^{-1} cm^{-3}. \tag{36}$$

The reaction rate per deuteron (D) is then

$$\Lambda^{^4He} = R^{^4He}/n_D = \Omega(6 \times 10^{11}) sec^{-1} \text{ per } D \ . \tag{37}$$

The observed excess heat production rate is $\sim 5W$. If the excess heat produced is due to reaction (1), the reaction rate is $R_{AZ}^{^4He} = 1.3 \times 10^{12}$ $(D + D)$ reactions/sec, and hence the reaction rate per D is

$$\Lambda_{AZ}^{^4He} = \frac{R_{AZ}^{^4He}}{N_T} = 0.76 \times 10^{-10} sec^{-1} \text{ per } D, \tag{38}$$

which is comparable to $\Lambda_{FP}^{^4He} \approx 10^{-10} sec^{-1}$ per D originally claimed by Fleischmann et al. [1]. Comparing Eq.(37) with Eq.(38), we infer that

$$\Omega < 10^{-22} \ . \tag{39}$$

Comparison of $\Lambda_{FP}^{^4He} \approx 10^{-10} sec^{-1}$ per D for reaction (1) with $\Lambda_{Jones}^{n} \approx 10^{-23} sec^{-1}$ per D for reaction $D(d,n)^3He$ claimed by Jones et al. [2], suggests that the S-factor for reaction (1) is greater by 10^{13} than that for reactions $D(d,p)T$ and $D(d,n)^3He$ and hence $B = 2.6 \times 10^{-9} sec$. For this case, we have

$$\Omega \approx 10^{-29} \ . \tag{40}$$

We note that $\Omega \approx 10^{-29} \sim 10^{-22}$ is much larger than the Gamow factor at ambient temperatures. Additional experimental measurements are needed to extract a more precise value of Ω.

5.2 Single-Trap Experiment

Recently, we suggested experiments for proof of the principle to test the proposed CQS nuclear fusion mechanism [15] based on the fusion rate R_t, Eq.(27).

In a recent experiment [19], $^9Be^+$ ions were confined in a cylindrical Penning trap consisting of an electrostatic quadrupolar potential and a uniform magnetic field. A typical density achieved is $\sim 4 \times 10^8 cm^{-3}$ with $N = 10^6$. If a similar density for deuterons, $n_D = n_B = 4 \times 10^8 cm^{-3}$ with $N = 10^6$ can be achieved in a same type of experiment, the fusion rate R_t, Eq.(27) is

$$R_t \approx \Omega B(1.35 \times 10^{19}) sec^{-2} \ . \tag{41}$$

For reactions, $D(d,n)\ ^3He$ and $D(d,p)T$, we have $B = 2.6 \times 10^{-22} sec$ (see Eq.(30)) and hence the fusion rate $R_t^{n+p}(\Omega)$ is from Eq.(41),

$$R_t^{n+p}(\Omega) \approx \Omega(3.5 \times 10^{-3}) sec^{-1} \ . \tag{42}$$

At room temperatures with $\Omega = 10^{-29}$ (see Eq.(40)), we have

$$R_t^{n+p}(10^{-29}) \approx 3.5 \times 10^{-32} sec^{-1}, \tag{43}$$

which implies that the effect is too small to be detected. On the other hand, if we can achieve $\Omega \approx 10^{-1}$ by cooling deuterons ($nK \sim mK$), then we have

$$R_t^{n+p}(10^{-1}) \approx 3.5 \times 10^{-4} sec^{-1}, \tag{44}$$

which is a detectable rate for neutrons. It is known that one can achieve temperatures of $\sim mK$ for the case of anti-protons by injecting electrons [20].

A more promising case is for reaction (1), $D + D \rightarrow {}^4He$. For this reaction, the inferred value of B is $B = 2.6 \times 10^{-9} sec$, and the fusion rate $R_t^{^4He}$ is from Eq.(41),

$$R_t^{^4He}(\Omega) \approx \Omega(3.5 \times 10^{10}) sec^{-1} \quad . \tag{45}$$

At room temperatures with $\Omega = 10^{-29}$, Eq.(45) yields

$$R_t^{^4He}(10^{-19}) \approx 3.5 \times 10^{-19} sec^{-1}, \tag{46}$$

which is again impossible to detect as in the case of Eq.(43). However, if we can achieve $\Omega \approx 10^{-10}$ by cooling deuterons in a trap with injection of positrons, we have from Eq.(45),

$$R_t^{^4He}(10^{-10}) \approx 3.5 sec^{-1}, \tag{47}$$

which is a detectable rate for ${}^4He$. Therefore, it is worthwhile to carry out ion-trap experments with cooled deuterons as tests of the proof of the principle for our CQS nuclear fusion mechanism.

6. Summary and Conclusions

Using the recently developed theoretical method ("Equivalent Linear Two-Body Method") [13], we have obtained an approximate ground-state solution of many-body Schrödinger equation for a system of N identical charged bosons confined in an isotropic harmonic oscillator potential. The solution is expected to be accurate for large N [13]. The solution is used to obtain theoretical formulae for estimating the probabilities and rates of nuclear fusion for N identical Bose nuclei confined in an ion trap. Our results show that the Coulomb interaction between two charged bosons is suppressed for the large N case. This is consistent with the conjecture made by Dirac [17] and used by Bogolubov [18] that each interacting neutral boson behaves as an independent particle in a common average background for the large N case. The fusion rate formula is applied to deuteron-deuteron fusion rates for deuterons trapped in metal atomic clusters. In the following, we summarize predictions and consequences of our theoretical formulation and Eqs.(27) and (28), for nuclear fusion of Bose nuclei (deuterons) confined in ion traps or trapped in metal powders (clusters).

a. The fusion rate R_t Eq.(27), and R, Eq.(28), does not depend on the Gamow factor, but instead depends on the probability of the ground-state occupation (Ω). Ω is expected to increase as the temperature decreases. This implies that the fusion rate increases as the temperature decreases. The experimental data suggest $\Omega < 10^{-22}$ [3-5] or $\Omega \approx 10^{-29}$ [1,2]. Although there have been some claims of observing higher fusion rates at higher temperatures from electrolysis experiments, they are not yet definitive and conclusive. Our contrary prediction can be tested by future experiments of Arata-Zhang type or single-trap type (described below in (d)).

b. The fusion rate R, Eq.(28), is proportional to n_D^2 where n_D is the deuteron density. Since metal powders or blacks can provide larger total surface area, they are more desirable and efficient systems for achieving steady high density states of deuterons in cluster-traps than bulk metals. This may explain the reproducible results of Arata-Zhang [3-5] who used Pd powders with $<r> \approx 40nm$, while others had difficulties in obtaining reproducible results from electrolysis experiments with heavy water using bulk metal cathodes.

c. Our theoretical formulation is based on deuterons (positive deuterium ions), but is also applicable to deuterion plasma (deuterons and electrons). We need transition metal (such as Pd, Ti, Nb, Zr, etc.) powders which can lower activation energies of D_2O or D_2 and convert them into deuterium ions or atoms efficiently as they make contact with and enter into the metal cluster (trap).

d. As a test of the proof of the principle for our CQS nuclear fusion mechanism, we propose single-trap experiments in which deuterons are confined in an ion trap and cooled by injection of positrons.

More detailed descriptions of some parts of this paper will be published elsewhere [21].

Appendix: Alternative Derivation

In this appendix, we describe an alternative derivation of the ground-state wavefunction and the fusion rate formula, Eqs.(24) and (25).

To describe ground-state properties of the system of the N Coulomb, interacting bosons, we start the following equation for the mean-field theory for bosons

$$[-\frac{\hbar^2}{2m}\Delta + \frac{m\omega^2}{2}r^2 + (N-1)e^2\int\frac{d\vec{r}'}{|\vec{r}-\vec{r}'|}|\tilde{\phi}(\vec{r}')|^2]\tilde{\phi}(\vec{r}) = \mu\tilde{\phi}(\vec{r}), \qquad (A-1)$$

where the chemical potential μ is related to the ground-state energy E and particle number N by the general thermodynamic identity

$$\mu = \frac{\partial E}{\partial N}. \qquad (A-2)$$

For the case of $N >> 1$ and $N\gamma_c >> 1$, where $\gamma_c = 2\sqrt{mc^2/\hbar\omega}$, the ground-state solution of Eq.(A-1) is found to be

$$|\tilde{\phi}(\vec{r})|^2 = \frac{3}{4\pi N\gamma_c}\theta((\gamma_c N)^{2/3} - r^2\frac{m\omega}{\hbar})(\frac{m\omega}{\hbar})^{3/2}, \qquad (A-3)$$

where θ denotes the positive unit step function. Straightforward calculations with $|\tilde{\phi}(\vec{r})|^2$ from Eq.(A-3) yield .

$$\mu = \frac{3}{2}\hbar\omega(\gamma_c N)^{2/3}, E = \frac{9}{10}\hbar\omega(\gamma_c)^{2/3}N^{5/3}. \qquad (A-4)$$

Substitution of Eq.(A-3) into Eq.(21) leads to the previous result for fusion rate given by Eqs.(24) and (25). From Eq.(A-3), we obtain the size d of the ground state for Bose nuclei as $d = \sqrt{\frac{\hbar}{m\omega}}(\gamma_c N)^{1/3}$, which is related to ω by the following relation for the case of large N,

$$\omega^2 = \alpha(\frac{\hbar c}{m})n_B, \qquad (A-5)$$

instead of Eq.(26). For this alternative derivation, all formulae for fusion reaction rates, Eqs.(27), (28), (31-37), (41-47) are to be multiplied by a factor of 2.

REFERENCES

[1] M. Fleischmann, S. Pons and M. Hawkins, J. Electroanal. Chem. **261**, 310 (1989); for some corrections see J. Electroanal. Chem. **263**, 187 (1989).

[2] S. Jones et al., Nature **338**, 737-740 (April 1989).

[3] Y. Arata and Y.-C. Zhang, Jpn. J. Appl. Phys. **37**, L1274 (1998).

[4] Y. Arata and Y.-C. Zhang, Jpn. J. Appl. Phys. **38**, L774 (1999).

[5] Y. Arata and Y.-C. Zhang, Proceedings of the Japan Academy, Vol. 75, Ser. B, No. 10 (1999), pp. 281-286.

[6] B.F. Bush, J.J. Lagowski, M.H. Miles, G.S. Ostrom; J. Electroanal. Chem., (1991) **304**, 271.

[7] B.F. Bush, J.J. Lagowski, M.H. Miles, Proceedings of 6th International Conference on Cold Fusion (ICCF-6), Hokkaido, Japan, October 13-18, 1996, Vol. 2 p, 622.

[8] B.F. Bush and J.J. Lagowski, Proceedings of 7th International Conference on Cold Fusion (ICCF-7), Vancouver, Canada, April 19-24, 1998.

[9] M.H. Miles, B.F. Bush, Proceedings of 4th International Conference on Cold Fusion (ICCF-4), Lahaina, Maui, Hawaii, December 6-9, 1993, Vol. 2, 6-1.

[10] L.C. Case, Proceedings of ICCF-7, 1998, pp. 48-50.

[11] R. Stringham et al., Proceedings of ICCF-7, 1998, pp. 361-365.

[12] Y.E. Kim and A.L. Zubarev, Proceedings of ICCF-7, 1998, pp. 186-191.

[13] Y.E. Kim and A.L. Zubarev, J. Phys. B: At. Mol. Opt. Phys. **33**, 55 (2000).

[14] Y.E. Kim and A.L. Zubarev, Fusion Technology **37**, 151 (2000).

[15] Y.E. Kim and A.L. Zubarev, "Effective Linear Two-Body Method for Many-Body Problems in Atomic and Nuclear Physics", invited paper presented at the First Asia-Pacific Conference on Few-Body Problems in Physics, Noda/Kashiwa, Japan, August 23-28, 1999, to be published in Few Body Systems Supplement.

[16] Y.E. Kim and A.L. Zubarev, Few-Body Systems Suppl. **8**, 324 (1995).

[17] P.A.M. Dirac, *"The Principles of Quantum Mechanics"* (second edition), Clarendon Press, Oxford 1935, Chapter XI, Section 62.

[18] N. Bogolubov, Journal of Physics **11**, 23 (1947).

[19] W.M. Itano et al., Science **279**, 686 (30 January 1998).

[20] J. Eades and F.J. Hartmann, Rev. Mod. Phys. **71**, 373 (1999).

[21] Y.E. Kim and A.L. Zubarev, "Ultra-Low Energy Nuclear Fusion of Bose Nuclei in Many-Body Environments", invited paper presented at Workshop on Anomalous Nuclear Fusion Reactions, Osaka University, March 17, 2000, to be published in Genshikaku-Kenkyu (Nuclear Physics Research).

Conference Proceedings Vol. 70
"ICCF8"
F. Scaramuzzi (Ed.)
SIF, Bologna, 2000

Theoretical Framework for Anomalous Heat and ^{4}He in Transition Metal Systems

Scott R. Chubb and Talbot A. Chubb
Research Systems, Inc., 9822 Pebble Weigh Ct., Burke. VA 22015-3378 USA

Introduction

Cold Fusion has been plagued with misconceptions about what is and is not possible, based on the "Laws" of Quantum Mechanics. An important reason for this is the seemingly impossibly large difference in length-scale between nuclear- and atomic- processes. In conventional fusion, these scales remain "so far apart" that they "effectively" don't "talk" to each other, usually. However, electromagnetic interactions (EMI's) have infinite range. For this reason, it is possible that EMI's "can" "explain" how this "apparent" problem can be eliminated.

A somewhat surprising feature of EMI's also is they can do this in the "seemingly" impossible situation in which "each of the particles" that is involved "effectively" has vanishingly small momentum. A key point in understanding how this can become possible is associated with how "momentum" and "length-scale" are related to each other. Although at high energy, the relationship between these quantities can be "viewed" as being localized, this is because when the associated Debroglie wavelengths ($\lambda_{Debroglie}$'s) of "individual particles" do not have appreciable overlap, the momentum p of an individual "particle" can be treated in terms of a classical picture, in which p=mv, where m is the mass of the particle, and v is its velocity.

As p-> 0, this picture breaks down because "uncertainties" in p and position (x) become intertwined with the electromagnetic field. For this reason, boundary effects and symmetry, through (implicit and explicit) EMI's lead to forms of coherence that explain well-known effects (Mossbauer effect, super-conductivity, Bragg-scattering, heat and electrical conductivity in solids) in which momentum can be shared by "many" "particles" "instantaneously." Because EMI's are also responsible for non-separable forms of coupling between electromagnetic and nuclear processes (in which the coordinates associated with these forms of forces depend on each other) in one form of reaction (D+D->^{4}He), it is theoretically possible that the two forms of interaction can become coupled. For this reason, it is also plausible that this form of interaction can become dominant in situations in which non-local, coherent effects that occur as p->0 (or when related limits, associated with large values of $\lambda_{Debroglie}$) become dominant.

An important point is that when the $\lambda_{Debroglie}$'s of many particles become sufficiently large (or are constrained by symmetry to particular values through the usual rules of Quantum Mechanics), coherent coupling between charged particles and an electromagnetic field can occur even in the limit in which the combined momentum of the particles becomes vanishingly small. The associated effect can explain how momenta can be transferred from an isolated location to many locations, all at once, without high energy being transmitted to any individual location. We explore the associated implications of this on Cold Fusion-related phenomena.

"Inside and Outside the Box" and the "Organizing Principles" of "Conventional Fusion"

Logical thought requires "rules." In physics, the logical "rules" follow from Newton's laws of motion, Maxwell's Equations, Quantum Mechanics, and Relativity. Because these "rules" provide a framework, often they can be self-limiting. For example, sometimes physicists misinterpret the "rules," simply because they are conditioned to look at them in a particular way. They become "used to" a particular "worldview." The "worldview" can be thought of as a kind of "box" that defines a "comfort zone." Often, the "box" is tied to the way we have learned a particular subject. Different people view the "box" in different ways. Kuhn[1] refers to it, abstractly, as it relates to science, as a "paradigm." Others have not been as open-minded[2].

Fig. 1 shows a pictorial representation of "conventional" fusion reactions super-posed on an idealized representation of the "box", associated with what is commonly viewed as "conventional" (labeled "inside the box") and "unconventional" (labeled "outside the box") science. In this schematic, all reactions originate from a configuration in which two deuterons (shown as proton-neutron pairs) overlap with each other in a manner that forms a configuration (shown in the center of the plot) that resembles an excited state of a ^{4}He nucleus. The two, dominant reactions (D+D->^{3}He+n, and D+D->^{3}H+p) that occur in free space are essentially "blind" to the presence of the electromagnetic interaction (EMI). For this reason, it is possible to treat these reactions within a framework in which the dependence of the reaction on electromagnetic interactions is independent of its dependence on the nuclear (strong force) interaction. This means that in these reactions, the associated wave functions describing the initial and final states do not couple the nuclear and electromagnetic interactions. As a result, the general reaction rate expression (which is described below) effectively "precludes" the "strong force" from "talking" to the "electromagnetic force," by construction. The figure schematically illustrates this point through the labels ("ignore E. M."),

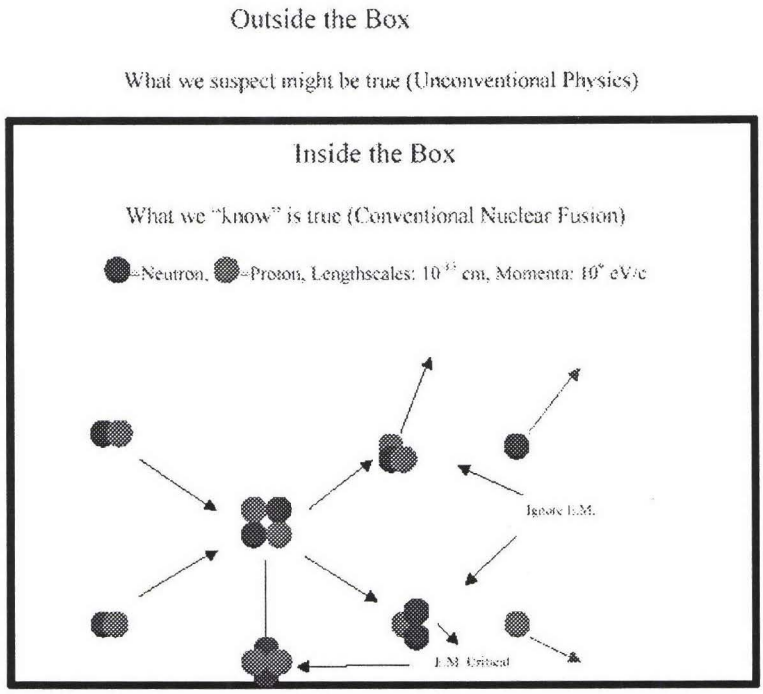

Fig. 1: Pictorial representation of conventional fusion reactions. Darkened and lightened circles, respectively represent neutrons and protons.

next to the arrows that are shown in the right portion of the figure. Also shown is the remaining fusion reaction (D+D->^{4}He). This reaction occurs rarely in conventional fusion. For this reason, in the figure it is shown as occurring at the "boundary" of the "box". A second reason we have drawn it at the boundary is that it violates a "paradigm" that many nuclear physicists believe to be valid: in conventional fusion, the strong and electromagnetic interactions remain uncoupled. For this reason, it is widely believed that the final (D+D->^{4}He) reaction should rarely occur and the two remaining

reactions should occur with roughly the same probability. However, the D+D->^{4}He does occur, and the reason that it is not frequently observed is well-understood: it violates energy-momentum conservation unless a high energy momentum gamma ray is emitted, and the associated EMI involves a complicated (quadrupolar) coupling between nucleon spins (that occurs as a second order electromagnetic process). Two important points are: 1. although this final reaction occurs infrequently relative the others, when it occurs, the "nuclear" and "electromagnetic" interactions do "talk to each other", and 2. it occurs rarely because the associated processes involve overlap between two "particles" at a single location.

Motivational Physics for Getting Outside the Box

Part of the confusion with the "box" associated with conventional nuclear physics involves the definition of momentum p: for a single charged particle, p does not equal mass (m) times velocity (v); the "rules" of the "box" are: for a particle possessing charge q, mv=p-q/cA, where A (the vector potential) is associated with the electromagnetic interaction, and c is the speed of light. Although this rule is based on classical physics, how and where it applies "seems" to have been a source of confusion. The "rule" follows from the "box" defined by classical physics. (Miss-assumptions about this rule not only "appear to have led to confusion about Cold Fusion" but to more serious problems. For example, Mills apparently has mistaken this equality[3] and misrepresented the Bohr theory, as a consequence.)

An example of the importance of this distinction occurs in the p->0 limit, when "many" particles "share" a common density ρ_o. When this occurs, mv, which is proportional to the current J (provided ρ_o is uniformly constant[4]), becomes proportional to A. But A, which is defined by the static wave equation ($-\nabla^2 A \equiv \frac{4\pi J}{c}$), then obeys a Helmholtz equation[4] ($-\nabla^2 A \equiv \frac{-4\pi q^2 \rho_o A}{mc^2}$) that results in A asymptotically vanishing beyond a critical coherence length, where J approaches a constant value. This occurs even in the absence of an applied electromagnetic field (EMF). The resulting picture explains the phenomenon of super-conductivity. It also explains how as p->0, super-conductivity not only is present, but because the current vanishes at some boundary, surrounding the region where superconductivity occurs, the effects of boundaries may result in the expulsion of magnetic flux when p=0 (the Meissner effect) or flux quantization[4], when p does not vanish but takes on values that are consistent with the associated rules (defined by "the box") associated with the requirements of quantum mechanics[4].

The basis of both phenomena is that p does not equal "mv"; in situations where the DeBroglie wavelengths of "particles" become sufficiently large, "particles" become "wavelike." In this kind of situation, the average value of the gradient of the phase of the associated collection of waves (which is described by the many-body wave function) defines the momentum. The important point is that the "phase of the many-body wave function," as opposed to a quantity related either directly to the current or to "mass x velocity" defines how the momentum behaves. When p->0, this quantity can be affected in ways that are non-local in character. This may occur because non-local changes in A can significantly alter the value of the phase. Because a priori it is not possible to predict if a solid is at rest or in motion, for example, its center-of-mass wave function can be altered by an arbitrary complex number. This introduces the possibility of an arbitrary gauge transformation in the definition of the A that applies inside and outside a solid. Because in the p->0 limit, it becomes possible to determine if the solid is in motion or at rest, the associated arbitrariness in "gauge" is removed. Not only does this mean that the associated "gauge symmetry" becomes broken, but physical effects (for example, the expulsion of magnetic flux, or spontaneous lattice recoil [as in the Mossbauer effect]) can occur. The resulting coherence can be viewed in different ways, within the framework (the "box") associated with a particular discipline.

In similar ways, effects of periodic order and other symmetries can become important in situations in which the wave-like character associated with large DeBroglie wavelengths becomes important. The important point is that because momentum is associated with wave-like behavior, it can change suddenly, in unexpected ways, on arbitrarily short time-scales. These changes can result in "instantaneous" changes in which large amounts of momentum coherently are shifted to many particles, and vice-versa. How or if this occurs is dictated by the dynamics of the many-body system.

More Precise Physics: Multiple Scattering

The exact problem is formidable. It involves solving the reaction rate problem for the (many-body) potential V that interacts with all charged particles. To understand how reaction rates in nuclear (as well as other) processes can be affected either through coherence that results as p->0 or (in a less restrictive sense) when symmetries constrain how p may vary during particular forms of interaction, it is not necessary to address all aspects of this problem. In particular, the associated coherence occurs as a result either of degeneracy or through the interactions between nearly degenerate states. The starting point of the analysis is general: we consider the problem of evaluating reaction rates, for a many-body system in which a perturbing potential V is present that asymptotically is assumed to have vanished in the distant past. Associated with the evaluation of reaction rate is the time evolution of the overlap $<E^{'-}|E^{+}>$ between an outwardly propagating many-body scattering state $|E^{+}>$ (defined by the assymptotic limit of the exact many-body state$|\Psi_E(t=time)>$: $|E^{+}> \equiv \lim_{t\to\infty}|\Psi_E(t)>$) with any of the possible initial, inwardly propagating states $|E^{'-}> (\equiv \lim_{t\to-\infty}|\Psi_{E'}(t=time)>)$. It follows from the asymptotic $(t\to\infty)$ limit of the well-known Lippmann-Schwinger equation that:

$$<E'^{-}(t)|E^{+}(t)>=<E'^{-}(0)|E^{-}(0)>+\frac{e^{\frac{-i(E-E'+i\varepsilon\hbar)t}{\hbar}}}{E-E'+i\varepsilon\hbar}<E'^{-}(0)|V|\Psi_E(0)> \qquad (1)$$

Here, implicitly, $t\to\infty$, with the infinitesimal variable ε approaching zero, constrained by $1/\varepsilon > t$.

In single-particle scattering theory, Eq. 1 is an integral representation of the Schroedinger equation. In many-body physics, it is equivalent to the Dyson equation, provided a "suitable" definition of V is employed. In fact, in practical applications involving many-body physics, V is never "known" exactly and is usually approximated using information provided by an approximate representation. Specifically, an important reason for using an approximate form for V is that usually neither V or $|\Psi_E(t)>$ is known explicitly. However, to address the more general problem of understanding how non-local interactions can evolve in many-body systems, it is not necessary to solve for either of these quantities. Instead, an alternative procedure, involving information associated with the underlying boundary conditions (and singular behavior of the wave function) may be employed. In this alternative formulation, "V" is replaced formally, using the kinetic energy operator $\hat{T}$ associated with the underlying many-body Schroedinger equations for $|\Psi_E(t)>$ and $|E^{-}(t)>$. This formal construction, which is a generalization of a standard, multiple-scattering technique[5,6], that has been applied in atomic, molecular, and solid state physics problems, in essence, relates the formal problem associated with scattering from a particular potential (as in Eq. 1) to a non-local momentum-balance problem. In this alternative problem, the matrix element $<E^{-}(t)|\ V\ |\Psi(t)>$ is transformed into a quantity involving $|\Psi_E(t)>$, $|E^{-}(t)>$ and the

derivatives of these quantities, evaluated at "boundaries" of the region, where V either becomes singular or vanishes.

Specifically, when $|\Psi_E(t)>$ satisfies the many-body Schroedinger equation associated with the many-body potential U, and energy E, it follows that

$$(H-\hat{T})|\Psi_E(t)>=(E-\hat{T})|\Psi_E(t)>"\equiv"U|\Psi_E>, \qquad (2)$$

where, in the coordinate representation, $\hat{T}=-\hbar^2\sum_i\frac{\nabla_i^2}{2m_i}$ (m_i is the mass of the i^{th} particle (i=1,...,n)) is the many-body kinetic energy operator, and we have used the condition that $|\Psi_E(t)>$ is an eigenstate of H. Since a similar relationship holds when $<E'^{-}(t)|$ obeys a comparable Schroedinger equation associated with potential U', it follows that in a formal sense since $<E'^{-}(t)|V|\Psi_E(t)>\equiv<E'^{-}(t)|U-U'|\Psi_E(t)>$, that

$$<E'^{-}(t)|V|\Psi_E(t)>=(E-E')<E'^{-}(t)|\Psi_E(t)>+$$
$$+\int d^3r_1\int d^3r_2...\int d^3r_n\ \{\hat{T}\Psi^{-*}_{E'}(r_1,r_2...,r_n,t)\}\Psi_E(r_1,r_2...,r_n,t)-\Psi^{-*}_{E'}(r_1,r_2...,r_n,t)\{\hat{T}\Psi_E(r_1,r_2...,r_n,t)\} \qquad ,(3)$$

where $\Psi_E(r_1,r_2,...,r_n,t)\equiv<r_1,r_2,...,r_n|\Psi_E(t)>$, and $\Psi^{-}_{E'}(r_1,r_2,...,r_n,t)\equiv<r_1,r_2,...,r_n|E'^{-}(t)>$ are coordinate representations of $|\Psi_E(t)>$ and $|E'^{-}(t)>$.

Superficially, it might appear that the second term in Eq. 3 vanishes. In fact, this is not the case because of the implicit boundary conditions associated with Eqs. 1 and 2. In particular, because both the unperturbed and perturbed Hamiltonians are both Hermitean, E and E' are finite and real. But this means that at points where U and/or U' become singular, comparable singularities occur in the terms that involve $\hat{T}$ on the left-sides of Eqs. 2 and 3. As a consequence, surface terms (from discontinuities in one or more components of the gradients of one or both of the many-body wave functions) occur in the second term from regions that bound the locations where singularities in U and/or U' are present. Also, because $|\Psi_E(t)>$ and $|E'^{-}(t)>$ are not required to vanish (and may have appreciable overlap) in regions where U=U', it also follows that the second term on the right-side of Eq. 3 reduces to a sum of surface terms (through Greens theorem) at the boundaries of this region.

To understand the possible rates of reaction in Cold Fusion, we examine the situations associated with Eq. 1 in which the many-body states associated with $|E'^{-}>$ and $|E^{-}>$ are different. Because these states are different, the overlap matrix element $<E'^{-}(0)|E^{-}(0)>$ vanishes. This means that

$$|<E'^{-}(t)|E^{+}(t)>|^2=\frac{e^{2\varepsilon t}}{(E-E'+i\varepsilon\hbar)(E-E'-i\varepsilon\hbar)}|<E'^{-}(0)|V|\Psi_E(0)>|^2 \qquad ,(4)$$

from which it follows that

$$\frac{\partial|<E'^{-}(t)|E^{+}(t)>|^2}{\partial t}=\lim_{\varepsilon\to 0}\frac{2\varepsilon}{(E-E'+i\varepsilon\hbar)(E-E'-i\varepsilon\hbar)}|<E'^{-}(0)|V|\Psi_E(0)>|^2$$
$$=\frac{2\pi}{\hbar}\delta(E-E')|<E'^{-}(0)|V|\Psi_E(0)>|^2$$

$$\equiv \frac{2\pi}{\hbar}\delta(E-E')\left|\sum_i \iiint_{boundaries_i} d^{3n-1}r_i \quad \frac{\hbar^2}{2m_i}\hat{n}_i \bullet \{\bar{\Psi}_{E'}^{*}\vec{\nabla}_i\Psi_E - \vec{\nabla}_i\bar{\Psi}_{E'}^{*}\Psi_E\}\right|^2$$

$$\equiv \frac{2\pi}{\hbar}\delta(E-E')\left|< E'|\vec{\partial}_n|\Psi_E >\right|^2 \qquad (5)$$

The total reaction rate R is constructed by summing the right side of Eq. 5 over all possible final (many-body) states $E_{\{k\}}$, in which the energy of each state is represented by a weighted sum of single-particle states:

$$E_{\{k\}} \equiv \sum_k n_k \varepsilon(k) \qquad (6)$$

Here, $\varepsilon(k)$ = energy of single-particle state possessing eigenvalue k; n_k = weighting factor that accounts for its degeneracy/occupation. In a many-body system, involving a macroscopic number of particles, $E_{\{k\}}$ can be quite large, and, in general, when a sum is taken over all final states, many large and small terms can be involved on the right-side of Eq. 5. However, in situations where large degeneracy occurs (and a small number of values of n_k can become large), a single term or a small number of terms can become dominant. An example of this kind of situation, for example, occurs when periodic order causes a large number of eigenvalues to be periodic functions with respect to the set of wave-vectors G (reciprocal lattice vectors) that define the fourier transform of the underlying (periodic) potential. In particular, this form of symmetry can cause a significant number of states $\varepsilon(k)$ to become degenerate (for example, $\varepsilon(k)$ can = $\varepsilon(k+G)$ for a large number N of values of G; in particular, N can ~ number of unit cells). For illustrative purposes, suppose $E=N\varepsilon(k)$. The resulting expression for the total reaction rate R is

$$R_{E'\to anything} = \frac{\partial P_{E'\to anything}}{\partial t} = \frac{2\pi}{\hbar}\sum_k \delta(\varepsilon(k) - \frac{E'}{N})\frac{|<E'^{-}(0)|\vec{\partial}_n|\Psi_{E(k)}(0)>|^2}{N} \qquad (7)$$

The point is that as a result of the degeneracy, the energy $\varepsilon(k)$ that appears in the delta function is a small quantity, and the square of the many-body matrix element has been reduced by a factor of N. This illustrates the general effect: an N-fold degeneracy can reduce the effective reaction rate by a factor of N. It literally is as if a small "piece" of the reaction is distributed between each of the N-possible states associated with the degeneracy. When the degeneracy is the result of periodic order, this is equivalent to the idea that the reaction has been reduced as a result of it's being "shared" between N different locations.

Acknowledgement

We would like to thank Robert Bass for providing critical comments concerning the present manuscript and Roy Swanson for his previous contributions.

References

[1] T. S. Kuhn, *The Structure of Scientific Revolutions.* (Univ. of Chicago Press, Chicago, 1962) *Vol II*, 10.

[2]R. L. Park, *Voodoo Science:the Road from Foolishness to Fraud. (Oxford Univeriy* Press, Oxford, 2000).

[3]Fractional quantum numbers (as in Mills's theory) require that the many-body wave-function become multi-valued in the semi-classical limit in which the expectation value of the many-body momentum ($\propto \nabla\phi$, $\phi \equiv$ many – body wave function phase) approaches the single-particle momentum.

[4]R.P. Feynman, R. B. Leighton, M. Sands, The Feynman Lectures on Physics. (*Addison Wesley Publishing, Inc.*, New York, 1965), v 3, c 21, pp. 7-13.

[5]A. Gonis and W.H. Butler, Multiple Scattering in Solids. (Springer-Verlag, N.Y., 2000), 350 pp.

[6] J. Korringa, Physica 13,392 (1947). W. Kohn and N. Rostoker, Phys. Rev. 94, 1111 (1954).

Conference Proceedings Vol. 70
"ICCF8"
F. Scaramuzzi (Ed.)
SIF, Bologna, 2000

DEUTERON FLUXING AND THE ION BAND STATE THEORY

Talbot A. Chubb and Scott R. Chubb
Research Systems, Inc., 5023 N. 38th St., Arlington, VA 22207 USA

Abstract

In Cold Fusion, confusion exists as a result of conflicting intuitive pictures, one based on local physics, the other on non-local physics. The local picture, based on particle-particle interaction, has played a dominant role. The non-local "less-intuitive" picture, based on the known behavior of solids, places greater emphasis on the behavior of matter distributions and their interaction with the associated environment. The resulting description is consistent with the known laws of physics and the behavior of hydrogen, deuterium (D^+) and tritons in transition metals. In the non-local picture, we examine consequences of fluxes of deuterons passing through the surfaces of transition metals as associated with the occupation of D^+ ion band states and possible nuclear energy release.

Introduction

Lattice Induced Nuclear Chemistry (LINC) explains[1] radiationless release of nuclear energy in a deuterided metal by a process in which deuterium converts to helium-4. This process occurs through self-interaction, based on a standard many-body formulation, provided coherent effects associated with periodic order (and the associated degeneracy) become important. Important features are embodied in the inherently non-local forms of interaction that may occur as a result of periodic order. In particular, coherence, broken gauge symmetry, as well as a number of non-local forms of interaction that are not usually considered in nuclear reactions, all may have consequence in periodically ordered systems. The explicit nature and significance of the associated interaction is considered in a separate paper that is included in this collection[2]. Because the non-local interaction can be related to the time evolution of the associated overlap between many-body wave functions[2], emphasis is placed on the wave functions and overlap characteristics. This provides an alternative framework that can be used to obtain insight into the associated physics.

In this paper, we use the non-local picture to obtain an intuitive understanding of phenomena associated with the breakdown of periodic order, especially the significance of non-equilibrium phenomena at locations where order breaks down and related effects. In the idealization of periodic order, the associated many-body system conforms to the periodicity of a host crystallite[1,3]. We emphasize that the assumed configuration of the deuterium matter is unlike that of chemical or interstitial hydrogen in normal metal hydrides.Different forms of matter

Figure 1 illustrates some of the forms which matter can assume in response to embedding environments. The distributions are portrayed by their charge and mass distributions in space. Figs. 1a and 1b illustrate independent particle configurations.

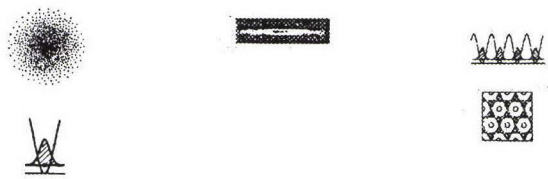

a) b) c) d)

Fig.1 Mass and charge density distributions of various forms of matter

Fig. 1a shows the mass density of the nucleus of an atom in free space. The nucleus is roughly spherically shaped with a radius of the order of fermis, appearing as a point on the scale of the Bohr atom. The bottom sketch of Fig. 1b shows the same nucleus when bound inside a metal. In the lowest vibration state the nucleus assumes a Gaussian distribution inside a parabolic potential well. The distribution is called the zero-point motion distribution. The top sketch of Fig. 1b shows the charge and mass density distribution of the electron bound in a hydrogen atom. The distribution is called the ground state electron orbital. Figs. 1c and 1d illustrate composite particle entities, in which independent particles have joined together to form a new single entity. Fig. 1c illustrates a Bose-Einstein condensate made up of sodium atoms in a magnetic trap. The top sketch of Fig. 1d illustrates a portion of a Bose-Einstein condensate made up of sodium atoms in an optical trap. The optical trap is created by interfering laser beams that create a sequence of potential wells within which the Bose-Einstein entity resides. The Bose-Einstein condensate is partitioned so that only a fraction of the mass and charge of each sodium atom resides in any one potential well created by the interfering laser beams. The bottom of Fig. 1d shows the charge and mass distribution of a hydrogen ion on the surface of Ni 111. It is a partitioned composite entity, which is described by a Bloch function. The ion band state attributes radiation-less deuteron fusion to the self-interaction of a partitioned composite particle entity described by a many-body deuteron wave function.

Observation suggests fluxing deuterons

The ion band state theory predicted the radiationless fusion of deuteron pairings within a many body-wave function so as to form helium-4. Observations of helium-4 in the electrolysis off-gasses in electrolytic deuterium-palladium experiments have demonstrated the production of helium-4 sourced at a rate of ~24 MeV per helium atom produced. Although these observations are in agreement with the theory, many experimenters say that heat production is a non-equilibrium process. McKubre states. "You need to maintain a flux of deuterons through the interface. The phenomenon that we are studying is not an equilibrium phenomenon. It is a phenomenon that is stimulated by departure from the steady state." In his critique of the ion band state theory Bob Bush says, "You have to have a deuteron wind." Arata and Zhang attribute the success of their DS-cathode experiments to a rapidly diffusing form of deuterium called "spill-over deuterium". Heat-producing catalytic experiments using gas-loaded Pd-on-carbon catalyst are carried out in containers that do not maintain a constant temperature over the catalyst bed,

which is conducive of a circulation of the deuterium through the bed. These experiments cause us to examine the role of deuteron fluxing in the observed heat production process.

A quantized matter field plus correlation

The physics of composite particle systems is modeled using second quantization theory in which a composite entity is described as a quantized matter field. In joining the composite entity, the separateness of the entering particles is lost. The quantized matter field is in turn described in terms of occupations of quantum states described by single particle wave functions. The occupations of the single particle states are called quasiparticles. The quasiparticles have the same charge and mass as that of the particles that joined into the composite entity. When the matter field is embedded in a metal crystal, the single particle states are solutions of the Schroedinger wave equation in which a charged particle is subject to a periodic potential provided by a host crystal lattice. The resulting wave functions are Bloch functions. When the many-body composite entity is composed of N_D deuterons in a crystallite containing N_{cell} unit cells of metal crystal, the lattice potential is modified by the distributed charge of the N_D added electrons provided by the N_D deuterium atoms and by the $(N_D\text{-}1)$ positive charges associated by the $(N_D\text{-}1)$ deuterons other than the test deuteron under consideration. The energy minimized Bloch function solution to this potential is called the mean field approximation wave function. The ion band state theory is concerned with small concentrations D^+_{Bloch}/Pd of Bloch function deuterons. At small concentrations using wave functions based on the bare lattice potential gives an adequate description of the system. It is important to note that this quantized matter field modeling is distinct from the modeling of a set independent particles subject to exchange. When all the quasiparticles are in the same state, all the single particle wave functions have the same distribution in physical space. This contrasts with and is inconsistent with the side-by-side distributions describing distinguishable, independent deuterons in a D_2 molecule.

Despite its success, the quantized matter field description of a many-body system composed of Bloch function ions in a lattice is an incomplete picture of a charged-particle many-body system. It does not contain the instantaneous point self-interaction between the multiple quasiparticles. The description does not include the point-particle interaction between quasiparticle pairs. To correct this deficiency point-particle interactions are added to the quantum field picture by including particle-particle correlation factors in the many-body wave function. For quasiparticle pairings inside metals the correlation factor modulates the strength of a 2-body wave equation in response to the point-particle self-interaction attraction or repulsion potential. The controlling self-interaction potential is the Coulomb repulsion between paired particles e^2/r_{12}. The correlation factor reduces the amplitude of the 2-particle wave function when particle separation r_{12} is small. "Where $particle_1$ is, $particle_2$ mostly isn't." The d-d correlation factor also includes the nuclear attraction between paired deuterons if the deuteron pairing has zero nuclear spin. There is no separation of the electrostatic and nuclear potentials. The attractive potential comes into play at small separation provided the correlation factor does not reduce the 2-particle wave function to zero amplitude at $|\mathbf{r}_{12}| = r_{nuc}$, where r_{nuc} is the range of the nuclear force. However, this condition never occurs as long as periodic symmetry iunbroken. When periodic symmetry is broken, energy minimization selects the side-by-side D_2 molecule configuration.

The paired quasiparticle wave function

The 2-particle wave function describing pairings of quasiparticles is a 6-dimensional function. Pairings of quasiparticles can be written in terms of a 2-body wave function of the form

$\Psi = \psi(\mathbf{r})\, g(\mathbf{r}_{12})$,

where $\mathbf{r}$ is the position vector in physical space and $\mathbf{r}_{12}$ is a separation vector in internal space. Here, $\psi(\mathbf{r})$ is a Bloch function in physical space and $g(\mathbf{r}_{12})$ is a Bloch function in separation space. In other words, $|\psi(\mathbf{r}+\mathbf{R}_j)| = |\psi(\mathbf{r})|$ and $|g(\mathbf{r}_{12}+\mathbf{R}_{12})| = ||g(\mathbf{r}_{12})|$, where $\mathbf{R}_j$ and $\mathbf{R}_{12}$ are independent Bravais lattice vectors. Figure 2 illustrates a possible form of $\psi(\mathbf{r})$ and $g(\mathbf{r}_{12})$. $\psi(\mathbf{r})$ has a maximum in each of N_{cell} unit cells of a crystallite in physical space, and has reduced amplitude at saddle points separating adjoining unit cells. $g(\mathbf{r}_{12})$ has a cusp-shaped minimum in each of N_{cell} unit cells of internal space in response to an $e^2/(N_{cell}^2\, r_{12})$ singularity in each of it N_{cell} coherence domain. Wave function Ψ transforms seamlessly into the 2-particle wave function

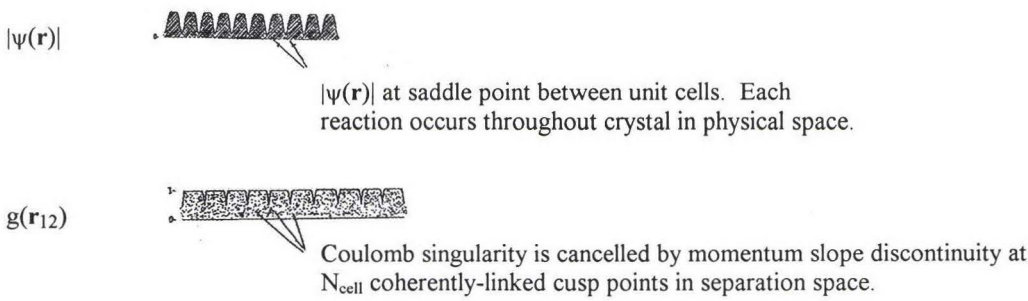

Fig. 2 Sketch of 2-quasiparticle wave function $\Psi = \psi(\mathbf{r})\, g(\mathbf{r}_{12})$ of Bloch function deuterons

describing a pair of independent non-interacting particles in the limit of large N_{cell} or of zero Coulombic potential self-interaction. The wave function is coherent over the N_{cell} volumes of physical and internal space. This means that calculation of physical quantities requires summing the contributions of both sets over N_{cell} unit cells.

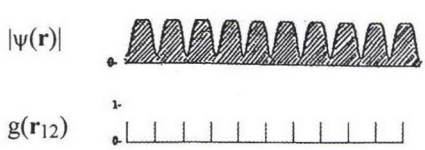

Fig. 3 The 2-quasiparticle wave function of Bloch function deuterons after coalescence

When a nuclear coalescence "reaction" occurs, a pairing of deuteron quasiparticles is replaced with a helium-4 nucleus in a reversible transition that preserves 2-particle Bloch symmetry. The periodic symmetry is preserved until irreversibility occurs by a dissipative process. The 2-deuteron wave function Ψ of Fig. 2 transitions reversibly into the coalesced form shown in Fig. 3. The cusps of function $g(\mathbf{r}_{12})$ become replaced with a repeated near-delta function configuration in which the deuterons are confined to a nuclear volume such that $|\mathbf{r}_{12}| < r_{nuc}$. The

coalescence occurs at the set of N_{cell} cusp points in $g(\mathbf{r}_{12})$. The cusp points are points at which internal momentum is discontinuous, allowing momentum to be transferred out of the coherent many-body entity. Coalescence causes only a small change in the charge density distribution in physical space. The spatial distribution $\psi(\mathbf{r})$ is slightly altered by a change in zero point motion caused by a change in the quantum of mass and charge, and is accompanied by a steepening of the charge gradient at the ordered domain's boundary in physical space. The change in charge density couples the nuclear configuration to the lattice, enabling momentum transfer to the embedding environment by electron and/or phonon scattering.

Intuitive Picture for Role of fluxing deuterons

A non-zero value of Ψ at $\mathbf{r}_{12} = 0$ permits an approximate calculation of reaction rate using time dependent perturbation theory, assuming that coupling to a dissipative medium converts each coalescence into an irreversible fusion reaction. Deuteron fluxing does not directly enter into this idealized, periodically-ordered picture. So what is the role of deuteron fluxing? In the real world, deuteron fluxing plays a role as a result of broken periodic order. In particular, as we have discussed elsewhere[2,3], in the presence of boundaries, coherent lattice recoil may result in non-local transfer of momentum, playing a dominant role in the associated channels for reaction.

An intuitive picture of a potentially key role played by fluxing deuterons is that of creating and maintaining a non-fluxing population of ion band state deuterons inside a set of small ordered domains inside a metal matrix. The domains may be area-like or volume-like. It is conjectured that in the deuterium-palladium system at high D/Pd ratio there can exist 2 forms of fluxing deuterons. The first form is a normal population of interstitial deuterons that diffuse down their concentration gradient by tunneling transitions into adjacent empty octahedral sites. But it is conjectured that there is a second population of wavelike deuterons that are described by Bloch functions with charge density distributions concentrated outside the charge density maxima of the normal interstitials, possibly having significant charge density within the tetrahedral site volumes. These deuterons have high tunneling rates between unit cells. We associated the spillover deuterium described by Arata and Zhang with this second population. This second population could be an important diffusing component in palladium at high D/Pd loading, where there is a scarcity of the empty sites needed for normal diffusion. It is speculated that this population could be formed on electrolysis cell cathodes at an overvoltaged interface between the electrolyte and the cathode surface.

This intuitive picture is based on transposing results from modeling by Jaksch et al. of atoms in an optical lattice.[4] The Jaksch modeling describes an array of potential wells created by interference between 2 standing waves from laser beams of slightly different wavelength. The superposition of the 2 standing waves creates an amplitude-modulated sequence of strong E-field volumes that serve as energy traps for cold polarizable atoms. Atoms collected in the section of the array where the traps have their greatest depth is modeled in terms of a periodic distribution of matter constrained to have an equal mass content in a sequence of adjoining traps. The partitioned matter field is studied as a function of potential well depth and tunneling rates across the barriers between adjacent traps. The modelers find that 2 types of composite matter can co-exist in such an array. Type 1 is called a superfluid and is characterized by a fractional occupation of each individual trap. Type 2 is called a Mott insulator, which is characterized by a common whole number occupation of each trap. When the trap depth is relatively shallow and the tunneling rate high, the superfluid matter type dominates. When the traps are deep and separated by higher barriers, type 2 matter type dominates. When both types of matter are present, the

different types of matter are spread out in different portions of the traps, i.e., where the Mott insulator charge density is relatively high, the superfluid matter density is relatively low, and vice versa. Transferring this picture to the metal lattice, we associate low density ion band state matter with the superfluid, and the normal interstitial deuterons at high D/Pd loading with the Mott insulator type of matter with single atom occupancy in each trap.

If this intuitive picture of high mobility Bloch function component of fluxing deuterons exists at high D/Pd ratio, we can analyze the deuterons using a boson version of the physics of electron current flow in metals. Treating such deuterons as quasiparticles of a quantized matter field, their time varying distribution in physical and momentum space is characterized by a distribution function $G(\mathbf{r},\mathbf{k},t)$ where $\mathbf{r}$ is a location in physical space and $\mathbf{k}$ is a momentum index identifying a wavelike state. The many-body medium is subject to scattering where there are discontinuities in the hosting lattice environment. Scatterings at inhomogeneities are responsible for the resistivity of metals to electron current flow at low temperature. The interface between a highly ordered crystallite and a less ordered metal matrix constitutes an inhomogeneity for fluxing deuterons. The inhomogeneity subjects the many-body system to scattering events, changing $G(\mathbf{r},\mathbf{k},t)$. Scattering events can remove deuterons from the fluxing population while adding deuterons to a non-fluxing distribution $N(\mathbf{k})$ within the ordered domain. With bosons there can be a build-up of the $\mathbf{k}=0$ zero-momentum population. This build up adds to a resident non-fluxing ion band state population within the crystallite. (A non-fluxing population can also exist when there is a balanced population of $+\mathbf{k}$ and $-\mathbf{k}$ state occupations.) A self-interacting long lasting $N(0)$ population provides a possible explanation for "heat-after-death".

In addition to its role in populating D^+ ion band states, a fluxing Bloch function population of deuterons may be able to directly interact nuclearly with a resident population of non-fluxing deuterons. The 2 populations share the same set of k momentum states when in the same volume, but with different occupation distributions. Occupants need not be in the same k-state to interact. Also, a fluxing Bloch function population of deuterons exists as a many-body system without the presence of a resident population and can nuclearly self-interact just like a resident population. However, the density of the fluxing Bloch function population is likely to be much lower than the density of the non-fluxing population. Experiments are needed to determine the direct heating role of a fluxing Bloch function population.

References

[1] S. R. Chubb and T. A. Chubb, in *Anomalous Nuclear Effects in Deuterium/Solid Systems*, AIP Conference Proceedings **228**, 691 (Amer. Inst. Phys., New York, 1991).

[2] S.R. Chubb and T. A. Chubb, "Theoretical Framework for Anomalous Heat and Helium-4 in Transition Metal Systems", This Proceedings.

[3] T. A. Chubb and S. R. Chubb, Fusion Technol. **20**, 93 (1991).

[4] D. Jaksch, C. Bruder, J.I. Cirac, C.W. Gardiner, and P. Zoller, Phys. Rev. Lett. **81**, 3108 (1998).

Conference Proceedings Vol. 70
"ICCF8"
F. Scaramuzzi (Ed.)
SIF, Bologna, 2000

A MODEL ANALYSIS ON LOW-ENERGY PHOTO-FISSION OF Pd ISOTOPES UNDER DYNAMIC CONDITION OF PdH(D)x

Akito TAKAHASHI, Masayuki OHTA and Tadahiko MIZUNO*

Osaka University, * Hokkaido University

Abstract: To explain the production of radiation-less fission-like foreign elements claimed by several electrolysis experiments (Mizuno, Miley, and so on) with Pd cathodes, a selective channel fission model by low-energy multi-photon excitation and collective deformation is proposed. Channel-dependent fission barriers are calculated based on liquid drop model potentials for about 530 scission channels of 6 Pd isotopes with positive Q-values. Mass-distribution , Z-distribution and non-natural isotopic ratios of fission fragments as stable isotopes by the present theory have shown qualitative agreements with the experiments.

1. INTRODUCTION

Mizuno[1], Miley[2], Ohmori[3], Iwamura[4] and others have reported anomalous production of radiation-less foreign elements (Fe, Cr, Ti, Ca, Cu, Zn, Si and so on) on cathode metals (Pd, for instance) of heavy-water or light-water electrolysis experiments. Anomaly was also reported for drastically non-natural isotopic ratios of foreign elements. They conceived a kind of fission phenomenon, but did not know mechanisms of excitation-to-fission, radiation-less fission-products (FP) and selected FP elements with non-natural isotopic ratios. Particle absorption reactions like Pd + p, Pd + n and Pd + d can not excite Pd isotopes over the lowest fission barriers (around 15MeV as shown in this paper) to induce fission, but induce radio-active compound nuclei and radiation (beta-rays, gamma-rays, neutrons and charged particles) which were not observed in experiments. If there were di-neutron capture, excitation near 15MeV would happen but we know that di-neutron state with meaningful life time (more than fs) never exists.

We propose here the possibility of fission by collective deformation of Pd nucleus absorbing simultaneously many low-energy photons (about 100 photons of 100keV, for instance) under the dynamic circumstance of Pd-cathode in electrochemical experiments, which may lead to selective channel fission for FP pairs within the lowest fission barrier band. Assuming the multi-photon E1 resonance absorption and collective nucleus deformation, scission-channel dependent fission barrier heights were calculated based on the liquid drop model potentials and fission products were analyzed. This is the first proposal of nuclear collective excitation with multi-photon absorption process.

2. THEORETICAL MODEL

Possible Photon Sources: Iwamura[4] and Fukuoka[5] have reported the observation of 10-100keV X-ray emission in their Pd/D_2O electrolysis experiments. Taking hint with these experiments, we assume here that very high flux (we may require 10^{21} to 10^{25} p/cm^2/s, assuming photo-absorption cross section in few hundreds mb) of virtual photons with 1-100keV would exist under the dynamic condition of PdD(H)x lattice or be irradiated (we consider X-ray laser irradiation interesting) on surface of Pd cathode. If we apply the scenario of coherent multi-body deuteron fusion[6], about 1000 QED-photons (10-100keV) per fusion were generated and one watt level (10^{11} fusions/s) coherent fusion can produce virtual photon flux of 10^{11}x1000x3x10^{10} = 3x10^{24} photons/cm^2/s. We assume that this extremely high flux of low-energy photons can induce the multi-photon E1 resonance absorption around 15MeV, by pumping up mechanism via nuclear excitation levels with relatively long life times (nano-sec to micro-sec) of Pd isotopes. By assuming photo-fission cross section of several tens mb, we may have about 10^{14} f/s/cc Pd-fission rate which is high enough to explain observed excess heat level and amount of "transmuted " products.

E1 Giant Resonance (EGR) and Fission: EGR of photo-nuclear reaction locates in 15-20 MeV region of photon energy. We assume the single level Breit-Wigner resonance cross section for P-wave with E_r = 15MeV and width Γ = 4MeV. We further assume that the multi-photon EGR can selectively deform Pd nucleus by the collective excitation process: Low energy photo-excitation can start with nuclear low-lying states (0.1 to few MeV) which are collective states (rotation and/or vibration states of E1 or E2 deformation), and then absorb more photons via E1 or E2 process within life-times of levels to go higher collective states (pumping-up). We consider that the excited energy goes to the total system (nucleus)of nucleons and can concentrate to each local nucleon (i.e., neutron) with very small probability. Hence neutron emission channels are suppressed and the collective deformation will lead nucleus to elliptic and then tandem (dumbbell) nuclear deformation which may exit to scission events. Scission channel is chaotic because of existence of so many possible combinations of FP pairs. We consider that deformation for fission is deferent from a scission FP pair to others and therefore each scission channel has own fission potential with different barrier height (channel-dependent fission barrier).

Liquid Drop Model: The distortion energy of collective nuclear deformation is given[7] by

$$\Delta E(r) = [\varepsilon(r)]^2 A^{2/3} \cdot (6.88 - 0.14Z^2/A) \quad ; \text{in fm and MeV units,} \qquad (1)$$

, where $\varepsilon(r)$ is the elliptic deformation coefficient given by

$$\varepsilon(r) = (R_1 + R_2 + r - 2R)/(2R_0) \qquad (2)$$

using the nuclear radius of Pd R_0, the nuclear radii of FPs R_1 and R_2 and relative distance r of FP_1 and FP_2 nuclei. The point-to-point Coulomb repulsive potential is given as,

$$V_c(r) = 1.44Z_1Z_2/r \quad ; \text{in fm and MeV units,} \qquad (3)$$

, where Z_1 and Z_2 are atomic numbers of FPs.

The first term of Eq.(1) right hand side shows the surface tension of liquid drop and corresponds to the degree of nuclear binding force by strong interaction, and the second term means the change of Coulomb repulsion energy by elliptic distortion. In tandem deformation, scission occurs at $r = R_1 + R_2 + \lambda_\pi$, with the range of strong interaction λ_π (wave length of pion), and at that moment the surface tension vanishes: The effective Coulomb energy E'_c at scission point can be estimated from the difference between $V_c(r)$

and the second term of Eq.(1). We can define the channel dependent fission barrier as,

$$E_{fi} = E'_{ci} - Q_i \quad (4)$$

, where Q_i is the Q-value of scission channel i. We have calculated E_{fi} values for about 530 scission channels with positive Q-values , for 6 Pd isotopes (Pd-102, Pd-104, Pd-105, Pd-106, Pd-108 and Pd-110). An example of E_f patterns is shown in Fi.g.1, for Pd-106, where E_f values are plotted as a function of paired two masses of FPs.

3. FISSION PRODUCTS

Selective Channel Fission: Fission channels with negative Q-values (including neutron and alpha-particle emission channels) have so large fission barriers as 30 – 50 MeV that we neglect those for the low-energy photo-fission (LEPF) with EGR of nuclear excitation energy $E_x > E_r = 15$MeV. With this excitation condition, limited number of scission channels have smaller fission barriers than E_x as we see an example in Fig.1, where the lowest fission barrier band (LB1) is drawn with the upper line of 11 MeV ($E_r - \Gamma = 15 - 4$) and the lower line of 18 MeV (near $E_r + \Gamma$). For scission channels below $E_f < E_x$, we have estimated tunnel fission probability using the WKB formula[7] and found that the effect of tunnel fission could not be neglected but small. Consequently, we select scission channels with $E_x = E_r$ and $E_x > E_r$ for the first order approximation. Within the LB1 band, there exist 20, 21, 23, 13, 12 and 5 scission channels, respectively for ^{102}Pd, ^{104}Pd, ^{105}Pd, ^{106}Pd, ^{108}Pd and ^{110}Pd. At present, we do not consider the difference in photo-nuclear excitations of different isotopes of Pd, and simply sum up fission products (FPs) of above 93 channels (SCF channels) within the LB1 band. For 1/3 of SCF channels, we have direct products of stable (radiation-less) FP elements. For rest 2/3 channels, we have finally stable FP elements after pure beta-decays (about 30 %) and short-lived beta-decays with partial gamma-ray emissions (about 40 %). Only several channels produce radio-isotopes as final products as ^{60}Fe (1.5×10^6 y: β-decay with 58.59keV γ-ray) and ^{42}Ar(32.9 y: pure β-decay). We list up the top 20 channels opening first in Table-1, from which we can extract the following important results: a) 11 channels out of 20 directly produce stable FP elements, b) dominant stable FPs are such even Z elements as Ti, Cr, Fe and Ca, c) naturally in-abundant isotopes like ^{44}Ca, ^{46}Ca, ^{48}Ca, ^{49}Ti, ^{50}Ti, ^{53}Cr, ^{54}Cr, ^{57}Fe and ^{58}Fe are dominantly produced. Iwamura reported [4] dominant production of Ca, Ti, Cr and Fe in their D_2O/multi-layered-Pd experiments with EDX and WDX analyses. The LEPF/SCF products of present theory agree very well with his experimental products.

Mass Distribution: Mass distribution of FPs within the LB1 for natural Pd was obtained by summing up isotopic data with weights of natural abundance rates(%) for 6 isotopes and is shown in Fig.2 compared with experimental EPMA data by Mizuno[1]. Mass distribution curve by the present LEPF/SCF theory has major peaks at A=49, 52 and 56 which respectively correspond to ^{49}Ti, ^{52}Cr and ^{56}Fe, and qualitatively agree well with Mizuno experiment. Mass distribution of LEPF/SCF for heavier elements (A>180) may have two peaks like uranium fission, as example for ^{197}Au is shown elsewhere[7]. We can apply the present theory to analyze two-peaked FP mass-spectra of neutron-induced uranium fission with E_x-dependence, which study is now under way by authors. This means that actinide fission (neutron-induced) is also by the selective channel fission.

Table-1: List of top 20 channels opening first by Pd LEPF

	(FP1)	(FP2)	(Q)	(Fission Barrier)
(1)	^{104}Pd →	^{50}Ti +	^{54}Cr + 18.96MeV	(E_f = 11.36MeV)
(2)	^{102}Pd →	^{50}Ti +	^{52}Cr + 18.91MeV	(E_f = 11.60MeV)
(3)	^{105}Pd →	^{51}Ti(5.8min)^{51}V +	^{54}Cr + 18.24MeV	(E_f = 11.98MeV)
(4)	^{105}Pd →	^{50}Ti +	^{55}Cr(3.5min)^{55}Mn + 18.12MeV	(E_f = 12.11MeV)
(5)	^{102}Pd →	^{48}Ti +	^{54}Cr + 17.49MeV	(E_f = 13.03MeV)
(6)	^{106}Pd →	^{48}Ca +	^{58}Fe + 16.46MeV	(E_f = 13.23MeV)
(7)	^{106}Pd →	^{50}Ti +	^{56}Cr(6min)^{56}Mn(2.6h)^{56}Fe + 16.81MeV	(E_f = 13.32MeV)
(8)	^{108}Pd →	^{48}Ca +	^{60}Fe(1.6x10^6 y)* + 16.10MeV	(E_f = 13.42MeV)
(9)	^{106}Pd →	^{52}Ti(1.7min)^{52}V(3.7min)^{52}Cr +	^{54}Cr + 16.49MeV	(E_f = 13.63MeV)
(10)	^{105}Pd →	^{47}Ca(4.5d)^{47}Sc(3.3d)^{47}Ti +	^{58}Fe + 16.07MeV	(E_f = 13.72MeV)
(11)	^{105}Pd →	^{48}Ca +	^{57}Fe + 15.98MeV	(E_f = 13.81MeV)
(12)	^{105}Pd →	^{52}Ti(1.7min)^{52}V(3.7min)^{52}Cr +	^{53}Cr + 16.33MeV	(E_f = 13.89MeV)
(13)	^{104}Pd →	^{46}Ca +	^{58}Fe + 15.89MeV	(E_f = 14.01MeV)
(14)	^{102}Pd →	^{51}V +	^{51}V + 16.47MeV	(E_f = 14.10MeV)
(15)	^{102}Pd →	^{46}Ca +	^{56}Fe + 15.81MeV	(E_f = 14.27MeV)
(16)	^{102}Pd →	^{44}Ca +	^{58}Fe + 15.69MeV	(E_f = 14.42MeV)
(17)	^{105}Pd →	^{46}Ca +	^{59}Fe(44d)^{59}Co + 15.38MeV	(E_f = 14.43MeV)
(18)	^{104}Pd →	^{48}Ca +	^{56}Fe + 15.42MeV	(E_f = 14.45MeV)
(19)	^{110}Pd →	^{48}Ca +	^{62}Fe(1.1min)^{62}Co(14min)^{62}Ni + 14.76MeV	(E_f = 14.59MeV)
(20)	^{102}Pd →	^{49}Ti +	^{53}Cr + 15.91MeV	(E_f = 14.60MeV)

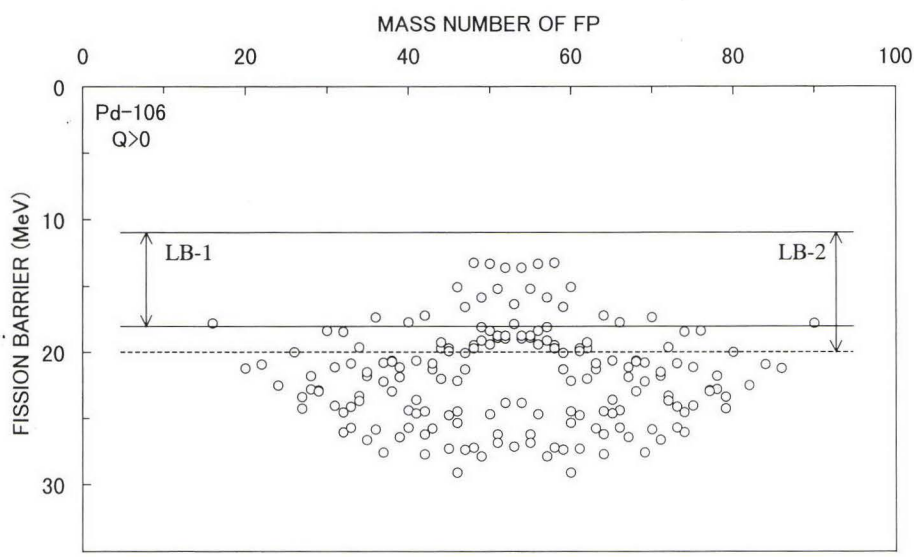

Fig.1: Map of channel-dependent fission barriers for Pd-106

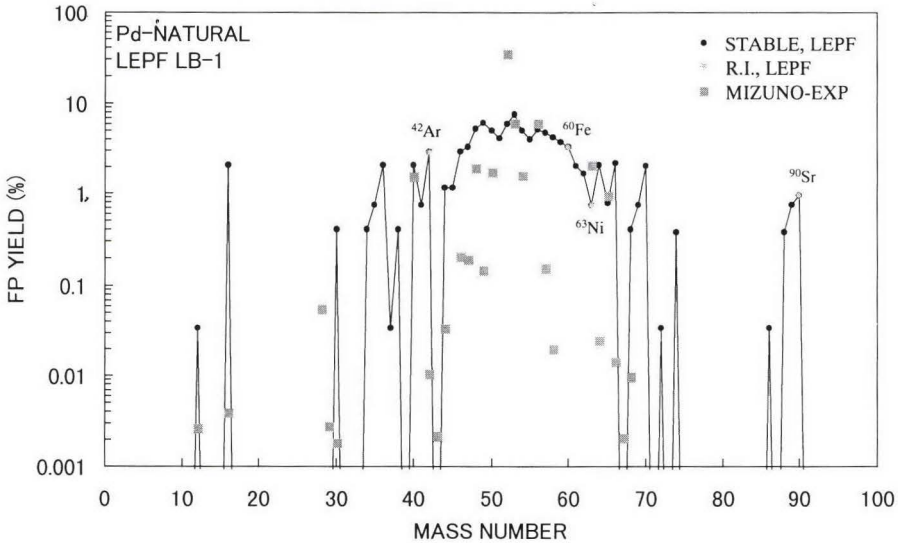

Fig.2: Mass distribution of Pd -LEPF

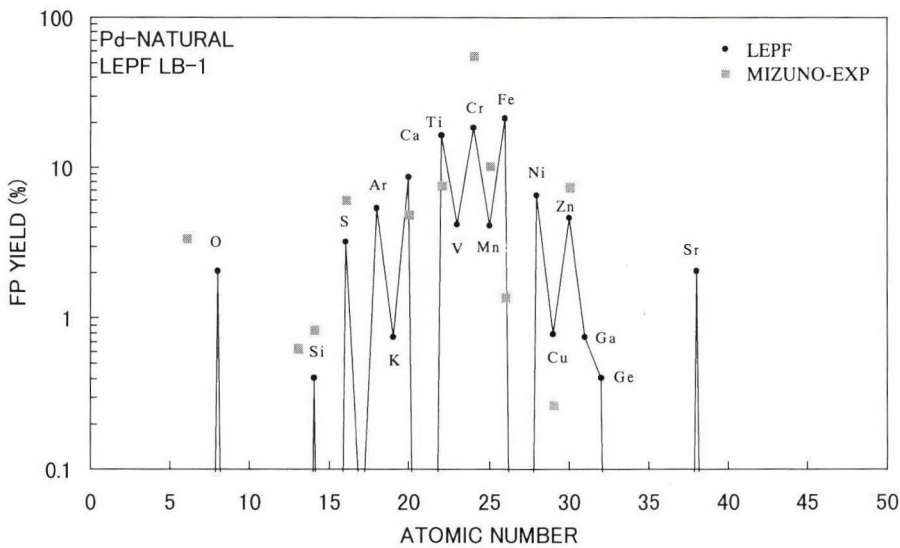

Fig.3: Elements (Z) distribution of Pd -LEPF

Elements (Z) Distribution: Results are shown in Fig.3, compared with the experimental EDX data by MIZUNO[1]. Stable FP elements for LB1 are distributed from Z = 8 (O) to Z = 40 (Zr). Fe, Cr and Ti are most dominant products, and are followed by Ca, Ni, Ar, Zn, Mn, V, S, Sr, O, Ga, K, Cu, Ge, and Si in the order of yield strength. Qualitative agreement is obtained with Mizuno's experimental data. Theoretical yield strength draws periodical peaks at even Z-values. The effect of nuclear shell structure, especially α-clustered nuclei like ^{16}O, ^{20}Ne, ^{28}Si, ^{48}Ca(double magic nucleus), ^{48}Ti, ^{52}Cr and ^{56}Fe by selective scission channels with low fission barriers will be the explanation to the even-Z effect.

Isotopic Ratios: Detail data for isotopic production is given elsewhere[7]. We reanalyzed[7] experimental data[1] for Ca and Ti, for which however we show only theoretical values. We only show results for 4 major elements. For Ca, ^{40}Ca/^{42}Ca/^{43}Ca/^{44}Ca/^{46}Ca/^{48}Ca ratio by LEPF/SCF-LB1 is 0.0/2.3/12/31.3/20.7/17.3, while the natural abundance ratio is 96.94/0.647/0.135/2.086/0.004/0.187. For Ti, ^{46}Ti/^{47}Ti/^{48}Ti/^{49}Ti/^{50}Ti ratio by LEPF/SCF-LB1 is 1.5/19.6/14.95/33.1/32.0, while the natural abundance ratio is 8.25/7.44/73.72/5.41/5.18. For Cr, ^{50}Cr/^{52}Cr/^{53}Cr/^{54}Cr ratio by LEPF/SCF-LB-1 is 0.3/37.9/31.5/30.3, while the natural abundance ratio is 4.34/83.79/9.5/2.36 and the Mizuno's SIMS data is 3/68/16/13. For Fe, ^{54}Fe/^{56}Fe/^{57}Fe/^{58}Fe ratio by LEPF/SCF-LB1 is 5.98/24.4/30.0/25.8, while the natural abundance ratio is 5.84/91.75/2.12/0.28 and the Iwamura's SIMS data is 0/45/41/14 compared with the Mizuno's data of 13/64/16/7. We can say that the present theory can qualitatively explain drastic change of isotopic ratios from natural ones, considering that experimental data are still scattered by conditions which are not clarified.

4. CONCLUSIONS

A fission model of Pd isotopes by the selective channel fission of low-energy multi-photon E1 resonance absorption has proposed and the results of model calculation have shown significant agreements with experimental foreign elements data by electrolyses. The present LEPF/SCF theory can be applied for possible low-energy photo-fission of elements heavier than A=100, and suggests a new method of nuclear-waste transmutation with much less radiation and energy production by largely positive Q-values. Detail description of the present work will be available elsewhere[7].

References:

1) T. Mizuno, et al.: Denki Kagaku, Vol.64, No.11 (1996) 1160
2) G.Miley, et al.: J. New Energy, Vol.1, No.3 (1996) 5
3) T. Ohmori, et al.: Fusion Technology, 33 (1998) 367
4) Y. Iwamura, et al.: Fusion Technology, 33 (1998) 476
5) H. Fukuoka, et al.: Proc. ICCF6, Toya Japan (1996) 425
6) A. Takahashi, et al.: Fusion Technology, 27 (1995) 71
7) A. Takahashi, M. Ohta and T. Mizuno: Production of Stable Isotopes by Selective Channel Photo-Fission of Pd, submitted to Fusion Technology (April 2000)

Conference Proceedings Vol. 70
"ICCF8"
F. Scaramuzzi (Ed.)
SIF, Bologna, 2000

Possible Mechanism of Coherent Multibody Fusion

Masayuki Ohta and Akito Takahashi

Department of Nuclear Engineering, Osaka University
Yamadaoka 2-1, Suita, Osaka, 565-0871, JAPAN

Abstract

From a point of view concerning electron-phonon interactions and electron-electron interactions, a mechanism inducing multibody fusion reactions is proposed. Because the coulomb repulsive force is screened by the deviation of charge like CDW caused by electron-phonon interactions and also by large effective mass of electron caused by electron-electron interactions, multibody fusion can be enhanced. For symmetry in the tetrahedral structure of Pd lattice, 2D fusion reacton is difficult to be enhanced, but 3D and 4D fusion reactions are possible to be enhanced.

1. Introduction

Unique fusion reactions in solid have been reported in a lot of experiments by electrolysis, discharge and beam-implantation using hydrogen-storage metal like Pd, Ti, etc. In these experiments, the productions of a large amount of heat, ^{4}He corresponding to excess heat, tritium and little amount of neutron were observed.

It is well known that the usual 2D fusion reaction is as follows:

$$\mathrm{D} + \mathrm{D} \rightarrow t\ (1.01\ \mathrm{MeV}) + p\ (3.02\ \mathrm{MeV}), \tag{1}$$

$$\mathrm{D} + \mathrm{D} \rightarrow {}^3\mathrm{He}\ (0.82\ \mathrm{MeV}) + n\ (2.45\ \mathrm{MeV}), \tag{2}$$

$$\mathrm{D} + \mathrm{D} \rightarrow {}^4\mathrm{He}\ (76.0\ \mathrm{keV}) + \gamma\ (23.8\ \mathrm{MeV}). \tag{3}$$

These branching ratio are $0.5/0.5/10^{-7}$ in turn from the top. In the usual 2D fusion reaction, the production rate of ^{4}He is very small, and this implies these phenomena can not be merely explained by the usual 2D fusion reaction.

Multibody fusion model was proposed to explain these anomolous phenomena.[1-3] This model assumes that multibody fusion reaction rate is enhanced in the transient process by the coherent motion of three or four hydrogen isotopes in Pd lattice. Fig.1 shows the geometry of hydrogen isotopes in Pd lattice, and it can be considered that the symmetry of the lattice realizes the situation inducing these reactions.

Nuclear products of 3D fusion reaction were predicted by the extension of established physics knowledge as follows:

$$\begin{aligned} \mathrm{3D} &\rightarrow {}^6\mathrm{Li}^*\ (\mathrm{E_i} = 25.3\ \mathrm{MeV} : 4-), \\ &\rightarrow {}^6\mathrm{Li}^*\ (\mathrm{E_i} = 2.18\ \mathrm{MeV} : 3+) + \gamma\ (23.2\ \mathrm{MeV}), \\ &\quad {}^6\mathrm{Li}^*\ (\mathrm{E_i} = 2.18\ \mathrm{MeV} : 3+) \rightarrow {}^6\mathrm{Li}\ (\mathrm{gs} : 1+) + \gamma\ (2.18\ \mathrm{MeV}), \\ &\qquad\qquad \rightarrow d + {}^4\mathrm{He} + 0.708\ \mathrm{MeV}. \end{aligned} \tag{4}$$

$$\mathrm{3D} \rightarrow t + {}^3\mathrm{He} + 9.5\ \mathrm{MeV}. \tag{5}$$

$$\mathrm{3D} \rightarrow d + {}^4\mathrm{He} + 23.8\ \mathrm{MeV}. \tag{6}$$

$$\mathrm{3D} \rightarrow n + p + {}^4\mathrm{He} + 20.1\ \mathrm{MeV}. \tag{7}$$

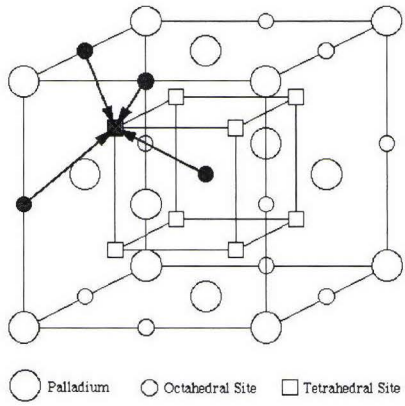

Figure 1: FCC lattice of PdD_x

Also, if 4D fusion reaction occurs, next reactions are expected:

$$\begin{aligned} 4D &\rightarrow {}^8Be^* \ (E_i = 47.6 \text{ MeV} : 3- \text{ or } 5-), \\ &\rightarrow {}^8Be^* \ (E_i : I\pi) + \gamma \ (47.6 \text{ MeV} - E_i), \\ &\quad {}^8Be^* \ (E_i : I\pi) \rightarrow {}^4He + {}^4He + E_i + 0.0918 \text{ MeV}. \qquad (8) \\ 4D &\rightarrow {}^8Be^* \ (47.6 \text{ MeV}) \rightarrow {}^8Be^*(gs : 0+) + \gamma \ (47.6 \text{ MeV}), \\ &\quad {}^8Be^*(gs : 0+) \rightarrow {}^4He + {}^4He + 0.0918 \text{ MeV}, \qquad (9) \end{aligned}$$

where possible values of E_i and $I\pi$ are $E_i = 25.5$ MeV : $I\pi = 4+$, 20.0 MeV : 2+, 16.6 MeV : 2+, 11.4 MeV : 2+, 3.04 MeV : 2+. The branching ratio of these reactions will be decided correctly only by experiments.

In this paper, we mentioned about the mechanism inducing these multibody fusion reactions from the point considering electron-phonon interactions and electron-electron interactions.

2. Interaction of Hydrogen Isotope with Lattice

M.C.H. McKubre et al. obtained the data that showed the correlation between excess heat and average loading ratio of cathod (D/Pd) from many experimental results.[4] Then, it was clarified that excess heat increased parabolically for $D/Pd \geq 0.85$. The problem of poor reproducibility pointed out in experiments of nuclear reaction in solid may be attributed to the condition that the loading ratio, D/Pd, was difficult to exceed the threshould value (≈ 0.85).

A deuteron in PdD_x with discrete energy levels is regarded as a quantum mechanical oscillator. But, generally, when the concentration of hydrogens in crystal is high, hydrogens are not well isolated oscillators, but become coupled-oscillators. Therefore, we assume that phenomena related with phonon occuring in hydrogen-storage metals of high-loading ratio may attribute to enhance fusion reactions particularly in solid, as we mention in Section 3.

In the electroconductive crystal, conduction electrons uniformly spread over the to whole crystal. When the deformation of crystal lattice is made, the spot of high atomic density attracts more electric charges than that of low one. So, the density wave of conduction electrons is created, as the crystal lattice makes periodic deformation. And, because positive feedback works between density wave of conduction electrons and lattice, the defomation of lattice grows still more. This is well known as Charge Density Wave (CDW). Thus, CDW is caused by the interaction between electron system and crystal lattice. The occurence of three dimentional CDW in PdD_x is also discussed by M. Fukuhara related to deuteron jumping.[5] The effects of electron-phonon interaction is known as the temperature-independence of electric resistance. And it is known that optical-mode phonon contributes to the temperature-independence of electric resistance in PdD_x.[6]

Transition metals which include hydrogen-storage metal like Pd and Ti, differ from simple metals in the point that ratio of volume occupied by closed shell in lattice is high. So, it is enough for simple metals to consider uniform sea of conduction electrons, but the influence of ions of lattice metal must be considered for transition metals.

Also, only from simple considerations, this increases the density of conduction electrons concerning screening, and affects to decrease the distance between ions. And as far as local site is concerned, the region that conduction electrons are possible to exist is small, then conduction become anisotoropic. So, CDW that is possible to develop in low-dimentional materials is produced easily and hydrogen oscillations of the feedback of the charged density become anisotoropic. It is said that hydrogens move under a certain order (coherence).

3. Possible Mechanism of Transient Coherent Motion

Based on the consideration in the previous section and by analogy with breathing mode, we mention here the mechanism of multibody fusion reactions. Tetrahedral structure of hydrogen isotopes in Fig.1 is converted to two-dimensional schematic view in Fig.2. In each figure, arrows show the direction of oscillation of hydrogen isotopes at any time.

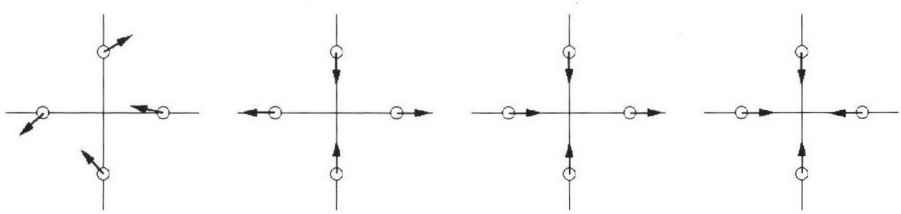

(a) incoherent (b) anti-coherent (c) coherent (d) coherent

Figure 2: Two-dimensional schematic view of coherent motion

Fig.2(a) corresponds to the situation that hydrogen isotopes in O-site oscillate ramdomly. The hydrogen isotopes are regarded as isolated oscillators located in O-site. These oscillators have no correlation each other (" incoherent"), and Fig.2(a) corresponds to the situation that hydrogen isotopes exist at low density in hydrogen

storage metal as mentioned in previous section. In this case, because no correlation exists between hydrogen isotopes, coherent motion does not occur and the deviation of charge like CDW is not also excited. In consequence, the screening of coulomb repulsive force is not enhanced and fusion reaction does not occur. This shows that fusion reactions in solid are not enhanced in random process, and it is consistent to conventinal physics.

Fig.2(b) corresponds to the situation that two hydrogen isotope pairs oscillate to opposite direction each other. In this case, hydrogen isotopes move with correlation. The closing hydrogen isotopes attemped to excite deviation of charge like CDW, but at the same time another hydrogen isotope pairs oscillating to opposite direction bring the charge out of there, then excitng effect is cancelled and CDW is not excited. This may be well understood by the superposition of CDW and that shifts half a period. So, on the site in the lattice of tetrahedral structure, coherent 2D fusion is difficult to occur. Here we call this condition as " anti-coherent".

Fig.2(c) corresponds to the situation that three hydrogen isotopes move to the T-site which is the center of the tetrahedral structure and one hydrogen moves to opposite direction. In this process, because the direction of one hydrogen isotope is oppsite, practically two hydrogen isotopes excite the deviation of charge. The deviation of charge is excited by net two hydrogen isotopes, but then three hydrogens squeeze simultaneously because of synchronous oscillation (" coherent"). It is considered that the occurred deviation of charge screens the coulomb repulsive force, and then leads to induce 3D fusion reacion.

Fig.2(d) shows that four hydrogen isotopes oscillate to same direction. Then, in this process, the deviation of charge like CDW is more enhanced. So, the coulomb repulsive force is screened, four hydrogen isotope is closed symcronously (" coherent") and 4D fusion reaction will occur. The coherent effect of nuclear strong interaction is disscussed elsewhere.[1]

4. DOS at Fermi Surface and Screening Effect

Deuterons have to approach each other to make fusion in solid. In this situation, two factors contribute to the enhancement of screening effect.

First, because of electron-phonon interactions, electrons at Fermi surface become heavy in metal. The electron energy ϵ_k is reduced by the factor $(1+\lambda)$, then the density of state (DOS) near the Fermi surface is enhanced by the factor $(1+\lambda)$.[7]

$$N^{\dagger}(E_F) \;=\; N(\epsilon_F)\,(1+\lambda). \tag{10}$$

where λ is the dimentionless electron-phonon coupling constant, given as follows:

$$\lambda \;=\; 2\int_0^{\omega_0} \frac{\alpha^2(\omega)\;F(\omega)}{\omega} \;=\; \frac{N(\epsilon_F)\langle I^2\rangle}{M\langle\omega^2\rangle}, \tag{11}$$

where ω_0 is the maximum phonon frequency, $\alpha^2(\omega)\;F(\omega)$ is the spectrum function of electron-phonon interaction. $N(\epsilon_F)$ is DOS at Fermi level, M is the mass of the atom, $\langle I^2\rangle$ is the average over the Fermi surface of the square of the electron matrix element and $\langle\omega^2\rangle$ is an average of the square of the phonon frequency.

Secondary, electron correlation is remarked especially in Pd. Recently, in the field of heavy electron systems, electron which effective mass is more than 1000 times of

free electron mass (m_0) is observed. It is the feature that heavy electron systems have inner f-electrons. Generally, effective mass of d-electrons of Pd is considered as about 10 times of m_0. Because electrons added to system by deuterating (hydrating) Pd screen the d-electrons of Pd, more heavy effective mass may be realized by analogy of heavy electron systems. High ratio of D(H)/Pd will make it more effective.

Considering this effect, Fermi level is described as,

$$E_F \sim \alpha\epsilon_F \qquad (\alpha = \frac{2V_{sd(f)}^2}{a^2}), \tag{12}$$

where $V_{sd(f)}$ is correlation parameter between conductrion electron and d(f)-electron, a is band separation between two bands.

Effective mass near Fermi level is given as next relation:

$$m^* \sim \frac{1}{\alpha}\, m \qquad \alpha \ll 1. \tag{13}$$

Specific heat of this system is defined by,

$$C_N = \frac{2\pi^2 k_B^2}{3} N^*(E_F) T, \tag{14}$$

and

$$N^*(E_F) \sim (1 + \frac{1}{\alpha})\ N(\epsilon_F). \tag{15}$$

The screening Coulomb potential (Thomas-Fermi potential) is written as,

$$\Phi(r) = \frac{\Delta Z e}{r}\ \exp(-\kappa r), \tag{16}$$

where κ is satisfied the next relation,

$$\kappa^2 = 4\pi e^2\, \frac{m^{\dagger,*}}{\pi^2\hbar^2}\ (3\pi^2 n_0)^{1/3} = 4\pi e^2\ N^{\dagger,*}(E_F), \tag{17}$$

where $N^{\dagger,*}(E_F)$ is DOS of quasi-particle at Fermi energy.

Considering electron-phonon interactions and electron-electron interactions, DOS at Fermi energy is represented in Eq.(10) and Eq.(15). Then next relation is obtained.

$$\kappa^2 = 4\pi e^2 (1 + \frac{1}{\alpha})(1 + \lambda)\ N(\epsilon_F). \tag{18}$$

And the effective screening radius is defined as κ^{-1}. So, the effective region of Coulomb potential become to be reduced by the factor $1/\sqrt{(1 + \frac{1}{\alpha})(1 + \lambda)}$. But to estimate multiboby fusion rate, the coherent effect of nuclear strong interaction must be conconsidered in addition to this effect. This is a task for future.

5. Discussion and Conclusion

In this paper, we proposed a possible mechanism of multibody fusion from the point of electron-phonon interactions and electron-electron interactions. The conventional physics for random reaction process can not explain these multibody fusion reaction.

But it is explained that because of the symmetry of crystal lattice, only 3D and 4D fusion reactions are enhanced and 2D fusion reaction is not enhanced, as the deviation of charge like CDW is induced. Of course, these reaction processes must be analyzed quantitatively by the method like molecular dynamics. V. Violante et al. discussed deuteron ion motion in Pd lattice about DD reaction.[9] But apparently CF phenomena cannot be explained only by DD reaction. It is a task to estimate the rate of 3D and 4D fusion reaction.

In the experiment of electrolysis, the existence of surface Li layer should be considered. Because of large ionization tendency of Alkali metal, Li tends to provide electrons to hydrogen isotope (or lattice element), then the number of electrons related to screening is increased.

Also, Low Energy Photo-Fission model was proposed.[8] This model assumes that many low energy photons excite Pd nuclei of lattice to induce fission. The mechanism of coherent multibody fusion proposed in this paper assumes the contribution of optical mode lattice vibration. The optical mode lattice vibration can be excited by photons, so the vibration may be excited by low energy photons. Thus, the origin of coherent multibody fusion and LEPF may be the same low energy photons.

The distance between deuterons in lattice can be reduced by screening of Coulomb force depended on effect of heavy electron system. If heavy electron system is realized by addition of element of lanthanoid, coherent multibody fusion is expected to be enhanced.

Recently, some experimental results suggesting 3D or 4D reactions have been obtained.[3] It is hoped that the phenomena are confirmed by a lot of experiments to obtain ratio of the reactions (2D/3D/4D). Then, by that, theoretical studies will develop still more.

References

[1] A. Takahashi et al., *Fusion Tech.*, **27**, 71 (1995).

[2] A. Takahashi, *Trans. Fusion Tech.*, **26**, 451 (1994).

[3] A. Takahashi et al., *Fusion Tech.*, **34**, 256 (1998).

[4] M.C.H. McKubre et al., *Frontier of Cold Fusion (Proc. ICCF3)*, 5 (1992).

[5] M. Fukuhara, *Fusion Tech.*, **34**, 151 (1998).

[6] J.P. Burger, Metal Hydrides, G. Bambakidis ed. (Plenum, 1981), p. 243.

[7] W.L. McMillan, *Phys. Rev.*, **167**, 331 (1968).

[8] A. Takahashi et al., " A Model Analysis on Low-Energy Photo-Fission of Pd Isotopes under Dynamic Condition of $PdH(D)_x$", *Proc. ICCF8* (in this issue).

[9] V. Violante et al., *Fusion Tech.*, **34**, 156 (1998).

Conference Proceedings Vol. 70
"ICCF8"
F. Scaramuzzi (Ed.)
SIF, Bologna, 2000

Hydrogen Isotopes Interaction Dynamics in Palladium Lattice

V. Violante[1], C. Sibilia[2], D. Di Gioacchino[3], M. McKubre[4], F. Tanzella[4], P. Tripodi[4]

[1]ENEA, Centro Ricerche di Frascati ,C.P. 65 - 00044 Frascati (Italy)
[2]La Sapienza Univ., Dip. Energetica, V. Scarpa, 14 Roma (Italy)
[3]INFN-LNF, Viale Enrico Fermi 40, 00044 Frascati (Italy)
[4]SRI Int., 333 Ravenswood Ave, 94025 Menlo Park, CA (USA)

Particles Dnamics Modeling

The dynamics of hydrogen isotopes within the lattice of metals like palladium and nickel is investigated assuming that the concentration of the gas in the metal, as atomic fraction, is close to unity and that coherent oscillations (plasmons) of the metal atom electrons, close to the Fermi level, occur [1-5].The aim of this work is to investigate the effect of the plasmon e.m. field both on the dynamics of the ions embedded in the lattice and on the nuclear decay of the compound ^{4}He* nucleus. The theory models D ions passing through a volume centered on a tetrahedral site in the fcc Pd lattice. The dc field configuration of this volume resembles that of an rf ion trap. For an assumed plasmon ac field of 10^{10} to 10^{11} V/cm at a frequency of 10^{15} to 10^{16} s^{-1} selected D ions called "shots" achieve keV energies relative to trapped ions near the trap center. The energizing dynamics and the field-stimulated decay of potential collision-product nuclei ^{4}He* are examined.

Hydrogen and deuterium within a metal lattice can be considered to be into a ionic state [6,7].

The oscillations of the electrons produce in the metal, on the lattice cell scale, an intense oscillating electric field (see Fig.1) that accelerates the ions entering the system "shot". The ions trajectories are studied by means of the equation of motion. The calculations show that, under proper initial conditions, the distance between two ions reduces below 0.1 Å (see Fig. 2 and Fig. 3). The equation of motion for the "shot" ions, assuming a lattice dipole signal, are:

$$\frac{d^2\bar{x}_i}{d\xi^2} = 8(1-\alpha)\frac{q_i \rho Ne}{m_i \Omega^2} I_0 \frac{\left(1+\bar{x}_i^2\right)}{\left(\gamma x_i^2 - l_0^2\right)^2}\cos(2\xi+\psi) + \frac{4q_i q_j}{m_i \Omega^2}\frac{\bar{x}_i - \bar{x}_j}{\left[\left(x_i-x_j\right)^2+\left(y_i-y_j\right)^2+\left(z_i-z_j\right)^2\right]^{3/2}}\beta$$

$$\frac{d^2\bar{y}_i}{d\xi^2} = \frac{4q_i q_j}{m_i \Omega^2}\frac{\bar{y}_i - \bar{y}_j}{\left[\left(x_i-x_j\right)^2+\left(y_i-y_j\right)^2+\left(z_i-z_j\right)^2\right]^{3/2}}\beta$$

$$\frac{d^2\bar{z}_i}{d\xi^2} = 8\alpha\frac{q_i \rho Ne}{m_i \Omega^2} I_0 \frac{\left(1+\bar{z}_i^2\right)}{\left(\gamma z_i^2 - l_0^2\right)^2}\cos(2\xi+\psi) + \frac{4q_i q_j}{m_i \Omega^2}\frac{\bar{z}_i - \bar{z}_j}{\left[\left(x_i-x_j\right)^2+\left(y_i-y_j\right)^2+\left(z_i-z_j\right)^2\right]^{3/2}}\beta$$

i,j=1,2 and *i≠j*.

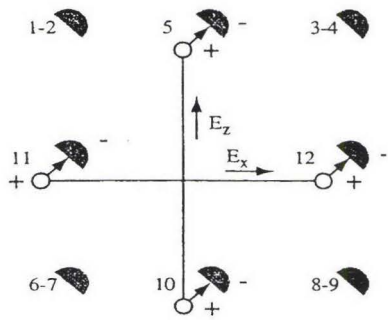

Fig.1 - Two dimensional view of the electronic clouds oscillations on a lattice cell plane

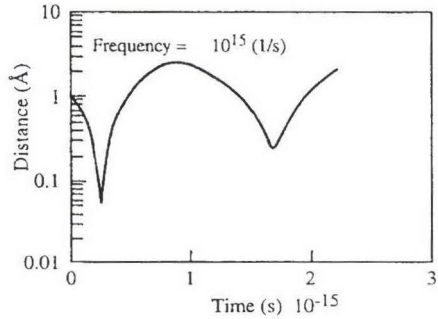

Fig. 2 - Evolution of the distance between two deuterons in the Pd lattice

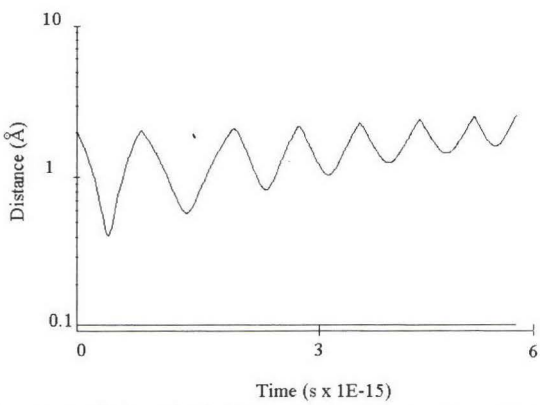

Fig. 3 Distance evolution with initial condition not inducing collision

x, y and z are the particle i dimensionless coordinates, q is the charge, l_o the lattice cell size, β the Thomas-Fermi screening factor, Ω the signal frequency (10^{15} s^{-1} for the plasmon), ψ a phase factor ξ the dimensionless time γ a numerical factor ($\cong 1$) avoiding singularity at the domain edges, e the electron charge, m_i the ion mass and ρN the oscillating charges acting at the edges of the domain.

The frequency of the alternating signal can be evaluated by considering the oscillating electrons as an ideal electron plasma.

$$\Omega \cong \frac{e}{m_e^{1/2}} n^{1/2} \approx \left(10^{16}\ s^{-1}\right)$$

The energy gained by the "shot" particle, due to the e.m. signal, is in the order of some keV.

^{4}He* decay

The effect of the plasmon e.m. field on the probability amplitude of an excited to ground state decay of the ^{4}He* nucleus has been studied by G. Preparata et al. [8], through the interaction potential given by the coupling between the nuclear current and the field potential vector.

The coupling between the excited ^{4}He nucleus and the e.m field existing within the lattice assumes the same parameters considered for the ions dynamics.

The nuclear current, in the excited nucleus, is considered to be created by the motion of a *single particle* (proton). The energy released by the excited nucleus is supposed to be transferred by a non radiative (stimulated) process, to a region of the lattice defined by the plasmons coherent behaviour: 100 ÷1000 Å. Such a region can be considered as an infinite reservoir that is not damaged or dramatically modified by the energy transfer or system recoil.

The excited α-particle cooling to the ground state (Helium-4) is mediated, in the proposed picture, by the Fermi electrons, participating as plasmons that release their energy towards phonons of the lattice [9] and low energy radiation emission (X rays).

According to the semi-classical approximation and by considering the coherence domain as an infinite reservoir we can assume that the distribution of the e.m. field is not strongly affected, over the coherence domain, by the excited nucleus decay, then the computation of the matrix element is carried out by means of the nucleus wave function in the initial and final state.

A fast transition is allowed since the decay is considered to take place through an electro-magnetic coupling between the excited nucleus and the e.m. field of the lattice coherence domain. Limiting the study to the interaction of the charge with the e.m. field the interaction term H_I becomes simply:

$$H_I = \frac{e}{m}\hat{p}\vec{A}$$

When the oscillations of the electron clouds develop along the z axis within the z-y plane, the potential vector becomes as:

$$\vec{A}(z,t) = \vec{A}_0 e^{\pm ikz - i\Omega t}$$

$$A_0 = \frac{E_0}{\Omega}$$

The state at a time *"t"* can be assumed to be represented by the overlapping of three states:

$$|\Psi(t)\rangle = C_0(t)e^{-i\omega_0 t}|0\rangle + C_1(t)e^{-i\omega_1 t}|1\rangle + C_2(t)e^{-i\omega_2 t}|2\rangle$$

where ω_0, ω_1, ω_2, are the energies (in units of $\hbar$) of the respective energy levels.

From the Schrödinger equation:

$$i\hbar\frac{\partial}{\partial t}|\Psi\rangle = (H_0 + A\cdot J)|\Psi\rangle$$

with the initial conditions: $C_0(0) = 1$, $C_1(0) = C_2(0) = 0$

the controlling step results to be the 0 –1 transition since $C_1 > C_2$

Mathematical handling gives the "stimulated" transition probability:

$$|a_{fi}|^2 \cong \gamma^2[3 - 2(\cos(\omega_{10}T) + \sin(\omega_{10}T))]$$

$$\gamma = -\frac{1}{\hbar^2}\frac{a^2}{(\omega_0 - \omega_1)^2}$$

and

$a \equiv \langle 1|H_I|0\rangle = (eA_0/m)\langle 1|\hat{p}|0\rangle$ so that: $\Omega = 10^{15}\,s^{-1} \Rightarrow |a_{fi}|^2 > 10^{-3}$;

$\Omega = 10^{16}\,s^{-1} \Rightarrow |a_{fi}|^2 < 10^{-5}$

where m is the proton mass, e the electron charge, $\hat{p}$ the momentum operator and T the interaction time.

It should be observed the important role played by the ratio E_0/Ω. If the ratio exceeds 0.01, both the stimulated transition probability and the reaction probability (from the ions dynamics calculation) become significant.

Reaction Channels

The probability P_i of a decay of a compound state into a generic channel i is given by:

$$P_i = \frac{\Gamma_i}{\Gamma} \quad ; \quad \Gamma = \sum_i \Gamma_i$$

and Γ_i is the appropriate partial width. The maximum value of the width is:

$$\Gamma^{max}_{D(D,n)^3He} = k_n R_N \frac{\hbar^2}{m_n R_N^2}$$

(k_n is the c.m. wave number of channel $n + {}^3He$ and R_N is the nuclear radius).

The result is close to the limit given by the uncertainty principle. We can assume this value for the stimulated transition process:

$$\Gamma_{st} = \Gamma^{max}$$

An approximate evaluation for $\Gamma_{(D,n)}$ can be carried out on the basis of a comparison between the cross section (deprived of the Gamow term) of the $D(D,n)^3He$ reaction and of the D-D reaction in the metal lattice. A rough estimate of the e.m. stimulated transition cross section can be carried out by means of the following well known relationship, using the principle of the detailed balance and using the transition matrix element above estimated:

$$\sigma_{st} \approx \frac{8\pi^3 \nu_{fi} V_N |a_{fi}|^2}{c}$$

ν_{fi} ($\cong 10^{21}$ - $10^{22}\,s^{-1}$) is the decay frequency and V_N the nuclear volume.

The calculations and the literature data give, for a frequency of the e.m. field in the order of 10^{15} (s^{-1}) and with a field peak value in the order of 10^{13} (V/m) (that is not far from the value calculated by the plasmon theory), the following result:

$$\chi = \frac{\sigma_{(D,n)}}{\sigma_{st}} \approx 10^{-4}$$

so that:

$$\Gamma_{(D,n)} = \chi \Gamma_{st}$$

The gamma emission channel width can be estimated by means of the well known relationship for an electric quadrupole decay:

$$\Gamma_\gamma = 4.8 \cdot 10^{-8} E_r^5 A^{4/3}$$

or we can assume that the vacuum channel probability ratio between the gamma emission and the (D,n),(D,p) channel maintains. In either case the computation leads to:

$P_{st}(=1) >> P_{(D,n)} >> P_{(D,\gamma)}$.

This result , even if indicative, is in reasonable accordance with the experimental results where neutrons and gamma ray have not been significantly observed above the natural

back ground .
A similar effect has been obtained, under the same conditions in the lattice, for the ^{3}He decay.

Tritium production

The experimental observations, however, show that in some cases the D(D,p)T channel is more likely than the D(D,n)^{3}He one. An analysis supportive of this apparent anomaly is carried out in the framework of this study. The problem can be approached by seeing if there is an e.m. field conditions that affects the D(D,p)T channel by acting on the proton emission from the nucleus.The nucleus can be considered as a square well with an external Coulomb potential within a region where an external field (perturbation) can be applied or not, see Fig. 4 (a square well potential is assumed for the neutron). The emission probability can be estimated by means of the particle wave function, in the space representation, by solving the Schrodinger equation:

$$-\frac{h^2}{2m}\nabla^2\Psi + \frac{1}{4\pi\varepsilon_0}\frac{q_1 q_2}{\vec{R} - R_N}\Psi + \hat{H}_I\Psi = E\Psi$$

$$H_I = \hat{A}\cdot\hat{J} = e\omega_{fi}R_N\hat{A}$$

where *m* the proton mass.
The same space dependence of the dipole signal, used for the dynamics analysis, is considered. The eigenvalue problem is numerically solved with the boundary condition that:
$\Psi = 0$ *at* $x = L$, where L is a distance larger than the distance covered by a particle leaving the nucleus with the light velocity.
Figure 5 shows the probability for the proton without external pertubation. The probability value is close to 10^{-5} and the proton is far away from the nucleus. Figure 6 shows the analogous picture for the neutron: the probability is always close to 10^{-5} (in accordance with the same probability for the two channels in the vacuum or within a plasma), the different shape of the surface plot is due to the Coulomb potential acting on the proton. There is an increase of the emission probability for the proton, of about 2 – 3 orders, even if the emitted particle is closer to the nucleus, and the effect is produced by applying an external perturbation (see Fig. 7). The localization probability doesn't change for the neutron in this case. By increasing again the external perturbation up to a value comparable with the value used in the previous calculation of the "stimulated" decay probability, we obtain a very high probability to have the proton in the nucleus, so that the "stimulated" decay becomes the dominant mechanism as seen above, see Fig. 8.

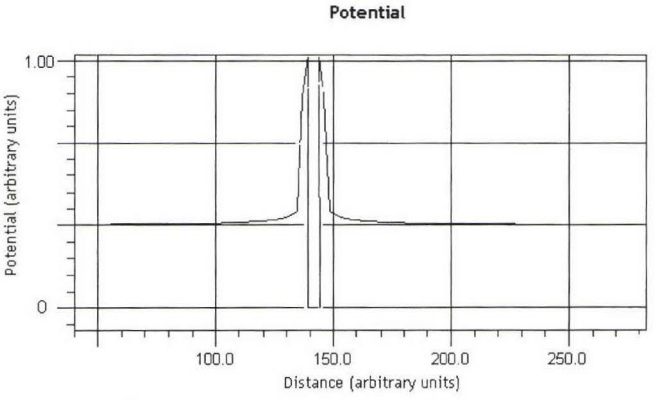

Fig. 4 - Square well and Coulombic potential

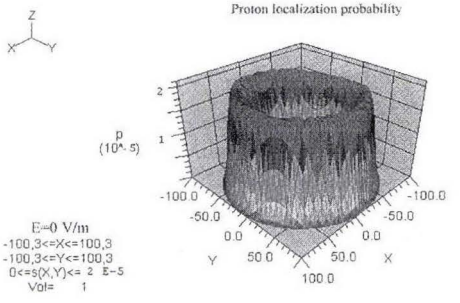

Fig. 5 - Proton localization probability without external field

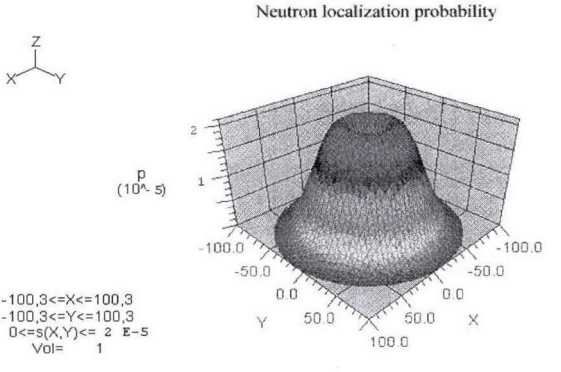

Fig. 6 - Neutron localization probability

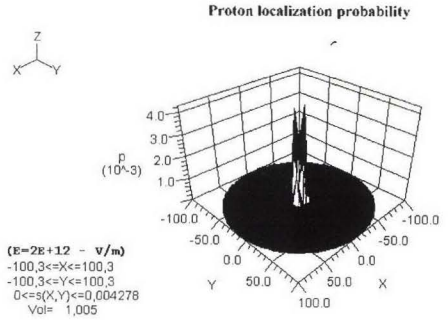

Fig. 7 - Proton localization probability

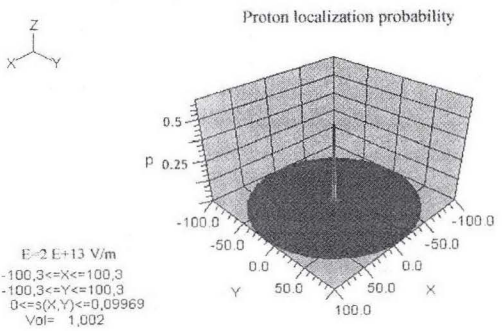

Fig. 8 - Proton localization probability with increased external field

Excess of Heat Production: Estimate

In the majority of cold fusion calorimetric experiments studying the Pd-D system, there has been observed an excess of heat production ranging between some watts for cubic centimeter up to some hundreds of watts for cubic centimeter of cathode (depending on the experimental conditions). The simulation suggests that approximately 1 collision occur over $10^4 \div 10^5$ particles entering a lattice with a target staying at rest in the tetrahedral sites. Two approximations have been considered in estimating the system reactivity:

i) D-D reaction in vacuum reactivity, with a decay channel in accordance with the results above reported;the power density Π is:

$$\Pi = n_{D1} n_{D2} \langle \sigma v \rangle \Delta E$$

where ΔE = 24 MeV, n_{D1} is the number of the particles that can participate in the dynamics, i.e. the colliding particles that can over come the activation energy barrier (E_b=0.32 eV) between the octahedral and tetrahedral sites, then:

$$n_{D1} = \Theta N_0 \exp(-E_b/kT)$$

Θ is the probability to have a "collision"; $n_{D2} \approx 10^{22}$ are the deuterons at rest in the tetrahedral sites.

ii) Estimate of the power density produced by the D-D reaction, for a d-wave process in Pd. Assuming that the particles population limiting the process are the particles n_{D1} then:

$\Pi = \Theta N_0 \exp(E_b / kT) \left| a_{fi} \right|^2 \nu_{fi} \exp(-2G_2) \Delta E$,

where ν_{fi} is the decay process frequency ($\cong 10^{21}$- 10^{22} 1/s), G_2 the Gamow factor for a d-wave process.

The calculations have been done for exchanged Coulomb potential energy (calculated with the dynamics analysis) values of 1 ,1.5 and 2 keV and for two different temperatures: 300 and 350 K.

Table 1 Power density values (kW/cm^3); values in brackets refer to the "in vacuum" estimate.

	1.1 keV	1.5 keV	2 keV
Temperature k	w/cm^3	w/cm^3	w/cm^3
300	0.95 (13)	68 (67)	2100 (260)
350	5.53 (76)	400 (394)	12000 (1520)

An increasing of the temperature of about 50 ° produces, if the deuterium concentration is not affected by that, an increasing of the excess of power of about a factor five.

Conclusions

The results reveal:

1) a possible mechanism producing collisions between deuterons, in the metal (Pd or Ni) lattice close to the tetrahedral sites;
2) a shift of the decay channel of the excited ($^4He^*$) nucleus is produced;
3) X rays and charged particles emission due to the not reacting ions having energy of some keV

- The mechanism is a consequence of the interaction of the e.m. field in the lattice due to the plasmons with the tetrahedral-site ions and the excited nuclei. An important role is played by the ratio:

$A_0 = E_0/\Omega$

-Where E_0 is [$10^{12} \div 10^{13}$ V/m] and $\Omega_{plasmon} \approx 10^{15}$ s^{-1}. The effective electron mass and the morthology of the surface, that modify the plasmon frequency, can significantly affect the process.

-The loading ratio and the temperature affect the excess of power production since they act on the number of reacting particles, while the field gradient, amplitude and frequency seem to have a role in tritium production. A temperature increase, that could produce a reduction of the number of deuterons in the lattice, increases the number density of the non-trapped particles producing collisions (changing the loading threshold). As a result the reactivity remains significant or increases.

References

[1] V. Violante, Lattice Ion Trap:, Confinement for Deuterons and Protons: Possible Interaction in Condensed Matter, Fusion Techn. **35** (1999) 361-368.

[2] J. M. Ziman, «Principles of the Theory of Solids», 2nd Edition, Cambridge at the University Press, 1972 (163-166).

[3] C. Kittel, «Quantum Theory of Solids», J. Wiley & Sons Inc. New York, London, 4th printing (1967), 36.

[4] A. M. Brodskii» Surface-Soliton Formation in Metal/Electrolyte Interface Electrodynamics», Elektrokhimiya, **22**, 2, (1986) 270.

[5] A.M. Brodskii and M.I. Urbakh, «Effect of Electrode Roughness on Photoemission During Surface-Plasmon Formation», Elektokimiya, **17**, 3, (1981) 302.

[6] B.C. Lamartine, T.W. Haas and J.S. Solomon, Appl. Surf. Science **4**, 537 (1980).

[7] R.C. Brouwer, R. Griessen, Phys. Rev. Lett. **62**, 1760 (1989).

[8] G. Preparata, Some Theoretical Ideas, Trans. Fusion Technology. **26**, 397 (Dec. 1994).

[9] P. L. Hagelstein, Anomalous Energy Transfer, Proc. Seventh Int Conf. on Cold Fusion Vancouver (Canada) Apr. 19-24 1998 (140).

Conference Proceedings Vol. 70
"ICCF8"
F. Scaramuzzi (Ed.)
SIF, Bologna, 2000

On the Reaction Product and Heat Correlation for LENRs

George H. Miley

LENR Lab, Dept. of Nuclear, Plasma and Radiological Engineering, University of Illinois,
103 S. Goodwin Avenue, Urbana, IL 61801 USA
Phone: (217) 333-3772 E-mail: g-miley@uiuc.edu

Abstract

"Low Energy Nuclear Reactions", or LENRs, typically involve electrolytes containing light water along with electrodes made of metals such as Ni, Ti and Pd. In these experiments a variety of reaction products (isotopes), with masses both higher and lower than that of the host electrode material, have been observed at the University of Illinois (U of IL). Related results, often termed "transmutation" studies, have been reported by other researchers. These observations suggest that proton-metal initiated reactions occur in such LENR cells. This paper discusses evidence that the production of these reaction products is correlated with the excess heat also frequently observed in LENR cells. Such a correlation for LENR reactions would be equivalent, in principle, to the correlation of He-4 with excess heat that is reported for heavy water-Pd experiments where a D-D reaction is postulated.

Introduction

Considerable research effort has been devoted to the establishment of a correlation between He-4 and excess heat from D-D reactions postulated to occur in Pons-Fleischmann type cold fusion cells. Good progress has been made and recent measurements of the reaction product He-4 have achieved levels where background helium is a less significant factor in interpretation of the results [1]. These results indicate, with a reasonable confidence level, that a direct correlation exists between He-4 production and excess heat, supporting the D-D reaction hypothesis.

In contrast, in the case of LENRs, a variety of reaction products (isotopes) with masses both higher and lower than that of host electrode material imply that proton-metal initiated reactions occur [2, 3]. Earlier G. Miley, et al. [3, 4] considered the possible correlation of these reaction products with the excess heat observed in these experiments. Additional results are presented here that further support this conjecture. Still, uncertainties in absolute values of both heat and product measurements leave open a fairly large error band for the correlation; thus, some important issues remain e.g. whether or not some reactions also occur in LENRs that involve electrolyte salts.

Indeed, as discussed later, due to the rich variety of conceivable contributing mechanisms in LENR experiments, the reaction product-heat relationship is less useful for specifying a unique reaction responsible for excess heat than is ^{4}He production in D_2O-Pd

cells. Still, the data provides important circumstantial evidence about the reacting species, hypothesized to be protons-metal atoms for LENRs.

Prior Reaction Product Measurements

The earlier measurements of LENR reaction products at the U of IL are described in references [2, 3]. Several precision analytical methods were used to analyze both the metal electrodes and electrolyte before and after runs. A characteristic result, shown in Fig. 1, indicates that a variety of reaction products occur with masses lying well below and above that of the base electrode metal (Ni and Pd in this figure, of cf. numbers defined in the references).

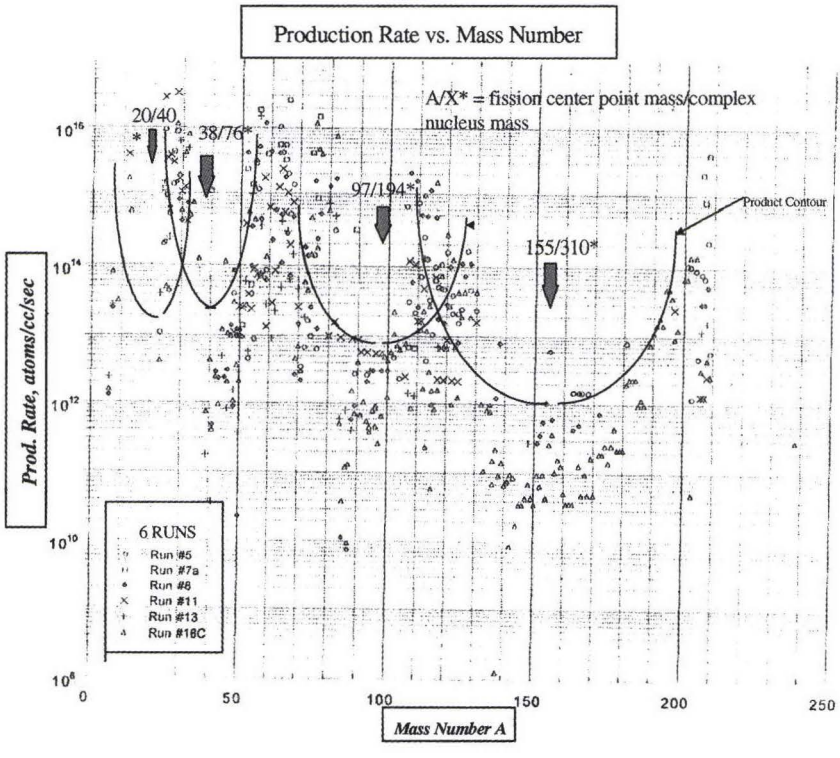

Figure 1. Reaction Product Yield vs. Mass Curve (from Ref. 3)

A striking pattern consistently observed in these measurements is that the high-yield reaction products occur in four mass ranges, roughly A = 20-30, 50-80, 110-130, and 190-210 [4].

Statistically significant shifts in isotope ratios from natural abundance are also observed for many of the products [2, 3]. Numerous precautions were taken to guard against impurities in these measurements (see references 2, 3). This includes use of special "clean" systems, blank runs, and precision diagnostics prior to and following runs. Consequently, the high-yield products (> 10^{13} atoms/cc-sec in Fig. 1) are well above background impurity limits, but some uncertainties due to possible impurities, especially in the electrolyte, still plague measurements of the lower yield products (< 10^{13} atoms/cc-sec in Fig. 1). For example, the yields of the high-yield products such as Ag and Cu in thin-film Ni cathodes typically exceeded the total amount (in weight) of impurity Ag and Cu found in the total system, (including both the electrodes and the electrolyte), by one or two orders of magnitude.

Other evidence of the nuclear basis for these results included the observation of low energy X-ray and/or beta emission from electrodes after a run and statistically significant shifts in isotope ratios for key elements. The general trends from these results are reasonably consistent with reaction product measurements by other workers (see the discussion and references in references 4, 5). However, others have often termed their work "transmutation studies" as opposed to "reaction product studies". For that reason, other studies have not generally focused on the total product yields or on correlations with heat.

Energy/Nucleon Balances

The measurements of reaction products shown in Fig. 1 used analytic techniques that were benchmarked via neutron activation analysis techniques to allow a determination of absolute values of the yields as well as trends. The "production rates" shown represent a time average over the experiment run-time since, with the present experimental arrangement, it was only possible to take samples at the beginning and end of a run. Likewise, the excess heat reported represented an average over the run, so that a comparison of these two results is consistent.

To test for a possible correlation, the measured product yields or Fig. 1 are used along with their respective binding energies to compute a theoretical "excess power", W_{excess}, as illustrated in Fig. 2.

$$\left[\sum_{RPs} (RP * BE/n) - \sum_{\substack{metal\ atom, \\ p\ burned}} (fuel * BE/n)\right]/run\ time = P_{out}$$

$$\Xi\ W_{excess}$$

Figure 2. Computation of Excess Power from measured reaction products and binding energies where:
RP = reaction product yield or atoms of product formed nuclei
BE /n= Binding energy per nucleon for RP or fuel
fuel = metal nuclei + protons reacted (from nucleon balance)
p = proton

The computation is straightforward but tedious due to the large number of reaction products produced. Basically, W_{excess} is computed by taking the product of all the isotope yield rates times their binding energies and subtracting the corresponding product for the "fuel". A key point is the determination of the amount of original material, that is consumed or "burned up." Since the decrease in the number of original metal atoms in the cathode is a small fraction of the original atoms, a direct measurement becomes imprecise (vs. the measure of new isotopes that differ from the base electrode material itself). However, the number "consumed" can be obtained from the measured products by invoking the basic requirement that nucleons are conserved in the reaction. A nucleon balance is performed by first computing the total number of nucleons in each of the measured reaction products. The basic assumption is that these nucleons come from the base electrode metal, e.g. Ni, plus the reacting protons. This calculation is done by first allotting the maximum number of reaction product nucleons to the metal nucleons. Then, any remaining nucleons are attributed to the protons, allowing for a variable proton/metal atom ratio to retain generality [6, 7]. This balance rests on the assumption that the protons plus the electrode metal (e.g. Ni in this case) are the reactants in LENR cells. This follows since protons in the light water electrolyte cannot react with themselves (as D-D reactions in heavy water electrolyte). Otherwise, this result does not rely on a knowledge of the reaction mechanism itself. While a counter view might assume the 'salt' employed in the electrolyte, e.g. Li_2SO_4, was involved in the reaction. There is no evidence for this in LENR reactions, and the fact that various workers have used different salts while still obtaining similar reaction products seems to rule out this possibility.

Product yield results from three runs (run numbers refer to experiments described in R. 2) where adequate information was available for this type of evaluation are summarized in Fig. 3.

Run Number (Ref. 2,3)	***Excess Power (W)***	
	Calculated	Measured
#7	1.9 ±0.6	4.0 ±0.8
#8	0.5 ±0.2	0.5 ±0.4
#18	0.7 ±0.3	0.6 ±0.4

Figure 3. Results from Energy Balance Calculations for Three Earlier Thin-Film Experiments. All experiments used Li_2SO_4 in H_2O for the electrolyte and thin-film Ni coated cathodes.

As seen from this figure, reasonably good agreement is obtained between the excess power measurement and the calculated values using the binding energy calculations described here. Two of the results show quite close agreement, but one has a mean measured value that is a factor of two larger than the calculated value. While these results are not definitive, still, in view of the many uncertainties in both of the calculated values (due to uncertainties in the yield measurements) and in the calorimetry, the agreement obtained strongly suggests a relation between products and excess heat.

More studies of this type are clearly needed to fully confirm the validity of this correlation. Still, this result, combined with the reaction product data itself, provides added evidence that proton-metal reactions are responsible for the anomalous isotope and heat phenomena observed in LENR experiments. The situation where heavy water is used instead of light water, as reported in some other LENR studies (e.g. see [5]), is less clear but again appears to involve proton-metal reactions. In that case, p-metal reactions could occur simultaneously with D-D reactions. More study is needed to resolve possible reactions involved this important regime.

Another way of viewing these data is to calculate the energy released (the observed excess heat times the run time) and divide by the number of Ni atoms reacted (based again on the number of nucleons associated with the measured quantities of reaction products observed). Then, for the runs of Fig 3, an energy release of order of 150 keV/Ni atom reacted is obtained. This value is consistent with nuclear as opposed to chemical processes. It is several orders of magnitude less than the energy released in neutron-induced fission, but is roughly in the range of "soft" fission releases predicted for LENR conditions [8].

These results also bear on an issue that is often raised about the LENR experiments: how can a positive excess power occur since the base metal involved, such as Ni, has a binding energy per nucleon near the peak of the binding energy-mass curve? In the present analysis this can be explained by noting that the "fuel" i.e. the reactants, are a mixture of protons and metal. Then the average binding energy of the reactants (p + metal) is reduced below that of the metal alone. As a result, there is an expanded range of reaction product masses lying around the mass of the base metal that offer a positive energy release, i.e. a positive Q-value for the reaction. Still, the fact that some reaction products lie outside of this range might seem to infer that reactions occur despite a negative Q-value, but then a very large input energy would be needed to drive the reactions. This dilemma is overcome, however, if the reaction occurs through multi-step excitation and/or formation of a compound nucleus which can split up or fission into a variety of reaction products of different masses [4, 8]. The energy balance requirement is that the formation energy of the compound nucleus must be supplied. Subsequently, the break-up energy is, in effect, shared among products.

Conclusion

Detailed energy and nucleon balance calculations for LENR experiments where reaction products were quantitatively measured have been shown to be generally consistent with corresponding excess heat measurements. Such data is only available for a few cases, so

additional experiments are needed to fully verify this correlation. However, the results to date support the hypothesis that proton-metal reactions are associated with the excess heat and reaction products observed in such LENR experiments.

Acknowledgement

Helpful discussions with H. Hora, M. Ragheb, W. Collins, D. Cravens, J. Patterson, and J. Kelly as well as colleagues in the LENR laboratory at the U of IL are gratefully acknowledged. Some data was taken from recent experiments supported by Cold Fusion Technology, Inc

References

[1] M. McKubre, and F. Tanzella, "The Correlation Between Heat and Helium in Experiments Performed at SRI", *Proceedings, Asti Workshop on Anomalous Effects in Hydrogen/Deuterium Loaded in Metals*, Asti, Italy, Oct 1999, to be published, Italian Physical Society.

[2] G. H. Miley and J. A. Patterson, "Nuclear Transmutations in Thin-Film Nickel Coatings Undergoing Electrolysis", *Journal of New Energy* 1 no. 3, p. 5 (1996).

[3] G. H. Miley, "Possible Evidence of Anomalous Energy Effects in H/D-Loaded Solids—Low Energy Nuclear Reactions (LENRs)," *Journal of New Energy*, 2, No. 3-4, pp.6-13, (1997).

[4] G. H. Miley, "Characteristics of Reaction Product Patterns in Thin Metallic Films Experiments," ", *Proceedings, Asti Workshop on Anomalous Effects in Hydrogen/Deuterium Loaded in Metals*, Asti, Italy, 77-87 (1997).

[5] G. H. Miley, G. Selvaggi, A. Tate, M. Okuniewski, M. J. Williams, D. Chicea, H. Hora, J. Kelly, "Advances in Thin-Film Electrode Experiments", *Proceedings, 8th International Conference on Cold Fusion,* ICCF-8, Villa Marigola, Lerici, Italy, May 21-26 (2000).

[6] H. Hora and G. H. Miley, "New Magic Numbers from Low Energy Nuclear Transmutations Predict Element $^{306}X_{126}$ for Compound Reactions", *Czechoslovak Journal of Physics*, 48, No. 9, 111-116 (1998).

[7] H. Hora, G. H. Miley, "Heavy Nuclide Synthesis by Neutrons in Astrophysics and by Screened Protons in Host Metals", *Czechoslovak Journal of Physics,* 50 no. 3, pp. 433-439 (2000).

[8] A. Takahashi, M. Ohta, and T. Mizuno, "A Model Analysis of Low-Energy Photo-Fission of Pd Isotopes Under Dynamic Condition of $PdH(D)_x$", these proceedings.

Conference Proceedings Vol. 70
"ICCF8"
F. Scaramuzzi (Ed.)
SIF, Bologna, 2000

LOW ENERGY NUCLEAR REACTIONS OF PROTONS IN HOST METALS

H.Hora[a], G.H. Miley[b] and J.C. Kelly[c]

[a]Dept. of Theoretical Physics, Univ. of New South Wales, Sydney 2052, Australia
[b]Low Energy Nuclear Reaction Laboratory, Univ. of Illinois, Urbana, Il 61801, USA
[c]School of Physics, Sydeny University, Sydney 2006, Australia

We present an explanation for the previously reported observations of low energy nuclear reactions (LENuR) of protons in host metals, such as nickel and palladium. These reactions occur at picometer separations with times of megaseconds. The endothermic production of heavy elements in the host metals follows a distribution similar to that calculated for the big bang and in supernova. The intense neutron background in these cases allows much smaller reaction distances and hence higher yields than for the proton reactions considered here. The relation to the nuclear magic numbers is similar for both the neutron and proton induced reactions.

1) Experimental Facts

Endothermic generation of heavy elements at LENuR of protons in layers of host metals were observed in 18 reproducible experiments[1] and further modified measurements[2] which independently were observed by other authors[3-5]. The experiments needed a several weeks interaction by electrolytically or gas/plasma loading the protons (deuterons) in the host metal. The experimental results indicated:
a) The mechanism was fully reproducible.
b) No pollution was involved since K-shell x-ray spectra uniquely identified such rare elements as thulium and terbium[6] which are so rare that any source of pollution can be completely excluded.
c) The reaction products were stable nuclides only (with one exception[3] where a radioactive platinum isotope may have been produced.
d) No neutron or gamma emission was detected within the limits of the instruments
e) The heat production was low but clearly detected[1,2] preferrably in multilayers of about 100 nm thickness being more than kW/cm^3 and more than 10keV per all atoms in the layers.
f) The nuclear reaction energy went into the heavy daughter nuclei which may have caused soft x-rays[5] and were detected as much larger tracks in CR39[7,8] than alpha particles produce.

g) The relative abundance of the elements generated by LENuR was similar to that of the endothermic element generation in the Universe as seen from typical examples in Fig. 1.

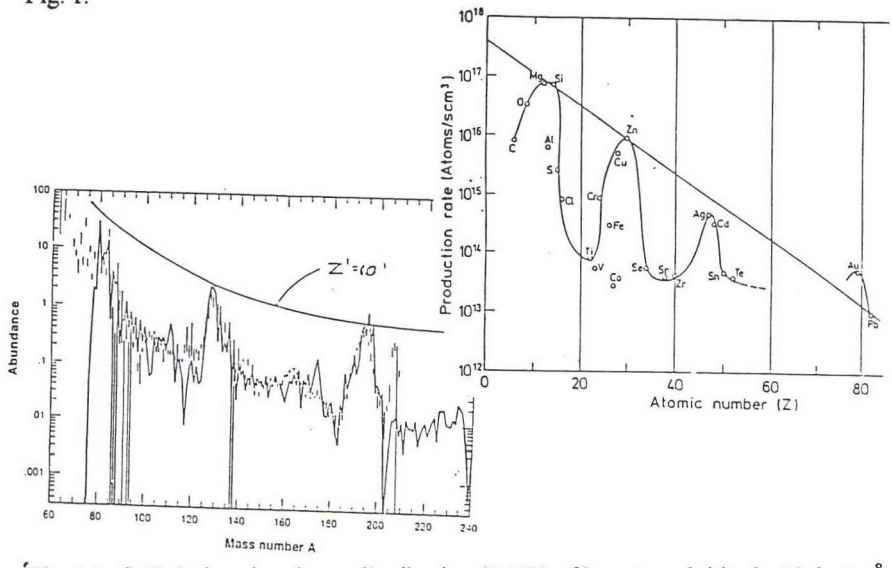

Fig. 1 Left: Relative abundance distribution (RAD) of heavy nuclei in the Universe[8] on the nucleon number A; right: same from LENuR reactions[10]

Further LENuR experiments are needed which measure more exactly the isotope ratios of the elements produced, to confirm more generally the less accurate examples so far observed of departures from the natural isotope ratios. Nuclear fission forms elements such as nickel or palladium into lower elements. The measurement of soft x-rays emitted from existing LENuR experimental arrangements is difficult but would be a valuable experiment to perform.

2) Analogy between endothermic heavy element generation by LENuR and in the Universe and New higher magic numbers

The most intriguing question is endothermic element synthesis generating heavy nuclei. In the Universe where the maximum binding energy per nucleon allows exothermic fusion reactions to make elements but generating the heavyer elements is a problem. It is assumed that nuclei, in a high concentration background of neutrons, follow a nuclear-chemical Boltzmann distribution. This is assumed to occure for a few seconds during supernova events and perhaps for femtoseconds with nuclear separation of femtometers[8], during the big bang. For this Boltzmann equilibrium there is the generation probability N(Z) for elements depending on the proton number Z of

$$N(Z) = N' \exp(-Z/Z') \qquad (1)$$

The neutron number is N (N = A-Z) and A is the nucleon number in the nucleus. It is interesting that the exponential increment

$$Z' = 10 \tag{1b}$$

provides the best fit, see Fig. 1 for the maxima of the abundance distribution in the Universe[8-10]. The same best fit was found for the measured abundance distribution in the case of LENuR, see Fig. 1.

The fact that this fit (2) is the best, was evaluated before[9,10] for the LENuR case, see Table 1 in Ref.[9]. The criterion was that the ratio $R(n) = N_{n+1}/N_n$ of the probabilities N for subsequent values Z_n representing the magic numbers of the nuclear shells Z_n = 2, 8, 20, 28, 50, 82, 126 where, however, special attention had to be given between the numbers 20 and 28, see Table 1 of Ref.[10]. This is an immediate foundation of the magic numbers from the exponential law (1) in contrast to the spin-orbit based explanation by Maria Goeppert-Meyer and Jensen et al[11]. Bagge (see Ref.[11]) had a *purely numerically speculative* derivation of magic numbers and arrived at the series

$$S_1 = \mathbf{2, 8, 20}, 40\ 70, 112,.... \tag{2a}$$

by using the sequence 2,3,4,5,..., and by using the sequence 1, 2, 3, 4, 5, ... to arrive at the series

$$S_2 = 2, 6, 14, \mathbf{28, 50, 82, 126} \tag{2b}$$

The question was, what causes the jump between these two series for the bold numbers to explain the observed magic numbers. Contrary to the spin-orbit explanation[11], our result[10] of the plots (1) with (1a) in the Fig. 1 for the element distribution in the Universe and for the LENuR reactions arrived at the jump immediately without any further explanation. This seems to be a remarkable property indicating a similarity of the endothermic synthesis of heavy nuclei in both cases.

The ratios R(n) result in the further remarkable relation[10] of

$$R(n) = 3^n \tag{3}$$

indicating that the (magic number determined) stable nuclear shells follow a threefold sequence, indicating a quark property. The analysis also predicts[10] magic numbers at (126, 180, 246, 324) rather than the earlier predicted numbers (114, 184, 228) where the agreement with the analysis[10] can be seen from Fig. 4 of Ref.[12]. Our new magic numbers are in agreement with the predictions of Rutz et al[13] based on the relativistic mean field Brueckner-Hartree-Fock calculations. Further agreement appears with the alpha decay line of superheavy elements (Fig. 6 of Ref. [12]) arriving at the relatively stable seaborgium-266. This whole synopsis underlines that the element

$$^{306}X_{126} \qquad (4)$$

should be especially stable since it includes the two magic numbers Z = 126 and the new number A-Z = 180. This all agrees with the measurements[14] of LENuR via a compound reaction with a nucleon number 153.

3) Phenomenological conclusion of picometer-megasecond reactions

We have shown the perfect consistency of the standard abundance distribution (SAD) of endothermic generated elements in the Universe with the results of LENuR of protons in host metals. This also is highly consistent with the derivation of new magic numbers and other results on super heavy elements (SHE) work.

We summarize now a general phenomenological result for the mechanism of nuclear reactions due to protons or deuterons in host metals. From the beginning it was assumed that the protons or deuterons can move nearly freely, within the host metal lattice, effectively as an exotic Maxwellian gas[15] where the short range nuclear reaction distance was considered. A quantitative relation for these distances d and the interaction time U was first published in 1990 (see Fig. 3 of Ref.[16]) and discussed in connection with the screening[17] necessary to allow such close approaches between charged nuclei to occur. The relation

$$U = 8.129 \times 10^4 \, d^{34.8} \text{ seconds} \qquad (5)$$

with d in picometers was derived where the distances and reaction times for hot fusion and for myonic fusion were taken from the experimental value.

This result was then used[17] in evaluating some of the very few repeatable, early D-D-reaction experiments in palladium to conclude that within orders of magnitudes the distance of the reacting neutrons had to be about 3 pm and the reaction time U about 10^5s. This is a reasonable range since K-shell electron capture radioactivity shows very similar times and distances: 20 h for ^{122}Xe with 0.97 pm Bohr radius, or 3.1 h for ^{47}Ti with 2.3 pm Bohr radius.

What is remarkable is that the shortest distance of 143 fm for the DD reaction at 10 eV is very much larger than the diameter of the proton or deuteron, of about one fm, and is very different from the usual nuclear reactions at a distance of a few fm for which MeV energy and much more is necessary for the colliding nuclei.

A first fully quantitative quantum theory explaining the very large distances involved in hot fusion reactions, is given very recently only by the results of X.Z. Li et al[18]. The extension of this theory to the reactions at a distance d of picometers[18] resulted in reaction times U of about 10^4 seconds. This is an excellent confirmation of our calculations from phenomenological conditions[10,16] that the low energy reactions of the protons with the nuclei in the host metals occur in a distance d of picometer and a reaction time of megaseconds.

The only question was how it is possible that the Coulomb repulsion of the pro-

tons is cut-off at a distance of about picometers. Initially it was calculated[17] that a screening by a factor 14 is necessary. This was considered to be occurring in the swimming electron layer of all metal surfaces or at the interface between metals of different Fermi energy. This is supported by several observations[1-6] that multi-layer structures result in higher LENuR effects. As an additional mechanism a Debye screening was based on a special interpretation of electron energy distribution and/or a dielectric shrinking of the proton potential[10].

For a reaction with a *picometer* radius, the necessary bonding of the nucleons in the internal potential well has such an exceedingly high number of bouncing oscillations[18] such that the reaction probability gives reaction times of 0.01 *megaseconds*. This agrees quite well with the above phenomenological analysis[10,17] . It is then a straight forward result that no neutron emission will occur. It should be mentioned that the predicted[19] and measured cluster emission from nuclei, e.g. of Ar emitted from U, is a cold process without further emission of gammas or neutrons.

4) Conclusion about the endothermic nuclear synthesis

The endothermic nuclear synthesis in the Universe was based on a nuclear-chemical Boltzmann equilibrium[8] of Eq. (1) where the high concentration of a neutron background between nuclei resulted in a balanced up and down of the size of the nuclei. This all occurred either within reaction times U of attoseconds in the case of the big-bang at nuclear distances d of few femtometers[8] or at the distances of dozens of femtometers and microsecond times at supernova conditions. In analogy to this, the endothermic nuclear synthesis at the low energy nuclear reactions LENuR occur not with the neutron background but with a background of picometer screened protons at the dense nuclear concentration of the host metals. Since the protons cannot have shorter reaction distances d than picometers - contrary to the neutrons in the Universe - the reaction times U are much longer in the range of megaseconds.

Though the nuclear energy generation at LENuR for the reactions is then spread to several weeks or months, the use of multilayer structures will permit the production of energy densities of 20 W/cm^3 or more[2] where the increase or the operational temperature of the host metal increases the reactivity as shown before in Fig. 3 of Ref.[17] and as measured recently[20].

References

1. G.H. Miley, G. Narne, M.J. Williams, J.A. Patterson, J. Nix, C. Cravens, and H. Hora, Progress in New Hydrogen Energy, M. Okamoto ed., (New Energy and Industrial technology, Tokyo 1997) p. 629
2. G.H. Miley et al. This conference ICCP8 Proceedings
3. T. Mizuno, T. Ohmorii, K. Akimoto, K. Kurokawa, K. Inoda, K. Azumi, S. Simokawa, and M. Enyo, Progress in New Hydrogen Energy, M. Okamoto ed., (NewEnergy and Industrial technology, Tokyo 1997) p. 665

4. T. Ohmori, T. Mizuno, and M. Enyo, *Progress in New Hydrogen Energy*, M. Okamoto ed., (New Energy and Industrial technology, Tokyo 1997) p. 670
5. Xing-Zhong Li and Huoji Tang (private Commun. Beijing, Sept. 1998); G.S. Qiao, X.L. Han, L.C. Kong, S.X. Zheng, H.F. Huang, Y.J. Yan, Q.L. Wu, Y. Deng, S.L. Lei and X.Z. Li, *Proceedings of the Seventh Conference on Cold Fusion Vancouver April 1998* (ENECO, Salt Lake City Utah, 1998) p. 314
6. Xing-Zhong Li, Guo Yi Tang et al. in Proc. Asti Meeting, Oct. 21-24, 1999 (Eds. W.F.M. Collins and R. George) Italian Physical Society, Conference Proceedings in print.
7. Y. Deng and X.Z. Li, presented at the Conf. Three Gorges, China, Oct. 6, 1998
8. K..L. Kratz et al Astrophys. J. 403, 216 (1993)
9. H. Hora, G.H. Miley, J.C. Kelly, and Y. Narne, Proceedings of the ICCF7 Conference Vancouver, April 1998, p. 147
10. H. Hora, Czechoslovak J. Phys. 48, 321 (1998); H. Hora, G.H. Miley and J.C. Kelly, Trans. Amer. Nucl. Soc., 78, 90 (1998)
11. O. Haxel, J.H.D. Jensen and H.E. Suess, Zeitschr. f. Physik 128, 295 (1950)
12. H. Hora, G.H. Miley, J.C. Kelly, G. Salvaggi, A. Tate, F. Osman, and R. Castillo, Fusion Technology 36, 331 (1999)
13. K. Rutz, M. Bender, T. Brevenich, T. Schilling, P.G. Reinhard, J.A. Maruhn and W. Greiner, Phys. Rev. C 56, 238 (1997)
14. H. Hora and G.H. Miley, Czechoslovak J. Phys. 48, 1111 (1998)
15. H. Hora, G.H. Miley, L. Cicchitelli, A. Scharmann, and W. Scheid, *Emerging Nuclear Energy Systems 1989 (Karlsruhe, July 1989) Proceedings*, U. von Möllendorf and B. Goel eds, (World Scientific Singapore 1989) p. 322; H. Hora, L. Cicchitelli, G.H. Miley, M. Ragheb, A. Scharmann and W. Scheid, Nuovo Cimento D 12, 393, (1990)
16. H. Hora, G.H. Miley, M. Ragheb and A. Scharmann, *World Hydrogen Energy Conference No.8, July 1990 Hawaii, Special Symposium Proceedings Cold Fusion* (Hawaii Natural Energy Institute, Univ. Hawaii 1990) p. 169
17. H. Hora, J.C. Kelly, J.U. Patel, M.A. Prelas, G.H. Miley, and J.W. Thomkins, Phys. Letters A175, 138 (1993)
18. Xing Zhong Li, Czechoslovak J. Phys. 49, 985 (1999); Xing. Zhong Li, Jian Tian, Ming-Yuan Mei and Chong Xin Li, Phys. Rev. C. 61, 024610 (2000)
19. R.K. Gupta, A. Sandulescu, and W. Greiner, Physics Letters 67B, 257 (1977)
20. S. Focardi et al. Nuovo Cimento 112A, 921 (1999)

Conference Proceedings Vol. 70
"ICCF8"
F. Scaramuzzi (Ed.)
SIF, Bologna, 2000

THE HYDREX CONCEPT – EFFECT ON HEAVY NUCLEI

J. Dufour, D. Murat, X. Dufour and J. Foos

CNAM. Laboratoire des Sciences Nucléaires 2 rue CONTE 75 003 Paris France

Introduction :

A growing body of evidences tends to prove that nuclear reactions can happen at room temperature, in certain metals containing one or several isotopes of hydrogen (light hydrogen and deuterium have mainly been tried), when these metals/metallic hydrides are submitted to various types of activation (electrolysis, passage of currents of various shapes and intensity, diffusion of hydrogen isotopes through the metal, ultrasonic waves, magnetic fields, laser light ...). The fact that nuclear reactions occur seems proven by :

- the overall exothermal effect, that cannot be accounted for by chemical reactions
- the appearance in the processed metallic lattice of new chemical species [1,2,3,4]
- the appearance of helium (3 and 4), of tritium and of charged particles [5,6].

These reactions are commonly referred to as CF reactions when helium seems to be the main reaction product and LENR reactions when other products are found.

A number of models have been proposed to explain these reactions [7,8]. We propose here a semi quantitative model, according to which CF and LENR reactions are essentially the same phenomenon : nuclear reactions catalysed at room temperature by a metastable state of hydrogen.

The system under study :

The system under study is a metallic lattice, loaded with hydrogen isotopes and submitted to various types of activation.
The metallic lattice is chosen among metals able to give an hydride with metallic properties, as palladium, nickel, titanium and uranium. This starting metallic lattice is generally well known as regards the chemical impurities it contains, but not at all as regards its lattice properties (it is certainly not a mono-crystal and few is known about its defects).
A wide range of activation means are applied : some tend to overload with hydrogen the metallic lattice beyond thermodynamic equilibrium (electrolysis of water is generally used [5,6]), some generate atomic hydrogen and protons that are contacted with the metallic lattice (electrical discharges in gaseous hydrogen are used for that case [10]) and other use chosen combinations of physical parameters that occur naturally in above mentioned activation means [1].
At this point, it is clear that the system under study is (from an epistemological point of view) very different from those that have made the success of solid state physics for the last 60 years : the purest compounds (with metallic or semi-conductive properties) were prepared as mono-crystals and submitted to the action of a thermal gradient, or an electrical field or a magnetic field ... The expected effect (heat transfer, current flow, Hall effect ...) always occurred. Representative data had then to be collected, and explained through the remarkable theories of solid state physics.

The system under consideration is not found as such in nature (contrary to metals and semi-conductors). If, as we think , the effects observed are true, this has three consequences :

-one needs a kind of working hypothesis (or pre-conceived idea or theory) to guide its efforts in the right direction to find the right parameters.
-it should not be considered as abnormal, that the reproducibility of the effects is still a major issue, since the right triggering parameters are still unknown.
-it is of paramount importance for the CF, LENR community to consider without pre-conceived idea, the various working hypothesis put forward, so that the maximum synergy can be achieved.

What kind of experimental results is needed to assess a theory :

Any theory should be assessed against a set of experimental data, which should cover 3 aspects :

- The excess energy
- The mass balance
- The radiation production

Many experimenters [5,6] have shown good correlations between excess energy and the production of a new chemical specie (generally $^{4}_{2}He$) and/or with radiation emission [9]. Emphasis will now be put on the mass balance, which is a very difficult and potentially misleading point.

Mass balance of the system under study :

It should be clearly realised, that in the field of CF and LENR, the mass balance is extremely difficult to achieve correctly. The starting system consists of a lattice containing various impurities, in which mixtures of various hydrogen isotopes (D2 with per cent amounts of H2 or H2 with ppm amounts of D2) are introduced. The final system is a lattice in which ppm amounts of new chemical species can be found, either $^{4}_{2}He$ (which can also be found in the hydrogen gas phase, if present), or/and "transmuted" nuclei. The mass balance is thus impossible to achieve, as in any reaction in which 2 bulk components (the hydrogen isotope and the lattice) can give ppm amounts of reaction products. This is just because no diminution (in the ppm range) of the bulk component(s) can be measured and put in front of the apparition (also in the ppm range) of reaction products.

We shall come back later to that point.

The hydrex concept :

Various author have proposed to explain CF and LENR by the action of an unusual combination between a proton and an electron : virtual neutron [10], tightly bound states due to the magnetic interaction between the nuclear spin of the proton and the spin of the electron [11]).

This last approach is interesting, because at very short distances the magnetic interaction is much stronger than the electrostatic one. But the emission of X radiations (in the tens of keV range) that would be the signature of such bound states has never been observed. The only possibility for this combination to exist, is thus a metastable state or resonance.

Indeed, it has been shown by a QED calculation [12] that resonances of long life time (s), nuclear dimensions (fm) and low energy of formation (eV) could exist. These resonances had been proposed to explain certain nuclear fusion reactions [13]. To explain our results we put forward the following working hypothesis : in a metal lattice and under proper conditions, the formation of such resonances (metastable states) could be favoured. We propose to call them HYDREX (DEUTEX in the case of deuterium) and we assume that they are actually formed in CF and LENR experiments. We note ${}_1^1\widetilde{H}$ the HYDREX and ${}_1^2\widetilde{H}$ the DEUTEX.
Assuming that HYDREX can be formed and is actually formed in CF and LENR experiments, doesn't say anything about how it is formed. But, some experimental data point to :

-the importance of variable electrical currents flowing through the lattice [1,5,6].
-the beneficial effect of diffusion of the hydrogen through the lattice [6]
-the beneficial effect of an external magnetic field. [1]
-the beneficial effect of a high current density at high frequency [14]
-the great importance of the type of lattice used and the defects in this lattice

These data provide some guidance to optimize the synthesis of HYDREX, which, however, is probably the crucial point, not yet completely mastered, in CF and LENR experiments.

The HYDREX-NUCLEUS cluster :

From its description, HYDREX is a nuclear-size electromagnetic metastable state of the proton/electron system. Its magnetic moment is likely to be of the order of the magnetic moment of the electron. It could be polarized in the strong electrostatic potential of a big nucleus (it could even be a permanent dipole).
In a region of the lattice where a sufficient number of HYDREX could be formed, a first HYDREX could attach to a nucleus of the lattice by electrostatic interaction, the proton staying out of the nucleus surface (strong electrostatic repulsion). Many other HYDREX could then attach (very rapidly and in a catastrophic way), to the same nucleus, now having the strong magnetic moment of the first HYDREX attached, yielding a H-N cluster (HYDREX-NUCLEUS cluster : see figure 1).

Figure 1a is a tentative visualisation of the (H-N) cluster when formed. The presence of a negative layer (electrons of HYDREX) close to the nucleus would increase the repulsion between its protons (by lowering the coulomb barrier of the nucleus - Figure 1b), thus increasing its instability. In other words, and from a

Figure 1a

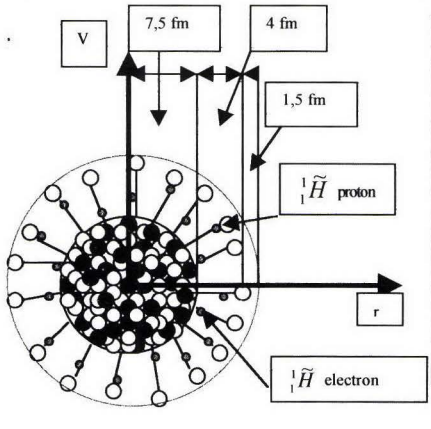

Figure 1b

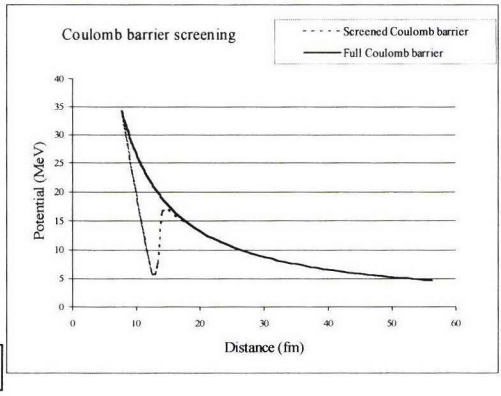

dynamic point of view, the loss of kinetic energy of the HYDREX attaching to the nucleus, would be compensated by the excitation energy gained by the nucleus. This exchange of energy (E_E) can be estimated to be in the order of some 1 MeV per HYDREX attached (when N is uranium).

The (H-N) cluster can be viewed as the equivalent of the "**compound nucleus**" considered in a classical nuclear reaction (one target, one projectile), but with much longer life time (fraction of seconds compared to some 10^{-16} seconds) and many more partners (HYDREX) at nuclear distance. A global many-body reaction between the excited nucleus and the surrounding HYDREX could then occur, when the excitation energy of the nucleus have reached a sufficient level (that is when a sufficient number of HYDREX have attached to it). The products of the reaction could be mainly α particles and a residual nucleus of mass smaller than that of the initial one. Due to the fact that this nuclear rearrangement is a many body reaction, the products formed should be stable products in their ground states, most of the reaction energy being carried away as kinetic energy by the alpha particles formed (de-excitation by evaporation rather than by radiation).

The overall nuclear reaction in the H-N cluster :

This reaction can be written as

$$ {}^{A}_{Z}N \quad + \quad n_1{}^{1}\widetilde{H} \rightarrow \boxed{\text{CLUSTER } {}^{A}_{Z}N^{*}, n_1{}^{1}\widetilde{H}} \rightarrow {}^{A'}_{Z'}N' \quad + \quad m_2{}^{4}H_e \qquad (1) $$

where ${}^{1}_{1}\widetilde{H}$ is the HYDREX form of hydrogen and ${}^{A}_{Z}N^{*}$ the excited nucleus.
A simple mass balance of the protons and neutrons involved in (**1**), yields :

$$ n = (A - A') - 2.(Z - Z') \quad \text{and} \quad m = \tfrac{1}{2}.[(A - A') - (Z - Z')] $$

The values of m and n allow the calculation (from mass loss) of the Q value of reaction (**1**). If $(A - A') - (Z - Z')$ is an odd number, an additional product may be formed : ${}^{3}_{2}H_e$ and (**1**) becomes (**1'**)

$$ {}^{A}_{Z}N + n_1{}^{1}\widetilde{H} \rightarrow {}^{A'}_{Z'}N' + m_2{}^{4}He + {}^{3}_{2}He \qquad (1') $$

with $n = (A - A') - 2.(Z - Z') + 1$ and $m = \tfrac{1}{2}.[(A - A') - (Z - Z') - 1]$

The Q values are in that case much lower and ${}^{3}_{2}H_e$ should thus be a minor product.

Application to the case of palladium :

Table 1 below gives the values of n, m, and Q when N is ${}^{110}_{46}Pd$ and for various residues of evaporation N', ranging from ${}^{74}_{34}Se$ to ${}^{50}_{24}Cr$ (The results are comparable for other isotopes of N and N',but the amplitude of the Q values are higher for the highest A value of N combined with the lowest A' value of N'). The energy available for the activation of nuclear reaction (**1**) is E_A estimated to be equal to n.E_E (E_E # 0.5 MeV for Pd).

The last column of table 1 gives the amount of the various nuclei N' found in experiment (3H06) [1]. It can be seen that there is a good fit between the amounts measured and the calculated Q values. Moreover, a

Table 1

N'	n	m	Q MeV	Q/m MeV/He	E_A MeV	N' produced (atom)
$^{50}_{24}Cr$	16	19	30,9	1,6	8,0	$1x10^{16}$
$^{55}_{25}Mn$	13	17	21,2	1,2	6,5	$<0.01x10^{16}$
$^{54}_{26}Fe$	16	18	39,5	2,2	8,0	$1,6.10^{16}$
$^{59}_{27}Co$	13	16	28,3	1,8	6,5	$<0.01x10^{16}$
$^{58}_{28}Ni$	16	17	46,0	2,7	8,0	$0.1x10^{16}$
$^{63}_{29}Cu$	13	15	43,3	2,9	6,5	$0.3x10^{16}$
$^{64}_{30}Zn$	14	15	42,0	2,8	7,0	$4.3x10^{16}$
$^{69}_{31}Ga$	11	13	28,0	2,2	5,5	$<0.01x10^{16}$
$^{70}_{32}Ge$	12	13	36,7	2,8	6,0	$<0.01x10^{16}$
$^{75}_{33}As$	9	11	22,0	2,0	4,5	$<0.01x10^{16}$
$^{74}_{34}Se$	12	12	40,9	3,4	6,0	$<0.01x10^{16}$

minimum energy of activation E_A of some 6.5 MeV seems to be needed for the reaction to start. Q/m gives an order of magnitude of the energy of the α paricles emitted. The Q values for the transmuted products are in the range 40 to 50 MeV. This is lower than that was measured in experiment 3H06 (130 MeV). This discrepancy could be due to the fact that the residue of evaporation could be 2 nuclei instead of 1 (for instance Zn and Mg). In that case the Q values are in the order of 70 to 80 MeV.

Application to the case of uranium :

In the case of uranium, Table 2 shows no clear maximum of the Q values computed for N' ranging from $^{232}_{90}Th$ to $^{168}_{70}Yb$. It is possible that 2 regimes can exist for reaction (**1**), depending on the rate of production of HYDREX : a regime with activation energy of some 13 to 14 MeV, where the local maximum of Q is for lead, and a regime with activation energy of some 20 MeV where the local maximum of Q is for Lu. This would be compatible with the experimental results.

Table 2

N'	N	m	Q MeV	Q/m MeV/He	E_A MeV
$^{168}_{70}Yb$	26	24	244,0	10,2	26
$^{175}_{71}Lu$	21	21	207,9	9,9	21
$^{174}_{72}Hf$	24	22	228,1	10,4	24
$^{180}_{73}Ta$	20	19,5	203,5	10,4	20
$^{180}_{74}W$	22	20	211,8	10,6	22
$^{185}_{75}Re$	19	18	188,9	10,5	19
$^{184}_{76}Os$	22	19	209,0	11,0	22
$^{191}_{77}Ir$	17	16	171,5	10,7	17
$^{190}_{78}Pt$	20	17	192,1	11,3	20
$^{197}_{19}Au$	15	14	156,2	11,2	15
$^{198}_{80}Hg$	16	14	163,5	11,7	16

N'	N	m	Q MeV	Q/m MeV/He	E_A MeV
$^{203}_{81}Tl$	13	12	141,0	11,7	13
$^{204}_{82}Pb$	14	12	147,7	12,3	14
$^{209}_{83}Bi$	11	10	123,4	12,3	11
$^{210}_{84}Po$	12	10	128,5	12,8	12
$^{226}_{88}Ra$	4	4	43,8	10,9	4
$^{232}_{90}Th$	2	2	21,9	11,0	2

Conclusion :

The HYDREX hypothesis describes CF and LENR as essentially the same phenomenon. It should be rather easy to check it by measuring the (ppm) amounts of ^4_2He and the (ppm) amounts of new nuclei in the same experiment, thus allowing a correct mass balance to be made. Moreover, for certain metals (uranium, nickel), the energy of the α particles formed should be in the range 6 to 10 MeV, and thus detectable.
Finally, one thing must be stressed : none of the above described nuclear reactions have their counterpart with DEUTEX (a specific DEUTEX reaction might be $^2_1H+^2_1\widetilde{H}\rightarrow^3_1H+^1_1H$ + 4,1MeV explaining small amounts of tritium). This could mean that HYDREX synthesis is easier when % amounts of hydrogen are treated in a lattice highly loaded with deuterium, as in deuterium experiments, than when hydrogen alone is present. When the synthesis of HYDREX is mastered, CF and LENR experiments should became fully reproducible, opening the way to **nuclear catalysis**.

[1] J.Dufour, D.Murat, X.Dufour and J.Foos Hydrex catalysed transmutation of uranium and palladium-Experimental part. *"Proceeding ICCF8"* (2000) to be published
[2] T.O Passel *"Proceedings 1CCF8"* (2000) to be published.
[3] X.Z Li *"Proceedings ICCF 8"* (2000) to be published.
[4] G.H Miley *"Proceedings ICCF8"* (2000) to be published
[5]M.H.Miles,B.Bush,K.Johnson Anomalous effects in deuterated systems *"Naval air warfare center weapons division China Lake,CA 93555-6100"* Sep.96
[6] M.McKubre, F.Tanzella,P.Tripodi,P,Hgelstein The emergence of a coherent explanation for anomalies observed in D/Pd and H/Pd systems. *"Proceedings ICCF8"* (2000) to be published.
[7]P.Hagelstein A model for fast ion emission in metal deuterides *"Proceeding ICCF8"* (2000) to be published
[8]V.Violante,C.Sibilia,D.Di Gioacchino,M.McKubre,F.Tanzella,P.Tripodi *"Proceeding ICCF8"* (2000) to be published
[9]D.Tuggle,T.Claytor,S.Taylor Tritium evolution from various morphologies of palladium *"Transaction of fusion technology ICCF4"* Dec.94 26 (221,231)
[10]J.Dufour Cold fusion by sparking in hydrogen isotopes *"Fusion Technology"* Sep. 1993 **24** (205-228)
[11]R.D.Dantanasijevic,D.Konjevic,Z.Maric,D.M.Sevic,J.P.Vigier,A.J.Jaric Cold fusion in terms of new quantum chemistry : the role of magnetic interactions in dense media *"Proceedings ICCF5"* Ap. 95 (505,522)
[12] J.R. Spence, J.P. Vary Electron-proton resonances at low energy from a relativistic two-body wave equation." *Phys Lett B"* 271 (1991) 27-31
[13]F.F.Meyer,J.R.Reitz *"Fusion technology"* **20** 1991 (367-372)
[14]F.Celani,A.Spalone,P.Tripodi,D. Di Gioacchino New kinds of electrolytic regimes and geometrical configurations to obtain anomalous results in Pd(M)-D systems *"Proceedings ICCF6"* Oct.96 Vol 1 (93,104)

Conference Proceedings Vol. 70
"ICCF8"
F. Scaramuzzi (Ed.)
SIF, Bologna, 2000

ON THE PROBABILITY OF COLLISION OF THE NUCLEI IN H_2 AND D_2 MOLECULES

LUIGI OLEARI
Dipartimento di Chimica Generale ed Inorganica, Chimica Analitica, Chimica Fisica
Parco Area delle Scienze, Università di Parma - 43100 Parma -Italy

Summary

It is shown that the collision of the nuclei is possible only in molecules with angular momentum quantum number $J = 0$. Moreover, it is pointed out that the motion correlation between electrons and nuclei has a decisive role on the probability of contact of the nuclei. A first calculation of the vibrational wave function within the Born-Oppenheimer approximation with a accurate Morse potential, i.e. with a full correlation of the electrons with respect to the nuclei and not vice versa, gives a probability density at $R = 0$ which ranges from 10^{-13} to 10^{-9} a_0^{-3} (it varies with the vibrational state) and hence a probability of collision from 10^{-25} to 10^{-20}. A second calculation, less accurate for the electronic part, in which the overall correlation is considered, gives a probability density $10^{-9} \div 10^{-5}$ a_0^{-3} and a probability of collision $10^{-20} \div 10^{-17}$. In both calculations the probability of collision increases remarkably by several orders of magnitude with the vibrational state.

Introduction

The main objection against Cold Fusion is based on the fact that two deuterons have to overcome an extremely high coulomb potential barrier before contact.

The answer to this objection can be found in the fact that usually a pair of deuterons is not isolated but is part of a system containing electrons (e.g. deuterium atoms in a metal (Pd,Ni)). In fact, in this case we have negative electron-deuteron electrostatic interactions that can counterbalance the positive deuteron-deuteron interaction. Since such compensation must occur especially when two deuterons are very close, it is clear that the possibility of contact depends in a decisive way on the correlation between the motions of the deuterons and of the electrons. Particularly, when the deuterons are very close, it depends on how great is the probability that one of the electrons is also very close. It is something like a three-body encounter, which has a much smaller probability than the two-body one. Therefore it is important to investigate the probability of contact of two deuterons in systems containing electrons and the extent of influence of the environment on this probability.

In this work, we studied the molecules H_2 and D_2 because they are relatively simple to be treated by quantum mechanics when an electron-nuclei correlation is introduced. As it is well known, these systems have been widely investigated and the related literature is very extensive. The classical treatment is based on the Born-Oppenheimer (BO) approximation, which considers the motion of the electrons with respect to successive fixed positions of the nuclei and the motion of the nuclei in an averaged potential due to the electrons. This is certainly a very good approach because it takes into account the correlation of the electrons with respect to the nuclei, which is preponderant, and neglects that of the nuclei with respect to the electrons, which is certainly much smaller. However, it is worth investigating the overall correlation, especially when the distance between the nuclei is short, in order to have information on the probability of collision of the nuclei. So far we have not found references in which the overall correlation between nuclei and electrons when the former are rather close is considered.

On the possibility of collision of the nuclei.

As it is known [1, 2, 3], the wave function (WF) of diatomic molecules can be written as a product of two functions, one related to the angular motion (a spherical harmonics Y_J^{MJ}) and the other related to the vibration and electron motions. In particular, in the cases of H_2 and D_2, we have:

$$\Psi = Y_J^{M_J}(\theta,\varphi)\psi(1,2;R)$$

where $\psi(1,2;R)$ is a solution of the following Schroedinger equation:

$$-\frac{1}{2m_r}\frac{1}{R^2}\frac{\partial}{\partial R}\left(R^2\frac{\partial\psi}{\partial R}\right)+\frac{J(J+1)}{2m_rR^2}\psi+\frac{1}{R}\psi+\hat{H}_{el}\psi=E\psi \qquad (1)$$

$$\hat{H}_{el}=-\frac{1}{2}\nabla^2_{(1)}-\frac{1}{2}\nabla^2_{(2)}+V_{ne}+V_{nn}+\frac{1}{r_{12}} \quad \text{with} \quad V_{ne}=-\left(\frac{1}{r_{1A}}+\frac{1}{r_{1B}}+\frac{1}{r_{2A}}+\frac{1}{r_{2B}}\right) \quad \text{and} \quad V_{nn}=\frac{1}{R} \qquad (2)$$

Here the equations are written in atomic units (a.u.)

$Y_J^{M_J}(\theta,\varphi)$ = spherical harmonic

1, 2: denote the electrons A,B: denote the nuclei

R= distance between the nuclei r_{iA} = distance between electron i and nucleus A

m_r= reduced mass of the nuclei relative to that of the electron

J = rotational quantum number

In connection with $\psi(1,2;R)$ we can define a «probability density» $p_k(R)$

$$p_k(R)=\int\left|\psi_{k,J=0}\right|^2 d\tau_{el} \qquad \text{in} \quad a_0^{-3} \quad (a_0 = \text{Bohr radius})$$

related to a vibrational state k and a nuclear distance R, and an overall probability of collision P_k:

$$P_k=\int_0^{2R_D} p_k(R)R^2\,dR\cong\frac{1}{3}(2R_D)^3\,p_k(R=0)$$

with $\int_0^{\infty} p_k(R)\,R^2\,dR=1$ and R_D =radius of deuteron in a_0.

It can be proved that when $J\neq0$, because of the presence of centrifugal potential term $J(J+1)/2m_rR^2$, it must hold $\psi(1,2;R=0)=0$ and hence $p_k(R=0)=0$ $P_k=0$

This means that in molecules with $J\neq0$ the probability of collision of the nuclei is zero. Conversely, with $J=0$ and the centrifugal potential term missing, it can be

$$J=0 \qquad \psi(1,2;R=0)\neq0 \qquad p_k(R=0)\neq0 \qquad P_k\neq0$$

There follows a nonzero probability of collision. (The situation is rather similar to that of the hydrogen atom. Only when the electron is in a *ns* orbital, i.e. zero angular momentum, the probability density on the nucleus is nonzero). Therefore, only those molecules in states with $J=0$ have to be considered for the nuclei collision.

There is another limiting factor of the probability of collision. As it is known, the deuterons have spin 1 and, in the case of D_2, their pairing gives quintet, triplet and singlet states. The quintet and singlet spin WF are even with respect to the exchange of the deuterons and the triplet is odd. Since deuterons are bosons and the overall WF must be even, it follows that the quintet and singlet states can combine only with rotational states

with J even and the triplet state with J odd [5]. In particular the state with $J = 0$ can exist only in the singlet and the quintet states. If, in an approximate estimate, we treat the D_2 molecule as a rigid rotator with a rotational constant $B_e = 30.429$ cm^{-1} [6] and assume a Boltzmann distribution among the rotational states, we have that at room temperature only 3 % of all molecules are in the singlet state with $J = 0$.

By re-writing eq.(1) as follows:

$$-\frac{1}{2m_r}\frac{1}{\psi}\frac{1}{R^2}\frac{\partial}{\partial R}\left(R^2\frac{\partial\psi}{\partial R}\right)-\frac{1}{\psi}\frac{1}{2}\left[\nabla^2_{(1)}+\nabla^2_{(2)}\right]\psi+V_{ne}+\frac{1}{r_{12}}+V_{nn}=E$$

it is evident that, when $R\to 0$, the term V_{nn} diverges to ∞ and must be counterbalanced by another term. If simultaneously the term V_{ne} does not diverge to $-\infty$, V_{nn} is counterbalanced by $-\frac{1}{\psi}\frac{1}{2m_r}\frac{1}{R^2}\frac{\partial}{\partial R}\left(R^2\frac{\partial\psi}{\partial R}\right)\Big|_{R\to 0}$. This means that, despite $\psi(1,2;R=0)\neq 0$, its absolute value and, hence, $p_k(R=0)$ are very small. Conversely, when simultaneously $V_{nn}\to\infty$ and $V_{ne}\to -\infty$, such that their sum does not diverge to $+\infty$, then the values of $|\psi(1,2;R=0)|$ and of $p_k(R=0)$ can be relatively much larger.

The above considerations show the important role of the correlation between the motion of the nuclei and that of the electrons for $R\to 0$.

The collision probability from the vibrational WF with BO approximation.

With $J = 0$, first we carried out a calculation on the vibrational motion within the BO approximation by considering a $W_{Morse}(R)$ potential as:

$$W_{Morse}(R)=\frac{1}{R}+W_{el}(R)$$

where, for the electronic energy $W_{el}(R)$, we have used the expansion:

$$W_{el}(R)=-1-\sum_i c_i\exp\left(-\gamma_i R^2\right)$$

obtained by a fitting of the accurate data of [7]. The RMS of the differences is $3.5\ 10^{-4}$ a.u.. The equation parameters are in Tab.1.

Tab. 1.

	1	2	3	4	5	6	7
c_i	0.190805	0.306305	0.317196	0.128746	0.289819	0.389849	0.34516
γ_i	15.591625	2.536481	0.840293	0.549720	0.266439	0.166776	0.0250

Moreover, we have assumed the vibrational WF expressed as a linear combination of two sets of functions:

$$\psi_k^{vibr}(R)=\sum_s c_{ks}\eta_s(R)+\sum_\rho c_{k\rho}\eta_\rho(R)$$

a) $\eta_s(R) = (R-R^\circ)^\nu \exp[-\beta^\circ(R-R^\circ)^2]$ with $R^\circ=1.401\ a_0$ (bond length), $\beta^\circ = 12.5\ a_0^{-2}$; $\nu = 0\div 8$ (integer). Linear combinations of this set approximate the WF of the lowest vibrational states in the range around the bond length distance. (Linear combinations of this set are also the WF of a harmonic oscillator)

b) $\eta_\rho(R)=(R-R_\rho°)^\nu \exp[-\beta_\rho°(R-R_\rho°)^2]$ with $\nu=0$, $R_\rho°=0.14\times n$, n=0÷8, and $\beta_\rho°=125\ a_0^{-2}$
These values of the parameters are properly chosen to take into account the motion of the nuclei at short distance.

The vibrational WF was calculated by solving the secular equation with the Hamiltonian:

$$\hat{H} = -\frac{1}{2m_r}\frac{1}{R^2}\frac{\partial}{\partial R}\left(R^2\frac{\partial \psi}{\partial R}\right) + W_{Morse}(R)$$

The evaluation of the matrix elements was done by numerical integration. Particular attention has been paid to accuracy because the probability density at $R = 0$ is a very small quantity. In Tab.2 we report the results in the case of D_2.

Tab.2.

		ground state	1st exc..state	2nd exc.state	3rd exc.state
Set a) only	$p_k\ a_0^{-3}$	3.0×10^{-22}	5.3×10^{-17}	1.0×10^{-14}	4.5×10^{-14}
	P_k	4.3×10^{-34}	7.6×10^{-29}	1.5×10^{-26}	6.5×10^{-26}
Set a)+b)	$p_k\ a_0^{-3}$	1.5×10^{-13}	3.1×10^{-13}	1.7×10^{-10}	7.5×10^{-10}
	P_k	2.1×10^{-25}	4.5×10^{-25}	2.5×10^{-22}	1.1×10^{-21}

where

$p_k = p_k(R=0) = |\psi_{vibr}|^2$ is the probability density at $R = 0$;

$P_k \approx (1/3)(2R_D)^3\ p_k(R=0)$ is the probability of collision (i.e. shorter distance than twice the deuteron radius R_D); $R_D = 4.32$ Fermi $= 8.16\times10^{-5}\ a_0$ [4]

Clearly, in the case with set a)+b) we have greater values of P_k.

An approach to a nuclei-electron «correlated» wave function.

In general terms, an approximate correlated WF of a system with several particles can be obtained by means of a linear combination of products of functions related to different sets of particles. Thus in the case of H_2 and D_2 molecules it can be written:

$$\psi(1,2;R) = \sum_i a_i \xi_i(R)\phi_i^{elet}(1,2;R) \qquad (3)$$

This means that, in connection to a given electronic function $\phi_i^{elet}(1,2;R)$, we have a correlated vibrational function $\xi_i(R)$. From the above considerations it is evident that, if, for instance, $\phi_i^{elet}(1,2;R)$ describes an electron distribution such that one of the electrons is very close to the nuclei or in the region between the nuclei for any value of R, such that $V_{ne}+V_{nn}<0$, we have, correspondingly, a relatively large value of $|\xi_i(R)|$, even if R is very short.

If we assume that the various $\xi_i(R)$ can be expressed as different linear combinations of a common basis set of functions $\eta_\rho(R)$:

$$\xi_i(R) = \sum_i b_{i,\rho}\eta_\rho(R) \qquad (4)$$

the expression of the WF becomes:

$$\psi(1,2;R) = \sum_{i,\rho} c_{i,\rho}\eta_\rho(R)\phi_i^{elet}(1,2;R) \qquad c_{i,\rho} = a_i b_{i,\rho}$$

In our calculation we have approximated the $\phi_i^{elet}(1,2;R)$ to properly symmetrized products of gaussian type orbitals (gto) and electron spin functions. For the products, we considered two schemes according to the conventional language of chemists: "covalent" when the two

gto belong to different nuclei and "ionic" when the gto belong to the same nucleus. Therefore the following: expressions have been used:

$$\psi = \sum_{\rho,r,s,u} c_{\rho,r,s,u}\, \eta_\rho(R)\, \phi^u_{r,s}(1,2;R) \tag{5}$$

where

$u = cov, ion$ (cov = covalent, ion = ionic)

$$\phi^{cov}_{r,s} = \left[\chi_{rA}(1)\chi_{sB}(2) + \chi_{sB}(1)\chi_{rA}(2) + \chi_{sA}(1)\chi_{rB}(2) + \chi_{rB}(1)\chi_{sA}(2)\right]\sigma$$

$$\phi^{ion}_{r,s} = \left[\chi_{rA}(1)\chi_{sA}(2) + \chi_{sA}(1)\chi_{rA}(2) + \chi_{sB}(1)\chi_{rB}(2) + \chi_{rB}(1)\chi_{sB}(2)\right]\sigma$$

$\sigma = \frac{1}{\sqrt{2}}\left[\alpha(1)\beta(2) - \beta(1)\alpha(2)\right]$ electron-spin function

$\alpha(i)$, $\beta(i)$ = one-electron spin functions

$$\begin{cases} \chi_{rA}(1) = \exp\left[-\alpha_r r_{1A}^2\right] & (s\text{-type}) \\ \chi_{rA}(1) = z_{1A}\exp\left[-\alpha_r r_{1A}^2\right] & (p\text{-type}) \end{cases}$$

χ_r = gaussian type orbital (gto) ;

It must be pointed out that a gto with a large value of the exponent a_r corresponds to an electron that moves very close to the nucleus. Therefore, when one of the above symmetrized expressions $\phi_{r,s}{}^u(1,2;R)$ has a gto with a large exponent, because of the counterbalance between V_{nn} and V_{ne}, it must have a correlated $\xi_{rs}{}^u(R)$ in eq.(3), and hence a proper combination of $\eta_\rho(R)$ in eq.(4), that does not become very small when $R \to 0$. It follows that the related product $\xi_{rs}{}^u(R)\ \phi_{r,s}{}^u(1,2;R)$ becomes a predominant term when $R \to 0$

With regard to the set of functions $\eta_\rho(R)$, we used the same choice of the above calculation with a Morse potential. Specifically with regard to the parameters:

set a): : $R_\rho^\circ = 1.401\ a_0$ $\beta_\rho = 12.5\ a_0^{-2}$ $\nu_\rho = 0 \div 5$.

set b) : $R_\rho^\circ = 0.14 \times n\ a_0$, n=0÷2 $\beta_\rho = 125\ a_0^{-2}$ $\nu_\rho = 0$

Even in this case, the WF was obtained by solving a secular equation. The evaluation of the matrix element has been done by carrying out analytically the integration related to electron co-ordinates and numerically with respect to R. Moreover particular attention has been paid to the accuracy of the numerical calculation.

Unfortunately in this calculation scheme the number of terms in eq.(5) increases quite rapidly with the basis sets of gto and of $\eta_\rho(R)$ functions. Moreover, the expansion (5) is slowly convergent and large basis sets should be used. Numerous calculations have been carried out with different basis sets. The most suitable values of the parameters α_r, i.e. gto exponents, and β_ρ, R_ρ°, ν_ρ of $\eta_\rho(R)$ have been determined.

We report here the results for D_2 related to a case with 8 gto, 6 η_ρ(R) of set a) and 3 η_ρ(R) of set b), which corresponds to a secular equation 720×720. The values of the related α_r parameters are in Table 3.

Tab. 3.

	1	2	3	4	5	6
s-type	0.168856	0.623913	3.42525	13.701	45	150
p –type	1.16	6	25			

The results of D_2 are given in Table 4. Those related to H_2 differ only very slightly.

Tab.4.

		ground state	1st exc..state	2nd exc.state	3rd exc.state
Set a) only	$p_k\, a_0^{-3}$	1.1×10^{-20}	7.8×10^{-18}	3.1×10^{-16}	1.9×10^{-16}
	P_k	1.7×10^{-32}	1.1×10^{-29}	4.5×10^{-28}	2.7×10^{-28}
Set a)+b)	$p_k\, a_0^{-3}$	6.9×10^{-9}	2.8×10^{-7}	1.7×10^{-5}	8.9×10^{-6}
	P_k	1.0×10^{-20}	4.0×10^{-19}	2.4×10^{-17}	1.3×10^{-17}

The values related to set a) only are rather similar to those obtained above with the Morse potential and with the adiabatic BO approximation. Conversely the values with set a)+b) are much greater than those of Tab.2. Clearly this proves the important role of the correlation between electrons and nuclei motions, in spite of the rather limited basis set. A new calculation project with a more extended basis is in progress. Unfortunately computer time increases very rapidly with the dimensions of the basis set.

Anyway, from our numerous calculations we have clear evidence that, when we increase the number of gto components with great exponents, there is also an increase in the probabilities $p_k(R=0)$. Therefore, we think that larger probabilities of collision can be obtained by extending the basis.

Conclusions

A first limitation of the probability of collision of the nuclei is due to the rotational motion and to the spin pairing of the nuclei. In some way, this can be partially overcome by «hindering» the rotation and by "catalysing" the transfer between the nuclear spin states. Perhaps this, to some extent, occurs already when D_2 is solved in transition metals.

With regard to the probability of collision when $J = 0$, we think that the above values are certainly reliable, at least, as an order of magnitude and, in any case, they are a lower boundary. A higher probability is expected with a larger basis set of functions.

It is worth pointing out that the probability of collision increases with the vibrational state, except few cases. Such an increase can be remarkable, even of several orders of magnitude.

Acknowledgements

This research has been carried out with financial contributions from the Italian C.N.R. (P.F.-MSTA II; contribution n. 99.01838.PF34) and MURST (COFIN 99).

References

[1] L.Pauling, E.B.Wilson, *Introduction to Quantum Mechanics*, McGraw Hill (1935) pag. 264-265 and 340-341.

[2] H.Eyring, J.Walter, G.E.Kimball, *Quantum Chemistry*, John Wiley & sons (1944) 8th. printing ed. (1958), pag 212-213 and 268.

[3] C.J.H.Schutte, *The Wave Mechanics of Atoms, Molecules and Ions*, Edward Arnold Publ. (1968), pag.82-86.

[4] Emilio Segre, *Nuclei e Particelle*, Zanichelli, 2nd ed. (1982), pag. 382.

[5] P.W.Atkins and R.S.Friedman, *Molecular Quantum Mechanics*, Oxford Univ.Press (1997), 3th Ed., pag. 334-335.

[6] G.Herzberg, *Molecular Spectra and Molecular Structure - I. Spectra of Diatomic Molecules*, Van Nostrand Company, 2nd Ed. (1966), pag. 533.

[7] W.Kolos and C.C.J.Roothaan, *Reviews of Modern Physics*, **32**, n.2, 219-232 (1960).

Conference Proceedings Vol. 70
"ICCF8"
F. Scaramuzzi (Ed.)
SIF, Bologna, 2000

Probability of deuteron-plasmon fusion at room temperature within microcracks of crystalline lattices with deuterium loading

Fulvio Frisone

Department of Physics, University of Catania, Corso Italia 57, 95129 Catania

CSFNSM - Catania -

Running Title: **Probability of deuteron-plasmon fusion at room temperature**

Abstract

This communication seeks to demonstrate that, at room temperature, the deformation of the crystalline lattice can influence the process of interaction of deuterons introduced within it. Calculations of this probability, in fact, showed an increase of at least 2-3 orders of magnitude with respect to the probability of fusion on the surface of the lattice. These phenomena open the way to the theoretical hypothesis of a kind of chain reaction, as a result of the deuterium loading and catalysed by microcracks formed in the structure by micro-explosions, can favour the process.

I. INTRODUCTION

This communication presents a study of the influence of temperature on the phenomenon of deuteron fusion within crystalline lattices with a CFC structure. We hypothesise that a kind of chain reaction, catalysed by the microcracks [1] which arise in the structure as the result of variations in the thermodynamic conditions or other causes, can favour the process. Here we aim to confirm the hypothesis regarding microcracks through quantitative theoretical estimations of the coefficient of structural deformation of the disturbed metal lattice, independent of time, obtained for different temperature values in the range 100-300 K. Thus, the length and depth of the microcracks, induced by micro-explosions and by lattice deformation on varying the temperature in the range 100-300 K, are analysed in Section II, and an attempt is made to evaluate their influence on deuteron fusion in impure lattices on varying the energy of the deuterons.

II. DEFORMATION IN CUBIC LATTICES

This section considers whether, and within what limits, the rate of fusion within a generic cubic lattice can be conditioned or influenced, not only by local lattice defects and other thermodynamic characteristics and conditions, but also by any "deformations" arising in the crystalline lattice as the result of varying the temperature. If this effectively occurs, it is not difficult to hypothesise that the energy produced by the micro-explosions within the microcracks could favour the creation of new microcracks which, in turn, would capture further deuterons by the same mechanism and thus trigger a kind of chain reaction. On the other hand, the formation of microcracks, provoked by the energy released during long periods of electrolysis with Deuterium, has already been observed experimentally in Palladium electrodes [6], but has until now been considered only a consequence of nuclear fusion. Our hypothesis is rather that this phenomenon could favour the process, enhancing the probability of fusion of the deutons absorbed by the metal lattice. We wish to analyse the internal perturbations "independent of time" which can occur following D_2 loading, and the consequent alteration in the properties of the metal. In fact, the loading does not simply produce an increase in the percentage of deuterium present, with a consequent disequilibrium in the "d" band; according to our hypothesis, this type of procedure also produces lattice deformations followed by dislocations which would cause microcracks in the structure. In the case of internal perturbation, in fact, it can happen that the interaction between the impurities present and the dislocations produced in the metal during a deformation significantly alters the electrical properties of the material. Then, as a result of the different arrangement of the atoms with respect to the non-perturbed lattice, certain special reactions can occur and incorporate the impurities in the nucleus of the dislocations [1]. An important effect on the reaction is represented by electronic screening due to the metal lattice. This effect, already studied by Rabinowitz [2], can be accounted for by means of a model in which the negative charge is distributed in the nucleons, and can be represented schematically supposing that q is uniformly distributed within a thin spherical shell whose radius, $R \geq r_1$, is equal to the effective range of the interaction between the nucleons, describable in terms of a shifted Coulomb potential [2]:

$$V = \left(k q^2 \right) \left[\, 1/r - 1/R \, \right] \qquad r_1 \leq r \leq R \tag{1}$$

In (1), q is the deuton charge, r_1 is the semi-classical point of inversion, $k = 1 / 4\pi \varepsilon_0$, and R is the nuclear radius. Then, $V = 0$ for $r > R$. The solution for the semi-classical tunnelling factor Λ is [2]:

$$\Lambda = D \exp \left[- 2 \gamma \left(r_1 \right) \right] \tag{2}$$

$$\gamma \left(r_1 \right) = \left(\pi / 2\hbar \right) \left[\left(2q^2 / 4\pi \varepsilon_0 \right) \mu r_2 \right]^{1/2} \tag{2'}$$

In equations (2) and (2'), D is a numerical constant of the order of unity, μ is the reduced effective mass of the deuton, r_2 is the classical point of inversion, and $\hbar$ is the reduced Planck constant. To take account of the effect of impurities present in the metal, the constant D is modified in (2), substituting the product $J\eta$, where J is the concentration of impurities and $\eta \cong 1$. The numerical calculation was performed using a

programme which takes account of the temperature contributions through the deuton interaction potential $V(r)$, which in this case can be expressed as:

$$V(r) = k_0 \frac{q^2}{r} \cdot M_d \left(V(r)_M - \frac{J\,k\,T\,R}{r} \right) \tag{3}$$

where $V(r)_M$ is the Morse potential, $k = 1/4\pi\varepsilon_0$, q is the charge of the deuton, M_d the reduced mass of the deuterium nuclei, T the absolute temperature at which the metal is held experimentally, J the concentration of impurities in the crystalline lattice [5], and R the nuclear radius. It is known that in the presence of interactions between deuterium nuclei and collective phonic excitations in the metal, the number of fusions λ_f in a gas consisting of λ deuterons with density ρ is given by:

$$\lambda = \lambda_f \frac{4\pi\rho\hbar}{\mu_d} \left\langle \frac{1}{p} \right\rangle \tag{4}$$

where μ_d is the reduced mass of the deuterium nuclei, p is their impulse, and where the parentheses $\langle\ \rangle$ represent the thermal mean. We can now consider, for convenience, a cubic lattice structure subjected to deformations and calculate the probability of fusion within a microcrack, Γ, on varying the temperature. Indicating the volume of a single cell by $d\Omega$, the deformation of the whole lattice is given by:

$$\Lambda_V = \left[\left(\iiint_{\Omega} \eta \left(\xi_{(r)} \left(\frac{1}{V} \right) \left(\frac{\partial V}{\partial T} \right)_P \right)^m d\Omega \right) \frac{1}{L} \int_0^L J\, c(r,t)\, dr \right] \tag{5}$$

where $\left(\frac{1}{V}\right)\left(\frac{\partial V}{\partial T}\right)_P$ represents the volume deformation coefficient of the crystalline lattice, maintaining the pressure constant and varying the temperature and time of exposure to the deuteron gas, in function of the micro-explosions within the microcrack; η is a parameter which depends on the lattice and electronic structure of the metal under consideration; m depends on the cubic symmetry [4] of the lattice, which is $\frac{1}{3}$. Integrating on the upper limit L, which is the length of the Pd sample, gives the medium loading level; $c(r,t)$ is the local concentration of d^+ ions in the Palladium at time t, in the three directions; and J the concentration of impurities.

Finally, $\xi_{(r)}$ is the number of dislocations. We are interested in the deformations of CFC type which occur in metals such as Pd at room temperature. We will try to evaluate the dislocation of ions in the crystalline lattice induced by the deformation in order to determine the effect of this phenomenon on deuteron fusion. We have already suggested that within a microcrack, the possible consequence of a dislocation under appropriate conditions, there could occur a greater number of events than on the surface. Setting the reference system as that of the centre of mass, the probability of fusion in a zone of the metal in which there is no microcrack, for example on the surface, can be written as [1]:

$$|P|^2_{sur} = \exp\left(-2 \int_0^{\alpha} \left(\sqrt{2[E - V(r)]/\hbar^2} \right)_{sur} dr \right) \tag{6}$$

where α is approximately 0.19Å, E is the total initial energy, substantially thermal in nature. Equation (6) refer to the process of fusion on the surface of the crystalline

lattice. The Coulomb potential $V(r)$, containing the temperature contribution, is given by the expression (1):

$$V(r) = k_0 \frac{q^2}{r} \cdot M_d \left(V(r)_M - \frac{J\ k T\ R}{r} \right) \qquad (7)$$

The same symbolism is adopted in this equation as that of (3). In equation (8), $V(r)_M$ is the Morse potential, given by:

$$V(r)_M = (J / \zeta) \left\{ \exp\left(-2\varphi(r - r_0) \right) - 2\exp\left(-\varphi\left(r - r_0 \right) \right) \right\} \qquad (8)$$

J indicates the concentration of impurities present in the metal, while the parameters φ and r_0 depend on the dynamic conditions of the system, ζ is a parameter, variable between 0.015 and 0.025, which depends on the structural characteristics of the lattice, the number of "d" band electrons and the type of lattice symmetry. If we divide equation (6) by (4) and multiply by (5), it follows that:

$$|\Gamma|^2_{wm} \simeq \frac{\exp\left(-2 \int_0^{\alpha} \left(\sqrt{2[E - V(r)]/\hbar^2} \right)_{wm} dr \right)}{\lambda \cdot \frac{4\pi\rho\hbar}{\mu_d} \cdot \langle \frac{1}{p} \rangle} \cdot \Lambda_V \qquad (9)$$

Expression (9) represents the probability of fusion of the deuterons within the microcrack. This is inversely proportional to the number of nuclei absorbed by the metal. In the context of the approximations made, the probability of fusion calculated is equal to the coefficient of corner deformation per unit of total deformation of the entire lattice. Using (9), and adopting the Morse potential, the probability of fusion within the microcrack, normalised to the number of events per minute, was calculated using a numerical simulation programme which employs the "WKB" method. The potential (8) with a "shell" potential of the type (1) modified as follows:

$$V = \left(k\ q^2 \right) \left((1/r) - \frac{K\ T}{J\varepsilon\ R} \right), \qquad r_1 \le r \le R \qquad (10)$$

where K T is the mean kinetic energy of the gas, ε is the vibrational energy which is typically of the order of some eV for the quantum states under consideration, and q is the deuton charge. Using expression (6), the probability of fusion on the surface was calculated to confirm, qualitatively, the enhancing effect. Using expression (9), the probability of fusion was calculated within a microcrack with loading, i.e. J = 0.8%. This means that as well as breaking the equilibrium of the "d" band, this procedure can also enhance the tunnelling effect within the microcrack.

III. CONCLUSIONS

The principal objective of this communication was that of demonstrating if and how the deformation of the crystalline lattice, at room temperature, can influence the process of fusion. In particular, we calculated the probability of fusion within a microcrack, comparing it with that calculated on the surface to evidence a possible enhancing effect.

With this aim, we have identified the probability of fusion within a microcrack with the deformation coefficient Γ, and performed a numerical simulation using the WKB method in the case of a model with cubic structure. The result is that, in effect, the presence of lattice deformation enhances the probability of fusion by at least 2-3 orders of magnitude compared with case of non-deformed lattices.

REFERENCES

[1] FRISONE F.: Nuovo Cimento D, 18, (1996) p. 1279.

[2] RABINOWITZ M.: Mod. Phys. Lett. B, 4, (1990) p. 233.

[3] Price Hirt J. and Lothe J.: in Theory of dislocation (McGraw Hill) 1968, p. 457.

[4] ASHCROFT N. W. AND MERMIN N. D.: in Solid State Physics (Saunders College, Philadelphia) 1986, pp. 492-509.

[5] GUTKIN M. YU AND OVID'KO I. A.: Philosophical Magazine A, 70, 4, 1994, pp. 561-575.

[6] HEUI KYEONG AN, *et al.*: Fusion Technology Vol. 27, 1995 p.27.

Conference Proceedings Vol. 70
"ICCF8"
F. Scaramuzzi (Ed.)
SIF, Bologna, 2000

THE COLD FUSION PHENOMENON AND PHYSICS OF NEUTRONS IN SOLIDS

H. Kozima

Cold Fusion Research Laboratory
Yatsu 597-16, Shizuoka 421-1202, JAPAN
Tel/Fax +81-54-278-0327, e-mail cf-lab.kozima@nifty.ne.jp

Abstract

Explanation of some phases of the cold fusion phenomenon (CFP) is given using Quantum Mechanics on the basis of recent development of physics of neutrons in solids. In the explanation, successful application of the TNCF model to various events in CFP has been used as a clue to treat the problems by Quantum Mechanics. Possibility of nuclear reactions between nuclei in solids is investigated. Physics of neutrons developed recently justifies the Premises in the TNCF model and gives a whole perspective of CFP.

1. Introduction

After the discovery of the neutron as a component of the nucleus by J. Chadwick in 1932, neutrons have been used in many ways as a tool to bombard nuclei in experiments of nuclear physics, as a catalyst to induce nuclear chain reactions of $^{235}_{92}$U in atomic pile, as a wave for structural analysis of materials and so on. The source of neutrons for these applications has been nuclei emitting neutrons spontaneously or by stimulation. The ambient neutrons generated in the outer atmosphere by cosmic ray have not been utilized with purpose even if tritium on the earth is produced mainly by them through collisions with deuterons in heavy water, minor component of water on the earth with a relative concentration of 0.015 %.

Recently, it has become common knowledge in nuclear physics that atomic nuclei have rather wide variation of Z/A ratio than known 20 years ago. The so-called exotic nuclei as $^{10}_{2}$He, $^{11}_{3}$Li, $^{32}_{11}$Na and so on [1] have been observed in free space by collision experiments in these 10 years. This fact gives us a hint to investigate physics of neutrons in solids which is not touched by physicists before due to the short life time of a free neutron of 886.7 $\pm$ 1.9 s.

The investigation of physics of neutrons in solids was performed by the present author[2 $\sim$ 5] and revealed their interesting features in solids with characteristic structure and composition which can be realized in experimental procedure in researches of the cold fusion phenomenon (CFP). The essential points of neutron physics in solids are explained in the next section.

Importance of behavior of neutrons in solids for physics of CFP should be emphasized here. The cold fusion phenomenon occurs in solids at near room temperature surrounded by ambient neutrons. By conventional logic of physics as discussed in Section 3, it is clear that Quantum Mechanics established in these more than 80 years is completely applicable to CFP which occurs in solids composed of atoms with the thermal energy of about 25 meV and mutual distance of 10^{-8} cm and of nuclear interactions taking place with an energy of about 1 MeV at a distance of about 10^{-13} cm . Then, it is also clear that CFP is most easily explained by reactions catalyzed by some neutral particle(s) in solids. The neutron should be a most hopeful candidate to it.

2. Neutrons in Solids

As pointed out in the preceding section, neutron is used widely as a tool of structural analysis in the neutron diffraction. In this case, neutron is wholly parallel to photon and electron as showing the wave nature of a quantum mechanical object. It should be noticed here that the particle nature of a quantum mechanical object will be revealed in which a position measurement is performed, or in such a corresponding event like an absorption by an atom or by a nucleus, as known in Quantum Mechanics as the contraction of wave packet. The frequency of the contraction is determined by a quantum mechanical probability depending on the wave functions of pertinent particles and their interaction.

2-1 Neutron Band and Local Coherence of Neutron Bloch Waves at Boundary Region

A phase of behavior of a neutron in a crystal lattice not noticed clearly until now is formation of a band structure in the energy spectrum of the neutron.[5] A neutron in a crystal interacts with nuclei in the crystal lattice (lattice nuclei) by the nuclear force. In a periodic potential of a lattice, the wave function of a neutron, expressed by a plane wave in free space, are modified by a factor with the same periods to those of the lattice and the energy spectrum becomes stratified to be a band structure.

Due to the strong interaction with very short range $\sim 10^{-13}$ cm of the nuclear force, a neutron band in the crystal lattice of attractive interaction becomes peculiar compared with the electron band popular in solid state physics. For an appropriate strength of the interaction constant, the lowest band above zero by a standard of free space has the energy minimum at a Brillouin zone boundary. The lowest band in the free space, in this case, is pulled into the negative energy region and represents trapped states. The concept of *the neutron affinity* of a nucleus defined to treat material aptitude for CFP[2] seems to reflect this property of nuclear interaction between a neutron and a lattice nucleus.

The larger the neutron affinity with a positive sign of a nucleus is, the stronger the attractive interaction potential of the nucleus for a neutron is, and the whole band structure of the energy spectrum of the neutron becomes lower in energy. We have noticed that all nuclei used in CF experiments have positive neutron affinities if they have shown positive results of CFP. This fact suggests strong correlation between the structure of the neutron band of a solid and occurrence of CFP in its.

If the energy minimum of a band above zero is at Brillouin zone edge, there appears *the local coherence* of wave functions of neutrons in the band. The local coherence makes the density of neutrons at the boundary region very high. The one-body approximation used to calculate the band structure of the energy spectrum fails here where we must take into our consideration the strong mutual nuclear interaction between neutrons.

The characteristics of the trapped neutron assumed in the Premises 1 and 2 of the TNCF model[2,10] may be interpreted as demonstration of the feature revealed by the occurrence of the local coherence and such related phenomena as the neutron drop investigated in the next subsection.

2-2 Neutron Drop $n_{A-Z}p_Z$

If the crystal contains many nuclei of hydrogen isotopes as metal hydrides or deuterides used in CF experiments, the high density neutrons in the boundary region can form a neutron drop $n_{A-Z}p_Z$ ($Z \ll A$) grown up from one of lattice nuclei or from a *n-p* or *n-d* cluster.

Some properties of the neutron drop can be investigated on the evaporation model of nuclear reaction.[6] In an equilibrium state, evaporation and condensation are reverse processes in balance and the same situation is also in quasi-equilibrium state we consider hereafter.

In the evaporation model, the evaporated neutron from a nucleus has the Maxwell energy distribution characterized by a temperature Θ defined by the level density of the residual nucleus. The thermal energy of $\sim 1/40$ eV in CF experiments is very small in the scale of that in nuclear reaction and the temperature Θ is almost constant for a neutron drop, a group

of many neutrons and a few protons or deuterons, supposed to be in the boundary region. The evaporation channel of the neutron drop is not known at present and we have to guess it from experimental data obtained in CF experiments if possible.

The formation of the neutron drop $n_{A-Z}p_Z$ ($N_p \equiv Z \ll N_n \equiv N = A - Z$), or the neutron cluster including several protons, is considered as follows. As the exotic nuclei are formed from ordinary nuclei in solids at crystal boundary where high density neutrons are, the neutron drops can be formed there from p or d as a seed when sufficient neutrons be supplied to increase neutron number N_n in the drop. One-body approximation which concluded local coherence of neutron waves in a band loses its validity if the strong interaction between nucleons is taken in.

To consider growth of the neutron drop as a result of condensation and evaporation processes of neutrons in a quasi-equilibrium state, we assume a situation where is a neutron drop with a number density of neutrons in it n_d and a radius R ($(4\pi/3)R^3 n_d = N_n$) in a boundary region of a solid where the neutron density is n_n. Motion of neutrons in and out of the drop is treated classically in this calculation and motion of N_p protons in it is neglected. Then, rate P_c of condensation of neutrons from outside is expressed as follows;

$$P_c = 0.35 n_n v_n 4\pi R^2 \eta, \tag{1}$$

where $0.35 n_n v_n$ is the neutron flux ($\mathrm{cm}^{-2}\mathrm{s}^{-1}$) onto the drop in the boundary region and η is a factor between 0 and 1 characterizing rate of capture by the drop.

On the other hand, the rate P_e of evaporation from the neutron drop in the evaporation model is written down as follows;[6]

$$P_e = \sum_b \int G_b(\varepsilon) d\varepsilon, \tag{2}$$

where the distribution function $G_b(\varepsilon)$ is the number of neutrons emitted through a channel b with an energy between ε and $\varepsilon + \mathrm{d}\varepsilon$. The sum is extended over all channel b and the integration is over the energy ε of the particle in the channel b . We do not have any information about the function $G_b(\varepsilon)$ at present and have to take an approximate form for P_e. Considering the complex energy dependence of neutron capture cross section of many nuclei in the thermal energy region and reciprocity theorem of nuclear reactions, we can only guess strong dependence of $G_b(\varepsilon)$ on ε.

It is natural, then, to assume that the neutron drop becomes less stable with increase of the radius R or of the number of neutrons N_n in it. We, therefore, assume that P_e measures stability of the neutron drop and reaches the limit at a definite maximum value R_M of R depending probably on the number of protons N_p in the drop. We assume following dependence of P_e on R ;

$$P_e = 0.35 n_d v_d 4\pi R^2 (\frac{R}{R_M})^\beta \quad (R \leq R_M), \tag{3}$$

where β is a constant depending probably on N_p to be determined later using experimental data and n_d and v_d are density and velocity of neutrons in the neutron drop, respectively ($4\pi R^3 n_d/3 = N_n$).

Putting $P_c = P_e$ in the quasi-equilibrium state, we obtain a relation between characteristic quantities of the neutron drop in the boundary layer with a neutron density n_n;

$$n_n v_n \eta = n_d v_d (\frac{R}{R_M})^\beta. \tag{4}$$

If the temperature in the drop is the same as that of neutrons in solids, i.e. $v_n = v_d$, the radius of the drop is given as

$$R = (\frac{\eta n_n}{n_d})^{1/\beta} R_M = (\frac{\eta n_n}{n_d})^{1/\beta} N_0^{1/3} r_0. \quad (5)$$

Here, N_0 is the maximum number of N_n or the number of neutrons in the largest drop with a radius R_M and r_0 is a constant with a value 1.5×10^{-13} cm = 1.5 fm;

$$R_M = r_0 N_0^{1/3} \quad (6)$$

if we assume the same density for the drop as the ordinary nuclei. R_M and β depend naturally on the number of protons N_p in the drop as explained already.

Then, we can express R as follows;

$$R = \frac{3}{4\pi}(\eta n_n)^{1/\beta} r_0^{(\beta-1)/\beta} N_0^{1/3} \quad (R \leq R_M). \quad (7)$$

It is probable that $N_0 \sim 27$ or ${N_0}^{1/3} \sim 3$ when $N_p = 1$ and then we have

$$R \sim \frac{9}{4\pi}(\eta n_n)^{1/\beta} r_0^{(\beta-1)/\beta} \quad (R \leq R_M). \quad (8)$$

R is insensitive to N_0. If we take $N_0 = 8$, then the factor of this relation shifts by a factor $2/3$ and becomes $(6/4\pi)$.

On the other hand, the neutron drop reduces to an ordinary nucleus when $A - Z \geq Z$, or $N_n \geq N_p$, and R should be larger than r_0;

$$(\frac{\eta n_n}{n_d})^{1/\beta} N_0^{1/3} r_0 > r_0, \quad (9)$$

or

$$n_n > \frac{1}{\eta} \frac{n_d}{N_0^{\beta/3}} \sim \frac{3}{4\pi\eta} r_0^3 N_0^{-\beta/3}. \quad (10)$$

From our analysis of experimental data in CF phenomenon, we can take the maximum value of n_n in the boundary regions as 10^{31} cm^{-3} [3] and from empirical formula in nuclear physics $n_d \sim 10^{38}$ cm^{-3}, and then the above relation gives a relation of N_0 and β ;

$$N_0^{\beta/3} \sim 10^7 \eta^{-1}. \quad (11)$$

If we take the maximum number N_0 of the neutrons in a drop with $N_p = 1$ as 27 as assumed above, Eq.(11) gives $3^\beta \sim 10^7 \eta^{-1}$ or $\beta \log 3 \sim 7 - \log\eta$:

$$\beta \sim 14.7 \quad (\text{when } \eta = 1). \quad (12)$$

It is interesting to notice that the average distance of about 0.5 pm (picometers) suggested by the maximum value 10^{31} cm^{-3} of n_n in the TNCF model is very close to the characteristic distances of 1 pm obtained in the heterogeneous models of Hora et al.[8] and X.Z. Li.[9]

3. Difficulty of a Nuclear Reaction between Charged Particles in Solids

After the discovery of the cold fusion phenomenon (CFP), or "nuclear reactions and accompanied events in solids with high density hydrogen isotopes", in 1989, there have been many works trying to show possibility of nuclear reactions between charged particles in the solids.

Almost all works of them are used to take up one (or several) experimental results as a goal to be proved assuming a special mechanism not noticed before as *a missing factor*

in the conventional physics. Due to the situation where occurs CFP, the assumed missing factors are related with phonons or electrons in the crystal lattice or are effects of the periodic potential on the deuteron in the sample solids.

As was pointed out in the Introduction, CFP occurs in solids composed of atoms with the thermal energy of about 25 meV and mutual distance of 10^{-8} cm while the nuclear interactions between a nucleus and a particle takes place with an energy of about 1 MeV at a distance of about 10^{-13} cm.

We would like to suggest here only difficulty of nuclear reactions between charged particles in solids because it is impossible to prove absence of a process or an effect to occur unless we know everything relevant to it and also the method to treat them.

First of all, the average energy of phonons excited in the solids is about an order of 25 meV and it is not possible to have their accumulation up to ~ 1 MeV with a finite probability. The difference is about 10^8 or eight orders of magnitude as easily estimated by a common sense of physics. Therefore, a nuclear reaction of charged particles in solids is not catalyzed by phonons.

Second, an electron confined in a small space with a linear dimension of $\delta x \sim 10^{-13}$ cm has a momentum of $\delta p \sim \hbar/\delta x$ and therefore a relevant energy $\delta E \sim (\delta p)^2/2m_e \sim 10$ GeV. Thus an electron and also a group of electrons can not screen the repulsive Coulomb interaction between two nuclei down to a distance where works the strong nuclear interaction.

Third, a proton (or a deuteron) in the lattice of a metal hydride is known to behave as a charged particle hopping around from an interstitial site to another even if it is possible to consider a band structure for the energy spectrum of a proton in a crystal. When two deuterons in the lattice interact with nuclear force, the situation considered in the above paragraph is applied to them and particle nature, one phase of duality of a quantum mechanical particle, appears and the wave nature disappears.

Thus, it is very difficult to find out an escape route for a nuclear reaction of two charged particles in solids even if its impossibility is not proved. The complicated nature of CFP

4. Conclusion

As is shown in the paper,[10] a phenomenological approach to CFP is effective in the present stage of investigation. The nuclear transmutation observed in CFP have been explained in consistent with other data with an adjustable parameter n_n of values 10^8 to 10^{12} cm^{-3}.[2,3,11]

By the success of the TNCF model and the liquid-drop model[7] in the analysis of data in CF phenomenon (CFP), it is probable that there are high density neutrons in the samples with positive results of CFP. We could give some information about a possible state of neutrons in the metal hydrides or deuterides, the neutron drop with radius R determined by parameters of the system as Eq.(7). The numerical factor β defined in Eq.(3) was determined by experimental facts as in Eq.(12) showing very strong dependence of evaporation rate on the radius of the drop. These conclusions depend strongly on the assumption made about nature of the neutron drop and should be considered as tentative ones.

With these reservations on the quantitative conclusions, we may be able to discuss qualitative nature of the neutron drop. The neutron drop $n_{A-Z}p_Z$ ($Z \ll A - Z$) and the exotic nuclei (extremely neutron-rich nuclei) are states of neutrons in the boundary region of metal hydrides (deuterides) formed through their interaction with protons and ordinary nuclei, respectively. It might be rather probable to form an exotic nucleus than a neutron drop if we consider probability of neutron capture by a deuteron (cross section $= 5.5 \times 10^{-4}$ barns) with that by appropriate nuclei in the material, i.e. $^{48}_{22}$Ti, $^{58}_{26}$Ni and $^{104}_{46}$Pd with cross sections of 7.8, 4.5 and 8.5 barns, respectively. This tendency is, probably, the cause of frequent observations of products of NT compared with tritium (and helium-4) in systems without

$^{6}_{3}$Li in recent experiments. Further, interaction of the neutron drop with the exotic nucleus should be taken in our consideration to understand CFP as a whole as Fisher[7] did in the explanation of NT_F.

The estimation given in this paper is based on the assumption that the CFP is real and indicate some states of matter described by Quantum Mechanics. A new phenomenon, if it is really new, should includes one or more factor not noticed before related with the phenomenon. This factor is not known or missing in past and may be called *a missing factor* as noticed already. The CFP should be resolved by a missing factor if it is a real one, according to the author's viewpoint. The missing factor of the CFP is trapped neutrons from the viewpoint of the TNCF model[2,10] and it is the polyneutron in Fisher's liquid-drop model[7] for NT_F.

The tentative estimation of several properties of the neutron drop in metal hydrides and deuterides based on experimental data in CFP and given in the preceding section should be revised by more elaborate calculations of many-body system with neutrons, hydrogen isotopes and lattice nuclei distributed heterogeneously in a solid.

There are plenty of space for developing new solid state-nuclear physics if existence of the neutron drop and the extremely neutron-rich nuclei (exotic nuclei) is confirmed in the boundary region of CF materials with positive results. The application of this science will produce great possibility of new energy and material sources.

One of effective methods to verify the existence of the neutron drop is, in the author's point of view, neutron diffraction investigation of CF materials which showed positive results. Another will be NMR investigation of trapped neutrons in the boundary region. Any method other than used in CF experiments will substantiate the results obtained hitherto in this field.

References

[1] A.A. Korsheninnikov et al.[^{10}He], *Phys. Lett.* **B326**, 31 (1994); T. Kobayashi et al.[^{11}Li], *Phys. Rev. Let.* **60**, 2599 (1988); T. Suzuki et al.[^{32}Na], *Phys. Rev. Lett.* **75**, 3241 (1995).

[2] H. Kozima, *Discovery of the Cold Fusion Phenomenon —Evolution of the Solid State - Nuclear Physics and the Energy Crisis in 21st Century*, Ohtake Shuppan KK., Tokyo, Japan, 1998.

[3] H. Kozima, K. Arai, M. Fujii, H. Kudoh, K. Yoshimoto and K. Kaki, "Nuclear Reactions in Surface Layers of Deuterium-Loaded Solids" *Fusion Technol.* **36**, 337 (1999).

[4] H. Kozima, "Neutron Drop; Condensation of Neutrons in Metal Hydrides and Deuterides", *Fusion Technol.* **37**, 253 (2000).

[5] H. Kozima, "Neutron Band in Solids", *J. Phys. Soc. Japan* **67**, 3310 (1998).

[6] J.M. Blatt and V.F. Weisskopf, *Theoretical Nuclear Physics*, John Wiley & Sons, New York, 1952.

[7] J.C. Fisher, "Liquid-Drop Model for Extremely Neutron Rich Nuclei" *Fusion Technol.* **34**, 66 (1998)

[8] H. Hora, G.H. Miley, J.C. Kelly, G. Salvaggi, A. Tate, F. Osman and R. Castillo, "Proton-Metal Reactions in Thin Films with Boltzmann Distribution similar to Nuclear Astrophysics" *Fusion Technol.* **36**, 331 (1999).

[9] X.Z. Li, "Solving the Puzzle of Excess Heat without Strong Nuclear Radiation" *Proc. ICCF5* (Office of ICCF5, Valbonne, France) p.285 (1995). See also X.Z. Li, *Czechoslovak J. Physics* **49**, 985 (1999).

[10] H. Kozima, "TNCF model - A Phenomenological Approach" *Proc. ICCF8* (to be published).

[11] H. Kozima, M. Ohta, K. Arai, M. Fujii, H. Kudoh and K. Yoshimoto, "Nuclear Transmutation in Solids explained by TNCF Model" *Proc. ICCF8* (to be published).

Conference Proceedings Vol. 70
"ICCF8"
F. Scaramuzzi (Ed.)
SIF, Bologna, 2000

NUCLEAR TRANAMUTATION IN SOLIDS EXPLAINED BY TNCF MODEL

H. Kozima, M. Ohta[1] , K. Arai[2] , M. Fujii[3] , H. Kudoh[3] and K. Yoshimoto[4]

Cold Fusion Research Laboratory
Yatsu 597-16, Shizuoka, 421-1202, JAPAN
Tel/Fax +81-54-278-0327, e-mail cf-lab.kozima@nifty.ne.jp

Abstract

It have been observed in these several years occurrence of nuclear transmutation (NT) of elements with the atomic number Z larger than 4 in the surface region of cathodes in electrolytic systems. The NT is divided into two types; NT_D explained by a decay of elements and NT_F by a fission of them. These experimental facts are explained by a model with an adjustable parameter n_n (TNCF model) consistently with other data in CFP.

1. Introduction

The cold fusion phenomenon (CFP) was declared its discovery in 1989 by Fleischmann and Pons (and Hawkins)[1] with an expectation of fusion of two deuterons in a palladium hydride PdD_x.

After controversial period on the reality of CFP in solids, there have appeared new data showing unexpected nuclear products of reactions between nuclei in the crystal lattice (the lattice nuclei) in or on the cathodes used in electrolytic experiments. It is now recognized that the nuclear transmutation (NT) occurs widely and frequently in a surface region of solids occluding hydrogen isotopes used in experiments of CFP.

The feature of NT is rather striking than its occurrence itself. The transmuted nuclei have been found in near-surface region with a width of few tens μm and the ratio of transmuted nuclei to that existed originally becomes very high reaching in typical cases to several tens %. Furthermore, atomic numbers of the transmuted nuclei shift from that of the original nucleus in the solids with very large variety from one to several tens. It is clear at a glance of these data that the transmuted nuclei result from decaying of the elements or from fission of them by some causes.

There had been a systematic explanation of various events of CFP by a model with a single adjustable parameter (TNCF model) proposed by the present author.[2] In the model, the fundamental premise is an existence of thermal neutrons trapped in solids inducing CFP and reactions of a neutron with a lattice nucleus are taken into explanation of these various events in CFP.[3,4]

To explain the whole spectra of NT, it is necessary to assume a simultaneous absorption of several neutrons by a lattice nucleus.[5,6] In this paper, NT as a whole, i.e. NT_D and NT_F, is explained by the TNCF model with extension of the Premises to allow the simultaneous reaction of neutrons with a lattice nucleus.

2. Experimental Facts of Nuclear Transmutation

Before explanation of NT by the TNCF model, we give a brief introduction of experimental data on NT_D and NT_F successively in this section.

[1] Present address: Department of Nuclear Engineering, Osaka University, Osaka.
[2] Present address: Materials and Energy Research Institute Tokyo Ltd., Tokyo.
[3] Present address: Department of Energy Engineering, Yokohama National University, Yokohama.
[4] Present address: Oki Software Co. Ltd., Tokyo.

2-1. Nuclear Transmutation by a Decay NT_D

The nuclear transmutation in solids has been observed in CF experiments from around 1994 by R.T. Bush et al., I. Savvatimova et al., M. Okamoto et al. and others in its NT_D form.

Data by R.T. Bush[7]

R. Bush observed the excess heat generation and nuclear transmutations $^{23}_{11}\mathrm{Na} \rightarrow {}^{24}_{12}\mathrm{Mg}$ and $^{39}_{19}\mathrm{K} \rightarrow {}^{40}_{20}\mathrm{Ca}$ in electrolytic systems Ni(alloy)/H/K(Na). It should be noticed that the decay time of $^{40}_{19}$K, formed by a reaction $n + {}^{39}_{19}\mathrm{K}$, into $^{40}_{20}$Ca by β -decay is known as $\sim 10^9$ y in nuclear physics.

Data by R.T. Bush and D.R. Eagleton[8]

R.T. Bush and R. Eagleton observed the excess heat and the nuclear transmutation of Rb into Sr in $Ni/H_2O + Rb_2CO_3$ system (with Ni sponge cathode). Natural abundance of $^{85}_{37}$Rb and $^{87}_{37}$Rb are 72.15 and 27.85 % and decay times of $^{86}_{37}$Rb and $^{88}_{37}$Rb are 19.5 d and 17.8 m, respectively. Observed decrease of the isotope ratio $^{88}_{38}\mathrm{Sr}/^{86}_{38}\mathrm{Sr}$ ($\equiv 1/\eta$) was from the original value of $1/\eta\,)_{orig} = 8.5$ to $1/\eta\,)_1 = 3.5$ when the excess heat was Q_1 and to $1/\eta\,)_2 = 2.7$ (the ordinate of point 2) when it was Q_2 ($= 5Q_1$).

Data by I. Savvatimova et al.[9]

I. Savvatimova and her collaborators measured the excess heat, NT (nuclear transmutation) of various isotopes and elements in the surface layer of the multi-layer cathodes in discharge experiments. After the discharge of 4 hours, the sample was analyzed its isotope composition about 3 months later. Here we take up only one data set of an increase of $^{107}_{47}$Ag from 20 to 5000 ppm in the glow discharge with D_2 gas and Pd cathode. The decay time of $^{107}_{46}$Pd formed by $n + {}^{106}_{46}$Pd into $^{107}_{47}$Ag is known as $\sim 10^6$ y in nuclear physics.

Data by T.O. Passell[10]

A Pd cathode used in an experiment with an electrolytic solution D_2O + 1.0M LiOD + 200 ppm Al producing the excess heat of 0.56 MJ was subjected upon comparison measurements of the prompt gamma activation analysis (PGAA) using thermal neutrons in beams from research reactors. A result showed an $\sim$ 18 % reduction in the boron impurity $^{10}_{5}$B.

Data by M. Okamoto et al.[11]

M. Okamoto et al. observed the excess heat and the changes of key and minor elements in the cathode. We take up here, the nuclear transmutation from Al into Si in the surface layer on the cathode in Pd/ D_2O + LiOD system. The change of the density of the elements (up to 80 % for Al) occurred in the surface layer with a thickness of ~ 1 μm.

Data by H. Yamada et al.[12]

To confirm the cold fusion phenomenon under glow discharge condition, a point-to-plane electrode configuration in slightly pressurized (2 atm) deuterium gas for highly non-uniform electric field was employed by Yamada et al. A neutron burst took place in 2 runs out of total 37 runs. X-ray photo-electron spectroscopy (XPS) was used to investigate black deposit observed covering the tip surfaces of two positive Pd electrodes which was used in the runs with neutron bursts to reveal the black deposit was carbon, mixed with palladium on the surface of palladium point electrode. The relative number of oxygen atom in the surface layer is the same order as that of carbon atom ($N_O/N_C \sim 1$).

Data by G. Miley et al.[13]

Miley et al. performed electrolysis experiment with an electrolytic solution 1M Li_2SO_4 + H_2O with a cathode composed of 1000 microspheres (ms's) coated by a Ni layer. The excess heat was 0.5 $\pm$ 0.4 W from 1000 ms's. The NT products were determined by NAA and SIMS (for $^{55}_{25}$Mn) for 1000 ms's (using only 10 ms's for analysis).

Data by J. Dash et al.[14]

There were two kinds of the Pd cathode used in the experiment by Dash et al. The Pd cathodes were (A) a cold-rolled 0.35 mm-thick polycrystalline sheet and (B) a 5.5 $\times$ 10^{-2}

mm thick foil. The anodes were Pt foils of 3×10^{-2} mm thickness in both cases. H_2O and D_2O were used. In the case A, several regions on the deformed Pd cathode gave EDS spectra which showed an appreciable amount of Pt and Au. The concentration of Au on the heavy-water cathode appeared to be greater than on the light-water cathode. In the case B, chemical composition was determined in regions which had topography suggestive of localized melting. The average surface composition of the entire area of the cathode was about 85 % Pd and 15 % Pt. In spectra from several points of the cathode, there are a predominant peak at 2.98 keV corresponding to Ag.

Data by R. Notoya[15]

In a series of experiments with Ni cathodes in H_2O (and D_2O) solution of electrolytes K_2CO_3, Notoya et al. observed the excess heat, NT and positron generation in the system by the observation of gamma ray spectrum. The observed new elements supposed to be results of NT were ${}^{A+1}_{20}Ca$ and ${}^{64}_{28}Ni$ in an electrolytic system Ni/H/K with a Ni plate cathode.

The experimental data sets introduced in this subsection as a whole suggest that there are nuclear transmutations in the surface layer of materials (electrodes) explained by an existence of thermal neutrons in them. Furthermore, it will be noticed in the analysis of these data that decay times of some unstable isotopes seem shortened largely from the values in normal states as explained in the next section.

2-2. Nuclear Transmutation by a Fission NT_F

The nuclear transmutation by a fission has been observed from around 1995 by J.O'M. Bockris et al., T. Mizuno et al., T. Ohmori et al., R. Notoya et al., G. Miley et al. and others.

Data by J.O'M. Bockris et al.[16]

Bockris and his collaborator performed an experiment in which hydrogen was electrolyzed from water in contact with a palladium electrode. Using XPS and EDA, it was determined that the concentration of the new elements (Mg, Al, Cl, K, Ca, Ti, Fe, Cu, Zn, and so on) was in the range $1 \sim 10$ atomic %. These elements have no relationship to the impurities in the solution.

Data by T. Mizuno et al.[17]

Mizuno et al. observed NT in the surface layers (thickness $\ell \leq 2$ μm) of Pd and other cathodes induced by electrolysis. The identification of isotopes was performed by several methods and many elements including Pt, Cu, Cr, Pd, and others were observed and showed shifts of isotope ratios from natural ones. We take up here only one data set of ${}^{52}_{24}Cr$ in Pd/D/Li system: isotope ratio of ${}^{52}_{24}Cr$ observed in the surface layer showed a reduction from 83.8 % (natural abundance) to 50 % through an electrolysis of 30 days.

Data by T. Ohmori et al.[18]

T. Ohmori et al. observed NT, i.e. increases of ${}^{57}_{26}Fe$ and ${}^{54}_{26}Fe$, generation of C and S, in light water electrolysis with electrodes Au and Pd and electrolytes Na_2SO_4, K_2CO_3 and KOH in H_2O. In the electrolysis with a gold electrode and an electrolyte Na_2SO_4 in H_2O for a week, a notable amount of iron atoms in the range of 1.0×10^{16} to 1.8×10^{17} atoms/cm^2 are detected at surface together with the generation of a certain amount of excess energy.

Data by Iwamura et al.[19]

Iwamura et al. measured the excess heat and nuclear products simultaneously in PdD_x ($0.8 \leq x$) system using a new type of experimental apparatus. The excess heat measured in the system with a Pd plate cathode ($25 \times 25 \times 1$ mm^3) was about 10 % at maximum for the input power of 40 W. Tritium was observed qualitatively with similar characteristics to the data obtained in the former experiments. New elements of Ti, Cr, and so forth were detected.

Data by G. Miley et al.[13]

The electrolytic experiments with cathodes of the packed-bed cell (about 1000 micro-

spheres (ms's)) in a electrolyte 1M $LiSO_4$ + H_2O were performed with nickel, palladium and Pd-Ni multilayer cathodes and titanium electrodes. We take in this paper only one data set, Run #11, where Pd thin-film of 200 μm was on the polystyrene microsphere. The analysis of the sample microspheres by NAA (Neutron Activation Analysis) after an experiment lasted 211 hours showed appearance of elements with yields of Al, Cu, V, Ni, Fe, Co, Cr, Zn and Ag with amounts (in 10^{-3} μg/ms) 233, 277, 4.06, 388, 153, 2.18, 60.4, 806 and 70.6, respectively. These amounts corresponds to number of atoms (in 10^{13}/ms) of 520, 262, 4.80, 398, 165, 223, 699, 742 and 39.4, respectively.

Data by G.S. Qiao et al.[20]

The experiment on the Pd/D_x and Pd/H_x systems were performed by Qiao et al. in a stainless steel Dewar with a piece of incandescent tungsten filament in it. The vacuum annealed palladium wire (900 °C in a pressure of 10^{-3} Pa for 3 hours) was sealed in the Dewar and hydrogen isotope gas with a pressure of less than 1 atm was filled. Comparison of the element composition after and before the experiment showed remarkable increase of Zn at points near the surface of the Pd wire. The large change of element composition of Pd and Zn, if it correlate, could only be explained by fission reactions, i.e. nuclear transmutation by a fission (NT_F), in the surface region of the sample.

The above experimental data sets introduced in this subsection suggest that there are nuclear transmutations by a fission in the surface layer of cathodes containing trapped neutrons. This fact could be understood that there is a nuclear fission of elements induced by the trapped thermal neutron (TN induced fission) in cold fusion materials not noticed until the CF phenomenon was observed even if these elements are stable against fission by an energetic neutron irradiated under several tens MeV in free space,

The decay time shortening explained in the subsection 1 and the threshold energy lowering of fission in the subsection 2 are new features of solid state - nuclear physics in complex systems composed of trapped neutrons and solids with the surface layer of an isotope with a large value of the mass number.

3. Explanation by the TNCF Model

The experimental data sets showing NT_D and NT_F in surface regions of materials used in CF experiments have successfully been analyzed by the TNCF model. A brief explanation of the analyses is given in this Section.

3-1. Premises related with NT explanation

The Premises of the TNCF model related with NT at the boundary region is Premises 1 and 2.[3,4]

3-2. Nuclear Transmutation by Decay NT_D

· Fundamental reactions used in the analysis of NT_D are such reactions between a trapped neutron and nuclei in the material followed by a beta or an alpha decay as follows:[3]

$$n + {}^{23}_{11}\mathrm{Na} = {}^{24}_{11}\mathrm{Na} = {}^{24}_{12}\mathrm{Mg} + e^- + \bar{\nu}_e, \quad (1)$$

$$n + {}^{39}_{19}\mathrm{K} = {}^{40}_{19}\mathrm{K} = {}^{40}_{20}\mathrm{Ca} + e^- + \bar{\nu}_e, \quad (2)$$

$$n + {}^{16}_{8}\mathrm{O} = {}^{17}_{8}\mathrm{O} = {}^{13}_{6}\mathrm{C} + {}^{4}_{2}\mathrm{He}. \quad (3)$$

These reactions with the assumption of the decay time shortening were used to analyze the data sets introduced in the subsection 2-1 and the results were tabulated in the Table 1 on the end of this section.

3-3. Nuclear Transmutation by Fission NT_F

As relevant nuclear reactions in nuclear transmutation by a fission (NT_F), we may take up a fission reaction with emission of several (say ν) neutrons induced by an energetic or a

Table 1: Analysis of NT data. Neutron Density n_n and Relations between the Numbers N_x of Event x Obtained by Theoretical Analysis of Experimental Data on TNCF Model ($N_Q \equiv Q$ (MeV)/5 (MeV)). Typical value of the surface vs. volume ratio $S/V(\mathrm{cm}^{-1})$ of the sample is tabulated, also.

Authors	System	S/V cm^{-1}	Measured Quantities	n_n cm^{-3}	Other Results (Remarks)
Bush[7]	Ni/H/K Ni/H/Na	~ 160 ~ 160	NT_D(Ca) NT_D(Mg)	5.3×10^{10} 5.3×10^{11}	$N_Q/N_{NT}\sim 3.5$ ifτ=0 for ^{40}K)
Bush[8]	Ni/H/Rb	$\sim 10^4$	NT_D(Sr)	1.6×10^7	$N_Q/N_{NT}\sim 3$
Savvatimova et al.[9]	Pd/D_2	100	NT_D(Ag)	9×10^{10}	
Passell[10]	Pd/D/Li	400	NT_D	1.1×10^9	N_{NT}/N_Q=2
Okamoto et al.[11]	Pd/D/Li	23	Q, NT_D $\ell_0 \sim 1$ μm	$\sim 10^{10}$	$N_Q/N_{NT}\sim 1.4$ (^{27}Al$\rightarrow$ ^{28}Si)
Yamada[12]	Pd/D_2	185	n , NT_D(C)	2.0×10^{12}	
Miley[13]	Pd/H/Li	150	NT_F(Ni,Zn,$\cdots\cdots$)	4.5×10^{12}	
Dash[14]	Pd/D,H_2SO_4	57	Q, NT_D	$\sim 10^{12}$	Pt $\rightarrow$ Au
Notoya[15]	Ni/D,H/K	3.4×10^4	NT_D(Ca)	1.4×10^9	(Sintered Ni)
Bockris et al.[16]	Pd/H/		NT_F(Mg,Si,Cs,Fe, etc. in 1μm layer)	3.0×10^{11}	Only Fe(10%of Pd) is taken up
Mizuno[17]	Pd/D/Li (If Cr in Pd)	3.4	Q, NT_D $\ell \leq 2$ μm)	2.6×10^8	τ=30d, Pd 1cm$\phi\times$ 10cm
Ohmori[18]	Au/H/K	200	Q, NT_F(Fe)	$\sim 10^{11}$	(Au plate)
Miley[13]	Ni/H/Li	50	NT_D(Fe,Cr,$\cdots$)	1.7×10^{12}	
Iwamura[19]	$PdD_x$and Pd /CaOPd_x/Pd	20	$Q\sim$ 1W,$N_{NT}/N_Q\sim 1$ NT_F(Ti, Fe, Cu etc.)	3.1×10^{10}	$(N_{NT}/N_Q)_{th}$= $1\sim 3$
Qiao[20]	Pd/H_2	185	NT_F(Zn)	3.8×10^{10}	(40%NT in 1y)

thermal neutron (and/or an energetic charged particle generated by a cold fusion reaction):

$$n\,(\varepsilon) + {}^{A}_{Z}\mathrm{M} = {}^{A-A'+1}_{Z-Z'}\mathrm{M} + {}^{A'}_{Z'}\mathrm{M}, \tag{4}$$

$$n\,(\varepsilon) + {}^{A}_{Z}\mathrm{M} = {}^{A'}_{Z-Z'}\mathrm{M}' + {}^{A''}_{Z'}\mathrm{M}'' + \nu\, n, \quad (A+1 = A' + A'' + \nu). \tag{5}$$

In the cold fusion, the possible maximum energy of a particle generated by a reaction assumed in the TNCF model is that of the neutron generated by a breeding reaction

$$t + d = {}^{4}_{2}\mathrm{He}\ (3.5\mathrm{MeV}) + n\ (14.1\mathrm{MeV}),$$

and is 14.1 MeV. Therefore, the experimental result showing NT_F should be an evidence of the lowering of threshold energies for fission reaction occurring in materials from those in vacuum.

The fission reactions illustrated above with the lowering of threshold energies were used to analyze the data sets introduced in the subsection 2-2 and the results were tabulated in the Table 1.

3-4. Determined values of n_n

As a result of analysis of a data set, it is possible to determine the parameter n_n defined in the TNCF model. The determined values of n_n are tabulated also in the Table 1 with other results.

4. Conclusion

It should be emphasized here that the single parameter n_n is determined uniquely even in such cases where are several events, e.g. the excess heat Q and NT, in a sample. This is

a strong support to the model and suggests that the model reflects some phases of physics of CFP in it. Meaning of the Premises 1 and 2 and also that of n_n, however, should be investigated in terms of the physics of neutrons in solids which will be given in another paper presented in this Conference.[21]

References

[1] M. Fleischmann, S. Pons and M. Hawkins, *J. Electroanal. Chem.* **261**, 301 (1989).

[2] H. Kozima, "Trapped Neutron Catalyzed Fusion of Deuterons and Protons in Inhomogeneous Solids", *Trans. Fusion Technol. (Proc. ICCF4)* **26**, 508 (1994). And also *Proc. ICCF4* (Dec. 6 - 9, 1993, Lahaina, Maui) Vol.**4**, p.5, EPRI TR-104188.

[3] H. Kozima, *Discovery of the Cold Fusion Phenomenon –Evolution of the Solid State - Nuclear Physics and the Energy Crisis in 21st Century* (in Japanese), Ohtake Shuppan KK., Tokyo, Japan, 1997.

[4] H. Kozima, "TNCF model - A Phenomenological Approach" *Proc. ICCF8* (to be published).

[5] J.C. Fisher, *Fusion Technol.* **36**, 66 (1998).

[6] H. Kozima et al., "Nuclear Reactions in Surface Layers of Deuterium-Loaded Solids", *Fusion Technol.* **36**, 337 (1999).

[7] R.T. Bush, *Fusion Technol.* **22**, 301 (1992).

[8] R.T. Bush and D.R. Eagleton, *Proc. ICCF4* (Dec. 6 - 9, 1993, Lahaina, Maui) Vol.**2**, p.13, EPRI TR-104188.

[9] I.B. Savvatimova et al., *Trans. Fusion Technol. (Proc. ICCF4)* **26**, 389 (1994).

[10] T.O. Passell, *Progress in New Hydrogen Energy (Proc. ICCF6)*, 282 (1996).

[11] M. Okamoto, H. Ogawa, Y. Yoshinaga, T. Kusunoki and O. Odawara, *Proc. ICCF4* (Dec. 6 - 9, 1993, Lahaina, Maui) Vol.**3**, p.14, EPRI TR-104188.

[12] H. Yamada, H. Nonaka, A. Dohi, H. Hirahara, T. Fujihara, X. Li and A. Chiba, *Progress in New Hydrogen Energy (Proc. ICCF6)*, 610 (1996).

[13] G.H. Miley, G. Narne, M.J. Williams, J.A. Patterson, J. Nix, D. Cravens and H. Hora, *Progress in New Hydrogen Energy (Proc. ICCF6)*, 629 (1996). *Cold Fusion* **20**, 71 (1996).

[14] J. Dash, *Progress in New Hydrogen Energy (Proc. ICCF6)*, 477 (1996).

[15] R. Notoya et al., *Progress in New Hydrogen Energy (Proc. ICCF6)*, 675 (1996).

[16] J.O'M. Bockris and Z. Minevski, *Infinite Energy* Nos. 5 & 6, 67 (1995-96).

[17] T. Mizuno, *Progress in New Hydrogen Energy (Proc. ICCF6)*, 665 (1996).

[18] T. Ohmori et al., *Fusion Technol.* **31**, 210 (1997)

[19] Y. Iwamura, T. Itoh, N. Gotoh, M. Sakano and I. Toyoda, *The Best Ever! (Proc. ICCF7)* (1998, Vancouver, Canada), 167 (1998).

[20] G.S. Qiao, X.M. Han, L.C. Kong and X.Z. Li, *J. New Energy* **2-2**, 48 (1997).

[21] H. Kozima, "The Cold Fusion Phenomenon and Physics of Neutrons in Solids", *Proc. ICCF8* (to be published).

Conference Proceedings Vol. 70
"ICCF8"
F. Scaramuzzi (Ed.)
SIF, Bologna, 2000

TNCF MODEL –A PHENOMENOLOGICAL APPROACH

H. Kozima

Cold Fusion Research Laboratory
Yatsu 597-16, Shizuoka 421-1202, JAPAN
Tel/Fax +81-54-278-0327, e-mail cf-lab.kozima@nifty.ne.jp

Abstract

The TNCF model for the cold fusion phenomenon (CFP) is explained as an example of the phenomenological approach with a single adjustable parameter for this complicated phenomenon composed of various events occurring in complex systems. Applied to many selected data sets, the model has given satisfactory explanations and therefore the Premises of the model may be taken as reflections of some phases of physics in the materials where occurred CFP. Selection of more than 60 data sets has a statistical meaning even if each data set may include some faults in it. Physical bases of the Premises are suggested upon physics of neutrons in solids.

1. Introduction

The cold fusion phenomenon (CFP), more precisely "nuclear reactions and accompanied events in solids with high density hydrogen isotopes", is an extremely complicated phenomenon occurring in complex systems composed of composite solids including hydrogen isotopes covered by surface layers of metals or oxides in ambient background radiations, especially neutrons.

After the discovery of some phases of its events in 1989,[1] there have been explored its various phases of the phenomenon, or events, ranging from the excess heat production, tritium and helium-4 generations, neutron and photon emissions with energies up to about 10 MeV and generation of transmuted nuclei with atomic numbers larger than 3. These events seems to have listed up all by now and are divided into two categories, direct or indirect, by their relation to assumed nuclear reactions to explain them: *the direct evidence* of nuclear reactions includes spatial distribution of transmuted nuclei and energy spectra of neutron and gamma photon, and *the indirect evidence* includes the excess heat unexplainable by chemical processes and amounts of generated tritium, helium-4, and transmuted nuclei.

Other remarkable characteristics of the phenomenon are its sporadic occurrence and qualitative reproducibility, characteristics of chaotic systems. These phases of CFP together with its various products should be explained finally by a theory.

There is a pile of these complicated experimental data in CFP accumulated in these eleven years waiting to be explained by one or other theories. As a working hypothesis, it is possible, of course, to consider these events in CFP be caused by several different mechanisms working in the same system. On the other hand, it is possible to seek a single cause as a fundamental mechanism for all events in CFP. Which viewpoint one takes in the research is a matter of one's aesthetics. A trial given in this paper belongs to the latter with phenomenological manner.

It should be explained briefly a characteristic of *the phenomenological approach* contrasted to the *fundamental approach* to avoid unnecessary confusion. In the fundamental approach, the logic to explain a phenomenon starts from established Principles and ends up with a

Mechanism (or a single functioned model) assumed to explain a phase of the phenomenon even if there appear several appropriate assumptions to proceed the logic or mathematics.

On the other hand in the *phenomenological approach*, the logic starts from Premises assumed in the Model to explain the phenomenon. The value of the Premises assumed irrespective of justification by principles are evaluated by the degree of success accomplished by the model in the explanation of the phenomenon. If the reality of the assumed Premises is established, then the Premises, are tried to justify on the bases of the Principles or the Principles are overthrown by the phenomenon, as illustrated by many famous examples in the history of science.

Next step to present the TNCF (trapped neutron catalyzed fusion) model, therefore, is the explanation of its Premises in terms of experimental facts.

2. Premises of the TNCF Model suggested by Experimental Facts

The cold fusion phenomenon (CFP) occurs in solids where a distance between particles is about 10^{-8} cm and an average energy of a particle is about 25 meV. On the other hand, nuclear reactions between charged particles which is realized at a mutual distance of 10^{-13} cm can only effectively occur when the mutual energy of reacting particles is above about 1 MeV. Therefore, a nuclear reaction in solids if it occurs in reality is not easily catalyzed by constituent charged particles in solids.

The TNCF model is a phenomenological one using a neutral particle, neutron, as a catalyst of nuclear reactions in solids and the basic Premises (assumptions) extracted from experimental data sets are summarized as follows in terms of relevant experimental facts:[2,3]

First, there are very many experimental data showing effects of the background neutron from the beginning of the discussion about reality of CFP. There have been no positive data without the background neutron. All attempts to verify or check the reality in ambient with almost no background neutron failed without exception. On the other hand, there are several data showing positive effects of thermal neutrons in CFP. These experimental facts result in the first Premise of the TNCF model:

Premise 1. We assume a priori existence of the quasi-stable trapped thermal neutrons with a density n_n in pertinent solids, to which the neutron is supplied essentially from the ambient neutron at first and then by breeding processes (explained below) in the sample.

The density n_n is a single adjustable parameter in the TNCF model which will be determined by an experimental data set using the supplementary premises which will be explained below concerning reactions between the trapped neutron and other particles in the solids. The quasi-stability of the trapped neutron means that the neutron trapped in the crystal does not decay until a strong perturbation destroys the stability while a free neutron decays with a time constant of 886.7 ± 1.9 s.

It is anticipated from this nature of CFP that the "inverse correlation of solar activity with a period of 11 years and neutron flux on the Earth" should reflect in an annual change of probability of success in experiments of CFP.

Second, there are experimental data showing localization of nuclear reactions responsible to CFP at crystal boundary or surface region, especially NT.[4] To explain this phase of CFP, it is necessary to assume localization of effective reactions between the trapped quasi-stable neutron and nuclei in the crystal lattice (lattice nuclei) which results in the Premise 2:

Premise 2. The trapped neutron in a solid reacts with another nucleus in the surface layer of the solid, where it suffers a strong perturbation. We express this property by taking the parameter (the instability parameter) ξ, defined in the relation (1) written down below, as $\xi = 1$, which means the interaction is the same as it is in vacuum.

We have to mention here that the instability parameter ξ in the surface layer is not known at all and it can be, as noticed recently, more than one ($1 \leq \xi$) making the determined

value of the parameter n_n smaller. This ambiguity is suggested by recent experimental data of various anomalous changes of decay character of radioactive isotopes and of unexpected fission products in the surface layer.

There are some experimental data sets observed in solids without surface layer or in volume far from the boundary region. To treat these data sets, it is necessary to assume reactions in solids expressed in the Premise 3:

Premise 3. The trapped neutron reacts with another perturbing nucleus in volume by a reaction rate given in the relation (1) below with a value of the instability parameter $\xi \leq 0.01$ due to its stability in the volume (except in special situations such as at very high temperature as 3000 K).

These three Premises are essential ones in the TNCF model. Following Premises 4 to 7 on the measured quantities of nuclear products and the excess heat are used to calculate reaction rates, for simplicity:

Premise 4. Product nuclei of a reaction lose all their kinetic energy in the sample except they go out without energy loss.

Premise 5. A nuclear product observed outside of the sample has the same energy as its initial (or original) one.

This means that if an energy spectrum of gamma-ray photon or neutron are observed outside, it reflects directly nuclear reactions in the solid sample. The same is for the distribution of a transmuted nucleus in the sample. Those spectra and the distributions of the transmuted nuclei are the direct information of the individual events of the nuclear reaction in the sample.

Premise 6. The amount of the excess heat is the total liberated energy in nuclear reactions dissipated in the sample except that brought out by nuclear products observed outside.

Premise 7. Tritium and helium measured in a system are accepted as all of them generated in the sample.

The amounts of the excess heat, tritium and helium are accumulated quantities reflecting nuclear reactions in the sample indirectly and are the indirect information of the individual events.

Furthermore, Premises 8 to 11 about structure of the sample and behavior of product particles are assumed for simplicity of calculation, as follows:

Premise 8. In electrolytic experiments, the thickness ℓ of the alkali metal layer on the cathode surface (surface layer) will be taken as $\ell = 1$ μm (though the experimental evidences show that it is $1 \sim 10$ μm).

Premise 9. The mean free path or path length ℓ_t of the triton with an energy 2.7 MeV generated by $n + {}^6\mathrm{Li}$ fusion reaction will be taken as $\ell_t = 1$ μm irrespective of material of the solid. Collision and fusion cross sections of the triton with nuclei in the sample will be taken as the same as those in vacuum.

Premise 10. Efficiency of detectors will be assumed as 100 % except otherwise described, i.e. the observed quantities are the same as those generated in the sample and to be observed by the detector in experiments if there are no description of its efficiency.

A premise will be made to calculate the number of events N_Q producing the excess heat Q.

Premise 11. In the calculation of the number of an event (a nuclear reaction) N_Q producing the excess heat Q, the average energy liberated in the reactions is assumed as 5 MeV unless the reaction is identified: N_Q = Excess heat Q (MeV)/ 5 (MeV).

The origin of the trapped thermal neutron can be considered as 1) the ambient background neutrons, the existence of which have been recognized widely in public, and 2) the neutrons breeded in the sample by chain nuclear reactions triggered by reactions of the trapped neutron

with perturbing nuclei, proposed in the TNCF model.

3. Reaction between the Trapped Neutron and Lattice Nuclei and its Effects

If the stability of the trapped thermal neutron is lost by a large perturbation in the surface layer or in volume, the number of reactions between the trapped neutron and lattice nuclei ${}^{A}_{Z}\mathrm{M}$ (trigger reactions) in a time τ may be calculated by the same formula as the usual collision process in vacuum but an instability parameter ξ:

$$P_f = 0.35 n_n v_n n_M V \sigma_{nM} \tau \xi, \tag{1}$$

where $0.35 n_n v_n$ is the flow density of the trapped thermal neutron per unit area and time, n_M is the density of the nucleus ${}^{A}_{Z}\mathrm{M}$, V is the volume where the reaction occurs, σ_{nM} is the cross section of the reaction determined in vacuum. The instability parameter ξ as taken into the relation (1) expresses an order of the stability of the trapped neutron in the region as explained in premises 2 and 3, and also in the next paragraph.

If a fusion reaction occurs between a trapped thermal neutron and one of lattice nuclei ${}^{A}_{Z}\mathrm{M}$ with a mass number A and an atomic number Z, there appears an excess energy Q and nuclear products as follows:

$$n + {}^{A}_{Z}\mathrm{M} = {}^{A+1-b}_{Z-a}\mathrm{M}' + {}^{b}_{a}\mathrm{M}'' + Q, \tag{2}$$

where ${}^{0}_{0}\mathrm{M} \equiv \gamma$, ${}^{1}_{0}\mathrm{M} \equiv n$, ${}^{1}_{1}\mathrm{M} \equiv p$, ${}^{2}_{1}\mathrm{M} \equiv d$, ${}^{3}_{1}\mathrm{M} \equiv t$, ${}^{4}_{2}\mathrm{M} \equiv {}^{4}\mathrm{He}$, etc.

The liberated energy Q may be measured as the excess heat by the attenuation of the nuclear products, γ and charged particles, as generated in the nuclear reaction. Otherwise, the nuclear products may be observed outside with an energy (we assume it as the original one, hereafter) or may induce succeeding nuclear reactions (breeding reactions) with one of other nuclei in the sample.

4. Explanation of Several Events in a Data Set with a Single Parameter n_n

In general, the number of events (reactions) N_{nM} in time τ between the trapped neutron and the lattice nuclei ${}^{A}_{Z}\mathrm{M}$ in a volume V of a reaction region is given by the similar relation as (1);

$$N_{nM} = 0.35 n_n v_n n_M V \sigma_{nM} \tau \xi, \tag{3}$$

where n_M is the density of the nucleus M, σ_{nM} is the cross section of the reaction and ξ is the instability parameter defined in Premises 2 and 3.

In cases where is a surface layer of Li metal on the cathode, the numbers of tritium N_t and helium-4 atoms N_{He} in n - ${}^{6}_{3}\mathrm{Li}$ reaction (2) are determined by the relation (3) and is also number of the events N_Q generating the excess heat of 4.8 MeV per a reaction;

$$N_t = N_{He} = N_Q \equiv Q \text{ (MeV)}/4.8 \text{ (MeV)}. \tag{4}$$

A relation between N_n and N_t in D/Li system with the surface layer of Li metal is, then, given as follows; when the n $-{}^{6}\mathrm{Li}$ reaction is predominant in an electrolytic system with D_2O, a neutron with an energy 14.1 MeV is generated by the reaction between a deuteron and a triton with an energy 2.7 MeV generated in the $n-{}^{6}_{3}\mathrm{Li}$ reaction:

$$t + d = {}^{4}_{2}\mathrm{He}\ (3.5\ \mathrm{MeV}) + n\ (14.1\ \mathrm{MeV}). \tag{5}$$

Number of this reaction is calculated by a relation (6) given below which determines a relation between N_n and N_t assuming half of the generated triton contribute the reaction (5),

$$N_n \sim N_t \ell_t n_d \sigma_{t-d}, \tag{6}$$

where $\ell_t \sim 1$ μm, $n_d = 6.8 \times 10^{22}$ x cm^{-3} (x = D/Pd) and $\sigma_{t-d} \sim 1.4 \times 10^{-1}$ b. For $x = 1$, we obtain a relation

$$N_n/N_t = 9.5 \times 10^{-7} \sim 10^{-6}, \quad (7)$$

$$\text{or } N_t/N_n = 1.1 \times 10^{6} \sim 10^{6}. \quad (8)$$

These quantitative results (4) and (8) on the numbers of events are compared with the lucky experimental data where observed several events in a sample simultaneously. Some of the results are shown in Table 1. In the case where the solid occluding hydrogen isotopes has

Table 1: Neutron Density n_n and Relations between the Numbers N_X of Event X Obtained by Theoretical Analysis of Experimental Data by TNCF Model ($N_Q \equiv Q$ (MeV)/5 (MeV)). Typical value of the surface vs. volume ratio S/V(cm^{-1}) of the sample is tabulated, also.

Authors	System	S/V cm^{-1}	Measured Quantities	n_n cm^{-3}	Other Results (Remarks)
Fleischmann et al.	Pd/D/Li	6 $\sim$ 40	Q, t, n $N_t/N_n \sim 4\times 10^7$ $N_Q/N_t \sim 0.25$	$\sim 10^9$	(Q =10W/cm^3) $N_t/N_n \sim 10^6$ $N_Q/N_t = 1.0$
Morrey et al.	Pd/D/Li	20	Q,^{4}He ^{4}He in $\ell \leq 25\mu$m	4.8×10^8	$N_Q/N_{He} \sim 5.4$ (If 3% ^{4}He in Pd)
Chien et al.	Pd/D/Li	4	^{4}He in surf. layer and t , no ^{3}He	1.8×10^6	$N_t/N_{He} \sim 1$(If few%^{4}He in Pd)
Takahashi et al.	Pd/D/Li	2.7	t, n $N_t/N_n \sim 6.7\times 10^4$	3×10^5	$N_t/N_n \sim$ 5.3×10^5
Miles et al.	Pd/D/Li	5	Q, ^{4}He (N_Q/N_{He}=1$\sim$ 10)	$\sim 10^{10}$	$N_Q/N_{He} \sim 5$
Okamoto et al.	Pd/D/Li	23	Q, NT$_D$ $\ell_0 \sim 1$ μm	$\sim 10^{10}$	$N_Q/N_{NT} \sim 1.4$ (^{27}Al $\rightarrow$ ^{28}Si)
Bockris et al.	Pd/D/Li	5.3	t,^{4}He;$N_t/N_{He} \sim 240$	3.2×10^6	$N_t/N_{He} \sim 8$
Cellucci et al.	Pd/D/Li	40	Q, ^{4}He N_Q/N_{He}=1$\sim$ 5	2.2×10^9	(IfQ =5W) N_Q/N_{He}=1
Iwamura et al.	PdD$_x$ and Pd/ CaOPd$_x$/Pd	20	$Q\sim$ 1W,$N_{NT}/N_Q \sim 1$ NT$_F$(Ti, Fe, Cu etc.)	3.1×10^{10}	$N_{NT}/N_Q)_{th}$=1 $\sim$ 3

no surface layers, we have to consider a trigger reaction between a trapped neutron and a deuteron (or a proton) in addition to those between a trapped neutron and one of lattice nuclei:

$$n + d = t\ (6.98\ \text{keV}) + \gamma\ (6.25\ \text{MeV}), \quad (9)$$

$$n + p = d\ (1.33\ \text{keV}) + \gamma\ (2.22\ \text{MeV}). \quad (10)$$

5. Conclusion –Values of n_n, Sporadic Occurrence and Qualitative Reproducibility of Events in CFP

Typical values of the adjustable parameter n_n determined by experimental data sets where observed several events in the same sample are shown in Table 1. Generally speaking, the values of n_n determined using experimental data sets more than 60 are between 10^8 and 10^{12} cm^{-3}. This is rather large value and its meaning assumed at first as a density of the trapped thermal neutrons in solids has to be reconsidered. This problem with others concerned with Premises will be discussed in relation with the evolution of the model in another paper presented in this Conference.[5]

It should be given here qualitative explanations of the two remarkable characteristics of CFP, sporadic occurrence and poor reproducibility of its events. In the following, we confine our discussion to electrolytic systems with electrolytes of alkali metals.

In the process of a CF experiment, there are many atomic processes with stochastic property: distribution of impurity atoms in the matrix metal, diffusion of hydrogen isotopes in it, deposition and diffusion of the electrolyte on and into the cathode, and so on. As a due result, the microscopic structure of the cathode becomes different from one to another even if the macroscopic condition of the electrolysis is the same. It should also be noticed the chaotic nature of CFP occurring in complex systems which induces inevitably the qualitative reproducibility.

In view of the TNCF model, the microscopic difference of the sample influences sensitively on the trapping of thermal neutrons in the cathode and also on the trigger and breeding reactions between the trapped neutron and one of lattice nuclei. Occurrence of a trigger reaction in the surface layer formed on the cathode is governed by statistical law and is characterized by a statistical reproducibility, or *qualitative reproducibility*. Even if there are enough background neutrons in ambiance, there occurs a situation with a various number of trapped neutrons from zero to the maximum value tolerated by the condition not to start the trigger reaction; these values correspond to from a null result to a positive result with maximum gain of products.

Thus, the reactions relevant to CFP are divided into trigger and breeding reactions in the TNCF model. When a trigger reaction is induced by one of trapped neutrons piled up in the sample, which may be in the form of neutron drops in a boundary region, the start of the succeeding breeding reaction multiplying trapped neutrons is governed by statistical law and also resulting products of CFP are. Occurrence of an events with a large yield is not frequent and is observed sporadically.

The qualitative reproducibility, sometimes called irreproducibility by mistake, and sporadic nature of events in CFP are explained consistently as above from TNCF point of view. We would like to notice again that the experimental trials done in large Laboratories in 1989 to confirm and prove reality of CFP are destined to fail due to elimination of background neutrons, among others, to improve S/N ratio in terms of conventional consideration in physics.

As a result of our investigation of CFP by the TNCF model, it is obligatory to measure and describe the background neutron density as one of experimental conditions in this field.

The TNCF model has shown its usefulness as explained in this paper using a neutral particle, neutron, as a agent which catalyzes nuclear reactions in solids and giving a systematic explanation of CFP even if the Premises assumed in the model is not verified yet.

References

[1] M. Fleischmann, S. Pons and M. Hawkins, *J. Electroanal. Chem.* **261**, 301 (1989).

[2] H. Kozima, *Discovery of the Cold Fusion Phenomenon –Evolution of the Solid State - Nuclear Physics and the Energy Crisis in 21st Century*, Ohtake Co. Inc., Tokyo, Japan, 1998.

[3]H. Kozima, K. Kaki and M. Ohta, "Anomalous Phenomenon in Solids Described by the TNCF Model", *Fusion Technology* **33**, 52 (1998).

[4] H. Kozima, M. Ohta, K. Arai, M. Fujii, H. Kudoh and K. Yoshimoto, "Nuclear Transmutation in Solids explained by TNCF Model" *Proc. ICCF8* (to be published)

[5] H. Kozima, "The Cold Fusion Phenomenon and Physics of Neutrons in Solids", *Proc. ICCF8* (to be published).

Conference Proceedings Vol. 70
"ICCF8"
F. Scaramuzzi (Ed.)
SIF, Bologna, 2000

THE COLD FUSION AS A SPACE-TIME ENERGY PUMPING PROCESS

ATHANASSIOS A. NASSIKAS

Technological Edu. Institute of Larissa.
10, Ethnikis Antistasseos Str. 41 335 Larissa Greece.
E-mail: a.a.nass@teilar.gr

Abstract

The purpose of this paper is to explain the cold fusion phenomena as a space-time energy pumping process on the basis of the hypothesis of the Quantum Space-Time; this hypothesis is based on *the unification of the physical meaning of the notions which derive either from the GRT or the QM.* An experiment is proposed to verify this cold fusion explanation.

1 Introduction

According to the GRT, a particle field consists of a particle matter and a spacetime continuum which surrounds this matter. According to the QM, a particle field is described by means of a matter (De Broglie) wave, which includes the notion of a particle matter. If we want to *unify the physical meaning of the notions which derive either from the GRT or the QM,* the following principles should be valid : *Principle I. "Any infinitesimal spacetime can be regarded as a matter wave". Principle II. "The energy of any oscillating infinitesimal spacetime is equivalent to its internal time" ;* where as internal time is defined a time τ of a phenomenon of comparison. The hypothesis of the Quantum Space-Time(QST) [1,2] is based on these principles and implies that space-time is stochastic and it can be regarded as matter -ether. However, matter can be either mass or charge. Thus, there exist both mass-gravitational (g) and charge-electromagnetic (em) spacetime. The (em) spacetime behaves as a (g) spacetime , since both are spacetime and obey the same principles I,II, but it is not. Thus, any time interval in the (em) spacetime is incomprehensible with respect to a coexisting (g) spacetime and it can be regarded as an imaginary number which is incomprehensible too. *According to principle II the energy of an infinitesimal (em) spacetime can be regarded as imaginary since it is equivalent to an (em) time interval. Therefore, in general, the electromagnetic energy can be regarded as imaginary.* A gravitational spacetime energy E_g can be converted into an electromagnetic spacetime energy E_{em} by means of photons and vice versa. Thus, in a closed system , the conservation principle can be applied as follows:

$$\overline{E}_g + \overline{E}_{em-g} = \text{constant} \quad (1)$$

where the em-g index indicates a gravitational space energy in such a way that $\overline{E}_{em} = i\overline{E}_{em-g}$ and the dash ($^{-}$) indicates the mean value. It is stressed that the energy of a system is a stochastic quantity, thus the mean value is meaningful . If we consider the Universe as a closed system which has been derived from zero, then the following equation applies:

$$\overline{E}_g{}^U + \overline{E}_{em-g}{}^U = 0 \quad (2)$$

where the superscript ^{U} indicates Universe quantities. In a particle field, the following equation is valid according to the QST hypothesis:

$$\langle E \rangle \langle V \rangle = hc \quad (3)$$

i.e., the product of the energy expectation value of a particle field multiplied by the expectation value of the volume which contains that energy, is equal to hc. In general, it can be proved that the volume $\overline{V}_g$ increase of a closed system has as a result the energy $\overline{E}_g$ decrease and vice versa. Thus, when $\overline{E}_g{}^U$ is very high, the volume $\overline{V}_g{}^U$ that contains $\overline{E}_g{}^U$ will be very low. Universe's expansion means increase of $\overline{V}_g{}^U$ and decrease of $\overline{E}_g{}^U$ as well as increase of $\overline{E}_{em-g}{}^U$ according to the equation (2). From the equation (2) it is derived that for positive value of $\overline{E}_g{}^U$ the $\overline{E}_{em-g}{}^U$ value will be negative. Thus, the Universe evolution is a process reverse to that of the Universe creation, and during this evolution the quantity $\overline{E}_g{}^U$ decreases tending to zero, while the quantity $\overline{E}_{em-g}{}^U$ increases tending also to zero. We can assume that the charge energy $\overline{E}_{em-g}{}^U$ is the charge energy sum of all the proton-electron couples regardless of whether they are joined or not. This means that the absolute value of the proton charge, assumed as negative energy, is greater than the electron charge – assumed as positive energy -, so that the total $\overline{E}_{em-g}{}^U$ will be negative. According to existing measurements, the proton charge is $4{,}803206815 \times 10^{-10}$ esu [3]. According to the existing data, the electron charge is $e = \sqrt{\alpha \hbar c} = 4{,}80319626 \cdot 10^{-10}$ esu [3]. When there is a tendency for increase and nullification of $\overline{E}_{em-g}{}^U$, this means that there is an approach and coincidence tendency between the positive and negative charges of the proton-electron couples. The electron charge, if considered as an imaginary mass, is not constant but it varies with its velocity; thus, when the electron approaches the proton, it will have a value able to neutralize it. Thus, the approach between electrons and protons has as a result the increase of $\overline{E}_{em-g}{}^U$ and due to equation (2), the decrease of $\overline{E}_g{}^U$. Consequently, we can assume that *during the approach between e^- + P, a gravitational space energy absorption takes place* . This might be compatible with the reaction [4]:

$$e^- + P \rightarrow n + \text{neutrino } -0{,}783MeV \quad (4)$$

which is endothermic. According to N. Kozyrev 's observations, the stars on which no nuclear reaction take place, are radiant and this radiation is proportional to the electrons

density at the radiating area [5,6]. This shows a relation between the radiation and the electron-proton couples mentioned.

2 Space-Time Energy Pump

We denote by E the energy level of an electron, excluding its rest energy, in a radius r in the hydrogen atom and by E_{el} the kinetic energy that the electron acquires during the free fall from radius $r=\infty$ to radius $r=r$. According to the QST hypothesis, matter is the spacetime itself and the energy E_{el} is the energy-matter of the space within which this energy exists. According to Classical Mechanics, the transfer from one energy level E_{el} to a higher one takes place through action of the proton field on the electron. *According to the QST hypothesis, there is no action from a far distance and the energy increase is caused only by matter increase.* Therefore, during the transfer from one level of energy E_{el1} to a higher level of energy E_{el2} which corresponds to a smaller radius r, we should have, according to the QST hypothesis, absorption of energy-matter by something that exists out of the space which encloses energy E_{el1}. Since the increase of E_{el} has as a consequence the decrease of the radius r, this means that this increase corresponds to e^-+P approach. According to what was mentioned above, the e^-+P approach has as a consequence the absorption of (g) space energy-matter δE_g; this energy according to the QST hypothesis, causes the increase of the level of energy E_{el}. By definition, it is valid that $E=-E_{el}$; therefore the transposition from E_{el1} to E_{el2} is equivalent to the transposition from the energy level $E_1=-E_{el1}$ to the energy level $E_2=-E_{el2}$. If E_1 and E_2 correspond to fundamental energy levels of the electron in the hydrogen atom, then, *as it is experimentally verified, photon emission will take place. Because of the* e^-+P *approach , as was above mentioned, gravitational energy* δE_g *absorption will occur.* Applying the energy conservation principle, we have as a result the following equations:

$$E_{el0}+E_{el1}+\delta E_g = E_{el0}+E_{el2}+h\nu,$$
$$\delta E_g = E_{el2}-E_{el1}+h\nu = (E_1-E_2)+(E_1-E_2) = 2(E_1-E_2) = 2(E_{el2}-E_{el1}) \quad (5)$$

Where E_{el0} is the total electron rest energy related both to mass and charge which charge is regarded as an imaginary mass. Thus, during the approach between e^- + P a gravitational space energy absorption δE_g takes place that fulfills eqn (5). This energy δE_g is converted partly into photons ($h\nu = E_{el2}-E_{el1} = \delta E_g/2$) and partly to energy increase in order to reach the energy E_{el2} ($E_{el2} = E_{el1}+\delta E_g/2 = E_{el1}+E_{el2}-E_{el1}$). According to this analysis the energy E_{el} takes in addition into account the energy δE_g; this is understood taking into consideration the relativistic changes of mass and load which is regarded as an imaginary mass. Taking into account the above mentioned, we conclude that the electron when approaching the proton increases in charge until it is valid that: $Q_{proton}=-Q_{electron}$ or $Q_{proton}+Q_{electron}=0$, a fact that corresponds to charge disappearance and -according to eqn(4)- to neutron and neutrino production.

After the 1st fundamental energy level of an electron in the hydrogen atom there is no permitted state other than the one corresponding to the elimination of the couple e^- + P and

to the neutron generation. *Thus , any other state can be regarded as unstable* . When reaching an unstable state E_2 lower than the fundamental E_1 in order that gravitational space absorption and photon emission are possible, the conditions of the equations (5) must be fulfilled. Consequently, it is valid: $E_1 - E_2 = h\nu$. Let's assume that a negative potential is imposed on the hydrogen atom. Due to the negative potential, no other permitted level interferes between the level $E_1 = -13{,}6\,eV$ and the level $E_\infty = 0$ and consequently the energy rejection must take place by photons of energy $-E_1$. Thus, it will be valid that:

$$E_1 - E_2 = -E_1 \quad \text{and} \quad E_2 = 2E_1 \tag{6}$$

Equation (6) can be extended to energy levels so that:

$$E_{k+1} = (k+1)E_1 \tag{7}$$

given that there is a difference $E_1 - E_{k+1} = -kE_1$, that is an integer multiple of $-E_1$ and consequently it can be rejected in the form of quanta with energy $-E_1$. Reaching the state E_{k+1}, a gravitational space absorption takes place according to eqn (5) so that we will have:

$$\delta E_{g\,k+1} = 2(E_1 - E_{k+1}) \tag{8}$$

Because of the equations (7,8) it is valid:

$$\delta E_{g\,k+1} = k\text{x}27{,}2\,eV \tag{9}$$

Equation (9) is similar to Mills' equation for the rejected energy during the conversion of hydrogen's atom into a stable state-hydrino[7] . Nevertheless, the levels E_{k+1} are unstable and different from those given by Mills. It is noted that eqn (9) has been derived from eqn (5) as if the states E_{k+1} were stable; however we cannot exclude graviton emission when electron moves from E_{k+1} to E_1. *Thus, we could regard this phenomenon as stochastic; the possibility for photon emission is reinforced by the Kozyrev star radiation which takes place under constant matter structure (without nuclear reactions)[6].*

On the basis of the aforementioned analysis, we can compose a space-time energy pump which can convert the ether's space-time energy into thermal energy or into mechanical or electrical work, by means of a system that displaces the electron of the E_1 fundamental level of the hydrogen atom to an unstable energy level E_{k+1} and returns it to the state E_1. In such a system gravitational space energy absorption $\delta E_{g\,k+1}$ will take place and its conversion into photons with simultaneous return of the electron to the stable situation E_1 under the condition that the aforementioned system imposes the energy level E_1 as the unique stable situation permitted.

3 Interpretation of the Cold Fusion Phenomena

During the heavy water electrolysis, heavy hydrogen is formed on the cathode and oxygen on the anode. When palladium is used as a cathode, the heavy hydrogen is absorbed inside the palladium. Because of the negative cathode potential, the heavy hydrogen electron is

on the 1st level and a force is exerted on it, pushing it towards the nucleus. Thus, an approach between e^- + P will take place by means of unstable states, in the same way as it has already been mentioned in Sec. 2. These unstable levels are probable to exist while the energy eigenvalue remains at the permitted energy level E_1. In this way, a space-time energy pump will be formed, having as a result the gravitational space energy pumping and the production of photons that heat the whole electrolytic system. The above mentioned are also effective in the case of light water electrolysis given that exactly the same mechanisms are being activated in the cases of both the heavy and the normal hydrogen. Thus, Mills' experiments [7] can be explained on the basis of the space -time energy pump; *this is an alternative explanation since hydrinos have not been detected.* The aforementioned concern an excess heat generated without any reaction. However, during the cold fusion phenomena there is detection of nuclear reaction products. All these can be explained on the basis of the following reactions[4]:

$$e^- + P \rightarrow n + \text{neutrino } -0{,}783\text{MeV} \quad (10)$$
$$e^- + D \rightarrow 2n + \text{neutrino } -0{,}783\text{MeV} \quad (11)$$

The energy of 0,783 MeV, according to Conte approved by Mizuno explanation [4], is covered by the electron capability to have – according to quantum mechanics – a presence probability under high energy as well as by the developing of an excess potential in very small distances between electron and proton. However, the energy of 783000 eV is difficult to be handled by means of low voltages. Thus, it is expected that the reactions (10,11) are significantly facilitated by the gravitational space energy absorption during the approach between e^- + P, which is not rejected but it is used for the creation of the next stable state (n + neutrino).

4 A Proposed Experiment

For the purposes of this chapter the following definitions are useful:
As reference spacetime is defined a Euclidean spacetime to which, through transformations of deformity, any field can correspond. Any magnitude of it will be denoted by the subscript $_0$. *As Hypothetical Measuring Field (*HMF) is defined a hypothetical field, which consists of the reference spacetime, in which at every point A_0 the real characteristics of the corresponding point A of the real field exist. In a HMF it is defined as *relative time* the ratio $tr = dt/dt_0$, where dt is an infinitesimal time of comparison.

According to the QST hypothesis we have that the gravitational acceleration $\vec{g}(r,t)$ at a point (r,t) of the HMF is [1,2,8]:

$$\vec{g}(r,t) = \frac{c^2}{P(r,t)}\nabla P(r,t) = \frac{c^2}{\overline{tr}(r,t)}\nabla \overline{tr}(r,t) \quad (12)$$

where $P(r,t)$ is the probability density of a matter system considered as a whole and $\overline{tr}(r,t)$ is the mean value, due to uncertainty, of relative time which correspond to (r,t) of the HMF; $\overline{tr}(r,t)$ is proportional to the HMF ether density at the point (r,t) [1]. Because of eqn (12), what is shown in Fig.1a will take place, that is the attraction on an object is attributed to the fact that the space time-ether under the object attracts the object more

than the upper one and that $\overline{tr}_2 > \overline{tr}_1$ [1,2,8]. If we reduce the ether energy density under the body[1,7], i.e. if we succeed in having $\overline{tr'}_2 < \overline{tr}_2$ then a weight loss of the object will take place as it is shown in Fig.1b

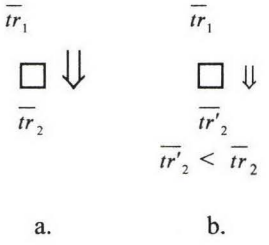

Fig.1

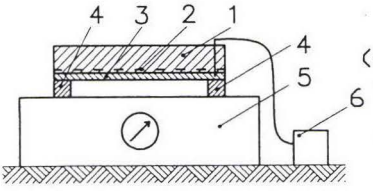

Fig.2

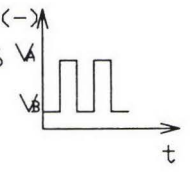

Fig.3

These can take place through the arrangement of fig.2 [9]. The nickel plate 1 is hydrogenated at its lower part 2. The already hydrogenated area 2 is covered by a layer of nickel plating 3. Through the insulating bars 4 the whole system lies on scales 5 . Through a production and regulation electric pulses system 6 negative voltage electric pulses of the form of fig. 3 are exercised on the parts 1 and 3. According to what was mentioned in Sec. 2,3 ether absorption will take place in the area 2. Ether will reach the area 2 through the less attracting area of nickel plating 3. Thus it is expected that what is shown in fig.1 will take place. A detectable weight loss is expected, through the scales 5, since the ether energy absorption is at the level of the excess heat, similar to Mills' one, at area 2.

REFFERENCES

[1] Nassikas, A.A.,1999. The Hypothesis of the Quantum Space Time - Aether. Accepted for publ. in Galilean Electrodynamics, Special Issues 2, 2000. Available at www. physical-congress. spb. ru

[2] Nassikas, A.A., 1997. The Hypothesis and the Equations of the Unified Matter Field. Infinite Energy - Cold Fusion Technology, Inc. Vol.3, No.13&No.14. Available at www. physical-congress. spb. ru

[3] Gervolin's, I.L., 1991. To Live Without Disasters. Higher Naval Engineering College. St. Petersburg.

[4] Mizuno, T., 1998. Nuclear Transmutation: The Reality of Cold Fusion. Infinite Energy Press. Concord, NH.

[5] Frolov, A., 1998. The Source of Excess Energy. Infinite Energy, Vol.(4) Issue 20.

[6] Dadaev, AN., 2000. Astrophysics and Causal Mechanics. Galilean Electrodynamics, Special Issues 2, 2000.

[7] Mills, R.L., 1991. Energy/matter Conversion Methods and Structures. International Patent Publication Number WO 92/10838. Infinite Energy, Vol.(3) Issue 17.

[8] Nassikas, A.A., 1994. The Hypothesis of the Unified Field and the Principle of its Dual Interpretation. III International Conference: "Problems of Space, Time, Gravitation". Russian Academy of Sciences. St. Petersburg, Russia. Available at www. physical-congress. spb. ru

[9] Nassikas, A.A., 1999. Space Time Energy Pump. Patent application No 990100439, Greek Organization of Industrial Property.

AUTHOR INDEX

AUTHOR INDEX